FATIGUE FAILURE AND CRACKING IN HIGH MAST POLES

by
Raka Goyal
Research Assistant

Hemant B. Dhonde
Research Assistant Professor

and

Mina Dawood
Assistant Professor

Research Project Number 0-6650
Fatigue Failure and Cracking in High Mast Poles

Performed in cooperation with the
Texas Department of Transportation
and the
Federal Highway Administration

October 2011
Published: March 2012

Department of Civil and Environmental Engineering
University of Houston
Houston, Texas

Technical Report Documentation Page

1. Report No.	2. Government Accession No.	3. Recipient's Catalog No.
FHWA/TX-12/0-6650-1		

4. Title and Subtitle	5. Report Date
FATIGUE FAILURE AND CRACKING IN HIGH MAST POLES	October 2011 Published: March 2012
	6. Performing Organization Code

7. Author(s)	8. Performing Organization Report No.
Raka Goyal, Hemant B. Dhonde, and Mina Dawood	Report 0-6650-1

9. Performing Organization Name and Address	10. Work Unit No. (TRAIS)
Department of Civil & Environmental Engineering Cullen College of Engineering University of Houston 4800 Calhoun Road Houston, TX 77204-4003	11. Contract or Grant No. Project 0-6650

12. Sponsoring Agency Name and Address	13. Type of Report and Period Covered
Texas Department of Transportation Research and Technology Implementation Office P.O. Box 5080 Austin, TX 78763-5080	Technical Report: September 2010–August 2011
	14. Sponsoring Agency Code

15. Supplementary Notes

Project performed in cooperation with the Texas Department of Transportation and the Federal Highway Administration.
Project Title: Fatigue Failure and Cracking in High Mast Poles
URL: http://tti.tamu.edu/documents/0-6650-1.pdf

16. Abstract

This report presents the findings of a comprehensive research project to investigate the fatigue cracking and failure of galvanized high mast illumination poles (HMIP). Ultrasonic inspection of poles throughout the state has revealed the presence of weld toe cracks at the shaft-to-base-plate connections of some galvanized poles that the Texas Department of Transportation (TxDOT) owns.

However, the effect of these galvanization-induced cracks on the fatigue life of the poles has not been clearly defined. The first phase of this research involved extensive review of published and unpublished data, to identify key factors that contribute to galvanization-induced cracking. Best fabrication practices to minimize such cracking are recommended. In the second phase, a comprehensive reliability analysis of several TxDOT pole configurations was conducted for different regions in Texas to predict the fatigue lives of the cracked poles. Critical pole configurations and locations are identified to facilitate cost-effective decisions related to inspection, repair, and replacement of poles.

17. Key Words	18. Distribution Statement
High Mast Illumination Pole, Galvanization, Fatigue Cracking, FEM Analysis, Fatigue Life	No restrictions. This document is available to the public through the NTIS: National Technical Information Service, Alexandria, Virginia 22312 http://www.ntis.gov

19. Security Classif. (of this report)	20. Security Classif. (of this page)	21. No. of Pages	22. Price
Unclassified	Unclassified	270	

Form DOT F 1700.7 (8-72) **Reproduction of completed page authorized**

FATIGUE FAILURE AND CRACKING IN HIGH MAST POLES

by

Raka Goyal
Research Assistant

Hemant B. Dhonde
Research Assistant Professor

and

Mina Dawood
Assistant Professor

Report 0-6650-1
Project 0-6650
Project Title: Fatigue Failure and Cracking in High Mast Poles

Performed in cooperation with the
Texas Department of Transportation
and the
Federal Highway Administration

October 2011
Published: March 2012

Department of Civil and Environmental Engineering
University of Houston
Houston, Texas

DISCLAIMER

This research was performed in cooperation with the Texas Department of Transportation and the U.S. Department of Transportation, Federal Highway Administration. The contents of this report reflect the views of the authors, who are responsible for the facts and accuracy of the data presented here. The contents do not necessarily reflect the official view or policies of the Federal Highway Administration (FHWA) or the Texas Department of Transportation (TxDOT). This report does not constitute a standard, specification, or regulation, nor is it intended for construction, bidding, or permit purposes.

TRADE NAMES/MANUFACTURERS' NOTICE

The United States Government and the State of Texas do not endorse products or manufacturers. Trade or manufacturers' names appear herein solely because they are considered essential to the object of this report. Trade names were used solely for information and not product endorsement.

ACKNOWLEDGMENTS

Project 0-6650 was conducted in cooperation with the Texas Department of Transportation and the U.S. Department of Transportation, Federal Highway Administration. The authors gratefully acknowledge the contributions of the project monitoring committee, which consisted of Tim Bradberry (Project Director), John Harper (Project Advisor), Teresa Michalk (Project Advisor), Jim Yang (Project Advisor), Yuan Zhao (Project Advisor), Sandra Kaderka (Contract Specialist), and Wade Odell (Research Engineer).

The researchers thank Mr. J. Wood of the North Texas Tollway Authority (NTTA) and Mr. E. Starnater of Lamb-Star Engineering for sharing their inspection data and invaluable experience.

TABLE OF CONTENTS

LIST OF FIGURES

LIST OF TABLES

1 INTRODUCTION

High Mast Illumination Poles (HMIP) are tall, slender tubular structures that state Departments of Transportation (DOTs) widely use to support illumination fixtures along the highways in the United States. HMIP are commonly manufactured using weathering steel or galvanized steel. The poles in the Texas Department of Transportation's (TxDOT) inventory are almost exclusively galvanized, consist of 8- or 12-sided cross-sections and range from 100 ft to 175 ft tall. There are approximately 5,000 HMIP currently installed around the state, mostly concentrated at intersections of major highways in urban areas, all of which have been galvanized.

1.1 Problem

There have been instances of fatigue failures of High Mast Illumination Poles in various states nationwide. Although no such failures have been reported in Texas, ultrasonic inspection has indicated the presence of weld toe cracks at the shaft-to-base-plate connections of some galvanized HMIP. These galvanization-induced cracks significantly decrease the fatigue life of welded details. However, the specific factors that cause galvanization-induced fatigue cracking are not well understood. Further, HMIP design details and fabrication processes have remained largely unchanged for the past 30 years. However, anecdotal evidence suggests that newer poles are more susceptible to this type of cracking than older poles. This report presents the preliminary findings of an ongoing research program to identify key factors that contribute to galvanization-induced cracking of TxDOT HMIP with particular attention to the pole-to-base-plate connection.

1.2 Scope

Many parameters can affect the formation of galvanization-induced cracks making identification of the key contributing factors a complex problem. These factors include steel chemistry, cold working, welding processes, chemistry of welding consumables, thermally induced residual stresses, galvanization processes, cleaning treatments, chemistry of galvanizing baths, and thermal shock during the galvanization process. The interaction between different factors at different stages during the fabrication and service life of the poles further complicates this problem. This report presents a synthesis of the available knowledge related to galvanization-induced cracking of HMIP. Specific factors that can contribute to cracking at various stages of

fabrication, and their potential interactions, are presented. Based on a survey of the existing literature and surveys of owners, fabricators, and galvanizers, this report presents recommended fabrication processes that can be used to help minimize the likelihood of galvanization-induced cracking of HMIP.

1.3 Layout of the Report

This report consists of six sections including this introductory section.

Section 2 discusses the main factors that contribute to galvanization-induced cracking at various stages of fabrication including cold working, welding, galvanizing, and material chemistry.

Section 3 presents the general framework of the analytical model that was adopted to predict the fatigue life of high mast poles with pre-existing cracks at the pole-to-base plate connection detail. The details of the dynamic structural analysis, fatigue analysis, and reliability analysis are presented.

Section 4 presents the results of the analysis that was conducted on various pole configurations at different locations throughout the state. Example results are presented in detail for a specific pole configuration. Detailed results for the remaining configurations are presented in the appendices.

Section 5 describes some of the available repair options that can be considered in lieu of replacing damaged poles. Representative costs of different repair and replacement alternatives are compared.

Section 6 summarizes the findings of the research project, presents relevant conclusions, and identifies specific areas requiring additional investigation.

2 BACKGROUND ON GALVANIZATION-INDUCED CRACKING

Galvanization-induced cracking is a phenomenon that is governed by the interaction between several complex parameters. High mast poles are typically subjected to a wide range of fabrication activities including cold-working, welding, and galvanization. Each of these steps has the potential to induce residual stresses in the steel, making it susceptible to cracking. Additionally, the thermal shocks associated with welding and galvanizing may also contribute to the formation of cracks. Further, the specific chemistry of the steel being used can also contribute to the potential for cracking, particularly when considering the interaction with welding consumables and the zinc and other elements in the galvanizing bath. The specific details of the base-plate connection may also promote or suppress cracking. The influence of each of these factors on the potential for galvanization-induced cracking is discussed in the following sections.

2.1 High Mast Illumination Poles—TxDOT Detail

The High Mast Illumination Pole inventory of Texas is comprised of 8-sided and 12-sided tapered poles with four pole heights: 100 ft, 125 ft, 150 ft, and 175 ft (see Figure 1). The designs are grouped into two categories on the basis of maximum design wind speeds: 100 mph and 80 mph. The bottom diameters of the pole shaft range from 24.625 inches to 37.375 inches, and the top diameters range from 7.75 inches to 7.875 inches The pole shaft tapers range from 0.16 inches/ft for the 8-sided 80 mph design to 0.19 in./ft for the 8-sided 100 mph design. The shaft is welded to a polygonal or round annular base plate with holes around the circumference for anchor bolt placement.

Figure 1. High Mast Illumination Pole (Rios, 2007).

The inner diameter of the base plate varies from 13 to 24 inches and the outer diameter from 37 inches to 52 inches. (TxDOT Standard Drawing HMIP-98). The number of anchor bolts to fix the base-plate to the concrete foundation also varies from 6 to 20 bolts. The TxDOT HMIP foundation is a drilled concrete shaft with depths ranging from 20 ft to 60 ft, depending on the Texas cone penetrometer test values (TxDOT drawings HMIF-98). The pole shaft supports a luminaire assembly (ring) arrangement fixed at its top. A winch arrangement at the bottom of the shaft accessed through a hatch in the shaft wall is used to raise and lower the light assembly for maintenance and replacement purposes (see Figure 2).

Figure 2. Winch System Access Hatch (Stam, 2009).

2.1.1 Shaft-to-Base-Plate Welding Details

The welded shaft-to-base plate connection of TxDOT HMIP is typically achieved with a full-penetration groove weld. Welding is done from both sides with back gouging and without a backing ring (see Figure 4). The TxDOT connection detail can be fabricated with or without an external collar or 'ground sleeve.' Two alternative ground sleeve details, shown in Figure 3, are specified and permitted for use. Using the standard detail, the pole shaft and ground sleeve are positioned over the base-plate together and welded through with a full-penetration groove weld. The alternative detail includes two welding steps. First, the shaft is positioned and welded to the base plate. Subsequently, the ground sleeve is positioned and welded to the base-plate separately (TxDOT Standard drawings HMIP-98). The two details differ in the root opening size of the ground sleeve to base-plate weld, which is 5/16 inches for the standard procedure and 0 inches for the alternative approach.

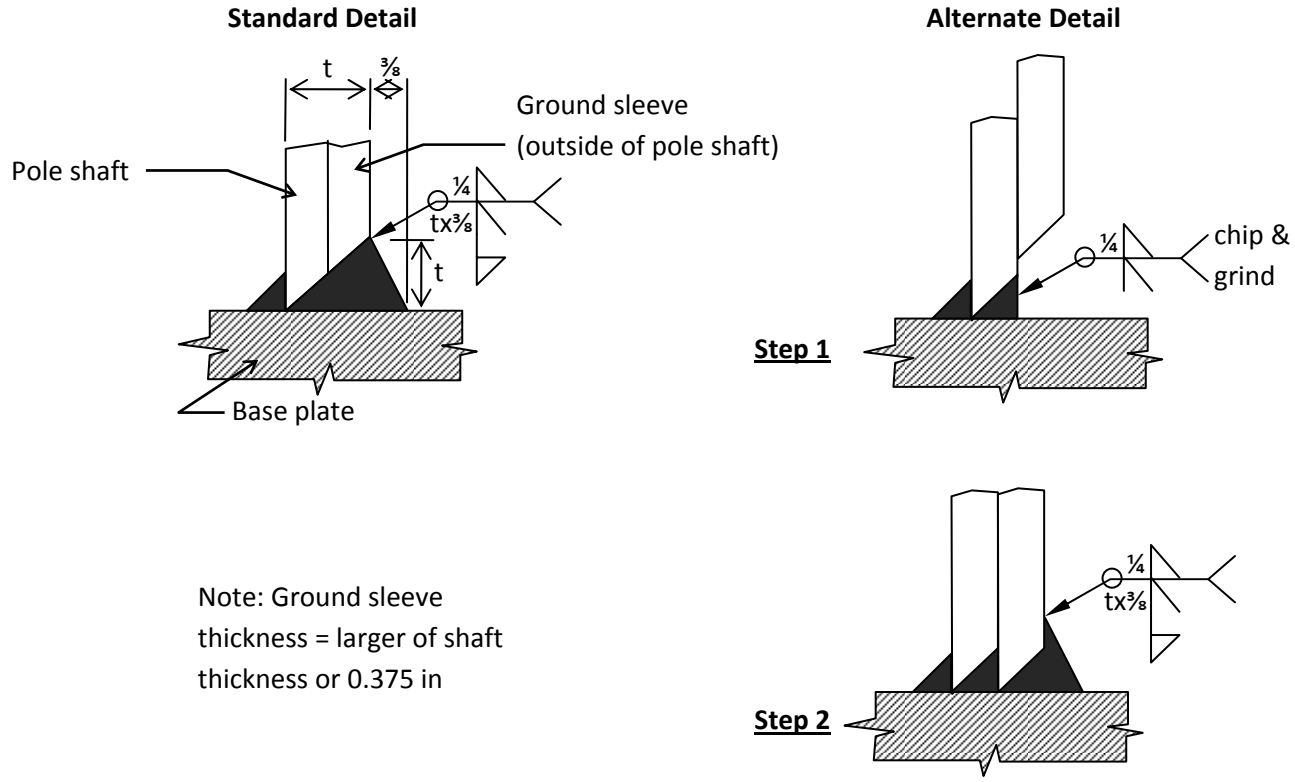

Figure 3. TxDOT Ground Sleeve Weld Details.

Several other base-plate connection details have been investigated and used in other states. Specifically, the socket detail (shown in Figure 5), and the continuous joint penetration (CJP) detail with a backing ring (shown in Figure 6) have been studied in detail. Wyoming DOT commonly uses

the latter detail. If a backing ring is used, it should be properly fillet welded around the upper edge to prevent ingress of acid into the space between the backing ring and the pole shaft. This ingress could cause accelerated corrosion of the pole base that inspectors would generally not detect.

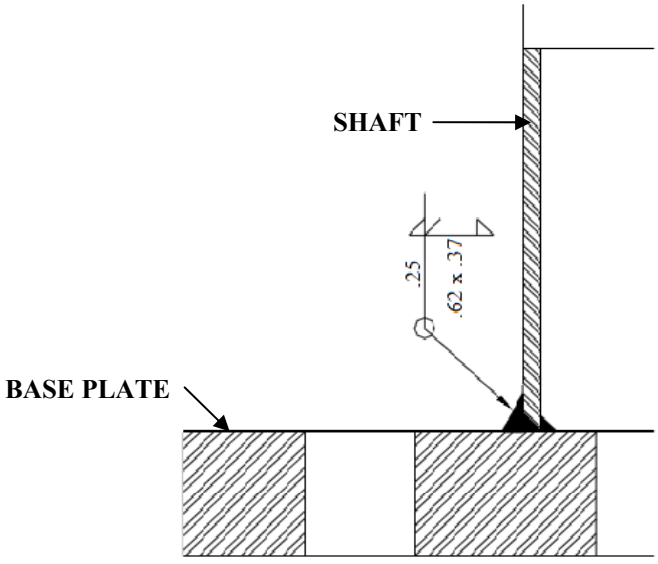

Figure 4. Texas Full Penetration Weld Detail without Ground Sleeve (Rios, 2007).

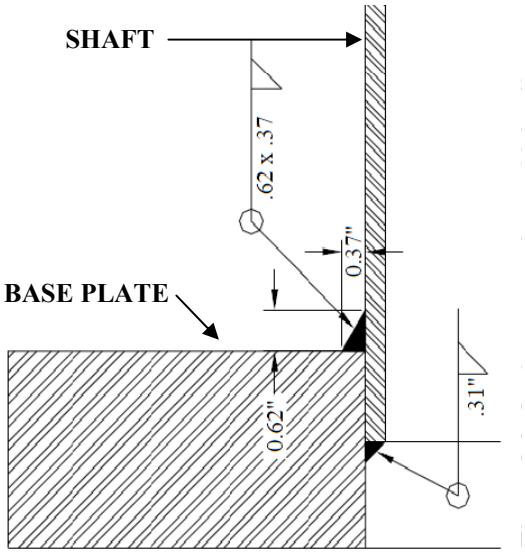

Figure 5. Fillet Welded Socket Connection Weld Detail (Rios, 2007).

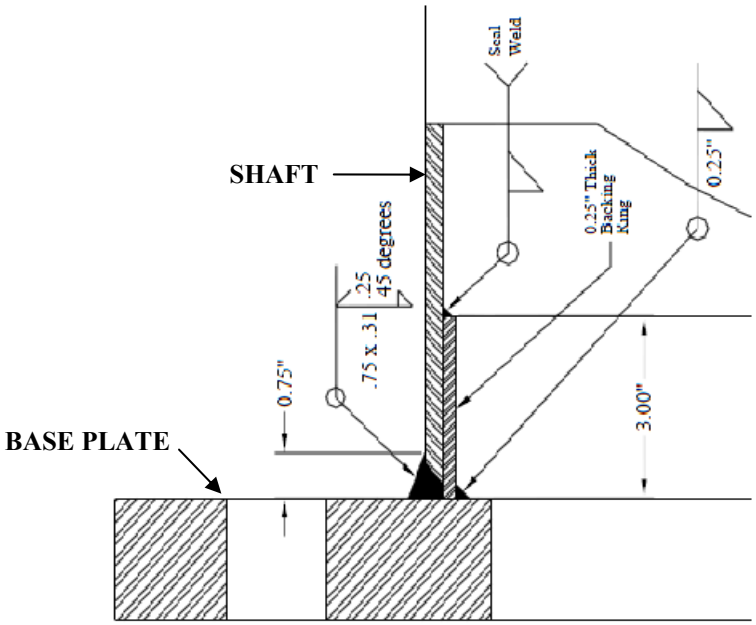

Figure 6. Wyoming Full Penetration Weld Detail with Backing Ring (Rios, 2007).

Several studies on HMIP base-plate connection details have been carried out in recent years at the University of Texas at Austin. These were based on testing of full-scale HMIP specimens with various connection details that followed AASHTO 2001 specifications. In general, full penetration welded connections showed marked improvements in fatigue resistance over fillet-welded socket connections. This effect was particularly significant for details with thicker base-plates and more anchor bolts. Neither of these factors was accounted for in the 2001 AASHTO specification (Rios, 2007). Also, galvanization was found to significantly undermine the fatigue resistance of welded details (Anderson, 2007). For a 2-inches base-plate thickness, the ungalvanized specimens tested in a previous phase of the study performed 10 times better under fatigue loading than the galvanized specimens tested in a later phase. Some of the observed difference in performance may be attributable to the difference in fabrication and testing of the details between phases.

The presence of geometric discontinuities such as holes, bends, and cavities can cause an increase in local stresses. This magnification of the stress at geometric discontinuities can be expressed by the elastic Stress Concentration Factor (SCF). It was found that for full penetration groove-welded details, the presence of a backing ring that is fillet-welded to the inside of the pole shaft can reduce the SCF of the connection detail by up to 20 percent, compared to a grove-welded detail without a backing ring. In

this regard, the backing ring performed similarly to an external collar. Further, the addition of a fillet weld at the top of the backing ring or providing a welded external collar resulted in stress concentrations forming at two locations, namely at the shaft-to-base plate weld and at the end of the backing ring or external collar, under the influence of applied loads. Base-plate thickness did not affect the hotspot stresses at the end of the collar. In general, if the welding details at the end of the backing ring or external collar were properly fabricated, the magnitude of the 'hot-spot' stresses were generally higher at the pole-to-base plate weld, although these were significantly lower than for the unstiffened pole details.

Ultrasonic testing and fatigue testing were also conducted on galvanized TxDOT poles with or without external collars (ground sleeves) and full penetration details. Poles with external collars were less likely to contain initial cracks. This was attributed to the lower ratio of volume of base plate to the volume of the first 12 inches of the shaft which resulted in more a uniform temperature distribution throughout the assembly. This more uniform temperature distribution is believed to have minimized the formation of cracks. Initial cracks were found to lower the fatigue life of poles without external collars. External collars were found to increase the section modulus at the base of the pole, thereby reducing the stress range and increasing the fatigue life of the pole (Pool, 2010). Testing suggested that the TxDOT details with and without ground sleeves corresponded to AASHTO Category C and E details, respectively. However, the external collar detail adds to the cost and difficulty of fabrication and also requires extra precautions during the galvanization process. Vent holes need to be drilled through the external collar to the pocket between the collar and the shaft wall to allow expanding air to escape during galvanizing. This essential step can be done only after the pickling stage; otherwise, the acidic pickling solution may get in through the holes and create severe corrosion hazard.

2.1.2 Materials and Fabrication

Specific materials to be used in the fabrication of HMIP are described in Texas Standard Specifications for Construction of Highways, Streets and Bridges. Generally, ASTM A572 or ASTM A588 steel is used to manufacture pole shafts, ground sleeves, and base plates. Due to thickness limitations, only grade 50 steel is permitted for use in the base-plates, whereas higher strength grade 55 steel is allowed for use in pole shafts and ground sleeves.

The shaft steel is usually manufactured in coils at the steel mills. The fabricators first decoil and then levelize the steel before bending (i.e., cold-working) it into polygonal shapes using brake presses. The two halves of the pole shaft are then joined together by seam welding. The pole has four to six sections that are slip fitted into each other at the time of installation. A CJP groove weld attaches the bottommost section to the annular base plate. The fabricator is required to get prior approval of welding procedure specifications (WPS) that are developed in accordance with the American Welding Society (AWS) codes. All the various components of the HMIP, including the anchor bolts, are hot-dip galvanized in accordance with ASTM A123 and ASTM A153 prior to fabrication.

2.1.3 Recommended Revisions to Existing TxDOT Details

The current base connection detail that TxDOT uses is generally quite robust. Some evidence suggests that the use of an internal backing ring, similar to the detail used in Wyoming, may improve the fatigue life of the connection. However, the correct performance of this detail depends on following several specific steps to prevent ingress of acid into the space between the backing ring and the pole shaft and to prevent distortion of the detail due to expansion of the air between these two elements. Based on these fabrication challenges, no changes to the connection detail are recommended. Further, the practice of using thick base plates and large numbers of anchor bolts is supported by other research that has been conducted to date. Therefore, it is strongly recommended to maintain the current practices. Similarly, it has been widely recommended to verify anchor bolt tightness during regular inspections. Research findings from a limited number of tests suggest that the presence of the ground sleeve reduces the likelihood of cracking at the base detail. The research further suggests that the presence of the ground sleeve also helps to improve the fatigue resistance of poles with pre-existing crack indications. As such, the use of the ground sleeve is strongly recommended.

2.2 Steel Chemistry

Steel is an alloy of iron (Fe) and carbon (C) with small amounts of other elements added to achieve different desirable properties. Cold working, heat treatment, and manufacturing processes further affect the properties of steel. As such, ASTM standards for different kinds of steel typically specify limitations on steel chemistry and mechanical properties of steels that are used for different applications. Seven different types of steel are currently found in different components of TxDOT maintained HMIP:

- ASTM A 572 – High-Strength Low-Alloy Columbium-Vanadium Structural Steel.
- ASTM A 588 – High- Strength Low-Alloy Structural Steel, up to 50 ksi [345 MPa] Minimum Yield Point, with Atmospheric Corrosion Resistance.
- ASTM A 607 – Steel, Sheet and Strip, High-Strength, Low-Alloy, Columbium or Vanadium, or Both, Hot-Rolled and Cold-Rolled.
- ASTM A 633 – Normalized High-Strength Low-Alloy Structural Steel Plates.
- ASTM A 1008 – Steel, Sheet, Cold-Rolled, Carbon, Structural, High-Strength Low-Alloy and High-Strength Low-Alloy with Improved Formability.
- ASTM A 1011 – Steel, Sheet and Strip, Hot-Rolled, Carbon, Structural, High-Strength Low-Alloy, High-Strength Low-Alloy with Improved Formability, and Ultra-High Strength.
- ASTM A 36 – Carbon Structural Steel.

2.2.1 Steel Manufacturing Processes

Steel manufacturing processes affect the properties of the materials. Steel making basically comprises purifying molten iron, which is saturated with carbon and contains undesirable amounts of other impurities like silicon (Si), manganese (Mn), phosphorus (P), nickel (Ni), copper (Cu), and sulfur (S). Steel manufacturing processes have evolved and changed over the years. The earliest steel making process, the Bessemer converter, is no longer in use. The Open Hearth (OH) process was largely used to manufacture steel from the 1920s to the 1960s when the Basic Oxygen (BO) process replaced it rapidly. Concurrently, the Electric Arc Furnace (EAF) method for secondary production of steel was also adopted. In the Basic Oxygen furnace, the charge has to be at least 70 percent molten iron ore, whereas the EAF method uses 100 percent scrap. EAF is the predominant method of producing steel structural shapes in the United States (Kinstler, 2003).

The steel composition varies with different processes and type and quantity of scrap used. The use of more and more scrap of highly variable quality from diverse sources results in higher alloy content in the finished steel and thereby increased hardness and reduced weldablility (Russell, 1976; Graville, 1975). Also, the EAF process is known to produce more free nitrogen in the steel, which accentuates the phenomenon of strain aging and increases the steel's susceptibility to cracking. This nitrogen needs to be balanced stoichiometrically with nitride-forming elements such as aluminum (Al), titanium (Ti), zirconium (Zr), vanadium (V), or boron (Bo). However, the consequences of having

nitrides instead of nitrogen are not so easily predicted. Aluminum nitride has been known to be associated with increased cracking tendency.

Because of these changes in the steel making industry in the past few decades, it has become increasingly important to monitor carefully the properties and chemical composition of steel to ensure crack-free performance.

2.2.2 Effect of Coiled Plate

The HMIP shaft steel is sourced from steel that is reeled into coils at the manufacturing facility at stress-relieving temperatures, depending on the thickness of the plate. These coils are then decoiled and levelized into flat plate before fabrication. A typical outcome of coiling is variation in mechanical properties in different regions of the coil due to differential cooling throughout the coil. The outer and inner laps cool more rapidly, whereas the central laps take more time in cooling from the coiling temperature to the ambient temperature. This typically results in higher yield and tensile strengths with reduced ductility of steel in the inner and outer laps. Aichinger (2006) suggested that using discrete plate instead of coils may be helpful in reducing the cracking incidences in the HMIP shaft-to-base plate connection. If coiled plate must be used, it should be cut and sized, such that critical welded details are made at the more ductile central-lap steel rather than at the ends of the coil.

2.2.3 Steel Strength and Toughness

Various studies (Nilsson, 1989; Pokhodnya, 2001; Poag, 2003) have demonstrated the susceptibility of high strength, low-alloy steels to embrittlement. The impact of yield strength of steel is to be noted on these embrittlement tendencies. It has been found that 50 ksi steel whose actual yield strength was within 10 percent of the minimum specified yield strength, displayed remarkable resistance to cracking under all adverse situations of cold working, welding, galvanizing, etc. Steel types with yield strengths in the range of 100 ksi were found to show 35 percent reduction in fatigue limit after hot-dip galvanizing, whereas no such reduction was observed in steel of low to medium strength level (42 ksi to 77 ksi).

In general, ASTM A 572 Grade 50 or 55 steel is used for both base plate and shaft fabrication. A recent HMIP fabricator response to a survey questionnaire revealed that Grade 50 is used for base plate, whereas shaft metal may be of Grade 55 or even Grade 65. A historical study of ASTM A572 standard shows that the Grade 55 steel was introduced only in the 1998 revision of the standard. It is

reasonable to assume that the use of higher grades in shaft steel would have started with the first upgrade from Grade 50 to Grade 55. The time period is relevant because cracks have been discovered in comparatively new HMIP manufactured in the past 10 years or so, much before the end of their projected fatigue life.

The ASTM A6 Supplementary requirement S18 has further limited to 95 ksi the maximum tensile strength of ASTM A572 Grade 50 and 55 steel. Similarly, the maximum tensile strength of Grade 60 and 65 steel is limited to 100 ksi and 105 ksi, respectively. The use of Grades 60 and 65 steel is restricted to riveted and bolted construction of bridges, but these types may be used for welded construction also in other applications. The use of lower grades of steel is acceptable for riveted, bolted, and welded applications for all types of structures. These restrictions are primarily implemented to minimize the potential for fatigue cracking in higher strength, lower toughness types of steel at welded details. In light of the observed cracking and fatigue failures of HMIP, it may be advisable to adopt similar limitations on strength and toughness of steels used for HMIP applications.

2.2.4 Steel Chemistry Related Parameters Affecting Cracking

'Weldability' and 'hardenability' are two terms closely related to cold cracking in welded steel structures. Weldability refers to the capacity of the steel to be welded easily using conventional welding practice. On the other hand, the sensitivity of steel to form brittle microstructures due to weld thermal cycles is known as hardenability. For carbon steel, hardness changes measurably with changes in the weld cooling rates. But for typical alloy steels, very little change in hardness occurs with cooling rate. Therefore, the slope of the hardening curve is very important in determining suitable crack-resistant welding procedures (see Figure 7).

Two aspects of the hardening curve are especially relevant. The first is the critical cooling rate that corresponds to a given level of hardness. The critical cooling rate is treated as a measure of the hardenability of steel and correlates very well with the steel chemical composition that is defined by the Carbon Equivalent (CE) value. Carbon Equivalent is a widely used method to normalize the effect of different alloying elements on the hardness of steel. When this approach is used, the alloy content is presented as the equivalent carbon content to achieve the same level of hardness as the alloyed steel.

One widely used CE value is shown in Eq. 1 (ASTM, 2007):

$$C.E. = C + Mn/6 + (Cr + Mo + V)/5 + (Ni + Cu)/15 \qquad \text{(Eq. 1)}$$

where

C = Carbon content of steel (%), **Mn** = Manganese content of steel (%).

Cr = Chromium content of steel (%), **Mo** = Molybdenum content of steel (%).

V = Vanadium content of steel (%), **Ni** = Nickel content of steel (%).

Cu = Copper content of steel (%).

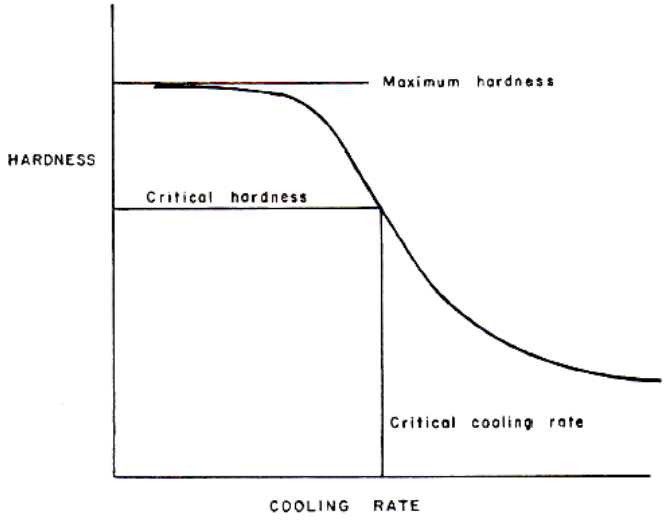

Figure 7. Typical Hardening Curve of Steel (Graville, 1975).

Carbon Equivalent is a suitable method of predicting the hardenability and cold cracking tendency of a wide range of commonly used carbon-manganese and low alloy steels. However, for low Carbon (<0.10 percent) low alloy steels, as used in manufacturing HMIP shaft steel, it might not be an accurate measure to assess cold cracking susceptibility (ASTM, 2007). This is because different chemical constituents of steel may not affect its hardness in the same way as they do its other embrittlement characteristics.

Steel's susceptibility to hydrogen embrittlement also increases with its increasing alloy content. However, a unique relation between susceptibility to hydrogen embrittlement and hardness does not exist. Thus, carbon (C), molybdenum (Mo), manganese (Mn), and chromium (Cr) increase the hydrogen embrittlement tendency of steels. While the presence of nickel (Ni) typically increases the

hardenability and the maximum hardness of steel, it is not detrimental with regard to hydrogen embrittlement. Therefore, a higher level of hardness in the weld Heat Affected Zone (HAZ) could be tolerated in a carbon-manganese steel containing nickel than in one containing chromium (Graville, 1975). As the steel composition affects hardenability, maximum hardness, and susceptibility to hydrogen embrittlement in different ways, it is very important to carefully control the types and amounts of alloying elements present in steel. To this end, supplementary requirement of the ASTM A6 standard, S31, can be used to specify a maximum CE value for the plates and shapes supplied, based on the heat analysis. The required chemical analysis as well as the CE value shall be reported.

Based on a number of hardening curves, a graph of Carbon content against Carbon Equivalent is plotted and three zones are identified, on the basis of which types of steel is classified (Graville, 1975) (see Figure 8):

- *Zone I* – These types of steel have low carbon and will not produce hard HAZs susceptible to cracking under normal circumstances.
- *Zone II* – Steel types with these compositions show steep hardening curves and the possibility of hardness control exists.
- *Zone III* – Hardness control is not possible and welding procedures must be designed on other principles.

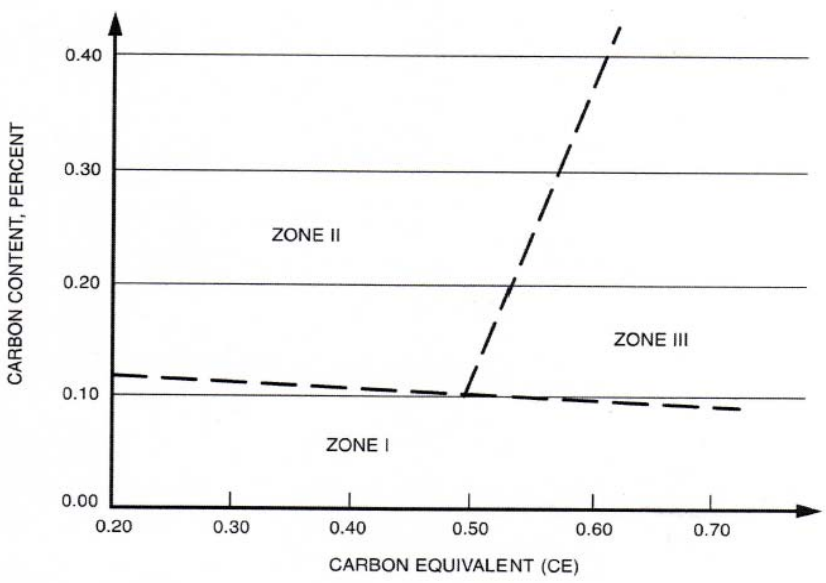

[CE = C + (Mn+Si)/6 + (Cr + Mo + V)/5 + (Ni + Cu)/15, where C = % Carbon, Mn = % Manganese, Si = % Silicon, Cr = % Chromium, Mo = % Molybdenum, V = % Vanadium, Ni = % Nickel and Cu = % Copper]

Figure 8. Zone Classification of Steels (AWS, 2010).

The shaft steel of TxDOT HMIP is a Zone I steel, whereas the base-plate steel is a Zone II steel. Based on this classification, weld preheat requirements to prevent cold cracking for different types of steel can be determined. For groove welds, the hydrogen control method of determining preheat is recommended. Section 2.4 of this report describes this method in detail.

Recently, researchers have found a correlation between the presence of small quantities of boron and susceptibility to Liquid Metal Assisted Cracking (LMAC). LMAC is a type of cracking that occurs in metals subjected to high stresses while dipped in another liquid metal, whereby the liquid metal penetrates the weakened grain boundaries of the immersed solid metal. LMAC is expected when steel types with yield strength higher than 50 ksi are used for welded structures (Mraz, 2009). The influence of steel chemical composition on hot-dip galvanized steel failure has been presented as the LMAC susceptibility parameter S_{LM-400} (Eqs. 2 and 3) based on percentages of carbon (C), silicon (Si), manganese (Mn), phosphorus (P), sulphur (S), copper (Cu), nickel (Ni), chromium (Cr), molybdenum (Mo), vanadium (V), niobium (Nb), titanium (Ti), aluminum (Al), nitrogen (N), and boron (B) (Mraz, 2009).

For Steel with C < 0.12%

$$S_{LM\text{-}400} = (201 - 370C - 22Si - 51Mn - 35P + 33S - 28Cu - 22Ni - 87Cr - 123Mo - 275V - 182Nb - 82Ti - 24Al - 1700N - 155000B) \quad \text{(Eq. 2)}$$

For Steel with C > 0.12%

$$S_{LM\text{-}400} = (227 - 320C - 10Si - 76Mn - 50Cu - 30Ni - 92Cr - 88Mo - 220V - 200Nb + 200Ti) \quad \text{(Eq. 3)}$$

The lower the value of $S_{LM\text{-}400}$, the higher the probability of LMAC. For transmission structures, which have similar configurations to, and are subjected to similar loading as HMIP, a $S_{LM\text{-}400}$ value greater than 30 is recommended. Metallographic examination of toe-cracks in transmission structures has not revealed LMAC as the failure mechanism (Aichinger, 2006). In the absence of specific guidance for HMIP, a similar limit may be appropriate. Sample calculations based on TxDOT mill certificates reveal an $S_{LM\text{-}400}$ value of more than 85 for pole shaft steel and 32 for base plate steel. As the $S_{LM\text{-}400}$ value is close to critical for base plate steel types, it is advisable to monitor this so it does not fall in the LMAC susceptible range. For ASTM A572 steel types, ASTM does not control the contents of alloy elements like molybdenum (Mo), chromium (Cr), copper (Cu), and nickel (Ni) that go into the calculation of $S_{LM\text{-}400}$ formula. It has been found that ASTM A572, Types V and I are preferable for use with regard to LMAC susceptibility rather than Type III that the mills prefer to produce (Aichinger, 2006). In any of the steel types used to manufacture HMIP, ASTM also does not control the other elements in the $S_{LM\text{-}400}$ formula like niobium (Nb), aluminum (Al), boron (B), and titanium (Ti).

Body-centered cubic metals (i.e., steel) lose most of the fracture resistance and ductility when temperature is lowered to below the Ductile-Brittle Transition Temperature (DBTT). This temperature is often the lowest temperature at which a structural engineering material can be considered useful. The transition temperature is also very sensitive to alloy composition and processing. The most dramatic and unexpected cause of brittle failure in ferrous alloys (i.e., steel) is their tendency to lose almost all of their toughness when the temperature drops below their DBTT. The DBTT is characterized by a sudden and dramatic drop in the energy absorbed by a metal subjected to impact loading. The DBTT is affected by a number of factors including heat treatment,

steel chemistry, and manufacturing processes. Therefore, typical values of DBTT cannot be clearly identified. As discussed later, cold working can also increase the DBTT of steel. Therefore, the expected service temperature for HMIP should be accounted for when selecting the steel. In order to minimize the effect of DBTT, it is recommended that steel types with DBTT well below the expected minimum service temperature of the HMIP be chosen.

Many variables in steel chemistry may influence cracking behavior, and the regular provisions in the material standards do not address some of these. Thus, the list of maximum allowable percentage content of various elements may not be exhaustive nor the minimum specified yield strengths sufficient to guard against the adverse effect of increased strength. The increasing use of scrap in steel production and the use of advanced technologies of rolling (discussed in detail in the next chapter), have obviously produced higher strength steel with lower tolerance to conventional fabrication practices. Therefore, it is imperative to control steel chemistry through specifying and enforcing all possible provisions in standards.

Different alloying elements affect the formation of galvanizing coatings on galvanized steel. Section 2.5 of this report presents the influence of steel chemistry on the galvanization products and relevant recommendations.

2.2.5 Recommendations to Minimize Cracking in HMIP

This section summarizes the various considerations that should be taken in specifying steel chemistry to minimize the potential for galvanization-induced toe-cracking in HMIP shaft-to-base plate welds:

- Since increasing carbon equivalency increases the hardness and brittleness of steels, the researchers recommend limiting the CE value of HMIP steels. They also recommend incorporating the S31 supplementary requirement of ASTM A6 into the TxDOT specifications.
- Similarly, since high-strength steel is typically more brittle, the researchers recommend adopting the S18 supplementary requirement of ASTM A6 for minimum tensile strength of ASTM A572 Grade 50/55 and Grade 60/65 steel in TxDOT specifications for the fabricators. These requirements were particularly developed for welded bridge details. However, since HMIP are heavily cold-worked, welded, and galvanized, making them susceptible to cracking, they also advise adopting these requirements.

- If feasible, it is advisable to specify Grade 50 steel for the HMIP in TxDOT specifications.
- To minimize susceptibility to liquid metal assisted cracking, it is advisable to specify susceptibility parameter SLM-400 value (Eqs. 2 and 3) higher than 30 for the HMIP in TxDOT specifications. An anecdotal review of available mill certificates suggests that this is more critical for base plate steel than for shaft steels.
- Specify the use of steels with lower Ductile-Brittle Transition Temperature, particularly for the HMIP erected in colder regions.
- In coiled steel, inner and outer laps tend to be harder and more brittle than central laps. As such, it is advisable that the steel at the bottom portion of the bottom pole segment be specified to be taken from the more ductile central laps. Alternatively, using a flat plate, rather than coiled, may also be effective.

2.3 Cold Working

Fabrication of High Mast Illumination Poles includes blanking, forming, seaming, and final assembly by welding before installation in the field. In particular, the pole shaft of the HMIP is made from levelized coil which is cold bent to make two halves of the pole. These two halves are then seam-welded together, which may require application of pressure due to lack-of-fit between the two halves. Longitudinally the pole has four to six sections, depending on the pole's height. These sections are slip fitted into each other at the time of installation in the field.

Toe cracking in HMIP has primarily been observed at the bend lines rather than at seam-welded corners. Fatigue testing of sample poles revealed that the bend lines without the longitudinal seam weld show cracking earlier than the seam welded edges (Pool, 2010). This suggests that the severe cold working at these locations affect the galvanization-induced cracking. Other researchers (Sandelin, 1954; McDonald, 1975; Kintsler, 2003) have reported similar findings. The incidence of cracking is found to be lower in poles with larger bend radii, compared to those with smaller bend radii (Aichinger, 2006). Therefore, it is important to design steel assemblies to minimize cold working and otherwise reduce areas of stress-concentrations like notches and other surface irregularities.

2.3.1 Cold Working Related Parameters Affecting Cracking

Cold working refers to plastic or permanent deformation at ambient temperatures rather than at elevated temperatures. The strain that results from such deformation is associated with the phenomenon known as *strain aging*. Strain aging is linked to the presence of free carbon and nitrogen atoms and their movement in the steel. As a result of strain aging, the yield point on the stress-strain curve of steel disappears after cold work and reappears at a higher stress. Ductility is lowered and notch sensitivity increases. Strain aging occurs very slowly at ambient temperatures but accelerates at high temperatures, a condition that the molten zinc galvanizing bath simulates. The strain aging effect produced in a period of six months at a temperature of 70°F, needs only 10 minutes at a temperature of 300°F. Strain aging causes a susceptibility to cracking, also known as strain-aging embrittlement. Cold working also makes steel more sensitive to other kinds of embrittlement. It is known that cold working can significantly increase the susceptibility of 'normal strength' (<150 ksi) steel to hydrogen embrittlement. Strain aging embrittlement can be avoided by hot working instead of cold working, or by heat treating the cold worked part at 1200 to 1300°F (McDonald, 1975; ASTM, 2007).

Fully de-oxidized or killed steel is less prone to strain aging owing to lesser amounts of free nitrogen and carbon in the material. Steel is fully deoxidized by adding strong deoxidizing agents like aluminum or silicon, to reduce oxygen content to such a level that no reaction occurs between carbon and oxygen during solidification. Semi-killed steel is incompletely de-oxidized steel containing sufficient oxygen to form enough carbon monoxide during solidification to offset solidification shrinkage. Rimmed steel is steel containing sufficient oxygen to give a continuous evolution of carbon monoxide during solidification, resulting in a case or rim of metal virtually free of voids (ASTM, 2007). Aluminum-killed steel is least susceptible to strain aging embrittlement (Sandelin, 1954).

Strain aging is also known to raise the DBTT of steel, which can be problematic in colder climates. The expected service temperature should therefore be accounted for when selecting the steel or method of fabrication. To minimize strain age embrittlement, it is recommended that steels with low DBTT be chosen.

Impact of Bend Radii on Cracking

Minimum bending radii are prescribed in various specifications and standards of ASTM and the AISC manual, but these are not consistent in all cases. It is generally recommended that the largest practical bend radii should be used, generally greater than three times the section thickness. If the bend radii must be smaller than this, it is preferable to hot bend the part. If hot bending is not possible, the cold bent part should be annealed or stress relieved before galvanizing (Sandelin, 1954; ASTM, 2007).

Bending radius has been identified as the single most important factor in causing cracking in galvanized HMIP (Sandelin, 1954; Kinstler, 2003). In one study, poles with 4-inch bend radii showed much lower incidence of cracking compared to similar poles with a 2-inches bend radii, although the 2-inches bend radii satisfied the minimum requirement of three times the section thickness specified in ASTM A143 (Aichinger, 2006). The shaft thicknesses of TxDOT HMIP range from 0.25 inches to 0.563 inches It is noted through the response of a TxDOT fabricator that 12-sided TXDOT poles are being manufactured with a bend radii of one inch due to the small diameter of the top of the pole. While pole standard bend radii are four inches the small diameter of the top section of the TxDOT poles cannot be fabricated with such a wide radius. This could be a critical factor contributing toward toe-cracking as smaller bend radii contribute to increased stress concentrations at the bends (Ocel, 2006). A feasible alternative may be to use four-inch bend radii for the bottom section of the pole shaft with smaller radii being used for higher sections. The influence of the resulting gaps at slip joints should be considered, but is not expected to be significant.

Thermal Treatment of Cold Worked Steel prior to Galvanizing

Various thermal treatments can be used to mitigate the effects of cold working. The thermal treatment that ASTM A143 recommends falls in three categories.

- For very heavy cold deformation, such as that occurring due to cold rolling, shearing, punching, sub-critical annealing at temperatures from 1200 to 1300°F is recommended.
- For less severe cold deformation as by cold bending and roll forming, the thermal treatment may be limited to stress relieving at a maximum of 1100°F.
- Lastly, the steel can also be fully normalized at temperatures from 1600 to 1700°F. The time at the temperature should approximately be one hour per inch of section thickness (ASTM,

2007). However, the costs associated with heat treatment of large pole sections may be prohibitive and other methods of minimizing embrittlement may be more suitable.

Rough Grinding of Corners and Other Measures to Prevent Stress Concentrations

Rough grinding of inside corners of bends has been known to significantly reduce cracking and even prevent the development of hidden microscopic cracks. It removes folds and surface roughness and also the hardest and most brittle material at the cold worked locations. These otherwise act as stress risers and crack nucleation sites increasing the risk of cracking manifold (Poag, 2003).

Other tips to reduce residual stresses are included in AGA's guide for fabrication of members to be hot-dip galvanized. Members should be accurately pre-formed so that it is not necessary to force spring or bend them in position during joining.

2.3.2 Recommendations to Minimize Cracking in HMIP

This section summarizes the various precautions to be taken and suggests improvements in cold working procedures to minimize the possibility of galvanization-induced toe-cracking in HMIP shaft-to-base plate welds:

- Bend radii of four inches and at least three times the pole thickness should be specified to prevent excessive cold working at bent corners. If smaller radii are required for upper sections of the pole, the four-inch minimum should be specified for the bottom pole segment only with tighter radii being permitted for higher segments in the shaft.
- If bend radii less than three times the thickness of shaft section are specified, hot bending is recommended to minimize the associated strain aging embrittlement.
- Rough grinding of cold worked bend corners in the crack-susceptible areas in HMIP is recommended. This process eliminates surface irregularities that act as stress risers and removes the most severely cold worked material at the bend locations. This is most critical at the bottom section of the pole near the pole-to-base plate connection.
- Assemblies should be accurately preformed to reduce residual stresses during fabrication of HMIP.

- Specifying the use of steel with low DBTT to account for strain aging effects is recommended, particularly for poles that are expected to experience low temperatures in service.
- The use of aluminum killed steel is recommended to reduce susceptibility to strain aging embrittlement. Most modern steels are aluminum killed.

2.4 Welding

Welding processes that have found commercial application in structural steel fabrication can be classified into two main categories:

- *Arc welding* defines a group of welding processes that involve heating the work pieces with an electric arc. It involves melting of both base metal and filler metals and is accompanied by some form of shielding. Shielded Metal Arc Welding (SMAW), Gas Metal Arc Welding (GMAW), Submerged Arc Welding (SAW), Flux Cored Arc Welding (FCAW), Electrogas Welding (EGW), Stud Welding, and Gas Tungsten Arc Welding are all classified as arc welding.
- *Resistance welding processes* generate thermal energy by passing electric current through the work pieces, with the addition of pressure. The longitudinal butt seam on Hollow Structural Sections (HSS) is typically welded with the resistance or induction seam welding process (RSEW). Electro Slag Welding (ESW) is sometimes classified in this category (Miller, 2006) AWS D1.1 classifies the following welding processes, based on the need for qualification testing:

- *Pre-qualified processes:* May be used with a prequalified Welding Procedure Specification (WPS); are not subject to qualification testing.
- *Code Approved processes:* Recognized by the code, but the WPS needs to be qualified by test.
- *Other:* WPS is qualified by test; however, the code does not provide specific testing criteria.

There are three essentials of any welding process:

- Atomic closeness, to the extent that metallic atoms can share a common electron cloud.
- Atomic cleanliness, or oxide-free surfaces, so that metallic atoms can attract other metallic atoms instead of oxygen.
- Shielding, to protect the molten metal in the weld pool from the atmosphere. Molten metal can dissolve large quantities of atmospheric gases like nitrogen and oxygen, which bubble out of the metal as it cools and solidifies. This process can compromise weld quality in various ways such as causing porosity or embrittlement due to the presence of nitrogen. The difference between welding processes is due to the various methods by which each process achieves the above requirements.

Submerged Metal Arc Welding (SMAW) is the earliest manual structural steel welding process that uses a coated electrode. The core of the electrode or filler is metallic, which melts and becomes part of the weld. The coating decomposes and provides shielding for the welding. An electric arc between the electrode and the materials being joined generates the heat for the welding. SMAW was used extensively for structural steel fabrication till 1960, after which FCAW became popular because it proved to be faster and more economical. Although SMAW is now not used for large, long welds, it is still preferred for its flexibility in some cases, including smaller field erection projects. SMAW is a reliable method of depositing high-quality welds and continues to be used for tack welding and repair welding.

Various filler metals and electrode coatings are available for SMAW. Only filler metals with low-hydrogen coatings are specified for use on steel with a minimum specified yield strength of 50 ksi or more. These produce welds and Heat Affected Zones that are more resistant to hydrogen-induced cracking, and are also more economical since they require lower levels of preheat. Non-low-hydrogen electrodes may be used in situations where hydrogen-induced cracking is not anticipated, such as in lower-strength steel or the use of higher preheat levels reduce cracking potential. Non-low hydrogen electrodes are better suited to welding on contaminated materials and handling poor fit-up conditions.

Flux Core Arc Welding (FCAW) uses a continuous tubular electrode that is fed from a coil through the electrode holder. The core of the electrode contains a flux that performs the same function as the coating in SMAW by forming an extensive slag cover over the weld bead. The continuity of the

electrode and the higher permissible amperages give FCAW a distinct advantage over SMAW. There are two types of FCAW:

- *Gas-shielded flux core (FCAW-G*), which uses an externally supplied shielding gas.
- *Self-shielded flux core (FCAW-S),* whereby the flux ingredients contained in the electrode core perform the shielding function entirely, without requiring external shielding gas.

FCAW filler metals are separately specified for carbon steel electrodes and for low-alloy steel materials. Some carbon steel electrodes are specified for making single-pass welds only and others for limited thickness welds. To reduce the probability of cracking at or near the weld, select an electrode that is consistent with the material type and fabrication processes being used.

While the FCAW process can be fully automated, semi-automatic FCAW is more prevalent. Semi-automatic FCAW-G is the most popular semi-automatic method for structural steel shop fabrication because of better arc action, good weld appearance and quality, and availability of higher strength electrodes. Short-run or difficult to access welds are generally made with semi-automatic FCAW (Miller D. K., 2006). However, the gas shield must be protected from wind and drafts; otherwise, porosity may form in the weld. Before the onset of porosity and at even lower wind speeds (less than five mph), there may be a decreased ductility and toughness. AWS D1.8 therefore limits the maximum wind velocity limited to three mph. Many cases of mast-arm-to-base-plate weld failures have been due to poor weld quality (Chen, 2003).

FCAW-S is used for field erection of all kinds of building components. Because of the compact size of FCAW-S guns, many ‘T’-shaped, ‘K’-shaped, and ‘Y’-shaped connections in hollow structural section construction are welded with FCAW-S. It is common to intermix various welding processes like SAW, FCAW-G, SMAW, and GMAW. However, FCAW-S should not be intermixed with other welding processes. Doing so may create an imbalance in the weld metal composition and may significantly affect Charpy V-Notch (CVN) toughness (FEMA, 1997; Quintana, 1998). Another limitation of FCAW-S is that its deposits are limited to 90 ksi tensile strength or less.

In ***Shielded Arc Welding***, the arc is invisible because it is covered or submerged by granular flux that is usually laid ahead of the advancing electrode and covers the arc. SAW allows high-welding currents and consequently higher rates of deposition and deeper penetration, leading to increased

productivity and economy in weld-metal. SAW welds have mechanical properties as good as the base material and are of high quality with good ductility and impact strength. SAW is typically an automated process. Semi-automatic application is also used; however, it requires very high welding skill, especially for multi-pass welds, as the welder cannot see the weld pool. Therefore, it is beneficial to use SAW for long straight seams. For joints that are not conducive to automated welding, it is better to use one of the open-arc processes. Also, SAW can only be used in flat or horizontal welding positions, making it more suitable for shop fabrication where weldments can be positioned suitably.

SAW fluxes may be active or neutral. Active fluxes have manganese and silicon added, whereas neutral fluxes do not. Manganese and silicon help welding on heavily rusted or scaled materials. Active fluxes are used for single-pass welding on such material. Some of the alloy in the active flux becomes part of the weld metal on melting and makes the weld more crack-resistant. If active fluxes are used for multi-pass welding, high voltages may lead to increased melting of flux and buildup of excessive alloy deposit in the weld, making the weld highly susceptible to cracking. Therefore, care should be exercised to use only neutral fluxes for multi-pass welding.

Gas Metal Arc Welding (GMAW) is similar to FCAW, except that the shielding is provided entirely by an externally supplied gas. GMAW uses a solid or metal cored electrode that leaves almost no slag, which simplifies cleaning. Also, GMAW welds have very low levels of diffusible hydrogen, reducing possibilities of cold cracking. Using GMAW for structural steel fabrication has increased because of the development of metal-cored electrodes that offer better resistance to mill scale and rust. The selection of shielding gas also plays an important role in the quality of weld. The processes which use CO_2 are called Metal Active Gas (MAG) , and those which use mainly argon are called Metal Inert Gas (MIG). CO_2 is generally more economical, but can result in excessive spatter. On the other hand, argon-based mixtures are less economical but generate less spatter.

GMAW is classified on the basis of modes of transfer of metal from the electrode to the weld pool. Four categories of GMAW are in commercial use for structural steel fabrication:

- *Short-Circuit Transfer* is where metal is transferred from the electrode to the weld pool through a series of repeated electrical short circuits. Short Circuit GMAW welding (GMAW-

S) is a low energy mode of transfer and suitable for thin gauge materials and all-position welding.

- *Globular Transfer* is a mode of transfer where the molten metal leaves the electrode in large drops or globs to join the weld pool and is associated with high concentrations of carbon dioxide shielding gas.
- *Spray Transfer* is a mode of transfer in which a fine spray of molten drops are transferred from the electrode to the weld pool. It is restricted to flat and horizontal positions. The shielding used for spray transfer is composed of at least 80 percent argon.
- *Pulsed Spray Transfer* uses a background low current to maintain the arc as well as a pulsing peak current applied anywhere between 100 to 400 times per second. The metal is transferred by each pulse as a single droplet.
- The spray transfer and pulsed spray transfer modes of metal transfer give welds of good quality and appearance as opposed to short-circuit and globular transfer. Special caution must be exercised if short circuit transfer mode is used on materials other than sheet metal, as it may lead to lack of fusion with base material and negligible weld strength. As in the case of FCAW-G, GMAW needs to be protected from wind and drafts; otherwise, mechanical properties of weld deposit may be adversely affected.

SMAW, FCAW, and SAW are all pre-qualified processes provided they conform to the AWS D1.1-Clause 3 provisions. In general, the FCAW or SAW processes are used in making the shaft-to-base plate connections. As early as 1974, research indicated that the SAW process resulted in more ductile connections because of its slower cooling rates. Thus, the SAW process is preferred to the FCAW process that generates comparatively more free hydrogen (Aichinger, 2006). While the pole-to-base weld has been commonly made using the SAW process over the past 30 years, the process has recently been automated rather than being a hand welding procedure (Aichinger, 2006). A regional fabricator also indicated that SAW welding was used for base-plate-to-shaft connections for shaft outer diameter equal to or more than 24 inches With one exception (100 ft, 80 mph, 8 sided pole design), all TxDOT pole shaft base sections have outer diameters equal to or greater than 24 inches. In the case of heavy weldments, such as those used in the pole-to-base plate weld, the AGA recommends the use of the SAW process (AGA, 2010).

2.4.1 Welding Related Parameters Affecting Cracking in HMIP

Weld cracks commonly form due to the shrinkage of the weld and surrounding base metal as they cool after being heated and expanded during the welding process Specifically, cracking occurs because the surrounding material restrains this shrinkage. The degree of restraint depends on several factors, including the volume of the surrounding material, the strength of the steel, the stiffness of the joint configuration, and the temperature and thermal gradients that exist within the steel. Therefore, due to the large thickness of the HMIP base plates, the high strength of the steels used, and the stiff 3-D geometry at the pole-to-base plate connection, the pole-to-base plate connection is highly restrained and may require special precautions during welding. These precautions include proper weld detailing, electrode selection, preheating and inter-pass heating, weld sequencing, and other special measures in order to prevent cracking (Miller, 2006).

Weld Cold Cracking

The toe weld cracking observed at the HMIP shaft-to-base-plate connection is a type of cold cracking or Heat Affected Zone cracking. Extensive research has been conducted to understand and ameliorate this kind of cracking. One of the earliest major studies indicated that cold cracks form as fine microcracks that are almost impossible to detect by non-destructive means and can be seen only under a microscope (Graville, 1975). Micro-cracks are often associated with non-metallic inclusions that provide sites for initiation.

Other research indicates that all welds exhibit microscopic undercuts, slag inclusions, or both along the weld toes that cannot be detected by normal inspection methods (Maddox, 1983). For plain materials, the fatigue life consists of crack initiation and crack propagation phases. However, for welded details, these weld imperfections act as crack initiators. Thus, the fatigue life of welded joints is only spent in crack propagation with essentially no time spent in the crack initiation stage. Therefore, the fatigue life of welded details is considerably shorter than that of unwelded material.

Later research confirmed that welding processes produce discontinuities that ultimately became stress concentrations, especially at the bend lines (Aichinger, 2006). It was further confirmed that the non-destructive testing NDT methods may not be completely reliable for the early detection of these microscopic crack features. Manual welding was recommended to ‘dress up’ the welds at the bend lines at the toe of the weld to reduce the potential for cracking. Dressing up of weld involves

remelting the weld toe to remove crack-like imperfections and shaping the weld to a more favorable profile.

Weld Reconditioning

Various methods of toe-reconditioning are suggested in order to remove or mitigate the pre-existing discontinuities and to restore the crack initiation phase, thereby increasing the fatigue life. Reconditioning may be done by toe-grinding or Gas Tungsten Arc Welding (GTAW)/Tungsten Inert Gas (TIG) dressing (AWS, 2010). GTAW (TIG) dressing is done by remelting the existing weld metal along the weld toe without the addition of filler metal. Peening is also used to retard the rate of crack propagation by introducing a compressive stress field at the weld toe. Specific guidelines are available for carrying out these procedures for given weld and base-metal thicknesses and the applicable fatigue categories. Combined treatment of toe grinding followed by hammer peening or GTAW (TIG) dressing can offer superior fatigue resistance for critical joints (AWS, 2010). However, peening must be carefully done in order to be effective. As such, peening is often avoided in structural steel welding applications because of the potential for incorrect application which has limited to no effectiveness (Miller, 2006).

Over the past decade, Ultrasonic Peening (UP) has been identified as the most efficient technique for increasing the fatigue life of welded elements. UP involves post-weld deformation treatment of the weld-toe by applying impacts at an ultrasonic frequency of about 27 kHz. The objectives of the UP procedure are to reduce stress concentrations by improving the weld profile and introduce compressive residual stresses at the treatment location (Roy, 2003). UP treatment of existing welded elements, suitably repaired for cracking, if any, provides the same advantage in enhancing the fatigue life of these elements as would treatment during or immediately after construction (Kudryavtsev, 2005). It has been found that hot-dip galvanizing after UP removes the benefit of UP (Palmatier, 2005). If UP is conducted after galvanizing, the damaged coating should be repaired using a zinc-rich paint with no apparent adverse effect (Koenigs, 2003). A study of a limited number of available Welding Procedure Specification indicates that HMIP fabricators in Texas are not employing any special methods for toe-reconditioning.

Weld Hydrogen Content

The relationship between weld cold cracking and the presence of hydrogen was noted as early as the 1940s. Subsequent research studies have confirmed the deleterious effect of hydrogen. Some fundamental factors that influence cracking are:

- Susceptibility of the weld metal or HAZ to hydrogen embrittlement which depends on its chemical composition and microstructure.
- Hydrogen content.
- Stress or strain level at the point of crack initiation.
- Temperature.

The methods of control may range from simply selecting consumables that promote a no-cracking weld condition to designing complex weld procedures involving pre-treatment of consumables and temperature control during and after welding. To a large extent, the development of low-hydrogen electrodes has helped mitigate cold cracking in welds (Graville, 1975). Other measures include keeping the base metal surfaces clean and filler metals dry or using post-weld heat treatments to remove excessive hydrogen (Miller D. K., 2006).

A number of studies have been carried out to explain the nature of hydrogen embrittlement in structural steels. A coherent explanation of this phenomenon has been presented by generalizing the results of such investigations carried out at the Paton Institute of Electric Welding, Ukrainian Academy of Sciences, Kiev (Pokhodnya, 2001). The unique characteristics of reversible hydrogen embrittlement are as follows:

- Hydrogen embrittlement is reversible. For hydrogen concentrations below a critical level, the affected mechanical properties of ferritic steel are recoverable with the removal of the hydrogen.
- Extra-low (< 1 cm^3/100 g of metal) hydrogen concentration can cause embrittlement.
- A temperature close to normal is the most favorable for the manifestation of reversible hydrogen embrittlement.
- The degree of embrittlement depends on the carbon content of the metal and the value, type, and distribution of stresses with stress concentrators enhancing the action of hydrogen.

The effect of several parameters on hydrogen embrittlement has been studied. These parameters included:

- Steel strength.
- Temperature.
- Heat treatment.
- Presence or absence of hydrogen.

It was found that the yield strength of the tested steel in the normal (that is, without heat treatment) and heat-treated states differed by several magnitudes. The results also indicated that the presence of dissolved hydrogen did not affect the yield strength of the steel types in the entire range of temperatures considered. However, as a result of structural changes with increase in temperature, the sensitivity of high-strength, low-alloy steel to the action of hydrogen increased substantially. Specimens with a mean hydrogen concentration of 3.0 cm^3/100 g ruptured almost immediately after yielding. On the other hand, the heat treatment of mild steel did not cause catastrophic fracture under the action of hydrogen.

The various hypotheses used thus far to explain hydrogen embrittlement (e.g., the pressure theory, the adsorption theory, and the decohesion theory), and the different phenomena that these hypotheses cannot explain, have been presented. This discussion brings out the complexity of the problem, especially in the absence of a clear-cut understanding of the micro-mechanisms of metal fracture under the action of hydrogen. The intensive emission of negative secondary ions recorded in experiments and the concept of micro-cleavage is used to explain the atomic mechanism of reversible hydrogen embrittlement. The localization of a negative charge on the surface of an ideally sharp incipient crack facilitates the rupture of maximally stressed interatomic bond by overcoming the limit strength of the lattice in the process of micro-cleavage at the tip of a microcrack. A decrease in the level of the normal stress, which is necessary for the crack to pass to autocatalytic propagation in a stress field, manifests itself as the embrittlement effect at the macro level. The movement of dislocations, which is an elementary act of plastic deformation and which initiates brittle fracture, is also the most efficient method of hydrogen transport in the bulk of the metal (Pokhodnya, 2001). Therefore, reduction in stress concentrations and protection from exposure to hydrogen become central to preventing hydrogen embrittlement of welded components.

Cold cracking has all the characteristic features of reversible hydrogen embrittlement. During welding of high-strength low alloy steel, the microstructure of the steel formed by special heat treatment during its manufacture is altered. The new structures that are formed are very sensitive to hydrogen; as such, special measures to limit the hydrogen content of the welds are called for. Cold cracks typically form at low temperatures—generally below 390°F—and frequently exhibit a delay phenomenon. Even after a joint has cooled to room temperature, there may be further lapse of time of a few minutes or several hours before cracking occurs. In some extreme cases, cracks have been observed to form several months after welding (Graville, 1975).

Preheating and Inter-Pass Heating

Preheating of the weld promotes a slower cooling rate that permits hydrogen to diffuse from the weld harmlessly without causing cracking. It also gives rise to a more ductile and crack-resistant metallurgical structure in the HAZ. Weld preheating also reduces shrinkage and raises some steel types above the temperature at which brittle fracture might occur during welding. It can dry moisture off damp surfaces and can also help ensure specific mechanical properties like the Charpy V-notch toughness. In addition to preheating, which is applied prior to welding, the inter-pass temperature should also be controlled. The inter-pass temperature refers to the base-metal temperature between welding passes; it should not fall below the preheat temperature to prevent reabsorption of hydrogen.

The minimum preheat and inter-pass temperatures are specified based on the category of steel, welding processes and thickness of members joined (AWS, 2010). However, these should not be considered all-encompassing or adequate in all cases. In general, preheat temperatures should be high enough to ensure sound welds (AWS, 2010). For cases where the risk of cracking is increased due to composition, restraint, hydrogen level, or lower welding heat input, two alternative methods are suggested for determining preheat namely (1) HAZ hardness control method and (2) Hydrogen control method (AWS, 2010).

The hardness control method is applicable to steel with very low alloy content and moderate carbon content. It is assumed that such steel types, if cooled slowly, will form a soft micro-structure that will be resistant to cracking below a critical hardness (Irving, 1992). This is achieved by controlling the cooling rate of the weld, a method that is restricted to use for fillet welds only.

The second approach focuses on the critical hydrogen content rather than on the hardness of the steel. It applies to modern alloyed steel with low carbon contents, where the microstructure does not change much with changes in cooling rate. The hydrogen control method involves calculation of a composition parameter P_{cm} similar to the carbon equivalent. A susceptibility index is then determined based on two factors: the composition parameter, and the filler metal diffusible hydrogen content. The welding code specifies three types of consumables ranging from H1 (Extra-low hydrogen with a diffusible hydrogen content of less than 5 ml/100 g) to H3 (Hydrogen Not Controlled consumables). Finally, the minimum preheat temperature can be determined from the restraint level, material thickness and susceptibility index (Irving, 1992) (AWS, 2010). Although three levels of restraint are described in the code, the selection of the restraint level is problematic and depends on engineering judgment.

As discussed previuosly, three zones of steel have been identified, on a plot of carbon content against carbon equivalent based on a number of hardening curves (Graville, 1975). The selection of the method for determining preheat is recommended on the basis of this classification (AWS, 2010). The hydrogen control method is recommended for Zone-I steel with low carbon that, though crack-resistant under normal circumstances, may still crack with high hydrogen or high restraint. This method is also recommended for groove welds in Zone-II steel types and all Zone-III steel types. Under Zone-II steel types, a minimum energy to control hardness (based on the hardness control method) may also be required for steel types with high carbon content.

From a study of mill certificates of steel used in TxDOT poles, it is apparent that the shaft steel falls in Zone-I and the steel types for base-plate and ground sleeves are classified in Zone-II. The latter turns out to be more critical in determining preheat. The preheat requirement calculated based on the alternative methods given in the AWS code is much higher for groove welds made in these steel types than the minimum preheat requirement specified in the code for this category. A sample calculation based on a set of WPS and mill certificates for a TxDOT HMIP shaft-to-base-plate FCAW connection by the Hydrogen Control method, gave a conservative value of preheat ranging from 300 to 320°F, considering low hydrogen consumables and medium to high restraint—for an ASTM A572 Grade 50 steel, 3-inch thick plate, $P_{cm} = 0.304$, Susceptibility Index (SI) = 4.64, SI Grouping = E. The actual minimum preheat specified was 250°F as per Category B of the AWS. This example illustrates that the minimum preheat values specified in the code may not be sufficient to adequately control

hydrogen content and prevent hydrogen embrittlement during welding. Moreover, the diffusible hydrogen content of the electrodes and shielding gases specified is generally found to be greater than 5 ml/100 g. Additionally, there appears to be no special emphasis on minimizing hydrogen content of consumables. These fabrication practices may lead to the formation of welds that are more susceptible to hydrogen embrittlement and HAZ cracking. The preferred practice should include the use of extra-low hydrogen consumables and specification of preheat requirements based on the hydrogen-control method as per AWS D1.1 Annex I.

The effectiveness of preheat in preventing cracking will depend on the area preheated and the method used. Preheat may be applied in a furnace or by using heating torches, electric strip heaters, or induction or radiant heaters, depending on the material thickness and size of the weldment. Carbon steel does not require precise temperature accuracy. However, maximum and minimum preheat temperatures must be followed closely for quenched and tempered steels. It is important to ensure that the required preheat/inter-pass temperature has been established before welding each pass (Funderburk, 1998).

In a previous study, Valmont Industries found variations in welding heat input that different fabricators used, ranging from 32 kilojoules per inch to 65 kilojoules per inch (Aichinger, 2006). In addition to suggesting dressing of welds at toe-lines and increasing preheat temperature to 400°F, which is consistent with the discussion in the preceding paragraphs, the study also recommended the reduction of welding heat input to below 65 kilojoules per inch.

Post-Weld Heat Treatment (PWHT) can be classified into two categories. The first category is done at approximately 302°F as an extension of preheat and with the intention of further removing hydrogen. The second type is a tempering process carried out by heating the component in a furnace at approximately 1125°F in order to temper microstructures as well as remove residual stresses (Irving, 1992). PWHT is often specified for thick materials like pressure vessels, and is an American Society of Mechanical Engineers (ASME) code requirement. It is a costly procedure and is generally not done for structural components.

Multi-Pass Welding

Multi-pass welding can lead to hardening of weldments and the associated HAZ. This hardening effect can be prevented by strategically selecting the weld sequence such that the HAZ of each weld

pass is tempered by a subsequent welding pass. For inter-pass tempering to take effect, the HAZ of the previous pass should not cool below about 210°F before the next pass is deposited. Also, the final weld pass should not touch the parent material. If the final pass of a multi-pass weld touches the parent material, a hardened HAZ may develop that will not benefit from the tempering effects of the subsequent passes. This may lead to toe cracking.

Figure 9 shows that this 'temper bead' technique has been effectively implemented to avoid toe cracking in high strength steel (Graville, 1975). The temper bead technique has been a subject of continuous research mainly for use in repair welding. It is thought of as a viable and less expensive alternative to Post-Weld Heat Treatment in effectively reducing the hardness and the size of the HAZ (Aloraier, 2004). Ways of detailing the exact procedure including the way heat input should be specified in the WPS are also documented (Sperko, 2005). This approach recommends adding an extra welding bead to the weld to provide a final tempering of the weld. This extra final tempering bead should be placed 1/8 inches to 3/16 inches away from the weld-toe in order to temper the un-tempered weld metal and HAZ. The final tempering bead can be subsequently removed by grinding to match the specified weld profile (Sperko, 2005).

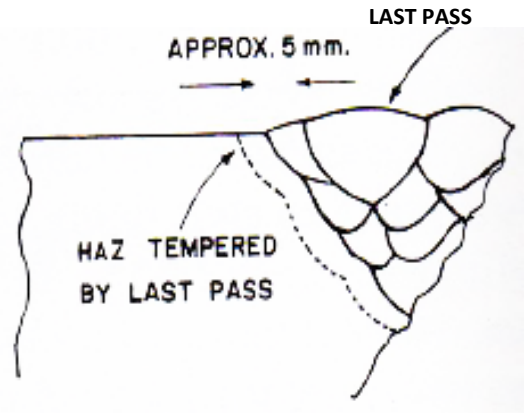

Figure 9. Temper Bead Welding (Graville, 1975).

2.4.2 Recommendations to Prevent/Minimize Cracking in HMIP

This section summarizes the various precautions that should be taken and suggested improvements in welding procedures to minimize the formation of galvanization-induced toe-cracks in HMIP shaft-to-base plate welds:

- Minimizing hydrogen content is essential to reduce the likelihood of hydrogen embrittlement and to minimize the potential for HAZ cracking. Hydrogen content can be reduced by using extra-low hydrogen consumables as specified in AWS D1.1 with diffusible hydrogen content of less than 5 ml/100 g. Additionally, base metal surfaces should be clean of grease, oil, rust, and debris; the weld filler material should be free of moisture. Low hydrogen electrodes should be used when SMAW is used to join steel types with yield strengths of 50 ksi or higher.
- Preheat requirement should be calculated according to the alternative hydrogen control method given in AWS D1.1 Annex I rather than following the code-specified minimum requirements. Ensure that preheat, as required, is properly established before welding. Next to using low hydrogen consumables, proper preheating can be considered the most effective method of reducing hydrogen content, thereby preventing hydrogen embrittlement.
- SAW welding process or other processes with MIG, TIG, or CO_2 shielding are preferable.
- If the SAW process is used, neutral fluxes should be used for multi-pass welding. Using active fluxes may lead to crack-sensitive welds owing to excessive alloy deposit.
- The use of semi-automated SAW requires very high welder skill since the weld pool cannot be seen during welding. Welder and welding operator qualification criteria are specified in the AWS welding code.
- The FCAW-S process should not be intermixed with other welding processes as this may create imbalance in the weld metal composition and lead to reduced Charpy V-notch toughness.
- When the FCAW-G and GMAW processes are used, the weld site should be protected from wind and drafts to prevent the formation of weld defects.
- If the GMAW process is used, the Short Circuit Transfer method of metal transfer should be avoided as it may lead to lack of fusion with the base material and result in poor weld strength.
- Temper bead welding techniques should be used to reduce the HAZ hardness and minimize the potential for cracking.
- Peening or other toe-reconditioning methods like toe-grinding or GTAW (TIG) dressing as per AWS D1.1 may be adopted to improve toe-profile for enhanced fatigue life. Ultrasonic peening may be implemented after hot-dip galvanizing along with repair of galvanizing with zinc-rich paint. However, care should be taken to ensure that peening is done properly.

2.5 Galvanizing

Essentially, the entire inventory of HMIP in Texas is comprised of hot-dip-galvanized poles. The universal use of hot-dip galvanizing is attributed to its excellent corrosion protection. However, a number of fatigue failures of HMIP have been reported in other states in recent years, and extensive research has been conducted to determine the causes of these failures. The failure is manifested as toe cracking at the base-plate-to-shaft welded connection. In Texas, although there have been no failures, internal toe cracking has been detected in some poles after galvanizing. Nilsson (1989) found that galvanizing is responsible for reducing the fatigue life of steel in general and these fracture-critical structures in particular (Anderson, 2007). Although no conclusive evidence holds galvanizing as solely responsible for the failures, the fact remains that such cracking occurs primarily in galvanized poles (Aichinger, 2006). As such, some of the typical components of hot-dip-galvanizing such as pickling, excessive temperature gradients, and zinc bath metal interactions with the steel need close scrutiny to assess their impact on cracking through processes like hydrogen embrittlement and liquid metal embrittlement.

2.5.1 Hot-Dip Galvanizing Process

The process of hot-dip-galvanizing has remained more or less the same for over a century except for improvements in efficiency over time due to mechanization of the material handling aspect. It is a dip-and-drain sequence that essentially has three steps; surface preparation, galvanizing, and inspection. Figure 9 illustrates the galvanization process. The steel assembly is hung on a wire and moved through the process using overhead cranes. The first step in the surface preparation process is typically a preliminary cleaning or degreasing in an aqueous caustic soda solution to remove dirt, oil, and organic residue.

While caustic cleaning is a common first step, not all galvanizers universally use it. Further cleaning is achieved by rinsing the component to remove any caustic residue, followed by dipping in a sulphuric acid or hydrochloric acid pickling solution to remove rust and mill scale. The cleaned pole is then dipped into an Ammonium-chloride or zinc-chloride based fluxing bath that removes any remaining oxides and coats the steel with a protective layer to prevent any further oxide formation. After the surface preparation, the steel is dipped into a molten zinc bath of at least 98 percent zinc at a temperature of 839 to 840°F. The temperatures and dipping times in various stages of the galvanizing process vary at different facilities, depending on the preferred practice at each facility. Additionally,

durations of dipping can vary within a given facility, depending on the cleanliness and size of the steel assembly being galvanized. Inspection is done as a last step of the galvanizing process—it is usually visual with the thickness of the coating being verified with a magnetic thickness gauge if required (AGA, 2009).

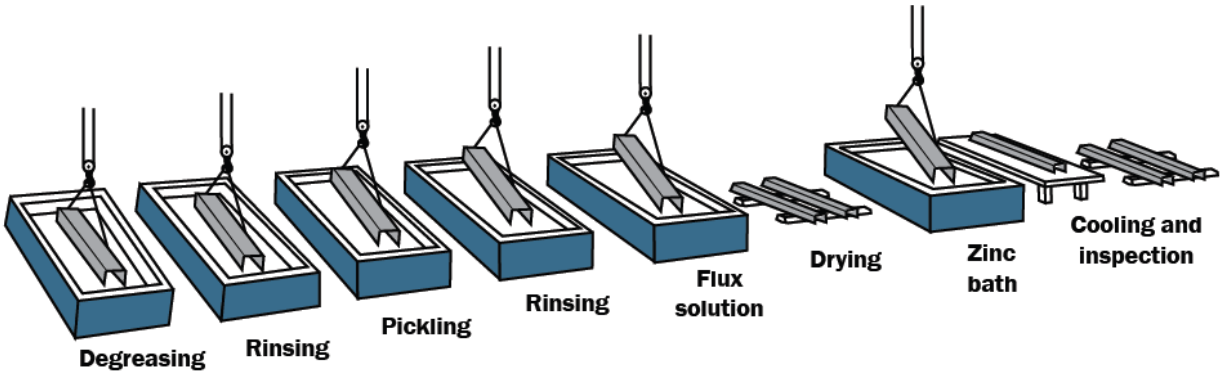

Figure 10. Galvanizing Process (AGA—www.galvanizeit.org).

2.5.2 Galvanizing Practice in Texas

The length of the bottom section of TxDOT standard HMIP ranges from 26.67 ft to 51.75 ft. According to the AGA, 13 galvanizers in Texas have kettle sizes more than 42 ft long, all capable of dipping most TxDOT-standard HMIP sections. These 13 fabricators were contacted to conduct an oral survey of their galvanizing procedures. Researchers collected specific details about the temperatures, chemical compositions, and durations of each of the galvanizing steps. They received eight responses, of which three fabricators claimed that they do not galvanize high mast poles. Table 1 summarizes the responses of the remaining five galvanizers. The durations of dipping in the pickling bath range from 15 minutes to one hour. Likewise, the durations of dipping in the zinc kettle range from as little as five minutes to almost an hour. Several of the galvanizers indicated that they generally quench galvanized parts if the customer allows them to do so. Quenching has been shown to increase the likelihood of cracking and is explicitly prohibited in the galvanization of TxDOT HMIP. Inspection of the survey results indicates that there is little variability in the duration of caustic cleaning and fluxing between different galvanizers. Similarly, the temperature of the zinc kettle is relatively constant between galvanizers. In contrast, the duration of pickling and the time spent in the

zinc kettle vary dramatically between galvanizers. The impact of these variations on the quality of galvanizing and its susceptibility to cracking will be discussed in the next section.

Table 1. Texas Galvanizer Survey Results.

Process Step	Time	Temperature	Remarks
Caustic Cleaning	Few minutes (3) None (2)	110°F–120°F (3)	-
Pickling	15 min. (1) 30–60 min. (4)	Ambient (2) 110°F–130°F (1) 140°F–150°F (2)	Hydrochloric acid (2) Sulphuric acid (3)
Flux Solution	Few minutes (5)	130°F (2) 140°F (1) 160°F (1) Unreported (1)	Ammonium chloride, Zinc chloride or mix
Zinc Kettle	5–6 min. (1) 10–12 min. (2) 15–30 min. (1) 30–45 min. (1)	832°F (1) 839°F–840°F (4)	Time increased for larger pieces Staging above kettle (few minutes)

Note: Figures in parentheses indicate the number of galvanizers following that practice out of a total of 5 galvanizers.

2.5.3 Galvanizing-Related Parameters Affecting Cracking in HMIP

Early studies on the behavior of structures during galvanizing focused on the effect of internal residual stresses that the significant temperature gradients of steel in the galvanizing kettles have induced. These temperature gradients can cause distortion and cracking of galvanized steel assemblies. Assemblies of parts with notably different thicknesses are likely to develop significant temperature differentials owing to variation in heating and cooling rates of thinner and thicker members. Increasing dipping and quenching times compounds this problem. The studies showed that peak thermal gradients could be controlled by minimizing the dipping time and using an angle of

dipping that maximized the rate of submergence of the steel assembly in the molten zinc bath. Quenching could be a major source of distortion, so therefore air cooling was preferable for crack-susceptible assemblies (Cresdee, 1993).

Maintaining balance at the fluxing stage of the galvanizing process has been shown to be an important factor in minimizing galvanization-induced cracking. Typical flux is an aqueous solution of $ZnCl_2$ and NH_4Cl heated to approximately 130°F. After being dipped in the flux solution, the steel is dried by evaporation before being dipped in the molten zinc bath. Complete evaporation, however, depends not only on time, temperature, and humidity of the surrounding environment, but also on the ratio of $ZnCl_2$ and NH_4Cl in the fluxing solution. If the flux film does not dry completely, the trapped moisture experiences flash evaporation resulting in dangerous spatter as the steel assembly first enters the galvanizing bath. This leads to slow immersion or intermittent immersion until the flash evaporation process is completed before the rest of the assembly is immersed in a similar fashion. Prolonging the immersion time worsens the thermal gradients and consequent strains inside the steel assembly. Therefore, care needs to be exercised during fluxing to prevent this, especially in steel types susceptible to cracking (Kinstler, 2003). The fluxing chemical reaction is also known to produce a zinc deposit prior to the actual galvanization and also to increase the hydrogen concentration in the steel (Carpio, 2010).

Abnormal Zinc Coatings

The corrosion-resistant hot-dip galvanized coating is formed by a metallurgical reaction between the steel and the molten zinc in the kettle. It is composed of a series of zinc-iron compound layers: gamma, delta and zeta, starting from the steel surface, and finally a layer of pure zinc at the outermost, known as the eta layer. The structure of the galvanized coating with regard to thickness of the various layers, its appearance and its physical properties such as adhesion to steel and brittleness, depend on the chemical composition of the steel being galvanized.

Steel with silicon content ranging from 0.04 to 0.15 percent or > 0.22 percent can produce galvanized coating growth rates much higher than those with silicon levels < 0.04 percent and 0.15 to 0.22 percent. Those types are known as reactive steel or *Sandelin* steel. Phosphorus has a similar effect, and phosphorus content of less than 0.4 percent is recommended. Even in cases where silicon and phosphorus are individually held to desirable limits, a combined effect between them can produce an

abnormal coating. Also, carbon content more than 0.25 percent and manganese more than 1.3 percent are known to produce atypical coatings characterized by accelerated growth of the compound layers with almost no eta layer. Although equally effective in preventing corrosion, such coatings are known to be more brittle and less adherent than normal coatings.

Cracks in the coating that penetrate through the entire thickness of the coating can propagate in the substrate. This occurs quite early in the fatigue life of the coated material. Beyond a certain threshold coating thickness, the fatigue life of a ferritic steel reduces with the increase in coating thickness. For example, for an applied stress of 39 ksi, the fatigue strength behavior of steel is not affected if the coating thickness does not exceed 60µm (0.00236 inches) (Vogt, 2001). A later study recommended galvanizing bath compositions, which would reduce the thickness of the brittle phases of the coating to improve its fatigue behavior. Recommended bath compositions such as Zn-Fe-Ti-0.012%Al and Zn-Fe-Ti-0.01%Al-0.037%Ni produced brittle layers of only 20 µm (0.000787 inches) and 23 µm (0.000905 inches), respectively (Camurri P., 2005).

Further, the inhomogeneity of the coating may give rise to a temperature differential within the coating itself leading to the development of residual stresses and subsequent crack formation. A study investigating this phenomenon found that the delta layer was the most brittle with the highest residual stress as compared to the gamma, zeta, and eta layers (Bigot, 1999). An earlier study linked the increase in silicon content of steel with the stability of the delta phase (Nilsson, 1989). Thus only steel types with silicon levels less than or equal to 0.04 percent or between 0.15 to 0.22 percent are recommended for galvanizing (AGA, 2010; ASTM, 2007). A study of typical mill certificates of TxDOT HMIP shows that the steel used in shaft and base plate of HMIP does not necessarily meet with this requirement. Also, there is noticeable variation in silicon content of shaft steel, base plate, and weld deposit at the shaft-to-base-plate welded connection. This may produce non-uniform thickness of galvanized coating. In such circumstances, abrasive blasting of entire assembly is recommended prior to galvanizing to improve the galvanizing quality (ASTM, 2007).

Besides the silicon present in steel, excessive silicon in weld filler material can also accelerate the growth of the hot-dip galvanized coating (AGA, 2010). Because some weld electrode metal contains nearly one percent silicon, the difference in coating thicknesses on the weld metal and structural steel can be significant. The use of low-silicon electrodes available for common welding

processes like SMAW, SAW, and FCAW is recommended. For example, weld rod material NR-203NiC+(E71T8-K2) with 0.04 percent silicon or NR-311(E70T-7) with 0.07 percent silicon are available for FCAW (AGA, 2002). Further, because weld flux and slag are insoluble in the chemical cleaning solutions used in the galvanizing process, it is recommended that these be removed by wire brush, flame-cleaning, chipping with a pick, grinding, or abrasive blast-cleaning. Uncoated and self-slagging electrodes may be used to prevent flux deposit (AGA, 2010).

Hydrogen Embrittlement

Research indicates that extended duration of pickling in an acidic bath can lead to excessive absorption of hydrogen into the steel, which may in turn lead to hydrogen embrittlement. Consequently, abrasive blast cleaning is generally preferable to acid pickling to minimize the potential for embrittlement. High temperatures, longer durations of pickling, and poor inhibition of the pickling acid may aggravate the effect. In high-strength steel (yield strength in the range of 100 ksi), the use of grit blasting instead of pickling was found to limit the reduction in fatigue limit of ungalvanized steel, after hot-dip galvanization, to only 12 percent instead of 35 percent with pickling (Nilsson, 1989). Hydrogen embrittlement is also a primary concern in steel types that have been severely cold worked prior to pickling, such as at the bent corners of HMIP poles. This concern is consistent with the observed pattern of cracking, which indicates that poles typically crack at the bent corners rather than at the longitudinally seam welded corners. To minimize hydrogen embrittlement at these locations, abrasive blast cleaning followed by flash pickling is recommended. The flash pickling is used to remove any traces of blast media before hot-dip galvanizing (ASTM, 2007).

The problems of residual stresses and hydrogen absorption in hot-dip galvanized welded steel assemblies have been simultaneously addressed using a technique known as strong shot peening cleaning (Hasegawa, 2009). In this technique, a large diameter steel shot (average diameter is 600 μm [0.0236 inches]) at a high projection pressure (58 psi or 0.4 MPa) is used to clean the welded joint. Specimens cleaned in this way needed just a minute each for pickling, rinsing, and fluxing before being dipped in the galvanizing bath for just a couple of minutes. The thickness and quality of the resulting coating were similar to those that would have been achieved in an hour of total process time including 30 minutes of pickling. Strong shot peening cleaning was found to increase the fatigue limit of welded joints, so that the subsequent effect of hot-dip galvanizing in reducing the fatigue limit

was, to a large extent, nullified. The improvement was considered a combined effect of increase in hardness of weld toe, relief in stress concentration, and increase of compressive residual stress. Also, the increase in surface roughness due to strong shot peening cleaning was thought to provide anchorage to the hot galvanized coating, making it more adherent to the steel surface.

Liquid Metal Assisted Cracking

Liquid Metal Assisted Cracking (LMAC) or Liquid Metal Embrittlement (LME) is the cracking phenomenon most closely identified with hot-dip galvanizing. It typically results in an inter-granular fracture coated with zinc at the location of a thermal or cold-forming process. For LMAC to occur, four components must be present:

- An embrittling metal (molten zinc).
- An embrittled metal (steel at welded connection).
- Forces acting on the affected component during contact with the embrittling metal (residual and thermal gradient stresses).
- Time in the galvanizing kettle (Kinstler, 2003).

Early experiments verified that the stress-strain curve of steel at a galvanizing temperature of 840°F showed sudden loss of ductility and brittle fracture in the presence of zinc, whereas no such effect was observed at the same temperature in the absence of zinc (see Figure 11). Thus, when stresses in a particular area due to cold forming, welding, or thermal gradients approach the yield stress, the steel may react by forming a small crack. This small crack absorbs the molten zinc along the grain boundaries in a wicking action. The liquid zinc breaks the bond between adjacent grains, thereby facilitating crack expansion and propagation. When the liquid zinc cools and solidifies, the cracks, which are filled with a thin film of zinc, are undetectable by visual inspection.

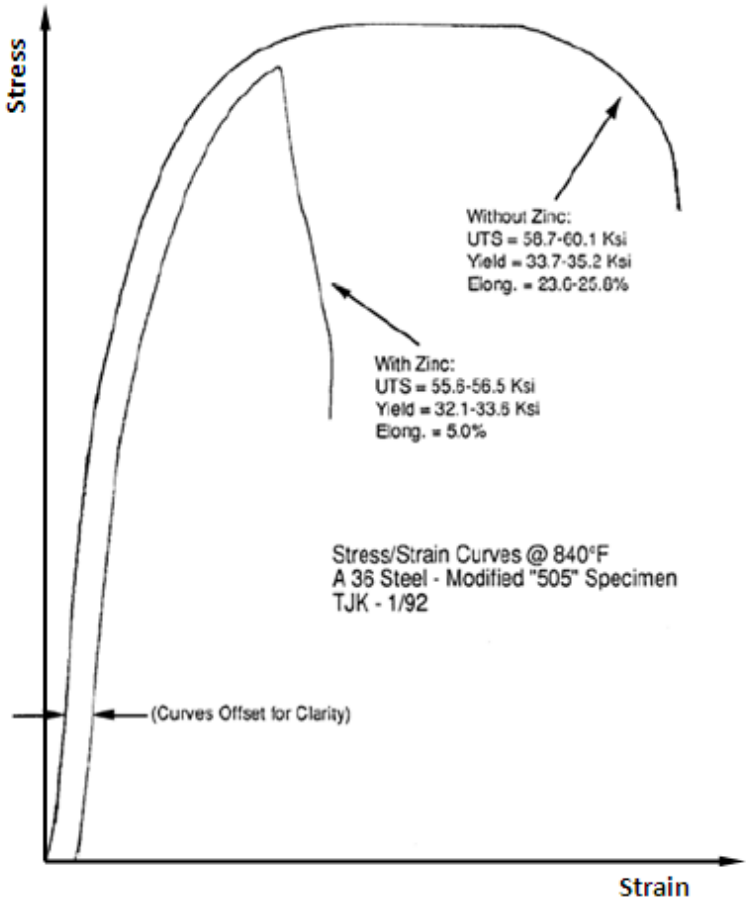

Figure 11. Stress/Strain Curve of Steel with and without Zinc at 840°F (Kinstler, 2003).

Although LMAC is widely accepted as the main fracture mechanism during hot-dip galvanizing (Kinstler, 2003), small scale-mechanisms that fully explain the cracking phenomena are not yet well understood or established (Carpio, 2010).

Different additives, such as lead (Pb), tin (Sn), nickel (Ni), and bismuth (Bi), have been used to control the reactivity of steel and enhance uniformity and appearance of the galvanized coating. The role of these additives in galvanization-induced cracking has been investigated. Lead was found to increase the incidence and severity of cracking (Poag, 2003). One grade of zinc, known as Prime Western (PW) Grade zinc, has a lead content of one percent. PW Grade zinc was used in most galvanizing plants until about 10 years ago, when the use of High Grade zinc with lower lead content became the standard practice(Kinstler, 2003). Bismuth can replace lead in enhancing the drainage characteristics of zinc. Tin and nickel, and sometimes vanadium and titanium, are

used to inhibit the reactivity of steel containing silicon. Aluminum in a certain range can enhance the brightness of the galvanized surface (Kinstler, 2003). However, levels of tin and bismuth above 0.2 percent were found to aggravate cracking. On the other hand, there was some evidence that nickel may be helpful in reducing cracking (Poag, 2003).

The crystallization points of all the galvanizing bath additives are lower than that of zinc. These elements remain liquid after zinc has solidified and may contribute to cracking. The accumulation of these additives within crack tips in various studies (Arata, 1982; Kinstler, 2003; Carpio, 2010; Mraz, 2009) proves this. Thus, in the case of galvanizing baths with 1.1 percent Tin (Sn), tin was found to react with steel to produce FeSn, a brittle intermetallic compound at crack tips. FeSn was thought to crack under plastic deformation and promote crack propagation by allowing more tin (Sn) and lead (Pb)-enriched liquid metal into the crack (Carpio, 2010).

Although the possibility of initiation of fracture due to local strain cannot be ruled out, the study of a large number of failures of zinc-coated steel products suggests hydrogen embrittlement as the most likely cause of fracture initiation (Mraz, 2009). The conclusion is based on microscopic examination of cracks that show trans-granular fracture close to fracture initiation, which is suggestive of hydrogen embrittlement. Trans-granular fracture is one that occurs through the grains, whereas inter-granular fracture occurs at the grain boundaries. Crack observation also revealed inter-granular fracture in the crack propagation direction. This led to the conclusion that while hydrogen embrittlement led to crack initiation, crack propagation was likely due to LME.

The addition of alloys like Bi and Sn is known to increase significantly the thermal gradients during dipping in the galvanizing bath as compared to the traditional bath compositions. This effect can be counteracted by increasing the dipping speed, which is very effective in lowering the thermal gradients. The adverse impact of low immersion speed is much more than that of alloy additions (Kinstler, 2003). Also, the time-to-crack or endurance of steel subjected to LME conditions depends on the stresses as well as on the temperature of the zinc bath. The time-to-crack increases with lower temperatures and lower loads. Therefore, it is beneficial to minimize the time in the galvanizing bath.

2.5.4 Recommendations to Prevent/Minimize Cracking in HMIP

This section summarizes the various precautions and modifications that can be adopted during the galvanizing process in order to minimize the occurrence of galvanization-induced toe-cracking in HMIP pole-to-base plate connections:

- Minimizing the immersion time in the zinc galvanizing bath may reduce chances of Liquid Metal Embrittlement. This can be achieved either by using a rapid speed of dipping in the galvanizing bath, or by optimizing the dipping angle of the pole shaft segments. This has the added benefit of reducing thermal gradients in the steel assembly, thereby further minimizing the cracking potential.
- The chemistry of the fluxing solution should be carefully monitored so as to achieve complete evaporation of the flux film before immersion in molten zinc. This is important to prevent dangerous spatter and consequent slow or intermittent immersion leading to aggravated thermal gradients.
- Silicon content in the steel of shaft, base-plate, and weld deposit should be kept below 0.04 percent or between 0.15 and 0.22 percent, to prevent the formation of abnormal and brittle coatings. Similarly, levels of carbon, phosphorus, and manganese should be limited to 0.25 percent, 0.4 percent, and 1.3 percent, respectively. Additionally, AGA guidelines for using low-silicon electrodes and uncoated or self-slagging electrodes should also be considered.
- Levels of tin (Sn) and bismuth (Bi) in the galvanizing bath should be limited to 0.2 percent as levels above this have been found to promote cracking. Bi and Sn are also known to significantly increase the thermal gradients during dipping in the galvanizing bath. The use of High Grade zinc with a lower concentration of lead is preferable to the use of Prime Western Grade Zinc. Titanium 0.1 to 0.16 percent and aluminum less than 0.1 percent are considered beneficial for reducing the coating thickness. Some galvanizing bath compositions such as Zn Fe-Ti-0.012%Al and Zn-Fe-Ti-0.01%Al-0.037%Ni reduce thickness of the brittle phases of galvanized coating and may therefore be preferred.

- As HMIP shaft-to-base plate connection has variable thicknesses and steel chemistries besides being severely cold worked, abrasive blasting followed by flash pickling of the shaft-to-base-plate welded connection prior to galvanizing is preferable to minimize the likelihood of hydrogen embrittlement due to exposure to acids.
- Excessive pickling temperature, longer duration of pickling, and poor inhibition of pickling acid increase absorption of hydrogen and, therefore, should be strictly controlled. Heating to 300°F after pickling helps in expelling hydrogen absorbed during the pickling process.
- Alternative techniques such as strong shot peening cleaning may be considered to drastically reduce the fluxing, pickling, and galvanizing durations and increase the fatigue limit of galvanized welded joints by improving hardness, increasing compressive residual stresses, and relieving stress concentrations.
- Quenching has been strongly connected to the formation of galvanization-induced cracks and therefore should not be permitted.

3 ANALYTICAL METHOD AND STRUCTURAL RESPONSE TO WIND LOADING

3.1 Introduction

A comprehensive analytical study was conducted to evaluate the response of HMIP to wind-induced vibrations and to assess the probability of failure of various configurations of HMIP used throughout Texas. Figure 11 presents the framework of the analysis. The individual steps of the analysis are described in detail in the following sections.

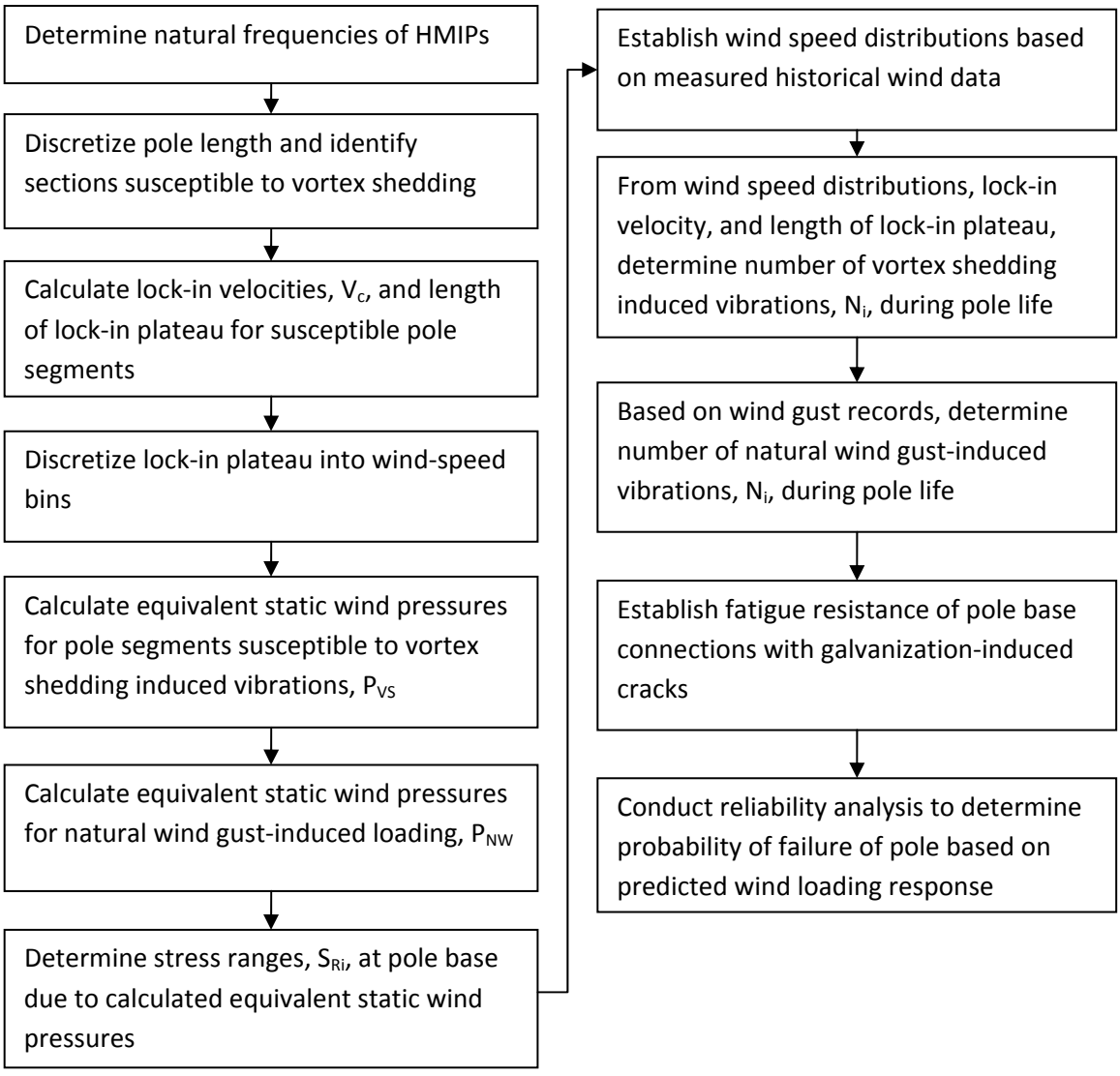

Figure 12. Analytical Framework to Determine Response of HMIP to Wind Loading and Associated Probability of Failure.

3.2 Modal Analysis of HMIP (Step 1)

The finite element analysis program SAP 2000 was used to conduct an Eigen value modal analysis of the HMIP studied in this research. Each pole was modeled using the four-noded 'thin shell' elements in SAP 2000. These elements have three translational and three rotational degrees of freedom at each node. The element is based on the classical 'Kirchhoff' formulation and does not include the effect of transverse shear deformations. The thickness of the shell elements was determined from the appropriate TxDOT standard HMIP details [TxDOT Drawing HMIP (2)-98, 1995]. A preliminary analysis indicated that the presence of the slip joints along the pole length had a negligible effect on the natural frequencies of the pole, typically less than one percent. As such, the slip joints were eliminated from the model. Instead, abrupt transitions between adjacent pole sections were modeled, and the locations of these abrupt transitions were taken at the mid-height of each slip joint.

Research has shown that for poles with thick base plates, the base can be accurately modeled as a fixed base (Foley et al., 2004). Since the standard TxDOT detail includes a three-inch thick base plate, a fixed base condition was considered for the HMIP in this study. The circular silo type storage structure template available in SAP was used to generate the tapered pole model. The number of angular divisions was made equal to the number of sides of the pole to generate an accurate representation of the multi-sided tapered pole. A maximum 48-inch edge length of the elements was specified in the vertical direction leading to element aspect ratios of approximately 6:1 at the base of the pole. To simulate the mass of the illumination ring at the top of the pole, a luminaire mass of 2.36 lb.s^2/in. (units of mass that are consistent with the unit system selected) was assigned as lumped mass distributed equally to each of the nodes at the top of the pole. The selected mass is equivalent to a total luminaire weight of 910 lb (Foley et al., 2004). Researchers conducted an eigen vector modal analysis and determined the first four natural frequencies and mode shapes of the poles.

The modeling approach was validated using two sets of data: (1) a numerical prediction of HML-67-006 Wisconsin pole design (Foley et al., 2004), and (2) the measured pole response of an actual HMIP in Iowa (Chang et al., 2009). The pole that Foley et al. modeled is a 150 ft tall, 8-sided pole with an octagonal base plate and 8 anchor rods at the base. This pole was selected for validation because it corresponded closely to the poles available in the TxDOT inventory. The first four

natural frequencies of the pole were predicted using the modeling procedure described above. Table 2 shows the comparison of the predicted natural frequencies with those of Foley et al.. Inspection of the table indicates that the predicted natural frequencies were in close agreement with those reported by Foley et al.

Table 2. Finite Element Model Calibration and Validation with Reported Values.

Mode	Current Model	Foley et al. (2004)	Difference
1st Mode	0.276	0.300	−8.0%
2nd Mode	1.130	1.155	−2.2%
3rd Mode	2.987	3.079	−3.0%
4th Mode	5.832	6.092	−4.3%

Further validation was done by modeling another HMIP located at the I-35/US-18 interchange, for which actual measured values of natural frequencies and stress ranges have been reported (Chang et al., 2009). The first four natural frequencies of the pole were predicted using the modeling procedure described above. Table 3 compares the predicted natural frequencies to those reported by Chang et al.. Finite element models were generated for all the 16 configurations of TxDOT poles and natural frequencies in the first three modes were recorded.

Table 3. Finite Element Model Calibration and Validation with Field Measured Values.

Mode	Current Model	Change et al. (2009)	Difference
1st Mode	0.3	0.3	-
2nd Mode	1.3	1.3	-
3rd Mode	3.4	3.3	+3.0%
4th Mode	6.6	6.4	+3.1%

3.3 Pole Segments Affected by Vortex Shedding (Step 2)

High mast lighting poles are susceptible to two types of wind-induced vibrations: vortex shedding induced vibrations and natural wind gust-induced vibrations (AASHTO, 2009). Vortex shedding is an across-wind response. When a cylindrical slender member is placed in a free wind stream, it

causes the wind stream to shed vortices on alternate sides of the cylinder as the flow passes around the member (Blevins, 1977). The manner in which the wind streamlines separate from the member and the tendency to form periodic and regularly shed vortices depends on a dimensionless parameter called the Reynold's number, as shown in Eq. 4:

$$Re = \frac{V \cdot D}{\nu} \qquad \text{(Eq. 4)}$$

where **ν** is the kinematic viscosity of air which is 1.615×10^{-4} ft^2/s, **V** is the mean velocity of the wind stream, and **D** is the dimension of the member presented to the wind stream. For subcritical flow ($300 \leq Re \leq 10^5$) and transcritical or hypercritical flow ($Re > 3.5 \times 10^6$), vortices are shed periodically and regularly. Such periodic or regular vortices exert an oscillating pressure on the member, which causes it to vibrate in a direction transverse to the flow direction. Therefore, a cylinder with a given diameter will only be susceptible to vortex shedding induced vibrations when the flow regime—that is, the free stream wind speed—is conducive to the shedding of these periodic vortices (Foley et al., 2004).

The vortex shedding behavior of tapered members is more complex than that of a prismatic cylinder. Due to the variation of the diameter of a tapered HMIP the Reynold's number of the pole also varies along its length for a given wind speed. Therefore, for a given constant wind speed, one portion of the pole may be susceptible to vortex shedding induced vibrations while another portion of the pole may not be. Similarly, the critical wind speed range over which the flow regime is conducive to the shedding of periodic vortices increases as the diameter of the pole decreases along the length of the pole. The fact that under typical flow conditions, wind speeds vary with elevation, further complicates this phenomenon.

The Canadian Highway Bridge Design Code (2006) applies a 'critical diameter' approach to simplify the calculation of the response for tapered poles. This approach suggests that a tapered pole can be reasonably assumed to behave in the same manner as a prismatic pole as long as the diameters of the pole are within ±10 percent of the critical diameter. Using this approach, the HMIP were divided into discrete segments in order to apply vortex-shedding pressures based on critical diameter approach. The critical diameter was the diameter at the middle of each segment. The vortex shedding response and the Reynold's number for each segment of the pole were evaluated based on this critical diameter. Thus, the top diameter of the pole was assumed to be

90 percent of the critical diameter for the topmost segment of the pole. The diameter at the bottom of the topmost segment was 110 percent of the critical diameter for this segment and 90 percent of the critical diameter for the following segment, and so on. Using this approach, the typical TxDOT HMIP were discretized into 6–8 segments.

3.4 Lock-in Velocity Range for Each Pole Segment (Step 3)

Under typical circumstances, the frequency of vortices shed around a bluff body, $\mathbf{f_s}$, is related to the projected dimension of the member perpendicular to the wind stream, **D**, and to the mean wind velocity, **V**, by a constant $\mathbf{S_n}$, known as the Strouhal number using Eq. 5,

$$f_s = \frac{S_n \cdot V}{D} \qquad \text{(Eq. 5)}$$

Thus, the frequency of shedding vortices increases linearly with the wind speed. However, as the vortex shedding frequency approaches one of the natural frequencies of the structure, a condition called 'lock-in' may occur. Figure 12 schematically illustrates this phenomenon. At lock-in, the vortex shedding frequency remains constant and equal to the natural frequency of the structure causing resonance of the structure in the across-wind direction. This is characterized by large amplitude and self-perpetuating vibrations that can subject the structure to unusually high stresses (Blevins, 1977; Simiu and Scanlan, 1986; Foley et al., 2004). This condition will persist until a limiting wind velocity, $\mathbf{V_e}$, is reached (Blevins, 1977; Chang et al., 2009). The wind velocity at which lock-in occurs is called the critical velocity $\mathbf{V_c}$. Thus, there is a range of wind speeds from $\mathbf{V_c}$ to $\mathbf{V_e}$ where there is the possibility of lock-in, just as there is a range of natural frequencies of the structure over which lock-in can occur.

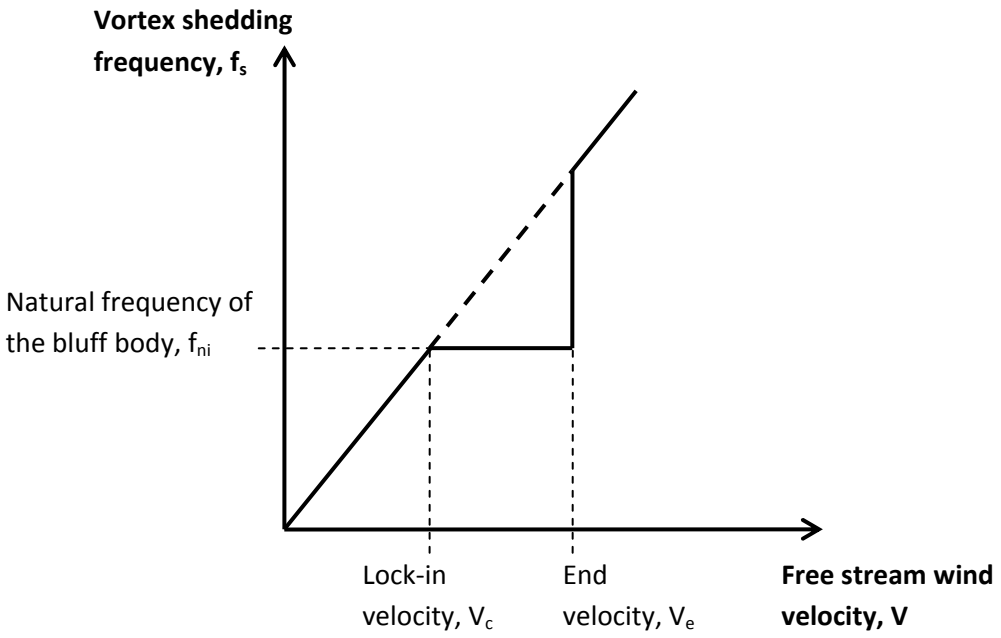

Figure 13. Vortex Shedding 'Lock-In.'

For each of the poles considered in this analysis, the critical wind velocity $\mathbf{V_c}$ was calculated for each segment of the pole based on the critical diameter of that segment and the natural frequencies of each pole in each of the first three modes of vibration (AASHTO, 2009):

$$V_c = 0.68\frac{f_n \cdot D}{S_n} \quad \text{(mph-3sec)} \qquad \text{(Eq. 6)}$$

where f_n is the natural frequency of the pole in Hz., D is the flat-to-flat width of the multisided pole cross-section and S_n is the Strouhal number (AASHTO, 2009). The calculated wind speed corresponds to a three-second average wind speed reported as hourly mean wind speed in miles per hour. The magnitudes of measured wind speeds are sensitive to the amount of time over which the wind speed is averaged. Typically, shorter averaging times yield higher wind speeds since the effects of gusts are more pronounced. Wind speeds can be converted to different averaging times following the procedure outlined in Chapter C26 of ASCE 7 (2010).

While the current AASHTO provisions include a method to calculate the lock-in velocity, $\mathbf{V_c}$, they do not incorporate a method to calculate the limiting, or end velocity, $\mathbf{V_e}$, of the lock-in plateau. However, several other sources indicate that lock-in terminates when the reduced velocity

approaches a value of seven (Blevins, 1977; Chang et al., 2009). The reduced velocity is a dimensionless parameter given by:

$$\text{Reduced velocity} = V_e/f_n D \qquad \text{(Eq. 7)}$$

The calculated end velocity, $\mathbf{V_e}$, was converted to a three-second gust speed by multiplying by a factor of 1.22 based on the assumption that the calculated value represented a 60-second average wind speed. The calculated end velocities determined using this approach for second mode vibrations were consistent with values measured and reported previously by others (Chang et al., 2009).

Thus, a lock-in plateau for vortex shedding, defined by $\mathbf{V_c}$ and $\mathbf{V_e}$, was established for each pole segment for each of the first three natural frequencies. It has been reported that tapered poles may exhibit vortex shedding vibrations in the second and third modes leading to significant accumulation of fatigue damage (Dexter et al., 2002; Chang et al., 2009).

3.5 Creation of Wind Speed Bins across the Lock-in Plateau (Step 4)

The lock-in plateau covered a wide range of wind speeds and, consequently, the stress ranges at the base of the pole differed significantly for $\mathbf{V_c}$ and $\mathbf{V_e}$. In order to assess fatigue damage accumulation more accurately, the range of wind speeds between V_c and V_e was divided equally into three 'bins' defined by $\mathbf{V_c=V_1, V_2, V_3}$ and $\mathbf{V_4=V_e}$. For each of the bins, the average wind speed was used to determine the equivalent static pressure range for that bin as described in the following section. The maximum and minimum wind speeds for a given bin were used, in conjunction with the statistical wind speed distribution, to determine the corresponding number of stress cycles at the base of the pole due to vibrations induced by vortices shed at a given segment height along the length of the pole, for a given range of wind speeds. This procedure is described in detail in the following sections.

3.6 Equivalent Static Wind Pressure Ranges, P_{vs}, for Vortex Shedding Induced Vibration (Step 5)

For vortex shedding induced vibrations at the critical wind speed, the current AASHTO guidelines recommend that the corresponding equivalent static pressure range, $\mathbf{P_{vs}}$, be calculated as (AASHTO, 2009):

$$P_{vs} = \frac{0.00256 V_c^2 C_d \ I_F}{2\beta} \quad \text{(psf)} \qquad \text{(Eq. 8)}$$

where $\mathbf{V_c}$ is the lock-in velocity expressed as a 3-second gust wind speed in miles per hour, $\mathbf{C_d}$ and $\mathbf{I_F}$ are the drag coefficient and the importance factor taken as 1.2 and 1, respectively, and $\boldsymbol{\beta}$ is the damping ratio of the poles taken as 0.005 (AASHTO, 2009). The same expression was used to calculate the corresponding equivalent static pressure for each of the wind speed bins defined in Step 4. However, rather than using the lock-in velocity, $\mathbf{V_c}$, the corresponding average three-second gust wind speeds for each of the wind-speed bins were used. Since the calculated equivalent static pressures were specific to a certain segment of the pole at a specific wind speed, the pressures were applied only to the specific pole segment under consideration for a given wind speed and natural frequency.

3.7 Equivalent Static Wind Pressure Ranges, P_{NW}, for Natural Wind Gust Induced Vibrations (Step 6)

Natural wind gusts, also called 'buffeting,' are an along-wind response. During long-term monitoring of HMIP, researchers have found that natural wind gusts cause along-wind vibrations of the pole in the first mode, giving rise to large stress ranges at the pole base (Chang et al., 2009).

The equivalent static pressure ranges for natural wind gusts were calculated as follows according to the current AASHTO (2009) provisions:

$$P_{NW} = 5.2 C_d I_F \quad \text{(psf)} \qquad \text{(Eq. 9)}$$

where $\mathbf{C_d}$ and $\mathbf{I_F}$ are the drag coefficient and the fatigue importance factor taken as 1.2 and 1, respectively. Unlike vortex shedding pressure ranges, the natural gust pressure ranges are independent of wind speed or pole diameter. As such, the natural wind gust associated pressures were applied to the entire height of the pole irrespective of the taper angle. Further, there was no

need to discretize the wind speed or establish wind speed bins since the natural gust induced pressures were independent of the free stream wind speed.

3.8 Calculation of Stress Ranges at the Base of the Pole (Step 7)

Reynold's numbers were calculated for all wind speeds for each segment of the pole for natural frequencies of all three modes. Vortex shedding loading in the form of equivalent static pressure ranges were applied only on those segments of the pole where the Reynolds number was conducive to shedding of regular and periodic vortices. Each of the calculated pressures were applied to the pole independently to capture the effect of vibrations induced by wind blowing at a particular speed and inducing vibrations of a specific segment of the pole at a specific height.

SAP models were loaded with appropriate wind load for wind speed, $\mathbf{V_1}$, for the first mode of vibration. For example, a typical pole may have been subdivided into eight segments along its height. However, due to the variation of the Reynold's number, only the top seven segments may have been susceptible to vortex shedding induced vibrations. Therefore, seven independent wind load cases were defined for the tapered pole with the appropriate equivalent static wind pressure, $\mathbf{P_{vs}}$, being applied to the corresponding segment of the pole. For each load case, the corresponding equivalent static pressure range was applied to the projected area of the relevant segment. The maximum stresses at the base of the pole were determined for each of the analyses. The stresses determined from the finite element analysis represented fatigue stress ranges since the applied loading represented an applied pressure range. As such, these stress ranges could be used directly in the fatigue analysis of the poles. Since the pole response was linear, the corresponding stress ranges for higher modes of vibrations and for higher wind speeds could be calculated by simple proportioning based on the appropriate equivalent static wind pressures.

For each of the poles, an additional load case was defined to determine the stresses associated with natural wind gusts. The equivalent static pressure range, $\mathbf{P_{NW}}$ was applied along the entire length of the pole and the analysis was conducted in a similar manner as previously described.

Individual analysis cases were defined for each of the wind load cases. Each global analysis was designed to be static and linear, to use stiffness at unstressed initial state, and set to run for all six translational and rotational degrees of freedom. The maximum stress ranges obtained at the base of the pole for each case were recorded.

The stress ranges for $\mathbf{V_2}$, $\mathbf{V_3}$, and $\mathbf{V_4}$ and for modes 2 and 3 were extrapolated linearly from these values based on ratio of the equivalent static pressure ranges. Further, stress ranges for poles with ground sleeve (GS) were calculated from the stress ranges for poles without GS by multiplying by the ratio of section moduli. All relevant stress ranges were thus obtained for 16 different pole configurations of various heights and design wind speeds, with and without ground sleeves.

The average stress ranges for each of the wind speed bins created as per Step 4 above were calculated by averaging out the stress ranges for $\mathbf{V_1 - V_2}$, $\mathbf{V_2 - V_3}$, and $\mathbf{V_3 - V_4}$ for bin 1, bin 2, and bin 3, respectively. These average stress ranges were used for reliability analysis as described in Step 12.

3.9 Wind Speed Distributions Based on Historical Wind Data (Step 8)

The majority of the HMIP in Texas are located in one of five metropolitan centers. Therefore, historical wind data were obtained from the National Oceanographic and Atmospheric Administration (NOAA) from airport locations in each of the five major centers in Texas : Dallas Fort Worth (DFW), San Antonio (SAT), Austin (RMMA), Houston (IAH), and El Paso (ELP). These locations and the surrounding areas with similar wind characteristics account for approximately 75 percent of the total TxDOT HMIP inventory. The archived data in the NOAA database included 2-minute mean wind speeds and directions, and gust speeds dating back over 40 years.

The wind data are comprised of hourly wind observations reported as per the following wind observation and reporting standards (OFCM, 2005):

- Wind direction—2-minute average in 10-degree increments with respect to the true north.
- Wind speed—2-minute average wind speed in knots.
- Wind gust—the maximum instantaneous speed in knots in the past 10 minutes.

Inspection of the wind data indicates that the wind in these five centers generally blows in a predominantly north-south (N-S) direction. Therefore, this direction was considered as the predominant direction for the vortex shedding effect that would induce pole vibrations in the transverse or east-west (E-W) direction. The natural wind gusts in the E-W direction were also considered as they would induce vibrations in the same direction. To simplify the analysis, the

wind roses were subdivided into four sectors, each centered on one of the cardinal directions. Wind blowing from any location within a given sector was conservatively considered to be aligned with the corresponding cardinal direction. This simplification is expected to be more representative for locations where the wind exhibits a distinct directionality. On the other hand, it is expected to be more conservative for locations where the wind direction is distributed more uniformly and does not exhibit clear directionality.

Accordingly, the measured wind data comprising hundreds of thousands of observations over 4–5 decades for each location were organized into N-S and E-W directions. The measured wind speed data were used to establish a probabilistic wind speed distribution for each location in the N-S and E-W directions. Log-normal distributions were fitted to the measured data to develop the wind speed distributions.

Also based on the number of observations, the percentages of time that the wind blew from the N-S and the E-W directions was determined. Further, the percentage of time that the wind was gusty in each direction was also calculated based on the number of recorded gust events in the entire data set. For a target pole design life, the time in seconds that the wind was blowing in the N-W direction within a given range of wind speeds was calculated based on the cumulative distribution functions of the respective log-normal distributions. Similarly, the time in seconds that the wind was gusty in the E-W direction was also calculated. These values are used in Steps 9 and 10 of the analysis, in conjunction with the appropriate natural frequencies, to determine the number of vibrations of the pole during its design life due to vortex shedding and natural wind gusts.

3.10 Number of Vortex Shedding Induced Vibrations during the Life of HMIP (Step 9)

The measured wind speed data were collected at a reference height, $\mathbf{z_{ref}}$, of 33 ft. The wind speeds, $\mathbf{V_z}$, at heights, **z**, other than the reference height can be obtained by using the power law (Foley et al., 2004),

$$V_z = V_{ref}\left(\frac{z}{z_{ref}}\right)^{\propto} \qquad \text{(Eq. 10)}$$

where $\mathbf{V_{ref}}$ is the wind velocity at the reference height. The power-law exponent $\boldsymbol{\alpha}$ depends on type of terrain and has a lower value for terrain with lesser obstructions. For HMIP, two types of terrain have been considered: Open terrain with $\boldsymbol{\alpha} = 0.15$ and Suburban/Urban terrain with $\boldsymbol{\alpha} = 0.25$. Thus, wind speeds in the lock-in plateau for various pole segments at different heights were adjusted to determine the corresponding wind speeds at the reference height by using the power law for both terrain types. The corresponding wind speed at the reference height was used to determine the probabilities of occurrence from the wind speed distributions established in Step 8 above.

The cumulative probabilities of wind speed being less than each of the lock-in velocities $\mathbf{V_1}$, $\mathbf{V_2}$, $\mathbf{V_3}$, and $\mathbf{V_4}$ (converted to equivalent speeds at reference height), were first calculated based on the lognormal distributions for the N-W direction for each of the five locations. The researchers found the probabilities of wind blowing in each of the bins as the difference of cumulative probabilities for the starting and ending wind speeds defining each bin. These probabilities multiplied by the total time in seconds that the wind was blowing in the N-S direction gave the time in seconds that the wind was blowing in each bin. This time in seconds multiplied by the natural frequency of the pole gave the number of vibrations or stress cycles induced at the base of the pole due to vortex shedding for wind blowing at speeds in that bin for that segment of the pole for each of the first three natural frequencies of vibration. So, for wind speed bin **i,** the number of stress cycles that are accumulated over a time period, **t**, due to vortex shedding induced vibrations, **N**, in the n^{th} mode is given by

$$N = [\Phi(V_{i+1}) - \Phi(V_i)]\ (f_n)\ (P_{N\text{-}S})\ (t) \qquad \text{(Eq. 11)}$$

where $\boldsymbol{\Phi()}$ is the cumulative distribution function for the wind speed distributions identified in step 8, $\mathbf{V_i}$ is the lower bound wind speed for the i^{th} bin, $\mathbf{V_{i+1}}$ is the upper bound wind speed for the i^{th} bin, $\mathbf{P_{N\text{-}S}}$ is the probability that wind blows in the N-S direction, and $\mathbf{f_n}$ is the n^{th} natural frequency of the pole.

3.11 Number of Natural Wind Gust Induced Vibrations during the Life of HMIP (Step 10)

The time in seconds that the wind was gusty in the E-W direction was determined as described in Step 8. Since natural wind gusts induce vibrations in the first mode of the pole, the calculated time was multiplied by the first natural frequency to determine the number of vibrations of the pole due to natural gusts during its design life. As mentioned earlier, the N-S direction (the predominant

wind direction) was considered for vortex shedding which other researchers have found to be critical in causing failure of poles due to vibrations in the second and third modes (Dexter, 2002). Accordingly, the number of natural wind gust-induced vibrations in the E-W direction, and the corresponding stress range at the pole base, were calculated and added to the effect of the vortex shedding induced vibrations to evaluate the cumulative fatigue damage at the pole base.

3.12 Fatigue Resistance of Pole Base Connection with Galvanization-Induced Cracks (Step 11)

The fatigue life of typical metallic details is commonly expressed as a function of the applied stress range as:

$$N = A \cdot S^{-m} \qquad \text{(Eq. 12)}$$

where **N** is the number of stress cycles, **S** is the applied stress range, and **A** and **m** are coefficients that are typically empirically determined (Fisher et al., 1998). Taking the logarithm of both sides of this equation and rearranging yields

$$\log S = \frac{\log A}{m} - \frac{\log N}{m} \qquad \text{(Eq. 13)}$$

This represents a linear relationship between log **S** and log **N**. The slope of the log-log relationship can be used to determine the exponent, **m**, of the fatigue life relationship while the **y**-intercept can be used to determine the value of the coefficient, **A**.

The fatigue resistance of cracked galvanized pole base connections was estimated based on results of tests on galvanized connections reported in available literature (Larsson and Westerlund, 1975; Stam et al., 2011). Larsson and Westerlund (1975) presented S-N curves for galvanized and ungalvanized welded steel specimens. Figure 14 plots the data from those tests along with best fit lines to the data. Inspection of the figure indicates that galvanizing the welded joints reduced their fatigue lives.

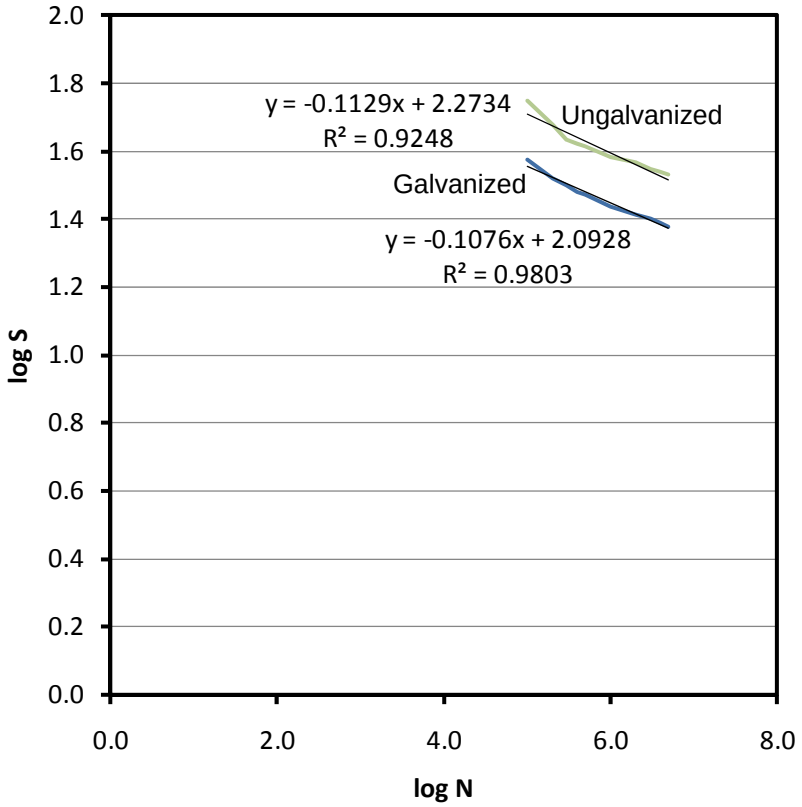

Figure 14. Fatigue Life Curves for Galvanized and Ungalvanized Welds.

While it was not explicitly stated, it can be inferred that this reduction was due to galvanization-induced cracking in the joints that could not be visually observed. Inspection of the figure further indicates that galvanization reduced the intercept of fatigue life curve, but had a minimal effect on the slope. From Figure 14 and applying Eq. 13, it can be seen that galvanization resulted in a minimal reduction of the exponent, **m**. Alternatively, galvanization of the joints resulted in an 80 percent reduction of the coefficient **A**. For AASHTO details, the exponent, **m**, is taken as 3 for all steel details while the coefficient **A** depends on the fatigue category of the detail, with lower values being assigned to details with shorter fatigue lives.

The groove-welded TxDOT base detail without a ground sleeve has been classified as an AASHTO Category E fatigue detail (AASHTO, 2009). Independent testing conducted by others (Stam et al., 2011) validated this point. Alternatively, testing indicates that the detail with a ground sleeve behaves as an AASHTO fatigue Category C detail (Stam et al., 2011). Figure 15 plots the fatigue life curves for AASHTO Category C and E details. The dashed lines in the figures illustrate the influence of an 80 percent reduction of the fatigue life coefficient, **A**.

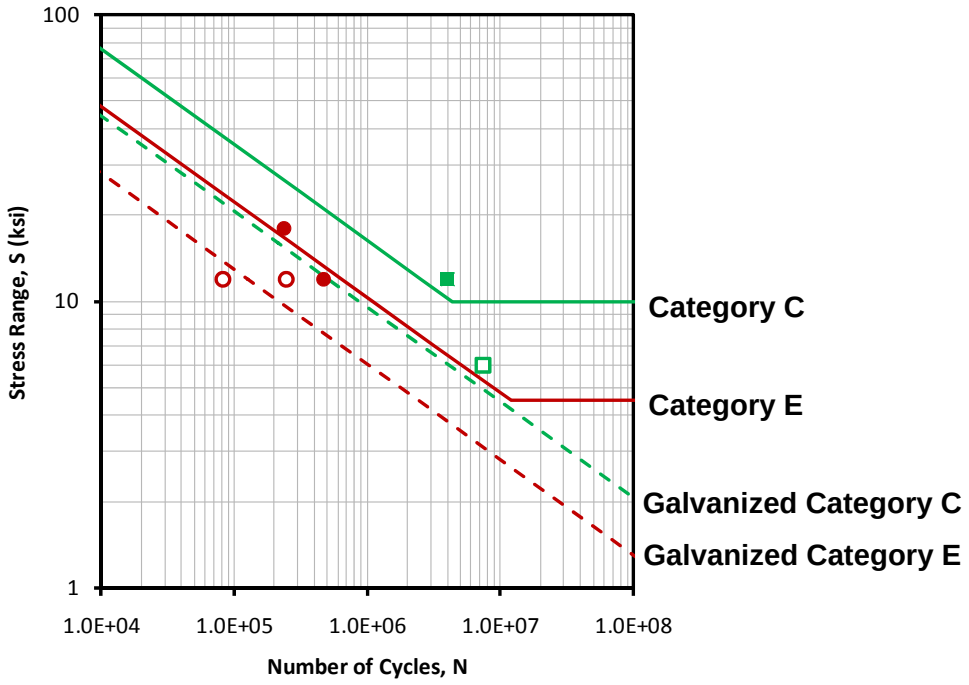

Figure 15. Results of Fatigue Tests of Various Pole Base Details.

The horizontal plateau on the S-N curves indicates the constant amplitude fatigue threshold of a given detail category. In addition to the 80 percent reduction of fatigue life, it is further assumed that details with pre-existing galvanization-induced cracks do not exhibit any constant amplitude fatigue threshold. Figure 15 plots the results of fatigue tests of various pole base details (Stam et al., 2011). Square markers indicate ground-sleeved details while circular markers indicate details without ground sleeves. Solid markers indicate ungalvanized details, or galvanized details without any pre-existing galvanization-induced crack indications, while hollow markers indicate galvanized details with pre-existing crack indications. Inspection of the figure indicates that the test data correspond well with the proposed 80 percent reduction of the fatigue life. Based on the results, Stam et al. recommended a fatigue life reduction of 50 percent be taken for galvanized details with pre-existing crack indications. The influence of the fatigue life reduction was considered in the current study.

Other research has indicated that the fatigue coefficient, **A**, can be represented as a log-normally distributed random variable. The mean, $\boldsymbol{\mu_A}$, and coefficient of variation, $\mathbf{CoV_A}$, of the coefficient **A** for the various AASHTO fatigue categories have been determined elsewhere (see Table 4) (Chung et al., 2003). Inspection of the data indicates that the relationship between the normalized mean,

μ_A/A, and the coefficient **A**, follows an approximately linear relationship within a specific range [see Figure 16(a)]. Similarly, within the same range, the coefficient of variation, CoV_A, is linearly related to the coefficient A [see Figure 16(b)]. The values of μ_A and CoV_A for galvanized details with pre-existing crack indications were extrapolated based on the tabulated data. Table 4 also gives the corresponding values of μ_A and CoV_A for 50 percent and 80 percent reduction of fatigue life. The mean values of **A** are significantly higher than the design values used in the AASHTO code. This is because the design values are necessarily low to provide an acceptably low probability of failure (typically within the range of 0.02 percent for most structural design codes).

Table 4. Fatigue Life Coefficient A and Its Distribution for Various Fatigue Categories.

Fatigue Category	A ($\times 10^8$ ksi^3)	μ_A ($\times 10^8$ ksi^3)	Coefficient of Variation
A	250.0	1500.0	0.54
B	120.0	785.0	0.35
C	44.0	110.0	0.15
D	22.0	47.6	0.25
E	11.0	20.1	0.26
Galv.w/ GS (80% red.)	8.8	16.1	0.28
Galv.no GS (80% red.)	2.2	3.7	0.30
Galv.w/ GS (50% red.)	22.0	46.0	0.23
Galv.no GS (50% red.)	5.5	9.7	0.29

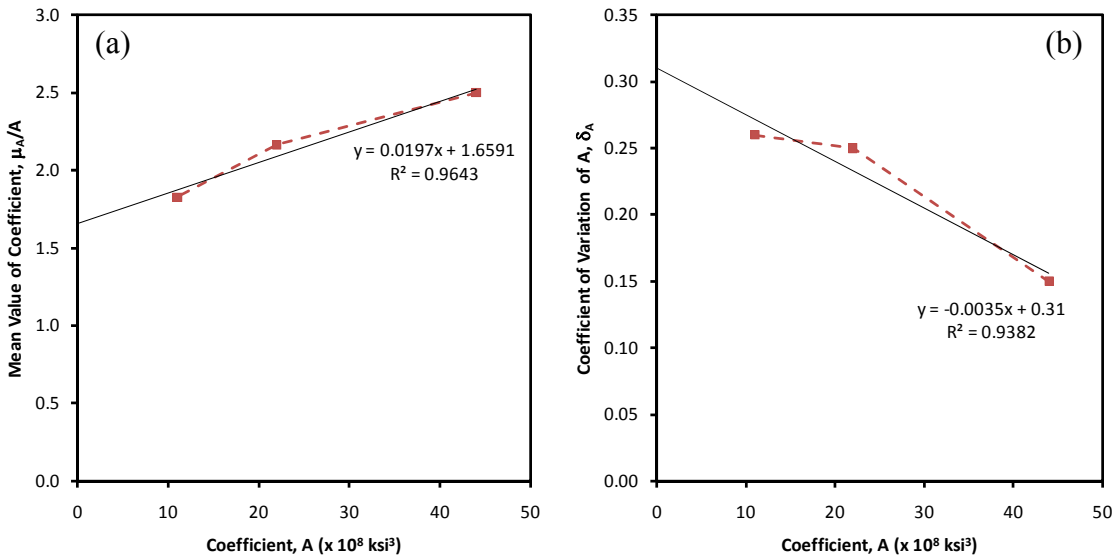

Figure 16. Values of (a) Mean and (b) Coefficient of Variation for Fatigue Coefficient A for Different Fatigue Categories.

3.13 Reliability Analysis to Determine Probability of Failure of Poles (Step 12)

The reliability analysis conducted in this step followed the basic framework presented by Chung et al. (2003) that was used to determine the reliability of fatigue-sensitive details in steel bridges. The stress range data obtained in Step 7 and the number of stress cycles for each stress range for vortex shedding and natural wind gusts calculated in Steps 9 and 10, were used to calculate the effective stress range $\mathbf{S_{RE}}$ as:

$$S_{RE} = \left\{\sum_{i=1}^{n} \gamma_i \cdot S_{R,i}^3\right\}^{1/3} \qquad \text{(Eq. 14)}$$

where $\boldsymbol{\gamma_i}$ is the ratio of the number of stress cycles for a given stress range, $\mathbf{S_{R,i}}$, to the total number of cycles that the pole experienced for all stress ranges. The effective stress ranges for each pole configuration for open and suburban terrains were thus calculated, considering the total number of stress cycles due to vortex shedding and natural wind gusts at the pole base in one year. Equations 12 and 14 were incorporated into Miner's rule to evaluate the cumulative fatigue damage at the pole base as (Chung et al., 2003):

$$D = \sum \frac{n_i}{N_i} = \sum \frac{\gamma_i \cdot N}{A \cdot S_{R,i}^{-3}} = \frac{N}{A} \sum \left[\gamma_i \cdot S_{R,i}^3\right] = \frac{N}{A} S_{RE}^3 \geq \Delta \qquad \text{(Eq. 15)}$$

where **D** is Miner's fatigue damage accumulation index, $\mathbf{n_i}$ is the actual number of stress cycles at a constant stress range $\mathbf{S_{R,i}}$ and $\mathbf{N_i}$ is the number of cycles that the pole base connection can sustain at the given stress range $\mathbf{S_{R,i}}$. For fatigue damage to occur, **D** should exceed the parameter **Δ**. For **D** = **Δ**, Chung et al. (2003) gives the fatigue life, $\mathbf{N_c}$, under variable amplitude loading with effective stress range, $\mathbf{S_{RE}}$:

$$\mathrm{N_c} = \frac{\mathrm{A} \cdot \Delta}{S_{RE}^3} \qquad \text{(Eq. 16)}$$

Just as **A** can be modeled by a log-normal distribution, **Δ** can also be modeled by a log-normal distribution with a mean value of 1.0 and a CoV of 0.30 (Chung et al., 2003). Further, the fatigue failure of a pole base connection can be defined to occur according to the limit state function:

$$g(X) = \mathrm{N_c} - \mathrm{N(Y)} \leq 0 \qquad \text{(Eq. 17)}$$

where **N(Y)** is the actual number of stress cycles to which the connection is subjected to over the life of the pole (Chung et al., 2003).

The probability of failure $\mathbf{P_f}$ of a given pole configuration can then be defined in terms of the reliability index β as:

$$P_f = P(g(X) \leq 0) = \Phi(-\beta) = 1 - \Phi(\beta) \qquad \text{(Eq. 18)}$$

where **ϕ** is a cumulative distribution function of a standard normal random variable. For a function of two log-normally distributed random variables, Chung et al. (2003) defines the reliability index as:

$$\beta = \frac{(\lambda_\Delta + \lambda_A) - 3lnS_{RE} - \ln(N)}{\sqrt{{\zeta_\Delta}^2 + {\zeta_A}^2}} \qquad \text{(Eq. 19)}$$

where the parameters $\boldsymbol{\lambda_\Delta}$, $\boldsymbol{\lambda_A}$, $\boldsymbol{\zeta_\Delta}$, and $\boldsymbol{\zeta_A}$ are defined in terms of mean, **μ**, and coefficient of variation, **δ**, of the randomly distributed variables **A** and **Δ** as follows:

$$\lambda_A = \ln(\mu_A) - \frac{\zeta_A^2}{2} \qquad \text{(Eq. 20)}$$

$$\lambda_\Delta = \ln(\mu_\Delta) - \frac{\zeta_\Delta^2}{2} \qquad \text{(Eq. 21)}$$

$$\zeta_A = \sqrt{\ln(1 + {\delta_A}^2)} \qquad \text{(Eq. 22)}$$

$$\zeta_\Delta = \sqrt{\ln(1 + {\delta_\Delta}^2)} \qquad \text{(Eq. 23)}$$

The values of λ_A and ζ_A were calculated for galvanized pole-to-base-plate connections of poles with and without ground sleeves respectively using the parameters defined in Step 11. Also, the values of λ_Δ and ζ_Δ were calculated. Thus, for each distinct, effective stress range calculated as per Eq. 14 for open and suburban terrains for poles with and without ground sleeves and for each of the five locations, the values of Reliability Index β were determined for various service lives of the pole up to the design life of 50 years. The corresponding values of probability of failure P_f were also calculated using Eq. 18. Thus, for an acceptable value of β or P_f, the fatigue life of a particular pole with any of the analyzed configurations and falling in any of the five wind zones considered above, was predicted.

4 ANALYTICAL RESULTS AND DISCUSSIONS

The analytical framework described in the previous chapter was used to evaluate the reliability of different HMIP designs in five major metropolitan centers throughout the state of Texas. The analysis results are summarized in this chapter. Each set of results is cross-referenced with respect to the relevant steps of the analysis. The complete results are presented for a single pole configuration. The example pole, designated HM-8-100-150, has an eight-sided cross-section, a design wind speed of 100 mph, and an overall height of 150 ft. The results for the remaining poles considered in the analysis are presented following a similar format in the appendices.

4.1 Natural Frequencies (Step 1)

The first three natural frequencies of vibration of the HMIP considered in this study were determined with an eigen value analysis using the SAP2000 commercial finite element analysis software package. Table 5 shows the calculated natural frequencies of vibration of the poles. Inspection of the table indicates that the calculated natural frequencies are consistent with several expected trends. The natural frequencies of all of the poles considered are higher for higher modes of vibration. Further, for a given design wind speed, the taller poles are more flexible and, therefore, exhibit lower frequencies of vibration compared to the shorter poles. Similarly, the poles designed for the higher, 100-mph wind speed have larger diameters and thickness than their 80-mph counterparts [TxDOT Drawing HMIP(2) -98].

Consequently, the stiffer poles, which were designed for higher wind speeds, exhibit higher natural frequencies of vibration. Combined with the independent validation of the model that was described in the previous chapter, the consistency of these trends provides a high degree of confidence in the accuracy of the analysis results. Each of the first three natural frequencies of vibration presented in Table 5 corresponds with three independent modes of vibration of the poles. Figure 17 gives the typical mode shapes for the example pole. The mode shapes were similar for all of the poles considered in the analysis.

Table 5. Pole Natural Frequencies.

# of sides	Wind speed (mph)	Height (ft)	HMIP Designation	f_1(Hz)	f_2(Hz)	f_3(Hz)
8	80	100	HM-8-80-100	0.482	2.076	5.810
		125	HM-8-80-125	0.397	1.562	4.137
		150	HM-8-80-150	0.340	1.251	3.143
		175	HM-8-80-175	0.296	1.023	2.480
	100	100	HM-8-100-100	0.570	2.415	6.391
		125	HM-8-100-125	0.475	1.803	4.611
		150	HM-8-100-150	0.410	1.433	3.559
		175	HM-8-100-175	0.358	1.170	2.842
12	80	100	HM-12-80-100	0.511	2.339	6.318
		125	HM-12-80-125	0.420	1.694	4.548
		150	HM-12-80-150	0.359	1.337	3.511
		175	HM-12-80-175	0.320	1.127	2.867
	100	100	HM-12-100-100	0.557	2.485	6.613
		125	HM-12-100-125	0.474	1.836	4.775
		150	HM-12-100-150	0.401	1.460	3.698
		175	HM-12-100-175	0.351	1.226	3.011

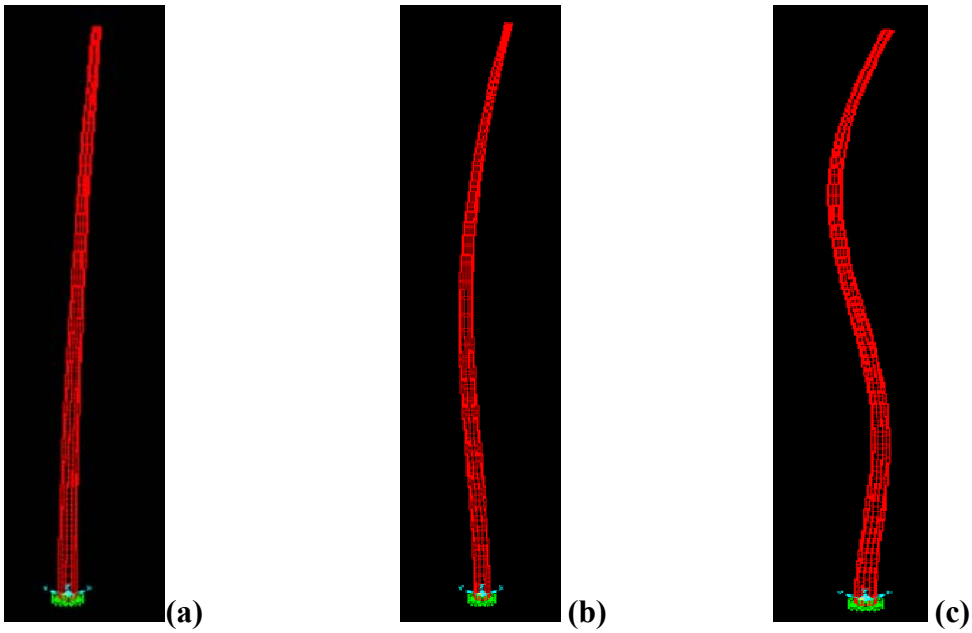

(a) (b) (c)

Figure 17. (a) First, (b) Second, and (c) Third Natural Vibration Modes of HMIP Wind.

4.2 Velocities Causing Vortex Shedding Induced Vibrations (Step 2 to Step 4)

Each of the poles was discretized into segments with top and bottom diameters within ±10 percent of the average diameter of that segment. This discretization resulted in each pole being subdivided into eight segments along the pole length, although the bottom segment was typically quite short. The vortex shedding characteristics of each segment were taken to be governed by the average diameter at the mid-height of the segment. For each segment, and for each mode of vibration, the lock-in velocity, $\mathbf{V_c}$ or $\mathbf{V_1}$, and the end velocity, $\mathbf{V_e}$ or $\mathbf{V_4}$, were calculated.

The lock-in plateau was discretized into three individual bins by defining two intermediate wind speeds, $\mathbf{V_2}$ and $\mathbf{V_3}$. Table 6 presents the critical wind speeds, $\mathbf{V_1}$ to $\mathbf{V_4}$, in the vortex-shedding lock-in plateau, at the mid-height of each of the segments of the HM-8-100-150 pole for the first three modal frequencies. The table also presents the corresponding Reynold's numbers associated with the specific wind speeds and average diameters of each of the segments.

The highlighted values in the table indicate Reynolds numbers and corresponding wind speeds that could potentially excite vortex shedding induced vibrations. Inspection of the table indicates that for lower vibration modes, the critical wind speeds are lower and fall within a broad spectrum of Reynolds numbers. Hence, vortex shedding vibrations are induced over a wider range of diameters closer to the base of the pole. As the vibration mode increases, the critical wind speeds are higher and the range of Reynolds numbers where the flow is conducive to exciting resonant vibrations reduces sharply. Thus, for higher modes beyond the third mode, the flow regime is too turbulent to cause vortex shedding induced vibrations. This is consistent with the reported effect of vortex shedding vibrations in HMIP predominantly in the second and third modes (Dexter et al., 2002; Chang et al., 2009).

Table 6. HM-8-100-150- Critical Wind Speeds and Reynold's Numbers Conducive to Vortex Shedding (Highlighted Values).

Mode	Segment	Avg. Diam. (in.)	Mid Ht. (ft)	V_1 (mph, 3s)	V_2 (mph, 3s)	V_3 (mph, 3s)	V_4 (mph, 3s)	Re_1	Re_2	Re_3	Re_4
								$300 \le Re \le 1.0 \times 10^5$ **$Re > 3.5 \times 10^6$**			
1st	1	8.750	145.	1.4	1.8	2.2	2.6	$9.0x10^3$	$1.2x10^4$	$1.4x10^4$	$1.7x10^4$
	2	10.694	134.	1.7	2.1	2.6	3.1	$1.3x10^4$	$1.7x10^4$	$2.1x10^4$	$2.5x10^4$
	3	13.071	121.	2.0	2.6	3.2	3.8	$2.0x10^4$	$2.6x10^4$	$3.2x10^4$	$3.8x10^4$
	4	15.976	105.	2.5	3.2	3.9	4.7	$3.0x10^4$	$3.9x10^4$	$4.8x10^4$	$5.7x10^4$
	5	19.526	83.7	3.0	3.9	4.8	5.7	$4.5x10^4$	$5.8x10^4$	$7.1x10^4$	$8.5x10^4$
	6	23.865	56.7	3.7	4.8	5.9	7.0	$6.7x10^4$	$8.7x10^4$	$1.1x10^5$	$1.3x10^5$
	7	29.168	22.6	4.5	5.9	7.2	8.5	$1.0x10^5$	$1.3x10^5$	$1.6x10^5$	$1.9x10^5$
	8	32.355	1.7	5.0	6.5	8.0	9.5	$1.2x10^5$	$1.6x10^5$	$2.0x10^5$	$2.3x10^5$
2nd	1	8.750	145.	4.7	6.1	7.5	9.0	$3.1x10^4$	$4.1x10^4$	$5.0x10^4$	$5.9x10^4$
	2	10.694	134.	5.8	7.5	9.2	10.9	$4.7x10^4$	$6.1x10^4$	$7.5x10^4$	$8.9x10^4$
	3	13.071	121.	7.1	9.2	11.3	13.4	$7.0x10^4$	$9.1x10^4$	$1.1x10^5$	$1.3x10^5$
	4	15.976	105.	8.6	11.2	13.8	16.3	$1.0x10^5$	$1.4x10^5$	$1.7x10^5$	$2.0x10^5$
	5	19.526	83.7	10.6	13.7	16.8	20.0	$1.6x10^5$	$2.0x10^5$	$2.5x10^5$	$3.0x10^5$
	6	23.865	56.7	12.9	16.8	20.6	24.4	$2.3x10^5$	$3.0x10^5$	$3.7x10^5$	$4.4x10^5$
	7	29.168	22.6	15.8	20.5	25.2	29.8	$3.5x10^5$	$4.5x10^5$	$5.6x10^5$	$6.6x10^5$
	8	32.355	1.7	17.5	22.7	27.9	33.1	$4.3x10^5$	$5.6x10^5$	$6.8x10^5$	$8.1x10^5$
3rd	1	8.750	145.	11.8	15.3	18.7	22.2	$7.8x10^4$	$1.0x10^5$	$1.2x10^5$	$1.5x10^5$
	2	10.694	134.	14.4	18.6	22.9	27.2	$1.2x10^5$	$1.5x10^5$	$1.9x10^5$	$2.2x10^5$
	3	13.071	121.	17.6	22.8	28.0	33.2	$1.7x10^5$	$2.3x10^5$	$2.8x10^5$	$3.3x10^5$
	4	15.976	105.	21.5	27.9	34.2	40.6	$2.6x10^5$	$3.4x10^5$	$4.1x10^5$	$4.9x10^5$
	5	19.526	83.7	26.3	34.0	41.8	49.6	$3.9x10^5$	$5.0x10^5$	$6.2x10^5$	$7.3x10^5$
	6	23.865	56.7	32.1	41.6	51.1	60.6	$5.8x10^5$	$7.5x10^5$	$9.3x10^5$	$1.1x10^6$
	7	29.168	22.6	39.2	50.9	62.5	74.1	$8.7x10^5$	$1.1x10^6$	$1.4x10^6$	$1.6x10^6$
	8	32.355	1.7	43.5	56.4	69.3	82.2	$1.1x10^6$	$1.4x10^6$	$1.7x10^6$	$2.0x10^6$

4.3 Equivalent Static Pressure Ranges for Vortex Shedding Induced Vibrations (Step 5)

The loading effect of periodically shed vortices can be represented by applying an equivalent static pressure range on the segment of the pole that is susceptible to vortex shedding induced vibrations. This pressure range is formulated in such a way that the stress range at the base of the pole due to the applied pressure range is equivalent to the stress range induced by the vortex shedding vibrations. Table 7 presents the equivalent static pressure ranges, $\mathbf{P_{vs,i}}$, due to vortex shedding for each segment of the pole caused by the critical wind velocities applicable to that segment. Generally, the amplitude of vibration—and, therefore, the stress range at the base of the pole—increases as the wind speed increases.

Table 7. HM-8-100-150- Static Pressure Ranges for Vortex Shedding.

Mode	Segment	Mid-Height (ft)	Critical wind velocities				Static pressure ranges			
			V_1 (mph, 3s)	V_2 (mph, 3s)	V_3 (mph, 3s)	V_4 (mph, 3s)	P_{vs1} (psf)	P_{vs2} (psf)	P_{vs3} (psf)	P_{vs4} (psf)
1st	1	145.3	1.4	1.8	2.2	2.6	0.56	0.95	1.4	2.0
	2	134.8	1.7	2.1	2.6	3.1	0.84	1.4	2.1	3.0
	3	121.9	2.0	2.6	3.2	3.8	1.3	2.1	3.2	4.5
	4	105.1	2.5	3.2	3.9	4.7	1.9	3.2	4.8	6.7
	5	83.7	3.0	3.9	4.8	5.7	2.8	4.7	7.1	10.0
	6	56.7	3.7	4.8	n/a	n/a	4.2	7.1	n/a	n/a
	7	22.6	4.5	n/a	n/a	n/a	6.3	n/a	n/a	n/a
2nd	1	145.3	4.7	6.1	7.5	9.0	6.9	11.6	17.5	24.6
	2	134.8	5.8	7.5	9.2	10.9	10.3	17.3	26.1	36.8
	3	121.9	7.1	9.2	n/a	n/a	15.4	25.9	n/a	n/a
	4	105.1	8.6	n/a	n/a	n/a	23.0	n/a	n/a	n/a
3rd	1	145.3	11.8	15.3	n/a	n/a	42.5	71.5	n/a	n/a

4.4 Equivalent Static Pressure Ranges for Natural Wind Gust Vibrations (Step 6)

The equivalent static pressure range for natural wind gusts was calculated according to the recommendations of the AASHTO provisions that are based on a yearly mean wind velocity of 11.2 mph, which is close to the mean wind speeds that were calculated for the five metropolitan areas considered in this study. The natural wind gust equivalent static pressure is independent of the vertical variation of the wind speed along the length of the pole and is independent of the pole diameter. As such, the calculated equivalent static pressure ranges for all of the poles considered in this study was equal to 6.24 psf.

4.5 Stress Ranges at the Base of the Pole (Step 7)

Researchers calculated the stress ranges at the base of the pole by applying calculated pressure ranges to the appropriate segment of the poles and conducting a static analysis in SAP2000. For several cases, the stresses were verified by simplified hand calculations. The SAP2000 analysis was conducted for one pressure range for each segment of the pole. Stresses due to different pressure ranges applied to the same segment of the pole were calculated by proportioning the stresses by the ratio of the applied pressures since the response was linear. Similarly, the reduced stresses in poles with ground sleeves were calculated by multiplying the stresses by the ratio of the section moduli.

Table 8 gives the stress ranges at the base of the HM-8-100-150 pole due to vortex shedding induced vibrations, with and without the ground sleeve detail. Inspection of the table indicates that, for a given segment of the pole, the corresponding stress ranges induced at the base due to higher modes of vibration are generally greater than those due lower modes of vibration. This is primarily because higher modes of vibration are excited at much higher wind speeds than lower modes of vibration. However, the magnitudes of the maximum induced stress ranges for each of the vibration modes are within a similar order of magnitude. This is consistent with measured stress ranges for higher order pole vibrations that others have reported (Chang et al., 2009). Inspection of the table also indicates that the addition of the ground sleeve at the base of the pole, reduces the stress ranges at that location by nearly 50 percent. This reduction in the induced stress range drastically increases the expected fatigue life of the poles as described later.

Table 8. HM-8-100-150- Vortex Shedding Stress Ranges at the Base of the Pole.

Mode	Segment	Mid-Height (ft)	Stress ranges for pole without ground sleeve				Stress ranges for pole with ground sleeve			
			S_{r1} (ksi)	S_{r2} (ksi)	S_{r3} (ksi)	S_{r4} (ksi)	S_{r1} (ksi)	S_{r2} (ksi)	S_{r3} (ksi)	S_{r4} (ksi)
1st	1	145.3	0.022	0.037	0.056	0.079	0.010	0.017	0.026	0.037
	2	134.8	0.036	0.060	0.091	0.128	0.017	0.028	0.043	0.060
	3	121.9	0.084	0.141	0.212	0.299	0.039	0.066	0.099	0.140
	4	105.1	0.150	0.253	0.381	0.537	0.070	0.118	0.178	0.251
	5	83.7	0.299	0.502	0.758	1.066	0.139	0.235	0.354	0.498
	6	56.7	0.442	0.743	n/a	n/a	0.206	0.347	n/a	n/a
	7	22.6	0.378	n/a	n/a	n/a	0.176	n/a	n/a	n/a
2nd	1	145.3	0.276	0.465	0.702	0.987	0.129	0.217	0.328	0.461
	2	134.8	0.439	0.738	1.115	1.568	0.205	0.345	0.521	0.733
	3	121.9	0.991	1.666	n/a	n/a	0.463	0.778	n/a	n/a
	4	105.1	1.823	n/a	n/a	n/a	0.852	n/a	n/a	n/a
3rd	1	145.3	1.700	2.859	n/a	n/a	0.794	1.336	n/a	n/a

Table 9 presents the average stress ranges due to vortex shedding induced vibrations for the three wind speed bins defined by $\mathbf{V_1 - V_2}$, $\mathbf{V_2 - V_3}$, and $\mathbf{V_3 - V_4}$, respectively.

Table 9. HM-8-100-150-Average Vortex Shedding Stress Ranges at Pole Base for Critical Wind Speeds within Respective Wind Speed Bins.

Mode	Segment	Mid-Height (ft)	Average Stress ranges for pole without ground sleeve			Average Stress ranges for pole with ground sleeve		
			S_{bin1} (ksi)	S_{bin2} (ksi)	S_{bin3} (ksi)	S_{bin1} (ksi)	S_{bin2} (ksi)	S_{bin3} (ksi)
1st	1	145.3	0.030	0.047	0.068	0.014	0.022	0.032
	2	134.8	0.048	0.076	0.110	0.023	0.035	0.051
	3	121.9	0.112	0.176	0.255	0.052	0.082	0.119
	4	105.1	0.201	0.317	0.459	0.094	0.148	0.214
	5	83.7	0.400	0.630	0.912	0.187	0.294	0.426
	6	56.7	0.592	0.743	n/a	0.277	0.347	n/a
	7	22.6	0.378	n/a	n/a	0.176	n/a	n/a
2nd	1	145.3	0.370	0.583	0.844	0.173	0.272	0.394
	2	134.8	0.589	0.926	1.341	0.275	0.433	0.627
	3	121.9	1.329	1.666	n/a	0.621	0.778	n/a
3rd	1	145.3	2.280	n/a	n/a	1.065	n/a	n/a

The stress range at the base of the poles due to natural wind gust induced vibrations was calculated by applying the equivalent static pressure range to the entire pole. Table 10 gives the calculated natural wind gust induced stress ranges for all of the poles considered in the analysis.

Table 10. Natural Wind Gust Static Pressure Ranges and Stress Ranges at Pole Base.

# of sides	Wind speed (mph)	Height (ft)	Natural Wind Gust Stress ranges (ksi)	
			Poles without ground sleeves	Poles with ground sleeves
8	80	150	4.089	1.908
		175	4.916	2.308
	100	150	3.026	1.414
		175	3.629	1.707
12	80	150	4.902	2.131
		175	4.919	2.361
	100	150	3.395	1.613
		175	3.610	1.712

Inspection of Table 10 indicates several relevant trends. For a given design wind speed, the calculated stress ranges are higher for taller poles. The larger surface area and moment arm of the taller poles induce larger moments at the base, resulting in higher stresses for these poles. For a given pole height, the poles designed for higher wind speeds are thicker and consequently have

higher section moduli than the poles designed for lower wind speeds. Consequently, the stress range at the base of the pole is reduced for poles designed for higher wind speeds. Similarly, the natural wind gust stress ranges for poles with ground sleeves are less than 50 percent of those without ground sleeves because of the increased section modulus due to presence of the ground sleeve.

4.6 Wind Speed Distributions (Step 8)

Wind roses and wind speed distributions were developed for five major metropolitan centers in Texas including Dallas/Fort Worth, San Antonio, Austin, Houston, and El Paso. Figure 18 gives the wind roses that illustrate the directionality of the wind in each of these regions. Inspection of Figure 18(a)–(d) indicates that although the specifics of the directionality of the wind in these five centers is somewhat different, it generally blows in a predominantly north-south (N-S) direction. Therefore, this direction was considered as the predominant direction for the vortex shedding effect that would induce pole vibrations in the transverse or east-west (E-W) direction. The natural wind gusts in the E-W direction were also considered as they would induce vibrations in the same direction.

Inspection of the wind rose in Figure 18(e) indicates that the character of the wind directionality in El Paso is quite different from that observed for the other four regions considered in the study. The wind speed distribution does not exhibit a clearly dominant direction. Rather, the wind direction is more evenly distributed. The more evenly distributed directionality of the wind would suggest that cracking would propagate more evenly around the circumference of a given pole. However, the number of damaging cycles in a given direction, and therefore the accumulation of damage, is expected to be lower than in cases when the wind blows from a single dominant direction. For the purposes of this study, the directionality of the wind was treated in a similar manner to that for the other four regions considered.

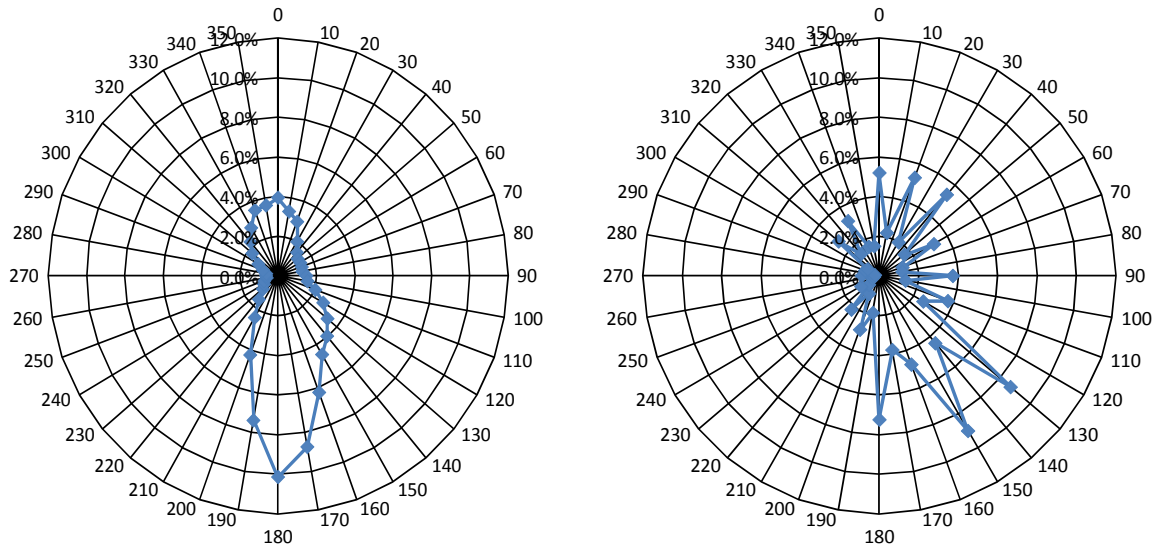

(a) Dallas/Fort Worth (DFW)

(b) San Antonio (SAT)

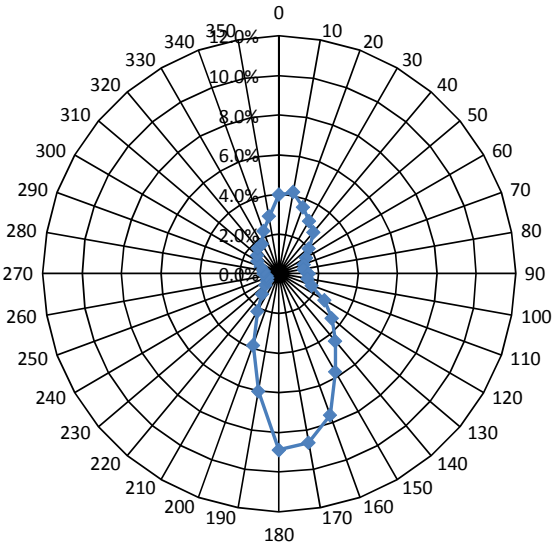

(c) Austin (RMMA)

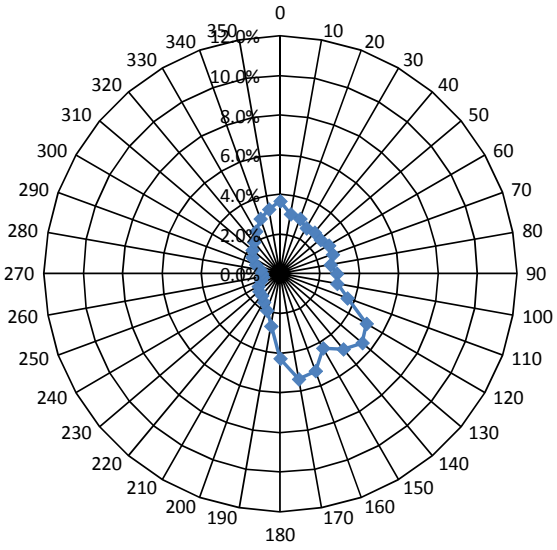

(d) Houston (IAH)

Figure 18. Wind Roses for (a) Dallas/Fort Worth, (b) San Antonio, (c) Austin, (d) Houston and (e) El Paso. Note: North = 0°

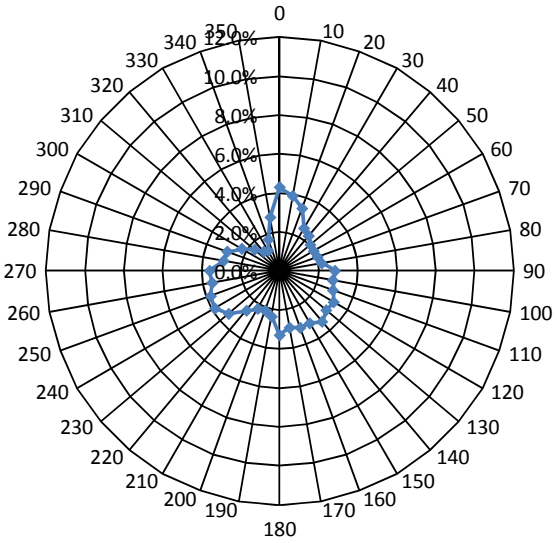

(e) El Paso (ELP)

Figure 18 (cont'd). Wind Roses for (a) Dallas/Fort Worth, (b) San Antonio, (c) Austin, (d) Houston and (e) El Paso. Note: North = 0°

To simplify the analysis, the wind rose was subdivided into four sectors, each centered on one of the cardinal directions. Wind blowing from any location within a given sector was considered to be aligned with the corresponding cardinal direction. This approach is believed to be conservative since it concentrates the accumulated damage due to the wind-induced vibrations rather than distributing it around the circumference of the pole. The measured wind speed data were used to establish a best-fit log-normal wind speed distribution for each location in the N-S and E-W directions as illustrated in Figure 19. The figure shows both the histograms of the measured wind speed data, and the corresponding best-fit log-normal distributions for each of the urban centers, decomposed into the principal N-S and E-W directions. Figure 18 also indicates a good correlation between the histograms of measured wind speeds and the corresponding log-normal distributions. The parameters of the log-normal distribution, including the mean, $\boldsymbol{\mu}$, and standard deviation, $\boldsymbol{\sigma}$, are also given in the figure. Based on the number of observations, the percentages of time that the wind blew from the N-S and the E-W directions were also determined. Further, the percentage of time that the wind was gusty in each direction was also calculated based on the number of recorded gust events in the entire data set. All these data are also given in Figure 19.

DFW
71% N-S
23% E-W
5% Calm

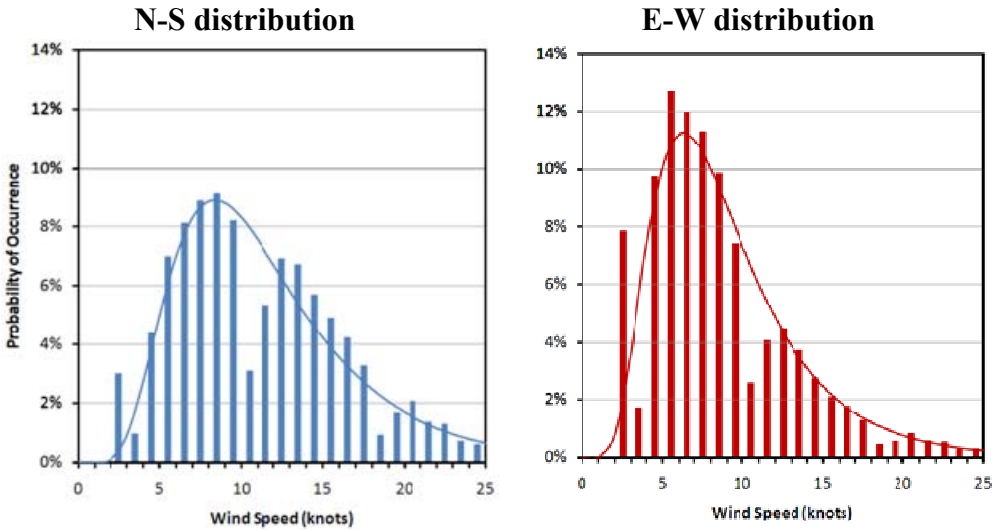

μ = 2.353, σ = 0.478, 9.18% gusts

μ = 2.089, σ = 0.496, 5.36% gusts

SAT
63% N-S
31% E-W
6% Calm

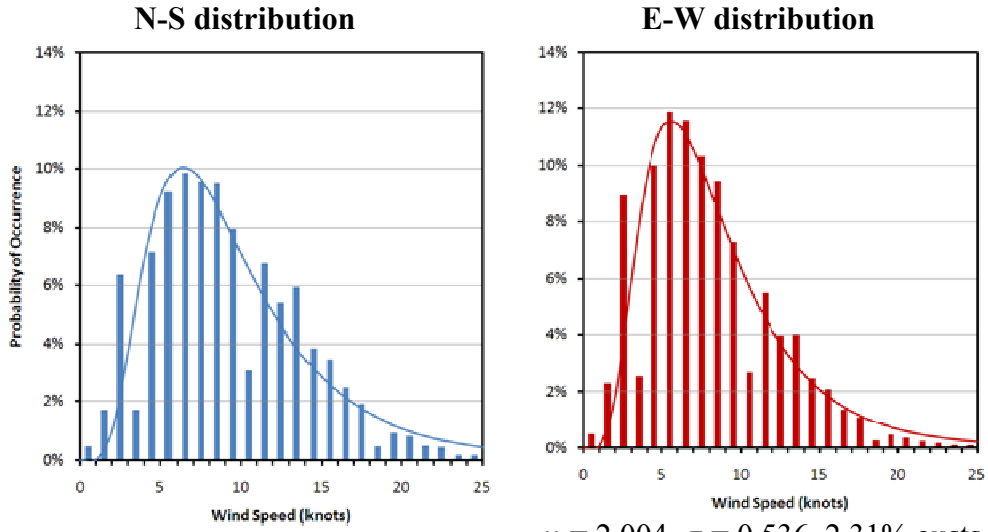

μ = 2.144, σ = 0.537, 5.22% gusts

μ = 2.004, σ = 0.536, 2.31% gusts

Figure 19. N-S and E-W Wind Distributions for (a) Dallas/Fort Worth, (b) San Antonio, (c) Austin, (d) Houston and (e) El Paso.

RMMA
66% N-S
22% E-W
12% Calm

N-S distribution

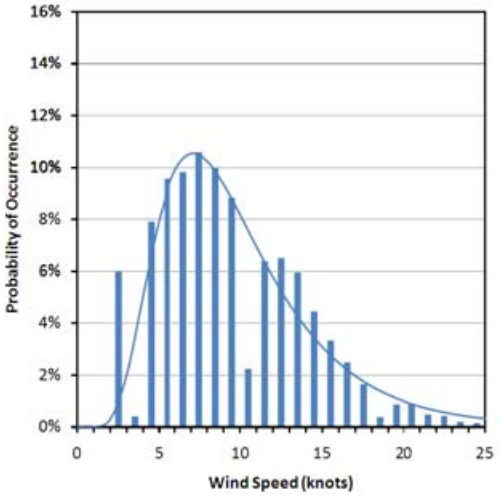

$\mu = 2.189$, $\sigma = 0.474$, 12.8% gusts

E-W distribution

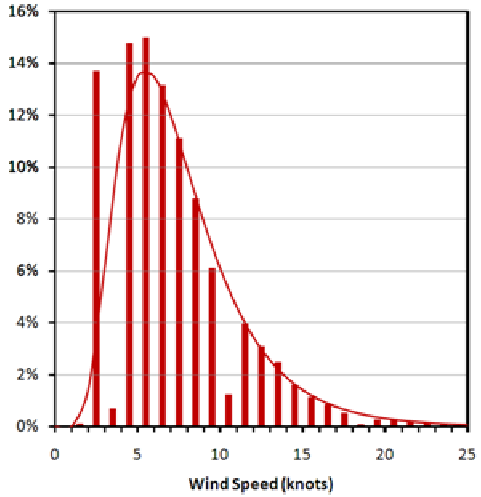

$\mu = 1.925$, $\sigma = 0.473$, 5.23% gusts

IAH
51% N-S
37% E-W
12% Calm

N-S distribution

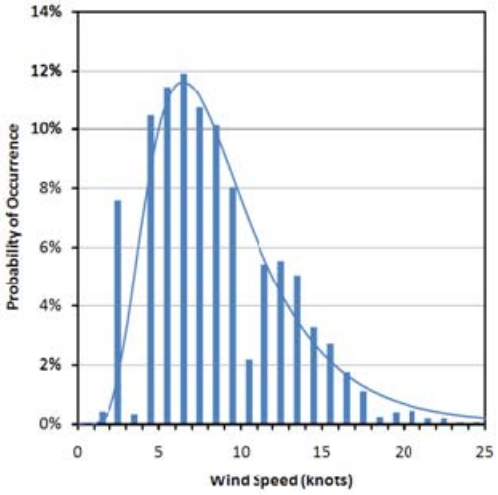

$\mu = 2.092$, $\sigma = 0.474$, 7.50% gusts

E-W distribution

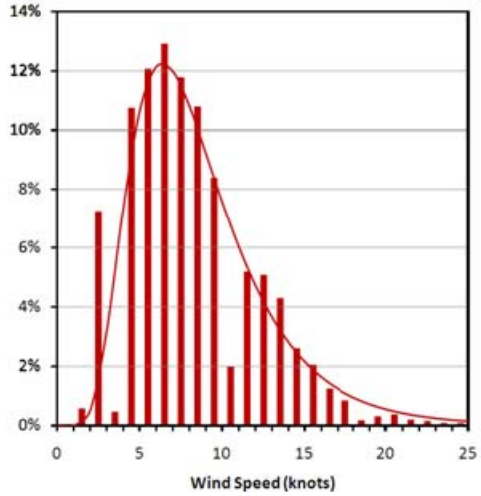

$\mu = 2.065$, $\sigma = 0.459$, 3.92% gusts

Figure 19 (cont'd): N-S and E-W Wind Distributions for (a) Dallas Fort Worth, (b) San Antonio, (c) Austin, (d) Houston and (e) El Paso.

ELP
42% N-S
45% E-W
13% Calm

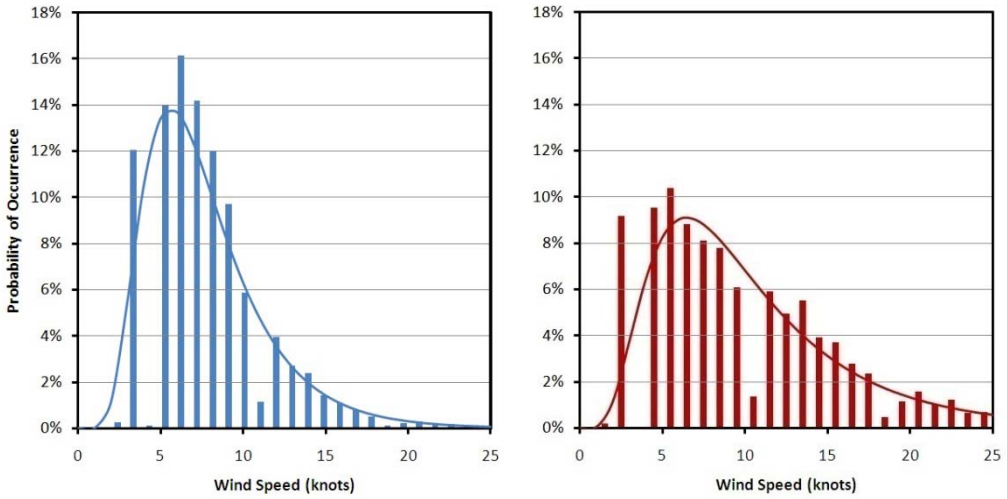

$\mu = 1.9389$, $\sigma = 0.46167$, 4.11% gusts $\mu = 2.1963$, $\sigma = 0.57618$, 17.3% gusts

Figure 19 (cont'd): N-S and E-W Wind Distributions for (a) Dallas Fort Worth, (b) San Antonio, (c) Austin, (d) Houston and (e) El Paso.

Comparison of the statistical data indicates that the mean wind speed in the N-S direction in El Paso is lower than that in the other major centers considered in this study. However, by comparison, the wind blows more frequently in the E-W direction and is gustier when blowing in the E-W direction. The data indicate that natural wind gusts in the E-W direction can be expected 7.79 percent of the time in El Paso. In the other four metropolitan centers considered in this study, wind gusts in the E-W direction can be expected from 0.72 percent to 1.45 percent of the time. That is, wind gusts in the E-W direction are 5–10 times more likely in El Paso than they are in any of the four other locations considered in this study. As such, natural wind gusts in the E-W direction are expected to play a more significant role in the accumulated wind damage for HMIP in El Paso compared to those in any of the other locations considered in this study.

4.7 Number of Applied Cycles for a Given Stress Range (Steps 9 and 10)

To evaluate the fatigue life of the poles, the number of wind-induced stress cycles was calculated for each of the stress ranges induced by vortex shedding and natural wind gusts. The calculated number of cycles for each of the wind load effects is presented in the following sections.

4.8 Vortex Shedding Induced Stress Cycles (Step 9)

For vortex shedding induced vibrations, the number of applied cycles for a given stress range was calculated based on the maximum and minimum wind speeds for the corresponding bin. Since the wind speed distributions for each of the five major metropolitan areas were measured at a reference height of 33 ft, the critical wind speeds at various heights along the pole were converted to wind speeds at the reference height of 33 ft using the power law described in the previous chapter. This conversion depends on the terrain surrounding the pole. The amount of time annually that the wind was blowing in each of the wind speed bins was determined, based on the cumulative distribution function of the wind speed for a given location. Since the corresponding natural frequency of the pole was known, researchers determined the number of cycles by multiplying the calculated duration by the appropriate natural frequency. Table 11 gives calculated number of stress cycles for the example pole, in open terrain near San Antonio for each of the vortex shedding wind speed bins and for each of the segments along the height of the pole. Appendix B shows data for other terrains and other locations along with the data for the remaining poles.

Table 11. HM-8-100-150—Number of Stress Cycles at Pole Base due to Vortex Shedding in Open Terrain, San Antonio.

Mode	Segment	Average Stress Range (ksi)			# of Vortex Shedding Induced Vibrations		
		Bin 1	Bin 2	Bin 3	N_{bin1}	N_{bin2}	N_{bin3}
1st	1	0.030	0.047	0.068	1.82×10^{5}	5.71×10^{5}	1.28×10^{6}
	2	0.048	0.076	0.110	5.79×10^{5}	1.57×10^{6}	3.12×10^{6}
	3	0.112	0.176	0.255	1.59×10^{6}	3.75×10^{6}	6.64×10^{6}
	4	0.201	0.317	0.459	3.78×10^{6}	7.77×10^{6}	1.23×10^{7}
	5	0.400	0.630	0.912	7.67×10^{6}	1.39×10^{7}	1.97×10^{7}
	6	0.592	0.743	-	1.30×10^{7}	2.11×10^{7}	-
	7	0.378	-	-	1.61×10^{7}	-	-
2nd	1	0.370	0.583	0.844	1.37×10^{8}	1.64×10^{8}	1.66×10^{8}
	2	0.589	0.926	1.341	1.94×10^{8}	2.00×10^{8}	1.80×10^{8}
	3	1.329	1.666	-	2.42×10^{8}	2.16×10^{8}	-
3rd	1	2.280	-	-	5.96×10^{8}	-	-

4.9 Natural Wind Gust Induced Stress Cycles (Step 10)

The number of natural wind gust-induced vibrations depends on the probability of occurrence of gusts and the first natural frequency of the pole. For each of the five locations considered in the

study, the probability of gusts given that the wind was blowing in E-W direction was determined. The research team calculated the probability that the wind was blowing in the E-W direction, and the amount of time that a gusty wind was blowing in the E-W direction annually. Since natural wind gusts induce first mode vibrations of the pole, the number of stress cycles can be determined by multiplying the calculated duration by the first natural frequency. Table 12 gives the number of natural wind gust-induced vibrations for the example pole in each of the five cities. The number of stress cycles induced due to natural wind gust is independent of the type of terrain. As discussed previously, inspection of Table 12 indicates that the number of natural wind gust induced vibrations experienced by a given pole configuration is 5–10 times greater in El Paso than in the other regions considered in this study.

Table 12. Number of Natural Gust Induced Stress Cycles for HM-8-100-150 Pole in Different Location.

	San Antonio	Dallas/Fort Worth	Austin	Houston	El Paso
# of cycles	4.63×10^{6}	8.13×10^{6}	7.53×10^{6}	9.38×10^{6}	5.01×10^{7}

4.10 Fatigue Life and Reliability Analysis of High Mast Poles (Steps 11 and 12)

The stress cycles presented in Table 11 and Table 12 and the stress ranges presented in Table 9 and Table 10 were combined to calculate the effective stress range, $\mathbf{S_{RE}}$, for the given pole configuration with and without ground sleeves for different locations and in different metropolitan centers (see Table 13). The effective stress range is representative of the magnitude of the loading acting on a given pole in a given location. It can be seen that the values of $\mathbf{S_{RE}}$ are the highest for DFW, which has the highest mean wind speed. The values are lower for suburban terrain in comparison to open terrain because of higher wind speeds in open terrain. The lower value of stress ranges in poles with ground sleeves is reflected in the lower values of S_{RE} for these poles in comparison to those without ground sleeves.

Table 13. HM-8-100-150—Effective Stress Ranges at Pole Base in Open or Suburban Terrain Located in One of the Five Urban Centers of Texas.

Location	Pole without ground sleeve		Pole with ground sleeve	
	Open terrain	Suburban terrain	Open terrain	Suburban terrain
	S_{RE} (ksi)	S_{RE} (ksi)	S_{RE} (ksi)	S_{RE} (ksi)
DFW	0.87	0.71	0.41	0.33
RMMA	0.68	0.54	0.32	0.25
SAT	0.62	0.50	0.29	0.23
IAH	0.58	0.44	0.27	0.21
ELP	0.42	0.31	0.2	0.15

As described in the previous section, the reliability of different HMIP in different locations depend on the statistical distributions of two parameters: the fatigue coefficient, **A**, and Miner's accumulated damage index, Δ. Table 14 gives the statistical parameters, μ, δ, ζ, and λ, of these variables for galvanized poles with and without ground sleeves. The statistical parameters of the coefficient **A** depend on the original fatigue category of the detail and the percentage of degradation due to galvanization that is assumed. In the current study, based on the findings of previous research (Stam et al., 2011), the undamaged ground sleeve base detail is assumed to behave as a Category C detail, while the details without ground sleeves are assumed to behave as a Category E detail. Two levels of galvanization-induced damage were considered: 50 percent and 80 percent. The relevant statistical parameters are presented in the table, and are independent of the pole design, location, and terrain.

Table 14. Parameters Representative of Fatigue Categories of Poles with Galvanization-Induced Cracking.

Parameter	Miner's Damage Index, Δ	With ground sleeve		Without ground sleeve	
		50% damage	80% damage	50% damage	80% damage
μ	1.00	46×10^8	1.61×10^9	9.7×10^8	3.75×10^8
δ	0.30	0.23	0.28	0.29	0.30
ζ	0.294	0.227	0.274	0.284	0.296
λ	−0.043	22.224	21.163	20.652	19.697

Based on these statistical parameters, the probability of failure and the reliability of different HMIP designs in different cities and for different exposure levels was calculated for service lives ranging from 1 year to 50 years. The probability of failure, $\mathbf{p_f}$, and reliability index, $\boldsymbol{\beta}$, for the example pole, HM-80-100-150, without a ground sleeve in San Antonio and assuming 80 percent reduction of the fatigue life due to the presence of a galvanization-induced crack are plotted for different service lives in Figure 1 (a) and (b), respectively.

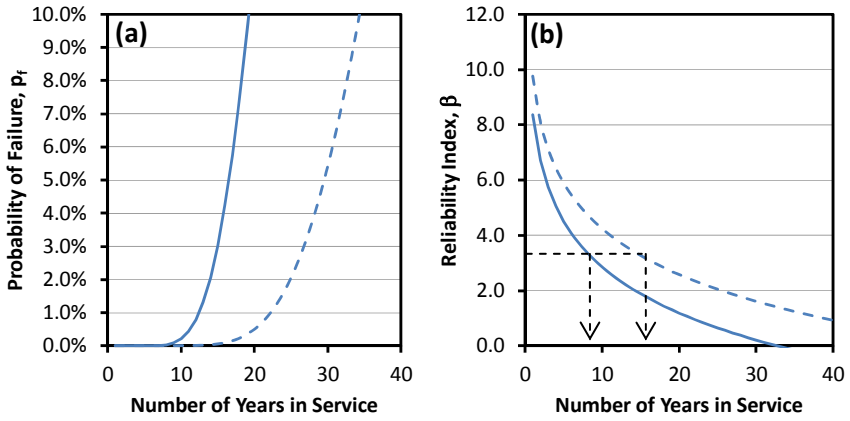

Figure 20. (a) Probability of Failure and (b) Reliability Indices for HM-80-100-150 Pole without Ground Sleeve in San Antonio.

The solid lines in the figure indicate the values for open terrain, while the dashed lines represent the behavior in suburban terrain. Inspection of the figure indicates that the probability of failure of poles in suburban terrains is substantially lower than that for poles in open terrain due to the reduction of the wind speed in these regions. Inspection of the figure further indicates that the probability of failure remains fairly low during the initial portion of the service life but begins to increase rapidly beyond a certain stage. This mirrors the behavior of the cumulative distribution function of log-normally distributed variables which are used to represent the random variables in this study. Figure 1(b) indicates that the reliability of the poles decreases with time. In the current study, a target reliability index of 3.5 was selected, which corresponds to a probability of failure of approximately 0.02 percent. This level of reliability was selected because it is consistent with the target reliability that the typical American bridge and structural design codes use (AASHTO, 2010; Barker et al., 2006).

Inspection of the figure indicates that the specified design pole, if located in San Antonio, would reach the target level of reliability in 7.6 years and 13.6 years in open and suburban terrain, respectively. At this stage, the probability of failure of the poles would be higher than is typically accepted for most American structural design codes. As such, some remedial measure should be implemented at this stage. These remedial measures could include a number of possible solutions ranging from relatively inexpensive and straightforward to the more expensive and involved. First, a more rigorous inspection of the pole base could be implemented to evaluate the rate of growth of galvanization-induced cracks. If continuous monitoring of the cracks indicates minimal crack propagation, it may be acceptable to leave the pole in service. However, the pole should be monitored regularly to assess the propagation of fatigue induced damage. Alternatively, if inspection indicates that the cracks have propagated but are still within an acceptable range, it may be appropriate to repair the base connection by removing the damaged portions of the weld and rewelding the connection. Finally, if the crack propagation has reached an unacceptable level, the pole may need to be replaced.

The calculated reliability index for the same pole design with a ground sleeve was greater than 300 years indicating that the presence of the ground sleeve significantly increased the 'safe' service life of the poles. This is due to two primary factors. First, the presence of the ground sleeve increased the fatigue life of the undamaged poles from a Category E detail to a Category C detail. Therefore, the fatigue lives of ground sleeved poles with pre-existing galvanization-induced cracks are much higher than that of poles without ground sleeves. Additionally, the presence of the ground sleeve helped to reduce the stress range at the base of the pole under the same load effects thereby significantly reducing the fatigue damage accumulation. A similar trend was observed for all of the pole configurations. In fact, all of the ground-sleeved poles had 'safe' serviceable lives to the target reliability index well above the target 50-year design life with the exception of the HM-12-80-150 configuration in open terrain in Dallas–Fort Worth, which had an expected fatigue life of 34.6 years. As such, the remaining discussion will focus on non-ground sleeved poles only.

The predicted 'safe' servicable lives for a reliability index of 3.5 for all the 150-ft and 175-ft tall poles without ground sleeves considered in this study in each of the five urban centers are given in Figure 21 (a) and (b) for open terrain and suburban terrain, respectively.

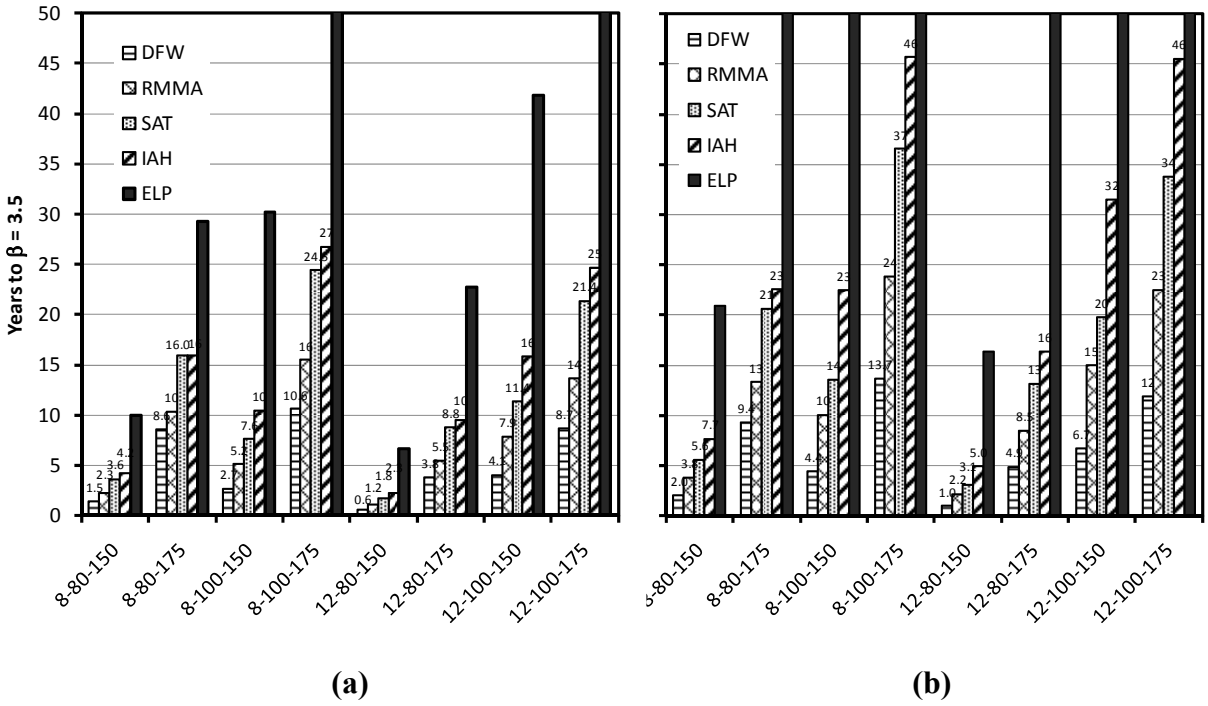

Figure 21. Fatigue Life of HMIP Located in (a) Open and (b) Suburban Terrains to Reach a Target Reliability index, β = 3.5.

Several factors in the analysis can affect the actual magnitude of the predicted 'safe' lives, and will be discussed later. As such, the predicted 'safe' lives do not necessarily represent absolute expected fatigue lives as there are several sources of uncertainty in the analysis that were not quantified. As such, the presented 'safe' lives should be considered in relative terms to direct maintenance and inspection decisions rather than being viewed as absolute measures of 'time to failure.'

Inspection of the figure indicates that poles located in the Dallas–Fort Worth metropolitan area have the lowest servicable lives. This is mainly due to the higher mean wind speeds in this region than in other parts of the state. The figures also indicate that for poles with a given number of sides and design wind speed, the 175-ft tall poles have a higher expected 'safe' lives than the 150-ft tall poles. This is consistent with the fact that the taller poles have a base section with greater moment of inertia and generally lower frequencies of vibration than the shorter poles yielding lower stress ranges and fewer stress cycles within a given time frame. The HM-12-80-150 and HM-8-80-150 configurations exhibit the lowest predicted fatigue lives. As such, these pole configurations should be carefully monitored. On the other hand the HM-8-100-175 and

HM-12-100-175 exhibit much higher predicted 'safe' lives, suggesting that they may be safely monitored using a longer inspection interval.

Inspection of Figure 21 also indicates that poles located in El Paso generally have a much longer predicted life than those located in the other four regions considered in this study. In fact, the predicted 'safe' life of several of the pole configurations exceeded the 50-year design life TxDOT typically uses. Unlike the other four regions considered in this study, the wind distribution in El Paso does not exhibit a strongly dominant direction; rather, the wind is more uniformly distributed. As such, poles are subjected to fewer vortex shedding-induced vibrations in one direction. Therefore, the accumulated damage, rather than being concentrated in one direction, is distributed more uniformly around the pole resulting in a lesser extent of fatigue damage in any given direction. Additionally, poles in El Paso are subjected to significantly more natural wind-gust induced fatigue cycles than poles in other regions. While these cycles impart the largest stress ranges to the poles, the number of accumulated natural wind gust-induced cycles is typically orders of magnitude lower than the number of vortex shedding induced cycles. Overall, the total accumulated damage due to natural wind gusts is typically much less than the damage accumulated due to vortex shedding induced vibrations.

4.11 Limitations of the Current Study

The current fatigue lives were calculated based on an assumed 80 percent degradation of the fatigue coefficient, **A**, of the galvanized details due to the presence of the galvanization-induced cracks. This is based on available research results for galvanization and other treatments of different types of welded connections, which do not exactly match the pole-to-base-plate connection details of HMIP. In a recent experimental research (Stam et al., 2011) where galvanized and ungalvanized HMIP specimens were tested in the laboratory over a period of three tofour years, the researchers proposed a 50 percent reduction of fatigue life based on a limited number of tests. If this value is adopted for the present analysis, it would increase the predicted 'safe/serviceable' life by 2.67 times for all of the poles considered where 'safe/servicable' means that the target reliability index, β, of 3.5 is not exceeded. Clearly, the expected 'safe' life to the target reliability index is particularly sensitive to the degree of degradation assumed. As such, more comprehensive data regarding the fatigue life of welded details with pre-existing galvanization-induced cracks are needed to provide an accurate

assessment of the reliability of the poles in the TxDOT inventory. Additionally it was assumed that the poles exhibited no constant amplitude fatigue threshold (CAFT); that is, all of the applied stress cycles were assumed to induce damage and cause crack propagation at the base of the pole. This may or may not be an appropriate assumption and requires further investigation. If poles with pre-existing cracks do exhibit a CAFT, the lower amplitude stress cycles may not induce any damage at the pole-to-base plate connection. This would reduce the number of damage-inducing cycles that the poles are subjected to thereby increasing the 'safe' life to the target reliability index. Based on the existing data available in the literature, more conservative values were selected for the current study to reflect a 'worst case' scenario. The conservative nature of the current analysis approach is highlighted by the fact that there have not been any reported failures of HMIP in Texas that were attributed to the presence of pre-existing cracks at the pole-to-base plate connection.

The results of this reliability analysis could be productively used to optimize inspection schedules. Thus, attention could be initially focused on poles with very low predicted fatigue lives by inspecting them frequently and assessing the rate and extent of crack propagation. Once the crack growth rate is more precisely known, a revised inspection period suitable for the particular pole configuration and location under consideration could be adopted.

The inherent variability of wind loading also adds additional complexity to the analysis. The current analysis adopted a simplified approach that can be conducted relatively quickly with limited computational resources. A more rigorous analysis, such as a non-linear dynamic time history analysis, could be adopted and may give a more accurate representation of the wind induced loading acting on the HMIP. However, any analysis results should be verified by field measurements to confirm the validity of the analysis to the extent possible. The current analysis assumed that all vibration modes act independently of one another for all wind speeds. Modal superposition may lead to constructive and destructive superposition of the maximum stress ranges. This effect was not considered in the current study and may also affect the predicted fatigue life of the poles.

The reliability analysis conducted in this study also depends on the selected value of the target reliability index, β, or the acceptable probability of failure, $\mathbf{p_f}$. Figure 22 gives the increase of the

probability of failure, $\mathbf{p_f}$, over time for the HMIP 8-100-150 pole configuration without a ground sleeve in open terrain in Houston. While the specific amount of time required to reach a given probability of failure varies for different pole configurations and locations, the general trend is consistent for all of the poles and locations considered in this study. Inspection of Figure 22(a) indicates that the increase of the probability of failure can be categorized into three phases. In the initial 'plateau' phase, the probability of failure remains relatively constant over time. A second phase follows, during which the probability of failure increases relatively rapidly over time. In the third phase, the probability of failure plateaus again at very high values.

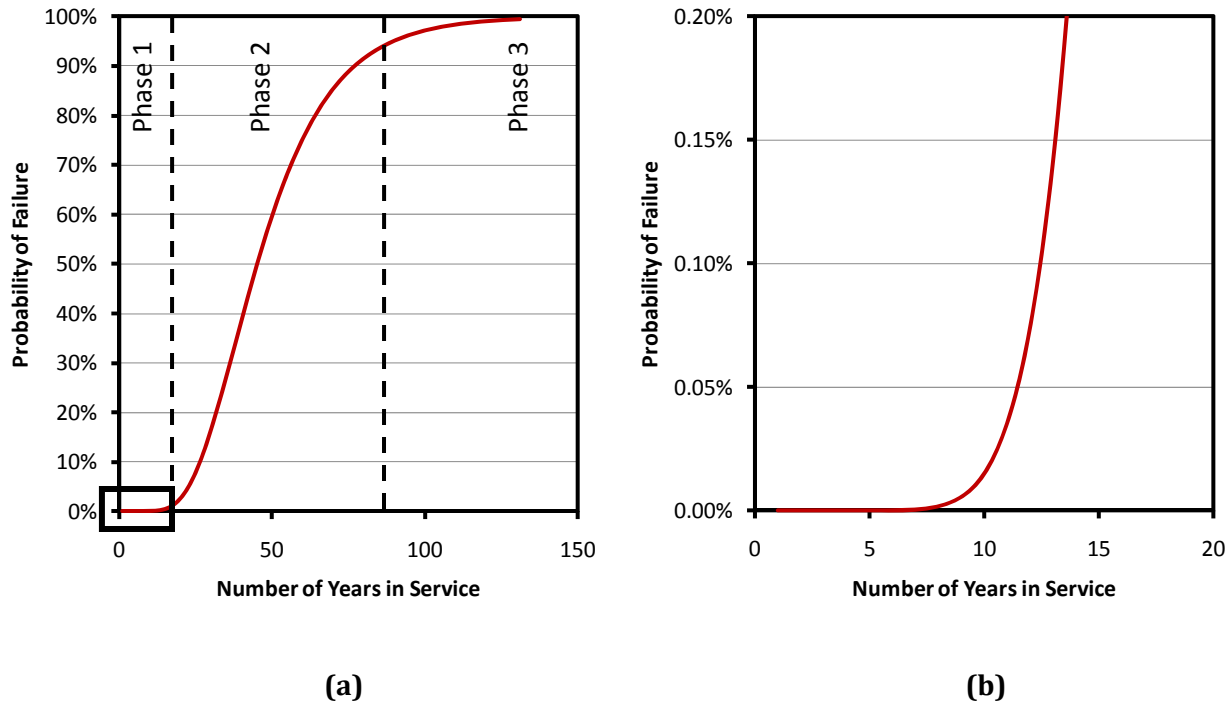

Figure 22. Increase of the Probability of Failure, $\mathbf{p_f}$, with Time for HMIP 8-100-150 without a Ground Sleeve in Open Terrain in Houston, TX (a) Overview, (b) Close-Up.

Ideally, the acceptable probability of failure, and the corresponding target reliability index, should be selected within the initial plateau range. This will help to avoid the possibility of a sudden increase of the expected probability of failure over a relatively short time. Figure 22 (b) plots a close-up view of this first plateau stage, and shows that the selected acceptable probability of failure of 0.02 percent already falls within the initial range of the second phase of the behavior. Increasing the acceptable probability of failure by 10 times to 0.2 percent, with a corresponding target reliability index of 2.88, would only increase the predicted 'safe' fatigue

life by 30 percent—from 10.5 years to 13.6 years. Similarly, increasing the acceptable probability of failure by another ten times to 2 percent, with a target reliability index of 2.0, would only increase the predicted 'safe' fatigue life to 19.2 years. A similar trend was observed for all of the poles considered in this analysis. As such, it can be seen that the predicted 'safe' fatigue life of the poles is not particularly sensitive to the specific value of the target reliability index, $\boldsymbol{\beta}$, selected, within the typical range of probabilities of failure, $\mathbf{p_f}$, that can be tolerated in typical structural applications.

5 REPAIR ALTERNATIVES AND REPAIR/REPLACEMENT COST ANALYSIS

5.1 Introduction

Detection of galvanization-induced cracks in HMIP represents a major practical challenge. Since these cracks can often be sub-visual, they require specialized inspection techniques to be detected. To maintain the integrity of the pole-to-base plate connection and to maximize the fatigue life of the connection, it is imperative to detect and repair these sub-surface cracks and the presence of incomplete weld fusion as soon as possible. This is because the fatigue life of a weldment is primarily based on the extent of crack propagation. Repair of cracks, particularly of those detected early in the sub-visual range, can extend the fatigue life of the damaged HMIP and is far more economical than replacement, which may be required if cracks are not identified early enough.

Numerous Non-Destructive Testing methods (NDT) are available in the market for detecting cracks in welded connections (Rizzo et al., 2010). Some of these NDT methods include:

- Visual Inspection.
- Liquid Penetrant.
- Eddy Current Testing.
- Acoustic Emission Testing.
- Electromechanical Impedance Testing.
- X-Ray Testing.
- Magnetic Particle Inspection.
- Conventional Ultrasonic Testing (UT).
- Enhanced Magnetic-Particle Testing (EMT).
- Advanced Ultrasonic Testing (AUT).

A literature review of the existing research has shown that many of the commonly used Non-Destructive Testing methods are incapable of detecting small, sub-visual cracks. Ultrasonic inspection after galvanizing of the base plate-to-shaft weld should be specified to prevent structures with pre-existing cracks from entering service. Such pre-existing cracks have been reported to be relatively shallow ($\leq {}^{3}/_{32}$ inches) in depth and shorter in lengths (1 to 3 inches) (Wood et al., 2005; Stam et al., 2011). In contrast, other states, including Florida, Colorado, and South Dakota reported the presence of more severe fatigue cracks which were about 25 percent of

total weld length. This extent of cracking could lead to total failure of a pole (Suksawang et al., 2009). Research shows that galvanization-induced shallow cracks at the toe of the base plate-to-shaft welds in HMIP can be easily repaired without jeopardizing the performance of the structure (Wood et al., 2005; Suksawang et al., 2009; Stam et al., 2011). Specialized Ultrasonic Testing procedures using small transducers must be employed, because coatings such as galvanization or paint can mask the sub-surface/sub-visual defects in metal and welds.

Normal UT methods of the poles as prescribed by AWSD1.1 are not sensitive enough to detect the existence of these sub-visual galvanization-induced cracks in pole-to-base plate connections. Consequently, Lamb-Star Engineering, a consultant for the North Texas Tollway Authority (NTTA), developed an advanced UT technique that involves several steps and the use of unique testing equipment and procedures (see Figure 23). The method that NTTA uses involves an initial inspection with an advanced UT method to provide a preliminary indication of the location and extent of cracking as illustrated in Figure 23 (a). This is followed by a more rigorous EMT to pin-point the location and extent of cracking as shown in Figure 23 (b). For illustrative purposes, the same sequence of tests was conducted after removal of the galvanization by grinding as shown in Figure 23 (c) and (d). NTTA has been successfully using this technique to detect subsurface cracks in HMIP since 2005. Certain researchers have reported that other methods of non-destructive testing were unable to detect sub-visual, galvanization-induced cracks (Stam et al., 2011; Wood et al., 2005). Early detection and repair of cracks is essential to maintain the fatigue performance of pole-to-base plate connection details.

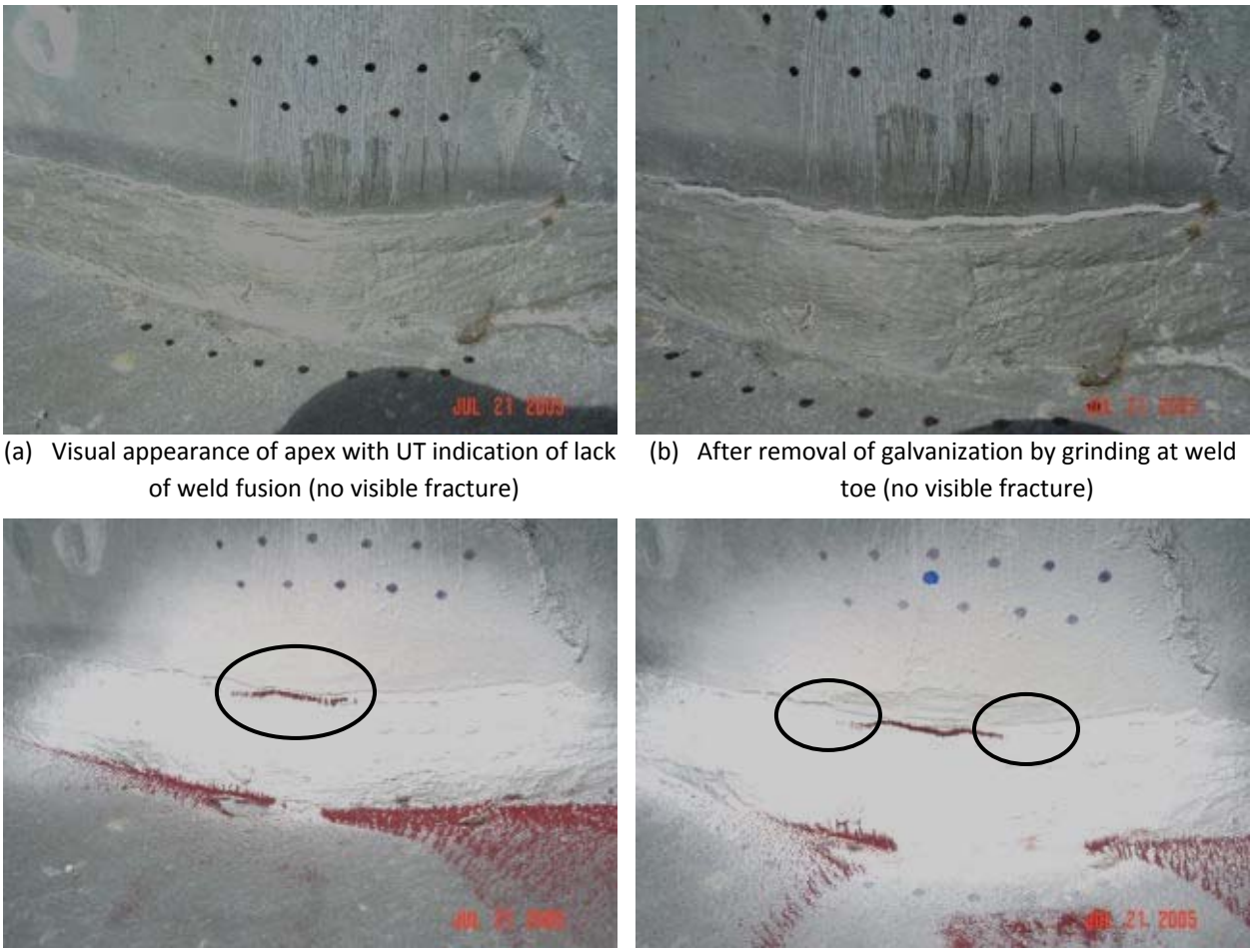

(a) Visual appearance of apex with UT indication of lack of weld fusion (no visible fracture)

(b) After removal of galvanization by grinding at weld toe (no visible fracture)

(c) Lack of fusion revealed by MPT (1/64" removed at weld toe)

(d) Through-wall fracture revealed coterminous to lack of fusion (1/32" removal depth at weld toe)

Figure 23. Optimized UT and Advanced EMT Methods Used for Early Detection of Cracking and Defects in HMIP (Courtesy Lamb-Star Engineering LP).

5.2 Repair Methods

Replacement of HMIP is a time-consuming and costly operation. As such, research has been conducted to identify various methods of repairing HMIP to postpone or prevent the need for replacement (Thomas et al., 2009; Suksawang et al., 2009). While some techniques are implemented as temporary measures, others have been shown to return poles to levels comparable to their initially intended design levels, if implemented properly. Figure 24 and 25 illustrate several techniques for repairing HMIP, including:

- Rewelding of cracks [Figure 24(a)].
- Steel Jacket Encasement [Figure 24(b)].

- Welded Plate Stiffeners [Figure 24(c)].
- Bolted Stiffeners [Figure 24(d)].
- Ultrasonic Impact Treatment (UIT) of cracks [Figure 25].

(a) Weld repair with toe dressing (prior to UIT) (courtesy Lamb-Star Engineering LP)

(b) Jacketing (courtesy Dr. Suksawang, Florida International University)

(c) Welded stiffeners (courtesy Dr. Suksawang, Florida International University)

(d) Bolted stiffeners (courtesy Dr. Suksawang, Florida International University)

Figure 24. Various Repair Methods for Fatigue Cracked HMIP.

The Florida Department of Transportation (FDOT) has adopted rewelding, due to its simplicity, to remediate the fatigue cracks in the HMIP (Suksawang et al., 2009). For temporary repairs, an additional fillet weld can be laid over the existing weld. However, this repair method is susceptible to reinitiation of cracks within a relatively short time. A more robust repair involves

first removing the entire length of the cracked weld, followed by rewelding onsite with a multi-pass weld to achieve a detail similar to the initial detail (Stam et al., 2011). As described in the previous section, a final inspection is advisable to confirm the quality of the repair. To maintain the corrosion resistance of the detail, the repaired weld should be painted with a zinc-rich paint, otherwise known as 'cold galvanizing.'

Steel jacketing typically requires the installation of a bolted jacket around the base section of the existing pole. The presence of the jacket increases the stiffness and section modulus of the base section of the pole, thereby reducing the stress range at the connection. This is generally a temporary measure and is susceptible to tampering. The jacket consist of two steel half pipes bolted together to form a jacket that encases the mast and the base welded to the base plate. The gaps between the jacket and mast can be sealed using non-shrink grout. Additionally, consideration must be given to maintain accessibility to the hand hole. This access can be achieved by leaving an opening in the jacket; however, in some applications, the presence of this opening may lead to the leakage of grout. Furthermore, HMIP base sections are typically different sizes which would require custom fabrication of jackets on an as-needed basis. Overall, jacketing has been deemed as an expensive and labor-intensive option that may not be practical for regular repairs (Suksawang et al., 2009).

As shown in Figure 24(c), welded plate stiffeners consist of triangular steel plates that are welded to the sides of the HMIP. Representative dimensions of these plates are in the range of 3/8 inches × 3-1/2 inches × 16 inches, and they are typically welded at the apex points of the pole. According to the FDOT experience, this repair method is easy to perform, although it requires substantially more welding than repair welding. The utilities near the pole should be shielded in the field to prevent damage, and the field welding requires strict quality control and assurance measures to avoid rough/uneven welds and undercutting (Suksawang et al., 2009). Additionally, galvanization must be removed prior to welding to avoid impurities in the weld and the release of possibly harmful fumes (Stam et al., 2011). This can be done using a flap-type sanding disk, which will remove the coating without damaging the parent metal.

The bolted stiffener repair method shown in Figure 24(d) consists of installing a composite stiffener fabricated from two triangular steel plates welded to a steel backing plate. The

dimensions of each stiffener are similar to those used in typical welded stiffener repairs. The backing plate can be directly bolted onto the HMIP at the base as shown. These stiffeners are typically installed on every other side of the pole section requiring six stiffener assemblies for 12-sided poles and four assemblies for eight-sided poles (Suksawang et al., 2009). Because of the gradual taper of HMIP and the buildup of the weld at the intersection between the base plate and the pole, detailing and installation of these assemblies can be challenging. For example, due to the taper of the poles and curvature near the apex points, the backing plate may not rest evenly against the pole section. Also, drilling holes on the pole mast represents a practical challenge and may lead to a reduction of the quality of the installation. Finally, accessibility to the inside of the pole in order to tighten the bolts may not be feasible, particularly on sides away from the hand hole at the pole base (Suksawang et al., 2009).

Since 2005, NTTA has effectively implemented UIT in the field on their HMIP as a means of improving the performance of rewelded details (Starnater E., 2009). Figure 25 illustrates this process. Upon verification that the repair welds exhibit no crack indications, the weld profile is enhanced through grinding, and fillet weld toe dressing. UIT is performed on the weld repair and top toe of the weld to enhance fatigue performance. This technique consists of applying mechanical impact through a pin at ultra-high frequency on the weld, imparting a localized but intense compressive stress that results into a uniform microstructure of the weld up to a depth of one inch. The UIT method involves a deformation treatment of the weld toe by a mechanical hammering at a specific frequency (200 Hz.) superimposed with ultrasonic treatment (27 kHz.). The objective of the treatment is to introduce beneficial compressive residual stresses at the weld toe and to reduce stress concentration by smoothing the weld toe profile. Upon completion of the weld repair and UIT, a spray-applied zinc-rich compound is applied to maintain corrosion resistance.

(a) UIT in progress

(b) Typical residual groove after UIT

(c) Repair weld made to improve fatigue life. The profile meets the requirements of AWS D1.1. Toe dressing has been performed at the weld toe

(d) Repair weld after application of UIT to both the face of the weld and toe

Figure 25. Ultrasonic Impact Treatment Repair for Fatigue Cracked HMIP (Courtesy Lamb-Starr Engineering LP).

UIT has been found effective in improving the fatigue resistance of some welded details. While some reports indicate that UIT can increase the fatigue resistance of a detail from Category E' to Category C (more than one order of magnitude) (Wood et al., 2005), others suggest a more modest increase of 2.5 times (Gunther et al., 2005). Research indicates that application of UIT to mast arm weld toes during the fabrication process helps to delay fatigue crack initiation (Koenigs, 2003). Successful UIT application during the fabrication process has also been found to extend the fatigue life of traffic signal mast arm welds in the field (Krishna et al., 2004). UIT should be applied after hot-dip galvanization, since temperatures above 570°F have been shown to undo the benefits of UIT (Mikheev et al., 1985; Statnikov et al., 2002). This has been attributed to the fact that extreme

heat relaxes the beneficial compressive stresses UIT had induced. The use of zinc-rich paint to repair the galvanizing that UIT had removed has been shown to not affect the performance of welds treated with UIT (Mikheev et al., 1985; Haagensen et al., 1998).

To date, all fractured HMIP on the NTTA system have been repaired, except for approximately 8 percent that are currently being monitored on a regular basis. A few structures are being monitored due to the number, size, and location of the detected crack indications relative to the toe of the weld. The majority of these defects have been detected near the root of the weld rather than at the weld toe. Since the NDT techniques that NTTA uses are highly sensitive, they are able to detect cracking at the very early stages. Thus, the cracks found are typically small and are always sub-visual. This early detection allows a more cost effective approach to repair since the damaged weld is removed and the poles are rewelded in-service. To date, these repaired defects have been innocuous and have not spread. On the other hand, if NTTA had waited until those defects were detected via traditional NDT techniques or through visual inspection, they may have been required to replace the pole. It would have been very difficult, if not impossible, to reproduce the full-penetration weld at that point in-service (Personal correspondence with E. Starnater, July 19, 2011).

5.3 Cost of Repair and Replacement of HMIP

Since repair welding is the preferred repair technique, cost assessment has focused on this specific repair alternative. Based on NTTA's input, the average cost to repair weld HMIP with crack indications at multiple apex points is $3400 per structure for weld repair. This includes removal of the weld, inspection using advanced NDT to confirm total removal of the crack, and rewelding in the field. The additional cost for UIT is $3000 per structure, including all apex points on the pole. Therefore, the total cost of enhanced NDT inspection, rewelding, and UIT of an HMIP is about $6400 per pole (Personal correspondence with E. Starnater, July 19, 2011).

In contrast, the cost of a complete pole replacement is approximately $25,000, which represents the cost of installing a new pole on an existing foundation. The estimated cost of removal and transportation of an existing pole is $10,000. Thus, the total expected cost of a single pole replacement is on the order of $35,000 (Personal correspondence with E. Starnater, July 19,

2011). TxDOT personnel provided a comparable cost of $32,550 based on recent contract bid costs (Personal communication, M. Smith, June 30, 2011).

Based on the findings of a limited series of tests, researchers have developed a preliminary framework for identifying candidate poles for reinspection, repair, or replacement (Stam et al., 2011). The selection criterion is based on the extent of damage, including crack length and crack depth. From these two parameters, poles can be classified as "Repair Critical" or "Replacement Critical" (see Table 15). Based on this framework, undamaged poles can be scheduled for reinspection within two years.

Table 15. Framework for Classification of HMIP Based on Extent of Observed Crack Damage.

Crack Length (in.) in HMIP	Crack Depth (in.)	Criteria Remark
No Cracks[1]	-	Reinspect[1] after 2 yrs.
Single or multiple cracks[1] ≤ 3	$\leq 3/32$	*Repair Critical—* Repair all cracks using UIT[1]
Single or multiple cracks[1] > 3	> 0	*Replacement Critical—* Replace with a new, uncracked pole or substantiate with full-scale testing

[1]Based on Advanced Ultrasonic Testing procedure

6 RECOMMENDATIONS, CONCLUSIONS, AND FUTURE WORK

6.1 Recommendations

Based on this research work consisting of an extensive literature search and surveys in the first half and a comprehensive analytical study in the second half, the following recommendations are presented aimed at minimizing the galvanization induced toe-cracking in HMIP in Texas.

6.1.1 Design and Geometry

Previous research studies have shown that the current TxDOT HMIP design details and specifications are quite robust. There is some evidence suggesting that the details that other state DOTs use may exhibit slightly better performance than the TxDOT details. However, the correct fabrication of these details requires careful and specific sequencing of various fabrication steps with the potential for errors or omissions. Errors in or omission of some of these fabrication steps could lead to damage of the detail or ingress of acid, which could cause accelerated corrosion in the critical base connection region. As such, no revisions to the current TxDOT details are recommended. Further, the current TxDOT practices of using thick base plates and many anchor bolts (typically more than eight) is recommended to be continued based on the documented benefits of these procedures. Inspection of anchor bolt tightness should be included as a part of the regular maintenance and inspection of the poles. Additionally, the research team believes that the ground sleeve detail should be mandatory rather than optional. The presence of the ground sleeve has been documented to significantly improve the fatigue life and reliability of the pole details.

6.1.2 Steel Chemistry

- Carbon Equivalent values of HMIP steel should be limited by incorporating the S31 supplementary requirement of ASTM A6 into the TxDOT specifications.
- HMIP are heavily cold-worked, welded, and galvanized, making them susceptible to cracking. Considering that high strength steel is known to aggravate this problem, researchers advised to also adopt the S18 supplementary requirement of ASTM A6 for minimum tensile strength of ASTM A572 Grade 50/55 and Grade 60/65 steel in TxDOT specifications for the fabricators. If feasible, Grade 50 steel should be specified for the HMIP in TxDOT specifications.

- To minimize susceptibility to liquid metal-assisted cracking, it is advisable to specify susceptibility parameter $\mathbf{S_{LM\text{-}400}}$ value higher than 30 for the HMIP steel in TxDOT specifications, especially for base plate steels.
- It is advisable to take the steel for the bottom portion of the bottom pole segment from the more ductile central laps of coiled steel.

6.1.3 Cold Working

- Bend radii of 4 inches and at least three times the pole thickness should be specified to prevent excessive cold working at bent corners. If smaller radii are required for upper sections of the pole, the 4- inches minimum should be specified for the bottom pole segment only with tighter radii being permitted for higher segments in the shaft.
- If bend radii less than three times the thickness of shaft section are specified, hot bending is recommended to minimize the associated strain aging embrittlement.
- Rough grinding of cold-worked bend corners in the crack susceptible areas near the pole-to-base plate connection in HMIP is recommended since it eliminates surface irregularities that act as stress risers and removes the most severely cold-worked material at the bend locations.
- Assemblies should be accurately preformed to reduce residual stresses during fabrication of HMIP.
- Specifying the use of steel with low Ductile-Brittle Transition Temperature to account for strain aging effects is recommended, particularly for poles that are expected to experience low temperatures in service.
- The use of aluminum-killed steel is recommended to reduce susceptibility to strain aging embrittlement. Most modern steel types are aluminum killed.

6.1.4 Welding Processes

- Minimizing hydrogen content is essential to reduce the likelihood of hydrogen embrittlement and to minimize the potential for HAZ cracking. Hydrogen content can be reduced by using extra-low hydrogen consumables as specified in AWS D1.1 with diffusible hydrogen content of less than 5 ml/100 g. Additionally, base metal surfaces should be clean of grease, oil, rust, and debris; weld filler material should be free of

moisture. Low hydrogen electrodes should be used when SMAW is used to join steel with yield strengths of 50 ksi or higher.

- Preheat requirement should be calculated according to the alternative hydrogen control method given in AWS D1.1 Annex I rather than following the code specified minimum requirements. Ensure that preheat, as required, is properly established before welding. Next to using low hydrogen consumables, proper preheating can be considered the most effective method of reducing hydrogen content and thereby preventing hydrogen embrittlement.
- SAW welding process or other processes with MIG, TIG, or CO_2 shielding are preferable.
- If the SAW process is used, neutral fluxes should be used for multi-pass welding. Using active fluxes may lead to crack-sensitive welds owing to excessive alloy deposit.
- The use of semi-automated SAW requires very high welder skill since the weld pool cannot be seen during welding. Welder and welding operator qualification criteria are specified in the AWS welding code.
- The FCAW-S process should not be intermixed with other welding processes since this may create imbalance in the weld metal composition and lead to reduced Charpy V-notch toughness.
- When the FCAW-G and GMAW processes are used, the weld site should be protected from wind and drafts to prevent the formation of weld defects.
- If the GMAW process is used, the Short Circuit Transfer method of metal transfer should be avoided since it may lead to lack of fusion with the base material and result in poor weld strength.
- Temper bead welding techniques may be used to reduce the HAZ hardness and minimize the potential for cracking. However, temper bead welding requires a significant amount of experience and expertise to be done properly. As such, this approach should be specified with caution to ensure that it is implemented correctly. Welder expertise in this technique should be well-documented.
- Peening or other toe-reconditioning methods like toe-grinding or GTAW (TIG) dressing as per AWS D1.1 may be adopted to improve toe-profile for enhanced fatigue life. Ultrasonic peening may be implemented after hot-dip galvanizing along with repair of

galvanizing with zinc-rich paint. However, care should be taken to ensure that peening is done properly to avoid improper application.

6.1.5 Galvanizing Processes

- Minimizing the immersion time in the zinc galvanizing bath may reduce the chances of Liquid Metal Embrittlement. This method involves using a rapid speed of dipping in the galvanizing bath or by optimizing the dipping angle of the pole shaft segments. It has the added benefit of reducing thermal gradients in the steel assembly, thereby further minimizing the cracking potential.
- The chemistry of the fluxing solution should be carefully monitored to achieve complete evaporation of the flux film before immersion in molten zinc. This is important to prevent dangerous spatter and consequent slow or intermittent immersion leading to aggravated thermal gradients.
- Silicon content in the steel of shaft, base-plate, and weld deposit should be kept below 0.04 percent or between 0.15 and 0.22 percent, to prevent the formation of abnormal and brittle coatings. Similarly, levels of carbon, phosphorus, and manganese should be limited to 0.25 percent, 0.4 percent, and 1.3 percent, respectively. Additionally, AGA guidelines for the use of low-silicon electrodes and uncoated or self-slagging electrodes should also be considered.
- Levels of tin (Sn) and bismuth (Bi) in the galvanizing bath should be limited to 0.2 percent because higher levels have been found to promote cracking. Bi and Sn are also known to significantly increase the thermal gradients during dipping in the galvanizing bath. The use of High Grade zinc with a lower concentration of lead is preferable to the use of Prime Western Grade Zinc. Titanium 0.1 to 0.16 percent and aluminum less than 0.1 percent are considered beneficial for reducing the coating thickness. Some galvanizing bath compositions such as Zn-Fe-Ti-0.012%Al andZn-Fe-Ti-0.01%Al-0.037%Ni reduce thickness of the brittle phases of galvanized coating and may therefore be preferred.
- As HMIP shaft-to-base plate connection has variable thicknesses and steel chemistries besides being severely cold worked, abrasive blasting followed by flash pickling of the shaft-to-base-plate welded connection prior to galvanizing is preferable to minimize the likelihood of hydrogen embrittlement due to exposure to acids.

- Excessive pickling temperature, longer duration of pickling, and poor inhibition of pickling acid increase absorption of hydrogen and therefore should be strictly controlled. Heating to 300ºF after pickling helps to expel hydrogen absorbed during that process.
- Alternative techniques like strong shot peening cleaning may be considered to drastically reduce the fluxing, pickling, and galvanizing durations, and increase the fatigue limit of galvanized welded joints by improving hardness, increasing compressive residual stresses, and relieving stress concentrations.
- Quenching has been strongly connected to the formation of galvanization-induced cracks and therefore should not be permitted.

6.1.6 Recommendations for Inspection Scheduling Based on Reliability Analysis

A comprehensive analysis approach was developed to predict the fatigue life, probability of failure, and reliability of HMIP with pre-existing galvanization-induced cracks. The analysis indicates that the presence of galvanization-induced cracks significantly affects the fatigue life of the poles and can reduce the fatigue coefficient, **A**, by up to 80 percent. The reliability analysis further emphasizes that the presence of the ground sleeve dramatically improves the fatigue life and performance of the pole details, improving the fatigue characteristics by approximately two categories from AASHTO Category E to AASHTO Category C. The analysis further illustrates that vortex shedding induced vibrations can impart significant stresses and significant numbers of fatigue cycles on the poles. The results of the analysis highlight several important trends in the behavior that can be used to prioritize inspections and maintenance of HMIP poles throughout the state. Notably, the wind characteristics in the Dallas/Fort Worth region are more aggressive than in the other major metropolitan areas in the state. As such, special attention should be focused on inspection of poles in this region because it may serve as a good indicator of trends that may develop in other parts of the state. More specifically, the analysis results indicate that:

- The HM-12-80-150 (No GS) is the most critical pole configuration having the lowest predicted fatigue life, followed by the HM-8-80-150 (No GS). Poles of these configurations with known pre-existing crack indicators should be inspected frequently and monitored closely for propagation of cracks. The HM-8-100-150 (No GS) and the HM-12-80-175 (No GS) poles, located in the Dallas area, should be similarly monitored.

- HM-8-100-150 (No GS) and HM-12-80-175 (No GS), located in wind areas of or similar to Austin and San Antonio, may be monitored less frequently. A similar schedule may be followed for HM-8-80-175 (No GS) and HM-12-100-150 (No GS), located in Dallas or similar wind regions.
- Pole configurations like the HM-8-100-175 and HM-12-100-175, especially those located in the Houston area, have predicted fatigue lives exceeding 20 years. These poles can be expected to perform well, although if regular inspections and monitoring indicate that cracks are propagating more rapidly than expected, earlier intervention may be advisable. This analysis focused only on 'regular' wind patterns. Special wind conditions and hurricane wind loading were not considered in this analysis. As such, specific attention should be paid to poles in hurricane regions after a hurricane event to ensure that their level of damage is still within an acceptable range.
- Based on fatigue life predictions reported in Chapter 4, poles located in suburban terrain generally exhibit significantly higher fatigue lives than those in open terrain because of the reduction of the wind speeds in these zones. While the reliability of these poles is generally higher, this should be tempered by the fact that the poles are generally located in regions of higher populations than poles in open terrain. Therefore, the higher consequences of failure should be considered when planning inspection and maintenance of these poles.
- All pole configurations with ground sleeves show remarkable fatigue resilience. The estimated fatigue life for the most critical configuration and location exceeds 30 years. Typical predicted fatigue lives for ground-sleeved poles are within the range of hundreds of years.

6.2 Conclusions

Based on the literature search and surveys carried out in the first half of this research work, the report presents the various aspects of the potential causes of galvanization-induced toe-cracking in HMIP. The problem of galvanization-induced toe-cracking in HMIP is a complex phenomenon and is known to occur due to an accumulative effect of multiple factors involved in the various stages of manufacturing and service of the HMIP. Recommendations are presented pertaining to every process involved in the manufacturing of HMIP, which would reduce HMIP susceptibility

to galvanization-induced toe-cracking. It is not expected that all of the recommendations presented herein can be feasibly adopted. However, these recommendations represent the best practice reported in the literature. Adoption of as many of these practices as feasible is expected to significantly minimize the occurrence of galvanization-induced cracking.

The reliability analysis is subject to inherent uncertainties and assumptions, e.g., not considering modal superposition in calculation of stress cycles, assuming 80 percent reduction in fatigue coefficient due to galvanization and ignoring the existence of constant amplitude fatigue limit for galvanized connections and assuming a target reliability index, β, of 3.5. Considering all these parameters, or changing some of these assumptions, may result in changes in the absolute values of predicted fatigue life for all the poles.

Although the absolute values of fatigue life will likely vary with change in the basic assumptions, the relative values, and therefore the prioritization of inspections and maintenance are not expected to change significantly. These form a valuable resource for optimizing the inspection schedules to make best use of available resources and for prioritizing repairs and replacement efforts where required. The plans made on this basis can be refined further at a later point, if required, according to inspection reports.

6.3 Future Work

The few experimental studies and field measurement data available for HMIP greatly benefited this research effort. However, significant future work is recommended to enhance the accuracy of the predictions in this study. The proposed future work includes:

- Additional field measurements by instrumenting TxDOT poles to further validate the analytical findings, including wind speed distributions, equivalent static pressure ranges, dynamic response of poles, and associated stress ranges due to wind load effects.
- The present research used equivalent static pressure values as specified in the current AASHTO provisions. The use of a more sophisticated analysis, such as a fully dynamic wind load analysis, or a non-linear time history analysis, may lead to a more rigorous understanding of the pole response, particularly when coupled with a larger database of measured pole behavior.

- The predicted fatigue life of galvanized details with pre-existing crack indicators is based on a very limited data set of experimental results. Additional research regarding the fatigue resistance of pole base details with pre-existing galvanization-induced cracks should be conducted. This research would provide more detailed information to develop more accurate fatigue models for the pre-cracked details.
- Due to limited time and resources, this analysis focused on a specific subclass of poles in the TxDOT inventory representing approximately 90 percent of the poles in the state. The remaining 10 percent of poles are shorter, generally 100 ft or 125 ft. The analysis of these poles is merited. Similarly, the analysis focused on five specific locations throughout the state, namely Dallas/Fort Worth, Austin, San Antonio, Houston, and El Paso. These five metropolitan areas and the surrounding regions with similar wind characteristics represent approximately 75 percent of the poles in the state. The wind behavior at other locations throughout the state should be considered. If the wind speed distributions are found to be substantially different than those in the five areas considered, a rigorous analysis should be conducted for these regions as well.
- The current analysis focused only on 'regular' wind behavior and did not consider special wind regions or hurricane-induced wind loading. The response of the poles to these more severe, and more complex, wind loads should be evaluated.
- The recommendations to minimize galvanization-induced cracking reported in this report are based on currently reported best practices. An experimental study and long-term monitoring plan of existing poles and new poles constructed using the proposed techniques would shed further light on the formation and propagation of galvanization-induced cracking and may provide additional insight into the specific factors that affect this behavior.

REFERENCES

AASHTO. (2010). *AASHTO LRFD Bridge design specifications* (5th edition). Washington, D.C: American Association of State Highway and Transportation Officials.

AASHTO. (2009). *AASHTO Standard Specifications for Structural Supports for Highway Signs, Luminaries, and Traffic Signals* (5th edition).

Abe, H., I. T. (1994). Study of HAZ cracking of hot-dip galvanizing steel bridges, IIW Doc. IX-1795-94.

AGA. (2010). *Design Guide—The Design of Products to be Hot-Dip Galvanized after Fabrication.* American Galvanizers Association.

AGA. (2009). *Hot-Dip Galvanizing for Sustainable Design.* American Galvanizers Association.

AGA. (2002). *Welding and Hot-Dip Galvanizing.* American Galvanizers Association .

Aichinger, R., and Higgins, W. (2006). Toe Cracks in Base Plate Welds—30 Years Later. *Electrical Transmission Line and Substation Structures: Structural Reliability in a Changing World—Proceedings of 2006 Electrical Transmission Conference* . American Society of Civil Engineers, pp. 274–285.

Aloraier, A. S., Ibrahim, R. N., and Ghojel, J. (2004). Eliminating post-weld heat treatment in repair welding by temper bead technique: role bead sequence in metallurgical changes. *Journal of Material Processing Technology* , pp. 392–400.

Anderson,T. H. (2007). Fatigue Life Investigation of Traffic Signal Mast-Arm Connection details. Department of Civil Engineering, The University of Texas at Austin.

Arata, Y., Akira, O., Okamoto, I., and Ogawa, H. (1982). Study on Liquid Metal Embrittlement of Carbon Steels (Report 1)—Penetration Behavior of Liquid Metal. *Transactions of JWRI, 11* (2), pp. 7–13.

ASTM. (2007). A 143/A 143M-03—Standard Practice for Safeguarding Against Embrittlement of Hot-Dip Galvanized Structural Steel Products and Procedure for Detecting Embrittlement. In

ASTM, *Annual Book of ASTM Standards, Section 1—Iron and Steel Products* (Vols. 01.06—Coated Steel Products) , pp. 26–28.

ASTM. (2007). A 385-05 - Standard Practice for Providing High-Quality Zinc Coatings (Hot-Dip). In ASTM, *Annual Book of ASTM Standards, Section 1—Iron and Steel Products* (Vols. 01.06- Coated Steel Products) , pp. 54–62.

ASTM. (2007). A 6/A 6M-06 Standard Specification for General Requirements for Rolled Structural Steel Bars, Plates, Shapes, and Sheet Piling. In ASTM, *Annual Book of ASTM Standards, Section 1—Iron and Steel Products* (Vols. 01.04—Steel-Structural, Reinforcing, Pressure Vessel, Railway) , pp. 13–71.

ASTM. (2007). *Annual Book of ASTM Standards, Section 1—Iron and Steel Products* (Vols. 01.06- Coated Steel Products).

ASTM. (2007). Annual Book of ASTM Standards, Section 1—Iron and Steel Products, Volume 01.04 - Steel—Structural, Reinforcing, Pressure Vessel, Railway.

AWS. (2010). *Commentary on Structural Welding Code—Steel.* American Welding Society.

AWS. (2010). *Structural Welding Code—Steel* (22nd ed.). Miami, FL, United States of America: American Welding Society.

Barker R. M., and Puckett, J. A. (2006). *Design of Highway Bridges: An LRFD Approach* (2nd edition).

Bigot, R., Iost, A. and Foct, J. (1999). Residual Stresses in Galvanizing. *Materials and Manufacturing Processes , 14* (3), pp. 413–426.

Blevins, R. D. (1977). *Flow-induced vibration*. New York: Van Nostrand Reinhold Company.

Camurri, C. P., Benavente, R. G., Roa, I. S., and Carrasco, C. C. (2005). Deformation and fatigue behavior of hot-dip galvanized coatings. *Materials Characterization, 55*, pp. 203–210.

Canadian Standards Association. (2006). Canadian highway bridge design code. Mississauga, ON: Canadian Standards Association.

Carpio, J., J.A. Casado, J.A. Alvarez, D. Mendez, and S.F. Gutierrez-Solana. (2010). Stress corrosion cracking of structural steels immersed in hot-dip galvanizing baths. *Engineering Failure Analysis, 17*, pp. 19–27.

Chang, B., Phares, B. M., Sarkar, P. P., and Wipf, T. J. (2009). Development of a procedures for fatigue design of slender support structures subjected to wind-induced vibration. *Transportation Research Board: Journal of the Transportation Research Board* , pp. 23–33.

Chen, G., Barker, M., Dharani, L. R., and Ramsay, C. (2003). *Signal Mast Arm Fatigue Failure Investigation.* Jefferson City, MO: Missouri Department of Transportation Research, Development and Technology.

Chung, H., L. Manuel., and K.H. Frank. (2003). Optimal inspection of fracture-critical steel trapezoidal girders. Report Number: FHWA/TX-04/0-2135-1. Austin, TX: Texas Department of Transportation.

Cresdee, R. B., Edwards, W. J., Thomas, P. J., and Voss, G. F. (1993). Analysis of beam distortion during hot dip galvanizing. *Materials Science and Technology, 9*, pp.161–167.

Dexter, R. J., and Ricker, M. J. (2002). NCHRP Report 469—Fatigue-Resistant Design of Cantilevered Signal, Sign, and Light Supports. Washington, D.C.: National Academy Press.

Frank, K. H., and Palmatier, A. H. (2005). *Repair of Galvanizing After UIT Application.* The University of Texas at Austin, Center for Transportation Research. Austin, TX: Texas Department of Transportation.

Fisher, J.W., G.L. Kulak, and I.F.C. Smith. (1998). A fatigue primer for structural engineers. Chicago, IL: National Steel Bridge Alliance.

Foley, C. M., Fournelle, R. A., Ginal, S. J., and Peronto, J. L. (2004). Structural Analysis of Sign Bridge Structures and Luminaire Supports. Madison, WI: Wisconsin Department of Transportation.

Funderburk, S. (1998, May). What is Preheat? The Lincoln Electric Company.

Graville, B. (1975). *The principles of cold cracking control in welds.* Montreal, Quebec, Canada: The Dominion Bridge Company, Limited.

Gunther, H. P., U. Kuhlmann, and A. Durr. "Rehabilitation of Welded Joints by Ultrasonic Impact Treatment (UIT)," IABSE Symposium Lisbon, 2005.

Haagensen, P. J., E. S. Statnikov, and L. Lopez-Martinez, "Introductory Fatigue Tests on Welded Joints in High Strength Steel and Aluminum Improved by Various Methods Including Ultrasonic Impact Treatment (UIT)," IIW, Doc. XIII-1748-98, 1998.

Hasegawa, M., Suzuki, H., and Miura, K. (2009). Effect of strong shot peening cleaning and hot-dip galvanizing on fatigue strength of steel welded joint. *Welding International, 23*, pp. 360–368.

Irving, B. (1992, July). Preheat: The Main Defense against Hydrogen Cracking. *Welding Journal*, pp. 25–31.

Kinstler, T. J. (2003). *Current Knowledge of the Cracking of Steels During Galvanizing—A Synthesis of the Available Technical Literature and Collective Experience for the American Institute of Steel Construction.* Springville, AL: GalvaScience LLC.

Koenigs, M. (2003, May). Fatigue Resistance of Traffic Signal Mast-Arm Connection Details. *MSE Thesis*. The University of Texas at Austin.

Krishna, K., P. E. Verma, E. S. Statnikov, and L. Theini, "Improving Service Life of Steel Bridges, Light Poles and Sign Structures Through the Use of Ultra Sonic Impact Treatment (UIT)," *Bridge Maintenance, Safety, Management and Costs*, Watanabe, Frangopol & Utsunomiya (eds.), Taylor and Francis Group, London, 2004.

Kudryavtsev, Y., Kleiman, J., Lugovskoy, A., Lobanov, L., Knysh, V., Voitenko, O., and Prokopenko, G. (2005). *IIW Document XIII-2076-05, Rehabilitation and Repair of Welded Elements and Structures by Ultrasonic Peening.* International Institute of Welding.

Larsson, B. and Westerlund, R. (1975). Fatigue tests on welded steel after hot-dip galvanizing. Metal Construction, pp. 92–97.

Maddox, S. J. (1983). *Improving the Fatigue Performance of Welded Joints.* Cambridge, England: The Welding Institute.

McDonald, R. D. (1975, January). Steel Embrittlement Problems Associated with Hot-Dip Galvanizing—Causes, Mechanisms, Controls, and Selected References. Canada.

Mikheev, P. P., A. Y. Nedoseka, I. V. Parkhomenko, A. Z. Kuz'menko, E. S. Statnikov, V. L. Senyukov, G. P. Chernetsov, and V. S. Skvortsov, "Effectiveness of Ultrasonic Treatment for Increasing the Fatigue Resistance of Welds," *Russian Ultrasonics*, Vol. 15, No. 4, 1985 pp. 70–75.

Miller, D. K. (2006). *AISC Steel Design Guide 21/ Welded Connections—A Primer for Engineers.* American Institute of Steel Construction, Inc.

Mraz, L., and Lesay, J. (2009). Problems with reliability and safety of hot-dip galvanized steel structures. *Soldagem Insp. São Paulo, 14*, pp. 184–190.

Nilsson, T., Engberg, G. and Trogen, H. (1989). Fatigue properties of hot-dip galvanized steels. *Scandinavian Journal of Metallurgy, 18*, pp. 166–175.

Ocel, J. M. (2006). The Behavior of Thin Hollow Structural Section (HSS) to Plate Connections. The University of Minnesota.

OFCM, (2005). Federal Meteorological Handbook No.1—Surface Weather Observations and Reports-FCM-H1-2005. Washington, D.C.: U.S. Department of Commerce/National Oceanic and Atmospheric Administration.

Palmatier, A. H. (2005, May). Ultrasonic Impact Treatment of Traffic Signal Mast Arm Welds. *MSE Thesis*. The University of Texas at Austin.

Poag, G., and Zervoudis, J. (2003). Influence of Various Parameters on Steel Cracking During Galvanizing. *AGA TechForum.* Kansas.

Pokhodnya, I. K., and Shvachko, V. I. (2001). Nature of Hydrogen Brittleness of Structural Steels. *Materials Science, 37* (2), pp. 241–251.

Pool, C. S. (2010). Effect of Galvanization on the Fatigue Strength of High Mast Illumination Poles. The University of Texas at Austin.

Richman, N. B.((2009). Fatigue Life Investigation of High Performance Mast Arm Base Plate Connections. Department of Civil Engineering, The University of Texas at Austin.

Rios, C. A. (2007, May). Fatigue Performance of Multi-Sided High-Mast Lighting Towers. The Department of Civil Engineering, The University of Texas at Austin.

Rizzo, P. and X. Zhu. "Sensing Technology for Damage Assessment of Sign Supports and Cantilever Poles," Final Report FHWA–PA–2010-10–PIT008, University of Pittsburgh, Pennsylvania Department of Transportation, August 31, 2010.

Roy, S. and Fisher, J. W. (2003). Fatigue resistance of welded details enhanced by Ultrasonic Impact Treatment (UIT). *International Journal of Fatigue, 25* (9-11), pp. 1239–1247.

Russell, C. S. and Vaughan, W. J. (1976). Steel Production: Processes, Products, and Residuals. The Johns Hopkins University Press.

Salmon C.G., Johnson, J. E., and Malhas, F. A. (2009). *Steel Structures—Design and Behaviour* (Fifth ed.). Upper Saddle River, NJ 07458: Pearson Education, Inc.

Sandelin, R. W. (1954). Bend Around Galvanizing Embrittlement. *Steel , 135* (22), p. 92.

Simiu, E. and R. Scanlan. (1996). Wind effects on structures (3rd edition). New York, NY: John Wiley and Sons.

Sperko, W. J. (2005, July). Exploring Temper Bead Welding. *Welding Journal*, pp. 37–40.

Stam, A. (2009, May). Fatigue Performance of Base Plate Connections Used in High Mast Lighting Towers. Department of Civil Engineering, The University of Texas at Austin.

Stam, A., N. Richman, C. Pool, C. Rios, T. Anderson, and K. Frank. (2011). Fatigue Life of Steel Base Plate to Pole Connections for Traffic Structures. Report Number FHWA/TX-11/9-1526-1. Austin, TX: Texas Department of Transportation.

Starnater, E., "Sam Rayburn Tollway—HMIP Repair and Ultrasonic Impact Treatment," NTTA Inspection and Repair Report, Prepared by Lamb-Star Engineering, L.P., Plano, TX, 2009.

Statnikov, E. S., V.O. Muktepavel, and A. Blomqvist. "Comparison of Ultrasonic Impact Treatment (UIT) and Other Fatigue Life Improvement Methods," Welding in the World, Vol. 46, No. 3–4, 2002, pp. 20–32.

Suksawang, N., B. Mintz, and A. Mirmiran. "Remedial Actions for Failed Pole/Base Plate Weld on High Mast Lighting Pole (HMLP)," Final Research Report- BD-015-23, Florida International University, Florida Department of Transportation, December 2009.

Thomas, M., S. Counsell, G. Taplin, G. Noyes-Brown, and J. Connal. "Fatigue Analysis and Repair of a High Mast Light Pole," 7th Austroads Bridge Conference, NZ Transportation Agency, Auckland, New Zealand, May 26–29, 2009.

TxDOT. (2004). Item 442—Metal for Structures, Standard Specifications for Construction and Maintenance of Highways, Streets, and Bridges. Texas Department of Transportation.

TxDOT Standard Drawings—

ftp://ftp.dot.state.tx.us/pub/txdot-info/cmd/cserve/standard/traffic/hmip-98.pdf

ftp://ftp.dot.state.tx.us/pub/txdot-info/cmd/cserve/standard/traffic/hmif98.pdf

Vogt, J. B., Boussac, O., and Foct, J. (2001) (2001). Prediction of fatigue resistance of a hot-dip galvanized steel. *Fatigue and Fracture of Engineering Materials and Structures, 23*, pp. 33–39.

Wood, J. C. and E. Starnater. "Overhead Structure Inspections," IBTTA Maintenance Fall Conference, October 16–19, 2005, Tampa, Florida.

APPENDICES

APPENDIX A:
HMIP STRESS RANGES AND STRESS CYCLES
(Steps 1 to 10)

								Equivalent Static Pressure Ranges						v(ft2/s)=	0.0001615	Stress ranges for pole with no GS			
Segment	Avg dia (in)	Mid ht. (ft)	f 1 (Hz)	V1 mph - 3s	V2 mph - 3s	V3 (mph - 3s	V4 mph - 3s	Pvs1 (psf)	Pvs2 (psf)	Pvs3 (psf)	Pvs4 (psf)	Re1 300≤Re≤1.0E+05 Re>3.5E+06	Re2	Re3	Re4	Sr1 (ksi)	Sr2 (ksi)	Sr3 (ksi)	Sr4 (ksi)
1	8.611	144.482	0.34	1.1	1.4	1.8	2.1	0.38	0.63	1.0	1.3	7.2E+03	9.4E+03	1.2E+04	1.4E+04	0.022	0.037	0.056	0.079
2	10.525	132.221	0.34	1.4	1.8	2.2	2.6	0.56	0.94	1.4	2.0	1.1E+04	1.4E+04	1.7E+04	2.0E+04	0.037	0.062	0.093	0.131
3	12.864	116.738	0.34	1.7	2.1	2.6	3.1	0.84	1.4	2.1	3.0	1.6E+04	2.1E+04	2.6E+04	3.0E+04	0.093	0.156	0.236	0.331
4	15.722	96.845	0.34	2.0	2.6	3.2	3.8	1.3	2.1	3.2	4.5	2.4E+04	3.1E+04	3.8E+04	4.6E+04	0.168	0.282	0.426	0.600
5	19.216	71.282	0.34	2.5	3.2	3.9	4.7	1.9	3.1	4.8	6.7	3.6E+04	4.7E+04	5.7E+04	6.8E+04	0.290	0.488	0.736	1.036
6	23.486	38.304	0.34	3.0	3.9	4.8	5.7	2.8	4.7	7.1	10.0	5.4E+04	7.0E+04	8.6E+04	1.0E+05	0.334	0.561	0.847	1.192
7	27.105	9.868	0.34	3.5	4.5	5.5	6.6	3.7	6.3	9.5	13.3	7.2E+04	9.3E+04	1.1E+05	1.4E+05	0.070	0.748		
	Pvs(windgust)		0.34					6.2								4.08922			
	Avg dia (in)	Mid ht. (ft)	f 2 (Hz)	V1 mph - 3s	V2 mph - 3s	V3 (mph - 3s	V4 mph - 3s	Pvs1 (psf)	Pvs2 (psf)	Pvs3 (psf)	Pvs4 (psf)	Re1 300≤Re≤1.0E+05 Re>3.5E+06	Re2	Re3	Re4	Sr1 (ksi)	Sr2 (ksi)	Sr3 (ksi)	Sr4 (ksi)
1	8.611	144.482	1.251	4.1	5.3	6.5	7.7	5.1	8.6	12.9	18.2	2.7E+04	3.4E+04	4.2E+04	5.0E+04	0.301	0.506	0.763	1.074
2	10.525	132.221	1.251	5.0	6.4	7.9	9.4	7.6	12.8	19.3	27.1	4.0E+04	5.1E+04	6.3E+04	7.5E+04	0.495	0.833	1.257	1.769
3	12.864	116.738	1.251	6.1	7.9	9.7	11.5	11.4	19.1	28.8	40.6	5.9E+04	7.7E+04	9.5E+04	1.1E+05	1.256	2.112	3.188	
4	15.722	96.845	1.251	7.4	9.6	11.8	14.0	17.0	28.5	43.1	60.6	8.9E+04	1.1E+05	1.4E+05	1.7E+05	2.273			
5	19.216	71.282	1.251	9.1	11.8	14.5	17.2	25.3	42.6	64.3	90.5	1.3E+05	1.7E+05	2.1E+05	2.5E+05				
6	23.486	38.304	1.251	11.1	14.4	17.7	21.0	37.8	63.6	96.1	135.2	2.0E+05	2.6E+05	3.2E+05	3.7E+05				
7	27.105	9.868	1.251	12.8	16.6	20.4	24.2	50.4	84.8	128.0	180.1	2.6E+05	3.4E+05	4.2E+05	5.0E+05				
	Avg dia (in)	Mid ht. (ft)	f 3 (Hz)	V1 mph - 3s	V2 mph - 3s	V3 (mph - 3s	V4 mph - 3s	Pvs1 (psf)	Pvs2 (psf)	Pvs3 (psf)	Pvs4 (psf)	Re1 300≤Re≤1.0E+05 Re>3.5E+06	Re2	Re3	Re4	Sr1 (ksi)	Sr2 (ksi)		
1	8.611	144.482	3.143	10.2	13.3	16.3	19.3	32.1	54.0	81.5	114.7	6.7E+04	8.7E+04	1.1E+05	1.3E+05	1.898	3.191		
2	10.525	132.221	3.143	12.5	16.2	19.9	23.6	48.0	80.7	121.8	171.4	1.0E+05	1.3E+05	1.6E+05	1.9E+05	3.126			
3	12.864	116.738	3.143	15.3	19.8	24.3	28.9	71.7	120.5	181.9	256.0	1.5E+05	1.9E+05	2.4E+05	2.8E+05				
4	15.722	96.845	3.143	18.7	24.2	29.7	35.3	107.1	180.0	271.8	382.4	2.2E+05	2.9E+05	3.5E+05	4.2E+05				
5	19.216	71.282	3.143	22.8	29.6	36.4	43.1	159.9	268.9	406.0	571.2	3.3E+05	4.3E+05	5.3E+05	6.3E+05				
6	23.486	38.304	3.143	27.9	36.2	44.4	52.7	238.9	401.7	606.5	853.3	5.0E+05	6.4E+05	7.9E+05	9.4E+05				
7	27.105	9.868	3.143	32.2	41.7	51.3	60.8	318.2	535.0	807.8	1136.6	6.6E+05	8.6E+05	1.1E+06	1.3E+06				

	Stress ranges for pole with GS				SAT (N-S)-Open Terrain probabilities								seconds in each bin			cycles in each bin		
Segment	Sr1 (ksi)	Sr2 (ksi)	Sr3 (ksi)	Sr4 (ksi)	P(V<V1)	P(V<V2)	P(V<V3)	P(V<V4)	(V1<V<V2	(V2<V<V3	(V3<V<V4)		t_bin1	t_bin2	t_bin3	N_bin1	N_bin2	N_bin3
1	0.010	0.017	0.026	0.037	0.00%	0.01%	0.05%	0.16%	0.01%	0.04%	0.10%		111931.09	408451.73	1039028	3.81E+04	1.39E+05	3.53E+05
2	0.017	0.029	0.043	0.061	0.01%	0.05%	0.18%	0.46%	0.04%	0.13%	0.29%		399627.67	1266682.5	2866308	1.36E+05	4.31E+05	9.75E+05
3	0.043	0.073	0.110	0.155	0.03%	0.15%	0.49%	1.18%	0.12%	0.34%	0.69%		1226919.1	3389467.8	6843012	4.17E+05	1.15E+06	2.33E+06
4	0.078	0.132	0.199	0.280	0.09%	0.41%	1.19%	2.61%	0.32%	0.78%	1.41%		3204333.4	7765312	14064439	1.09E+06	2.64E+06	4.78E+06
5	0.135	0.228	0.344	0.483	0.23%	0.93%	2.43%	4.90%	0.70%	1.51%	2.47%		6948949.9	14967020	24587618	2.36E+06	5.09E+06	8.36E+06
6	0.156	0.262	0.395	0.556	0.42%	1.56%	3.82%	7.29%	1.14%	2.26%	3.47%		11343253	22502944	34537587	3.86E+06	7.65E+06	1.17E+07
7	0.033	0.349			0.30%	1.17%	2.98%	5.87%	0.87%	1.81%	2.89%		8665729.7	18000983	28699386	2.95E+06		
	1.90777											E-W G	11298933			3841637.3		
	Sr1 (ksi)	Sr2 (ksi)	Sr3 (ksi)	Sr4 (ksi)	P(V<V1)	P(V<V2)	P(V<V3)	P(V<V4)	(V1<V<V2	(V2<V<V3	(V3<V<V4)		t_bin1	t_bin2	t_bin3	N_bin1	N_bin2	N_bin3
1	0.140	0.236	0.356	0.501	4.35%	10.98%	19.92%	29.92%	6.62%	8.95%	10.00%		65865708	88939346	99401994	8.24E+07	1.11E+08	1.24E+08
2	0.231	0.388	0.587	0.825	8.65%	18.97%	31.00%	42.93%	10.32%	12.04%	11.93%		102557698	119665748	1.19E+08	1.28E+08	1.50E+08	1.48E+08
3	0.586	0.985	1.487		15.30%	29.44%	43.76%	56.38%	14.15%	14.31%	12.62%		140666314	142308581		1.76E+08	1.78E+08	
4	1.060				24.11%	41.32%	56.52%	68.50%	17.21%	15.19%	11.98%							
5					33.92%	52.73%	67.43%	77.92%	18.82%	14.70%	10.49%							
6					41.50%	60.59%	74.28%	83.39%	19.09%	13.69%	9.11%							
7					37.20%	56.23%	70.54%	80.45%	19.03%	14.32%	9.91%							
	Sr1 (ksi)	Sr2 (ksi)			P(V<V1)	P(V<V2)	P(V<V3)	P(V<V4)	(V1<V<V2	(V2<V<V3	(V3<V<V4)		t_bin1	t_bin2	t_bin3	N_bin1	N_bin2	N_bin3
1	0.886	1.489			50.12%	68.66%	80.78%	88.25%	18.55%	12.11%	7.47%		184383846			5.80E+08		
2	1.458				63.74%	79.81%	88.84%	93.77%	16.07%	9.03%	4.93%							
3					75.50%	87.97%	94.03%	96.96%	12.48%	6.05%	2.93%							
4					84.41%	93.25%	96.98%	98.59%	8.84%	3.73%	1.61%							
5					90.31%	96.27%	98.48%	99.35%	5.96%	2.22%	0.87%							
6					93.31%	97.63%	99.10%	99.64%	4.32%	1.47%	0.54%							
7					91.73%	96.93%	98.79%	99.49%	5.20%	1.86%	0.70%							

	Avg Sr (No GS)			Avg Sr (w/GS)			SAT(N-S)-Suburban Terrain probabilities							seconds in each bin			cycles in each bin		
Segment	S_bin1	S_bin2	S_bin3	S_bin1	S_bin2	S_bin3	P(V<V1)	P(V<V2)	P(V<V3)	P(V<V4)	(V1<V<V2	(V2<V<V3	(V3<V<V4	t_bin1	t_bin2	t_bin3	N_bin1	N_bin2	N_bin3
1	0.030	0.047	0.068	0.014	0.022	0.032	0.01%	0.04%	0.14%	0.37%	0.03%	0.10%	0.23%	308228	1006632	2E+06	1.05E+05	3.42E+05	7.94E+05
2	0.049	0.077	0.112	0.023	0.036	0.052	0.02%	0.12%	0.39%	0.95%	0.10%	0.27%	0.57%	949781	2711018	6E+06	3.23E+05	9.22E+05	1.91E+06
3	0.124	0.196	0.283	0.058	0.091	0.132	0.07%	0.32%	0.95%	2.13%	0.25%	0.63%	1.18%	2501711	6279766	1E+07	8.51E+05	2.14E+06	3.98E+06
4	0.225	0.354	0.513	0.105	0.165	0.239	0.17%	0.73%	1.97%	4.08%	0.56%	1.24%	2.10%	5539074	1.2E+07	2E+07	1.88E+06	4.20E+06	7.12E+06
5	0.389	0.612	0.886	0.181	0.286	0.413	0.35%	1.35%	3.37%	6.54%	1.00%	2.02%	3.17%	9910701	2E+07	3E+07	3.37E+06	6.84E+06	1.07E+07
6	0.448	0.704	1.020	0.209	0.329	0.476	0.45%	1.67%	4.06%	7.69%	1.22%	2.39%	3.63%	1.2E+07	2.4E+07	4E+07	4.12E+06	8.07E+06	1.23E+07
7	0.409			0.191			0.15%	0.64%	1.75%	3.67%	0.49%	1.11%	1.92%	4863402	1.1E+07	2E+07	1.65E+06		
	4.089			1.908															
	S_bin1	S_bin2	S_bin3	S_bin1	S_bin2	S_bin3	P(V<V1)	P(V<V2)	P(V<V3)	P(V<V4)	(V1<V<V2	(V2<V<V3	(V3<V<V4	t_bin1	t_bin2	t_bin3	N_bin1	N_bin2	N_bin3
1	0.403	0.634	0.919	0.188	0.296	0.429	7.55%	17.03%	28.45%	40.06%	9.49%	11.42%	11.61%	9.4E+07	1.1E+08	1E+08	1.18E+08	1.42E+08	1.44E+08
2	0.664	1.045	1.513	0.310	0.488	0.706	13.48%	26.74%	40.61%	53.20%	13.26%	13.88%	12.58%	1.3E+08	1.4E+08	1E+08	1.65E+08	1.73E+08	1.56E+08
3	1.684	2.650		0.786	1.236		21.51%	38.00%	53.11%	65.38%	16.49%	15.10%	12.27%	1.6E+08	1.5E+08		2.05E+08	1.88E+08	
4							30.77%	49.24%	64.22%	75.24%	18.47%	14.98%	11.02%						
5							39.30%	58.39%	72.41%	81.94%	19.09%	14.03%	9.52%						
6							42.58%	61.65%	75.16%	84.07%	19.07%	13.51%	8.91%						
7							29.07%	47.29%	62.38%	73.67%	18.22%	15.09%	11.29%						
	S_bin1	S_bin2	S_bin3	S_bin1			P(V<V1)	P(V<V2)	P(V<V3)	P(V<V4)	(V1<V<V2	(V2<V<V3	(V3<V<V4	t_bin1	t_bin2	t_bin3	N_bin1	N_bin2	N_bin3
1	2.545			1.187			60.94%	77.67%	87.38%	92.81%	16.73%	9.71%	5.44%	1.7E+08			5.23E+08		
2							72.90%	86.28%	93.01%	96.36%	13.38%	6.73%	3.35%						
3							82.26%	92.05%	96.34%	98.26%	9.79%	4.29%	1.91%						
4							88.72%	95.50%	98.12%	99.17%	6.78%	2.62%	1.06%						
5							92.54%	97.29%	98.95%	99.57%	4.75%	1.66%	0.62%						
6							93.66%	97.78%	99.17%	99.66%	4.12%	1.39%	0.50%						
7							87.75%	95.01%	97.88%	99.05%	7.26%	2.87%	1.17%						

	DFW(N-S)-Open Terrain probabilities								seconds in each bin			cycles in each bin			
Segment	P(V<V1)	P(V<V2)	P(V<V3)	P(V<V4)	P(V1<V<V2)	P(V2<V<V3)	P(V3<V<V4)		t_bin1	t_bin2	t_bin3	N_bin1	N_bin2	N_bin3	
1	0.00%	0.00%	0.00%	0.01%	0.00%	0.00%	0.01%		2856.76482	18634.9993	74480.38116	9.71E+02	6.34E+03	2.53E+04	
2	0.00%	0.00%	0.01%	0.04%	0.00%	0.01%	0.03%		16826.5169	92156.3389	318267.2372	5.72E+03	3.13E+04	1.08E+05	
3	0.00%	0.01%	0.04%	0.14%	0.01%	0.03%	0.10%		81511.3463	376411.851	1127387.977	2.77E+04	1.28E+05	3.83E+05	
4	0.00%	0.03%	0.14%	0.44%	0.03%	0.11%	0.29%		319242.232	1252986.14	3276825.518	1.09E+05	4.26E+05	1.11E+06	
5	0.01%	0.10%	0.39%	1.07%	0.09%	0.29%	0.68%		973087.041	3299147.6	7637273.439	3.31E+05	1.12E+06	2.60E+06	
6	0.03%	0.21%	0.75%	1.90%	0.18%	0.54%	1.15%		1987251.57	6083386.95	12934819.46	6.76E+05	2.07E+06	4.40E+06	
7	0.02%	0.14%	0.53%	1.39%	0.12%	0.39%	0.86%		1341094.29	4346907.99	9692994.446	4.56E+05			
								E-W Gusts	19820567.7			6738993.018			
	P(V<V1)	P(V<V2)	P(V<V3)	P(V<V4)	P(V1<V<V2)	P(V2<V<V3)	P(V3<V<V4)		t_bin1	t_bin2	t_bin3	N_bin1	N_bin2	N_bin3	
1	0.91%	3.44%	8.26%	15.14%	2.54%	4.82%	6.88%		28502178.3	54079267.1	77303328.05	3.57E+07	6.77E+07	9.67E+07	
2	2.44%	7.68%	15.98%	26.17%	5.24%	8.29%	10.20%		58884321.1	93140358.9	114536991.1	7.37E+07	1.17E+08	1.43E+08	
3	5.59%	14.78%	26.95%	39.86%	9.19%	12.16%	12.92%		103177054	136599587		1.29E+08	1.71E+08		
4	10.97%	24.69%	40.02%	54.16%	13.72%	15.33%	14.15%								
5	18.29%	35.93%	52.83%	66.58%	17.64%	16.90%	13.76%								
6	24.85%	44.62%	61.64%	74.33%	19.77%	17.02%	12.69%								
7	21.04%	39.70%	56.76%	70.11%	18.66%	17.06%	13.36%								
	P(V<V1)	P(V<V2)	P(V<V3)	P(V<V4)	P(V1<V<V2)	P(V2<V<V3)	P(V3<V<V4)		t_bin1	t_bin2	t_bin3	N_bin1	N_bin2	N_bin3	
1	33.20%	54.37%	70.58%	81.56%	21.16%	16.21%	10.98%		237648391			7.47E+08			
2	48.33%	69.22%	82.47%	90.16%	20.89%	13.25%	7.69%								
3	63.27%	81.14%	90.57%	95.27%	17.87%	9.43%	4.71%								
4	75.82%	89.34%	95.31%	97.90%	13.51%	5.98%	2.59%								
5	84.72%	94.16%	97.72%	99.08%	9.44%	3.56%	1.36%								
6	89.43%	96.36%	98.70%	99.51%	6.93%	2.34%	0.81%								
7	86.94%	95.23%	98.21%	99.30%	8.29%	2.98%	1.09%								

	DFW (N-S)-Suburban Terrain probabilities								seconds in each bin			cycles in each bin		
Segment	P(V<V1)	P(V<V2)	P(V<V3)	P(V<V4)	P(V1<V<V2)	P(V2<V<V3)	P(V3<V<V4)		t_bin1	t_bin2	t_bin3	N_bin1	N_bin2	N_bin3
1	0.00%	0.00%	0.01%	0.03%	0.00%	0.01%	0.02%		11702.6677	66517.025	236953.6792	3.98E+03	2.26E+04	8.06E+04
2	0.00%	0.01%	0.03%	0.11%	0.01%	0.02%	0.08%		56778.6431	273052.16	845975.9842	1.93E+04	9.28E+04	2.88E+05
3	0.00%	0.02%	0.10%	0.33%	0.02%	0.08%	0.22%		224159.726	919089.27	2492784.396	7.62E+04	3.12E+05	8.48E+05
4	0.01%	0.07%	0.29%	0.82%	0.06%	0.22%	0.53%		700964.681	2484896.6	5969952.817	2.38E+05	8.45E+05	2.03E+06
5	0.03%	0.17%	0.63%	1.63%	0.15%	0.46%	1.00%		1631097.47	5140077.9	11196103.5	5.55E+05	1.75E+06	3.81E+06
6	0.04%	0.23%	0.82%	2.05%	0.19%	0.59%	1.23%		2185478.59	6595952	13860093.92	7.43E+05	2.24E+06	4.71E+06
7	0.01%	0.06%	0.25%	0.71%	0.05%	0.19%	0.46%		581077.86	2111845.8	5180064.864	1.98E+05		
	P(V<V1)	P(V<V2)	P(V<V3)	P(V<V4)	P(V1<V<V2)	P(V2<V<V3)	P(V3<V<V4)		t_bin1	t_bin2	t_bin3	N_bin1	N_bin2	N_bin3
1	2.00%	6.55%	14.04%	23.54%	4.55%	7.49%	9.50%		51130168.7	84062771	106730094.2	6.40E+07	1.05E+08	1.34E+08
2	4.65%	12.79%	24.04%	36.42%	8.15%	11.25%	12.37%		91483623.3	126356373	138927713.4	1.14E+08	1.58E+08	1.74E+08
3	9.25%	21.73%	36.32%	50.30%	12.48%	14.59%	13.98%		140114357	163828873		1.75E+08	2.05E+08	
4	15.80%	32.31%	48.90%	62.93%	16.52%	16.59%	14.03%							
5	22.87%	42.11%	59.18%	72.23%	19.24%	17.08%	13.05%							
6	25.85%	45.85%	62.83%	75.33%	20.01%	16.97%	12.50%							
7	14.50%	30.36%	46.71%	60.83%	15.86%	16.35%	14.12%							
	P(V<V1)	P(V<V2)	P(V<V3)	P(V<V4)	P(V1<V<V2)	P(V2<V<V3)	P(V3<V<V4)		t_bin1	t_bin2	t_bin3	N_bin1	N_bin2	N_bin3
1	45.02%	66.23%	80.24%	88.64%	21.21%	14.01%	8.40%		238200483			7.49E+08		
2	59.82%	78.60%	88.95%	94.31%	18.78%	10.35%	5.36%							
3	72.70%	87.44%	94.28%	97.36%	14.75%	6.84%	3.08%							
4	82.28%	92.92%	97.14%	98.81%	10.64%	4.22%	1.67%							
5	88.21%	95.82%	98.47%	99.41%	7.60%	2.65%	0.95%							
6	89.99%	96.60%	98.80%	99.55%	6.61%	2.20%	0.76%							
7	80.81%	92.15%	96.76%	98.62%	11.33%	4.61%	1.87%							

		IAH (N-S)-Open Terrain probabilities								seconds in each bin			cycles in each bin		
Segment		P(V<V1)	P(V<V2)	P(V<V3)	P(V<V4)	P(V1<V<V2)	P(V2<V<V3)	P(V3<V<V4)		t_bin1	t_bin2	t_bin3	N_bin1	N_bin2	N_bin3
1		0.00%	0.00%	0.02%	0.06%	0.00%	0.01%	0.04%		20006.6297	105457.399	351804.39	6.80E+03	3.59E+04	1.20E+05
2		0.00%	0.01%	0.07%	0.22%	0.01%	0.05%	0.16%		98052.7638	432214.535	1241894.26	3.33E+04	1.47E+05	4.22E+05
3		0.01%	0.06%	0.24%	0.70%	0.05%	0.18%	0.46%		396405.816	1467424.35	3645090.44	1.35E+05	4.99E+05	1.24E+06
4		0.03%	0.19%	0.70%	1.81%	0.16%	0.51%	1.11%		1305024.5	4089978.24	8843910.94	4.44E+05	1.39E+06	3.01E+06
5		0.09%	0.52%	1.67%	3.85%	0.43%	1.15%	2.19%		3398701.8	9168189.91	17499727.6	1.16E+06	3.12E+06	5.95E+06
6		0.20%	0.97%	2.86%	6.17%	0.78%	1.89%	3.31%		6215885.05	15101272.6	26423646.9	2.11E+06	5.13E+06	8.98E+06
7		0.13%	0.69%	2.13%	4.77%	0.56%	1.44%	2.64%		4462210.72	11494974	21116617.8	1.52E+06		
									E-W Gusts	22874716.9			7777403.7		
		P(V<V1)	P(V<V2)	P(V<V3)	P(V<V4)	P(V1<V<V2)	P(V2<V<V3)	P(V3<V<V4)		t_bin1	t_bin2	t_bin3	N_bin1	N_bin2	N_bin3
1		3.35%	9.96%	19.81%	31.28%	6.62%	9.84%	11.47%		52897113.3	78680536.1	91701869.1	6.62E+07	9.84E+07	1.15E+08
2		7.54%	18.73%	32.53%	46.32%	11.19%	13.80%	13.79%		89416499.1	110342611	110241875	1.12E+08	1.38E+08	1.38E+08
3		14.63%	30.73%	47.27%	61.49%	16.09%	16.54%	14.22%		128630726	132227140		1.61E+08	1.65E+08	
4		24.58%	44.47%	61.64%	74.43%	19.89%	17.17%	12.79%							
5		35.91%	57.44%	73.33%	83.73%	21.54%	15.89%	10.40%							
6		44.67%	66.08%	80.23%	88.69%	21.41%	14.15%	8.47%							
7		39.71%	61.32%	76.51%	86.07%	21.61%	15.19%	9.56%							
		P(V<V1)	P(V<V2)	P(V<V3)	P(V<V4)	P(V1<V<V2)	P(V2<V<V3)	P(V3<V<V4)		t_bin1	t_bin2	t_bin3	N_bin1	N_bin2	N_bin3
1		54.51%	74.60%	86.37%	92.75%	20.09%	11.77%	6.38%		160587800			5.05E+08		
2		69.46%	85.49%	93.22%	96.81%	16.03%	7.74%	3.58%							
3		81.41%	92.53%	96.97%	98.74%	11.12%	4.44%	1.76%							
4		89.58%	96.46%	98.75%	99.54%	6.88%	2.29%	0.79%							
5		94.35%	98.35%	99.49%	99.83%	4.01%	1.13%	0.34%							
6		96.50%	99.09%	99.74%	99.92%	2.59%	0.65%	0.18%							
7		95.40%	98.72%	99.62%	99.88%	3.33%	0.90%	0.26%							

		IAH (N-S)-Suburban Terrain probabilities								seconds in each bin			cycles in each bin		
Segment		P(V<V1)	P(V<V2)	P(V<V3)	P(V<V4)	P(V1<V<V2)	P(V2<V<V3)	P(V3<V<V4)		t_bin1	t_bin2	t_bin3	N_bin1	N_bin2	N_bin3
1		0.00%	0.01%	0.05%	0.17%	0.01%	0.04%	0.12%		70917.6882	324701.1645	963008.7262	2.41E+04	1.10E+05	3.27E+05
2		0.00%	0.04%	0.18%	0.54%	0.04%	0.14%	0.36%		288295.403	1112463.353	2860679.674	9.80E+04	3.78E+05	9.73E+05
3		0.02%	0.14%	0.53%	1.42%	0.12%	0.39%	0.88%		960223.278	3147077.777	7063313.256	3.26E+05	1.07E+06	2.40E+06
4		0.07%	0.39%	1.29%	3.09%	0.32%	0.91%	1.80%		2568691.17	7253063.364	14380145.67	8.73E+05	2.47E+06	4.89E+06
5		0.16%	0.82%	2.47%	5.42%	0.66%	1.65%	2.96%		5264477.99	13175817.62	23630886.94	1.79E+06	4.48E+06	8.03E+06
6		0.22%	1.06%	3.07%	6.56%	0.84%	2.02%	3.49%		6731731.62	16118383.25	27864833.24	2.29E+06	5.48E+06	9.47E+06
7		0.05%	0.33%	1.12%	2.73%	0.27%	0.79%	1.61%		2187174.33	6335398.202	12830139.5	7.44E+05		
		P(V<V1)	P(V<V2)	P(V<V3)	P(V<V4)	P(V1<V<V2)	P(V2<V<V3)	P(V3<V<V4)		t_bin1	t_bin2	t_bin3	N_bin1	N_bin2	N_bin3
1		6.42%	16.56%	29.57%	43.01%	10.14%	13.02%	13.44%		81030421	104042253.4	107403387.6	1.01E+08	1.30E+08	1.34E+08
2		12.64%	27.60%	43.65%	57.96%	14.96%	16.06%	14.31%		119543526	128347145.8	114344462.7	1.50E+08	1.61E+08	1.43E+08
3		21.61%	40.64%	57.86%	71.19%	19.03%	17.22%	13.33%		152118920	137637103.8		1.90E+08	1.72E+08	
4		32.26%	53.52%	69.97%	81.17%	21.25%	16.45%	11.20%							
5		42.14%	63.69%	78.39%	87.41%	21.56%	14.69%	9.02%							
6		45.92%	67.23%	81.09%	89.29%	21.31%	13.87%	8.19%							
7		30.30%	51.31%	68.01%	79.63%	21.01%	16.70%	11.62%							
		P(V<V1)	P(V<V2)	P(V<V3)	P(V<V4)	P(V1<V<V2)	P(V2<V<V3)	P(V3<V<V4)		t_bin1	t_bin2	t_bin3	N_bin1	N_bin2	N_bin3
1		66.46%	83.49%	92.06%	96.16%	17.03%	8.57%	4.10%		136125349			4.28E+08		
2		78.87%	91.16%	96.29%	98.41%	12.29%	5.13%	2.11%							
3		87.70%	95.62%	98.40%	99.39%	7.93%	2.77%	0.99%							
4		93.13%	97.90%	99.32%	99.77%	4.78%	1.42%	0.44%							
5		95.97%	98.92%	99.68%	99.90%	2.95%	0.77%	0.22%							
6		96.73%	99.16%	99.76%	99.93%	2.43%	0.60%	0.16%							
7		92.36%	97.61%	99.21%	99.72%	5.25%	1.60%	0.51%							

		RMMA (N-S)-Open Terrain probabilities								seconds in each bin			cycles in each bin			
Segment		P(V<V1)	P(V<V2)	P(V<V3)	P(V<V4)	P(V1<V<V2)	P(V2<V<V3)	P(V3<V<V4)		t_bin1	t_bin2	t_bin3	N_bin1	N_bin2	N_bin3	
1		0.00%	0.00%	0.01%	0.03%	0.00%	0.01%	0.02%		11134.65	63977.68	229479.9	3.79E+03	2.18E+04	7.80E+04	
2		0.00%	0.01%	0.03%	0.12%	0.01%	0.03%	0.08%		58778.32	282697.7	874015.1	2.00E+04	9.61E+04	2.97E+05	
3		0.00%	0.03%	0.13%	0.39%	0.02%	0.10%	0.26%		255499.6	1032984	2762964	8.69E+04	3.51E+05	9.39E+05	
4		0.01%	0.10%	0.40%	1.09%	0.09%	0.30%	0.69%		901353.3	3088170	7195507	3.06E+05	1.05E+06	2.45E+06	
5		0.05%	0.29%	0.99%	2.45%	0.24%	0.71%	1.45%		2498151	7373588	15175549	8.49E+05	2.51E+06	5.16E+06	
6		0.10%	0.56%	1.78%	4.07%	0.46%	1.22%	2.30%		4771583	12692226	23957028	1.62E+06	4.32E+06	8.15E+06	
7		0.07%	0.39%	1.29%	3.08%	0.32%	0.90%	1.79%		3343159	9425949	18674385	1.14E+06			
									E-W Gusts	18359523			6242237.74			
		P(V<V1)	P(V<V2)	P(V<V3)	P(V<V4)	P(V1<V<V2)	P(V2<V<V3)	P(V3<V<V4)		t_bin1	t_bin2	t_bin3	N_bin1	N_bin2	N_bin3	
1		2.10%	6.87%	14.66%	24.47%	4.77%	7.79%	9.82%		49748391	81269256	1.02E+08	6.22E+07	1.02E+08	1.28E+08	
2		5.07%	13.77%	25.59%	38.36%	8.71%	11.81%	12.77%		90831735	1.23E+08	1.33E+08	1.14E+08	1.54E+08	1.67E+08	
3		10.48%	23.99%	39.27%	53.49%	13.50%	15.28%	14.23%		1.41E+08	1.59E+08		1.76E+08	1.99E+08		
4		18.66%	36.59%	53.65%	67.43%	17.93%	17.06%	13.77%								
5		28.63%	49.34%	66.20%	78.17%	20.71%	16.86%	11.97%								
6		36.78%	58.32%	74.04%	84.25%	21.54%	15.72%	10.21%								
7		32.12%	53.32%	69.77%	81.00%	21.21%	16.45%	11.23%								
		P(V<V1)	P(V<V2)	P(V<V3)	P(V<V4)	P(V1<V<V2)	P(V2<V<V3)	P(V3<V<V4)		t_bin1	t_bin2	t_bin3	N_bin1	N_bin2	N_bin3	
1		46.38%	67.61%	81.36%	89.46%	21.23%	13.75%	8.10%		2.22E+08			6.96E+08			
2		61.95%	80.29%	90.09%	95.02%	18.34%	9.80%	4.93%								
3		75.43%	89.17%	95.26%	97.88%	13.75%	6.08%	2.63%								
4		85.36%	94.52%	97.90%	99.17%	9.16%	3.39%	1.26%								
5		91.59%	97.29%	99.09%	99.67%	5.70%	1.79%	0.59%								
6		94.57%	98.43%	99.52%	99.84%	3.86%	1.08%	0.32%								
7		93.03%	97.86%	99.31%	99.76%	4.83%	1.44%	0.45%								

	RMMA (N-S)-Suburban Terrain probabilities								seconds in each bin			cycles in each bin			
Segment	P(V<V1)	P(V<V2)	P(V<V3)	P(V<V4)	P(V1<V<V2)	P(V2<V<V3)	P(V3<V<V4)		t_bin1	t_bin2	t_bin3	N_bin1	N_bin2	N_bin3	
1	0.00%	0.00%	0.02%	0.09%	0.00%	0.02%	0.06%		41846.86434	209010.4305	666894.8008	1.42E+04	7.11E+04	2.27E+05	
2	0.00%	0.02%	0.09%	0.30%	0.02%	0.07%	0.20%		182641.2069	769542.7385	2130439.455	6.21E+04	2.62E+05	7.24E+05	
3	0.01%	0.07%	0.30%	0.84%	0.06%	0.22%	0.54%		651000.0184	2331884.053	5638474.113	2.21E+05	7.93E+05	1.92E+06	
4	0.03%	0.21%	0.76%	1.93%	0.18%	0.55%	1.17%		1852620.274	5722251.907	12230400.95	6.30E+05	1.95E+06	4.16E+06	
5	0.08%	0.46%	1.51%	3.54%	0.38%	1.05%	2.03%		3991729.078	10936274	21155893.42	1.36E+06	3.72E+06	7.19E+06	
6	0.11%	0.61%	1.92%	4.35%	0.50%	1.31%	2.44%		5198821.065	13630219.23	25420342.63	1.77E+06	4.63E+06	8.64E+06	
7	0.03%	0.18%	0.65%	1.68%	0.15%	0.47%	1.03%		1560844.69	4944875.571	10794359.01	5.31E+05			
	P(V<V1)	P(V<V2)	P(V<V3)	P(V<V4)	P(V1<V<V2)	P(V2<V<V3)	P(V3<V<V4)		t_bin1	t_bin2	t_bin3	N_bin1	N_bin2	N_bin3	
1	4.25%	12.01%	22.97%	35.21%	7.76%	10.96%	12.24%		80976666.78	114301772.3	127646788.4	1.01E+08	1.43E+08	1.60E+08	
2	8.92%	21.25%	35.81%	49.87%	12.33%	14.57%	14.05%		128605733.8	151974126.5	146587980.6	1.61E+08	1.90E+08	1.83E+08	
3	16.15%	32.98%	49.76%	63.84%	16.83%	16.78%	14.07%		175585580.3	175061832.3		2.20E+08	2.19E+08		
4	25.35%	45.39%	62.50%	75.14%	20.04%	17.11%	12.63%								
5	34.39%	55.80%	71.91%	82.65%	21.41%	16.12%	10.73%								
6	37.97%	59.55%	75.05%	84.99%	21.57%	15.50%	9.94%								
7	23.61%	43.20%	60.38%	73.35%	19.60%	17.18%	12.96%								
	P(V<V1)	P(V<V2)	P(V<V3)	P(V<V4)	P(V1<V<V2)	P(V2<V<V3)	P(V3<V<V4)		t_bin1	t_bin2	t_bin3	N_bin1	N_bin2	N_bin3	
1	58.73%	77.88%	88.55%	94.09%	19.16%	10.66%	5.55%		199882915			6.28E+08			
2	72.47%	87.38%	94.28%	97.38%	14.91%	6.90%	3.09%								
3	83.00%	93.35%	97.36%	98.92%	10.34%	4.01%	1.56%								
4	89.96%	96.61%	98.81%	99.56%	6.66%	2.20%	0.75%								
5	93.83%	98.16%	99.42%	99.80%	4.33%	1.26%	0.39%								
6	94.91%	98.55%	99.56%	99.86%	3.64%	1.01%	0.30%								
7	88.94%	96.18%	98.63%	99.49%	7.23%	2.46%	0.86%								

	ELP (N-S)Open Terrain probabilities								seconds in each bin			cycles in each bin			
Segment	P(V<V1)	P(V<V2)	P(V<V3)	P(V<V4)	P(V1<V<V2)	P(V2<V<V3)	P(V3<V<V4)		t_bin1	t_bin2	t_bin3	N_bin1	N_bin2	N_bin3	
1	0.00%	0.01%	0.04%	0.14%	0.01%	0.03%	0.10%		43067.4222	213778.1352	672765.2	1.46E+04	7.27E+04	2.29E+05	
2	0.00%	0.03%	0.16%	0.49%	0.03%	0.12%	0.33%		200550.115	824635.4171	2217593	6.82E+04	2.80E+05	7.54E+05	
3	0.02%	0.13%	0.52%	1.43%	0.11%	0.39%	0.90%		765778.216	2619828.888	6043459	2.60E+05	8.91E+05	2.05E+06	
4	0.07%	0.42%	1.44%	3.47%	0.35%	1.02%	2.03%		2372044.23	6809110.393	13571944	8.06E+05	2.32E+06	4.61E+06	
5	0.21%	1.08%	3.21%	6.93%	0.87%	2.13%	3.72%		5816858.92	14255884.78	24914279	1.98E+06	4.85E+06	8.47E+06	
6	0.43%	1.95%	5.28%	10.60%	1.52%	3.33%	5.32%		10171259	22322378.65	35594320	3.46E+06	7.59E+06	1.21E+07	
7	0.29%	1.41%	4.02%	8.41%	1.12%	2.61%	4.38%		7489739.55	17485161.84	29348954	2.55E+06			
								E-W Gusts	122120226			4.15E+07			
	P(V<V1)	P(V<V2)	P(V<V3)	P(V<V4)	P(V1<V<V2)	P(V2<V<V3)	P(V3<V<V4)		t_bin1	t_bin2	t_bin3	N_bin1	N_bin2	N_bin3	
1	6.09%	16.25%	29.53%	43.32%	10.16%	13.28%	13.79%		67992691.9	88909532.89	92357377	8.51E+07	1.11E+08	1.16E+08	
2	12.69%	28.15%	44.74%	59.39%	15.46%	16.59%	14.65%		103496291	111104012.9	98095478	1.29E+08	1.39E+08	1.23E+08	
3	22.75%	42.69%	60.33%	73.62%	19.94%	17.64%	13.29%		133485314	118134589.6		1.67E+08	1.48E+08		
4	35.45%	57.52%	73.76%	84.27%	22.07%	16.24%	10.51%								
5	48.49%	70.01%	83.42%	91.00%	21.53%	13.41%	7.58%								
6	57.73%	77.57%	88.57%	94.22%	19.84%	11.00%	5.65%								
7	52.58%	73.48%	85.85%	92.56%	20.90%	12.37%	6.71%								
	P(V<V1)	P(V<V2)	P(V<V3)	P(V<V4)	P(V1<V<V2)	P(V2<V<V3)	P(V3<V<V4)		t_bin1	t_bin2	t_bin3	N_bin1	N_bin2	N_bin3	
1	67.31%	84.40%	92.75%	96.62%	17.10%	8.35%	3.87%		114465689			3.60E+08			
2	80.35%	92.18%	96.88%	98.72%	11.82%	4.70%	1.84%								
3	89.41%	96.49%	98.80%	99.57%	7.09%	2.31%	0.77%								
4	94.76%	98.56%	99.57%	99.87%	3.79%	1.02%	0.29%								
5	97.49%	99.41%	99.85%	99.96%	1.93%	0.44%	0.11%								
6	98.57%	99.70%	99.93%	99.98%	1.13%	0.23%	0.05%								
7	98.03%	99.56%	99.89%	99.97%	1.53%	0.33%	0.08%								

	ELP (N-S)Suburban Terrain probabilities								seconds in each bin			cycles in each bin		
Segment	P(V<V1)	P(V<V2)	P(V<V3)	P(V<V4)	P(V1<V<V2)	P(V2<V<V3)	P(V3<V<V4)		t_bin1	t_bin2	t_bin3	N_bin1	N_bin2	N_bin3
1	0.00%	0.02%	0.12%	0.38%	0.02%	0.09%	0.26%		146725.61	627928.727	1745915.7	4.99E+04	2.13E+05	5.94E+05
2	0.01%	0.10%	0.40%	1.12%	0.08%	0.30%	0.72%		564903.21	2019022.82	4830461.6	1.92E+05	6.86E+05	1.64E+06
3	0.05%	0.31%	1.11%	2.77%	0.27%	0.80%	1.65%		1775221.9	5341968.34	11073894	6.04E+05	1.82E+06	3.77E+06
4	0.15%	0.82%	2.54%	5.67%	0.67%	1.72%	3.13%		4479958.8	11521175.9	20957340	1.52E+06	3.92E+06	7.13E+06
5	0.35%	1.66%	4.61%	9.44%	1.30%	2.95%	4.83%		8727129.1	19763076.8	32344428	2.97E+06	6.72E+06	1.10E+07
6	0.47%	2.11%	5.64%	11.20%	1.63%	3.53%	5.56%		10944789	23654385.6	37241152	3.72E+06	8.04E+06	1.27E+07
7	0.13%	0.70%	2.22%	5.05%	0.58%	1.52%	2.83%		3854175.7	10182075.7	18940377	1.31E+06		
	P(V<V1)	P(V<V2)	P(V<V3)	P(V<V4)	P(V1<V<V2)	P(V2<V<V3)	P(V3<V<V4)		t_bin1	t_bin2	t_bin3	N_bin1	N_bin2	N_bin3
1	10.99%	25.32%	41.36%	56.03%	14.33%	16.04%	14.66%		95957896	107422847	98176435	1.20E+08	1.34E+08	1.23E+08
2	20.03%	39.06%	56.69%	70.48%	19.03%	17.63%	13.79%		127395699	118048307	92351059	1.59E+08	1.48E+08	1.16E+08
3	31.80%	53.56%	70.39%	81.74%	21.76%	16.83%	11.35%		145712120	112678895		1.82E+08	1.41E+08	
4	44.44%	66.38%	80.76%	89.23%	21.94%	14.38%	8.47%							
5	55.13%	75.54%	87.24%	93.42%	20.41%	11.70%	6.18%							
6	58.99%	78.52%	89.18%	94.59%	19.54%	10.66%	5.41%							
7	42.20%	64.28%	79.17%	88.14%	22.08%	14.89%	8.97%							
	P(V<V1)	P(V<V2)	P(V<V3)	P(V<V4)	P(V1<V<V2)	P(V2<V<V3)	P(V3<V<V4)		t_bin1	t_bin2	t_bin3	N_bin1	N_bin2	N_bin3
1	77.88%	90.84%	96.22%	98.41%	12.96%	5.38%	2.19%		86757697			2.73E+08		
2	87.59%	95.71%	98.48%	99.44%	8.11%	2.77%	0.96%							
3	93.60%	98.15%	99.43%	99.81%	4.55%	1.29%	0.38%							
4	96.82%	99.22%	99.79%	99.94%	2.40%	0.57%	0.15%							
5	98.32%	99.64%	99.91%	99.98%	1.32%	0.27%	0.06%							
6	98.69%	99.73%	99.94%	99.98%	1.04%	0.21%	0.05%							
7	96.40%	99.09%	99.75%	99.93%	2.69%	0.66%	0.18%							

								Equivalent Static Pressure Ranges						v(ft2/s)=	0.0001615 Stress ranges for pole with no GS			
Segment	Avg dia (in)	Mid ht. (ft)	f 1 (Hz)	V1 mph - 3s	V2 mph - 3s	V3 mph - 3	V4 mph - 3s	Pvs1 (psf)	Pvs2 (psf)	Pvs3 (psf)	Pvs4 (psf)	Re1 300≤Re≤1.0E+05 Re>3.5E+06	Re2	Re3	Re4	Sr1 (ksi)	Sr2 (ksi)	Sr3 (ksi)	Sr4 (ksi)
1	8.611	169.482	0.296	1.0	1.2	1.5	1.8	0.28	0.48	0.7	1.0	6.3E+03	8.2E+03	1.0E+04	1.2E+04	0.016	0.026	0.040	0.056
2	10.525	157.221	0.296	1.2	1.5	1.9	2.2	0.43	0.72	1.1	1.5	9.4E+03	1.2E+04	1.5E+04	1.8E+04	0.027	0.046	0.070	0.098
3	12.864	141.738	0.296	1.4	1.9	2.3	2.7	0.64	1.1	1.6	2.3	1.4E+04	1.8E+04	2.2E+04	2.7E+04	0.071	0.119	0.179	0.252
4	15.722	121.845	0.296	1.8	2.3	2.8	3.3	0.9	1.6	2.4	3.4	2.1E+04	2.7E+04	3.3E+04	4.0E+04	0.127	0.214	0.323	0.455
5	19.216	96.282	0.296	2.1	2.8	3.4	4.1	1.4	2.4	3.6	5.1	3.1E+04	4.1E+04	5.0E+04	5.9E+04	0.239	0.402	0.607	0.854
6	23.486	62.977	0.296	2.6	3.4	4.2	5.0	2.1	3.6	5.4	7.6	4.7E+04	6.1E+04	7.5E+04	8.8E+04	0.373	0.627	0.947	1.332
7	28.542	22.041	0.296	3.2	4.1	5.1	6.0	3.1	5.3	7.9	11.2	6.9E+04	9.0E+04	1.1E+05	1.3E+05	0.234	0.926		
		Pvs(windgu	0.296					6.2								4.916			
Segment	Avg dia (in)	Mid ht. (ft)	f (2nd) (Hz)	V1 mph - 3s	V2 mph - 3s	V3 mph - 3	V4 mph - 3s	Pvs1 (psf)	Pvs2 (psf)	Pvs3 (psf)	Pvs4 (psf)	Re1 00≤Re≤1.0E+05 Re>3.5E+06	Re2	Re3	Re4	Sr1 (ksi)	Sr2 (ksi)	Sr3 (ksi)	Sr4 (ksi)
1	8.611	169.482	1.023	3.3	4.3	5.3	6.3	3.4	5.7	8.6	12.2	2.2E+04	2.8E+04	3.5E+04	4.1E+04	0.187	0.315	0.475	0.669
2	10.525	157.221	1.023	4.1	5.3	6.5	7.7	5.1	8.5	12.9	18.2	3.2E+04	4.2E+04	5.2E+04	6.1E+04	0.328	0.551	0.832	1.171
3	12.864	141.738	1.023	5.0	6.4	7.9	9.4	7.6	12.8	19.3	27.1	4.9E+04	6.3E+04	7.7E+04	9.2E+04	0.843	1.417	2.139	3.010
4	15.722	121.845	1.023	6.1	7.9	9.7	11.5	11.3	19.1	28.8	40.5	7.2E+04	9.4E+04	1.2E+05	1.4E+05	1.522	2.558		
5	19.216	96.282	1.023	7.4	9.6	11.8	14.0	16.9	28.5	43.0	60.5	1.1E+05	1.4E+05	1.7E+05	2.0E+05				
6	23.486	62.977	1.023	9.1	11.8	14.5	17.2	25.3	42.6	64.3	90.4	1.6E+05	2.1E+05	2.6E+05	3.1E+05				
7	28.542	22.041	1.023	11.0	14.3	17.6	20.8	37.4	62.8	94.9	133.5	2.4E+05	3.1E+05	3.8E+05	4.5E+05				
Segment	Avg dia (in)	Mid ht. (ft)	f 3 (Hz)	V1 mph - 3s	V2 mph - 3s	V3 mph - 3	V4 mph - 3s	Pvs1 (psf)	Pvs2 (psf)	Pvs3 (psf)	Pvs4 (psf)	Re1 00≤Re≤1.0E+05 Re>3.5E+06	Re2	Re3	Re4	Sr1 (ksi)	Sr2 (ksi)	Sr3 (ksi)	Sr4 (ksi)
1	8.611	169.482	2.48	8.1	10.5	12.9	15.2	20.0	33.6	50.8	71.4	5.3E+04	6.8E+04	8.4E+04	1.0E+05	1.101	1.850	2.794	3.931
2	10.525	157.221	2.48	9.9	12.8	15.7	18.6	29.9	50.2	75.8	106.7	7.9E+04	1.0E+05	1.3E+05	1.5E+05	1.926	3.238		
3	12.864	141.738	2.48	12.1	15.6	19.2	22.8	44.6	75.0	113.3	159.4	1.2E+05	1.5E+05	1.9E+05	2.2E+05				
4	15.722	121.845	2.48	14.7	19.1	23.5	27.8	66.7	112.1	169.2	238.1	1.8E+05	2.3E+05	2.8E+05	3.3E+05				
5	19.216	96.282	2.48	18.0	23.3	28.7	34.0	99.6	167.4	252.8	355.7	2.6E+05	3.4E+05	4.2E+05	5.0E+05				
6	23.486	62.977	2.48	22.0	28.5	35.1	41.6	148.7	250.1	377.6	531.3	3.9E+05	5.1E+05	6.2E+05	7.4E+05				
7	28.542	22.041	2.48	26.7	34.7	42.6	50.5	219.7	369.3	557.7	784.7	5.8E+05	7.5E+05	9.2E+05	1.1E+06				

	Stress ranges for pole with GS				SAT (N-S)-Open Terrain probabilities								seconds in each bin			cycles in each bin		
Segment	Sr1 (ksi)	Sr2 (ksi)	Sr3 (ksi)	Sr4 (ksi)	P(V<V1)	P(V<V2)	P(V<V3)	P(V<V4)	(V1<V<V2	(V2<V<V3	(V3<V<V4		t_bin1	t_bin2	t_bin3	N_bin1	N_bin2	N_bin3
1	0.007	0.012	0.019	0.026	0.00%	0.01%	0.02%	0.08%	0.00%	0.02%	0.05%		48434.9898	192596.058	526202.99	1.43E+04	5.70E+04	1.56E+05
2	0.013	0.022	0.033	0.046	0.00%	0.02%	0.09%	0.25%	0.02%	0.07%	0.16%		188668.559	650898.91	1580298.9	5.58E+04	1.93E+05	4.68E+05
3	0.033	0.056	0.084	0.118	0.01%	0.08%	0.27%	0.68%	0.06%	0.19%	0.41%		633318.786	1900564.65	4109789.3	1.87E+05	5.63E+05	1.22E+06
4	0.060	0.101	0.152	0.214	0.04%	0.23%	0.71%	1.63%	0.18%	0.48%	0.93%		1817698.7	4767521.87	9219697.2	5.38E+05	1.41E+06	2.73E+06
5	0.112	0.189	0.285	0.401	0.13%	0.57%	1.59%	3.38%	0.44%	1.02%	1.78%		4395194.4	10166352.7	17716361	1.30E+06	3.01E+06	5.24E+06
6	0.175	0.294			0.29%	1.15%	2.93%	5.78%	0.86%	1.78%	2.85%		8513188.88	17736561	28347136	2.52E+06	5.25E+06	8.39E+06
7	0.110				0.36%	1.37%	3.43%	6.64%	1.01%	2.05%	3.21%		10089177.2	20425479.5	31879418	2.99E+06		
	2.3079											E-W	11298933.3			3344484.25		
Segment	Sr1 (ksi)	Sr2 (ksi)	Sr3 (ksi)	Sr4 (ksi)	P(V<V1)	P(V<V2)	P(V<V3)	P(V<V4)	(V1<V<V2	(V2<V<V3	(V3<V<V4		t_bin1	t_bin2	t_bin3	N_bin1	N_bin2	N_bin3
1	0.088	0.148	0.223	0.314	2.06%	5.97%	12.02%	19.59%	3.90%	6.05%	7.57%		38819340.6	60140493.4	75267130	3.97E+07	6.15E+07	7.70E+07
2	0.154	0.259	0.391	0.550	4.57%	11.41%	20.56%	30.71%	6.84%	9.15%	10.15%		68028273.8	90996482.7	100914578	6.96E+07	9.31E+07	1.03E+08
3	0.396	0.665	1.004	1.413	8.95%	19.47%	31.66%	43.66%	10.52%	12.19%	12.00%		104636515	121150571		1.07E+08	1.24E+08	
4	0.714	1.201			15.56%	29.82%	44.19%	56.81%	14.27%	14.37%	12.62%							
5					24.03%	41.22%	56.41%	68.41%	17.19%	15.19%	11.99%							
6					32.62%	51.32%	66.14%	76.85%	18.69%	14.83%	10.71%							
7					35.18%	54.09%	68.66%	78.92%	18.92%	14.56%	10.27%							
Segment	Sr1 (ksi)	Sr2 (ksi)	Sr3 (ksi)	Sr4 (ksi)	P(V<V1)	P(V<V2)	P(V<V3)	P(V<V4)	(V1<V<V2	(V2<V<V3	(V3<V<V4		t_bin1	t_bin2	t_bin3	N_bin1	N_bin2	N_bin3
1	0.517	0.869	1.3	1.8	34.70%	53.59%	68.20%	78.56%	18.88%	14.62%	10.35%		187747485			4.66E+08		
2	0.904	1.520			48.37%	67.09%	79.55%	87.36%	18.72%	12.46%	7.80%							
3					61.93%	78.43%	87.90%	93.16%	16.51%	9.47%	5.26%							
4					73.72%	86.82%	93.34%	96.56%	13.10%	6.51%	3.22%							
5					82.70%	92.30%	96.48%	98.33%	9.60%	4.18%	1.85%							
6					88.44%	95.36%	98.05%	99.14%	6.92%	2.69%	1.09%							
7					89.74%	96.00%	98.36%	99.29%	6.26%	2.36%	0.93%							

	Avg Sr (No GS)			Avg Sr (w/GS)			SAT(N-S)-Suburban Terrain probabilities							seconds in each bin			cycles in each bin		
Segment	S_bin1	S_bin2	S_bin3	S_bin1	S_bin2	S_bin3	P(V<V1)	P(V<V2)	P(V<V3)	P(V<V4)	(V1<V<V2	(V2<V<V3	(V3<V<V4	t_bin1	t_bin2	t_bin3	N_bin1	N_bin2	N_bin3
1	0.021	0.033	0.048	0.010	0.016	0.022	0.00%	0.02%	0.07%	0.21%	0.02%	0.06%	0.14%	157919	555469.1	1370491	4.67E+04	1.64E+05	4.06E+05
2	0.037	0.058	0.084	0.017	0.027	0.039	0.01%	0.06%	0.23%	0.59%	0.05%	0.16%	0.36%	527915	1619312	3565810	1.56E+05	4.79E+05	1.06E+06
3	0.095	0.149	0.216	0.044	0.070	0.101	0.04%	0.19%	0.60%	1.41%	0.15%	0.41%	0.81%	1513745	4068534	8028994	4.48E+05	1.20E+06	2.38E+06
4	0.171	0.269	0.389	0.080	0.126	0.183	0.10%	0.47%	1.35%	2.92%	0.37%	0.88%	1.57%	3679577	8739133	1.6E+07	1.09E+06	2.59E+06	4.61E+06
5	0.321	0.505	0.731	0.150	0.237	0.343	0.25%	0.99%	2.58%	5.17%	0.75%	1.59%	2.59%	7408953	15793028	2.6E+07	2.19E+06	4.67E+06	7.61E+06
6	0.500	0.787	1.140	0.235	0.294		0.42%	1.56%	3.83%	7.31%	1.14%	2.27%	3.48%	1.1E+07	22553448	3.5E+07	3.37E+06	6.68E+06	1.02E+07
7	0.580			0.110			0.29%	1.13%	2.90%	5.72%	0.85%	1.76%	2.83%	8401965	17543163	2.8E+07	2.49E+06		
	4.916			2.3079															
Segment	S_bin1	S_bin2	S_bin3	S_bin1	S_bin2	S_bin3	P(V<V1)	P(V<V2)	P(V<V3)	P(V<V4)	(V1<V<V2	(V2<V<V3	(V3<V<V4	t_bin1	t_bin2	t_bin3	N_bin1	N_bin2	N_bin3
1	0.251	0.395	0.572	0.118	0.186	0.269	4.12%	10.51%	19.22%	29.05%	6.38%	8.71%	9.82%	6.3E+07	86631378	9.8E+07	6.49E+07	8.86E+07	9.99E+07
2	0.439	0.692	1.001	0.206	0.325	0.470	8.11%	18.02%	29.76%	41.54%	9.91%	11.74%	11.78%	9.9E+07	1.17E+08	1.2E+08	1.01E+08	1.19E+08	1.20E+08
3	1.130	1.778		0.530	0.835		14.17%	27.78%	41.83%	54.44%	13.61%	14.06%	12.61%	1.4E+08	1.4E+08		1.38E+08	1.43E+08	
4							22.07%	38.73%	53.86%	66.08%	16.66%	15.13%	12.22%						
5							30.64%	49.10%	64.08%	75.12%	18.45%	14.99%	11.04%						
6							37.07%	56.09%	70.42%	80.35%	19.02%	14.33%	9.93%						
7							32.43%	51.10%	65.95%	76.69%	18.67%	14.84%	10.74%						
Segment	S_bin1	S_bin2	S_bin3	S_bin1	S_bin2	S_bin3	P(V<V1)	P(V<V2)	P(V<V3)	P(V<V4)	(V1<V<V2	(V2<V<V3	(V3<V<V4	t_bin1	t_bin2	t_bin3	N_bin1	N_bin2	N_bin3
1	1.476			0.693			46.46%	65.34%	78.17%	86.34%	18.88%	12.83%	8.17%	1.9E+08			4.66E+08		
2							59.85%	76.82%	86.78%	92.42%	16.97%	9.96%	5.64%						
3							71.73%	85.50%	92.53%	96.07%	13.77%	7.03%	3.55%						
4							81.00%	91.33%	95.95%	98.04%	10.33%	4.62%	2.09%						
5							87.32%	94.79%	97.77%	99.00%	7.47%	2.98%	1.23%						
6							90.62%	96.41%	98.55%	99.38%	5.80%	2.14%	0.83%						
7							88.33%	95.31%	98.02%	99.13%	6.97%	2.72%	1.10%						

	DFW(N-S)-Open Terrain probabilities								seconds in each bin			cycles in each bin			
Segment	P(V<V1)	P(V<V2)	P(V<V3)	P(V<V4)	P(V1<V<V2)	P(V2<V<V3)	P(V3<V<V4)		t_bin1	t_bin2	t_bin3	N_bin1	N_bin2	N_bin3	
1	0.00%	0.00%	0.00%	0.00%	0.00%	0.00%	0.00%		895.9503611	6501.78295	28408.7614	2.65E+02	1.92E+03	8.41E+03	
2	0.00%	0.00%	0.00%	0.02%	0.00%	0.00%	0.01%		5902.204746	35910.1211	135407.651	1.75E+03	1.06E+04	4.01E+04	
3	0.00%	0.00%	0.02%	0.07%	0.00%	0.01%	0.05%		32093.93061	164239.467	535952.803	9.50E+03	4.86E+04	1.59E+05	
4	0.00%	0.01%	0.07%	0.22%	0.01%	0.05%	0.16%		142279.0587	616034.092	1748510.44	4.21E+04	1.82E+05	5.18E+05	
5	0.01%	0.05%	0.22%	0.63%	0.04%	0.17%	0.41%		502308.0181	1860698.6	4637100.49	1.49E+05	5.51E+05	1.37E+06	
6	0.02%	0.14%	0.51%	1.36%	0.12%	0.38%	0.85%		1306862.89	4251561.04	9509452.87	3.87E+05	1.26E+06	2.81E+06	
7	0.03%	0.18%	0.64%	1.66%	0.15%	0.47%	1.02%		1674185.352	5255879.71	11412248.8	4.96E+05			
								E-W Gusts	19820567.7			5866888			
Segment	P(V<V1)	P(V<V2)	P(V<V3)	P(V<V4)	P(V1<V<V2)	P(V2<V<V3)	P(V3<V<V4)		t_bin1	t_bin2	t_bin3	N_bin1	N_bin2	N_bin3	
1	0.31%	1.42%	3.93%	8.05%	1.11%	2.50%	4.12%		12491863.05	28122151.6	46320314.1	1.28E+07	2.88E+07	4.74E+07	
2	0.97%	3.64%	8.65%	15.75%	2.67%	5.01%	7.09%		30010664.17	56276181.5	79664742.7	3.07E+07	5.76E+07	8.15E+07	
3	2.56%	7.98%	16.48%	26.85%	5.43%	8.50%	10.37%		60928976.34	95449789.9		6.23E+07	9.76E+07		
4	5.73%	15.07%	27.36%	40.34%	9.33%	12.29%	12.98%								
5	10.91%	24.60%	39.90%	54.05%	13.68%	15.31%	14.15%								
6	17.25%	34.44%	51.23%	65.12%	17.19%	16.79%	13.88%								
7	19.33%	37.38%	54.36%	67.97%	18.05%	16.98%	13.62%								
Segment	P(V<V1)	P(V<V2)	P(V<V3)	P(V<V4)	P(V1<V<V2)	P(V2<V<V3)	P(V3<V<V4)		t_bin1	t_bin2	t_bin3	N_bin1	N_bin2	N_bin3	
1	18.94%	36.83%	53.79%	67.46%	17.90%	16.96%	13.67%		200975588			4.98E+08			
2	31.43%	52.41%	68.85%	80.21%	20.97%	16.45%	11.36%								
3	46.18%	67.29%	81.04%	89.19%	21.12%	13.75%	8.15%								
4	60.90%	79.41%	89.47%	94.62%	18.51%	10.06%	5.15%								
5	73.33%	87.84%	94.50%	97.48%	14.50%	6.66%	2.97%								
6	81.85%	92.70%	97.03%	98.75%	10.85%	4.33%	1.72%								
7	83.85%	93.73%	97.52%	98.99%	9.88%	3.79%	1.46%								

	DFW (N-S)-Suburban Terrain probabilities								seconds in each bin			cycles in each bin		
Segment	P(V<V1)	P(V<V2)	P(V<V3)	P(V<V4)	P(V1<V<V2)	P(V2<V<V3)	P(V3<V<V4)		t_bin1	t_bin2	t_bin3	N_bin1	N_bin2	N_bin3
1	0.00%	0.00%	0.00%	0.01%	0.00%	0.00%	0.01%		4608.001	28718	110485.5	1.36E+03	8.50E+03	3.27E+04
2	0.00%	0.00%	0.01%	0.05%	0.00%	0.01%	0.04%		24855.56	130700.1	436291.7	7.36E+03	3.87E+04	1.29E+05
3	0.00%	0.01%	0.05%	0.18%	0.01%	0.04%	0.13%		109745.1	489805	1425863	3.25E+04	1.45E+05	4.22E+05
4	0.00%	0.04%	0.17%	0.51%	0.03%	0.13%	0.34%		389180.3	1489750	3815620	1.15E+05	4.41E+05	1.13E+06
5	0.02%	0.11%	0.43%	1.16%	0.10%	0.32%	0.73%		1067901	3574237	8185758	3.16E+05	1.06E+06	2.42E+06
6	0.03%	0.21%	0.75%	1.91%	0.18%	0.54%	1.16%		1995181	6104051	12972374	5.91E+05	1.81E+06	3.84E+06
7	0.02%	0.13%	0.51%	1.34%	0.11%	0.37%	0.83%		1282087	4182304	9375722	3.79E+05		
Segment	P(V<V1)	P(V<V2)	P(V<V3)	P(V<V4)	P(V1<V<V2)	P(V2<V<V3)	P(V3<V<V4)		t_bin1	t_bin2	t_bin3	N_bin1	N_bin2	N_bin3
1	0.84%	3.23%	7.83%	14.48%	2.39%	4.60%	6.65%		26877341	51673833	74676591	2.75E+07	5.29E+07	7.64E+07
2	2.22%	7.12%	15.02%	24.89%	4.90%	7.90%	9.87%		55061170	88729587	1.11E+08	5.63E+07	9.08E+07	1.13E+08
3	5.00%	13.54%	25.16%	37.75%	8.55%	11.61%	12.59%		95968301	1.3E+08		9.82E+07	1.33E+08	
4	9.61%	22.36%	37.12%	51.15%	12.75%	14.76%	14.03%							
5	15.70%	32.17%	48.74%	62.77%	16.47%	16.57%	14.04%							
6	20.92%	39.55%	56.60%	69.98%	18.62%	17.06%	13.38%							
7	17.10%	34.22%	51.00%	64.89%	17.13%	16.77%	13.90%							
Segment	P(V<V1)	P(V<V2)	P(V<V3)	P(V<V4)	P(V1<V<V2)	P(V2<V<V3)	P(V3<V<V4)		t_bin1	t_bin2	t_bin3	N_bin1	N_bin2	N_bin3
1	29.54%	50.25%	66.92%	78.68%	20.71%	16.67%	11.76%		2.33E+08			5.77E+08		
2	43.77%	65.07%	79.35%	88.02%	21.30%	14.28%	8.67%							
3	58.28%	77.43%	88.19%	93.85%	19.15%	10.76%	5.66%							
4	70.89%	86.30%	93.64%	97.02%	15.42%	7.34%	3.37%							
5	80.15%	91.79%	96.58%	98.54%	11.64%	4.79%	1.96%							
6	85.20%	94.40%	97.83%	99.13%	9.20%	3.44%	1.30%							
7	81.69%	92.61%	96.99%	98.73%	10.92%	4.37%	1.75%							

Segment		IAH (N-S)-Open Terrain probabilities								seconds in each bin			cycles in each bin			
		P(V<V1)	P(V<V2)	P(V<V3)	P(V<V4)	P(V1<V<V2)	P(V2<V<V3)	P(V3<V<V4)		t_bin1	t_bin2	t_bin3	N_bin1	N_bin2	N_bin3	
1		0.00%	0.00%	0.01%	0.02%	0.00%	0.01%	0.02%		7013.195	41224.29	150634.8	2.08E+03	1.22E+04	4.46E+04	
2		0.00%	0.01%	0.03%	0.10%	0.00%	0.02%	0.07%		38422.54	188603	592834.8	1.14E+04	5.58E+04	1.75E+05	
3		0.00%	0.02%	0.11%	0.36%	0.02%	0.09%	0.24%		174065.3	715795.2	1940934	5.15E+04	2.12E+05	5.75E+05	
4		0.01%	0.09%	0.37%	1.03%	0.08%	0.28%	0.66%		646012.2	2238763	5263689	1.91E+05	6.63E+05	1.56E+06	
5		0.05%	0.29%	1.00%	2.47%	0.24%	0.71%	1.47%		1929813	5700149	11732702	5.71E+05	1.69E+06	3.47E+06	
6		0.13%	0.67%	2.08%	4.69%	0.55%	1.41%	2.60%		4365616	11288607	20802560	1.29E+06	3.34E+06	6.16E+06	
7		0.16%	0.84%	2.52%	5.52%	0.67%	1.68%	3.00%		5381426	13416235	23984475	1.59E+06			
										0	0	0				
									E-W Gusts	22874717			6770916.19			
Segment		P(V<V1)	P(V<V2)	P(V<V3)	P(V<V4)	P(V1<V<V2)	P(V2<V<V3)	P(V3<V<V4)		t_bin1	t_bin2	t_bin3	N_bin1	N_bin2	N_bin3	
1		1.37%	4.87%	11.07%	19.43%	3.50%	6.20%	8.36%		27966770	49577483	66803254	2.86E+07	5.07E+07	6.83E+07	
2		3.54%	10.42%	20.53%	32.19%	6.88%	10.11%	11.66%		54981366	80800266	93239100	5.62E+07	8.27E+07	9.54E+07	
3		7.84%	19.29%	33.29%	47.15%	11.45%	13.99%	13.87%		91540102	1.12E+08		9.36E+07	1.14E+08		
4		14.92%	31.16%	47.76%	61.96%	16.24%	16.60%	14.20%								
5		24.49%	44.35%	61.53%	74.33%	19.86%	17.17%	12.81%								
6		34.41%	55.86%	71.99%	82.72%	21.45%	16.13%	10.73%								
7		37.37%	58.96%	74.59%	84.67%	21.59%	15.63%	10.08%								
Segment		P(V<V1)	P(V<V2)	P(V<V3)	P(V<V4)	P(V1<V<V2)	P(V2<V<V3)	P(V3<V<V4)		t_bin1	t_bin2	t_bin3	N_bin1	N_bin2	N_bin3	
1		36.82%	58.40%	74.12%	84.32%	21.58%	15.73%	10.20%		1.72E+08			4.28E+08			
2		52.53%	72.97%	85.25%	92.04%	20.45%	12.27%	6.79%								
3		67.52%	84.21%	92.48%	96.40%	16.69%	8.27%	3.92%								
4		79.68%	91.60%	96.52%	98.52%	11.92%	4.91%	2.00%								
5		88.09%	95.80%	98.47%	99.42%	7.71%	2.67%	0.95%								
6		92.90%	97.82%	99.29%	99.75%	4.91%	1.47%	0.46%								
7		93.92%	98.20%	99.43%	99.81%	4.28%	1.23%	0.38%								

	IAH (N-S)-Suburban Terrain probabilities								seconds in each bin			cycles in each bin			
Segment	P(V<V1)	P(V<V2)	P(V<V3)	P(V<V4)	P(V1<V<V2)	P(V2<V<V3)	P(V3<V<V4)		t_bin1	t_bin2	t_bin3	N_bin1	N_bin2	N_bin3	
1	0.00%	0.00%	0.02%	0.09%	0.00%	0.02%	0.06%		30764.16	154769.4	496576	9.11E+03	4.58E+04	1.47E+05	
2	0.00%	0.02%	0.09%	0.30%	0.02%	0.07%	0.20%		138740.4	586614.5	1627967	4.11E+04	1.74E+05	4.82E+05	
3	0.01%	0.07%	0.30%	0.86%	0.06%	0.23%	0.56%		514678.9	1839894	4439283	1.52E+05	5.45E+05	1.31E+06	
4	0.04%	0.23%	0.82%	2.07%	0.19%	0.59%	1.25%		1548819	4731250	10014717	4.58E+05	1.40E+06	2.96E+06	
5	0.10%	0.56%	1.79%	4.10%	0.46%	1.23%	2.31%		3678379	9792441	18487193	1.09E+06	2.90E+06	5.47E+06	
6	0.20%	0.98%	2.87%	6.18%	0.78%	1.89%	3.31%		6236696	15142653	26482722	1.85E+06	4.48E+06	7.84E+06	
7	0.12%	0.66%	2.05%	4.63%	0.54%	1.39%	2.57%		4295430	11138083	20572707	1.27E+06			
Segment	P(V<V1)	P(V<V2)	P(V<V3)	P(V<V4)	P(V1<V<V2)	P(V2<V<V3)	P(V3<V<V4)		t_bin1	t_bin2	t_bin3	N_bin1	N_bin2	N_bin3	
1	3.14%	9.47%	19.01%	30.27%	6.33%	9.55%	11.25%		50610717	76306258	89935138	5.18E+07	7.81E+07	9.20E+07	
2	6.98%	17.66%	31.09%	44.72%	10.68%	13.43%	13.63%		85349426	1.07E+08	1.09E+08	8.73E+07	1.10E+08	1.11E+08	
3	13.39%	28.80%	45.06%	59.34%	15.40%	16.26%	14.29%		1.23E+08	1.3E+08		1.26E+08	1.33E+08		
4	22.24%	41.47%	58.70%	71.92%	19.23%	17.22%	13.22%								
5	32.11%	53.35%	69.82%	81.05%	21.24%	16.47%	11.23%								
6	39.56%	61.17%	76.39%	85.98%	21.62%	15.22%	9.59%								
7	34.19%	55.62%	71.78%	82.56%	21.43%	16.16%	10.78%								
Segment	P(V<V1)	P(V<V2)	P(V<V3)	P(V<V4)	P(V1<V<V2)	P(V2<V<V3)	P(V3<V<V4)		t_bin1	t_bin2	t_bin3	N_bin1	N_bin2	N_bin3	
1	50.36%	71.14%	83.96%	91.20%	20.79%	12.81%	7.24%		1.66E+08			4.12E+08			
2	65.29%	82.68%	91.57%	95.88%	17.40%	8.89%	4.31%								
3	77.70%	90.50%	95.96%	98.24%	12.80%	5.45%	2.28%								
4	86.57%	95.10%	98.17%	99.29%	8.54%	3.07%	1.12%								
5	92.01%	97.47%	99.16%	99.70%	5.46%	1.69%	0.55%								
6	94.58%	98.44%	99.52%	99.84%	3.86%	1.08%	0.32%								
7	92.82%	97.79%	99.28%	99.75%	4.96%	1.49%	0.47%								

	RMMA (N-S)-Open Terrain probabilities								seconds in each bin			cycles in each bin			
Segment	P(V<V1)	P(V<V2)	P(V<V3)	P(V<V4)	P(V1<V<V2)	P(V2<V<V3)	P(V3<V<V4)		t_bin1	t_bin2	t_bin3	N_bin1	N_bin2	N_bin3	
1	0.00%	0.00%	0.00%	0.01%	0.00%	0.00%	0.01%		3730.501	23889.47	93816.46	1.10E+03	7.07E+03	2.78E+04	
2	0.00%	0.00%	0.01%	0.05%	0.00%	0.01%	0.04%		22026.1	117899.8	398581	6.52E+03	3.49E+04	1.18E+05	
3	0.00%	0.01%	0.06%	0.19%	0.01%	0.05%	0.13%		107398.5	482065.7	1406907	3.18E+04	1.43E+05	4.16E+05	
4	0.01%	0.05%	0.20%	0.60%	0.04%	0.16%	0.39%		427945	1620341	4103352	1.27E+05	4.80E+05	1.21E+06	
5	0.02%	0.15%	0.58%	1.51%	0.13%	0.42%	0.94%		1366067	4412635	9789427	4.04E+05	1.31E+06	2.90E+06	
6	0.06%	0.38%	1.26%	3.02%	0.31%	0.89%	1.76%		3265680	9242056	18367193	9.67E+05	2.74E+06	5.44E+06	
7	0.08%	0.48%	1.55%	3.61%	0.39%	1.07%	2.06%		4086989	11154064	21507978	1.21E+06			
								E-W Gusts	18359523			5434418.74			
Segment	P(V<V1)	P(V<V2)	P(V<V3)	P(V<V4)	P(V1<V<V2)	P(V2<V<V3)	P(V3<V<V4)		t_bin1	t_bin2	t_bin3	N_bin1	N_bin2	N_bin3	
1	0.80%	3.15%	7.71%	14.35%	2.34%	4.56%	6.64%		24461790	47571893	69244301	2.50E+07	4.87E+07	7.08E+07	
2	2.23%	7.21%	15.25%	25.29%	4.98%	8.04%	10.03%		51966807	83882115	1.05E+08	5.32E+07	8.58E+07	1.07E+08	
3	5.29%	14.24%	26.26%	39.16%	8.95%	12.03%	12.89%		93369244	1.25E+08		9.55E+07	1.28E+08		
4	10.71%	24.37%	39.75%	53.99%	13.66%	15.37%	14.24%								
5	18.58%	36.48%	53.54%	67.32%	17.90%	17.06%	13.79%								
6	27.27%	47.73%	64.71%	76.96%	20.46%	16.98%	12.25%								
7	29.96%	50.89%	67.61%	79.30%	20.93%	16.72%	11.69%								
Segment	P(V<V1)	P(V<V2)	P(V<V3)	P(V<V4)	P(V1<V<V2)	P(V2<V<V3)	P(V3<V<V4)		t_bin1	t_bin2	t_bin3	N_bin1	N_bin2	N_bin3	
1	29.46%	50.31%	67.09%	78.88%	20.85%	16.77%	11.80%		2.18E+08			5.40E+08			
2	44.41%	65.81%	80.00%	88.53%	21.40%	14.19%	8.53%								
3	59.86%	78.74%	89.10%	94.43%	18.88%	10.36%	5.33%								
4	73.40%	87.96%	94.60%	97.54%	14.55%	6.64%	2.94%								
5	83.49%	93.59%	97.48%	98.97%	10.10%	3.88%	1.50%								
6	89.66%	96.49%	98.76%	99.54%	6.83%	2.27%	0.78%								
7	91.01%	97.06%	98.99%	99.64%	6.04%	1.93%	0.64%								

	RMMA (N-S)-Suburban Terrain probabilities								seconds in each bin				cycles in each bin			
Segment	P(V<V1)	P(V<V2)	P(V<V3)	P(V<V4)	P(V1<V<V2)	P(V2<V<V3)	P(V3<V<V4)		t_bin1	t_bin2	t_bin3		N_bin1	N_bin2	N_bin3	
1	0.00%	0.00%	0.01%	0.04%	0.00%	0.01%	0.03%		17456.71053	95754.29253	330395.1536		5.17E+03	2.83E+04	9.78E+04	
2	0.00%	0.01%	0.05%	0.16%	0.01%	0.04%	0.11%		84620.18853	390470.9777	1166186.667		2.50E+04	1.16E+05	3.45E+05	
3	0.00%	0.04%	0.16%	0.49%	0.03%	0.13%	0.33%		336575.1303	1314353.874	3415273.53		9.96E+04	3.89E+05	1.01E+06	
4	0.02%	0.12%	0.47%	1.26%	0.10%	0.35%	0.79%		1081175.227	3611105.431	8237351.493		3.20E+05	1.07E+06	2.44E+06	
5	0.05%	0.31%	1.07%	2.62%	0.26%	0.76%	1.55%		2718577.914	7919544.892	16122152.03		8.05E+05	2.34E+06	4.77E+06	
6	0.10%	0.56%	1.78%	4.08%	0.46%	1.22%	2.30%		4788762.316	12730250.53	24016775.8		1.42E+06	3.77E+06	7.11E+06	
7	0.06%	0.37%	1.24%	2.98%	0.31%	0.87%	1.74%		3209469.38	9108145.482	18142763.83		9.50E+05			
Segment	P(V<V1)	P(V<V2)	P(V<V3)	P(V<V4)	P(V1<V<V2)	P(V2<V<V3)	P(V3<V<V4)		t_bin1	t_bin2	t_bin3		N_bin1	N_bin2	N_bin3	
1	1.96%	6.50%	14.01%	23.58%	4.54%	7.51%	9.57%		47332532.86	78370208.07	99851629.61		4.84E+07	8.02E+07	1.02E+08	
2	4.66%	12.91%	24.31%	36.83%	8.25%	11.40%	12.52%		86019659.72	118963709.5	130631161.9		8.80E+07	1.22E+08	1.34E+08	
3	9.51%	22.29%	37.15%	51.28%	12.79%	14.86%	14.13%		133388516.8	154994647.2			1.36E+08	1.59E+08		
4	16.68%	33.76%	50.62%	64.64%	17.08%	16.86%	14.02%									
5	25.22%	45.23%	62.34%	75.00%	20.01%	17.12%	12.66%									
6	31.98%	53.17%	69.63%	80.89%	21.19%	16.47%	11.26%									
7	27.07%	47.49%	64.49%	76.78%	20.42%	17.00%	12.29%									
Segment	P(V<V1)	P(V<V2)	P(V<V3)	P(V<V4)	P(V1<V<V2)	P(V2<V<V3)	P(V3<V<V4)		t_bin1	t_bin2	t_bin3		N_bin1	N_bin2	N_bin3	
1	42.27%	63.79%	78.44%	87.44%	21.52%	14.65%	8.99%		224500636.4				5.57E+08			
2	57.48%	76.93%	87.92%	93.71%	19.45%	10.99%	5.79%									
3	71.13%	86.54%	93.81%	97.12%	15.41%	7.27%	3.31%									
4	81.61%	92.62%	97.01%	98.75%	11.02%	4.39%	1.74%									
5	88.48%	95.97%	98.54%	99.45%	7.49%	2.57%	0.90%									
6	91.91%	97.42%	99.14%	99.69%	5.51%	1.72%	0.56%									
7	89.55%	96.44%	98.74%	99.53%	6.89%	2.30%	0.79%									

	ELP (N-S)Open Terrain probabilities								seconds in each bin			cycles in each bin			
Segment	P(V<V1)	P(V<V2)	P(V<V3)	P(V<V4)	P(V1<V<V2)	P(V2<V<V3)	P(V3<V<V4)		t_bin1	t_bin2	t_bin3	N_bin1	N_bin2	N_bin3	
1	0.00%	0.00%	0.02%	0.06%	0.00%	0.01%	0.04%		15517.32	86388.69	299223.2	4.59E+03	2.56E+04	8.86E+04	
2	0.00%	0.01%	0.07%	0.23%	0.01%	0.06%	0.16%		81115.36	373544.7	1104166	2.40E+04	1.11E+05	3.27E+05	
3	0.01%	0.06%	0.26%	0.76%	0.05%	0.20%	0.50%		348317.1	1331206	3367916	1.03E+05	3.94E+05	9.97E+05	
4	0.03%	0.21%	0.79%	2.06%	0.18%	0.58%	1.27%		1219119	3890726	8470208	3.61E+05	1.15E+06	2.51E+06	
5	0.11%	0.62%	2.00%	4.61%	0.51%	1.38%	2.61%		3427318	9242708	17489858	1.01E+06	2.74E+06	5.18E+06	
6	0.28%	1.38%	3.95%	8.28%	1.10%	2.57%	4.33%		7339417	17202465	28969925	2.17E+06	5.09E+06	8.58E+06	
7	0.36%	1.69%	4.69%	9.59%	1.33%	3.00%	4.89%		8905942	20085459	32760291	2.64E+06			
								E-W Gusts	1.22E+08			3.61E+07			
Segment	P(V<V1)	P(V<V2)	P(V<V3)	P(V<V4)	P(V1<V<V2)	P(V2<V<V3)	P(V3<V<V4)		t_bin1	t_bin2	t_bin3	N_bin1	N_bin2	N_bin3	
1	2.67%	8.56%	17.83%	29.04%	5.89%	9.26%	11.22%		39415174	62031551	75093100	4.03E+07	6.35E+07	7.68E+07	
2	6.42%	16.90%	30.44%	44.36%	10.49%	13.54%	13.92%		70209730	90646569	93177419	7.18E+07	9.27E+07	9.53E+07	
3	13.14%	28.87%	45.59%	60.22%	15.73%	16.71%	14.63%		1.05E+08	1.12E+08		1.08E+08	1.14E+08		
4	23.14%	43.19%	60.82%	74.04%	20.05%	17.63%	13.22%								
5	35.34%	57.40%	73.66%	84.20%	22.06%	16.26%	10.54%								
6	46.84%	68.56%	82.37%	90.31%	21.72%	13.81%	7.94%								
7	50.07%	71.38%	84.40%	91.63%	21.31%	13.01%	7.24%								
Segment	P(V<V1)	P(V<V2)	P(V<V3)	P(V<V4)	P(V1<V<V2)	P(V2<V<V3)	P(V3<V<V4)		t_bin1	t_bin2	t_bin3	N_bin1	N_bin2	N_bin3	
1	49.48%	70.88%	84.04%	91.40%	21.39%	13.16%	7.36%		1.43E+08			3.55E+08			
2	65.44%	83.15%	92.02%	96.21%	17.71%	8.87%	4.20%								
3	78.76%	91.32%	96.46%	98.53%	12.56%	5.14%	2.06%								
4	88.18%	95.96%	98.58%	99.48%	7.79%	2.62%	0.90%								
5	93.85%	98.23%	99.46%	99.83%	4.39%	1.23%	0.36%								
6	96.70%	99.18%	99.78%	99.94%	2.48%	0.60%	0.16%								
7	97.26%	99.35%	99.83%	99.95%	2.09%	0.48%	0.12%								

	ELP (N-S)Suburban Terrain probabilities								seconds in each bin			cycles in each bin		
Segment	P(V<V1)	P(V<V2)	P(V<V3)	P(V<V4)	P(V1<V<V2)	P(V2<V<V3)	P(V3<V<V4)		t_bin1	t_bin2	t_bin3	N_bin1	N_bin2	N_bin3
1	0.00%	0.01%	0.06%	0.20%	0.01%	0.05%	0.14%		65394.27	309044.5	933472.1	1.94E+04	9.15E+04	2.76E+05
2	0.01%	0.05%	0.21%	0.64%	0.04%	0.16%	0.43%		280108.6	1102335	2857834	8.29E+04	3.26E+05	8.46E+05
3	0.02%	0.17%	0.65%	1.74%	0.15%	0.48%	1.08%		982149.8	3238737	7245684	2.91E+05	9.59E+05	2.14E+06
4	0.09%	0.50%	1.66%	3.93%	0.42%	1.16%	2.27%		2787366	7788128	15178393	8.25E+05	2.31E+06	4.49E+06
5	0.23%	1.17%	3.43%	7.33%	0.94%	2.26%	3.90%		6260774	15131619	26140508	1.85E+06	4.48E+06	7.74E+06
6	0.43%	1.96%	5.30%	10.62%	1.52%	3.34%	5.33%		10202590	22376831	35662222	3.02E+06	6.62E+06	1.06E+07
7	0.28%	1.36%	3.90%	8.18%	1.08%	2.54%	4.29%		7230002	16995832	28691816	2.14E+06		
Segment	P(V<V1)	P(V<V2)	P(V<V3)	P(V<V4)	P(V1<V<V2)	P(V2<V<V3)	P(V3<V<V4)		t_bin1	t_bin2	t_bin3	N_bin1	N_bin2	N_bin3
1	5.74%	15.53%	28.51%	42.16%	9.79%	12.98%	13.65%		65532450	86927005	91370074	6.70E+07	8.89E+07	9.35E+07
2	11.85%	26.77%	43.11%	57.78%	14.92%	16.34%	14.67%		99885978	1.09E+08	98224052	1.02E+08	1.12E+08	1.00E+08
3	21.07%	40.46%	58.12%	71.73%	19.40%	17.65%	13.61%		1.3E+08	1.18E+08		1.33E+08	1.21E+08	
4	32.59%	54.44%	71.15%	82.32%	21.85%	16.71%	11.17%							
5	44.27%	66.22%	80.64%	89.15%	21.95%	14.42%	8.51%							
6	52.42%	73.35%	85.76%	92.50%	20.93%	12.41%	6.74%							
7	46.59%	68.34%	82.21%	90.20%	21.75%	13.87%	7.99%							
Segment	P(V<V1)	P(V<V2)	P(V<V3)	P(V<V4)	P(V1<V<V2)	P(V2<V<V3)	P(V3<V<V4)		t_bin1	t_bin2	t_bin3	N_bin1	N_bin2	N_bin3
1	63.36%	81.71%	91.16%	95.73%	18.34%	9.45%	4.57%		1.23E+08			3.05E+08		
2	76.90%	90.29%	95.95%	98.28%	13.39%	5.66%	2.33%							
3	86.74%	95.32%	98.31%	99.37%	8.58%	2.99%	1.05%							
4	92.88%	97.88%	99.34%	99.78%	5.00%	1.46%	0.44%							
5	96.20%	99.03%	99.73%	99.92%	2.83%	0.70%	0.19%							
6	97.61%	99.45%	99.86%	99.96%	1.84%	0.41%	0.10%							
7	96.66%	99.17%	99.78%	99.93%	2.51%	0.61%	0.16%							

						Equivalent Static Pressure Ranges							v(ft2/s)=	0.0001615	Stress ranges for pole with no GS				
Segment	Avg dia (in)	Mid ht. (ft)	f 1 (Hz)	V1 (mph - 3s)	V2 (mph - 3s)	V3 (mph - 3s)	V4 (mph - 3s)	Pvs1 (psf)	Pvs2 (psf)	Pvs3 (psf)	Pvs4 (psf)	Re1 300≤Re≤1.0E+05 Re>3.5E+06	Re2	Re3	Re4	Sr1 (ksi)	Sr2 (ksi)	Sr3 (ksi)	Sr4 (ksi)
1	8.750	145.298	0.41	1.4	1.8	2.2	2.6	0.56	0.95	1.4	2.0	9.0E+03	1.2E+04	1.4E+04	1.7E+04	0.022	0.037	0.056	0.079
2	10.694	134.849	0.41	1.7	2.1	2.6	3.1	0.84	1.4	2.1	3.0	1.3E+04	1.7E+04	2.1E+04	2.5E+04	0.036	0.060	0.091	0.128
3	13.071	121.891	0.41	2.0	2.6	3.2	3.8	1.3	2.1	3.2	4.5	2.0E+04	2.6E+04	3.2E+04	3.8E+04	0.084	0.141	0.212	0.299
4	15.976	105.113	0.41	2.5	3.2	3.9	4.7	1.9	3.2	4.8	6.7	3.0E+04	3.9E+04	4.8E+04	5.7E+04	0.150	0.253	0.381	0.537
5	19.526	83.699	0.41	3.0	3.9	4.8	5.7	2.8	4.7	7.1	10.0	4.5E+04	5.8E+04	7.1E+04	8.5E+04	0.299	0.502	0.758	1.066
6	23.865	56.742	0.41	3.7	4.8	5.9	7.0	4.2	7.1	10.7	15.0	6.7E+04	8.7E+04	1.1E+05	1.3E+05	0.442	0.743		
7	29.168	22.559	0.41	4.5	5.9	7.2	8.5	6.3	10.5	15.9	22.4	1.0E+05	1.3E+05	1.6E+05	1.9E+05	0.378			
8	32.355	1.743	0.41	5.0	6.5	8.0	9.5	7.7	13.0	19.6	27.6	1.2E+05	1.6E+05	2.0E+05	2.3E+05				
			0.41			PNW(windgust)		6.24								3.026			
	Avg dia (in)	Mid ht. (ft)	f 2 (Hz)	V1 (mph - 3s)	V2 (mph - 3s)	V3 (mph - 3s)	V4 (mph - 3s)	Pvs1 (psf)	Pvs2 (psf)	Pvs3 (psf)	Pvs4 (psf)	Re1 300≤Re≤1.0E+05 Re>3.5E+06	Re2	Re3	Re4	Sr1 (ksi)	Sr2 (ksi)	Sr3 (ksi)	Sr4 (ksi)
1	8.750	145.298	1.433	4.7	6.1	7.5	9.0	6.9	11.6	17.5	24.6	3.1E+04	4.1E+04	5.0E+04	5.9E+04	0.276	0.465	0.702	0.987
2	10.694	134.849	1.433	5.8	7.5	9.2	10.9	10.3	17.3	26.1	36.8	4.7E+04	6.1E+04	7.5E+04	8.9E+04	0.439	0.738	1.115	1.568
3	13.071	121.891	1.433	7.1	9.2	11.3	13.4	15.4	25.9	39.0	54.9	7.0E+04	9.1E+04	1.1E+05	1.3E+05	0.991	1.666		
4	15.976	105.113	1.433	8.6	11.2	13.8	16.3	23.0	38.6	58.3	82.1	1.0E+05	1.4E+05	1.7E+05	2.0E+05	1.823			
5	19.526	83.699	1.433	10.6	13.7	16.8	20.0	34.3	57.7	87.1	122.6	1.6E+05	2.0E+05	2.5E+05	3.0E+05				
6	23.865	56.742	1.433	12.9	16.8	20.6	24.4	51.3	86.2	130.2	183.2	2.3E+05	3.0E+05	3.7E+05	4.4E+05				
7	29.168	22.559	1.433	15.8	20.5	25.2	29.8	76.6	128.8	194.5	273.6	3.5E+05	4.5E+05	5.6E+05	6.6E+05				
8	32.355	1.743	1.433	17.5	22.7	27.9	33.1	94.2	158.5	239.3	336.7	4.3E+05	5.6E+05	6.8E+05	8.1E+05				
	Avg dia (in)	Mid ht. (ft)	f 3 (Hz)	V1 (mph - 3s)	V2 (mph - 3s)	V3 (mph - 3s)	V4 (mph - 3s)	Pvs1 (psf)	Pvs2 (psf)	Pvs3 (psf)	Pvs4 (psf)	Re1 300≤Re≤1.0E+05 Re>3.5E+06	Re2	Re3	Re4	Sr1 (ksi)	Sr2 (ksi)		
1	8.750	145.298	3.559	11.8	15.3	18.7	22.2	42.5	71.5	107.9	151.9	7.8E+04	1.0E+05	1.2E+05	1.5E+05	1.700	2.859		
2	10.694	134.849	3.559	14.4	18.6	22.9	27.2	63.5	106.8	161.2	226.9	1.2E+05	1.5E+05	1.9E+05	2.2E+05				
3	13.071	121.891	3.559	17.6	22.8	28.0	33.2	94.9	159.5	240.9	338.9	1.7E+05	2.3E+05	2.8E+05	3.3E+05				
4	15.976	105.113	3.559	21.5	27.9	34.2	40.6	141.7	238.3	359.8	506.3	2.6E+05	3.4E+05	4.1E+05	4.9E+05				
5	19.526	83.699	3.559	26.3	34.0	41.8	49.6	211.7	356.0	537.5	756.3	3.9E+05	5.0E+05	6.2E+05	7.3E+05				
6	23.865	56.742	3.559	32.1	41.6	51.1	60.6	316.3	531.8	802.9	1129.8	5.8E+05	7.5E+05	9.3E+05	1.1E+06				
7	29.168	22.559	3.559	39.2	50.9	62.5	74.1	472.5	794.4	1199.4	1687.7	8.7E+05	1.1E+06	1.4E+06	1.6E+06				
8	32.355	1.743	3.559	43.5	56.4	69.3	82.2	581.3	977.4	1475.9	2076.6	1.1E+06	1.4E+06	1.7E+06	2.0E+06				

	Stress ranges for pole with GS				SAT (N-S)-Open Terrain probabilities								seconds in each bin			cycles in each bin		
Segment	Sr1 (ksi)	Sr2 (ksi)	Sr3 (ksi)	Sr4 (ksi)	P(V<V1)	P(V<V2)	P(V<V3)	P(V<V4)	P(V1<V<V2)	P(V2<V<V3)	P(V3<V<V4)		t_bin1	t_bin2	t_bin3	N_bin1	N_bin2	N_bin3
1	0.010	0.017	0.026	0.037	0.01%	0.05%	0.19%	0.51%	0.04%	0.14%	0.31%		445006.7017	1392887.61	3119143.039	1.82E+05	5.71E+05	1.28E+06
2	0.017	0.028	0.043	0.060	0.03%	0.18%	0.56%	1.33%	0.14%	0.39%	0.77%		1412038.525	3830108.949	7616118.426	5.79E+05	1.57E+06	3.12E+06
3	0.039	0.066	0.099	0.140	0.11%	0.50%	1.42%	3.05%	0.39%	0.92%	1.63%		3885574.861	9154508.034	16198000.41	1.59E+06	3.75E+06	6.64E+06
4	0.070	0.118	0.178	0.251	0.32%	1.25%	3.15%	6.16%	0.93%	1.91%	3.01%		9212391.368	18941043.38	29942850.58	3.78E+06	7.77E+06	1.23E+07
5	0.139	0.235	0.354	0.498	0.79%	2.67%	6.07%	10.91%	1.88%	3.40%	4.84%		18696984.47	33833798.8	48131384.02	7.67E+06	1.39E+07	1.97E+07
6	0.206	0.347			1.57%	4.77%	9.95%	16.69%	3.20%	5.18%	6.74%		31780708.04	51536815.45	66973739.42	1.30E+07	2.11E+07	2.75E+07
7	0.176				2.09%	6.04%	12.14%	19.75%	3.95%	6.10%	7.62%		39228325.86	60624052.43	75717919.58	1.61E+07		
8					0.53%	1.91%	4.55%	8.50%	1.38%	2.64%	3.95%		13710721.81	26295898.81	39247879.58			
	1.414											E-W Gusts	11298933.27			4.63E+06		
	Sr1 (ksi)	Sr2 (ksi)	Sr3 (ksi)	Sr4 (ksi)	P(V<V1)	P(V<V2)	P(V<V3)	P(V<V4)	P(V1<V<V2)	P(V2<V<V3)	P(V3<V<V4)		t_bin1	t_bin2	t_bin3	N_bin1	N_bin2	N_bin3
1	0.129	0.217	0.328	0.461	7.68%	17.27%	28.76%	40.42%	9.59%	11.50%	11.65%		95337436.02	114297999.9	115845361.9	1.37E+08	1.64E+08	1.66E+08
2	0.205	0.345	0.521	0.733	14.13%	27.72%	41.77%	54.38%	13.59%	14.05%	12.61%		135138489	139670903.2	125332994.2	1.94E+08	2.00E+08	1.80E+08
3	0.463	0.778			23.29%	40.29%	55.46%	67.55%	17.00%	15.18%	12.08%		168980302	150902370.6		2.42E+08	2.16E+08	
4	0.852				34.56%	53.43%	68.06%	78.44%	18.87%	14.63%	10.38%							
5					46.51%	65.39%	78.21%	86.37%	18.88%	12.82%	8.16%							
6					57.04%	74.56%	85.18%	91.34%	17.52%	10.62%	6.16%							
7					61.54%	78.13%	87.70%	93.03%	16.60%	9.56%	5.33%							
8					40.97%	60.06%	73.84%	83.05%	19.10%	13.77%	9.21%							
	Sr1 (ksi)	Sr2 (ksi)			P(V<V1)	P(V<V2)	P(V<V3)	P(V<V4)	P(V1<V<V2)	P(V2<V<V3)	P(V3<V<V4)		t_bin1	t_bin2	t_bin3	N_bin1	N_bin2	N_bin3
1	0.794	1.336			60.47%	77.31%	87.12%	92.65%	16.83%	9.82%	5.52%		167367853.2			5.96E+08		
2					73.18%	86.47%	93.12%	96.43%	13.29%	6.65%	3.31%							
3					83.23%	92.60%	96.64%	98.41%	9.37%	4.04%	1.78%							
4					90.24%	96.24%	98.47%	99.34%	6.00%	2.23%	0.87%							
5					94.58%	98.16%	99.33%	99.74%	3.59%	1.17%	0.41%							
6					96.93%	99.07%	99.69%	99.89%	2.14%	0.62%	0.20%							
7					97.65%	99.32%	99.78%	99.92%	1.68%	0.46%	0.14%							
8					92.84%	97.43%	99.01%	99.60%	4.58%	1.59%	0.58%							

	Avg Sr (No GS)			Avg Sr (w/GS)			SAT(N-S)-Suburban Terrain probabilities							seconds in each bin			cycles in each bin		
Segment	S_bin1	S_bin2	S_bin3	S_bin1	S_bin2	S_bin3	P(V<V1)	P(V<V2)	P(V<V3)	P(V<V4)	P(V1<V<V2	P(V2<V<V3)	P(V3<V<V4)	t_bin1	t_bin2	t_bin3	N_bin1	N_bin2	N_bin3
1	0.030	0.047	0.068	0.014	0.022	0.032	0.03%	0.14%	0.45%	1.09%	0.11%	0.31%	0.64%	1109668.758	3105426.51	6337116.786	4.55E+05	1.27E+06	2.60E+06
2	0.048	0.076	0.110	0.023	0.035	0.051	0.08%	0.39%	1.15%	2.52%	0.31%	0.75%	1.37%	3076542.725	7499457.24	13649029.29	1.26E+06	3.07E+06	5.60E+06
3	0.112	0.176	0.255	0.052	0.082	0.119	0.24%	0.99%	2.57%	5.15%	0.74%	1.58%	2.58%	7388765.725	15756989.77	25673524.37	3.03E+06	6.46E+06	1.05E+07
4	0.201	0.317	0.459	0.094	0.148	0.214	0.60%	2.14%	5.02%	9.25%	1.53%	2.88%	4.23%	15226367.19	28646461.59	42082309.15	6.24E+06	1.17E+07	1.73E+07
5	0.400	0.630	0.912	0.187	0.294	0.426	1.25%	3.93%	8.44%	14.50%	2.68%	4.52%	6.06%	26654905.57	44899689.78	60206995.68	1.09E+07	1.84E+07	2.47E+07
6	0.592	0.743		0.277	0.347		2.02%	5.86%	11.83%	19.33%	3.84%	5.97%	7.50%	38195997.63	59400194.42	74573894.18	1.57E+07	2.44E+07	3.06E+07
7	0.378			0.176			1.76%	5.24%	10.77%	17.84%	3.48%	5.53%	7.08%	34551795.74	54989859.69	70365152.94	1.42E+07		
8							0.10%	0.44%	1.26%	2.75%	0.34%	0.82%	1.48%	3416043.551	8201924.36	14741533.41			
	3.026			1.414															
	S_bin1	S_bin2	S_bin3	S_bin1	S_bin2	S_bin3	P(V<V1)	P(V<V2)	P(V<V3)	P(V<V4)	P(V1<V<V2	P(V2<V<V3)	P(V3<V<V4)	t_bin1	t_bin2	t_bin3	N_bin1	N_bin2	N_bin3
1	0.370	0.583	0.844	0.173	0.272	0.394	12.48%	25.21%	38.80%	51.32%	12.73%	13.59%	12.52%	126561850.9	135111345.8	124503219.9	1.81E+08	1.94E+08	1.78E+08
2	0.589	0.926	1.341	0.275	0.433	0.627	20.82%	37.10%	52.16%	64.50%	16.28%	15.06%	12.34%	161833233	149716917.3	122690859.3	2.32E+08	2.15E+08	1.76E+08
3	1.329	1.666		0.621	0.778		31.34%	49.89%	64.82%	75.75%	18.55%	14.93%	10.93%	184390342.2	148483345.6		2.64E+08	2.13E+08	
4							42.79%	61.85%	75.33%	84.20%	19.06%	13.48%	8.87%						
5							53.41%	71.53%	82.96%	89.80%	18.12%	11.42%	6.84%						
6							60.96%	77.69%	87.39%	92.82%	16.73%	9.70%	5.43%						
7							58.81%	75.99%	86.20%	92.03%	17.18%	10.21%	5.83%						
8							21.90%	38.51%	53.63%	65.87%	16.61%	15.12%	12.24%						
	S_bin1	S_bin2	S_bin3	S_bin1			P(V<V1)	P(V<V2)	P(V<V3)	P(V<V4)	P(V1<V<V2	P(V2<V<V3)	P(V3<V<V4)	t_bin1	t_bin2	t_bin3	N_bin1	N_bin2	N_bin3
1	2.280			1.065			70.59%	84.73%	92.04%	95.78%	14.14%	7.32%	3.74%	140568958.5			5.00E+08		
2							81.06%	91.36%	95.97%	98.05%	10.30%	4.60%	2.09%						
3							88.62%	95.45%	98.09%	99.16%	6.83%	2.65%	1.07%						
4							93.46%	97.69%	99.13%	99.65%	4.23%	1.43%	0.52%						
5							96.23%	98.81%	99.59%	99.85%	2.58%	0.78%	0.26%						
6							97.56%	99.29%	99.77%	99.92%	1.73%	0.48%	0.15%						
7							97.23%	99.18%	99.73%	99.90%	1.95%	0.55%	0.17%						
8							82.04%	91.93%	96.28%	98.22%	9.89%	4.35%	1.94%						

	DFW(N-S)-Open Terrain probabilities								seconds in each bin			cycles in each bin			
Segment	P(V<V1)	P(V<V2)	P(V<V3)	P(V<V4)	P(V1<V<V2)	P(V2<V<V3)	P(V3<V<V4)		t_bin1	t_bin2	t_bin3	N_bin1	N_bin2	N_bin3	
1	0.00%	0.00%	0.01%	0.04%	0.00%	0.01%	0.03%		19561.64	105476.8	359551.6	8.02E+03	4.32E+04	1.47E+05	
2	0.00%	0.01%	0.05%	0.17%	0.01%	0.04%	0.12%		99446.23	448916.3	1319292	4.08E+04	1.84E+05	5.41E+05	
3	0.01%	0.04%	0.18%	0.55%	0.04%	0.14%	0.36%		420810.7	1594834	4050937	1.73E+05	6.54E+05	1.66E+06	
4	0.02%	0.15%	0.57%	1.49%	0.13%	0.42%	0.92%		1466129	4691962	10351939	6.01E+05	1.92E+06	4.24E+06	
5	0.08%	0.45%	1.46%	3.41%	0.37%	1.01%	1.95%		4153474	11342328	21931520	1.70E+06	4.65E+06	8.99E+06	
6	0.21%	1.03%	2.99%	6.36%	0.82%	1.95%	3.37%		9207586	21939898	37881501	3.78E+06	9.00E+06	1.55E+07	
7	0.32%	1.45%	3.99%	8.15%	1.13%	2.54%	4.17%		12694225	28489979	46806619	5.20E+06			
8	0.05%	0.28%	0.97%	2.37%	0.23%	0.69%	1.41%		2625228	7706021	15822709				
								E-W Gusts	19820568			8.13E+06			
	P(V<V1)	P(V<V2)	P(V<V3)	P(V<V4)	P(V1<V<V2)	P(V2<V<V3)	P(V3<V<V4)		t_bin1	t_bin2	t_bin3	N_bin1	N_bin2	N_bin3	
1	2.05%	6.69%	14.27%	23.87%	4.64%	7.59%	9.59%		52068136	85188842	1.08E+08	7.46E+07	1.22E+08	1.54E+08	
2	4.98%	13.51%	25.10%	37.68%	8.53%	11.59%	12.58%		95736796	1.3E+08	1.41E+08	1.37E+08	1.87E+08	2.02E+08	
3	10.41%	23.75%	38.86%	52.97%	13.34%	15.11%	14.11%		1.5E+08	1.7E+08		2.15E+08	2.43E+08		
4	18.82%	36.67%	53.61%	67.30%	17.85%	16.95%	13.69%								
5	29.60%	50.32%	66.98%	78.72%	20.72%	16.66%	11.74%								
6	40.60%	62.02%	76.96%	86.32%	21.42%	14.94%	9.37%								
7	45.72%	66.88%	80.73%	88.98%	21.16%	13.85%	8.25%								
8	24.37%	44.01%	61.06%	73.84%	19.65%	17.04%	12.78%								
	P(V<V1)	P(V<V2)	P(V<V3)	P(V<V4)	P(V1<V<V2)	P(V2<V<V3)	P(V3<V<V4)		t_bin1	t_bin2	t_bin3	N_bin1	N_bin2	N_bin3	
1	44.48%	65.73%	79.86%	88.38%	21.25%	14.13%	8.52%		2.39E+08			8.49E+08			
2	60.18%	78.87%	89.13%	94.42%	18.69%	10.26%	5.29%								
3	74.10%	88.31%	94.76%	97.61%	14.21%	6.45%	2.85%								
4	84.62%	94.11%	97.70%	99.07%	9.49%	3.59%	1.37%								
5	91.45%	97.21%	99.05%	99.65%	5.77%	1.84%	0.61%								
6	95.22%	98.65%	99.59%	99.86%	3.43%	0.94%	0.28%								
7	96.39%	99.04%	99.72%	99.91%	2.65%	0.68%	0.19%								
8	88.69%	96.03%	98.56%	99.45%	7.34%	2.53%	0.89%								

DFW (N-S)-Suburban Terrain probabilities									seconds in each bin			cycles in each bin		
Segment	P(V<V1)	P(V<V2)	P(V<V3)	P(V<V4)	P(V1<V<V2)	P(V2<V<V3)	P(V3<V<V4)		t_bin1	t_bin2	t_bin3	N_bin1	N_bin2	N_bin3
1	0.00%	0.01%	0.04%	0.13%	0.01%	0.03%	0.09%		70723.31	331874	1007387	2.90E+04	1.36E+05	4.13E+05
2	0.00%	0.03%	0.14%	0.42%	0.03%	0.11%	0.28%		301186.8	1190754	3133023	1.23E+05	4.88E+05	1.28E+06
3	0.02%	0.11%	0.43%	1.15%	0.09%	0.32%	0.73%		1063681	3562074	8161648	4.36E+05	1.46E+06	3.35E+06
4	0.06%	0.33%	1.11%	2.68%	0.27%	0.78%	1.57%		3064176	8782109	17677420	1.26E+06	3.60E+06	7.25E+06
5	0.15%	0.78%	2.35%	5.17%	0.63%	1.57%	2.82%		7058449	17633075	31663996	2.89E+06	7.23E+06	1.30E+07
6	0.30%	1.39%	3.84%	7.90%	1.09%	2.45%	4.06%		12185846	27563268	45578226	5.00E+06	1.13E+07	1.87E+07
7	0.25%	1.18%	3.35%	7.02%	0.93%	2.17%	3.67%		10455443	24339211	41218849	4.29E+06		
8	0.00%	0.04%	0.16%	0.47%	0.03%	0.12%	0.31%		349863.7	1357449	3516100			
	P(V<V1)	P(V<V2)	P(V<V3)	P(V<V4)	P(V1<V<V2)	P(V2<V<V3)	P(V3<V<V4)		t_bin1	t_bin2	t_bin3	N_bin1	N_bin2	N_bin3
1	4.15%	11.72%	22.43%	34.45%	7.57%	10.71%	12.02%		84953207	1.2E+08	1.35E+08	1.22E+08	1.72E+08	1.93E+08
2	8.82%	20.95%	35.32%	49.24%	12.13%	14.37%	13.91%		1.36E+08	1.61E+08	1.56E+08	1.95E+08	2.31E+08	2.24E+08
3	16.24%	32.97%	49.63%	63.61%	16.73%	16.66%	13.99%		1.88E+08	1.87E+08		2.69E+08	2.68E+08	
4	26.04%	46.09%	63.05%	75.51%	20.05%	16.96%	12.46%							
5	36.65%	58.03%	73.70%	83.93%	21.39%	15.67%	10.23%							
6	45.05%	66.26%	80.26%	88.65%	21.21%	14.00%	8.40%							
7	42.58%	63.94%	78.47%	87.40%	21.36%	14.53%	8.93%							
8	9.50%	22.17%	36.88%	50.90%	12.67%	14.71%	14.02%							
	P(V<V1)	P(V<V2)	P(V<V3)	P(V<V4)	P(V1<V<V2)	P(V2<V<V3)	P(V3<V<V4)		t_bin1	t_bin2	t_bin3	N_bin1	N_bin2	N_bin3
1	56.81%	76.29%	87.43%	93.38%	19.47%	11.14%	5.95%		2.19E+08			7.78E+08		
2	70.98%	86.36%	93.68%	97.03%	15.38%	7.31%	3.36%							
3	82.12%	92.84%	97.10%	98.79%	10.72%	4.26%	1.69%							
4	89.66%	96.46%	98.74%	99.53%	6.79%	2.28%	0.79%							
5	94.10%	98.25%	99.44%	99.81%	4.14%	1.20%	0.37%							
6	96.25%	98.99%	99.71%	99.91%	2.75%	0.71%	0.20%							
7	95.71%	98.81%	99.65%	99.89%	3.11%	0.83%	0.24%							
8	72.39%	87.25%	94.18%	97.30%	14.86%	6.92%	3.13%							

		IAH (N-S)-Open Terrain probabilities								seconds in each bin			cycles in each bin		
Segment		P(V<V1)	P(V<V2)	P(V<V3)	P(V<V4)	P(V1<V<V2)	P(V2<V<V3)	P(V3<V<V4)		t_bin1	t_bin2	t_bin3	N_bin1	N_bin2	N_bin3
1		0.00%	0.02%	0.08%	0.25%	0.01%	0.06%	0.17%		112126.8	486421.1	1379145	4.60E+04	1.99E+05	5.65E+05
2		0.01%	0.07%	0.28%	0.80%	0.06%	0.21%	0.52%		472065.8	1707322	4159575	1.94E+05	7.00E+05	1.71E+06
3		0.04%	0.25%	0.87%	2.19%	0.21%	0.63%	1.32%		1656863	5009825	10514571	6.79E+05	2.05E+06	4.31E+06
4		0.14%	0.74%	2.27%	5.06%	0.60%	1.53%	2.78%		4811497	12233810	22231156	1.97E+06	5.02E+06	9.11E+06
5		0.42%	1.86%	4.96%	9.89%	1.44%	3.10%	4.93%		11478110	24804482	39382991	4.71E+06	1.02E+07	1.61E+07
6		0.99%	3.73%	8.89%	16.18%	2.74%	5.16%	7.29%		21934018	41215858	58280802	8.99E+06	1.69E+07	2.39E+07
7		1.39%	4.93%	11.20%	19.61%	3.54%	6.26%	8.42%		28324386	50053296	67268554	1.16E+07		
8		0.26%	1.24%	3.53%	7.38%	0.98%	2.28%	3.86%		7846465	18259889	30829303			
									E-W Gusts	22874717			9.38E+06		
		P(V<V1)	P(V<V2)	P(V<V3)	P(V<V4)	P(V1<V<V2)	P(V2<V<V3)	P(V3<V<V4)		t_bin1	t_bin2	t_bin3	N_bin1	N_bin2	N_bin3
1		6.55%	16.82%	29.94%	43.43%	10.27%	13.12%	13.49%		82074050	1.05E+08	1.08E+08	1.18E+08	1.50E+08	1.54E+08
2		13.36%	28.74%	44.99%	59.27%	15.38%	16.25%	14.29%		1.23E+08	1.3E+08	1.14E+08	1.76E+08	1.86E+08	1.64E+08
3		23.64%	43.28%	60.48%	73.45%	19.64%	17.20%	12.97%		1.57E+08	1.38E+08		2.25E+08	1.97E+08	
4		36.65%	58.22%	73.98%	84.21%	21.57%	15.76%	10.24%							
5		50.42%	71.20%	84.00%	91.23%	20.78%	12.80%	7.23%							
6		62.22%	80.51%	90.23%	95.11%	18.29%	9.73%	4.88%							
7		67.10%	83.93%	92.31%	96.30%	16.82%	8.39%	3.99%							
8		44.06%	65.52%	79.80%	88.40%	21.45%	14.28%	8.60%							
		P(V<V1)	P(V<V2)	P(V<V3)	P(V<V4)	P(V1<V<V2)	P(V2<V<V3)	P(V3<V<V4)		t_bin1	t_bin2	t_bin3	N_bin1	N_bin2	N_bin3
1		65.96%	83.15%	91.85%	96.04%	17.19%	8.70%	4.19%		1.37E+08			4.89E+08		
2		79.14%	91.31%	96.37%	98.44%	12.17%	5.06%	2.08%							
3		88.55%	96.01%	98.56%	99.46%	7.46%	2.55%	0.89%							
4		94.30%	98.34%	99.48%	99.83%	4.04%	1.15%	0.35%							
5		97.33%	99.34%	99.82%	99.95%	2.01%	0.48%	0.12%							
6		98.72%	99.73%	99.94%	99.98%	1.01%	0.21%	0.05%							
7		99.10%	99.82%	99.96%	99.99%	0.72%	0.14%	0.03%							
8		96.18%	98.98%	99.71%	99.91%	2.81%	0.72%	0.20%							

Segment	IAH (N-S)-Suburban Terrain probabilities							seconds in each bin			cycles in each bin		
	P(V<V1)	P(V<V2)	P(V<V3)	P(V<V4)	P(V1<V<V2)	P(V2<V<V3)	P(V3<V<V4)	t_bin1	t_bin2	t_bin3	N_bin1	N_bin2	N_bin3
1	0.01%	0.05%	0.21%	0.63%	0.04%	0.16%	0.41%	349860.6	1316562	3315408	1.43E+05	5.40E+05	1.36E+06
2	0.03%	0.18%	0.67%	1.74%	0.16%	0.49%	1.07%	1240854	3917956	8524661	5.09E+05	1.61E+06	3.50E+06
3	0.10%	0.56%	1.78%	4.09%	0.46%	1.22%	2.31%	3666021	9765056	18444151	1.50E+06	4.00E+06	7.56E+06
4	0.31%	1.42%	3.96%	8.15%	1.12%	2.54%	4.19%	8924160	20265258	33526478	3.66E+06	8.31E+06	1.37E+07
5	0.74%	2.96%	7.33%	13.76%	2.21%	4.37%	6.43%	17704285	34920567	51402572	7.26E+06	1.43E+07	2.11E+07
6	1.33%	4.76%	10.87%	19.14%	3.43%	6.11%	8.27%	27423132	48850166	66088031	1.12E+07	2.00E+07	2.71E+07
7	1.13%	4.17%	9.74%	17.47%	3.04%	5.57%	7.73%	24280429	44546842	61755929	9.95E+06		
8	0.03%	0.21%	0.76%	1.93%	0.18%	0.55%	1.17%	1412654	4375376	9368609			
	P(V<V1)	P(V<V2)	P(V<V3)	P(V<V4)	P(V1<V<V2)	P(V2<V<V3)	P(V3<V<V4)	t_bin1	t_bin2	t_bin3	N_bin1	N_bin2	N_bin3
1	11.57%	25.84%	41.56%	55.86%	14.27%	15.72%	14.30%	1.14E+08	1.26E+08	1.14E+08	1.64E+08	1.80E+08	1.64E+08
2	20.83%	39.60%	56.80%	70.26%	18.77%	17.20%	13.46%	1.5E+08	1.38E+08	1.08E+08	2.15E+08	1.97E+08	1.54E+08
3	32.92%	54.25%	70.60%	81.66%	21.32%	16.35%	11.06%	1.7E+08	1.31E+08		2.44E+08	1.87E+08	
4	46.16%	67.44%	81.25%	89.40%	21.29%	13.81%	8.14%						
5	58.20%	77.51%	88.31%	93.96%	19.31%	10.80%	5.65%						
6	66.48%	83.50%	92.06%	96.16%	17.02%	8.56%	4.10%						
7	64.15%	81.89%	91.09%	95.61%	17.74%	9.20%	4.52%						
8	22.05%	41.22%	58.45%	71.70%	19.17%	17.22%	13.25%						
	P(V<V1)	P(V<V2)	P(V<V3)	P(V<V4)	P(V1<V<V2)	P(V2<V<V3)	P(V3<V<V4)	t_bin1	t_bin2	t_bin3	N_bin1	N_bin2	N_bin3
1	76.56%	89.85%	95.62%	98.07%	13.29%	5.77%	2.45%	1.06E+08			3.78E+08		
2	86.62%	95.13%	98.18%	99.29%	8.51%	3.05%	1.11%						
3	93.04%	97.87%	99.31%	99.76%	4.83%	1.44%	0.45%						
4	96.60%	99.12%	99.75%	99.92%	2.52%	0.63%	0.17%						
5	98.33%	99.63%	99.91%	99.97%	1.29%	0.28%	0.07%						
6	99.05%	99.81%	99.96%	99.99%	0.76%	0.15%	0.03%						
7	98.88%	99.77%	99.95%	99.99%	0.89%	0.18%	0.04%						
8	87.51%	95.54%	98.36%	99.37%	8.03%	2.82%	1.01%						

	RMMA (N-S)-Open Terrain probabilities								seconds in each bin			cycles in each bin			
Segment	P(V<V1)	P(V<V2)	P(V<V3)	P(V<V4)	P(V1<V<V2)	P(V2<V<V3)	P(V3<V<V4)		t_bin1	t_bin2	t_bin3	N_bin1	N_bin2	N_bin3	
1	0.00%	0.01%	0.04%	0.13%	0.01%	0.03%	0.09%		67662.49	320298.2	977219.6	2.77E+04	1.31E+05	4.01E+05	
2	0.00%	0.03%	0.15%	0.45%	0.03%	0.12%	0.31%		307219.2	1213686	3184282	1.26E+05	4.98E+05	1.31E+06	
3	0.02%	0.13%	0.50%	1.33%	0.11%	0.37%	0.83%		1161514	3840215	8686168	4.76E+05	1.57E+06	3.56E+06	
4	0.07%	0.42%	1.39%	3.28%	0.35%	0.97%	1.89%		3624445	10087125	19769575	1.49E+06	4.14E+06	8.11E+06	
5	0.23%	1.12%	3.22%	6.81%	0.89%	2.10%	3.60%		9249228	21899953	37528476	3.79E+06	8.98E+06	1.54E+07	
6	0.57%	2.36%	6.06%	11.71%	1.80%	3.70%	5.65%		18728113	38592173	58934323	7.68E+06	1.58E+07	2.42E+07	
7	0.82%	3.20%	7.81%	14.50%	2.38%	4.61%	6.69%		24806936	48092141	69820038	1.02E+07			
8	0.14%	0.73%	2.22%	4.95%	0.59%	1.50%	2.73%		6131690	15627281	28467335				
								E-W Gusts	18359523			7.53E+06			
	P(V<V1)	P(V<V2)	P(V<V3)	P(V<V4)	P(V1<V<V2)	P(V2<V<V3)	P(V3<V<V4)		t_bin1	t_bin2	t_bin3	N_bin1	N_bin2	N_bin3	
1	4.35%	12.23%	23.29%	35.60%	7.88%	11.07%	12.31%		82188983	1.15E+08	1.28E+08	1.18E+08	1.65E+08	1.84E+08	
2	9.48%	22.24%	37.08%	51.21%	12.76%	14.84%	14.13%		1.33E+08	1.55E+08	1.47E+08	1.91E+08	2.22E+08	2.11E+08	
3	17.86%	35.46%	52.45%	66.33%	17.60%	16.99%	13.88%		1.84E+08	1.77E+08		2.63E+08	2.54E+08		
4	29.31%	50.13%	66.92%	78.75%	20.83%	16.79%	11.83%								
5	42.33%	63.85%	78.49%	87.47%	21.52%	14.64%	8.98%								
6	54.25%	74.36%	86.19%	92.63%	20.11%	11.83%	6.44%								
7	59.41%	78.41%	88.89%	94.30%	18.99%	10.48%	5.42%								
8	36.20%	57.72%	73.54%	83.87%	21.52%	15.82%	10.33%								
	P(V<V1)	P(V<V2)	P(V<V3)	P(V<V4)	P(V1<V<V2)	P(V2<V<V3)	P(V3<V<V4)		t_bin1	t_bin2	t_bin3	N_bin1	N_bin2	N_bin3	
1	58.19%	77.47%	88.28%	93.93%	19.28%	10.80%	5.65%		2.01E+08			7.16E+08			
2	72.78%	87.58%	94.39%	97.43%	14.79%	6.81%	3.04%								
3	84.07%	93.89%	97.61%	99.04%	9.81%	3.73%	1.42%								
4	91.52%	97.27%	99.08%	99.67%	5.74%	1.81%	0.59%								
5	95.77%	98.85%	99.66%	99.89%	3.08%	0.81%	0.23%								
6	97.86%	99.50%	99.87%	99.96%	1.64%	0.37%	0.09%								
7	98.45%	99.66%	99.92%	99.98%	1.21%	0.26%	0.06%								
8	94.12%	98.27%	99.46%	99.82%	4.15%	1.19%	0.36%								

	RMMA (N-S)-Suburban Terrain probabilities								seconds in each bin			cycles in each bin			
Segment	P(V<V1)	P(V<V2)	P(V<V3)	P(V<V4)	P(V1<V<V2)	P(V2<V<V3)	P(V3<V<V4)		t_bin1	t_bin2	t_bin3	N_bin1	N_bin2	N_bin3	
1	0.00%	0.02%	0.11%	0.35%	0.02%	0.09%	0.24%		223966.9037	920401.8003	2495583.306	9.18E+04	3.77E+05	1.02E+06	
2	0.01%	0.09%	0.38%	1.04%	0.08%	0.28%	0.66%		854384.2687	2949016.71	6913813.802	3.50E+05	1.21E+06	2.83E+06	
3	0.05%	0.31%	1.07%	2.61%	0.26%	0.76%	1.54%		2708809.039	7895519.749	16080752.83	1.11E+06	3.24E+06	6.59E+06	
4	0.16%	0.84%	2.52%	5.52%	0.68%	1.68%	3.00%		7045034.891	17523167.13	31281884.16	2.89E+06	7.18E+06	1.28E+07	
5	0.42%	1.84%	4.91%	9.79%	1.42%	3.07%	4.88%		14816235.57	32038102.96	50919581.58	6.07E+06	1.31E+07	2.09E+07	
6	0.78%	3.08%	7.56%	14.11%	2.29%	4.48%	6.55%		23938195.32	46778575.49	68362011.65	9.81E+06	1.92E+07	2.80E+07	
7	0.66%	2.66%	6.70%	12.75%	2.01%	4.04%	6.05%		20937752.2	42132341.68	63085766.98	8.58E+06			
8	0.02%	0.11%	0.43%	1.16%	0.09%	0.32%	0.73%		980480.1057	3320107.14	7660738.201				
	P(V<V1)	P(V<V2)	P(V<V3)	P(V<V4)	P(V1<V<V2)	P(V2<V<V3)	P(V3<V<V4)		t_bin1	t_bin2	t_bin3	N_bin1	N_bin2	N_bin3	
1	8.09%	19.73%	33.85%	47.74%	11.64%	14.11%	13.90%		121470941.3	147210461.7	144974369.1	1.74E+08	2.11E+08	2.08E+08	
2	15.50%	32.01%	48.69%	62.82%	16.51%	16.68%	14.13%		172257128.9	173965775.7	147459547.4	2.47E+08	2.49E+08	2.11E+08	
3	25.94%	46.12%	63.19%	75.71%	20.18%	17.08%	12.52%		210538658.3	178143204.9		3.02E+08	2.55E+08		
4	38.20%	59.78%	75.24%	85.13%	21.58%	15.46%	9.89%								
5	50.11%	70.91%	83.77%	91.07%	20.79%	12.86%	7.30%								
6	58.75%	77.90%	88.56%	94.10%	19.15%	10.66%	5.54%								
7	56.28%	75.98%	87.29%	93.32%	19.71%	11.31%	6.03%								
8	16.52%	33.53%	50.36%	64.40%	17.01%	16.83%	14.04%								
	P(V<V1)	P(V<V2)	P(V<V3)	P(V<V4)	P(V1<V<V2)	P(V2<V<V3)	P(V3<V<V4)		t_bin1	t_bin2	t_bin3	N_bin1	N_bin2	N_bin3	
1	69.82%	85.70%	93.34%	96.87%	15.88%	7.64%	3.53%		165688483.3			5.90E+08			
2	81.68%	92.66%	97.03%	98.76%	10.98%	4.37%	1.73%								
3	89.85%	96.57%	98.79%	99.55%	6.72%	2.23%	0.76%								
4	94.72%	98.48%	99.53%	99.85%	3.77%	1.05%	0.31%								
5	97.26%	99.32%	99.82%	99.94%	2.06%	0.49%	0.13%								
6	98.38%	99.64%	99.91%	99.98%	1.26%	0.27%	0.07%								
7	98.11%	99.57%	99.89%	99.97%	1.46%	0.32%	0.08%								
8	82.77%	93.23%	97.30%	98.89%	10.46%	4.08%	1.59%								

	ELP (N-S)Open Terrain probabilities								seconds in each bin			cycles in each bin		
Segment	P(V<V1)	P(V<V2)	P(V<V3)	P(V<V4)	P(V1<V<V2)	P(V2<V<V3)	P(V3<V<V4)		t_bin1	t_bin2	t_bin3	N_bin1	N_bin2	N_bin3
1	0.00%	0.04%	0.18%	0.54%	0.03%	0.14%	0.37%		228207.9	922708.2	2446743	9.36E+04	3.78E+05	1.00E+06
2	0.02%	0.16%	0.61%	1.63%	0.14%	0.45%	1.02%		904549.5	3019661	6824972	3.71E+05	1.24E+06	2.80E+06
3	0.09%	0.54%	1.76%	4.13%	0.44%	1.23%	2.37%		2969903	8209227	15856313	1.22E+06	3.37E+06	6.50E+06
4	0.32%	1.52%	4.28%	8.86%	1.20%	2.76%	4.58%		8030842	18491746	30685235	3.29E+06	7.58E+06	1.26E+07
5	0.90%	3.56%	8.72%	16.14%	2.66%	5.16%	7.43%		17811965	34549110	49725907	7.30E+06	1.42E+07	2.04E+07
6	1.97%	6.73%	14.68%	24.82%	4.75%	7.96%	10.13%		31828119	53268318	67850225	1.30E+07	2.18E+07	2.78E+07
7	2.72%	8.67%	18.01%	29.28%	5.95%	9.34%	11.27%		39855373	62515819	75471233	1.63E+07		
8	0.57%	2.45%	6.39%	12.45%	1.88%	3.95%	6.06%		12595942	26417192	40566830			
								E-W Gusts	1.22E+08			5.01E+07		
	P(V<V1)	P(V<V2)	P(V<V3)	P(V<V4)	P(V1<V<V2)	P(V2<V<V3)	P(V3<V<V4)		t_bin1	t_bin2	t_bin3	N_bin1	N_bin2	N_bin3
1	11.19%	25.67%	41.79%	56.45%	14.47%	16.12%	14.67%		96915907	1.08E+08	98205782	1.39E+08	1.55E+08	1.41E+08
2	21.01%	40.39%	58.04%	71.66%	19.38%	17.65%	13.62%		1.3E+08	1.18E+08	91186803	1.86E+08	1.69E+08	1.31E+08
3	34.31%	56.30%	72.74%	83.52%	22.00%	16.44%	10.78%		1.47E+08	1.1E+08		2.11E+08	1.58E+08	
4	49.30%	70.72%	83.93%	91.33%	21.42%	13.21%	7.40%							
5	63.42%	81.75%	91.18%	95.75%	18.33%	9.43%	4.56%							
6	74.26%	88.77%	95.16%	97.88%	14.50%	6.39%	2.72%							
7	78.42%	91.14%	96.37%	98.48%	12.72%	5.24%	2.11%							
8	57.11%	77.09%	88.26%	94.04%	19.98%	11.17%	5.78%							
	P(V<V1)	P(V<V2)	P(V<V3)	P(V<V4)	P(V1<V<V2)	P(V2<V<V3)	P(V3<V<V4)		t_bin1	t_bin2	t_bin3	N_bin1	N_bin2	N_bin3
1	77.46%	90.61%	96.11%	98.35%	13.14%	5.50%	2.25%		88010481			3.13E+08		
2	87.79%	95.79%	98.51%	99.45%	8.00%	2.72%	0.94%							
3	94.14%	98.34%	99.50%	99.84%	4.20%	1.16%	0.34%							
4	97.46%	99.41%	99.85%	99.96%	1.95%	0.44%	0.11%							
5	98.97%	99.80%	99.96%	99.99%	0.83%	0.16%	0.03%							
6	99.56%	99.93%	99.99%	100.00%	0.36%	0.06%	0.01%							
7	99.71%	99.95%	99.99%	100.00%	0.25%	0.04%	0.01%							
8	98.42%	99.67%	99.92%	99.98%	1.25%	0.25%	0.06%							

		ELP (N-S)Suburban Terrain probabilities								seconds in each bin			cycles in each bin		
Segment		P(V<V1)	P(V<V2)	P(V<V3)	P(V<V4)	P(V1<V<V2)	P(V2<V<V3)	P(V3<V<V4)		t_bin1	t_bin2	t_bin3	N_bin1	N_bin2	N_bin3
1		0.02%	0.12%	0.47%	1.30%	0.10%	0.35%	0.83%		679703.6	2365930	5537014	2.79E+05	9.70E+05	2.27E+06
2		0.07%	0.40%	1.38%	3.34%	0.34%	0.98%	1.96%		2261865	6544038	13129147	9.27E+05	2.68E+06	5.38E+06
3		0.23%	1.16%	3.42%	7.31%	0.93%	2.25%	3.90%		6241221	15093351	26087309	2.56E+06	6.19E+06	1.07E+07
4		0.66%	2.78%	7.10%	13.60%	2.12%	4.32%	6.50%		14168135	28956481	43523172	5.81E+06	1.19E+07	1.78E+07
5		1.52%	5.45%	12.37%	21.56%	3.93%	6.92%	9.20%		26307660	46340718	61580159	1.08E+07	1.90E+07	2.52E+07
6		2.61%	8.40%	17.55%	28.68%	5.79%	9.15%	11.13%		38744038	61288366	74508291	1.59E+07	2.51E+07	3.05E+07
7		2.24%	7.44%	15.93%	26.51%	5.20%	8.49%	10.59%		34816511	56817431	70875137	1.43E+07		
8		0.08%	0.46%	1.54%	3.68%	0.38%	1.08%	2.14%		2556014	7246550	14295188			
		P(V<V1)	P(V<V2)	P(V<V3)	P(V<V4)	P(V1<V<V2)	P(V2<V<V3)	P(V3<V<V4)		t_bin1	t_bin2	t_bin3	N_bin1	N_bin2	N_bin3
1		18.53%	36.97%	54.53%	68.56%	18.44%	17.55%	14.04%		1.23E+08	1.18E+08	93994278	1.77E+08	1.68E+08	1.35E+08
2		30.82%	52.46%	69.43%	81.00%	21.64%	16.97%	11.57%		1.45E+08	1.14E+08	77478739	2.08E+08	1.63E+08	1.11E+08
3		45.18%	67.06%	81.27%	89.58%	21.88%	14.21%	8.31%		1.47E+08	95130886		2.10E+08	1.36E+08	
4		59.23%	78.70%	89.29%	94.65%	19.48%	10.59%	5.36%							
5		70.70%	86.59%	93.99%	97.28%	15.89%	7.39%	3.29%							
6		77.90%	90.85%	96.23%	98.41%	12.95%	5.38%	2.18%							
7		75.93%	89.74%	95.66%	98.14%	13.81%	5.93%	2.47%							
8		32.35%	54.17%	70.92%	82.14%	21.82%	16.75%	11.22%							
		P(V<V1)	P(V<V2)	P(V<V3)	P(V<V4)	P(V1<V<V2)	P(V2<V<V3)	P(V3<V<V4)		t_bin1	t_bin2	t_bin3	N_bin1	N_bin2	N_bin3
1		85.88%	94.93%	98.14%	99.29%	9.04%	3.21%	1.15%		60546486			2.15E+08		
2		92.91%	97.89%	99.34%	99.78%	4.98%	1.45%	0.44%							
3		96.78%	99.21%	99.79%	99.94%	2.43%	0.58%	0.15%							
4		98.62%	99.72%	99.93%	99.98%	1.09%	0.22%	0.05%							
5		99.41%	99.90%	99.98%	100.00%	0.49%	0.08%	0.02%							
6		99.69%	99.95%	99.99%	100.00%	0.26%	0.04%	0.01%							
7		99.63%	99.94%	99.99%	100.00%	0.31%	0.05%	0.01%							
8		93.48%	98.10%	99.42%	99.81%	4.62%	1.31%	0.39%							

Segment	Avg dia (in)	Mid ht. (ft)	f 1 (Hz)	V1 nph - 3	V2 nph - 3	V3 nph - 3	V4 nph - 3	Pvs1 (psf)	Pvs2 (psf)	Pvs3 (psf)	Pvs4 (psf)	Re1 300≤Re≤1.0E+05 Re>3.5E+06	Re2	Re3	Re4	Sr1 (ksi)	Sr2 (ksi)	Sr3 (ksi)	Sr4 (ksi)
				Equivalent Static Pressure Ranges										v(ft2/s)=	0.0001615	Stress ranges for pole with no GS			
1	8.750	170.298	0.358	1.2	1.5	1.9	2.2	0.43	0.72	1.1	1.5	7.9E+03	1.0E+04	1.3E+04	1.5E+04	0.016	0.027	0.041	0.058
2	10.694	159.849	0.358	1.4	1.9	2.3	2.7	0.64	1.08	1.6	2.3	1.2E+04	1.5E+04	1.9E+04	2.2E+04	0.019	0.032	0.048	0.068
3	13.071	146.891	0.358	1.8	2.3	2.8	3.3	0.96	1.6	2.4	3.4	1.8E+04	2.3E+04	2.8E+04	3.3E+04	0.063	0.107	0.161	0.226
4	15.976	130.113	0.358	2.2	2.8	3.4	4.1	1.4	2.4	3.6	5.1	2.6E+04	3.4E+04	4.2E+04	4.9E+04	0.112	0.189	0.285	0.401
5	19.526	108.853	0.358	2.6	3.4	4.2	5.0	2.1	3.6	5.4	7.7	3.9E+04	5.1E+04	6.2E+04	7.4E+04	0.240	0.403	0.609	0.856
6	23.865	81.897	0.358	3.2	4.2	5.1	6.1	3.2	5.4	8.1	11.4	5.8E+04	7.6E+04	9.3E+04	1.1E+05	0.378	0.635	0.959	
7	29.168	46.689	0.358	3.9	5.1	6.3	7.5	4.8	8.0	12.1	17.1	8.7E+04	1.1E+05	1.4E+05	1.6E+05	0.561			
8	34.105	13.373	0.358	4.6	6.0	7.3	8.7	6.5	11.0	16.6	23.3	1.2E+05	1.5E+05	1.9E+05	2.3E+05				
		Pvs(windgu	0.358					6.2								3.6293			
	Avg dia (in)	Mid ht. (ft)	f 2 (Hz)	V1 nph - 3	V2 nph - 3	V3 nph - 3	V4 nph - 3	Pvs1 (psf)	Pvs2 (psf)	Pvs3 (psf)	Pvs4 (psf)	Re1 300≤Re≤1.0E+05 Re>3.5E+06	Re2	Re3	Re4	Sr1 (ksi)	Sr2 (ksi)	Sr3 (ksi)	Sr4 (ksi)
1	8.750	170.298	1.17	3.9	5.0	6.2	7.3	4.6	7.7	11.7	16.4	2.6E+04	3.3E+04	4.1E+04	4.9E+04	0.174	0.293	0.443	0.623
2	10.694	159.849	1.17	4.7	6.1	7.5	8.9	6.9	11.5	17.4	24.5	3.8E+04	5.0E+04	6.1E+04	7.2E+04	0.202	0.340	0.514	0.723
3	13.071	146.891	1.17	5.8	7.5	9.2	10.9	10.3	17.2	26.0	36.6	5.7E+04	7.4E+04	9.1E+04	1.1E+05	0.677	1.138	1.718	
4	15.976	130.113	1.17	7.1	9.2	11.3	13.3	15.3	25.8	38.9	54.7	8.6E+04	1.1E+05	1.4E+05	1.6E+05	1.200			
5	19.526	108.853	1.17	8.6	11.2	13.8	16.3	22.9	38.5	58.1	81.7	1.3E+05	1.7E+05	2.0E+05	2.4E+05				
6	23.865	81.897	1.17	10.5	13.7	16.8	19.9	34.2	57.5	86.8	122.1	1.9E+05	2.5E+05	3.0E+05	3.6E+05				
7	29.168	46.689	1.17	12.9	16.7	20.5	24.4	51.1	85.9	129.6	182.4	2.9E+05	3.7E+05	4.5E+05	5.4E+05				
8	34.105	13.373	1.17	15.1	19.5	24.0	28.5	69.8	117.4	177.2	249.4	3.9E+05	5.1E+05	6.2E+05	7.4E+05				
	Avg dia (in)	Mid ht. (ft)	f 3 (Hz)	V1 nph - 3	V2 nph - 3	V3 nph - 3	V4 nph - 3	Pvs1 (psf)	Pvs2 (psf)	Pvs3 (psf)	Pvs4 (psf)	Re1 300≤Re≤1.0E+05 Re>3.5E+06	Re2	Re3	Re4	Sr1 (ksi)	Sr2 (ksi)		
1	8.750	170.298	2.842	9.4	12.2	15.0	17.8	27.1	45.6	68.8	96.8	6.2E+04	8.1E+04	9.9E+04	1.2E+05	1.029	1.731	2.613	
2	10.694	159.849	2.842	11.5	14.9	18.3	21.7	40.5	68.1	102.8	144.7	9.3E+04	1.2E+05	1.5E+05	1.8E+05	1.194			
3	13.071	146.891	2.842	14.0	18.2	22.4	26.5	60.5	101.7	153.6	216.1	1.4E+05	1.8E+05	2.2E+05	2.6E+05				
4	15.976	130.113	2.842	17.2	22.2	27.3	32.4	90.4	152.0	229.4	322.8	2.1E+05	2.7E+05	3.3E+05	3.9E+05				
5	19.526	108.853	2.842	21.0	27.2	33.4	39.6	135.0	227.0	342.7	482.3	3.1E+05	4.0E+05	4.9E+05	5.9E+05				
6	23.865	81.897	2.842	25.6	33.2	40.8	48.4	201.7	339.1	512.0	720.4	4.6E+05	6.0E+05	7.4E+05	8.8E+05				
7	29.168	46.689	2.842	31.3	40.6	49.9	59.2	301.3	506.5	764.8	1076.2	6.9E+05	9.0E+05	1.1E+06	1.3E+06				
8	34.105	13.373	2.842	36.6	47.5	58.3	69.2	411.9	692.5	1045.7	1471.3	9.5E+05	1.2E+06	1.5E+06	1.8E+06				

	Stress ranges for pole with GS				SAT (N-S)-Open Terrain probabilities								seconds in each bin			cycles in each bin		
Segment	Sr1 (ksi)	Sr2 (ksi)	Sr3 (ksi)	Sr4 (ksi)	P(V<V1)	P(V<V2)	P(V<V3)	P(V<V4)	›(V1<V<V2›	(V2<V<V3	(V3<V<V4)		t_bin1	t_bin2	t_bin3	N_bin1	N_bin2	N_bin3
1	0.008	0.013	0.019	0.027	0.00%	0.03%	0.10%	0.27%	0.02%	0.07%	0.17%		212593	723861	2E+06	7.61E+04	2.59E+05	6.22E+05
2	0.009	0.015	0.023	0.032	0.02%	0.09%	0.31%	0.77%	0.07%	0.22%	0.46%		732607	2E+06	5E+06	2.62E+05	7.73E+05	1.65E+06
3	0.030	0.050	0.076	0.106	0.06%	0.28%	0.84%	1.91%	0.22%	0.56%	1.07%		2190675	6E+06	1E+07	7.84E+05	2.01E+06	3.80E+06
4	0.053	0.089	0.134	0.189	0.18%	0.74%	2.01%	4.15%	0.57%	1.27%	2.14%		5654650	1E+07	2E+07	2.02E+06	4.51E+06	7.60E+06
5	0.113	0.190	0.286	0.403	0.47%	1.74%	4.20%	7.92%	1.26%	2.46%	3.72%		1.3E+07	2E+07	4E+07	4.50E+06	8.76E+06	1.33E+07
6	0.178	0.299	0.451		1.07%	3.46%	7.58%	13.21%	2.39%	4.12%	5.64%		2.4E+07	4E+07	6E+07	8.50E+06	1.47E+07	2.01E+07
7	0.264				1.86%	5.47%	11.17%	18.41%	3.61%	5.70%	7.24%		3.6E+07	6E+07	7E+07	1.29E+07		
8					1.61%	4.86%	10.11%	16.91%	3.25%	5.25%	6.80%		3.2E+07	5E+07	7E+07			
	1.7066											E-W	1.1E+07			4045018.1		
	Sr1 (ksi)	Sr2 (ksi)	Sr3 (ksi)	Sr4 (ksi)	P(V<V1)	P(V<V2)	P(V<V3)	P(V<V4)	›(V1<V<V2›	(V2<V<V3	(V3<V<V4)		t_bin1	t_bin2	t_bin3	N_bin1	N_bin2	N_bin3
1	0.082	0.138	0.208	0.293	3.92%	10.09%	18.59%	28.25%	6.17%	8.50%	9.66%		6.1E+07	8E+07	1E+08	7.17E+07	9.89E+07	1.12E+08
2	0.095	0.160	0.242	0.340	8.01%	17.86%	29.54%	41.30%	9.84%	11.69%	11.75%		9.8E+07	1E+08	1E+08	1.15E+08	1.36E+08	1.37E+08
3	0.318	0.535	0.808		14.58%	28.40%	42.55%	55.17%	13.81%	14.16%	12.62%		1.4E+08	1E+08		1.61E+08	1.65E+08	
4	0.564				23.73%	40.84%	56.03%	68.06%	17.11%	15.19%	12.03%							
5					34.77%	53.66%	68.27%	78.61%	18.89%	14.61%	10.34%							
6					46.12%	65.02%	77.91%	86.15%	18.90%	12.89%	8.23%							
7					54.74%	72.66%	83.79%	90.38%	17.92%	11.13%	6.59%							
8					52.43%	70.69%	82.32%	89.35%	18.26%	11.63%	7.03%							
	Sr1 (ksi)	Sr2 (ksi)			P(V<V1)	P(V<V2)	P(V<V3)	P(V<V4)	›(V1<V<V2›	(V2<V<V3	(V3<V<V4)		t_bin1	t_bin2	t_bin3	N_bin1	N_bin2	N_bin3
1	0.484	0.814	1.2		45.67%	64.61%	77.58%	85.90%	18.93%	12.97%	8.32%		1.9E+08			5.35E+08		
2	0.561				59.75%	76.74%	86.73%	92.38%	16.99%	9.99%	5.65%							
3					72.47%	86.00%	92.83%	96.26%	13.53%	6.84%	3.42%							
4					82.54%	92.21%	96.43%	98.30%	9.67%	4.22%	1.87%							
5					89.61%	95.94%	98.33%	99.27%	6.32%	2.39%	0.95%							
6					93.99%	97.92%	99.23%	99.69%	3.93%	1.31%	0.47%							
7					96.17%	98.79%	99.58%	99.84%	2.62%	0.79%	0.26%							
8					95.66%	98.59%	99.50%	99.81%	2.94%	0.91%	0.31%							

	Avg Sr (No GS)			Avg Sr (w/GS)			SAT(N-S)-Suburban Terrain probabilities							seconds in each bin			cycles in each bin		
Segment	S_bin1	S_bin2	S_bin3	S_bin1	S_bin2	S_bin3	P(V<V1)	P(V<V2)	P(V<V3)	P(V<V4)	(V1<V<V2	(V2<V<V3	(V3<V<V4	t_bin1	t_bin2	t_bin3	N_bin1	N_bin2	N_bin3
1	0.022	0.034	0.050	0.010	0.016	0.023	0.01%	0.08%	0.26%	0.67%	0.06%	0.19%	0.41%	619546	2E+06	4E+06	221797	667380	1446339
2	0.025	0.040	0.058	0.012	0.019	0.027	0.05%	0.23%	0.72%	1.66%	0.19%	0.49%	0.94%	2E+06	5E+06	9E+06	663007	1734575	3347408
3	0.085	0.134	0.194	0.040	0.063	0.091	0.14%	0.63%	1.73%	3.63%	0.48%	1.10%	1.90%	5E+06	1E+07	2E+07	1718342	3921942	6759481
4	0.151	0.237	0.343	0.071	0.111	0.161	0.39%	1.46%	3.62%	6.96%	1.08%	2.16%	3.34%	1E+07	2E+07	3E+07	3832910	7680696	11886802
5	0.321	0.506	0.733	0.151	0.238	0.344	0.88%	2.94%	6.60%	11.74%	2.06%	3.66%	5.13%	2E+07	4E+07	5E+07	7330628	1.3E+07	18267978
6	0.506	0.797	0.959	0.238	0.375	0.451	1.65%	4.96%	10.29%	17.17%	3.31%	5.33%	6.88%	3E+07	5E+07	7E+07	1.2E+07	1.9E+07	24490995
7	0.561			0.264			2.17%	6.22%	12.45%	20.18%	4.05%	6.22%	7.73%	4E+07	6E+07	8E+07	1.4E+07		
8							1.04%	3.39%	7.44%	13.01%	2.34%	4.06%	5.57%	2E+07	4E+07	6E+07			
	3.629			1.707															
	S_bin1	S_bin2	S_bin3	S_bin1	S_bin2	S_bin3	P(V<V1)	P(V<V2)	P(V<V3)	P(V<V4)	(V1<V<V2	(V2<V<V3	(V3<V<V4	t_bin1	t_bin2	t_bin3	N_bin1	N_bin2	N_bin3
1	0.234	0.368	0.533	0.110	0.173	0.251	7.29%	16.57%	27.83%	39.35%	9.28%	11.26%	11.52%	9E+07	1E+08	1E+08	1.1E+08	1.3E+08	1.34E+08
2	0.271	0.427	0.618	0.128	0.201	0.291	13.33%	26.52%	40.36%	52.94%	13.19%	13.84%	12.58%	1E+08	1E+08	1E+08	1.5E+08	1.6E+08	1.46E+08
3	0.907	1.428		0.427	0.672		21.87%	38.46%	53.59%	65.83%	16.60%	15.12%	12.24%	2E+08	2E+08		1.9E+08	1.8E+08	
4							32.29%	50.94%	65.80%	76.57%	18.66%	14.86%	10.77%						
5							43.28%	62.32%	75.72%	84.50%	19.05%	13.40%	8.77%						
6							52.86%	71.06%	82.60%	89.55%	18.20%	11.54%	6.95%						
7							57.29%	74.76%	85.32%	91.43%	17.48%	10.56%	6.11%						
8							45.74%	64.67%	77.63%	85.93%	18.93%	12.96%	8.31%						
	S_bin1	S_bin2	S_bin3	S_bin1			P(V<V1)	P(V<V2)	P(V<V3)	P(V<V4)	(V1<V<V2	(V2<V<V3	(V3<V<V4	t_bin1	t_bin2	t_bin3	N_bin1	N_bin2	N_bin3
1	1.380			0.649			57.79%	75.18%	85.62%	91.64%	17.38%	10.44%	6.02%	2E+08			4.9E+08		
2							70.56%	84.71%	92.03%	95.77%	14.15%	7.33%	3.74%						
3							80.91%	91.28%	95.92%	98.03%	10.37%	4.64%	2.11%						
4							88.33%	95.30%	98.02%	99.12%	6.97%	2.72%	1.10%						
5							93.08%	97.53%	99.06%	99.62%	4.45%	1.53%	0.56%						
6							95.75%	98.63%	99.52%	99.82%	2.88%	0.89%	0.30%						
7							96.67%	98.98%	99.65%	99.87%	2.30%	0.68%	0.22%						
8							93.87%	97.87%	99.20%	99.68%	4.00%	1.33%	0.48%						

DFW(N-S)-Open Terrain probabilities									seconds in each bin			cycles in each bin			
Segment	P(V<V1)	P(V<V2)	P(V<V3)	P(V<V4)	P(V1<V<V2)	P(V2<V<V3)	P(V3<V<V4)		t_bin1	t_bin2	t_bin3	N_bin1	N_bin2	N_bin3	
1	0.00%	0.00%	0.00%	0.02%	0.00%	0.00%	0.01%		6969.902	41720.03	155185.3	2.50E+03	1.49E+04	5.56E+04	
2	0.00%	0.00%	0.02%	0.08%	0.00%	0.02%	0.06%		39387.03	197163.5	631648.3	1.41E+04	7.06E+04	2.26E+05	
3	0.00%	0.02%	0.09%	0.28%	0.02%	0.07%	0.19%		185524.9	778297.6	2151618	6.64E+04	2.79E+05	7.70E+05	
4	0.01%	0.07%	0.30%	0.84%	0.06%	0.23%	0.54%		722178.9	2549888	6105730	2.59E+05	9.13E+05	2.19E+06	
5	0.04%	0.24%	0.86%	2.14%	0.21%	0.62%	1.28%		2308847	6910950	14422526	8.27E+05	2.47E+06	5.16E+06	
6	0.12%	0.65%	2.01%	4.51%	0.53%	1.36%	2.50%		5930398	15265718	28103765	2.12E+06	5.47E+06	1.01E+07	
7	0.27%	1.26%	3.53%	7.35%	0.99%	2.27%	3.82%		11095283	25544497	42864660	3.97E+06			
8	0.22%	1.06%	3.05%	6.48%	0.84%	1.99%	3.43%		9434663	22381570	38502201				
								E-W Gusts	19820568			7095763.2			
	P(V<V1)	P(V<V2)	P(V<V3)	P(V<V4)	P(V1<V<V2)	P(V2<V<V3)	P(V3<V<V4)		t_bin1	t_bin2	t_bin3	N_bin1	N_bin2	N_bin3	
1	0.78%	3.05%	7.45%	13.89%	2.27%	4.41%	6.44%		25436516	49505133	72270399	2.98E+07	5.79E+07	8.46E+07	
2	2.18%	7.02%	14.86%	24.67%	4.84%	7.83%	9.81%		54405921	87961156	1.1E+08	6.37E+07	1.03E+08	1.29E+08	
3	5.22%	14.00%	25.82%	38.54%	8.78%	11.82%	12.72%		98643029	1.33E+08		1.15E+08	1.55E+08		
4	10.71%	24.25%	39.48%	53.61%	13.54%	15.23%	14.13%								
5	19.00%	36.91%	53.87%	67.54%	17.92%	16.96%	13.66%								
6	29.21%	49.87%	66.57%	78.39%	20.66%	16.70%	11.82%								
7	38.07%	59.50%	74.91%	84.83%	21.43%	15.42%	9.92%								
8	35.61%	56.95%	72.79%	83.25%	21.34%	15.84%	10.46%								
	P(V<V1)	P(V<V2)	P(V<V3)	P(V<V4)	P(V1<V<V2)	P(V2<V<V3)	P(V3<V<V4)		t_bin1	t_bin2	t_bin3	N_bin1	N_bin2	N_bin3	
1	28.78%	49.36%	66.11%	78.02%	20.59%	16.75%	11.91%		2.31E+08			6.57E+08			
2	43.66%	64.96%	79.27%	87.96%	21.30%	14.30%	8.70%								
3	59.25%	78.17%	88.67%	94.14%	18.92%	10.50%	5.47%								
4	73.11%	87.70%	94.42%	97.43%	14.59%	6.73%	3.01%								
5	83.65%	93.63%	97.47%	98.96%	9.98%	3.85%	1.49%								
6	90.51%	96.82%	98.89%	99.59%	6.31%	2.07%	0.70%								
7	94.00%	98.21%	99.43%	99.81%	4.21%	1.22%	0.38%								
8	93.18%	97.90%	99.31%	99.76%	4.72%	1.42%	0.45%								

DFW (N-S)-Suburban Terrain probabilities									seconds in each bin			cycles in each bin			
Segment	P(V<V1)	P(V<V2)	P(V<V3)	P(V<V4)	P(V1<V<V2)	P(V2<V<V3)	P(V3<V<V4)		t_bin1	t_bin2	t_bin3	N_bin1	N_bin2	N_bin3	
1	0.00%	0.00%	0.02%	0.06%	0.00%	0.01%	0.05%		31117.63	159770.5	522810.3	1.11E+04	5.72E+04	1.87E+05	
2	0.00%	0.01%	0.07%	0.23%	0.01%	0.06%	0.16%		146105.3	630622.8	1785248	5.23E+04	2.26E+05	6.39E+05	
3	0.01%	0.06%	0.24%	0.70%	0.05%	0.18%	0.45%		570172.3	2077383	5106126	2.04E+05	7.44E+05	1.83E+06	
4	0.03%	0.19%	0.70%	1.78%	0.16%	0.50%	1.08%		1826050	5660228	12160899	6.54E+05	2.03E+06	4.35E+06	
5	0.09%	0.52%	1.65%	3.80%	0.42%	1.13%	2.15%		4755327	12701839	24112996	1.70E+06	4.55E+06	8.63E+06	
6	0.23%	1.09%	3.14%	6.63%	0.87%	2.04%	3.50%		9721266	22935726	39276853	3.48E+06	8.21E+06	1.41E+07	
7	0.34%	1.51%	4.14%	8.42%	1.18%	2.62%	4.28%		13224414	29447257	48064575	4.73E+06			
8	0.12%	0.63%	1.96%	4.41%	0.51%	1.33%	2.45%		5761204	14903174	27548451				
	P(V<V1)	P(V<V2)	P(V<V3)	P(V<V4)	P(V1<V<V2)	P(V2<V<V3)	P(V3<V<V4)		t_bin1	t_bin2	t_bin3	N_bin1	N_bin2	N_bin3	
1	1.90%	6.29%	13.58%	22.91%	4.39%	7.29%	9.33%		49320175	81866912	1.05E+08	5.77E+07	9.58E+07	1.23E+08	
2	4.57%	12.64%	23.82%	36.14%	8.06%	11.18%	12.32%		90564799	1.26E+08	1.38E+08	1.06E+08	1.47E+08	1.62E+08	
3	9.48%	22.13%	36.83%	50.85%	12.65%	14.70%	14.01%		1.42E+08	1.65E+08		1.66E+08	1.93E+08		
4	16.98%	34.05%	50.81%	64.72%	17.07%	16.76%	13.91%								
5	26.49%	46.64%	63.58%	75.95%	20.15%	16.93%	12.37%								
6	36.06%	57.42%	73.18%	83.54%	21.36%	15.77%	10.36%								
7	40.87%	62.29%	77.17%	86.48%	21.42%	14.88%	9.31%								
8	28.84%	49.44%	66.18%	78.08%	20.60%	16.74%	11.90%								
	P(V<V1)	P(V<V2)	P(V<V3)	P(V<V4)	P(V1<V<V2)	P(V2<V<V3)	P(V3<V<V4)		t_bin1	t_bin2	t_bin3	N_bin1	N_bin2	N_bin3	
1	41.44%	62.84%	77.61%	86.79%	21.40%	14.77%	9.18%		2.4E+08			6.83E+08			
2	56.78%	76.26%	87.41%	93.37%	19.48%	11.15%	5.95%								
3	70.77%	86.23%	93.60%	96.99%	15.46%	7.37%	3.39%								
4	81.68%	92.61%	96.99%	98.73%	10.93%	4.38%	1.75%								
5	89.07%	96.20%	98.63%	99.48%	7.13%	2.43%	0.85%								
6	93.34%	97.96%	99.34%	99.77%	4.62%	1.38%	0.43%								
7	94.82%	98.50%	99.54%	99.85%	3.69%	1.03%	0.31%								
8	90.32%	96.74%	98.86%	99.58%	6.42%	2.11%	0.72%								

IAH (N-S)-Open Terrain probabilities									seconds in each bin			cycles in each bin			
Segment	P(V<V1)	P(V<V2)	P(V<V3)	P(V<V4)	P(V1<V<V2)	P(V2<V<V3)	P(V3<V<V4)		t_bin1	t_bin2	t_bin3	N_bin1	N_bin2	N_bin3	
1	0.00%	0.01%	0.03%	0.12%	0.01%	0.03%	0.08%		44601.8	215312	667425.7	1.60E+04	7.71E+04	2.39E+05	
2	0.00%	0.03%	0.13%	0.41%	0.03%	0.10%	0.28%		208683.2	838992.4	2232554	7.47E+04	3.00E+05	7.99E+05	
3	0.02%	0.12%	0.46%	1.24%	0.10%	0.34%	0.78%		814420.5	2732542	6253847	2.92E+05	9.78E+05	2.24E+06	
4	0.07%	0.40%	1.32%	3.16%	0.33%	0.93%	1.83%		2635071	7410088	14641520	9.43E+05	2.65E+06	5.24E+06	
5	0.23%	1.11%	3.20%	6.80%	0.88%	2.09%	3.59%		7048382	16734234	28726781	2.52E+06	5.99E+06	1.03E+07	
6	0.62%	2.54%	6.45%	12.36%	1.92%	3.91%	5.91%		15368530	31259531	47200550	5.50E+06	1.12E+07	1.69E+07	
7	1.20%	4.39%	10.17%	18.10%	3.18%	5.78%	7.93%		25456641	46177730	63418181	9.11E+06			
8	1.01%	3.81%	9.04%	16.42%	2.80%	5.23%	7.37%		22366462	41837839	58938025				
								E-W Gusts	22874717			8189148.6			
	P(V<V1)	P(V<V2)	P(V<V3)	P(V<V4)	P(V1<V<V2)	P(V2<V<V3)	P(V3<V<V4)		t_bin1	t_bin2	t_bin3	N_bin1	N_bin2	N_bin3	
1	2.95%	9.03%	18.30%	29.34%	6.07%	9.27%	11.04%		48545418	74116268	88263848	5.68E+07	8.67E+07	1.03E+08	
2	6.89%	17.48%	30.84%	44.44%	10.59%	13.36%	13.60%		84639381	1.07E+08	1.09E+08	9.90E+07	1.25E+08	1.27E+08	
3	13.85%	29.51%	45.89%	60.15%	15.66%	16.37%	14.27%		1.25E+08	1.31E+08		1.46E+08	1.53E+08		
4	24.14%	43.92%	61.10%	73.98%	19.77%	17.19%	12.87%								
5	36.90%	58.48%	74.19%	84.37%	21.58%	15.71%	10.18%								
6	49.97%	70.81%	83.72%	91.05%	20.84%	12.91%	7.33%								
7	59.68%	78.63%	89.04%	94.40%	18.95%	10.41%	5.36%								
8	57.11%	76.66%	87.76%	93.62%	19.55%	11.09%	5.86%								
	P(V<V1)	P(V<V2)	P(V<V3)	P(V<V4)	P(V1<V<V2)	P(V2<V<V3)	P(V3<V<V4)		t_bin1	t_bin2	t_bin3	N_bin1	N_bin2	N_bin3	
1	49.46%	70.37%	83.40%	90.84%	20.91%	13.03%	7.43%		1.67E+08			4.75E+08			
2	65.18%	82.61%	91.53%	95.86%	17.43%	8.92%	4.33%								
3	78.44%	90.92%	96.17%	98.35%	12.48%	5.25%	2.18%								
4	87.95%	95.74%	98.45%	99.41%	7.79%	2.71%	0.96%								
5	93.82%	98.16%	99.42%	99.80%	4.34%	1.26%	0.38%								
6	96.95%	99.23%	99.79%	99.94%	2.28%	0.56%	0.15%								
7	98.30%	99.62%	99.90%	99.97%	1.32%	0.29%	0.07%								
8	98.00%	99.54%	99.88%	99.97%	1.54%	0.34%	0.09%								

	IAH (N-S)-Suburban Terrain probabilities								seconds in each bin			cycles in each bin			
Segment	P(V<V1)	P(V<V2)	P(V<V3)	P(V<V4)	P(V1<V<V2)	P(V2<V<V3)	P(V3<V<V4)		t_bin1	t_bin2	t_bin3	N_bin1	N_bin2	N_bin3	
1	0.00%	0.02%	0.11%	0.35%	0.02%	0.09%	0.24%		169362.2	698814.3	1900242	6.06E+04	2.50E+05	6.80E+05	
2	0.01%	0.10%	0.38%	1.05%	0.08%	0.29%	0.67%		661171.4	2283961	5355632	2.37E+05	8.18E+05	1.92E+06	
3	0.05%	0.32%	1.10%	2.69%	0.27%	0.78%	1.59%		2151884	6249115	12682313	7.70E+05	2.24E+06	4.54E+06	
4	0.18%	0.90%	2.69%	5.84%	0.72%	1.78%	3.15%		5789436	14246595	25194808	2.07E+06	5.10E+06	9.02E+06	
5	0.49%	2.09%	5.48%	10.77%	1.60%	3.39%	5.28%		12829158	27102526	42230023	4.59E+06	9.70E+06	1.51E+07	
6	1.05%	3.91%	9.24%	16.72%	2.87%	5.33%	7.48%		22908711	42612497	59751180	8.20E+06	1.53E+07	2.14E+07	
7	1.45%	5.11%	11.53%	20.09%	3.66%	6.42%	8.56%		29254430	51281156	68459850	1.05E+07			
8	0.60%	2.48%	6.32%	12.14%	1.88%	3.84%	5.82%		15010089	30684558	46526115				
	P(V<V1)	P(V<V2)	P(V<V3)	P(V<V4)	P(V1<V<V2)	P(V2<V<V3)	P(V3<V<V4)		t_bin1	t_bin2	t_bin3	N_bin1	N_bin2	N_bin3	
1	6.16%	16.05%	28.86%	42.20%	9.88%	12.81%	13.34%		78992631	1.02E+08	1.07E+08	9.24E+07	1.20E+08	1.25E+08	
2	12.49%	27.35%	43.36%	57.67%	14.86%	16.01%	14.31%		1.19E+08	1.28E+08	1.14E+08	1.39E+08	1.50E+08	1.34E+08	
3	22.01%	41.17%	58.39%	71.65%	19.16%	17.22%	13.26%		1.53E+08	1.38E+08		1.79E+08	1.61E+08		
4	34.02%	55.43%	71.63%	82.44%	21.42%	16.19%	10.82%								
5	46.72%	67.95%	81.63%	89.65%	21.23%	13.68%	8.02%								
6	57.58%	77.03%	88.00%	93.77%	19.45%	10.97%	5.77%								
7	62.49%	80.70%	90.35%	95.18%	18.21%	9.65%	4.83%								
8	49.54%	70.44%	83.45%	90.87%	20.90%	13.01%	7.42%								
	P(V<V1)	P(V<V2)	P(V<V3)	P(V<V4)	P(V1<V<V2)	P(V2<V<V3)	P(V3<V<V4)		t_bin1	t_bin2	t_bin3	N_bin1	N_bin2	N_bin3	
1	63.04%	81.10%	90.60%	95.33%	18.06%	9.50%	4.72%		1.44E+08			4.10E+08			
2	76.53%	89.83%	95.61%	98.07%	13.30%	5.78%	2.46%								
3	86.49%	95.06%	98.15%	99.28%	8.58%	3.09%	1.13%								
4	92.82%	97.78%	99.28%	99.75%	4.97%	1.49%	0.47%								
5	96.34%	99.04%	99.72%	99.91%	2.69%	0.69%	0.19%								
6	98.06%	99.55%	99.89%	99.97%	1.50%	0.33%	0.08%								
7	98.58%	99.69%	99.93%	99.98%	1.11%	0.23%	0.05%								
8	96.87%	99.21%	99.78%	99.93%	2.33%	0.57%	0.15%								

RMMA (N-S)-Open Terrain probabilities									seconds in each bin			cycles in each bin			
Segment	P(V<V1)	P(V<V2)	P(V<V3)	P(V<V4)	P(V1<V<V2)	P(V2<V<V3)	P(V3<V<V4)		t_bin1	t_bin2	t_bin3	N_bin1	N_bin2	N_bin3	
1	0.00%	0.00%	0.02%	0.06%	0.00%	0.01%	0.04%		25746.23	135544.3	451922.6	9.22E+03	4.85E+04	1.62E+05	
2	0.00%	0.01%	0.07%	0.23%	0.01%	0.05%	0.16%		129970.9	570430.7	1633898	4.65E+04	2.04E+05	5.85E+05	
3	0.01%	0.06%	0.25%	0.73%	0.05%	0.19%	0.47%		546801.4	2004839	4942767	1.96E+05	7.18E+05	1.77E+06	
4	0.03%	0.22%	0.78%	1.97%	0.18%	0.56%	1.20%		1903728	5856221	12474406	6.82E+05	2.10E+06	4.47E+06	
5	0.12%	0.64%	2.01%	4.53%	0.52%	1.36%	2.52%		5462512	14201513	26301193	1.96E+06	5.08E+06	9.42E+06	
6	0.34%	1.56%	4.28%	8.70%	1.22%	2.71%	4.42%		12698871	28311143	46150603	4.55E+06	1.01E+07	1.65E+07	
7	0.70%	2.82%	7.02%	13.26%	2.11%	4.21%	6.24%		22055367	43883587	65096750	7.90E+06			
8	0.58%	2.42%	6.18%	11.90%	1.83%	3.76%	5.72%		19133313	39249461	59714072				
								E-W Gusts	18359523			6572709.15			
	P(V<V1)	P(V<V2)	P(V<V3)	P(V<V4)	P(V1<V<V2)	P(V2<V<V3)	P(V3<V<V4)		t_bin1	t_bin2	t_bin3	N_bin1	N_bin2	N_bin3	
1	1.84%	6.17%	13.42%	22.77%	4.33%	7.26%	9.34%		45166349	75721365	97476117	5.28E+07	8.86E+07	1.14E+08	
2	4.59%	12.76%	24.09%	36.56%	8.17%	11.33%	12.48%		85185882	1.18E+08	1.3E+08	9.97E+07	1.38E+08	1.52E+08	
3	9.86%	22.92%	37.94%	52.11%	13.05%	15.02%	14.17%		1.36E+08	1.57E+08		1.59E+08	1.83E+08		
4	18.28%	36.06%	53.10%	66.92%	17.78%	17.03%	13.82%								
5	29.53%	50.40%	67.16%	78.94%	20.86%	16.77%	11.78%								
6	41.89%	63.42%	78.16%	87.24%	21.53%	14.73%	9.08%								
7	51.62%	72.19%	84.68%	91.67%	20.57%	12.49%	6.98%								
8	49.00%	69.94%	83.08%	90.61%	20.94%	13.13%	7.54%								
	P(V<V1)	P(V<V2)	P(V<V3)	P(V<V4)	P(V1<V<V2)	P(V2<V<V3)	P(V3<V<V4)		t_bin1	t_bin2	t_bin3	N_bin1	N_bin2	N_bin3	
1	41.39%	62.94%	77.78%	86.97%	21.55%	14.84%	9.19%		2.25E+08			6.39E+08			
2	57.37%	76.84%	87.86%	93.67%	19.47%	11.02%	5.82%								
3	71.97%	87.07%	94.11%	97.28%	15.10%	7.04%	3.17%								
4	83.32%	93.51%	97.44%	98.95%	10.19%	3.93%	1.52%								
5	90.88%	97.00%	98.97%	99.63%	6.12%	1.97%	0.66%								
6	95.22%	98.66%	99.60%	99.87%	3.44%	0.94%	0.27%								
7	97.21%	99.31%	99.81%	99.94%	2.10%	0.50%	0.13%								
8	96.76%	99.17%	99.77%	99.93%	2.41%	0.60%	0.16%								

	RMMA (N-S)-Suburban Terrain probabilities								seconds in each bin			cycles in each bin		
Segment	P(V<V1)	P(V<V2)	P(V<V3)	P(V<V4)	P(V1<V<V2)	P(V2<V<V3)	P(V3<V<V4)		t_bin1	t_bin2	t_bin3	N_bin1	N_bin2	N_bin3
1	0.00%	0.01%	0.06%	0.19%	0.01%	0.05%	0.13%		104349.8976	469960.151	1375431.934	3.74E+04	1.68E+05	4.92E+05
2	0.01%	0.05%	0.21%	0.61%	0.04%	0.16%	0.40%		438570.6882	1655286.619	4180724.087	1.57E+05	5.93E+05	1.50E+06
3	0.03%	0.17%	0.64%	1.66%	0.15%	0.47%	1.02%		1534034.01	4872290.284	10658408.09	5.49E+05	1.74E+06	3.82E+06
4	0.09%	0.52%	1.66%	3.84%	0.42%	1.14%	2.18%		4420676.463	11909521.46	22718826.96	1.58E+06	4.26E+06	8.13E+06
5	0.27%	1.27%	3.58%	7.48%	1.00%	2.32%	3.89%		10435493.26	24158159.43	40631049.65	3.74E+06	8.65E+06	1.45E+07
6	0.60%	2.49%	6.33%	12.14%	1.88%	3.84%	5.82%		19642714.23	40070508.68	60682271.96	7.03E+06	1.43E+07	2.17E+07
7	0.86%	3.32%	8.06%	14.90%	2.46%	4.74%	6.83%		25707185.09	49439253.06	71300442.91	9.20E+06		
8	0.33%	1.52%	4.18%	8.53%	1.19%	2.66%	4.35%		12376863.04	27731645.62	45393980.41			
	P(V<V1)	P(V<V2)	P(V<V3)	P(V<V4)	P(V1<V<V2)	P(V2<V<V3)	P(V3<V<V4)		t_bin1	t_bin2	t_bin3	N_bin1	N_bin2	N_bin3
1	4.07%	11.60%	22.35%	34.44%	7.54%	10.74%	12.09%		78620868.06	112065180.1	126161520.5	9.20E+07	1.31E+08	1.48E+08
2	8.80%	21.03%	35.54%	49.57%	12.23%	14.51%	14.03%		127614170.8	151330486.8	146387943.4	1.49E+08	1.77E+08	1.71E+08
3	16.49%	33.48%	50.31%	64.35%	16.99%	16.83%	14.04%		177254089.8	175573511		2.07E+08	2.05E+08	
4	26.92%	47.31%	64.32%	76.64%	20.39%	17.01%	12.32%							
5	38.74%	60.32%	75.68%	85.45%	21.58%	15.36%	9.77%							
6	49.48%	70.36%	83.38%	90.81%	20.88%	13.02%	7.43%							
7	54.53%	74.59%	86.35%	92.73%	20.06%	11.76%	6.38%							
8	41.47%	63.02%	77.84%	87.01%	21.55%	14.82%	9.17%							
	P(V<V1)	P(V<V2)	P(V<V3)	P(V<V4)	P(V1<V<V2)	P(V2<V<V3)	P(V3<V<V4)		t_bin1	t_bin2	t_bin3	N_bin1	N_bin2	N_bin3
1	55.12%	75.06%	86.67%	92.93%	19.94%	11.61%	6.27%		208078244.8			5.91E+08		
2	69.79%	85.68%	93.33%	96.86%	15.89%	7.64%	3.53%							
3	81.51%	92.57%	96.99%	98.74%	11.06%	4.42%	1.75%							
4	89.55%	96.44%	98.74%	99.53%	6.89%	2.30%	0.79%							
5	94.35%	98.35%	99.49%	99.83%	4.00%	1.13%	0.34%							
6	96.84%	99.19%	99.77%	99.93%	2.35%	0.58%	0.16%							
7	97.64%	99.43%	99.85%	99.96%	1.79%	0.42%	0.11%							
8	95.11%	98.62%	99.58%	99.86%	3.51%	0.96%	0.28%							

ELP (N-S)Open Terrain probabilities									seconds in each bin			cycles in each bin		
Segment	P(V<V1)	P(V<V2)	P(V<V3)	P(V<V4)	P(V1<V<V2)	P(V2<V<V3)	P(V3<V<V4)		t_bin1	t_bin2	t_bin3	N_bin1	N_bin2	N_bin3
1	0.00%	0.02%	0.08%	0.26%	0.01%	0.06%	0.18%		93715.91	424055.5	1235216	3.36E+04	1.52E+05	4.42E+05
2	0.01%	0.07%	0.30%	0.87%	0.06%	0.23%	0.57%		414531.1	1547030	3837075	1.48E+05	5.54E+05	1.37E+06
3	0.04%	0.27%	0.97%	2.45%	0.23%	0.70%	1.48%		1518856	4684858	9913575	5.44E+05	1.68E+06	3.55E+06
4	0.16%	0.84%	2.60%	5.78%	0.69%	1.75%	3.18%		4588055	11748334	21293978	1.64E+06	4.21E+06	7.62E+06
5	0.50%	2.21%	5.86%	11.57%	1.71%	3.65%	5.71%		11416565	24454569	38216582	4.09E+06	8.75E+06	1.37E+07
6	1.28%	4.74%	11.04%	19.63%	3.46%	6.30%	8.60%		23177224	42172236	57566458	8.30E+06	1.51E+07	2.06E+07
7	2.38%	7.80%	16.54%	27.34%	5.42%	8.74%	10.80%		36296197	58526795	72287485	1.30E+07		
8	2.02%	6.86%	14.91%	25.14%	4.84%	8.06%	10.22%		32382654	53937002	68429731			
								E-W Gusts	1.22E+08			4.37E+07		
	P(V<V1)	P(V<V2)	P(V<V3)	P(V<V4)	P(V1<V<V2)	P(V2<V<V3)	P(V3<V<V4)		t_bin1	t_bin2	t_bin3	N_bin1	N_bin2	N_bin3
1	5.44%	14.89%	27.59%	41.09%	9.45%	12.70%	13.50%		63284332	85064326	90395033	7.40E+07	9.95E+07	1.06E+08
2	11.70%	26.53%	42.82%	57.49%	14.82%	16.30%	14.67%		99246839	1.09E+08	98229471	1.16E+08	1.28E+08	1.15E+08
3	21.69%	41.29%	58.95%	72.45%	19.60%	17.66%	13.49%		1.31E+08	1.18E+08		1.54E+08	1.38E+08	
4	34.92%	56.96%	73.29%	83.93%	22.04%	16.33%	10.64%							
5	49.57%	70.95%	84.09%	91.44%	21.38%	13.14%	7.34%							
6	62.98%	81.44%	91.00%	95.64%	18.45%	9.56%	4.64%							
7	72.02%	87.42%	94.44%	97.51%	15.39%	7.02%	3.08%							
8	69.71%	85.96%	93.64%	97.09%	16.26%	7.67%	3.46%							
	P(V<V1)	P(V<V2)	P(V<V3)	P(V<V4)	P(V1<V<V2)	P(V2<V<V3)	P(V3<V<V4)		t_bin1	t_bin2	t_bin3	N_bin1	N_bin2	N_bin3
1	62.49%	81.09%	90.78%	95.52%	18.60%	9.69%	4.74%		1.25E+08			3.54E+08		
2	76.81%	90.24%	95.92%	98.26%	13.43%	5.68%	2.34%							
3	87.28%	95.57%	98.42%	99.41%	8.29%	2.85%	0.99%							
4	93.76%	98.20%	99.45%	99.82%	4.44%	1.25%	0.37%							
5	97.20%	99.33%	99.83%	99.95%	2.13%	0.49%	0.12%							
6	98.79%	99.76%	99.94%	99.99%	0.97%	0.19%	0.04%							
7	99.39%	99.89%	99.98%	99.99%	0.50%	0.09%	0.02%							
8	99.26%	99.87%	99.97%	99.99%	0.60%	0.11%	0.02%							

ELP (N-S)Suburban Terrain probabilities									seconds in each bin			cycles in each bin		
Segment	P(V<V1)	P(V<V2)	P(V<V3)	P(V<V4)	P(V1<V<V2)	P(V2<V<V3)	P(V3<V<V4)		t_bin1	t_bin2	t_bin3	N_bin1	N_bin2	N_bin3
1	0.01%	0.06%	0.25%	0.75%	0.05%	0.19%	0.49%		339275.7	1301279	3301999	1.21E+05	4.66E+05	1.18E+06
2	0.03%	0.22%	0.81%	2.10%	0.19%	0.59%	1.29%		1246277	3963982	8605434	4.46E+05	1.42E+06	3.08E+06
3	0.12%	0.69%	2.19%	4.99%	0.57%	1.50%	2.80%		3795881	10055105	18746110	1.36E+06	3.60E+06	6.71E+06
4	0.40%	1.82%	4.98%	10.09%	1.42%	3.17%	5.10%		9526877	21192629	34174050	3.41E+06	7.59E+06	1.22E+07
5	1.02%	3.97%	9.54%	17.40%	2.94%	5.57%	7.86%		19698487	37305034	52638247	7.05E+06	1.34E+07	1.88E+07
6	2.08%	7.02%	15.20%	25.53%	4.94%	8.18%	10.33%		33075551	54765969	69141951	1.18E+07	1.96E+07	2.48E+07
7	2.83%	8.95%	18.48%	29.89%	6.12%	9.52%	11.42%		40995477	63758482	76430940	1.47E+07		
8	1.24%	4.63%	10.83%	19.33%	3.39%	6.20%	8.50%		22691160	41507739	56909287			
	P(V<V1)	P(V<V2)	P(V<V3)	P(V<V4)	P(V1<V<V2)	P(V2<V<V3)	P(V3<V<V4)		t_bin1	t_bin2	t_bin3	N_bin1	N_bin2	N_bin3
1	10.59%	24.64%	40.53%	55.18%	14.05%	15.89%	14.65%		94071074	1.06E+08	98085538	1.10E+08	1.24E+08	1.15E+08
2	19.82%	38.77%	56.39%	70.22%	18.95%	17.62%	13.83%		1.27E+08	1.18E+08	92593277	1.48E+08	1.38E+08	1.08E+08
3	32.30%	54.12%	70.87%	82.11%	21.82%	16.75%	11.24%		1.46E+08	1.12E+08		1.71E+08	1.31E+08	
4	46.40%	68.17%	82.09%	90.12%	21.77%	13.92%	8.03%							
5	59.78%	79.12%	89.56%	94.81%	19.33%	10.44%	5.25%							
6	70.14%	86.24%	93.79%	97.18%	16.10%	7.55%	3.39%							
7	74.50%	88.90%	95.23%	97.92%	14.41%	6.33%	2.69%							
8	62.56%	81.14%	90.81%	95.54%	18.58%	9.67%	4.72%							
	P(V<V1)	P(V<V2)	P(V<V3)	P(V<V4)	P(V1<V<V2)	P(V2<V<V3)	P(V3<V<V4)		t_bin1	t_bin2	t_bin3	N_bin1	N_bin2	N_bin3
1	74.98%	89.19%	95.38%	97.99%	14.21%	6.19%	2.62%		95131878			2.70E+08		
2	85.86%	94.92%	98.14%	99.29%	9.05%	3.22%	1.15%							
3	92.83%	97.86%	99.33%	99.78%	5.03%	1.47%	0.45%							
4	96.65%	99.17%	99.78%	99.93%	2.52%	0.61%	0.16%							
5	98.50%	99.69%	99.93%	99.98%	1.19%	0.24%	0.05%							
6	99.29%	99.87%	99.97%	99.99%	0.58%	0.10%	0.02%							
7	99.51%	99.92%	99.98%	100.00%	0.41%	0.07%	0.01%							
8	98.75%	99.75%	99.94%	99.99%	0.99%	0.19%	0.04%							

								Equivalent Static Pressure Ranges						v(ft2/s)=	0.0001615	Stress ranges for pole with no GS			
Segment	Avg dia (in)	Mid ht. (ft)	f 1 (Hz)	V1 mph - 3s	V2 mph - 3s	V3 mph - 3s	V4 mph - 3s	Pvs1 (psf)	Pvs2 (psf)	Pvs3 (psf)	Pvs4 (psf)	Re1 300≤Re≤1.0E+05 Re>3.5E+06	Re2	Re3	Re4	Sr1 (ksi)	Sr2 (ksi)	Sr3 (ksi)	Sr4 (ksi)
1	8.611	145.008	0.359	1.2	1.5	1.9	2.2	0.42	0.70	1.1	1.5	7.6E+03	9.9E+03	1.2E+04	1.4E+04	0.026	0.044	0.067	0.094
2	10.525	133.914	0.359	1.4	1.9	2.3	2.7	0.63	1.05	1.6	2.2	1.1E+04	1.5E+04	1.8E+04	2.2E+04	0.045	0.076	0.114	0.161
3	12.864	120.355	0.359	1.7	2.3	2.8	3.3	0.93	1.6	2.4	3.3	1.7E+04	2.2E+04	2.7E+04	3.2E+04	0.097	0.162	0.245	0.345
4	15.722	103.602	0.359	2.1	2.8	3.4	4.0	1.4	2.3	3.5	5.0	2.5E+04	3.3E+04	4.1E+04	4.8E+04	0.188	0.316	0.477	0.672
5	19.216	82.457	0.359	2.6	3.4	4.2	4.9	2.1	3.5	5.3	7.5	3.8E+04	4.9E+04	6.1E+04	7.2E+04	0.377	0.633	0.956	1.346
6	23.486	56.147	0.359	3.2	4.1	5.1	6.0	3.1	5.2	7.9	11.1	5.7E+04	7.4E+04	9.0E+04	1.1E+05	0.511	0.860	1.298	
7	28.705	24.064	0.359	3.9	5.0	6.2	7.4	4.7	7.8	11.8	16.6	8.5E+04	1.1E+05	1.4E+05	1.6E+05	0.499			
8	32.100	3.221	0.359	4.4	5.6	6.9	8.2	5.8	9.8	14.8	20.8	1.1E+05	1.4E+05	1.7E+05	2.0E+05				
		Pvs(windg	0.359					6.24								4.90227			
	Avg dia (in)	Mid ht. (ft)	f 2 (Hz)	V1 mph - 3s	V2 mph - 3s	V3 mph - 3s	V4 mph - 3s	Pvs1 (psf)	Pvs2 (psf)	Pvs3 (psf)	Pvs4 (psf)	Re1 300≤Re≤1.0E+05 Re>3.5E+06	Re2	Re3	Re4	Sr1 (ksi)	Sr2 (ksi)	Sr3 (ksi)	Sr4 (ksi)
1	8.611	145.008	1.337	4.3	5.6	6.9	8.2	5.8	9.8	14.8	20.8	2.8E+04	3.7E+04	4.5E+04	5.4E+04	0.366	0.615	0.929	1.307
2	10.525	133.914	1.337	5.3	6.9	8.5	10.0	8.7	14.6	22.0	31.0	4.2E+04	5.5E+04	6.8E+04	8.0E+04	0.618	1.039	1.569	2.208
3	12.864	120.355	1.337	6.5	8.4	10.4	12.3	13.0	21.8	32.9	46.3	6.3E+04	8.2E+04	1.0E+05	1.2E+05	1.345	2.261	3.413	
4	15.722	103.602	1.337	7.9	10.3	12.7	15.0	19.4	32.6	49.2	69.2	9.5E+04	1.2E+05	1.5E+05	1.8E+05	2.604			
5	19.216	82.457	1.337	9.7	12.6	15.5	18.3	28.9	48.7	73.5	103.4	1.4E+05	1.8E+05	2.3E+05	2.7E+05				
6	23.486	56.147	1.337	11.9	15.4	18.9	22.4	43.2	72.7	109.7	154.4	2.1E+05	2.7E+05	3.4E+05	4.0E+05				
7	28.705	24.064	1.337	14.5	18.8	23.1	27.4	64.6	108.6	163.9	230.7	3.2E+05	4.1E+05	5.0E+05	6.0E+05				
8	32.100	3.221	1.337	16.2	21.0	25.8	30.6	80.8	135.8	205.0	288.5	3.9E+05	5.1E+05	6.3E+05	7.5E+05				
	Avg dia (in)	Mid ht. (ft)	f 3 (Hz)	V1 mph - 3s	V2 mph - 3s	V3 mph - 3s	V4 mph - 3s	Pvs1 (psf)	Pvs2 (psf)	Pvs3 (psf)	Pvs4 (psf)	Re1 300≤Re≤1.0E+05 Re>3.5E+06	Re2	Re3	Re4	Sr1 (ksi)	Sr2 (ksi)		
1	8.611	145.008	3.511	11.4	14.8	18.2	21.6	40.1	67.4	101.7	143.2	7.5E+04	9.7E+04	1.2E+05	1.4E+05	2.531	4.255		
2	10.525	133.914	3.511	14.0	18.1	22.2	26.4	59.9	100.7	152.0	213.8	1.1E+05	1.4E+05	1.8E+05	2.1E+05				
3	12.864	120.355	3.511	17.1	22.1	27.2	32.2	89.4	150.4	227.0	319.4	1.7E+05	2.2E+05	2.7E+05	3.1E+05				
4	15.722	103.602	3.511	20.9	27.0	33.2	39.4	133.6	224.6	339.1	477.2	2.5E+05	3.2E+05	4.0E+05	4.7E+05				
5	19.216	82.457	3.511	25.5	33.0	40.6	48.2	199.6	335.5	506.6	712.9	3.7E+05	4.8E+05	5.9E+05	7.0E+05				
6	23.486	56.147	3.511	31.2	40.4	49.6	58.9	298.1	501.2	756.8	1064.9	5.5E+05	7.2E+05	8.8E+05	1.0E+06				
7	28.705	24.064	3.511	38.1	49.4	60.7	72.0	445.3	748.7	1130.5	1590.7	8.3E+05	1.1E+06	1.3E+06	1.6E+06				
8	32.100	3.221	3.511	42.6	55.2	67.8	80.5	556.9	936.3	1413.8	1989.3	1.0E+06	1.3E+06	1.7E+06	2.0E+06				

Segment	Stress ranges for pole with GS SAT (N-S)-Open Terrain probabilities												seconds in each bin			cycles in each bin		
	Sr1 (ksi)	Sr2 (ksi)	Sr3 (ksi)	Sr4 (ksi)	P(V<V1)	P(V<V2)	P(V<V3)	P(V<V4)	(V1<V<V2	(V2<V<V3	(V3<V<V4)		t_bin1	t_bin2	t_bin3	N_bin1	N_bin2	N_bin3
1	0.011	0.019	0.029	0.041	0.00%	0.02%	0.08%	0.22%	0.02%	0.06%	0.14%		164564.831	576266.691	1416537.61	5.91E+04	2.07E+05	5.09E+05
2	0.020	0.033	0.050	0.070	0.01%	0.07%	0.24%	0.63%	0.06%	0.17%	0.38%		572205.052	1738323.47	3797362.1	2.05E+05	6.24E+05	1.36E+06
3	0.042	0.071	0.107	0.150	0.04%	0.22%	0.67%	1.56%	0.17%	0.46%	0.89%		1722387.73	4550386.71	8852797.35	6.18E+05	1.63E+06	3.18E+06
4	0.082	0.137	0.208	0.292	0.13%	0.58%	1.62%	3.42%	0.45%	1.04%	1.80%		4468732.29	10310624.1	17930604.5	1.60E+06	3.70E+06	6.44E+06
5	0.164	0.275	0.416	0.585	0.35%	1.34%	3.36%	6.52%	0.99%	2.02%	3.16%		9875637.46	20066485.8	31414018.8	3.55E+06	7.20E+06	1.13E+07
6	0.222	0.374	0.564		0.75%	2.57%	5.89%	10.63%	1.82%	3.32%	4.74%		18107021.8	32969625.3	47142276	6.50E+06	1.18E+07	1.69E+07
7	0.217				1.09%	3.51%	7.68%	13.36%	2.42%	4.17%	5.69%		24073385.1	41420823.5	56522901.3	8.64E+06		
8					0.41%	1.52%	3.75%	7.18%	1.12%	2.23%	3.43%		11119326.6	22135715.8	34071942.1			
	2.1311											E-W Gus	11298933.3			4056317		
	Sr1 (ksi)	Sr2 (ksi)	Sr3 (ksi)	Sr4 (ksi)	P(V<V1)	P(V<V2)	P(V<V3)	P(V<V4)	(V1<V<V2	(V2<V<V3	(V3<V<V4)		t_bin1	t_bin2	t_bin3	N_bin1	N_bin2	N_bin3
1	0.159	0.267	0.404	0.568	5.63%	13.50%	23.59%	34.39%	7.87%	10.09%	10.80%		78235724.1	100274001	107365158	1.05E+08	1.34E+08	1.44E+08
2	0.269	0.452	0.682	0.960	10.84%	22.61%	35.63%	47.97%	11.77%	13.02%	12.35%		117021666	129426439	122777040	1.56E+08	1.73E+08	1.64E+08
3	0.585	0.983	1.484		18.63%	34.15%	49.01%	61.52%	15.52%	14.85%	12.51%		154352198	147660918		2.06E+08	1.97E+08	
4	1.132				28.77%	46.94%	62.04%	73.38%	18.17%	15.10%	11.34%							
5					40.11%	59.21%	73.11%	82.48%	19.10%	13.90%	9.37%							
6					50.63%	69.11%	81.12%	88.49%	18.49%	12.01%	7.37%							
7					56.06%	73.76%	84.60%	90.94%	17.70%	10.84%	6.34%							
8					42.05%	61.13%	74.73%	83.74%	19.08%	13.60%	9.01%							
	Sr1 (ksi)	Sr2 (ksi)			P(V<V1)	P(V<V2)	P(V<V3)	P(V<V4)	(V1<V<V2	(V2<V<V3	(V3<V<V4)		t_bin1	t_bin2	t_bin3	N_bin1	N_bin2	N_bin3
1	1.100	1.850			58.32%	75.60%	85.92%	91.84%	17.28%	10.32%	5.92%		171800571			6.03E+08		
2					71.26%	85.19%	92.33%	95.96%	13.92%	7.15%	3.62%							
3					81.72%	91.74%	96.18%	98.17%	10.03%	4.43%	1.99%							
4					89.18%	95.72%	98.23%	99.23%	6.54%	2.50%	1.00%							
5					93.89%	97.88%	99.21%	99.68%	3.98%	1.33%	0.48%							
6					96.50%	98.91%	99.63%	99.86%	2.41%	0.72%	0.23%							
7					97.43%	99.25%	99.76%	99.91%	1.82%	0.51%	0.16%							
8					94.47%	98.12%	99.31%	99.73%	3.65%	1.19%	0.42%							

	Avg Sr (No GS)			Avg Sr (w/GS)			SAT(N-S)-Suburban Terrain probabilities							seconds in each bin			cycles in each bin		
Segment	S_bin1	S_bin2	S_bin3	S_bin1	S_bin2	S_bin3	P(V<V1)	P(V<V2)	P(V<V3)	P(V<V4)	P(V1<V<V2)	P(V2<V<V3)	P(V3<V<V4)	t_bin1	t_bin2	t_bin3	N_bin1	N_bin2	N_bin3
1	0.035	0.056	0.081	0.015	0.024	0.035	0.01%	0.05%	0.19%	0.50%	0.04%	0.14%	0.31%	441856	1384179	3E+06	1.59E+05	4.97E+05	1.11E+06
2	0.060	0.095	0.138	0.026	0.041	0.060	0.03%	0.17%	0.53%	1.27%	0.13%	0.37%	0.73%	1334086	3645656	7E+06	4.79E+05	1.31E+06	2.62E+06
3	0.129	0.204	0.295	0.056	0.089	0.128	0.10%	0.45%	1.29%	2.79%	0.35%	0.84%	1.50%	3479080	8331039	1E+07	1.25E+06	2.99E+06	5.36E+06
4	0.252	0.397	0.575	0.110	0.172	0.250	0.26%	1.04%	2.70%	5.38%	0.78%	1.66%	2.68%	7785898	1.6E+07	3E+07	2.80E+06	5.91E+06	9.56E+06
5	0.505	0.795	1.151	0.220	0.346	0.500	0.58%	2.05%	4.85%	8.98%	1.48%	2.80%	4.13%	1.5E+07	2.8E+07	4E+07	5.27E+06	9.98E+06	1.47E+07
6	0.685	1.079	1.298	0.298	0.469	0.564	0.99%	3.23%	7.14%	12.56%	2.24%	3.92%	5.42%	2.2E+07	3.9E+07	5E+07	8.00E+06	1.40E+07	1.93E+07
7	0.499			0.217			0.93%	3.08%	6.87%	12.14%	2.15%	3.79%	5.27%	2.1E+07	3.8E+07	5E+07	7.67E+06		
8							0.10%	0.47%	1.34%	2.90%	0.37%	0.87%	1.56%	3650924	8681046	2E+07			
	4.902			2.1311															
	S_bin1	S_bin2	S_bin3	S_bin1	S_bin2	S_bin3	P(V<V1)	P(V<V2)	P(V<V3)	P(V<V4)	P(V1<V<V2)	P(V2<V<V3)	P(V3<V<V4)	t_bin1	t_bin2	t_bin3	N_bin1	N_bin2	N_bin3
1	0.490	0.772	1.118	0.213	0.336	0.486	9.49%	20.40%	32.84%	44.97%	10.90%	12.45%	12.12%	1.1E+08	1.2E+08	1E+08	1.45E+08	1.65E+08	1.61E+08
2	0.829	1.304	1.889	0.360	0.567	0.821	16.49%	31.16%	45.70%	58.31%	14.68%	14.54%	12.60%	1.5E+08	1.4E+08	1E+08	1.95E+08	1.93E+08	1.68E+08
3	1.803	2.837		0.784	1.233		25.76%	43.35%	58.54%	70.32%	17.59%	15.20%	11.77%	1.7E+08	1.5E+08		2.34E+08	2.02E+08	
4							36.42%	55.41%	69.83%	79.87%	18.99%	14.41%	10.05%						
5							46.81%	65.66%	78.43%	86.53%	18.85%	12.76%	8.10%						
6							54.56%	72.51%	83.68%	90.30%	17.95%	11.17%	6.63%						
7							53.74%	71.81%	83.16%	89.94%	18.07%	11.35%	6.78%						
8							26.32%	44.03%	59.22%	70.91%	17.71%	15.19%	11.70%						
	S_bin1	S_bin2	S_bin3	S_bin1			P(V<V1)	P(V<V2)	P(V<V3)	P(V<V4)	P(V1<V<V2)	P(V2<V<V3)	P(V3<V<V4)	t_bin1	t_bin2	t_bin3	N_bin1	N_bin2	N_bin3
1	3.393			1.475			68.63%	83.37%	91.18%	95.25%	14.74%	7.82%	4.07%	1.5E+08			5.14E+08		
2							79.44%	90.41%	95.43%	97.76%	10.97%	5.03%	2.32%						
3							87.40%	94.83%	97.79%	99.01%	7.43%	2.96%	1.22%						
4							92.63%	97.33%	98.97%	99.58%	4.70%	1.64%	0.61%						
5							95.69%	98.61%	99.51%	99.81%	2.91%	0.90%	0.30%						
6							97.20%	99.17%	99.73%	99.90%	1.97%	0.56%	0.18%						
7							97.06%	99.12%	99.71%	99.89%	2.06%	0.59%	0.19%						
8							87.75%	95.01%	97.88%	99.05%	7.26%	2.87%	1.17%						

	DFW(N-S)-Open Terrain probabilities								seconds in each bin			cycles in each bin			
Segment	P(V<V1)	P(V<V2)	P(V<V3)	P(V<V4)	P(V1<V<V2)	P(V2<V<V3)	P(V3<V<V4)		t_bin1	t_bin2	t_bin3	N_bin1	N_bin2	N_bin3	
1	0.00%	0.00%	0.00%	0.01%	0.00%	0.00%	0.01%		4879.89	30244.42	115820.4	1.75E+03	1.09E+04	4.16E+04	
2	0.00%	0.00%	0.02%	0.06%	0.00%	0.01%	0.04%		27830.8	144604.2	477905.1	9.99E+03	5.19E+04	1.72E+05	
3	0.00%	0.01%	0.06%	0.21%	0.01%	0.05%	0.15%		131803.7	575833.3	1646714	4.73E+04	2.07E+05	5.91E+05	
4	0.01%	0.05%	0.22%	0.64%	0.05%	0.17%	0.42%		514438.1	1899723	4722116	1.85E+05	6.82E+05	1.70E+06	
5	0.03%	0.17%	0.63%	1.62%	0.14%	0.46%	0.99%		1622676	5117387	11153657	5.83E+05	1.84E+06	4.00E+06	
6	0.08%	0.43%	1.40%	3.29%	0.35%	0.97%	1.89%		3960310	10898331	21208151	1.42E+06	3.91E+06	7.61E+06	
7	0.13%	0.67%	2.05%	4.59%	0.54%	1.38%	2.54%		6056790	15535207	28514737	2.17E+06			
8	0.03%	0.20%	0.73%	1.86%	0.17%	0.53%	1.13%		1930048	5933906	12662506				
								E-W Gusts	19820568			7115583.8			
	P(V<V1)	P(V<V2)	P(V<V3)	P(V<V4)	P(V1<V<V2)	P(V2<V<V3)	P(V3<V<V4)		t_bin1	t_bin2	t_bin3	N_bin1	N_bin2	N_bin3	
1	1.31%	4.66%	10.61%	18.68%	3.35%	5.95%	8.06%		37593399	66843501	90548222	5.03E+07	8.94E+07	1.21E+08	
2	3.38%	9.96%	19.70%	31.04%	6.58%	9.74%	11.34%		73920091	1.09E+08	1.27E+08	9.88E+07	1.46E+08	1.70E+08	
3	7.48%	18.49%	32.07%	45.69%	11.01%	13.59%	13.62%		1.24E+08	1.53E+08		1.65E+08	2.04E+08		
4	14.28%	30.02%	46.31%	60.45%	15.74%	16.30%	14.14%								
5	23.59%	43.04%	60.10%	73.02%	19.44%	17.06%	12.92%								
6	33.73%	54.93%	71.07%	81.94%	21.21%	16.13%	10.87%								
7	39.52%	60.95%	76.10%	85.70%	21.44%	15.15%	9.60%								
8	25.35%	45.24%	62.24%	74.84%	19.89%	17.00%	12.59%								
	P(V<V1)	P(V<V2)	P(V<V3)	P(V<V4)	P(V1<V<V2)	P(V2<V<V3)	P(V3<V<V4)		t_bin1	t_bin2	t_bin3	N_bin1	N_bin2	N_bin3	
1	42.02%	63.41%	78.06%	87.11%	21.38%	14.65%	9.05%		2.4E+08			8.43E+08			
2	57.69%	76.97%	87.88%	93.66%	19.28%	10.92%	5.77%								
3	71.92%	86.96%	94.01%	97.22%	15.04%	7.05%	3.20%								
4	82.99%	93.29%	97.31%	98.89%	10.30%	4.03%	1.58%								
5	90.36%	96.76%	98.86%	99.58%	6.40%	2.11%	0.72%								
6	94.54%	98.40%	99.50%	99.83%	3.87%	1.10%	0.33%								
7	96.04%	98.93%	99.68%	99.90%	2.88%	0.76%	0.22%								
8	91.28%	97.14%	99.02%	99.64%	5.86%	1.88%	0.63%								

	DFW (N-S)-Suburban Terrain probabilities								seconds in each bin			cycles in each bin		
Segment	P(V<V1)	P(V<V2)	P(V<V3)	P(V<V4)	P(V1<V<V2)	P(V2<V<V3)	P(V3<V<V4)		t_bin1	t_bin2	t_bin3	N_bin1	N_bin2	N_bin3
1	0.00%	0.00%	0.01%	0.04%	0.00%	0.01%	0.03%		19367.86	104540.2	356667.3	6.95E+03	3.75E+04	1.28E+05
2	0.00%	0.01%	0.05%	0.16%	0.01%	0.04%	0.11%		91763.52	418073.4	1238141	3.29E+04	1.50E+05	4.44E+05
3	0.00%	0.04%	0.16%	0.48%	0.03%	0.12%	0.32%		359148.6	1388870	3587580	1.29E+05	4.99E+05	1.29E+06
4	0.02%	0.12%	0.46%	1.23%	0.10%	0.34%	0.77%		1147700	3802832	8636571	4.12E+05	1.37E+06	3.10E+06
5	0.05%	0.31%	1.06%	2.57%	0.26%	0.75%	1.51%		2902224	8388466	17004018	1.04E+06	3.01E+06	6.10E+06
6	0.11%	0.59%	1.85%	4.19%	0.48%	1.26%	2.34%		5395215	14111629	26326048	1.94E+06	5.07E+06	9.45E+06
7	0.10%	0.55%	1.74%	3.99%	0.45%	1.19%	2.24%		5061666	13381053	25185144	1.82E+06		
8	0.00%	0.04%	0.17%	0.51%	0.03%	0.13%	0.34%		384842.4	1475247	3782968			
	P(V<V1)	P(V<V2)	P(V<V3)	P(V<V4)	P(V1<V<V2)	P(V2<V<V3)	P(V3<V<V4)		t_bin1	t_bin2	t_bin3	N_bin1	N_bin2	N_bin3
1	2.79%	8.55%	17.42%	28.10%	5.76%	8.87%	10.67%		64719037	99643119	1.2E+08	8.65E+07	1.33E+08	1.60E+08
2	6.25%	16.10%	28.81%	42.02%	9.85%	12.71%	13.21%		1.11E+08	1.43E+08	1.48E+08	1.48E+08	1.91E+08	1.98E+08
3	12.10%	26.56%	42.28%	56.47%	14.46%	15.72%	14.19%		1.62E+08	1.77E+08		2.17E+08	2.36E+08	
4	20.37%	38.81%	55.84%	69.30%	18.43%	17.04%	13.46%							
5	29.89%	50.65%	67.28%	78.96%	20.76%	16.63%	11.68%							
6	37.88%	59.30%	74.75%	84.71%	21.42%	15.45%	9.96%							
7	36.99%	58.39%	74.00%	84.15%	21.40%	15.61%	10.16%							
8	12.49%	27.20%	43.04%	57.23%	14.71%	15.84%	14.19%							
	P(V<V1)	P(V<V2)	P(V<V3)	P(V<V4)	P(V1<V<V2)	P(V2<V<V3)	P(V3<V<V4)		t_bin1	t_bin2	t_bin3	N_bin1	N_bin2	N_bin3
1	54.33%	74.30%	86.08%	92.53%	19.97%	11.78%	6.45%		2.24E+08			7.88E+08		
2	68.69%	84.88%	92.82%	96.56%	16.18%	7.94%	3.74%							
3	80.27%	91.86%	96.61%	98.55%	11.58%	4.76%	1.94%							
4	88.36%	95.88%	98.49%	99.42%	7.52%	2.61%	0.93%							
5	93.24%	97.92%	99.32%	99.76%	4.68%	1.40%	0.44%							
6	95.66%	98.80%	99.64%	99.88%	3.14%	0.84%	0.24%							
7	95.44%	98.72%	99.61%	99.87%	3.28%	0.89%	0.26%							
8	80.81%	92.14%	96.76%	98.62%	11.34%	4.61%	1.87%							

		IAH (N-S)-Open Terrain probabilities								seconds in each bin			cycles in each bin		
Segment		P(V<V1)	P(V<V2)	P(V<V3)	P(V<V4)	P(V1<V<V2)	P(V2<V<V3)	P(V3<V<V4)		t_bin1	t_bin2	t_bin3	N_bin1	N_bin2	N_bin3
1		0.00%	0.00%	0.02%	0.09%	0.00%	0.02%	0.06%		32390.45	162030.1	517417.5	1.16E+04	5.82E+04	1.86E+05
2		0.00%	0.02%	0.10%	0.32%	0.02%	0.08%	0.22%		153392.8	640672.6	1759917	5.51E+04	2.30E+05	6.32E+05
3		0.01%	0.09%	0.35%	0.98%	0.08%	0.26%	0.63%		604219.5	2113299	5006963	2.17E+05	7.59E+05	1.80E+06
4		0.05%	0.29%	1.02%	2.51%	0.25%	0.73%	1.49%		1969832	5799870	11906402	7.07E+05	2.08E+06	4.27E+06
5		0.16%	0.81%	2.46%	5.40%	0.66%	1.64%	2.95%		5241557	13128568	23561225	1.88E+06	4.71E+06	8.46E+06
6		0.40%	1.78%	4.79%	9.60%	1.38%	3.01%	4.81%		11036141	24038191	38416772	3.96E+06	8.63E+06	1.38E+07
7		0.63%	2.59%	6.55%	12.52%	1.96%	3.96%	5.97%		15634838	31684353	47696269	5.61E+06		
8		0.19%	0.95%	2.80%	6.05%	0.76%	1.85%	3.25%		6065304	14800963	25993770			
									E-W Gusts	22874717			8212023.36		
		P(V<V1)	P(V<V2)	P(V<V3)	P(V<V4)	P(V1<V<V2)	P(V2<V<V3)	P(V3<V<V4)		t_bin1	t_bin2	t_bin3	N_bin1	N_bin2	N_bin3
1		4.54%	12.67%	23.98%	36.45%	8.13%	11.31%	12.47%		64955419	90386040	99704312	8.68E+07	1.21E+08	1.33E+08
2		9.81%	22.86%	37.89%	52.08%	13.04%	15.03%	14.19%		1.04E+08	1.2E+08	1.13E+08	1.39E+08	1.61E+08	1.52E+08
3		18.35%	36.18%	53.25%	67.08%	17.84%	17.07%	13.83%		1.43E+08	1.36E+08		1.91E+08	1.82E+08	
4		29.95%	50.91%	67.65%	79.34%	20.96%	16.74%	11.70%							
5		43.08%	64.59%	79.08%	87.90%	21.51%	14.50%	8.81%							
6		55.08%	75.06%	86.68%	92.95%	19.98%	11.62%	6.27%							
7		61.14%	79.72%	89.74%	94.82%	18.58%	10.02%	5.08%							
8		45.30%	66.66%	80.67%	89.00%	21.36%	14.00%	8.33%							
		P(V<V1)	P(V<V2)	P(V<V3)	P(V<V4)	P(V1<V<V2)	P(V2<V<V3)	P(V3<V<V4)		t_bin1	t_bin2	t_bin3	N_bin1	N_bin2	N_bin3
1		63.61%	81.51%	90.86%	95.47%	17.89%	9.35%	4.62%		1.43E+08			5.02E+08		
2		77.24%	90.24%	95.82%	98.17%	13.00%	5.58%	2.35%							
3		87.22%	95.40%	98.30%	99.35%	8.19%	2.90%	1.04%							
4		93.49%	98.04%	99.37%	99.79%	4.55%	1.34%	0.41%							
5		96.89%	99.21%	99.78%	99.93%	2.32%	0.57%	0.15%							
6		98.49%	99.67%	99.92%	99.98%	1.18%	0.25%	0.06%							
7		98.99%	99.80%	99.95%	99.99%	0.81%	0.16%	0.04%							
8		97.26%	99.32%	99.82%	99.95%	2.06%	0.49%	0.13%							

Segment		IAH (N-S)-Suburban Terrain probabilities								seconds in each bin			cycles in each bin			
		P(V<V1)	P(V<V2)	P(V<V3)	P(V<V4)	P(V1<V<V2)	P(V2<V<V3)	P(V3<V<V4)		t_bin1	t_bin2	t_bin3	N_bin1	N_bin2	N_bin3	
1		0.00%	0.02%	0.08%	0.25%	0.01%	0.06%	0.17%		111137.7	482641.4	1369639	3.99E+04	1.73E+05	4.92E+05	
2		0.01%	0.06%	0.26%	0.76%	0.06%	0.20%	0.49%		439896.5	1606069	3943799	1.58E+05	5.77E+05	1.42E+06	
3		0.03%	0.21%	0.77%	1.96%	0.18%	0.56%	1.19%		1445008	4460442	9523851	5.19E+05	1.60E+06	3.42E+06	
4		0.11%	0.60%	1.89%	4.30%	0.49%	1.29%	2.41%		3910532	10303590	19286076	1.40E+06	3.70E+06	6.92E+06	
5		0.29%	1.36%	3.80%	7.88%	1.07%	2.44%	4.07%		8530243	19539125	32558191	3.06E+06	7.01E+06	1.17E+07	
6		0.56%	2.34%	6.02%	11.65%	1.78%	3.68%	5.63%		14226789	29414993	45022379	5.11E+06	1.06E+07	1.62E+07	
7		0.52%	2.21%	5.74%	11.20%	1.69%	3.53%	5.45%		13502929	28225139	43594398	4.85E+06			
8		0.04%	0.23%	0.81%	2.06%	0.19%	0.59%	1.24%		1533901	4692527	9944834				
		P(V<V1)	P(V<V2)	P(V<V3)	P(V<V4)	P(V1<V<V2)	P(V2<V<V3)	P(V3<V<V4)		t_bin1	t_bin2	t_bin3	N_bin1	N_bin2	N_bin3	
1		8.41%	20.34%	34.66%	48.65%	11.93%	14.32%	13.99%		95385555	1.14E+08	1.12E+08	1.28E+08	1.53E+08	1.49E+08	
2		15.95%	32.72%	49.50%	63.61%	16.76%	16.78%	14.11%		1.34E+08	1.34E+08	1.13E+08	1.79E+08	1.79E+08	1.51E+08	
3		26.47%	46.80%	63.86%	76.28%	20.33%	17.06%	12.42%		1.63E+08	1.36E+08		2.17E+08	1.82E+08		
4		38.81%	60.42%	75.79%	85.54%	21.62%	15.36%	9.76%								
5		50.76%	71.48%	84.20%	91.36%	20.73%	12.72%	7.16%								
6		59.48%	78.48%	88.94%	94.34%	19.00%	10.47%	5.40%								
7		58.56%	77.79%	88.49%	94.07%	19.22%	10.71%	5.58%								
8		27.11%	47.58%	64.59%	76.88%	20.47%	17.02%	12.29%								
		P(V<V1)	P(V<V2)	P(V<V3)	P(V<V4)	P(V1<V<V2)	P(V2<V<V3)	P(V3<V<V4)		t_bin1	t_bin2	t_bin3	N_bin1	N_bin2	N_bin3	
1		74.56%	88.68%	95.00%	97.75%	14.11%	6.32%	2.76%		1.13E+08			3.96E+08			
2		85.14%	94.42%	97.86%	99.15%	9.28%	3.44%	1.29%								
3		92.07%	97.49%	99.17%	99.71%	5.42%	1.67%	0.54%								
4		96.03%	98.94%	99.69%	99.90%	2.90%	0.75%	0.21%								
5		98.02%	99.54%	99.88%	99.97%	1.52%	0.34%	0.08%								
6		98.87%	99.77%	99.94%	99.99%	0.90%	0.18%	0.04%								
7		98.79%	99.75%	99.94%	99.98%	0.95%	0.19%	0.04%								
8		92.36%	97.60%	99.21%	99.72%	5.25%	1.60%	0.51%								

	RMMA (N-S)-Open Terrain probabilities								seconds in each bin			cycles in each bin			
Segment	P(V<V1)	P(V<V2)	P(V<V3)	P(V<V4)	P(V1<V<V2)	P(V2<V<V3)	P(V3<V<V4)		t_bin1	t_bin2	t_bin3	N_bin1	N_bin2	N_bin3	
1	0.00%	0.00%	0.01%	0.04%	0.00%	0.01%	0.03%		18422.84	100485.7	345091.6	6.61E+03	3.61E+04	1.24E+05	
2	0.00%	0.01%	0.05%	0.17%	0.01%	0.04%	0.12%		94034.01	428657.7	1267289	3.38E+04	1.54E+05	4.55E+05	
3	0.01%	0.04%	0.19%	0.56%	0.04%	0.15%	0.37%		398732.3	1523617	3887967	1.43E+05	5.47E+05	1.40E+06	
4	0.02%	0.16%	0.59%	1.54%	0.13%	0.43%	0.95%		1396238	4495849	9947808	5.01E+05	1.61E+06	3.57E+06	
5	0.08%	0.46%	1.51%	3.53%	0.38%	1.04%	2.02%		3973080	10893522	21086617	1.43E+06	3.91E+06	7.57E+06	
6	0.22%	1.07%	3.10%	6.59%	0.85%	2.03%	3.50%		8864076	21153129	36485294	3.18E+06	7.59E+06	1.31E+07	
7	0.35%	1.59%	4.35%	8.83%	1.24%	2.75%	4.48%		12938627	28740336	46708278	4.64E+06			
8	0.10%	0.54%	1.73%	3.99%	0.45%	1.19%	2.25%		4647433	12416625	23522873				
								E-W Gusts	18359523			6591068.67			
	P(V<V1)	P(V<V2)	P(V<V3)	P(V<V4)	P(V1<V<V2)	P(V2<V<V3)	P(V3<V<V4)		t_bin1	t_bin2	t_bin3	N_bin1	N_bin2	N_bin3	
1	2.92%	8.94%	18.15%	29.12%	6.02%	9.20%	10.98%		62793715	96007119	1.15E+08	8.40E+07	1.28E+08	1.53E+08	
2	6.76%	17.20%	30.44%	43.97%	10.44%	13.24%	13.53%		1.09E+08	1.38E+08	1.41E+08	1.46E+08	1.85E+08	1.89E+08	
3	13.46%	28.88%	45.13%	59.39%	15.42%	16.25%	14.26%		1.61E+08	1.69E+08		2.15E+08	2.27E+08		
4	23.30%	42.81%	60.00%	73.02%	19.51%	17.19%	13.02%								
5	35.27%	56.74%	72.71%	83.25%	21.47%	15.97%	10.54%								
6	46.95%	68.13%	81.75%	89.72%	21.18%	13.62%	7.97%								
7	53.13%	73.45%	85.56%	92.23%	20.32%	12.11%	6.67%								
8	37.38%	58.94%	74.56%	84.63%	21.56%	15.61%	10.07%								
	P(V<V1)	P(V<V2)	P(V<V3)	P(V<V4)	P(V1<V<V2)	P(V2<V<V3)	P(V3<V<V4)		t_bin1	t_bin2	t_bin3	N_bin1	N_bin2	N_bin3	
1	55.71%	75.54%	86.99%	93.14%	19.82%	11.45%	6.14%		2.07E+08			7.26E+08			
2	70.60%	86.20%	93.62%	97.02%	15.60%	7.42%	3.40%								
3	82.41%	93.04%	97.21%	98.85%	10.63%	4.17%	1.64%								
4	90.44%	96.82%	98.90%	99.60%	6.38%	2.08%	0.70%								
5	95.13%	98.63%	99.59%	99.87%	3.50%	0.96%	0.28%								
6	97.50%	99.39%	99.84%	99.95%	1.90%	0.45%	0.12%								
7	98.28%	99.61%	99.90%	99.97%	1.34%	0.29%	0.07%								
8	95.67%	98.81%	99.65%	99.89%	3.14%	0.83%	0.24%								

	RMMA (N-S)-Suburban Terrain probabilities								seconds in each bin			cycles in each bin			
Segment	P(V<V1)	P(V<V2)	P(V<V3)	P(V<V4)	P(V1<V<V2)	P(V2<V<V3)	P(V3<V<V4)		t_bin1	t_bin2	t_bin3	N_bin1	N_bin2	N_bin3	
1	0.00%	0.01%	0.04%	0.13%	0.01%	0.03%	0.09%		67036.09146	317667.6553	970046.9523	2.41E+04	1.14E+05	3.48E+05	
2	0.00%	0.03%	0.14%	0.43%	0.03%	0.11%	0.29%		285163.1247	1137178.777	3007001.486	1.02E+05	4.08E+05	1.08E+06	
3	0.02%	0.11%	0.44%	1.18%	0.10%	0.32%	0.75%		1004347.874	3389488.663	7798912.515	3.61E+05	1.22E+06	2.80E+06	
4	0.06%	0.33%	1.14%	2.76%	0.28%	0.80%	1.62%		2902553.37	8369198.735	16892793.13	1.04E+06	3.00E+06	6.06E+06	
5	0.16%	0.80%	2.41%	5.31%	0.64%	1.61%	2.90%		6709951.104	16833892.27	30266881.82	2.41E+06	6.04E+06	1.09E+07	
6	0.31%	1.43%	3.97%	8.16%	1.12%	2.54%	4.19%		11676008.84	26457809.77	43715708.54	4.19E+06	9.50E+06	1.57E+07	
7	0.29%	1.35%	3.77%	7.81%	1.06%	2.42%	4.04%		11031883	25271192.56	42133088.64	3.96E+06			
8	0.02%	0.12%	0.46%	1.25%	0.10%	0.34%	0.78%		1070111.956	3579348.618	8174790.703				
	P(V<V1)	P(V<V2)	P(V<V3)	P(V<V4)	P(V1<V<V2)	P(V2<V<V3)	P(V3<V<V4)		t_bin1	t_bin2	t_bin3	N_bin1	N_bin2	N_bin3	
1	5.71%	15.10%	27.50%	40.61%	9.39%	12.40%	13.11%		98008736.04	129383682.3	136725088.2	1.31E+08	1.73E+08	1.83E+08	
2	11.53%	25.75%	41.43%	55.71%	14.22%	15.68%	14.28%		148382305.2	163539274.6	148948827.3	1.98E+08	2.19E+08	1.99E+08	
3	20.27%	38.82%	55.98%	69.51%	18.54%	17.16%	13.54%		193462627.6	179010953.1		2.59E+08	2.39E+08		
4	31.29%	52.39%	68.95%	80.36%	21.11%	16.56%	11.41%								
5	42.66%	64.16%	78.74%	87.64%	21.50%	14.57%	8.91%								
6	51.42%	72.02%	84.56%	91.59%	20.60%	12.54%	7.03%								
7	50.48%	71.22%	84.00%	91.22%	20.74%	12.77%	7.22%								
8	20.83%	39.57%	56.75%	70.19%	18.74%	17.18%	13.45%								
	P(V<V1)	P(V<V2)	P(V<V3)	P(V<V4)	P(V1<V<V2)	P(V2<V<V3)	P(V3<V<V4)		t_bin1	t_bin2	t_bin3	N_bin1	N_bin2	N_bin3	
1	67.58%	84.22%	92.48%	96.39%	16.65%	8.26%	3.91%		173680102.4			6.10E+08			
2	79.87%	91.70%	96.56%	98.53%	11.82%	4.86%	1.98%								
3	88.57%	96.01%	98.56%	99.46%	7.44%	2.55%	0.90%								
4	93.92%	98.20%	99.43%	99.81%	4.28%	1.23%	0.38%								
5	96.79%	99.18%	99.77%	99.93%	2.39%	0.59%	0.16%								
6	98.08%	99.56%	99.89%	99.97%	1.48%	0.33%	0.08%								
7	97.97%	99.53%	99.88%	99.97%	1.56%	0.35%	0.09%								
8	88.94%	96.17%	98.63%	99.49%	7.23%	2.46%	0.86%								

	ELP (N-S)Open Terrain probabilities								seconds in each bin			cycles in each bin			
Segment	P(V<V1)	P(V<V2)	P(V<V3)	P(V<V4)	P(V1<V<V2)	P(V2<V<V3)	P(V3<V<V4)		t_bin1	t_bin2	t_bin3	N_bin1	N_bin2	N_bin3	
1	0.00%	0.01%	0.06%	0.20%	0.01%	0.05%	0.14%		68743.36	322939.2	970592.2	2.47E+04	1.16E+05	3.48E+05	
2	0.01%	0.05%	0.23%	0.69%	0.05%	0.18%	0.46%		308487.1	1198457	3073780	1.11E+05	4.30E+05	1.10E+06	
3	0.03%	0.20%	0.75%	1.96%	0.17%	0.55%	1.21%		1144046	3686735	8091244	4.11E+05	1.32E+06	2.90E+06	
4	0.11%	0.63%	2.04%	4.68%	0.52%	1.40%	2.65%		3493963	9390882	17720742	1.25E+06	3.37E+06	6.36E+06	
5	0.35%	1.65%	4.59%	9.41%	1.30%	2.94%	4.82%		8692039	19699621	32262344	3.12E+06	7.07E+06	1.16E+07	
6	0.85%	3.42%	8.44%	15.72%	2.57%	5.02%	7.28%		17188962	33619236	48722427	6.17E+06	1.21E+07	1.75E+07	
7	1.30%	4.82%	11.19%	19.86%	3.52%	6.37%	8.67%		23537342	42661458	58047196	8.45E+06			
8	0.42%	1.90%	5.18%	10.42%	1.49%	3.27%	5.24%		9944246	21926529	35099182				
								E-W Gusts	1.22E+08			4.38E+07			
	P(V<V1)	P(V<V2)	P(V<V3)	P(V<V4)	P(V1<V<V2)	P(V2<V<V3)	P(V3<V<V4)		t_bin1	t_bin2	t_bin3	N_bin1	N_bin2	N_bin3	
1	8.05%	20.07%	34.72%	49.08%	12.02%	14.65%	14.36%		80490414	98096633	96152608	1.08E+08	1.31E+08	1.29E+08	
2	16.03%	33.35%	50.64%	65.02%	17.31%	17.29%	14.38%		1.16E+08	1.16E+08	96290869	1.55E+08	1.55E+08	1.29E+08	
3	27.66%	48.79%	66.13%	78.40%	21.13%	17.34%	12.27%		1.41E+08	1.16E+08		1.89E+08	1.55E+08		
4	41.79%	63.89%	78.87%	87.93%	22.10%	14.98%	9.07%								
5	56.09%	76.30%	87.75%	93.73%	20.21%	11.44%	5.98%								
6	67.84%	84.75%	92.95%	96.73%	16.92%	8.20%	3.78%								
7	73.32%	88.20%	94.86%	97.73%	14.88%	6.66%	2.87%								
8	58.37%	78.05%	88.88%	94.41%	19.69%	10.83%	5.53%								
	P(V<V1)	P(V<V2)	P(V<V3)	P(V<V4)	P(V1<V<V2)	P(V2<V<V3)	P(V3<V<V4)		t_bin1	t_bin2	t_bin3	N_bin1	N_bin2	N_bin3	
1	75.47%	89.47%	95.53%	98.07%	14.00%	6.05%	2.54%		93755434			3.29E+08			
2	86.39%	95.16%	98.24%	99.34%	8.77%	3.08%	1.09%								
3	93.30%	98.03%	99.39%	99.80%	4.74%	1.36%	0.41%								
4	97.02%	99.28%	99.81%	99.94%	2.26%	0.53%	0.14%								
5	98.76%	99.75%	99.94%	99.99%	0.99%	0.19%	0.04%								
6	99.47%	99.91%	99.98%	100.00%	0.44%	0.07%	0.01%								
7	99.67%	99.95%	99.99%	100.00%	0.28%	0.04%	0.01%								
8	98.93%	99.79%	99.95%	99.99%	0.86%	0.16%	0.03%								

	ELP(N-S)Suburban Terrain probabilities								seconds in each bin			cycles in each bin		
Segment	P(V<V1)	P(V<V2)	P(V<V3)	P(V<V4)	P(V1<V<V2)	P(V2<V<V3)	P(V3<V<V4)		t_bin1	t_bin2	t_bin3	N_bin1	N_bin2	N_bin3
1	0.00%	0.04%	0.17%	0.54%	0.03%	0.14%	0.36%		226269.2	915891.4	2430930	8.12E+04	3.29E+05	8.73E+05
2	0.02%	0.15%	0.57%	1.54%	0.13%	0.43%	0.97%		845708.9	2851459	6498453	3.04E+05	1.02E+06	2.33E+06
3	0.08%	0.47%	1.57%	3.74%	0.39%	1.10%	2.17%		2611122	7376388	14508129	9.37E+05	2.65E+06	5.21E+06
4	0.25%	1.24%	3.61%	7.66%	0.99%	2.37%	4.05%		6627010	15843428	27123867	2.38E+06	5.69E+06	9.74E+06
5	0.63%	2.66%	6.85%	13.19%	2.03%	4.19%	6.34%		13596057	28042146	42469283	4.88E+06	1.01E+07	1.52E+07
6	1.16%	4.39%	10.37%	18.65%	3.23%	5.98%	8.28%		21623417	40030747	55431066	7.76E+06	1.44E+07	1.99E+07
7	1.09%	4.17%	9.94%	18.01%	3.08%	5.77%	8.07%		20629708	38634069	54010652	7.41E+06		
8	0.08%	0.50%	1.65%	3.90%	0.41%	1.15%	2.25%		2762091	7729400	15083247			
	P(V<V1)	P(V<V2)	P(V<V3)	P(V<V4)	P(V1<V<V2)	P(V2<V<V3)	P(V3<V<V4)		t_bin1	t_bin2	t_bin3	N_bin1	N_bin2	N_bin3
1	13.98%	30.20%	47.12%	61.70%	16.23%	16.92%	14.58%		1.09E+08	1.13E+08	97615668	1.45E+08	1.51E+08	1.31E+08
2	24.52%	44.95%	62.53%	75.46%	20.43%	17.58%	12.94%		1.37E+08	1.18E+08	86628262	1.83E+08	1.57E+08	1.16E+08
3	37.72%	59.87%	75.68%	85.68%	22.15%	15.82%	10.00%		1.48E+08	1.06E+08		1.98E+08	1.42E+08	
4	51.62%	72.69%	85.31%	92.21%	21.07%	12.62%	6.91%							
5	63.75%	81.98%	91.32%	95.82%	18.23%	9.34%	4.50%							
6	71.85%	87.31%	94.38%	97.48%	15.46%	7.07%	3.11%							
7	71.03%	86.80%	94.10%	97.34%	15.77%	7.30%	3.24%							
8	38.49%	60.64%	76.31%	86.13%	22.16%	15.67%	9.82%							
	P(V<V1)	P(V<V2)	P(V<V3)	P(V<V4)	P(V1<V<V2)	P(V2<V<V3)	P(V3<V<V4)		t_bin1	t_bin2	t_bin3	N_bin1	N_bin2	N_bin3
1	84.38%	94.21%	97.83%	99.15%	9.84%	3.61%	1.33%		65853883			2.31E+08		
2	91.95%	97.53%	99.20%	99.73%	5.58%	1.68%	0.52%							
3	96.23%	99.04%	99.73%	99.92%	2.81%	0.70%	0.19%							
4	98.35%	99.65%	99.92%	99.98%	1.30%	0.27%	0.06%							
5	99.27%	99.87%	99.97%	99.99%	0.60%	0.10%	0.02%							
6	99.62%	99.94%	99.99%	100.00%	0.32%	0.05%	0.01%							
7	99.59%	99.93%	99.99%	100.00%	0.34%	0.05%	0.01%							
8	96.40%	99.09%	99.75%	99.93%	2.69%	0.66%	0.18%							

HM-12-80-175						Equivalent Static Pressure Ranges						v(ft2/s)=	0.0001615	Stress ranges for pole with no GS				
Segment	Avg dia (in)	Mid ht. (ft)	f 1 (Hz)	V1 (mph - 3s)	V2 (mph - 3s)	V3 (mph - 3s)	V4 (mph - 3s)	Pvs1 (psf)	Pvs2 (psf)	Pvs3 (psf)	Pvs4 (psf)	Re1 300≤Re≤1.0E+05 Re>3.5E+06	Re2	Re3	Re4	Sr1 (ksi)	Sr2 (ksi)	Sr3 (ksi)	Sr4 (ksi)
1	8.611	170.008	0.32	1.0	1.3	1.7	2.0	0.33	0.56	0.8	1.2	6.8E+03	8.8E+03	1.1E+04	1.3E+04	0.017	0.028	0.043	0.060
2	10.525	158.914	0.32	1.3	1.6	2.0	2.4	0.50	0.84	1.3	1.8	1.0E+04	1.3E+04	1.6E+04	1.9E+04	0.029	0.049	0.074	0.104
3	12.864	145.355	0.32	1.6	2.0	2.5	2.9	0.74	1.2	1.9	2.7	1.5E+04	2.0E+04	2.4E+04	2.9E+04	0.063	0.106	0.160	0.225
4	15.722	128.602	0.32	1.9	2.5	3.0	3.6	1.1	1.9	2.8	4.0	2.3E+04	2.9E+04	3.6E+04	4.3E+04	0.125	0.210	0.317	0.446
5	19.216	107.457	0.32	2.3	3.0	3.7	4.4	1.7	2.8	4.2	5.9	3.4E+04	4.4E+04	5.4E+04	6.4E+04	0.231	0.389	0.587	0.826
6	23.486	81.034	0.32	2.8	3.7	4.5	5.4	2.5	4.2	6.3	8.8	5.1E+04	6.6E+04	8.1E+04	9.6E+04	0.422	0.709	1.071	1.507
7	28.705	48.437	0.32	3.5	4.5	5.5	6.6	3.7	6.2	9.4	13.2	7.6E+04	9.8E+04	1.2E+05	1.4E+05	0.509	1.059		
8	33.913	15.207	0.32	4.1	5.3	6.5	7.7	5.2	8.7	13.1	18.4	1.1E+05	1.4E+05	1.7E+05	2.0E+05				
		Pvs(windgu	0.32					6.2								4.91859			
Segment	Avg dia (in)	Mid ht. (ft)	f (2nd) (Hz)	V1 (mph - 3s)	V2 (mph - 3s)	V3 (mph - 3s)	V4 (mph - 3s)	Pvs1 (psf)	Pvs2 (psf)	Pvs3 (psf)	Pvs4 (psf)	Re1 00≤Re≤1.0E+05 Re>3.5E+06	Re2	Re3	Re4	Sr1 (ksi)	Sr2 (ksi)	Sr3 (ksi)	Sr4 (ksi)
1	8.611	170.008	1.127	3.7	4.8	5.8	6.9	4.13	6.94	10.5	14.7	2.4E+04	3.1E+04	3.8E+04	4.5E+04	0.208	0.349	0.527	0.742
2	10.525	158.914	1.127	4.5	5.8	7.1	8.5	6.17	10.37	15.7	22.0	3.6E+04	4.6E+04	5.7E+04	6.8E+04	0.359	0.604	0.912	1.284
3	12.864	145.355	1.127	5.5	7.1	8.7	10.4	9.2	15.5	23.4	32.9	5.3E+04	6.9E+04	8.5E+04	1.0E+05	0.783	1.316	1.987	2.796
4	15.722	128.602	1.127	6.7	8.7	10.7	12.7	13.8	23.1	34.9	49.2	8.0E+04	1.0E+05	1.3E+05	1.5E+05	1.550	2.605		
5	19.216	107.457	1.127	8.2	10.6	13.0	15.5	20.6	34.6	52.2	73.4	1.2E+05	1.5E+05	1.9E+05	2.3E+05				
6	23.486	81.034	1.127	10.0	13.0	15.9	18.9	30.7	51.6	78.0	109.7	1.8E+05	2.3E+05	2.8E+05	3.4E+05				
7	28.705	48.437	1.127	12.2	15.8	19.5	23.1	45.9	77.1	116.5	163.9	2.7E+05	3.5E+05	4.2E+05	5.0E+05				
8	33.913	15.207	1.127	14.4	18.7	23.0	27.3	64.0	107.7	162.6	228.8	3.7E+05	4.8E+05	5.9E+05	7.0E+05				
Segment	Avg dia (in)	Mid ht. (ft)	f 3 (Hz)	V1 (mph - 3s)	V2 (mph - 3s)	V3 (mph - 3s)	V4 (mph - 3s)	Pvs1 (psf)	Pvs2 (psf)	Pvs3 (psf)	Pvs4 (psf)	Re1 00≤Re≤1.0E+05 Re>3.5E+06	Re2	Re3	Re4	Sr1 (ksi)	Sr2 (ksi)	Sr3 (ksi)	Sr4
1	8.611	170.008	2.867	9.3	12.1	14.9	17.6	26.7	44.9	67.8	95.5	6.1E+04	7.9E+04	9.7E+04	1.2E+05	1.344	2.260	3.412	
2	10.525	158.914	2.867	11.4	14.8	18.2	21.5	39.9	67.1	101.3	142.6	9.1E+04	1.2E+05	1.4E+05	1.7E+05	2.326			
3	12.864	145.355	2.867	13.9	18.1	22.2	26.3	59.6	100.3	151.4	213.0	1.4E+05	1.8E+05	2.2E+05	2.6E+05				
4	15.722	128.602	2.867	17.0	22.1	27.1	32.2	89.1	149.8	226.1	318.2	2.0E+05	2.6E+05	3.2E+05	3.8E+05				
5	19.216	107.457	2.867	20.8	27.0	33.2	39.3	133.1	223.7	337.8	475.3	3.0E+05	3.9E+05	4.8E+05	5.7E+05				
6	23.486	81.034	2.867	25.4	33.0	40.5	48.1	198.8	334.2	504.6	710.1	4.5E+05	5.9E+05	7.2E+05	8.6E+05				
7	28.705	48.437	2.867	31.1	40.3	49.5	58.8	296.9	499.3	753.8	1060.7	6.8E+05	8.8E+05	1.1E+06	1.3E+06				
8	33.913	15.207	2.867	36.7	47.6	58.5	69.4	414.5	696.8	1052.2	1480.5	9.4E+05	1.2E+06	1.5E+06	1.8E+06				

HM-12-80-	Stress ranges for pole with GS				SAT (N-S)-Open Terrain probabilities								seconds in each bin			cycles in each bin		
Segment	Sr1 (ksi)	Sr2 (ksi)	Sr3 (ksi)	Sr4 (ksi)	P(V<V1)	P(V<V2)	P(V<V3)	P(V<V4)	P(V1<V<V2)	P(V2<V<V3)	P(V3<V<V4)		t_bin1	t_bin2	t_bin3	N_bin1	N_bin2	N_bin3
1	0.008	0.014	0.020	0.029	0.00%	0.01%	0.04%	0.13%	0.01%	0.03%	0.08%		86320.84032	323668.5324	842158.9154	2.76E+04	1.04E+05	2.69E+05
2	0.014	0.023	0.035	0.050	0.01%	0.04%	0.14%	0.39%	0.03%	0.11%	0.24%		322076.4333	1046598.043	2417749.343	1.03E+05	3.35E+05	7.74E+05
3	0.030	0.051	0.077	0.108	0.02%	0.13%	0.42%	1.03%	0.10%	0.30%	0.61%		1041661.419	2938724.436	6037206.334	3.33E+05	9.40E+05	1.93E+06
4	0.060	0.101	0.152	0.214	0.08%	0.37%	1.09%	2.41%	0.29%	0.72%	1.32%		2911605.737	7153611.095	13104936.36	9.32E+05	2.29E+06	4.19E+06
5	0.111	0.187	0.282	0.396	0.23%	0.93%	2.44%	4.92%	0.70%	1.51%	2.48%		6980074.634	15023233.77	24665266.62	2.23E+06	4.81E+06	7.89E+06
6	0.202	0.340	0.514	0.723	0.55%	1.98%	4.69%	8.72%	1.42%	2.72%	4.03%		14162295.98	27002160.44	40106023.88	4.53E+06	8.64E+06	1.28E+07
7	0.244	0.508			1.04%	3.37%	7.41%	12.96%	2.33%	4.04%	5.55%		23178339.11	40191243.34	55197024.64	7.42E+06		
8					1.00%	3.27%	7.23%	12.69%	2.27%	3.96%	5.46%		22566291.86	39343139.27	54275060.28			
	2.360605											E-W Gusts	11298933.27			3615658.6		
Segment	Sr1 (ksi)	Sr2 (ksi)	Sr3 (ksi)	Sr4 (ksi)	P(V<V1)	P(V<V2)	P(V<V3)	P(V<V4)	P(V1<V<V2)	P(V2<V<V3)	P(V3<V<V4)		t_bin1	t_bin2	t_bin3	N_bin1	N_bin2	N_bin3
1	0.100	0.168	0.253	0.356	3.15%	8.43%	16.03%	24.97%	5.29%	7.60%	8.94%		52577439.64	75544399.29	88857795.39	5.93E+07	8.51E+07	1.00E+08
2	0.173	0.290	0.438	0.616	6.61%	15.34%	26.15%	37.41%	8.73%	10.81%	11.26%		86777021.22	107510424.8	111947338.8	9.78E+07	1.21E+08	1.26E+08
3	0.376	0.632	0.954	1.342	12.37%	25.03%	38.58%	51.10%	12.67%	13.55%	12.51%		125923065.6	134750304.8		1.42E+08	1.52E+08	
4	0.744	1.250			20.68%	36.91%	51.96%	64.31%	16.23%	15.05%	12.35%							
5					31.05%	49.56%	64.51%	75.49%	18.51%	14.96%	10.97%							
6					42.08%	61.16%	74.76%	83.76%	19.08%	13.60%	9.00%							
7					51.19%	69.61%	81.50%	88.77%	18.42%	11.89%	7.26%							
8					50.67%	69.15%	81.15%	88.52%	18.48%	12.00%	7.36%							
Segment	Sr1 (ksi)	Sr2 (ksi)	Sr3 (ksi)	Sr4	P(V<V1)	P(V<V2)	P(V<V3)	P(V<V4)	P(V1<V<V2)	P(V2<V<V3)	P(V3<V<V4)		t_bin1	t_bin2	t_bin3	N_bin1	N_bin2	N_bin3
1	0.645	1.084	1.6		45.12%	64.09%	77.16%	85.58%	18.97%	13.07%	8.42%		188560642.7			5.41E+08		
2	1.116				59.17%	76.28%	86.40%	92.17%	17.11%	10.13%	5.76%							
3					71.92%	85.63%	92.61%	96.12%	13.71%	6.98%	3.51%							
4					82.11%	91.97%	96.30%	98.23%	9.86%	4.33%	1.93%							
5					89.30%	95.78%	98.25%	99.24%	6.48%	2.47%	0.98%							
6					93.79%	97.83%	99.19%	99.68%	4.04%	1.35%	0.49%							
7					96.14%	98.78%	99.58%	99.84%	2.64%	0.80%	0.26%							
8					96.03%	98.74%	99.56%	99.84%	2.71%	0.82%	0.27%							

HM-12-80-	Avg Sr (No GS)			Avg Sr (w/GS)			SAT(N-S)-Suburban Terrain probabilities							seconds in each bin			cycles in each bin		
Segment	S_bin1	S_bin2	S_bin3	S_bin1	S_bin2	S_bin3	P(V<V1)	P(V<V2)	P(V<V3)	P(V<V4)	P(V1<V<V2)	P(V2<V<V3)	P(V3<V<V4)	t_bin1	t_bin2	t_bin3	N_bin1	N_bin2	N_bin3
1	0.022	0.035	0.051	0.011	0.017	0.025	0.00%	0.03%	0.12%	0.33%	0.03%	0.09%	0.21%	269968	895021.2	2102283	8.64E+04	2.86E+05	6.73E+05
2	0.039	0.061	0.089	0.019	0.029	0.042	0.02%	0.11%	0.36%	0.89%	0.09%	0.25%	0.53%	869517.2	2509565	5253859	2.78E+05	8.03E+05	1.68E+06
3	0.085	0.133	0.193	0.041	0.064	0.093	0.06%	0.31%	0.92%	2.07%	0.24%	0.61%	1.15%	2423911	6111400	11438125	7.76E+05	1.96E+06	3.66E+06
4	0.167	0.264	0.382	0.080	0.127	0.183	0.18%	0.77%	2.07%	4.25%	0.59%	1.30%	2.18%	5824148	12901384	21692036	1.86E+06	4.13E+06	6.94E+06
5	0.310	0.488	0.706	0.149	0.234	0.339	0.44%	1.64%	4.00%	7.60%	1.20%	2.36%	3.59%	11925552	23450708	35731260	3.82E+06	7.50E+06	1.14E+07
6	0.565	0.890	1.289	0.271	0.427	0.619	0.88%	2.93%	6.57%	11.69%	2.05%	3.65%	5.12%	20371241	36250276	50859862	6.52E+06	1.16E+07	1.63E+07
7	0.784			0.376			1.25%	3.94%	8.47%	14.53%	2.69%	4.53%	6.07%	26729508	44998794	60310524	8.55E+06		
8							0.68%	2.35%	5.45%	9.93%	1.67%	3.10%	4.49%	16636046	30784343	44608405			
	4.919			2.3606															
Segment	S_bin1	S_bin2	S_bin3	S_bin1	S_bin2	S_bin3	P(V<V1)	P(V<V2)	P(V<V3)	P(V<V4)	P(V1<V<V2)	P(V2<V<V3)	P(V3<V<V4)	t_bin1	t_bin2	t_bin3	N_bin1	N_bin2	N_bin3
1	0.278	0.438	0.635	0.134	0.210	0.305	6.00%	14.20%	24.57%	35.55%	8.20%	10.37%	10.98%	81513312	1.03E+08	1.09E+08	9.19E+07	1.16E+08	1.23E+08
2	0.482	0.758	1.098	0.231	0.364	0.527	11.26%	23.28%	36.46%	48.86%	12.03%	13.18%	12.40%	1.2E+08	1.31E+08	1.23E+08	1.35E+08	1.48E+08	1.39E+08
3	1.049	1.652		0.504	0.793		18.92%	34.55%	49.43%	61.92%	15.63%	14.88%	12.49%	1.55E+08	1.48E+08		1.75E+08	1.67E+08	
4							28.62%	46.76%	61.87%	73.23%	18.15%	15.11%	11.36%						
5							39.17%	58.26%	72.30%	81.85%	19.09%	14.04%	9.54%						
6							48.70%	67.39%	79.79%	87.53%	18.69%	12.40%	7.74%						
7							54.03%	72.06%	83.35%	90.07%	18.03%	11.29%	6.72%						
8							44.93%	63.91%	77.01%	85.47%	18.98%	13.11%	8.46%						
Segment	S_bin1	S_bin2	S_bin3	S_bin1	S_bin2	S_bin3	P(V<V1)	P(V<V2)	P(V<V3)	P(V<V4)	P(V1<V<V2)	P(V2<V<V3)	P(V3<V<V4)	t_bin1	t_bin2	t_bin3	N_bin1	N_bin2	N_bin3
1	1.802			0.865			57.24%	74.72%	85.29%	91.42%	17.49%	10.57%	6.12%	1.74E+08			4.98E+08		
2							70.00%	84.32%	91.79%	95.63%	14.32%	7.47%	3.84%						
3							80.41%	90.98%	95.75%	97.94%	10.57%	4.77%	2.18%						
4							87.95%	95.11%	97.93%	99.08%	7.16%	2.82%	1.15%						
5							92.82%	97.42%	99.01%	99.59%	4.60%	1.59%	0.59%						
6							95.59%	98.57%	99.49%	99.81%	2.98%	0.93%	0.31%						
7							96.70%	98.99%	99.66%	99.87%	2.29%	0.67%	0.22%						
8							94.63%	98.18%	99.34%	99.74%	3.56%	1.15%	0.40%						

HM-12-80- DFW(N-S)-Open Terrain probabilities									seconds in each bin			cycles in each bin			
Segment	P(V<V1)	P(V<V2)	P(V<V3)	P(V<V4)	P(V1<V<V2)	P(V2<V<V3)	P(V3<V<V4)		t_bin1	t_bin2	t_bin3	N_bin1	N_bin2	N_bin3	
1	0.00%	0.00%	0.00%	0.01%	0.00%	0.00%	0.00%		1992.632	13443.76	55267.73	6.38E+02	4.30E+03	1.77E+04	
2	0.00%	0.00%	0.01%	0.03%	0.00%	0.01%	0.02%		12443.81	70290.73	249098	3.98E+03	2.25E+04	7.97E+04	
3	0.00%	0.01%	0.03%	0.12%	0.01%	0.03%	0.08%		64680.63	306573.1	938398.5	2.07E+04	9.81E+04	3.00E+05	
4	0.00%	0.03%	0.13%	0.39%	0.02%	0.10%	0.26%		278372.2	1111385	2948165	8.91E+04	3.56E+05	9.43E+05	
5	0.01%	0.10%	0.40%	1.08%	0.09%	0.30%	0.68%		979411.8	3317622	7674323	3.13E+05	1.06E+06	2.46E+06	
6	0.05%	0.29%	1.01%	2.47%	0.25%	0.71%	1.46%		2753585	8023752	16374952	8.81E+05	2.57E+06	5.24E+06	
7	0.12%	0.63%	1.95%	4.39%	0.51%	1.32%	2.44%		5722525	14820000	27420653	1.83E+06			
8	0.11%	0.60%	1.88%	4.25%	0.49%	1.28%	2.38%		5497878	14334698	26671953				
								E-W Gusts	19820568			6342581.66			
Segment	P(V<V1)	P(V<V2)	P(V<V3)	P(V<V4)	P(V1<V<V2)	P(V2<V<V3)	P(V3<V<V4)		t_bin1	t_bin2	t_bin3	N_bin1	N_bin2	N_bin3	
1	0.57%	2.35%	5.99%	11.55%	1.78%	3.65%	5.56%		19974529	40944541	62397930	2.25E+07	4.61E+07	7.03E+07	
2	1.65%	5.62%	12.38%	21.22%	3.97%	6.76%	8.84%		44537964	75913874	99301657	5.02E+07	8.56E+07	1.12E+08	
3	4.10%	11.59%	22.24%	34.21%	7.50%	10.65%	11.97%		84184177	1.2E+08		9.49E+07	1.35E+08		
4	8.73%	20.79%	35.11%	49.01%	12.06%	14.32%	13.90%								
5	16.01%	32.63%	49.25%	63.26%	16.62%	16.62%	14.01%								
6	25.38%	45.28%	62.28%	74.87%	19.90%	17.00%	12.59%								
7	34.31%	55.57%	71.61%	82.35%	21.26%	16.05%	10.74%								
8	33.77%	54.98%	71.11%	81.97%	21.21%	16.13%	10.86%								
Segment	P(V<V1)	P(V<V2)	P(V<V3)	P(V<V4)	P(V1<V<V2)	P(V2<V<V3)	P(V3<V<V4)		t_bin1	t_bin2	t_bin3	N_bin1	N_bin2	N_bin3	
1	28.24%	48.74%	65.53%	77.56%	20.49%	16.80%	12.02%		2.3E+08			6.60E+08			
2	42.99%	64.33%	78.78%	87.62%	21.34%	14.45%	8.84%								
3	58.53%	77.62%	88.31%	93.92%	19.09%	10.69%	5.61%								
4	72.48%	87.31%	94.21%	97.32%	14.83%	6.90%	3.11%								
5	83.17%	93.38%	97.36%	98.91%	10.21%	3.98%	1.55%								
6	90.19%	96.69%	98.83%	99.57%	6.49%	2.15%	0.73%								
7	93.96%	98.19%	99.42%	99.80%	4.24%	1.23%	0.38%								
8	93.78%	98.12%	99.40%	99.79%	4.35%	1.27%	0.40%								

HM-12-80- DFW (N-S)-Suburban Terrain probabilities									seconds in each bin			cycles in each bin		
Segment	P(V<V1)	P(V<V2)	P(V<V3)	P(V<V4)	P(V1<V<V2)	P(V2<V<V3)	P(V3<V<V4)		t_bin1	t_bin2	t_bin3	N_bin1	N_bin2	N_bin3
1	0.00%	0.00%	0.01%	0.02%	0.00%	0.01%	0.02%		9725.58788	56319.326	203774.726	3.11E+03	1.80E+04	6.52E+04
2	0.00%	0.00%	0.03%	0.09%	0.00%	0.02%	0.07%		50133.1255	244431.02	766042.792	1.60E+04	7.82E+04	2.45E+05
3	0.00%	0.02%	0.10%	0.31%	0.02%	0.08%	0.21%		214286.714	883437.4	2407065.21	6.86E+04	2.83E+05	7.70E+05
4	0.01%	0.08%	0.31%	0.87%	0.07%	0.24%	0.56%		753653.972	2645795.5	6305174.7	2.41E+05	8.47E+05	2.02E+06
5	0.04%	0.23%	0.80%	2.02%	0.19%	0.58%	1.21%		2138594.44	6475456.6	13643725	6.84E+05	2.07E+06	4.37E+06
6	0.09%	0.51%	1.64%	3.77%	0.42%	1.12%	2.14%		4718899.85	12620523	23983871.6	1.51E+06	4.04E+06	7.67E+06
7	0.15%	0.79%	2.36%	5.19%	0.63%	1.58%	2.83%		7088213.49	17694445	31754847.6	2.27E+06		
8	0.06%	0.38%	1.25%	2.98%	0.31%	0.87%	1.73%		3492810.13	9806636.6	19404705.4			
Segment	P(V<V1)	P(V<V2)	P(V<V3)	P(V<V4)	P(V1<V<V2)	P(V2<V<V3)	P(V3<V<V4)		t_bin1	t_bin2	t_bin3	N_bin1	N_bin2	N_bin3
1	1.44%	5.01%	11.28%	19.64%	3.58%	6.26%	8.37%		40192582.8	70301032	93946774.9	4.53E+07	7.92E+07	1.06E+08
2	3.57%	10.41%	20.41%	31.93%	6.84%	10.00%	11.52%		76768355.2	112267584	129397761	8.65E+07	1.27E+08	1.46E+08
3	7.65%	18.81%	32.50%	46.17%	11.16%	13.70%	13.67%		125277509	153809688		1.41E+08	1.73E+08	
4	14.16%	29.84%	46.11%	60.25%	15.68%	16.27%	14.14%							
5	22.76%	41.96%	59.04%	72.11%	19.20%	17.08%	13.07%							
6	31.76%	52.77%	69.18%	80.47%	21.01%	16.41%	11.29%							
7	37.31%	58.72%	74.27%	84.36%	21.41%	15.55%	10.09%							
8	28.06%	48.52%	65.34%	77.39%	20.46%	16.81%	12.06%							
Segment	P(V<V1)	P(V<V2)	P(V<V3)	P(V<V4)	P(V1<V<V2)	P(V2<V<V3)	P(V3<V<V4)		t_bin1	t_bin2	t_bin3	N_bin1	N_bin2	N_bin3
1	40.81%	62.23%	77.13%	86.44%	21.42%	14.89%	9.32%		240536859			6.90E+08		
2	56.06%	75.69%	87.03%	93.13%	19.63%	11.34%	6.10%							
3	70.05%	85.77%	93.34%	96.85%	15.71%	7.57%	3.51%							
4	81.11%	92.31%	96.84%	98.66%	11.19%	4.53%	1.82%							
5	88.65%	96.01%	98.55%	99.45%	7.36%	2.54%	0.90%							
6	93.06%	97.85%	99.30%	99.75%	4.79%	1.44%	0.46%							
7	94.86%	98.52%	99.54%	99.85%	3.66%	1.02%	0.31%							
8	91.53%	97.24%	99.06%	99.66%	5.72%	1.82%	0.60%							

HM-12-80-		IAH (N-S)-Open Terrain probabilities								seconds in each bin			cycles in each bin		
Segment		P(V<V1)	P(V<V2)	P(V<V3)	P(V<V4)	P(V1<V<V2)	P(V2<V<V3)	P(V3<V<V4)		t_bin1	t_bin2	t_bin3	N_bin1	N_bin2	N_bin3
1		0.00%	0.00%	0.01%	0.05%	0.00%	0.01%	0.03%		14455.69869	78869.97488	270795.075	4.63E+03	2.52E+04	8.67E+04
2		0.00%	0.01%	0.05%	0.18%	0.01%	0.04%	0.13%		74915.74822	340829.1759	1005483.44	2.40E+04	1.09E+05	3.22E+05
3		0.01%	0.05%	0.20%	0.59%	0.04%	0.15%	0.39%		323393.3825	1229502.803	3122744.22	1.03E+05	3.93E+05	9.99E+05
4		0.03%	0.17%	0.63%	1.65%	0.14%	0.46%	1.01%		1158952.954	3696243.823	8109683.12	3.71E+05	1.18E+06	2.60E+06
5		0.09%	0.52%	1.67%	3.87%	0.43%	1.15%	2.20%		3417495.642	9210442.101	17566988.4	1.09E+06	2.95E+06	5.62E+06
6		0.28%	1.30%	3.66%	7.61%	1.02%	2.36%	3.96%		8164955.684	18858788.11	31642452.7	2.61E+06	6.03E+06	1.01E+07
7		0.60%	2.46%	6.28%	12.09%	1.87%	3.82%	5.80%		14927828.04	30552081.09	46370144.1	4.78E+06		
8		0.57%	2.38%	6.10%	11.79%	1.81%	3.72%	5.69%		14447636.1	29774792.28	45450602.8			
									E-W Gusts	22874716.87			7319909.4		
Segment		P(V<V1)	P(V<V2)	P(V<V3)	P(V<V4)	P(V1<V<V2)	P(V2<V<V3)	P(V3<V<V4)		t_bin1	t_bin2	t_bin3	N_bin1	N_bin2	N_bin3
1		2.27%	7.32%	15.45%	25.56%	5.05%	8.13%	10.12%		40355476.16	64980716.39	80864355.5	4.55E+07	7.32E+07	9.11E+07
2		5.49%	14.68%	26.93%	39.96%	9.19%	12.24%	13.03%		73450245.39	97866895.9	104160581	8.28E+07	1.10E+08	1.17E+08
3		11.44%	25.64%	41.31%	55.61%	14.19%	15.68%	14.30%		113439412.8	125308726.6		1.28E+08	1.41E+08	
4		20.66%	39.37%	56.57%	70.06%	18.71%	17.20%	13.49%							
5		32.58%	53.87%	70.28%	81.41%	21.29%	16.40%	11.13%							
6		45.34%	66.70%	80.70%	89.01%	21.36%	14.00%	8.32%							
7		55.72%	75.57%	87.02%	93.16%	19.85%	11.46%	6.14%							
8		55.13%	75.10%	86.71%	92.97%	19.97%	11.61%	6.26%							
Segment		P(V<V1)	P(V<V2)	P(V<V3)	P(V<V4)	P(V1<V<V2)	P(V2<V<V3)	P(V3<V<V4)		t_bin1	t_bin2	t_bin3	N_bin1	N_bin2	N_bin3
1		48.83%	69.82%	83.01%	90.57%	20.99%	13.18%	7.57%		167805446.6			4.81E+08		
2		64.54%	82.17%	91.26%	95.70%	17.62%	9.09%	4.45%							
3		77.89%	90.61%	96.01%	98.27%	12.72%	5.40%	2.26%							
4		87.57%	95.56%	98.37%	99.38%	8.00%	2.81%	1.00%							
5		93.58%	98.07%	99.39%	99.79%	4.49%	1.31%	0.41%							
6		96.82%	99.19%	99.77%	99.93%	2.37%	0.59%	0.16%							
7		98.28%	99.61%	99.90%	99.97%	1.33%	0.29%	0.07%							
8		98.22%	99.60%	99.90%	99.97%	1.38%	0.30%	0.07%							

HM-12-80-		IAH (N-S)-Suburban Terrain probabilities								seconds in each bin			cycles in each bin			
Segment		P(V<V1)	P(V<V2)	P(V<V3)	P(V<V4)	P(V1<V<V2)	P(V2<V<V3)	P(V3<V<V4)		t_bin1	t_bin2	t_bin3	N_bin1	N_bin2	N_bin3	
1		0.00%	0.01%	0.04%	0.15%	0.01%	0.04%	0.11%		60105.37	280493.4	845240.3	1.92E+04	8.98E+04	2.70E+05	
2		0.00%	0.04%	0.16%	0.49%	0.03%	0.13%	0.33%		258296.6	1010831	2630010	8.27E+04	3.23E+05	8.42E+05	
3		0.02%	0.13%	0.52%	1.37%	0.12%	0.38%	0.86%		923328.1	3043190	6862146	2.95E+05	9.74E+05	2.20E+06	
4		0.07%	0.41%	1.37%	3.25%	0.34%	0.96%	1.88%		2732984	7640379	15022931	8.75E+05	2.44E+06	4.81E+06	
5		0.21%	1.04%	3.03%	6.47%	0.83%	1.99%	3.44%		6610532	15880986	27530452	2.12E+06	5.08E+06	8.81E+06	
6		0.49%	2.08%	5.45%	10.72%	1.59%	3.37%	5.26%		12748440	26967026	42064194	4.08E+06	8.63E+06	1.35E+07	
7		0.75%	2.97%	7.35%	13.79%	2.22%	4.38%	6.44%		17764729	35013435	51507153	5.68E+06			
8		0.35%	1.60%	4.37%	8.86%	1.24%	2.77%	4.50%		9947794	22118010	35956462				
Segment		P(V<V1)	P(V<V2)	P(V<V3)	P(V<V4)	P(V1<V<V2)	P(V2<V<V3)	P(V3<V<V4)		t_bin1	t_bin2	t_bin3	N_bin1	N_bin2	N_bin3	
1		4.90%	13.43%	25.10%	37.80%	8.53%	11.67%	12.70%		68200715	93315599	1.02E+08	7.69E+07	1.05E+08	1.14E+08	
2		10.26%	23.63%	38.85%	53.09%	13.37%	15.22%	14.23%		1.07E+08	1.22E+08	1.14E+08	1.20E+08	1.37E+08	1.28E+08	
3		18.67%	36.64%	53.73%	67.52%	17.97%	17.09%	13.79%		1.44E+08	1.37E+08		1.62E+08	1.54E+08		
4		29.77%	50.70%	67.46%	79.20%	20.93%	16.76%	11.74%								
5		41.99%	63.55%	78.28%	87.33%	21.56%	14.73%	9.05%								
6		52.90%	73.28%	85.46%	92.18%	20.38%	12.18%	6.71%								
7		58.89%	78.04%	88.66%	94.17%	19.14%	10.62%	5.51%								
8		48.61%	69.63%	82.87%	90.48%	21.02%	13.24%	7.61%								
Segment		P(V<V1)	P(V<V2)	P(V<V3)	P(V<V4)	P(V1<V<V2)	P(V2<V<V3)	P(V3<V<V4)		t_bin1	t_bin2	t_bin3	N_bin1	N_bin2	N_bin3	
1		62.43%	80.66%	90.33%	95.17%	18.23%	9.67%	4.84%		1.46E+08			4.18E+08			
2		75.96%	89.50%	95.44%	97.98%	13.54%	5.94%	2.54%								
3		86.03%	94.85%	98.06%	99.24%	8.82%	3.21%	1.18%								
4		92.52%	97.67%	99.23%	99.73%	5.15%	1.57%	0.50%								
5		96.16%	98.98%	99.71%	99.91%	2.82%	0.73%	0.20%								
6		97.95%	99.52%	99.88%	99.96%	1.57%	0.35%	0.09%								
7		98.60%	99.70%	99.93%	99.98%	1.10%	0.23%	0.05%								
8		97.36%	99.35%	99.83%	99.95%	1.99%	0.47%	0.12%								

HM-12-80- RMMA (N-S)-Open Terrain probabilities									seconds in each bin			cycles in each bin			
Segment	P(V<V1)	P(V<V2)	P(V<V3)	P(V<V4)	P(V1<V<V2)	P(V2<V<V3)	P(V3<V<V4)		t_bin1	t_bin2	t_bin3	N_bin1	N_bin2	N_bin3	
1	0.00%	0.00%	0.01%	0.02%	0.00%	0.00%	0.02%		7930.96901	47159.4707	174072.043	2.54E+03	1.51E+04	5.57E+04	
2	0.00%	0.00%	0.03%	0.09%	0.00%	0.02%	0.07%		44323.1038	219980.705	698195.726	1.42E+04	7.04E+04	2.23E+05	
3	0.00%	0.02%	0.10%	0.33%	0.02%	0.08%	0.22%		206144.08	855837.926	2340337.62	6.60E+04	2.74E+05	7.49E+05	
4	0.01%	0.09%	0.35%	0.98%	0.08%	0.27%	0.63%		794676.391	2770413.68	6549259.31	2.54E+05	8.87E+05	2.10E+06	
5	0.05%	0.29%	1.00%	2.46%	0.24%	0.71%	1.46%		2512920.79	7410427.21	15239814.5	8.04E+05	2.37E+06	4.88E+06	
6	0.15%	0.76%	2.31%	5.12%	0.61%	1.55%	2.81%		6400486.07	16190942	29311672.2	2.05E+06	5.18E+06	9.38E+06	
7	0.33%	1.51%	4.16%	8.49%	1.18%	2.65%	4.33%		12303076.6	27598354	45219347.7	3.94E+06			
8	0.32%	1.45%	4.03%	8.26%	1.14%	2.57%	4.24%		11873212.4	26818015.1	44192412.1				
								E-W Gusts	18359522.8			5875047.28			
Segment	P(V<V1)	P(V<V2)	P(V<V3)	P(V<V4)	P(V1<V<V2)	P(V2<V<V3)	P(V3<V<V4)		t_bin1	t_bin2	t_bin3	N_bin1	N_bin2	N_bin3	
1	1.38%	4.90%	11.13%	19.50%	3.52%	6.22%	8.37%		36729623.7	64921243.3	87310482.1	4.14E+07	7.32E+07	9.84E+07	
2	3.59%	10.52%	20.67%	32.35%	6.93%	10.15%	11.68%		72288774	105861649	121865972	8.15E+07	1.19E+08	1.37E+08	
3	8.00%	19.56%	33.61%	47.49%	11.56%	14.05%	13.88%		120617219	146619930		1.36E+08	1.65E+08		
4	15.36%	31.81%	48.46%	62.60%	16.44%	16.65%	14.15%								
5	25.64%	45.75%	62.84%	75.42%	20.11%	17.09%	12.58%								
6	37.42%	58.98%	74.59%	84.65%	21.56%	15.60%	10.06%								
7	47.59%	68.70%	82.17%	90.01%	21.11%	13.47%	7.84%								
8	47.00%	68.17%	81.78%	89.74%	21.17%	13.61%	7.96%								
Segment	P(V<V1)	P(V<V2)	P(V<V3)	P(V<V4)	P(V1<V<V2)	P(V2<V<V3)	P(V3<V<V4)		t_bin1	t_bin2	t_bin3	N_bin1	N_bin2	N_bin3	
1	40.78%	62.35%	77.31%	86.63%	21.57%	14.96%	9.32%		225002361			6.45E+08			
2	56.69%	76.31%	87.51%	93.46%	19.62%	11.20%	5.95%								
3	71.34%	86.68%	93.89%	97.17%	15.33%	7.21%	3.27%								
4	82.84%	93.26%	97.32%	98.90%	10.42%	4.06%	1.58%								
5	90.56%	96.87%	98.92%	99.61%	6.31%	2.05%	0.69%								
6	95.03%	98.60%	99.57%	99.86%	3.56%	0.98%	0.29%								
7	97.18%	99.30%	99.81%	99.94%	2.11%	0.51%	0.13%								
8	97.09%	99.27%	99.80%	99.94%	2.18%	0.53%	0.14%								

HM-12-80- RMMA (N-S)-Suburban Terrain probabilities									seconds in each bin			cycles in each bin			
Segment	P(V<V1)	P(V<V2)	P(V<V3)	P(V<V4)	P(V1<V<V2)	P(V2<V<V3)	P(V3<V<V4)		t_bin1	t_bin2	t_bin3	N_bin1	N_bin2	N_bin3	
1	0.00%	0.00%	0.02%	0.08%	0.00%	0.02%	0.06%		35187.02296	179111.2436	580616.2633	1.13E+04	5.73E+04	1.86E+05	
2	0.00%	0.02%	0.08%	0.27%	0.02%	0.07%	0.19%		162682.7093	695108.8394	1946969.053	5.21E+04	2.22E+05	6.23E+05	
3	0.01%	0.07%	0.28%	0.81%	0.06%	0.22%	0.52%		624529.137	2249584.603	5464826.907	2.00E+05	7.20E+05	1.75E+06	
4	0.04%	0.22%	0.81%	2.03%	0.19%	0.58%	1.23%		1979288.278	6053180.387	12831399.87	6.33E+05	1.94E+06	4.11E+06	
5	0.11%	0.60%	1.88%	4.29%	0.49%	1.29%	2.40%		5098176.176	13410665.92	25079765.34	1.63E+06	4.29E+06	8.03E+06	
6	0.27%	1.26%	3.56%	7.44%	0.99%	2.30%	3.88%		10364255.54	24024249.15	40449159.72	3.32E+06	7.69E+06	1.29E+07	
7	0.42%	1.85%	4.93%	9.82%	1.43%	3.08%	4.89%		14871451.46	32133466.27	51039488.7	4.76E+06			
8	0.19%	0.95%	2.80%	6.04%	0.76%	1.85%	3.24%		7922110.297	19295739.37	33851437.13				
Segment	P(V<V1)	P(V<V2)	P(V<V3)	P(V<V4)	P(V1<V<V2)	P(V2<V<V3)	P(V3<V<V4)		t_bin1	t_bin2	t_bin3	N_bin1	N_bin2	N_bin3	
1	3.17%	9.53%	19.10%	30.36%	6.36%	9.57%	11.26%		66391332.02	99821957.12	117441819.8	7.48E+07	1.12E+08	1.32E+08	
2	7.09%	17.85%	31.33%	44.97%	10.76%	13.48%	13.64%		112234697.8	140589347.5	142277123.9	1.26E+08	1.58E+08	1.60E+08	
3	13.73%	29.29%	45.60%	59.85%	15.57%	16.31%	14.25%		162386041.5	170170265.9		1.83E+08	1.92E+08		
4	23.14%	42.61%	59.80%	72.85%	19.47%	17.19%	13.05%								
5	34.25%	55.65%	71.79%	82.55%	21.40%	16.14%	10.76%								
6	44.78%	66.15%	80.26%	88.70%	21.37%	14.11%	8.45%								
7	50.82%	71.51%	84.20%	91.35%	20.69%	12.69%	7.15%								
8	40.57%	62.14%	77.15%	86.51%	21.57%	15.00%	9.37%								
Segment	P(V<V1)	P(V<V2)	P(V<V3)	P(V<V4)	P(V1<V<V2)	P(V2<V<V3)	P(V3<V<V4)		t_bin1	t_bin2	t_bin3	N_bin1	N_bin2	N_bin3	
1	54.48%	74.55%	86.32%	92.71%	20.07%	11.77%	6.40%		209376594.5			6.00E+08			
2	69.15%	85.26%	93.09%	96.73%	16.12%	7.82%	3.64%								
3	80.95%	92.28%	96.84%	98.67%	11.32%	4.57%	1.83%								
4	89.15%	96.27%	98.67%	99.50%	7.11%	2.40%	0.83%								
5	94.10%	98.26%	99.45%	99.82%	4.16%	1.19%	0.36%								
6	96.69%	99.15%	99.76%	99.93%	2.45%	0.61%	0.17%								
7	97.67%	99.44%	99.85%	99.96%	1.77%	0.41%	0.10%								
8	95.82%	98.86%	99.67%	99.89%	3.04%	0.80%	0.23%								

HM-12-80- ELP (N-S)Open Terrain probabilities									seconds in each bin			cycles in each bin			
Segment	P(V<V1)	P(V<V2)	P(V<V3)	P(V<V4)	P(V1<V<V2)	P(V2<V<V3)	P(V3<V<V4)		t_bin1	t_bin2	t_bin3	N_bin1	N_bin2	N_bin3	
1	0.00%	0.01%	0.03%	0.11%	0.00%	0.02%	0.08%		31399.204	161618.71	524273.98	1.00E+04	5.17E+04	1.68E+05	
2	0.00%	0.03%	0.12%	0.40%	0.02%	0.10%	0.27%		154702.75	657642.8	1818327.3	4.95E+04	2.10E+05	5.82E+05	
3	0.01%	0.11%	0.44%	1.22%	0.09%	0.33%	0.78%		630491.25	2218460.6	5238839.4	2.02E+05	7.10E+05	1.68E+06	
4	0.06%	0.38%	1.30%	3.18%	0.32%	0.93%	1.87%		2120679.2	6200758.7	12550364	6.79E+05	1.98E+06	4.02E+06	
5	0.21%	1.09%	3.22%	6.96%	0.87%	2.14%	3.73%		5846785.5	14315388	24998187	1.87E+06	4.58E+06	8.00E+06	
6	0.60%	2.55%	6.61%	12.80%	1.95%	4.06%	6.19%		13062920	27180232	41464951	4.18E+06	8.70E+06	1.33E+07	
7	1.23%	4.60%	10.78%	19.26%	3.37%	6.18%	8.48%		22579388	41354247	56756796	7.23E+06			
8	1.18%	4.46%	10.50%	18.84%	3.27%	6.04%	8.34%		21925244	40450708	55853852				
								E-W Gusts	122120226			3.91E+07			
Segment	P(V<V1)	P(V<V2)	P(V<V3)	P(V<V4)	P(V1<V<V2)	P(V2<V<V3)	P(V3<V<V4)		t_bin1	t_bin2	t_bin3	N_bin1	N_bin2	N_bin3	
1	4.27%	12.35%	23.84%	36.64%	8.08%	11.49%	12.79%		54118637	76949933	85656337	6.10E+07	8.67E+07	9.65E+07	
2	9.55%	22.82%	38.26%	52.84%	13.27%	15.45%	14.58%		88830943	103411544	97605048	1.00E+08	1.17E+08	1.10E+08	
3	18.36%	36.72%	54.26%	68.33%	18.37%	17.54%	14.07%		122986716	117442177		1.39E+08	1.32E+08		
4	30.61%	52.22%	69.22%	80.84%	21.61%	16.99%	11.62%								
5	44.80%	66.71%	81.01%	89.40%	21.91%	14.30%	8.39%								
6	58.40%	78.08%	88.90%	94.42%	19.68%	10.82%	5.52%								
7	68.43%	85.14%	93.17%	96.85%	16.71%	8.03%	3.67%								
8	67.88%	84.78%	92.97%	96.74%	16.90%	8.19%	3.77%								
Segment	P(V<V1)	P(V<V2)	P(V<V3)	P(V<V4)	P(V1<V<V2)	P(V2<V<V3)	P(V3<V<V4)		t_bin1	t_bin2	t_bin3	N_bin1	N_bin2	N_bin3	
1	61.87%	80.64%	90.51%	95.36%	18.77%	9.87%	4.85%		125686190			3.60E+08			
2	76.27%	89.93%	95.76%	98.19%	13.66%	5.83%	2.42%								
3	86.88%	95.38%	98.34%	99.38%	8.51%	2.96%	1.04%								
4	93.52%	98.12%	99.42%	99.81%	4.60%	1.31%	0.39%								
5	97.07%	99.29%	99.81%	99.95%	2.22%	0.52%	0.13%								
6	98.73%	99.74%	99.94%	99.98%	1.01%	0.20%	0.04%								
7	99.38%	99.89%	99.98%	99.99%	0.51%	0.09%	0.02%								
8	99.36%	99.89%	99.98%	99.99%	0.53%	0.09%	0.02%								

HM-12-80- ELP (N-S)Suburban Terrain probabilities									seconds in each bin			cycles in each bin		
Segment	P(V<V1)	P(V<V2)	P(V<V3)	P(V<V4)	P(V1<V<V2)	P(V2<V<V3)	P(V3<V<V4)		t_bin1	t_bin2	t_bin3	N_bin1	N_bin2	N_bin3
1	0.00%	0.02%	0.10%	0.33%	0.02%	0.08%	0.23%		125058.8	546057.1	1543936	4.00E+04	1.75E+05	4.94E+05
2	0.01%	0.09%	0.36%	1.03%	0.08%	0.28%	0.67%		508520.7	1844651	4468166	1.63E+05	5.90E+05	1.43E+06
3	0.05%	0.30%	1.08%	2.69%	0.26%	0.77%	1.61%		1710598	5178046	10787078	5.47E+05	1.66E+06	3.45E+06
4	0.16%	0.87%	2.68%	5.93%	0.71%	1.80%	3.25%		4747103	12080487	21783481	1.52E+06	3.87E+06	6.97E+06
5	0.46%	2.07%	5.56%	11.06%	1.61%	3.49%	5.51%		10763610	23344671	36860843	3.44E+06	7.47E+06	1.18E+07
6	1.02%	3.94%	9.49%	17.33%	2.93%	5.55%	7.84%		19586509	37143865	52470420	6.27E+06	1.19E+07	1.68E+07
7	1.52%	5.46%	12.40%	21.61%	3.94%	6.94%	9.21%		26387852	46445084	61678283	8.44E+06		
8	0.75%	3.09%	7.76%	14.65%	2.34%	4.67%	6.89%		15641656	31264170	46132092			
Segment	P(V<V1)	P(V<V2)	P(V<V3)	P(V<V4)	P(V1<V<V2)	P(V2<V<V3)	P(V3<V<V4)		t_bin1	t_bin2	t_bin3	N_bin1	N_bin2	N_bin3
1	8.61%	21.11%	36.08%	50.54%	12.50%	14.97%	14.46%		83721185	1E+08	96815665	9.44E+07	1.13E+08	1.09E+08
2	16.67%	34.30%	51.67%	65.97%	17.62%	17.37%	14.30%		1.18E+08	1.16E+08	95763583	1.33E+08	1.31E+08	1.08E+08
3	28.07%	49.28%	66.58%	78.76%	21.21%	17.30%	12.18%		1.42E+08	1.16E+08		1.60E+08	1.31E+08	
4	41.59%	63.70%	78.72%	87.83%	22.11%	15.02%	9.11%							
5	54.97%	75.42%	87.16%	93.37%	20.45%	11.74%	6.21%							
6	65.79%	83.39%	92.16%	96.29%	17.59%	8.77%	4.13%							
7	71.32%	86.98%	94.20%	97.39%	15.66%	7.22%	3.19%							
8	61.66%	80.49%	90.42%	95.31%	18.83%	9.92%	4.89%							
Segment	P(V<V1)	P(V<V2)	P(V<V3)	P(V<V4)	P(V1<V<V2)	P(V2<V<V3)	P(V3<V<V4)		t_bin1	t_bin2	t_bin3	N_bin1	N_bin2	N_bin3
1	74.45%	88.88%	95.22%	97.91%	14.43%	6.34%	2.70%		96600517			2.77E+08		
2	85.44%	94.72%	98.05%	99.25%	9.28%	3.33%	1.20%							
3	92.53%	97.75%	99.29%	99.76%	5.22%	1.54%	0.47%							
4	96.49%	99.12%	99.76%	99.93%	2.63%	0.64%	0.17%							
5	98.41%	99.66%	99.92%	99.98%	1.25%	0.26%	0.06%							
6	99.24%	99.86%	99.97%	99.99%	0.62%	0.11%	0.02%							
7	99.51%	99.92%	99.98%	100.00%	0.40%	0.07%	0.01%							
8	98.98%	99.80%	99.96%	99.99%	0.82%	0.15%	0.03%							

								Equivalent Static Pressure Ranges						v(ft2/s)=	0.0001615	Stress ranges for pole with no GS			
Segment	Avg dia (in)	Mid ht. (ft)	f 1 (Hz)	V1 (mph - 3s)	V2 (mph - 3s)	V3 (mph - 3s)	V4 (mph - 3s)	Pvs1 (psf)	Pvs2 (psf)	Pvs3 (psf)	Pvs4 (psf)	Re1 300≤Re≤1.0E+05 Re>3.5E+06	Re2	Re3	Re4	Sr1 (ksi)	Sr2 (ksi)	Sr3 (ksi)	Sr4 (ksi)
1	8.750	145.205	0.401	1.3	1.7	2.1	2.5	0.54	0.91	1.4	1.9	8.8E+03	1.1E+04	1.4E+04	1.7E+04	0.024	0.040	0.060	0.085
2	10.694	134.549	0.401	1.6	2.1	2.6	3.1	0.81	1.36	2.0	2.9	1.3E+04	1.7E+04	2.1E+04	2.5E+04	0.039	0.066	0.100	0.140
3	13.071	121.526	0.401	2.0	2.6	3.2	3.7	1.20	2.0	3.1	4.3	2.0E+04	2.5E+04	3.1E+04	3.7E+04	0.064	0.107	0.162	0.227
4	15.976	105.443	0.401	2.4	3.1	3.9	4.6	1.8	3.0	4.6	6.4	2.9E+04	3.8E+04	4.7E+04	5.5E+04	0.167	0.282	0.425	0.598
5	19.526	84.834	0.401	3.0	3.8	4.7	5.6	2.7	4.5	6.8	9.6	4.4E+04	5.7E+04	7.0E+04	8.3E+04	0.283	0.475	0.718	1.010
6	23.865	58.879	0.401	3.6	4.7	5.8	6.8	4.0	6.8	10.2	14.3	6.5E+04	8.5E+04	1.0E+05	1.2E+05	0.486	0.817	1.234	
7	29.168	27.260	0.401	4.4	5.7	7.0	8.4	6.0	10.1	15.2	21.4	9.8E+04	1.3E+05	1.6E+05	1.8E+05	0.441			
8	32.917	4.953	0.401	5.0	6.5	7.9	9.4	7.6	12.8	19.4	27.3	1.2E+05	1.6E+05	2.0E+05	2.4E+05				
		Pvs(windgu	0.401					6.2								3.395422			
	Avg dia (in)	Mid ht. (ft)	f 2 (Hz)	V1 (mph - 3s)	V2 (mph - 3s)	V3 (mph - 3s)	V4 (mph - 3s)	Pvs1 (psf)	Pvs2 (psf)	Pvs3 (psf)	Pvs4 (psf)	Re1 300≤Re≤1.0E+05 Re>3.5E+06	Re2	Re3	Re4	Sr1 (ksi)	Sr2 (ksi)	Sr3 (ksi)	Sr4 (ksi)
1	8.750	145.205	1.46	4.8	6.3	7.7	9.1	7.2	12.0	18.2	25.6	3.2E+04	4.2E+04	5.1E+04	6.1E+04	0.310	0.522	0.788	1.109
2	10.694	134.549	1.46	5.9	7.6	9.4	11.1	10.7	18.0	27.1	38.2	4.8E+04	6.2E+04	7.6E+04	9.0E+04	0.685	1.151	1.738	2.445
3	13.071	121.526	1.46	7.2	9.3	11.5	13.6	16.0	26.8	40.5	57.0	7.1E+04	9.3E+04	1.1E+05	1.4E+05	1.119	1.881		
4	15.976	105.443	1.46	8.8	11.4	14.0	16.7	23.9	40.1	60.6	85.2	1.1E+05	1.4E+05	1.7E+05	2.0E+05				
5	19.526	84.834	1.46	10.8	14.0	17.2	20.4	35.6	59.9	90.5	127.3	1.6E+05	2.1E+05	2.5E+05	3.0E+05				
6	23.865	58.879	1.46	13.2	17.1	21.0	24.9	53.2	89.5	135.1	190.1	2.4E+05	3.1E+05	3.8E+05	4.5E+05				
7	29.168	27.260	1.46	16.1	20.9	25.6	30.4	79.5	133.7	201.9	284.0	3.6E+05	4.6E+05	5.7E+05	6.7E+05				
8	32.917	4.953	1.46	18.2	23.5	28.9	34.3	101.3	170.3	257.1	361.7	4.5E+05	5.9E+05	7.2E+05	8.6E+05				
	Avg dia (in)	Mid ht. (ft)	f 3 (Hz)	V1 (mph - 3s)	V2 (mph - 3s)	V3 (mph - 3s)	V4 (mph - 3s)	Pvs1 (psf)	Pvs2 (psf)	Pvs3 (psf)	Pvs4 (psf)	Re1 300≤Re≤1.0E+05 Re>3.5E+06	Re2	Re3	Re4	Sr1 (ksi)	Sr2 (ksi)		
1	8.750	145.205	3.698	12.2	15.9	19.5	23.1	45.9	77.2	116.5	164.0	8.1E+04	1.1E+05	1.3E+05	1.5E+05	1.977			
2	10.694	134.549	3.698	14.9	19.4	23.8	28.2	68.6	115.3	174.1	244.9	1.2E+05	1.6E+05	1.9E+05	2.3E+05				
3	13.071	121.526	3.698	18.3	23.7	29.1	34.5	102.4	172.2	260.1	365.9	1.8E+05	2.3E+05	2.9E+05	3.4E+05				
4	15.976	105.443	3.698	22.3	28.9	35.6	42.2	153.0	257.3	388.5	546.6	2.7E+05	3.5E+05	4.3E+05	5.1E+05				
5	19.526	84.834	3.698	27.3	35.4	43.5	51.6	228.6	384.3	580.3	816.5	4.0E+05	5.2E+05	6.4E+05	7.6E+05				
6	23.865	58.879	3.698	33.3	43.2	53.1	63.0	341.5	574.1	866.9	1219.7	6.0E+05	7.8E+05	9.6E+05	1.1E+06				
7	29.168	27.260	3.698	40.7	52.8	64.9	77.0	510.1	857.6	1295.0	1822.1	9.0E+05	1.2E+06	1.4E+06	1.7E+06				
8	32.917	4.953	3.698	46.0	59.6	73.3	86.9	649.7	1092.3	1649.3	2320.6	1.1E+06	1.5E+06	1.8E+06	2.2E+06				

	Stress ranges for pole with GS				SAT (N-S)-Open Terrain probabilities								seconds in each bin			cycles in each bin		
Segment	Sr1 (ksi)	Sr2 (ksi)	Sr3 (ksi)	Sr4 (ksi)	P(V<V1)	P(V<V2)	P(V<V3)	P(V<V4)	P(V1<V<V2)	P(V2<V<V3)	P(V3<V<V4)		t_bin1	t_bin2	t_bin3	N_bin1	N_bin2	N_bin3
1	0.011	0.019	0.029	0.040	0.01%	0.05%	0.17%	0.45%	0.04%	0.12%	0.28%		385371.0775	1226662.306	2785497.284	1.55E+05	4.92E+05	1.12E+06
2	0.019	0.031	0.047	0.067	0.03%	0.15%	0.50%	1.19%	0.12%	0.34%	0.69%		1238786.637	3417993.133	6893478.461	4.97E+05	1.37E+06	2.76E+06
3	0.030	0.051	0.077	0.108	0.10%	0.44%	1.28%	2.77%	0.35%	0.83%	1.50%		3455539.203	8282868.429	14866381.18	1.39E+06	3.32E+06	5.96E+06
4	0.080	0.134	0.202	0.284	0.28%	1.12%	2.88%	5.69%	0.84%	1.75%	2.81%		8341503.204	17437816.65	27947819.13	3.34E+06	6.99E+06	1.12E+07
5	0.134	0.226	0.341	0.480	0.71%	2.44%	5.63%	10.22%	1.73%	3.19%	4.59%		17246565.42	31696770	45672163.68	6.92E+06	1.27E+07	1.83E+07
6	0.231	0.388	0.586		1.46%	4.47%	9.42%	15.93%	3.01%	4.95%	6.50%		29975292.02	49237663.42	64667371.69	1.20E+07	1.97E+07	2.59E+07
7	0.210				2.15%	6.18%	12.37%	20.07%	4.03%	6.19%	7.70%		40029374.6	61566259.03	76591691.77	1.61E+07		
8					1.15%	3.66%	7.96%	13.79%	2.52%	4.30%	5.82%		25030609.7	42722223.29	57912559.42			
	1.612897											E-W Gusts	11298933.27			4530872.2		
	Sr1 (ksi)	Sr2 (ksi)	Sr3 (ksi)	Sr4 (ksi)	P(V<V1)	P(V<V2)	P(V<V3)	P(V<V4)	P(V1<V<V2)	P(V2<V<V3)	P(V3<V<V4)		t_bin1	t_bin2	t_bin3	N_bin1	N_bin2	N_bin3
1	0.147	0.248	0.374	0.527	8.19%	18.17%	29.95%	41.76%	9.98%	11.79%	11.81%		99186680.78	117200270.3	117380225	1.45E+08	1.71E+08	1.71E+08
2	0.325	0.547	0.825	1.162	14.91%	28.88%	43.11%	55.73%	13.97%	14.23%	12.62%		138876745.3	141481939.6	125468114.9	2.03E+08	2.07E+08	1.83E+08
3	0.531	0.893			24.34%	41.60%	56.80%	68.76%	17.26%	15.20%	11.96%		171644589.3	151090994.9		2.51E+08	2.21E+08	
4					35.88%	54.84%	69.32%	79.47%	18.96%	14.48%	10.14%							
5					48.05%	66.80%	79.32%	87.19%	18.75%	12.52%	7.87%							
6					58.80%	75.98%	86.20%	92.03%	17.18%	10.21%	5.83%							
7					64.84%	80.63%	89.39%	94.12%	15.79%	8.76%	4.73%							
8					55.17%	73.02%	84.05%	90.56%	17.85%	11.04%	6.51%							
	Sr1 (ksi)	Sr2 (ksi)			P(V<V1)	P(V<V2)	P(V<V3)	P(V<V4)	P(V1<V<V2)	P(V2<V<V3)	P(V3<V<V4)		t_bin1	t_bin2	t_bin3	N_bin1	N_bin2	N_bin3
1	0.939				63.18%	79.39%	88.56%	93.59%	16.21%	9.17%	5.03%		161151078.6			5.96E+08		
2					75.45%	87.94%	94.01%	96.95%	12.49%	6.07%	2.94%							
3					84.94%	93.54%	97.13%	98.67%	8.60%	3.59%	1.54%							
4					91.43%	96.79%	98.73%	99.46%	5.36%	1.94%	0.74%							
5					95.35%	98.47%	99.46%	99.79%	3.12%	0.98%	0.33%							
6					97.45%	99.26%	99.76%	99.91%	1.80%	0.50%	0.16%							
7					98.26%	99.52%	99.85%	99.95%	1.27%	0.33%	0.10%							
8					96.85%	99.04%	99.68%	99.88%	2.19%	0.64%	0.20%							

	Avg Sr (No GS)			Avg Sr (w/GS)			SAT(N-S)-Suburban Terrain probabilities							seconds in each bin			cycles in each bin		
Segment	S_bin1	S_bin2	S_bin3	S_bin1	S_bin2	S_bin3	P(V<V1)	P(V<V2)	P(V<V3)	P(V<V4)	P(V1<V<V2)	P(V2<V<V3)	P(V3<V<V4)	t_bin1	t_bin2	t_bin3	N_bin1	N_bin2	N_bin3
1	0.032	0.050	0.073	0.015	0.024	0.035	0.02%	0.12%	0.40%	0.97%	0.10%	0.28%	0.58%	971454.4	2765001	5722139	3.90E+05	1.11E+06	2.29E+06
2	0.053	0.083	0.120	0.025	0.039	0.057	0.07%	0.35%	1.03%	2.28%	0.27%	0.68%	1.26%	2725074	6758596	12478155	1.09E+06	2.71E+06	5.00E+06
3	0.085	0.134	0.194	0.041	0.064	0.092	0.21%	0.88%	2.33%	4.72%	0.67%	1.45%	2.39%	6627952	14384420	23779389	2.66E+06	5.77E+06	9.54E+06
4	0.224	0.353	0.512	0.107	0.168	0.243	0.54%	1.94%	4.62%	8.61%	1.40%	2.68%	3.99%	13923804	26629804	39654301	5.58E+06	1.07E+07	1.59E+07
5	0.379	0.596	0.864	0.180	0.283	0.410	1.14%	3.64%	7.91%	13.72%	2.50%	4.27%	5.80%	24868807	42503211	57679666	9.97E+06	1.70E+07	2.31E+07
6	0.652	1.026	1.234	0.310	0.487	0.586	1.90%	5.58%	11.36%	18.68%	3.68%	5.78%	7.32%	36587230	57470839	72749430	1.47E+07	2.30E+07	2.92E+07
7	0.441			0.210			1.97%	5.76%	11.66%	19.09%	3.78%	5.90%	7.43%	37594616	58682161	73897906	1.51E+07		
8							0.43%	1.60%	3.92%	7.45%	1.17%	2.31%	3.54%	11651014	23005136	35171516			
	3.395			1.612897															
	S_bin1	S_bin2	S_bin3	S_bin1	S_bin2	S_bin3	P(V<V1)	P(V<V2)	P(V<V3)	P(V<V4)	P(V1<V<V2)	P(V2<V<V3)	P(V3<V<V4)	t_bin1	t_bin2	t_bin3	N_bin1	N_bin2	N_bin3
1	0.416	0.655	0.948	0.198	0.311	0.450	13.20%	26.32%	40.13%	52.70%	13.12%	13.80%	12.57%	1.3E+08	1.37E+08	1.25E+08	1.90E+08	2.00E+08	1.82E+08
2	0.918	1.444	2.091	0.436	0.686	0.993	21.80%	38.38%	53.50%	65.75%	16.58%	15.12%	12.25%	1.65E+08	1.5E+08	1.22E+08	2.41E+08	2.19E+08	1.78E+08
3	1.500	1.881		0.712	0.893		32.53%	51.22%	66.05%	76.78%	18.68%	14.83%	10.73%	1.86E+08	1.47E+08		2.71E+08	2.15E+08	
4							44.21%	63.23%	76.46%	85.06%	19.01%	13.23%	8.60%						
5							55.04%	72.91%	83.97%	90.51%	17.87%	11.07%	6.53%						
6							62.94%	79.20%	88.43%	93.51%	16.27%	9.23%	5.07%						
7							63.51%	79.64%	88.73%	93.70%	16.13%	9.09%	4.97%						
8							41.18%	60.27%	74.01%	83.18%	19.09%	13.74%	9.17%						
	S_bin1	S_bin2	S_bin3	S_bin1			P(V<V1)	P(V<V2)	P(V<V3)	P(V<V4)	P(V1<V<V2)	P(V2<V<V3)	P(V3<V<V4)	t_bin1	t_bin2	t_bin3	N_bin1	N_bin2	N_bin3
1	1.977			0.939			72.98%	86.34%	93.04%	96.38%	13.36%	6.70%	3.34%	1.33E+08			4.91E+08		
2							82.90%	92.42%	96.54%	98.36%	9.52%	4.12%	1.82%						
3							89.91%	96.08%	98.39%	99.31%	6.17%	2.32%	0.91%						
4							94.34%	98.06%	99.29%	99.72%	3.73%	1.22%	0.43%						
5							96.83%	99.03%	99.68%	99.88%	2.21%	0.64%	0.21%						
6							98.03%	99.45%	99.83%	99.94%	1.42%	0.38%	0.11%						
7							98.10%	99.47%	99.84%	99.94%	1.38%	0.36%	0.11%						
8							93.40%	97.67%	99.12%	99.64%	4.27%	1.45%	0.53%						

	DFW(N-S)-Open Terrain probabilities								seconds in each bin			cycles in each bin			
Segment	P(V<V1)	P(V<V2)	P(V<V3)	P(V<V4)	P(V1<V<V2)	P(V2<V<V3)	P(V3<V<V4)		t_bin1	t_bin2	t_bin3	N_bin1	N_bin2	N_bin3	
1	0.00%	0.00%	0.01%	0.04%	0.00%	0.01%	0.03%		15992.43	88048.34	305413.9	6.41E+03	3.53E+04	1.22E+05	
2	0.00%	0.01%	0.04%	0.14%	0.01%	0.03%	0.10%		82628.58	380981.7	1139604	3.31E+04	1.53E+05	4.57E+05	
3	0.00%	0.04%	0.16%	0.48%	0.03%	0.12%	0.32%		355672.3	1377119	3560874	1.43E+05	5.52E+05	1.43E+06	
4	0.02%	0.13%	0.50%	1.33%	0.11%	0.37%	0.83%		1268684	4144749	9303060	5.09E+05	1.66E+06	3.73E+06	
5	0.07%	0.40%	1.31%	3.11%	0.33%	0.91%	1.79%		3684372	10257022	20153147	1.48E+06	4.11E+06	8.08E+06	
6	0.19%	0.94%	2.76%	5.94%	0.75%	1.82%	3.18%		8426759	20402701	35697667	3.38E+06	8.18E+06	1.43E+07	
7	0.33%	1.50%	4.10%	8.35%	1.17%	2.60%	4.25%		13094193	29212986	47757733	5.25E+06			
8	0.14%	0.71%	2.16%	4.80%	0.57%	1.45%	2.64%		6421745	16307144	29683650				
								E-W Gusts	19820568			7948048			
	P(V<V1)	P(V<V2)	P(V<V3)	P(V<V4)	P(V1<V<V2)	P(V2<V<V3)	P(V3<V<V4)		t_bin1	t_bin2	t_bin3	N_bin1	N_bin2	N_bin3	
1	2.25%	7.21%	15.17%	25.09%	4.96%	7.96%	9.92%		55647548	89414108	1.11E+08	8.12E+07	1.31E+08	1.63E+08	
2	5.39%	14.36%	26.34%	39.15%	8.97%	11.98%	12.81%		1.01E+08	1.35E+08	1.44E+08	1.47E+08	1.96E+08	2.10E+08	
3	11.12%	24.95%	40.33%	54.49%	13.83%	15.38%	14.16%		1.55E+08	1.73E+08		2.27E+08	2.52E+08		
4	19.92%	38.18%	55.20%	68.73%	18.27%	17.02%	13.53%								
5	31.11%	52.04%	68.53%	79.96%	20.93%	16.49%	11.43%								
6	42.57%	63.93%	78.47%	87.40%	21.36%	14.53%	8.93%								
7	49.64%	70.37%	83.31%	90.72%	20.73%	12.94%	7.42%								
8	38.54%	59.97%	75.30%	85.12%	21.43%	15.33%	9.82%								
	P(V<V1)	P(V<V2)	P(V<V3)	P(V<V4)	P(V1<V<V2)	P(V2<V<V3)	P(V3<V<V4)		t_bin1	t_bin2	t_bin3	N_bin1	N_bin2	N_bin3	
1	47.66%	68.63%	82.03%	89.87%	20.97%	13.41%	7.84%		2.35E+08			8.71E+08			
2	63.21%	81.10%	90.54%	95.26%	17.88%	9.44%	4.72%								
3	76.60%	89.79%	95.55%	98.02%	13.19%	5.76%	2.47%								
4	86.46%	95.00%	98.11%	99.25%	8.54%	3.10%	1.15%								
5	92.69%	97.71%	99.24%	99.73%	5.02%	1.53%	0.49%								
6	96.07%	98.93%	99.69%	99.90%	2.87%	0.75%	0.21%								
7	97.36%	99.34%	99.82%	99.95%	1.98%	0.48%	0.13%								
8	95.10%	98.60%	99.57%	99.86%	3.51%	0.97%	0.29%								

DFW (N-S)-Suburban Terrain probabilities									seconds in each bin			cycles in each bin		
Segment	P(V<V1)	P(V<V2)	P(V<V3)	P(V<V4)	P(V1<V<V2)	P(V2<V<V3)	P(V3<V<V4)		t_bin1	t_bin2	t_bin3	N_bin1	N_bin2	N_bin3
1	0.00%	0.01%	0.03%	0.11%	0.01%	0.03%	0.08%		58614.85	280888.5	867692.4	2.35E+04	1.13E+05	3.48E+05
2	0.00%	0.03%	0.12%	0.36%	0.02%	0.09%	0.24%		253252.8	1022974	2740186	1.02E+05	4.10E+05	1.10E+06
3	0.01%	0.09%	0.37%	1.02%	0.08%	0.28%	0.65%		908637.1	3109815	7255720	3.64E+05	1.25E+06	2.91E+06
4	0.05%	0.29%	0.99%	2.42%	0.24%	0.70%	1.43%		2685536	7855635	16083250	1.08E+06	3.15E+06	6.45E+06
5	0.13%	0.70%	2.14%	4.77%	0.57%	1.44%	2.63%		6359517	16176160	29486156	2.55E+06	6.49E+06	1.18E+07
6	0.28%	1.29%	3.62%	7.51%	1.02%	2.33%	3.89%		11409546	26130707	43658067	4.58E+06	1.05E+07	1.75E+07
7	0.29%	1.35%	3.76%	7.75%	1.06%	2.41%	3.99%		11893372	27026079	44861264	4.77E+06		
8	0.03%	0.22%	0.78%	1.96%	0.18%	0.56%	1.19%		2066777	6290009	13309361			
	P(V<V1)	P(V<V2)	P(V<V3)	P(V<V4)	P(V1<V<V2)	P(V2<V<V3)	P(V3<V<V4)		t_bin1	t_bin2	t_bin3	N_bin1	N_bin2	N_bin3
1	4.51%	12.50%	23.61%	35.89%	7.99%	11.11%	12.28%		89712997	1.25E+08	1.38E+08	1.31E+08	1.82E+08	2.01E+08
2	9.44%	22.06%	36.74%	50.75%	12.62%	14.68%	14.01%		1.42E+08	1.65E+08	1.57E+08	2.07E+08	2.41E+08	2.30E+08
3	17.18%	34.34%	51.12%	65.01%	17.16%	16.78%	13.89%		1.93E+08	1.88E+08		2.81E+08	2.75E+08	
4	27.38%	47.71%	64.58%	76.78%	20.33%	16.87%	12.20%							
5	38.40%	59.83%	75.18%	85.03%	21.43%	15.36%	9.85%							
6	47.37%	68.36%	81.84%	89.74%	21.00%	13.48%	7.90%							
7	48.05%	68.97%	82.29%	90.04%	20.92%	13.32%	7.75%							
8	24.56%	44.25%	61.29%	74.03%	19.70%	17.03%	12.74%							
	P(V<V1)	P(V<V2)	P(V<V3)	P(V<V4)	P(V1<V<V2)	P(V2<V<V3)	P(V3<V<V4)		t_bin1	t_bin2	t_bin3	N_bin1	N_bin2	N_bin3
1	59.93%	78.68%	89.01%	94.34%	18.75%	10.32%	5.34%		2.11E+08			7.79E+08		
2	73.62%	88.02%	94.60%	97.53%	14.39%	6.58%	2.93%							
3	84.10%	93.85%	97.58%	99.01%	9.75%	3.73%	1.43%							
4	91.06%	97.05%	98.98%	99.63%	5.99%	1.93%	0.65%							
5	95.06%	98.59%	99.57%	99.86%	3.53%	0.98%	0.29%							
6	96.99%	99.23%	99.78%	99.93%	2.24%	0.55%	0.15%							
7	97.11%	99.27%	99.80%	99.94%	2.16%	0.53%	0.14%							
8	89.57%	96.42%	98.72%	99.52%	6.85%	2.30%	0.80%							

		IAH (N-S)-Open Terrain probabilities								seconds in each bin			cycles in each bin		
Segment		P(V<V1)	P(V<V2)	P(V<V3)	P(V<V4)	P(V1<V<V2)	P(V2<V<V3)	P(V3<V<V4)		t_bin1	t_bin2	t_bin3	N_bin1	N_bin2	N_bin3
1		0.00%	0.01%	0.07%	0.21%	0.01%	0.05%	0.15%		93709.34	415289.3	1198613	3.76E+04	1.67E+05	4.81E+05
2		0.01%	0.06%	0.24%	0.70%	0.05%	0.19%	0.46%		401178.6	1482744	3678290	1.61E+05	5.95E+05	1.47E+06
3		0.03%	0.21%	0.77%	1.95%	0.18%	0.55%	1.18%		1432910	4428670	9465929	5.75E+05	1.78E+06	3.80E+06
4		0.12%	0.66%	2.04%	4.60%	0.53%	1.38%	2.56%		4257364	11056240	20447451	1.71E+06	4.43E+06	8.20E+06
5		0.37%	1.67%	4.54%	9.17%	1.30%	2.87%	4.63%		10397088	22916615	36986656	4.17E+06	9.19E+06	1.48E+07
6		0.90%	3.45%	8.33%	15.33%	2.56%	4.88%	7.00%		20427072	39018344	55927316	8.19E+06	1.56E+07	2.24E+07
7		1.44%	5.07%	11.45%	19.98%	3.63%	6.38%	8.53%		29026911	50982047	68170895	1.16E+07		
8		0.67%	2.72%	6.84%	12.98%	2.05%	4.11%	6.14%		16397061	32889458	49090711			
									E-W Gusts	22874717			9172761		
		P(V<V1)	P(V<V2)	P(V<V3)	P(V<V4)	P(V1<V<V2)	P(V2<V<V3)	P(V3<V<V4)		t_bin1	t_bin2	t_bin3	N_bin1	N_bin2	N_bin3
1		7.07%	17.83%	31.32%	44.97%	10.76%	13.49%	13.66%		85981566	1.08E+08	1.09E+08	1.26E+08	1.57E+08	1.59E+08
2		14.21%	30.07%	46.52%	60.77%	15.86%	16.45%	14.25%		1.27E+08	1.32E+08	1.14E+08	1.85E+08	1.92E+08	1.66E+08
3		24.84%	44.79%	61.95%	74.69%	19.95%	17.16%	12.74%		1.59E+08	1.37E+08		2.33E+08	2.00E+08	
4		38.18%	59.79%	75.27%	85.17%	21.61%	15.48%	9.90%							
5		52.16%	72.67%	85.04%	91.90%	20.51%	12.37%	6.87%							
6		64.14%	81.88%	91.09%	95.61%	17.74%	9.20%	4.52%							
7		70.61%	86.23%	93.65%	97.04%	15.62%	7.42%	3.39%							
8		60.15%	78.99%	89.27%	94.54%	18.83%	10.28%	5.27%							
		#VALUE! #VALUE!	P(V<V2)	P(V<V3)	P(V<V4)	P(V1<V<V2)	P(V2<V<V3)	P(V3<V<V4)		t_bin1	t_bin2	t_bin3	N_bin1	N_bin2	N_bin3
1		68.86%	85.10%	93.00%	96.68%	16.23%	7.90%	3.69%		1.3E+08			4.80E+08		
2		81.37%	92.51%	96.96%	98.73%	11.14%	4.45%	1.77%							
3		90.03%	96.65%	98.83%	99.57%	6.62%	2.18%	0.74%							
4		95.17%	98.65%	99.59%	99.87%	3.47%	0.95%	0.28%							
5		97.81%	99.48%	99.87%	99.96%	1.67%	0.38%	0.10%							
6		99.00%	99.80%	99.95%	99.99%	0.80%	0.16%	0.03%							
7		99.39%	99.89%	99.98%	99.99%	0.50%	0.09%	0.02%							
8		98.68%	99.72%	99.93%	99.98%	1.04%	0.21%	0.05%							

		IAH (N-S)-Suburban Terrain probabilities								seconds in each bin			cycles in each bin			
Segment		P(V<V1)	P(V<V2)	P(V<V3)	P(V<V4)	P(V1<V<V2)	P(V2<V<V3)	P(V3<V<V4)		t_bin1	t_bin2	t_bin3	N_bin1	N_bin2	N_bin3	
1		0.01%	0.04%	0.18%	0.55%	0.04%	0.14%	0.37%		296503.8	1140008	2922686	1.19E+05	4.57E+05	1.17E+06	
2		0.02%	0.16%	0.59%	1.54%	0.13%	0.43%	0.96%		1067638	3445982	7636252	4.28E+05	1.38E+06	3.06E+06	
3		0.09%	0.49%	1.58%	3.68%	0.40%	1.09%	2.10%		3206007	8732330	16802159	1.29E+06	3.50E+06	6.74E+06	
4		0.27%	1.27%	3.59%	7.49%	1.00%	2.32%	3.91%		7996467	18542636	31214033	3.21E+06	7.44E+06	1.25E+07	
5		0.67%	2.70%	6.79%	12.90%	2.04%	4.09%	6.11%		16267787	32686179	48856703	6.52E+06	1.31E+07	1.96E+07	
6		1.24%	4.50%	10.37%	18.40%	3.26%	5.88%	8.03%		26028125	46961223	64207798	1.04E+07	1.88E+07	2.57E+07	
7		1.30%	4.66%	10.69%	18.87%	3.37%	6.02%	8.18%		26900283	48146047	65391010	1.08E+07			
8		0.20%	1.01%	2.95%	6.33%	0.80%	1.94%	3.38%		6423920	15513593	27010589				
		P(V<V1)	P(V<V2)	P(V<V3)	P(V<V4)	P(V1<V<V2)	P(V2<V<V3)	P(V3<V<V4)		t_bin1	t_bin2	t_bin3	N_bin1	N_bin2	N_bin3	
1		12.35%	27.12%	43.09%	57.40%	14.77%	15.97%	14.31%		1.18E+08	1.28E+08	1.14E+08	1.72E+08	1.86E+08	1.67E+08	
2		21.94%	41.08%	58.30%	71.57%	19.14%	17.22%	13.27%		1.53E+08	1.38E+08	1.06E+08	2.23E+08	2.01E+08	1.55E+08	
3		34.30%	55.74%	71.89%	82.64%	21.44%	16.15%	10.75%		1.71E+08	1.29E+08		2.50E+08	1.88E+08		
4		47.79%	68.91%	82.34%	90.13%	21.12%	13.43%	7.79%								
5		60.01%	78.88%	89.20%	94.50%	18.87%	10.32%	5.30%								
6		68.60%	84.93%	92.90%	96.63%	16.32%	7.97%	3.73%								
7		69.21%	85.32%	93.13%	96.76%	16.11%	7.81%	3.63%								
8		44.31%	65.74%	79.97%	88.52%	21.44%	14.23%	8.55%								
		P(V<V1)	P(V<V2)	P(V<V3)	P(V<V4)	P(V1<V<V2)	P(V2<V<V3)	P(V3<V<V4)		t_bin1	t_bin2	t_bin3	N_bin1	N_bin2	N_bin3	
1		78.96%	91.21%	96.32%	98.42%	12.25%	5.11%	2.10%		97919737			3.62E+08			
2		88.27%	95.88%	98.51%	99.43%	7.61%	2.63%	0.93%								
3		94.04%	98.24%	99.45%	99.82%	4.20%	1.20%	0.37%								
4		97.18%	99.30%	99.81%	99.94%	2.12%	0.51%	0.13%								
5		98.67%	99.72%	99.93%	99.98%	1.05%	0.22%	0.05%								
6		99.28%	99.86%	99.97%	99.99%	0.58%	0.11%	0.02%								
7		99.31%	99.87%	99.97%	99.99%	0.56%	0.10%	0.02%								
8		96.56%	99.11%	99.75%	99.92%	2.55%	0.64%	0.18%								

	RMMA (N-S)-Open Terrain probabilities								seconds in each bin			cycles in each bin			
Segment	P(V<V1)	P(V<V2)	P(V<V3)	P(V<V4)	P(V1<V<V2)	P(V2<V<V3)	P(V3<V<V4)		t_bin1	t_bin2	t_bin3	N_bin1	N_bin2	N_bin3	
1	0.00%	0.01%	0.03%	0.11%	0.01%	0.03%	0.08%		56049.68	271015.4	841634.8	2.25E+04	1.09E+05	3.37E+05	
2	0.00%	0.03%	0.13%	0.40%	0.02%	0.10%	0.27%		258745.8	1044464	2790005	1.04E+05	4.19E+05	1.12E+06	
3	0.02%	0.11%	0.43%	1.18%	0.10%	0.32%	0.74%		995418.4	3363562	7747331	3.99E+05	1.35E+06	3.11E+06	
4	0.06%	0.37%	1.23%	2.96%	0.30%	0.87%	1.73%		3179015	9035414	18020606	1.27E+06	3.62E+06	7.23E+06	
5	0.20%	1.00%	2.92%	6.27%	0.80%	1.92%	3.35%		8309833	20065767	34950370	3.33E+06	8.05E+06	1.40E+07	
6	0.51%	2.17%	5.65%	11.03%	1.66%	3.48%	5.38%		17323532	36283833	56162261	6.95E+06	1.45E+07	2.25E+07	
7	0.85%	3.29%	8.00%	14.80%	2.44%	4.71%	6.80%		25486606	49110484	70940516	1.02E+07			
8	0.38%	1.68%	4.56%	9.18%	1.31%	2.87%	4.63%		13627243	29962557	48284049				
								E-W Gusts	18359523			7362169			
	P(V<V1)	P(V<V2)	P(V<V3)	P(V<V4)	P(V1<V<V2)	P(V2<V<V3)	P(V3<V<V4)		t_bin1	t_bin2	t_bin3	N_bin1	N_bin2	N_bin3	
1	4.72%	13.04%	24.51%	37.07%	8.32%	11.47%	12.56%		86763530	1.2E+08	1.31E+08	1.27E+08	1.75E+08	1.91E+08	
2	10.15%	23.41%	38.55%	52.75%	13.26%	15.14%	14.20%		1.38E+08	1.58E+08	1.48E+08	2.02E+08	2.31E+08	2.16E+08	
3	18.88%	36.90%	53.98%	67.72%	18.02%	17.08%	13.74%		1.88E+08	1.78E+08		2.74E+08	2.60E+08		
4	30.71%	51.74%	68.37%	79.90%	21.03%	16.63%	11.53%								
5	44.05%	65.47%	79.74%	88.35%	21.42%	14.27%	8.60%								
6	56.27%	75.98%	87.29%	93.32%	19.71%	11.31%	6.03%								
7	63.21%	81.20%	90.65%	95.35%	17.99%	9.45%	4.70%								
8	52.11%	72.60%	84.97%	91.85%	20.49%	12.37%	6.88%								
	P(V<V1)	P(V<V2)	P(V<V3)	P(V<V4)	P(V1<V<V2)	P(V2<V<V3)	P(V3<V<V4)		t_bin1	t_bin2	t_bin3	N_bin1	N_bin2	N_bin3	
1	61.31%	79.82%	89.79%	94.84%	18.51%	9.97%	5.05%		1.93E+08			7.14E+08			
2	75.38%	89.14%	95.24%	97.88%	13.77%	6.10%	2.64%								
3	85.93%	94.79%	98.03%	99.22%	8.86%	3.23%	1.20%								
4	92.72%	97.74%	99.26%	99.74%	5.02%	1.52%	0.48%								
5	96.48%	99.08%	99.74%	99.92%	2.60%	0.66%	0.18%								
6	98.29%	99.62%	99.90%	99.97%	1.33%	0.29%	0.07%								
7	98.92%	99.78%	99.95%	99.99%	0.86%	0.17%	0.04%								
8	97.79%	99.48%	99.86%	99.96%	1.68%	0.39%	0.10%								

	RMMA (N-S)-Suburban Terrain probabilities								seconds in each bin			cycles in each bin			
Segment	P(V<V1)	P(V<V2)	P(V<V3)	P(V<V4)	P(V1<V<V2)	P(V2<V<V3)	P(V3<V<V4)		t_bin1	t_bin2	t_bin3	N_bin1	N_bin2	N_bin3	
1	0.00%	0.02%	0.10%	0.30%	0.02%	0.08%	0.21%		188123.7456	789797.9033	2179966.435	7.54E+04	3.17E+05	8.74E+05	
2	0.01%	0.08%	0.33%	0.91%	0.07%	0.25%	0.59%		728437.5866	2569865.91	6135638.92	2.92E+05	1.03E+06	2.46E+06	
3	0.04%	0.27%	0.94%	2.33%	0.22%	0.67%	1.39%		2347090.196	6994551.188	14510903.42	9.41E+05	2.80E+06	5.82E+06	
4	0.14%	0.74%	2.27%	5.03%	0.60%	1.52%	2.77%		6258166.711	15893118.08	28866366.53	2.51E+06	6.37E+06	1.16E+07	
5	0.37%	1.67%	4.52%	9.12%	1.29%	2.85%	4.60%		13510206.17	29755904.86	48018882.98	5.42E+06	1.19E+07	1.93E+07	
6	0.72%	2.89%	7.18%	13.51%	2.17%	4.29%	6.33%		22600713.99	44729072.39	66057881.32	9.06E+06	1.79E+07	2.65E+07	
7	0.76%	3.01%	7.42%	13.89%	2.25%	4.41%	6.47%		23435873.69	46012773.47	67505279.95	9.40E+06			
8	0.11%	0.58%	1.83%	4.19%	0.47%	1.25%	2.35%		4943527.807	13071631.02	24551540.95				
	P(V<V1)	P(V<V2)	P(V<V3)	P(V<V4)	P(V1<V<V2)	P(V2<V<V3)	P(V3<V<V4)		t_bin1	t_bin2	t_bin3	N_bin1	N_bin2	N_bin3	
1	8.69%	20.84%	35.28%	49.30%	12.14%	14.45%	14.01%		126691364.8	150726128.4	146194773.2	1.85E+08	2.20E+08	2.13E+08	
2	16.43%	33.39%	50.21%	64.26%	16.96%	16.82%	14.05%		176952869.7	175483055.6	146536513	2.58E+08	2.56E+08	2.14E+08	
3	27.18%	47.62%	64.61%	76.88%	20.44%	16.99%	12.27%		213290556.9	177227006		3.11E+08	2.59E+08		
4	39.77%	61.36%	76.52%	86.06%	21.58%	15.16%	9.54%								
5	51.97%	72.48%	84.89%	91.80%	20.51%	12.41%	6.91%								
6	61.02%	79.61%	89.66%	94.76%	18.59%	10.05%	5.11%								
7	61.68%	80.09%	89.96%	94.94%	18.41%	9.87%	4.98%								
8	36.43%	57.96%	73.74%	84.02%	21.53%	15.78%	10.28%								
	P(V<V1)	P(V<V2)	P(V<V3)	P(V<V4)	P(V1<V<V2)	P(V2<V<V3)	P(V3<V<V4)		t_bin1	t_bin2	t_bin3	N_bin1	N_bin2	N_bin3	
1	72.57%	87.44%	94.32%	97.39%	14.88%	6.88%	3.08%		155200108.6			5.74E+08			
2	83.71%	93.71%	97.53%	99.00%	9.99%	3.82%	1.47%								
3	91.18%	97.13%	99.02%	99.65%	5.94%	1.89%	0.63%								
4	95.55%	98.77%	99.63%	99.88%	3.22%	0.86%	0.25%								
5	97.77%	99.47%	99.86%	99.96%	1.70%	0.39%	0.10%								
6	98.74%	99.73%	99.94%	99.98%	0.99%	0.20%	0.05%								
7	98.80%	99.75%	99.94%	99.98%	0.95%	0.19%	0.04%								
8	94.66%	98.46%	99.53%	99.84%	3.80%	1.06%	0.32%								

	ELP (N-S)Open Terrain probabilities								seconds in each bin			cycles in each bin			
Segment	P(V<V1)	P(V<V2)	P(V<V3)	P(V<V4)	P(V1<V<V2)	P(V2<V<V3)	P(V3<V<V4)		t_bin1	t_bin2	t_bin3	N_bin1	N_bin2	N_bin3	
1	0.00%	0.03%	0.15%	0.47%	0.03%	0.12%	0.32%		191981.4	793871.6	2144946	7.70E+04	3.18E+05	8.60E+05	
2	0.02%	0.13%	0.53%	1.44%	0.12%	0.40%	0.91%		774572.4	2645501	6094205	3.11E+05	1.06E+06	2.44E+06	
3	0.08%	0.46%	1.56%	3.71%	0.39%	1.09%	2.16%		2590525	7327922	14428734	1.04E+06	2.94E+06	5.79E+06	
4	0.28%	1.35%	3.87%	8.13%	1.07%	2.52%	4.26%		7170592	16883325	28540012	2.88E+06	6.77E+06	1.14E+07	
5	0.80%	3.23%	8.04%	15.10%	2.43%	4.82%	7.05%		16282746	32248055	47222919	6.53E+06	1.29E+07	1.89E+07	
6	1.81%	6.27%	13.87%	23.69%	4.46%	7.60%	9.82%		29881855	50883440	65746865	1.20E+07	2.04E+07	2.64E+07	
7	2.80%	8.88%	18.36%	29.74%	6.08%	9.48%	11.38%		40717195	63456696	76199276	1.63E+07			
8	1.38%	5.05%	11.63%	20.50%	3.67%	6.58%	8.87%		24563419	44041282	59389104				
								E-W Gusts	1.22E+08			4.90E+07			
	P(V<V1)	P(V<V2)	P(V<V3)	P(V<V4)	P(V1<V<V2)	P(V2<V<V3)	P(V3<V<V4)		t_bin1	t_bin2	t_bin3	N_bin1	N_bin2	N_bin3	
1	11.98%	26.98%	43.36%	58.03%	15.00%	16.38%	14.67%		1E+08	1.1E+08	98214919	1.47E+08	1.60E+08	1.43E+08	
2	22.18%	41.94%	59.59%	72.99%	19.76%	17.65%	13.40%		1.32E+08	1.18E+08	89738520	1.93E+08	1.73E+08	1.31E+08	
3	35.77%	57.85%	74.03%	84.48%	22.08%	16.18%	10.44%		1.48E+08	1.08E+08		2.16E+08	1.58E+08		
4	50.95%	72.13%	84.92%	91.97%	21.17%	12.79%	7.05%								
5	65.09%	82.91%	91.88%	96.14%	17.82%	8.97%	4.26%								
6	75.92%	89.74%	95.66%	98.14%	13.81%	5.93%	2.47%								
7	81.28%	92.66%	97.11%	98.83%	11.38%	4.45%	1.72%								
8	72.45%	87.68%	94.58%	97.59%	15.23%	6.90%	3.01%								
	P(V<V1)	P(V<V2)	P(V<V3)	P(V<V4)	P(V1<V<V2)	P(V2<V<V3)	P(V3<V<V4)		t_bin1	t_bin2	t_bin3	N_bin1	N_bin2	N_bin3	
1	79.87%	91.92%	96.75%	98.66%	12.05%	4.84%	1.91%		80691218			2.98E+08			
2	89.38%	96.48%	98.80%	99.57%	7.11%	2.31%	0.77%								
3	95.04%	98.65%	99.61%	99.88%	3.61%	0.96%	0.27%								
4	97.92%	99.53%	99.88%	99.97%	1.62%	0.35%	0.08%								
5	99.18%	99.85%	99.97%	99.99%	0.67%	0.12%	0.02%								
6	99.67%	99.95%	99.99%	100.00%	0.28%	0.04%	0.01%								
7	99.81%	99.97%	100.00%	100.00%	0.16%	0.02%	0.00%								
8	99.55%	99.92%	99.99%	100.00%	0.38%	0.06%	0.01%								

	ELP (N-S)Suburban Terrain probabilities								seconds in each bin			cycles in each bin		
Segment	P(V<V1)	P(V<V2)	P(V<V3)	P(V<V4)	P(V1<V<V2)	P(V2<V<V3)	P(V3<V<V4)		t_bin1	t_bin2	t_bin3	N_bin1	N_bin2	N_bin3
1	0.01%	0.10%	0.41%	1.14%	0.09%	0.31%	0.74%		580277.6	2066087	4927388	2.33E+05	8.29E+05	1.98E+06
2	0.06%	0.35%	1.22%	2.99%	0.29%	0.87%	1.78%		1962473	5810957	11885449	7.87E+05	2.33E+06	4.77E+06
3	0.20%	1.02%	3.06%	6.65%	0.82%	2.04%	3.59%		5509188	13640070	24040665	2.21E+06	5.47E+06	9.64E+06
4	0.58%	2.50%	6.49%	12.62%	1.91%	4.00%	6.12%		12816132	26777940	40992507	5.14E+06	1.07E+07	1.64E+07
5	1.37%	5.01%	11.55%	20.39%	3.64%	6.54%	8.84%		24389873	43809351	59164981	9.78E+06	1.76E+07	2.37E+07
6	2.44%	7.97%	16.83%	27.73%	5.53%	8.86%	10.90%		37010874	59341470	72950453	1.48E+07	2.38E+07	2.93E+07
7	2.55%	8.24%	17.28%	28.32%	5.69%	9.05%	11.04%		38096317	60565479	73934225	1.53E+07		
8	0.45%	2.01%	5.43%	10.85%	1.57%	3.41%	5.42%		10483976	22863952	36267442			
	P(V<V1)	P(V<V2)	P(V<V3)	P(V<V4)	P(V1<V<V2)	P(V2<V<V3)	P(V3<V<V4)		t_bin1	t_bin2	t_bin3	N_bin1	N_bin2	N_bin3
1	19.62%	38.50%	56.11%	69.97%	18.87%	17.62%	13.86%		1.26E+08	1.18E+08	92814729	1.85E+08	1.72E+08	1.36E+08
2	32.21%	54.02%	70.79%	82.04%	21.81%	16.77%	11.26%		1.46E+08	1.12E+08	75367239	2.13E+08	1.64E+08	1.10E+08
3	46.72%	68.45%	82.30%	90.26%	21.73%	13.84%	7.96%		1.46E+08	92678918		2.12E+08	1.35E+08	
4	60.85%	79.90%	90.05%	95.10%	19.05%	10.15%	5.05%							
5	72.32%	87.60%	94.54%	97.57%	15.28%	6.94%	3.03%							
6	79.65%	91.80%	96.70%	98.64%	12.15%	4.89%	1.94%							
7	80.15%	92.07%	96.83%	98.70%	11.92%	4.76%	1.87%							
8	57.35%	77.28%	88.38%	94.11%	19.93%	11.10%	5.73%							
	P(V<V1)	P(V<V2)	P(V<V3)	P(V<V4)	P(V1<V<V2)	P(V2<V<V3)	P(V3<V<V4)		t_bin1	t_bin2	t_bin3	N_bin1	N_bin2	N_bin3
1	87.65%	95.73%	98.49%	99.44%	8.08%	2.75%	0.95%		54102481			2.00E+08		
2	93.96%	98.27%	99.48%	99.83%	4.32%	1.20%	0.35%							
3	97.32%	99.37%	99.84%	99.95%	2.04%	0.47%	0.12%							
4	98.89%	99.78%	99.95%	99.99%	0.89%	0.17%	0.04%							
5	99.54%	99.92%	99.98%	100.00%	0.38%	0.06%	0.01%							
6	99.78%	99.97%	99.99%	100.00%	0.19%	0.03%	0.00%							
7	99.79%	99.97%	99.99%	100.00%	0.18%	0.03%	0.00%							
8	98.60%	99.71%	99.93%	99.98%	1.11%	0.22%	0.05%							

								Equivalent Static Pressure Ranges						v(ft2/s)=	0.0001615	Stress ranges for pole with no GS			
Segment	Avg dia (in)	Mid ht. (ft)	f 1 (Hz)	V1 (mph - 3s)	V2 (mph - 3s)	V3 (mph - 3s)	V4 (mph - 3s)	Pvs1 (psf)	Pvs2 (psf)	Pvs3 (psf)	Pvs4 (psf)	Re1 300≤Re≤1.0E+05 Re>3.5E+06	Re2	Re3	Re4	Sr1 (ksi)	Sr2 (ksi)	Sr3 (ksi)	Sr4 (ksi)
1	8.750	170.205	0.351	1.2	1.5	1.8	2.2	0.41	0.70	1.0	1.5	7.7E+03	1.0E+04	1.2E+04	1.5E+04	0.015	0.025	0.038	0.053
2	10.694	159.549	0.351	1.4	1.8	2.3	2.7	0.62	1.04	1.6	2.2	1.2E+04	1.5E+04	1.8E+04	2.2E+04	0.026	0.043	0.065	0.092
3	13.071	146.526	0.351	1.7	2.2	2.8	3.3	0.92	1.6	2.3	3.3	1.7E+04	2.2E+04	2.7E+04	3.2E+04	0.043	0.071	0.108	0.152
4	15.976	130.443	0.351	2.1	2.7	3.4	4.0	1.4	2.3	3.5	4.9	2.6E+04	3.3E+04	4.1E+04	4.9E+04	0.116	0.195	0.294	0.414
5	19.526	109.834	0.351	2.6	3.4	4.1	4.9	2.1	3.5	5.2	7.4	3.8E+04	5.0E+04	6.1E+04	7.2E+04	0.211	0.355	0.536	0.754
6	23.865	83.792	0.351	3.2	4.1	5.0	6.0	3.1	5.2	7.8	11.0	5.7E+04	7.4E+04	9.1E+04	1.1E+05	0.390	0.656	0.991	
7	29.168	51.657	0.351	3.9	5.0	6.2	7.3	4.6	7.7	11.7	16.4	8.6E+04	1.1E+05	1.4E+05	1.6E+05	0.497			
8	34.730	16.938	0.351	4.6	6.0	7.3	8.7	6.5	11.0	16.5	23.3	1.2E+05	1.6E+05	1.9E+05	2.3E+05				
		Pvs(windgu	0.351					6.2								3.610148			
	Avg dia (in)	Mid ht. (ft)	f 2 (Hz)	V1 (mph - 3s)	V2 (mph - 3s)	V3 (mph - 3s)	V4 (mph - 3s)	Pvs1 (psf)	Pvs2 (psf)	Pvs3 (psf)	Pvs4 (psf)	Re1 300≤Re≤1.0E+05 Re>3.5E+06	Re2	Re3	Re4	Sr1 (ksi)	Sr2 (ksi)	Sr3 (ksi)	Sr4 (ksi)
1	8.750	170.205	1.226	4.1	5.3	6.5	7.7	5.0	8.5	12.8	18.0	2.7E+04	3.5E+04	4.3E+04	5.1E+04	0.181	0.304	0.459	0.645
2	10.694	159.549	1.226	5.0	6.4	7.9	9.4	7.5	12.7	19.1	26.9	4.0E+04	5.2E+04	6.4E+04	7.6E+04	0.314	0.528	0.798	1.123
3	13.071	146.526	1.226	6.1	7.8	9.6	11.4	11.3	18.9	28.6	40.2	6.0E+04	7.8E+04	9.6E+04	1.1E+05	0.519	0.872	1.316	
4	15.976	130.443	1.226	7.4	9.6	11.8	14.0	16.8	28.3	42.7	60.1	9.0E+04	1.2E+05	1.4E+05	1.7E+05	1.414			
5	19.526	109.834	1.226	9.0	11.7	14.4	17.1	25.1	42.2	63.8	89.7	1.3E+05	1.7E+05	2.1E+05	2.5E+05				
6	23.865	83.792	1.226	11.1	14.3	17.6	20.9	37.5	63.1	95.3	134.1	2.0E+05	2.6E+05	3.2E+05	3.8E+05				
7	29.168	51.657	1.226	13.5	17.5	21.5	25.5	56.1	94.3	142.3	200.3	3.0E+05	3.9E+05	4.8E+05	5.6E+05				
8	34.730	16.938	1.226	16.1	20.9	25.6	30.4	79.5	133.6	201.8	283.9	4.2E+05	5.5E+05	6.8E+05	8.0E+05				
	Avg dia (in)	Mid ht. (ft)	f 3 (Hz)	V1 (mph - 3s)	V2 (mph - 3s)	V3 (mph - 3s)	V4 (mph - 3s)	Pvs1 (psf)	Pvs2 (psf)	Pvs3 (psf)	Pvs4 (psf)	Re1 300≤Re≤1.0E+05 Re>3.5E+06	Re2	Re3	Re4	Sr1 (ksi)	Sr2 (ksi)		
1	8.750	170.205	3.011	10.0	12.9	15.9	18.8	30.4	51.2	77.3	108.7	6.6E+04	8.6E+04	1.1E+05	1.2E+05	1.090	1.833		
2	10.694	159.549	3.011	12.2	15.8	19.4	23.0	45.5	76.4	115.4	162.4	9.9E+04	1.3E+05	1.6E+05	1.9E+05	1.895			
3	13.071	146.526	3.011	14.9	19.3	23.7	28.1	67.9	114.2	172.4	242.6	1.5E+05	1.9E+05	2.3E+05	2.8E+05				
4	15.976	130.443	3.011	18.2	23.6	29.0	34.3	101.4	170.6	257.5	362.4	2.2E+05	2.9E+05	3.5E+05	4.2E+05				
5	19.526	109.834	3.011	22.2	28.8	35.4	42.0	151.5	254.8	384.7	541.3	3.3E+05	4.3E+05	5.2E+05	6.2E+05				
6	23.865	83.792	3.011	27.1	35.2	43.3	51.3	226.4	380.6	574.7	808.6	4.9E+05	6.4E+05	7.8E+05	9.3E+05				
7	29.168	51.657	3.011	33.2	43.0	52.9	62.7	338.2	568.6	858.5	1208.0	7.3E+05	9.5E+05	1.2E+06	1.4E+06				
8	34.730	16.938	3.011	39.5	51.2	62.9	74.7	479.4	806.1	1217.1	1712.6	1.0E+06	1.3E+06	1.7E+06	2.0E+06				

	Stress ranges for pole with GS				SAT (N-S)-Open Terrain probabilities								seconds in each bin			cycles in each bin		
Segment	Sr1 (ksi)	Sr2 (ksi)	Sr3 (ksi)	Sr4 (ksi)	P(V<V1)	P(V<V2)	P(V<V3)	P(V<V4)	P(V1<V<V2)	P(V2<V<V3)	P(V3<V<V4)		t_bin1	t_bin2	t_bin3	N_bin1	N_bin2	N_bin3
1	0.007	0.012	0.018	0.025	0.00%	0.02%	0.09%	0.24%	0.02%	0.06%	0.16%		185663.045	641657.6074	1560140.904	6.52E+04	2.25E+05	5.48E+05
2	0.012	0.021	0.031	0.044	0.01%	0.08%	0.27%	0.69%	0.07%	0.19%	0.42%		647307.933	1937401.438	4180235.653	2.27E+05	6.80E+05	1.47E+06
3	0.020	0.034	0.051	0.072	0.05%	0.25%	0.76%	1.74%	0.20%	0.51%	0.98%		1959559.546	5087529.705	9755859.218	6.88E+05	1.79E+06	3.42E+06
4	0.055	0.092	0.140	0.196	0.16%	0.67%	1.84%	3.84%	0.52%	1.17%	2.00%		5140801.607	11610640.47	19837596.7	1.80E+06	4.08E+06	6.96E+06
5	0.100	0.168	0.254	0.358	0.43%	1.60%	3.90%	7.43%	1.17%	2.31%	3.53%		11602829.72	22926701.76	35072721.24	4.07E+06	8.05E+06	1.23E+07
6	0.185	0.311	0.470		0.99%	3.23%	7.15%	12.57%	2.24%	3.92%	5.42%		22315180.43	38993424.1	53893096.76	7.83E+06	1.37E+07	1.89E+07
7	0.236				1.82%	5.38%	11.01%	18.18%	3.56%	5.63%	7.18%		35373855.9	55997348.86	71338595.34	1.24E+07		
8					1.88%	5.53%	11.26%	18.54%	3.65%	5.74%	7.28%		36249265.89	57062030.07	72359527.92			
	1.712224											E-W Gusts	11298933.27			3965925.6		
	Sr1 (ksi)	Sr2 (ksi)	Sr3 (ksi)	Sr4 (ksi)	P(V<V1)	P(V<V2)	P(V<V3)	P(V<V4)	P(V1<V<V2)	P(V2<V<V3)	P(V3<V<V4)		t_bin1	t_bin2	t_bin3	N_bin1	N_bin2	N_bin3
1	0.086	0.144	0.218	0.306	4.72%	11.71%	21.00%	31.25%	6.99%	9.29%	10.25%		69518272.25	92394831.26	101926073.8	8.52E+07	1.13E+08	1.25E+08
2	0.149	0.251	0.378	0.532	9.38%	20.20%	32.60%	44.69%	10.82%	12.39%	12.10%		107611069.1	123227767	120279075.5	1.32E+08	1.51E+08	1.47E+08
3	0.246	0.413	0.624		16.65%	31.39%	45.96%	58.56%	14.74%	14.57%	12.60%		146577114	144841377.4		1.80E+08	1.78E+08	
4	0.671				26.52%	44.28%	59.46%	71.13%	17.75%	15.18%	11.67%							
5					38.14%	57.20%	71.39%	81.12%	19.06%	14.19%	9.73%							
6					49.84%	68.41%	80.58%	88.11%	18.58%	12.17%	7.52%							
7					59.26%	76.35%	86.45%	92.20%	17.09%	10.10%	5.75%							
8					59.79%	76.77%	86.75%	92.40%	16.98%	9.98%	5.65%							
	Sr1 (ksi)	Sr2 (ksi)			P(V<V1)	P(V<V2)	P(V<V3)	P(V<V4)	P(V1<V<V2)	P(V2<V<V3)	P(V3<V<V4)		t_bin1	t_bin2	t_bin3	N_bin1	N_bin2	N_bin3
1	0.517	0.869			49.95%	68.51%	80.66%	88.16%	18.56%	12.15%	7.50%		184573878.7			5.56E+08		
2	0.899				63.83%	79.88%	88.89%	93.80%	16.05%	9.01%	4.91%							
3					75.91%	88.24%	94.18%	97.05%	12.32%	5.95%	2.87%							
4					85.19%	93.67%	97.20%	98.71%	8.49%	3.53%	1.51%							
5					91.46%	96.81%	98.73%	99.47%	5.34%	1.93%	0.73%							
6					95.23%	98.43%	99.44%	99.78%	3.20%	1.01%	0.35%							
7					97.17%	99.16%	99.72%	99.90%	1.99%	0.57%	0.18%							
8					97.25%	99.19%	99.73%	99.90%	1.93%	0.55%	0.17%							

	Avg Sr (No GS)			Avg Sr (w/GS)			SAT(N-S)-Suburban Terrain probabilities							seconds in each bin			cycles in each bin		
Segment	S_bin1	S_bin2	S_bin3	S_bin1	S_bin2	S_bin3	P(V<V1)	P(V<V2)	P(V<V3)	P(V<V4)	P(V1<V<V2)	P(V2<V<V3)	P(V3<V<V4)	t_bin1	t_bin2	t_bin3	N_bin1	N_bin2	N_bin3
1	0.020	0.031	0.045	0.009	0.015	0.021	0.01%	0.07%	0.23%	0.60%	0.06%	0.17%	0.37%	546901.5	1670486	3665633	1.92E+05	5.86E+05	1.29E+06
2	0.035	0.054	0.079	0.016	0.026	0.037	0.04%	0.21%	0.65%	1.51%	0.17%	0.44%	0.86%	1652268	4389481	8579216	5.80E+05	1.54E+06	3.01E+06
3	0.057	0.090	0.130	0.027	0.043	0.062	0.13%	0.56%	1.57%	3.34%	0.44%	1.01%	1.76%	4332076	10042186	17531536	1.52E+06	3.52E+06	6.15E+06
4	0.155	0.245	0.354	0.074	0.116	0.168	0.35%	1.34%	3.35%	6.50%	0.99%	2.01%	3.15%	9833030	19994664	31320688	3.45E+06	7.02E+06	1.10E+07
5	0.283	0.446	0.645	0.134	0.211	0.306	0.81%	2.73%	6.20%	11.11%	1.92%	3.46%	4.91%	19118933	34447735	48829748	6.71E+06	1.21E+07	1.71E+07
6	0.523	0.823	0.991	0.248	0.391	0.470	1.55%	4.70%	9.83%	16.52%	3.16%	5.13%	6.68%	31371072	51018670	66457378	1.10E+07	1.79E+07	2.33E+07
7	0.497			0.236			2.22%	6.35%	12.66%	20.47%	4.13%	6.31%	7.81%	41015642	62717532	77651160	1.44E+07		
8							1.38%	4.27%	9.07%	15.41%	2.89%	4.80%	6.34%	28765486	47674015	63076233			
	3.610			1.712224															
	S_bin1	S_bin2	S_bin3	S_bin1	S_bin2	S_bin3	P(V<V1)	P(V<V2)	P(V<V3)	P(V<V4)	P(V1<V<V2)	P(V2<V<V3)	P(V3<V<V4)	t_bin1	t_bin2	t_bin3	N_bin1	N_bin2	N_bin3
1	0.242	0.381	0.552	0.115	0.181	0.262	8.57%	18.82%	30.81%	42.72%	10.25%	11.99%	11.91%	1.02E+08	1.19E+08	1.18E+08	1.25E+08	1.46E+08	1.45E+08
2	0.421	0.663	0.960	0.200	0.314	0.455	15.28%	29.42%	43.73%	56.35%	14.14%	14.31%	12.62%	1.41E+08	1.42E+08	1.25E+08	1.72E+08	1.74E+08	1.54E+08
3	0.695	1.094		0.330	0.519		24.48%	41.78%	56.98%	68.92%	17.30%	15.20%	11.94%	1.72E+08	1.51E+08		2.11E+08	1.85E+08	
4							35.51%	54.45%	68.98%	79.18%	18.94%	14.52%	10.21%						
5							46.88%	65.73%	78.48%	86.57%	18.85%	12.75%	8.09%						
6							56.72%	74.30%	84.99%	91.21%	17.58%	10.69%	6.22%						
7							62.46%	78.84%	88.19%	93.35%	16.38%	9.34%	5.16%						
8							54.92%	72.81%	83.90%	90.46%	17.89%	11.09%	6.56%						
	S_bin1	S_bin2	S_bin3	S_bin1			P(V<V1)	P(V<V2)	P(V<V3)	P(V<V4)	P(V1<V<V2)	P(V2<V<V3)	P(V3<V<V4)	t_bin1	t_bin2	t_bin3	N_bin1	N_bin2	N_bin3
1	1.461			0.693			61.94%	78.44%	87.91%	93.17%	16.50%	9.47%	5.25%	1.64E+08			4.94E+08		
2							74.12%	87.09%	93.50%	96.65%	12.96%	6.41%	3.15%						
3							83.67%	92.84%	96.77%	98.48%	9.18%	3.92%	1.71%						
4							90.32%	96.28%	98.49%	99.35%	5.95%	2.21%	0.86%						
5							94.45%	98.11%	99.31%	99.73%	3.66%	1.20%	0.42%						
6							96.72%	98.99%	99.66%	99.88%	2.28%	0.67%	0.21%						
7							97.67%	99.33%	99.79%	99.92%	1.66%	0.46%	0.14%						
8							96.37%	98.87%	99.61%	99.86%	2.50%	0.75%	0.24%						

	DFW(N-S)-Open Terrain probabilities								seconds in each bin			cycles in each bin			
Segment	P(V<V1)	P(V<V2)	P(V<V3)	P(V<V4)	P(V1<V<V2	P(V2<V<V3	P(V3<V<V4)		t_bin1	t_bin2	t_bin3	N_bin1	N_bin2	N_bin3	
1	0.00%	0.00%	0.00%	0.02%	0.00%	0.00%	0.01%		5771.728	35193.01	132945.92	2.03E+03	1.24E+04	4.67E+04	
2	0.00%	0.00%	0.02%	0.07%	0.00%	0.02%	0.05%		33094.57	168803.8	549335.83	1.16E+04	5.93E+04	1.93E+05	
3	0.00%	0.02%	0.08%	0.25%	0.01%	0.06%	0.17%		158313.6	676850.9	1900981.1	5.56E+04	2.38E+05	6.67E+05	
4	0.01%	0.06%	0.27%	0.76%	0.06%	0.20%	0.49%		629430.6	2263543	5503515.4	2.21E+05	7.95E+05	1.93E+06	
5	0.03%	0.22%	0.77%	1.95%	0.18%	0.56%	1.18%		2054257	6257571	13250701	7.21E+05	2.20E+06	4.65E+06	
6	0.11%	0.59%	1.85%	4.20%	0.48%	1.26%	2.35%		5406639	14136492	26364659	1.90E+06	4.96E+06	9.25E+06	
7	0.26%	1.23%	3.46%	7.22%	0.97%	2.23%	3.76%		10836985	25059865	42205273	3.80E+06			
8	0.27%	1.28%	3.58%	7.43%	1.00%	2.30%	3.85%		11248947	25831598	43253805				
								E-W Gusts	19820568			6957019.263			
	P(V<V1)	P(V<V2)	P(V<V3)	P(V<V4)	P(V1<V<V2	P(V2<V<V3	P(V3<V<V4)		t_bin1	t_bin2	t_bin3	N_bin1	N_bin2	N_bin3	
1	1.02%	3.78%	8.93%	16.17%	2.77%	5.15%	7.24%		31069804	57798720	81280715	3.81E+07	7.09E+07	9.97E+07	
2	2.74%	8.43%	17.23%	27.84%	5.69%	8.80%	10.61%		63920647	98769043	119134040	7.84E+07	1.21E+08	1.46E+08	
3	6.34%	16.28%	29.05%	42.30%	9.94%	12.78%	13.24%		1.12E+08	1.43E+08		1.37E+08	1.76E+08		
4	12.64%	27.44%	43.32%	57.51%	14.80%	15.88%	14.19%								
5	21.85%	40.77%	57.85%	71.07%	18.93%	17.07%	13.23%								
6	32.92%	54.05%	70.30%	81.34%	21.14%	16.25%	11.04%								
7	43.09%	64.43%	78.85%	87.68%	21.34%	14.42%	8.82%								
8	43.69%	65.00%	79.29%	87.98%	21.30%	14.30%	8.69%								
	P(V<V1)	P(V<V2)	P(V<V3)	P(V<V4)	P(V1<V<V2	P(V2<V<V3	P(V3<V<V4)		t_bin1	t_bin2	t_bin3	N_bin1	N_bin2	N_bin3	
1	33.03%	54.17%	70.41%	81.43%	21.15%	16.24%	11.02%		2.37E+08			7.15E+08			
2	48.43%	69.31%	82.54%	90.21%	20.88%	13.23%	7.67%								
3	63.84%	81.54%	90.82%	95.42%	17.71%	9.27%	4.60%								
4	76.97%	90.00%	95.67%	98.08%	13.04%	5.66%	2.41%								
5	86.52%	95.03%	98.12%	99.26%	8.51%	3.09%	1.14%								
6	92.49%	97.63%	99.21%	99.72%	5.14%	1.58%	0.51%								
7	95.61%	98.78%	99.63%	99.88%	3.17%	0.85%	0.25%								
8	95.75%	98.83%	99.65%	99.89%	3.08%	0.82%	0.24%								

	DFW (N-S)-Suburban Terrain probabilities								seconds in each bin			cycles in each bin		
Segment	P(V<V1)	P(V<V2)	P(V<V3)	P(V<V4)	P(V1<V<V2)	P(V2<V<V3)	P(V3<V<V4)		t_bin1	t_bin2	t_bin3	N_bin1	N_bin2	N_bin3
1	0.00%	0.00%	0.01%	0.06%	0.00%	0.01%	0.04%		26118.93	136625.8	454081.8	9.17E+03	4.80E+04	1.59E+05
2	0.00%	0.01%	0.06%	0.20%	0.01%	0.05%	0.14%		124254.3	546611.3	1572176	4.36E+04	1.92E+05	5.52E+05
3	0.01%	0.05%	0.21%	0.62%	0.04%	0.16%	0.41%		491969.8	1827333	4564214	1.73E+05	6.41E+05	1.60E+06
4	0.03%	0.17%	0.62%	1.61%	0.14%	0.45%	0.99%		1612463	5089841	11102087	5.66E+05	1.79E+06	3.90E+06
5	0.08%	0.47%	1.50%	3.50%	0.38%	1.04%	2.00%		4293585	11661962	22448850	1.51E+06	4.09E+06	7.88E+06
6	0.21%	1.01%	2.93%	6.26%	0.80%	1.92%	3.33%		9028177	21589270	37386633	3.17E+06	7.58E+06	1.31E+07
7	0.35%	1.56%	4.24%	8.60%	1.21%	2.68%	4.36%		13593196	30107773	48926223	4.77E+06		
8	0.18%	0.88%	2.61%	5.66%	0.71%	1.73%	3.05%		7917953	19384702	34230430			
	P(V<V1)	P(V<V2)	P(V<V3)	P(V<V4)	P(V1<V<V2)	P(V2<V<V3)	P(V3<V<V4)		t_bin1	t_bin2	t_bin3	N_bin1	N_bin2	N_bin3
1	2.40%	7.59%	15.83%	25.98%	5.19%	8.23%	10.15%		58287864	92460258	1.14E+08	7.15E+07	1.13E+08	1.40E+08
2	5.58%	14.76%	26.92%	39.83%	9.18%	12.16%	12.91%		1.03E+08	1.37E+08	1.45E+08	1.26E+08	1.67E+08	1.78E+08
3	11.22%	25.11%	40.53%	54.69%	13.89%	15.42%	14.16%		1.56E+08	1.73E+08		1.91E+08	2.12E+08	
4	19.61%	37.76%	54.76%	68.34%	18.15%	17.00%	13.58%							
5	29.96%	50.73%	67.36%	79.02%	20.77%	16.62%	11.67%							
6	40.24%	61.67%	76.68%	86.12%	21.43%	15.01%	9.44%							
7	46.81%	67.86%	81.47%	89.48%	21.05%	13.60%	8.02%							
8	38.27%	59.70%	75.08%	84.95%	21.43%	15.38%	9.88%							
	P(V<V1)	P(V<V2)	P(V<V3)	P(V<V4)	P(V1<V<V2)	P(V2<V<V3)	P(V3<V<V4)		t_bin1	t_bin2	t_bin3	N_bin1	N_bin2	N_bin3
1	46.19%	67.30%	81.05%	89.20%	21.11%	13.75%	8.15%		2.37E+08			7.14E+08		
2	61.43%	79.80%	89.72%	94.78%	18.37%	9.92%	5.05%							
3	74.74%	88.69%	94.97%	97.72%	13.95%	6.28%	2.75%							
4	84.75%	94.17%	97.73%	99.08%	9.43%	3.56%	1.35%							
5	91.24%	97.13%	99.01%	99.64%	5.89%	1.89%	0.63%							
6	94.89%	98.53%	99.55%	99.85%	3.64%	1.02%	0.30%							
7	96.42%	99.05%	99.73%	99.91%	2.63%	0.68%	0.19%							
8	94.33%	98.33%	99.47%	99.82%	4.00%	1.15%	0.35%							

		IAH (N-S)-Open Terrain probabilities								seconds in each bin			cycles in each bin		
Segment		P(V<V1)	P(V<V2)	P(V<V3)	P(V<V4)	P(V1<V<V2)	P(V2<V<V3)	P(V3<V<V4)		t_bin1	t_bin2	t_bin3	N_bin1	N_bin2	N_bin3
1		0.00%	0.01%	0.03%	0.10%	0.00%	0.02%	0.07%		37659.412	185270.31	583445.746	1.32E+04	6.50E+04	2.05E+05
2		0.00%	0.03%	0.12%	0.36%	0.02%	0.09%	0.25%		178867.78	733070.87	1982202.77	6.28E+04	2.57E+05	6.96E+05
3		0.01%	0.10%	0.41%	1.11%	0.09%	0.30%	0.71%		709182.68	2426079.2	5642939.71	2.49E+05	8.52E+05	1.98E+06
4		0.06%	0.35%	1.19%	2.88%	0.29%	0.84%	1.69%		2342419	6712058.8	13471149.8	8.22E+05	2.36E+06	4.73E+06
5		0.20%	1.00%	2.93%	6.30%	0.80%	1.93%	3.37%		6391268.3	15449071	26918988.4	2.24E+06	5.42E+06	9.45E+06
6		0.56%	2.34%	6.03%	11.67%	1.78%	3.68%	5.64%		14251409	29455177	45070286.3	5.00E+06	1.03E+07	1.58E+07
7		1.17%	4.30%	9.99%	17.85%	3.13%	5.70%	7.85%		24983895	45525241	62756180.1	8.77E+06		
8		1.22%	4.44%	10.27%	18.25%	3.22%	5.83%	7.98%		25736577	46562231	63806407.6			
									E-W Gusts	22874717			8029025.62		
		P(V<V1)	P(V<V2)	P(V<V3)	P(V<V4)	P(V1<V<V2)	P(V2<V<V3)	P(V3<V<V4)		t_bin1	t_bin2	t_bin3	N_bin1	N_bin2	N_bin3
1		3.68%	10.74%	21.03%	32.82%	7.06%	10.29%	11.79%		56423643	82242759	94263355.2	6.92E+07	1.01E+08	1.16E+08
2		8.29%	20.12%	34.38%	48.34%	11.83%	14.26%	13.96%		94585114	113951016	111616686	1.16E+08	1.40E+08	1.37E+08
3		16.13%	32.98%	49.79%	63.88%	16.85%	16.81%	14.09%		134681831	134335788		1.65E+08	1.65E+08	
4		27.35%	47.87%	64.86%	77.10%	20.51%	17.00%	12.24%							
5		40.79%	62.39%	77.36%	86.68%	21.60%	14.97%	9.32%							
6		54.19%	74.34%	86.19%	92.64%	20.15%	11.85%	6.45%							
7		64.64%	82.24%	91.30%	95.73%	17.59%	9.06%	4.43%							
8		65.21%	82.63%	91.54%	95.87%	17.42%	8.91%	4.33%							
		P(V<V1)	P(V<V2)	P(V<V3)	P(V<V4)	P(V1<V<V2)	P(V2<V<V3)	P(V3<V<V4)		t_bin1	t_bin2	t_bin3	N_bin1	N_bin2	N_bin3
1		54.31%	74.44%	86.26%	92.68%	20.13%	11.82%	6.42%		160884555			4.84E+08		
2		69.55%	85.55%	93.26%	96.83%	16.00%	7.71%	3.57%							
3		81.82%	92.74%	97.08%	98.79%	10.93%	4.33%	1.71%							
4		90.24%	96.74%	98.87%	99.59%	6.50%	2.13%	0.72%							
5		95.20%	98.66%	99.60%	99.87%	3.46%	0.94%	0.27%							
6		97.74%	99.46%	99.86%	99.96%	1.72%	0.40%	0.10%							
7		98.85%	99.76%	99.94%	99.99%	0.91%	0.18%	0.04%							
8		98.89%	99.77%	99.95%	99.99%	0.88%	0.17%	0.04%							

		IAH (N-S)-Suburban Terrain probabilities								seconds in each bin			cycles in each bin			
Segment		P(V<V1)	P(V<V2)	P(V<V3)	P(V<V4)	P(V1<V<V2)	P(V2<V<V3)	P(V3<V<V4)		t_bin1	t_bin2	t_bin3	N_bin1	N_bin2	N_bin3	
1		0.00%	0.02%	0.10%	0.31%	0.02%	0.08%	0.21%		144986.51	609746.73	1684613.42	5.09E+04	2.14E+05	5.91E+05	
2		0.01%	0.08%	0.34%	0.94%	0.07%	0.25%	0.60%		573821.1	2021213.9	4817068.99	2.01E+05	7.09E+05	1.69E+06	
3		0.05%	0.28%	0.99%	2.43%	0.24%	0.70%	1.45%		1895588.1	5614576.3	11583206.4	6.65E+05	1.97E+06	4.07E+06	
4		0.16%	0.81%	2.44%	5.38%	0.65%	1.64%	2.94%		5213730.1	13071146	23476488.8	1.83E+06	4.59E+06	8.24E+06	
5		0.44%	1.92%	5.09%	10.10%	1.48%	3.17%	5.01%		11796056	25351184	40067077.1	4.14E+06	8.90E+06	1.41E+07	
6		0.97%	3.67%	8.76%	15.99%	2.70%	5.09%	7.23%		21590547	40719148	57753151.8	7.58E+06	1.43E+07	2.03E+07	
7		1.50%	5.24%	11.76%	20.42%	3.74%	6.52%	8.67%		29895607	52119744	69265713.6	1.05E+07			
8		0.84%	3.27%	7.97%	14.76%	2.43%	4.70%	6.79%		19427466	37533730	54308922.7				
		P(V<V1)	P(V<V2)	P(V<V3)	P(V<V4)	P(V1<V<V2)	P(V2<V<V3)	P(V3<V<V4)		t_bin1	t_bin2	t_bin3	N_bin1	N_bin2	N_bin3	
1		7.45%	18.56%	32.31%	46.08%	11.11%	13.75%	13.77%		88790350	109891266	110056175	1.09E+08	1.35E+08	1.35E+08	
2		14.61%	30.70%	47.23%	61.45%	16.08%	16.54%	14.22%		128546380	132194921	113674780	1.58E+08	1.62E+08	1.39E+08	
3		25.01%	45.00%	62.15%	74.86%	19.99%	17.15%	12.71%		159819204	137091566		1.96E+08	1.68E+08		
4		37.75%	59.36%	74.92%	84.91%	21.60%	15.56%	9.99%								
5		50.84%	71.56%	84.25%	91.39%	20.72%	12.69%	7.14%								
6		61.87%	80.25%	90.07%	95.02%	18.38%	9.82%	4.94%								
7		68.10%	84.59%	92.70%	96.52%	16.49%	8.11%	3.82%								
8		59.88%	78.78%	89.14%	94.46%	18.90%	10.36%	5.32%								
		P(V<V1)	P(V<V2)	P(V<V3)	P(V<V4)	P(V1<V<V2)	P(V2<V<V3)	P(V3<V<V4)		t_bin1	t_bin2	t_bin3	N_bin1	N_bin2	N_bin3	
1		67.53%	84.22%	92.48%	96.40%	16.68%	8.27%	3.91%		133339747			4.01E+08			
2		80.08%	91.82%	96.62%	98.57%	11.74%	4.80%	1.95%								
3		88.94%	96.18%	98.63%	99.49%	7.24%	2.46%	0.85%								
4		94.36%	98.36%	99.49%	99.83%	4.00%	1.13%	0.34%								
5		97.25%	99.32%	99.81%	99.94%	2.07%	0.50%	0.13%								
6		98.61%	99.70%	99.93%	99.98%	1.09%	0.23%	0.05%								
7		99.11%	99.82%	99.96%	99.99%	0.72%	0.14%	0.03%								
8		98.41%	99.65%	99.91%	99.98%	1.24%	0.26%	0.06%								

	RMMA (N-S)-Open Terrain probabilities								seconds in each bin			cycles in each bin			
Segment	P(V<V1)	P(V<V2)	P(V<V3)	P(V<V4)	P(V1<V<V2)	P(V2<V<V3)	P(V3<V<V4)		t_bin1	t_bin2	t_bin3	N_bin1	N_bin2	N_bin3	
1	0.00%	0.00%	0.01%	0.05%	0.00%	0.01%	0.04%		21568.6242	115707.74	391896.619	7.57E+03	4.06E+04	1.38E+05	
2	0.00%	0.01%	0.06%	0.20%	0.01%	0.05%	0.14%		110516.053	494400.7	1438879.23	3.88E+04	1.74E+05	5.05E+05	
3	0.01%	0.05%	0.22%	0.64%	0.05%	0.17%	0.42%		472323.104	1765506.4	4423275.88	1.66E+05	6.20E+05	1.55E+06	
4	0.03%	0.19%	0.69%	1.79%	0.16%	0.50%	1.09%		1679155.89	5262780.1	11385928.7	5.89E+05	1.85E+06	4.00E+06	
5	0.11%	0.58%	1.82%	4.17%	0.47%	1.25%	2.34%		4916508.14	13012184	24458628.2	1.73E+06	4.57E+06	8.58E+06	
6	0.31%	1.43%	3.97%	8.17%	1.12%	2.54%	4.20%		11697977.3	26498007	43768990.9	4.11E+06	9.30E+06	1.54E+07	
7	0.68%	2.75%	6.89%	13.06%	2.07%	4.14%	6.16%		21605390.2	43181537	64293873.6	7.58E+06			
8	0.71%	2.85%	7.10%	13.38%	2.14%	4.25%	6.28%		22322311.3	44298174	65568828.3				
								E-W Gusts	18359522.8			6444192.49			
	P(V<V1)	P(V<V2)	P(V<V3)	P(V<V4)	P(V1<V<V2)	P(V2<V<V3)	P(V3<V<V4)		t_bin1	t_bin2	t_bin3	N_bin1	N_bin2	N_bin3	
1	2.33%	7.46%	15.67%	25.84%	5.13%	8.21%	10.18%		53510886.2	85673798	106168102	6.56E+07	1.05E+08	1.30E+08	
2	5.62%	14.92%	27.24%	40.31%	9.30%	12.32%	13.06%		97038221.4	128573998	136281726	1.19E+08	1.58E+08	1.67E+08	
3	11.67%	25.99%	41.71%	55.99%	14.32%	15.72%	14.28%		149350126	164041045		1.83E+08	2.01E+08		
4	21.04%	39.85%	57.03%	70.44%	18.81%	17.18%	13.41%								
5	33.13%	54.43%	70.74%	81.75%	21.31%	16.31%	11.01%								
6	46.06%	67.33%	81.15%	89.31%	21.26%	13.82%	8.17%								
7	56.80%	76.40%	87.57%	93.49%	19.60%	11.17%	5.93%								
8	57.40%	76.86%	87.88%	93.69%	19.46%	11.01%	5.81%								
	P(V<V1)	P(V<V2)	P(V<V3)	P(V<V4)	P(V1<V<V2)	P(V2<V<V3)	P(V3<V<V4)		t_bin1	t_bin2	t_bin3	N_bin1	N_bin2	N_bin3	
1	46.18%	67.44%	81.23%	89.37%	21.25%	13.79%	8.14%		221727459			6.68E+08			
2	62.05%	80.36%	90.13%	95.04%	18.31%	9.77%	4.91%								
3	75.90%	89.45%	95.40%	97.96%	13.55%	5.95%	2.56%								
4	86.20%	94.92%	98.09%	99.25%	8.72%	3.16%	1.16%								
5	92.76%	97.76%	99.27%	99.74%	5.00%	1.51%	0.48%								
6	96.37%	99.05%	99.73%	99.91%	2.67%	0.68%	0.19%								
7	98.06%	99.55%	99.88%	99.97%	1.49%	0.33%	0.08%								
8	98.13%	99.57%	99.89%	99.97%	1.44%	0.32%	0.08%								

	RMMA (N-S)-Suburban Terrain probabilities								seconds in each bin			cycles in each bin			
Segment	P(V<V1)	P(V<V2)	P(V<V3)	P(V<V4)	P(V1<V<V2)	P(V2<V<V3)	P(V3<V<V4)		t_bin1	t_bin2	t_bin3	N_bin1	N_bin2	N_bin3	
1	0.00%	0.01%	0.05%	0.16%	0.01%	0.04%	0.12%		88626.89463	406785.2853	1209517.994	3.11E+04	1.43E+05	4.25E+05	
2	0.00%	0.04%	0.18%	0.54%	0.04%	0.14%	0.36%		377562.2162	1452896.903	3729286.406	1.33E+05	5.10E+05	1.31E+06	
3	0.02%	0.15%	0.57%	1.49%	0.13%	0.42%	0.93%		1340299.653	4341330.203	9653324.224	4.70E+05	1.52E+06	3.39E+06	
4	0.08%	0.46%	1.50%	3.51%	0.38%	1.04%	2.01%		3950446.976	10841588.07	21002388.45	1.39E+06	3.81E+06	7.37E+06	
5	0.24%	1.15%	3.30%	6.97%	0.91%	2.15%	3.67%		9527205.36	22434675.47	38270047.12	3.34E+06	7.87E+06	1.34E+07	
6	0.55%	2.32%	5.97%	11.56%	1.76%	3.65%	5.59%		18406951.81	38068511.97	58310093.72	6.46E+06	1.34E+07	2.05E+07	
7	0.89%	3.41%	8.24%	15.17%	2.52%	4.83%	6.93%		26330013.07	50363088.39	72307135.39	9.24E+06			
8	0.48%	2.05%	5.38%	10.58%	1.57%	3.33%	5.20%		16398361.71	34736717.78	54274095.46				
	P(V<V1)	P(V<V2)	P(V<V3)	P(V<V4)	P(V1<V<V2)	P(V2<V<V3)	P(V3<V<V4)		t_bin1	t_bin2	t_bin3	N_bin1	N_bin2	N_bin3	
1	5.00%	13.64%	25.39%	38.12%	8.64%	11.75%	12.73%		90086831.18	122601531.4	132851925.8	1.10E+08	1.50E+08	1.63E+08	
2	10.47%	23.96%	39.23%	53.46%	13.49%	15.28%	14.23%		140764968.7	159376522.1	148408291.1	1.73E+08	1.95E+08	1.82E+08	
3	19.02%	37.09%	54.18%	67.91%	18.07%	17.09%	13.72%		188563111.5	178297824.7		2.31E+08	2.19E+08		
4	30.32%	51.29%	67.97%	79.59%	20.98%	16.68%	11.62%								
5	42.75%	64.24%	78.80%	87.69%	21.50%	14.55%	8.89%								
6	53.89%	74.07%	85.99%	92.51%	20.18%	11.92%	6.52%								
7	60.48%	79.21%	89.40%	94.61%	18.73%	10.19%	5.21%								
8	51.83%	72.37%	84.81%	91.75%	20.53%	12.44%	6.94%								
	P(V<V1)	P(V<V2)	P(V<V3)	P(V<V4)	P(V1<V<V2)	P(V2<V<V3)	P(V3<V<V4)		t_bin1	t_bin2	t_bin3	N_bin1	N_bin2	N_bin3	
1	59.88%	78.75%	89.11%	94.44%	18.88%	10.36%	5.33%		196962250.3			5.93E+08			
2	73.86%	88.24%	94.75%	97.62%	14.37%	6.52%	2.87%								
3	84.55%	94.12%	97.72%	99.09%	9.57%	3.60%	1.36%								
4	91.61%	97.30%	99.09%	99.68%	5.69%	1.79%	0.59%								
5	95.65%	98.81%	99.65%	99.89%	3.15%	0.84%	0.24%								
6	97.68%	99.45%	99.85%	99.96%	1.76%	0.41%	0.10%								
7	98.46%	99.66%	99.92%	99.98%	1.20%	0.25%	0.06%								
8	97.38%	99.36%	99.83%	99.95%	1.97%	0.47%	0.12%								

	ELP (N-S)Open Terrain probabilities								seconds in each bin			cycles in each bin		
Segment	P(V<V1)	P(V<V2)	P(V<V3)	P(V<V4)	P(V1<V<V2)	P(V2<V<V3)	P(V3<V<V4)		t_bin1	t_bin2	t_bin3	N_bin1	N_bin2	N_bin3
1	0.00%	0.01%	0.07%	0.23%	0.01%	0.05%	0.16%		79554.28262	367218.035	1087597.98	2.79E+04	1.29E+05	3.82E+05
2	0.01%	0.06%	0.26%	0.78%	0.05%	0.20%	0.51%		357537.457	1361606.256	3434650.1	1.25E+05	4.78E+05	1.21E+06
3	0.03%	0.23%	0.86%	2.21%	0.20%	0.63%	1.35%		1332049.72	4193555.94	9026368.38	4.68E+05	1.47E+06	3.17E+06
4	0.14%	0.75%	2.35%	5.31%	0.61%	1.60%	2.95%		4109772.886	10734169.82	19778864	1.44E+06	3.77E+06	6.94E+06
5	0.45%	2.00%	5.41%	10.81%	1.56%	3.40%	5.40%		10434962.83	22779349.85	36162613.3	3.66E+06	8.00E+06	1.27E+07
6	1.16%	4.40%	10.38%	18.67%	3.23%	5.99%	8.29%		21657095.38	40077704.12	55478437	7.60E+06	1.41E+07	1.95E+07
7	2.32%	7.65%	16.29%	27.01%	5.33%	8.64%	10.71%		35702907.99	57845117.59	71727714.5	1.25E+07		
8	2.41%	7.88%	16.68%	27.53%	5.47%	8.80%	10.85%		36646618.15	58927125.55	72614085.1			
								E-W Gusts	122120226.5			4.29E+07		
	P(V<V1)	P(V<V2)	P(V<V3)	P(V<V4)	P(V1<V<V2)	P(V2<V<V3)	P(V3<V<V4)		t_bin1	t_bin2	t_bin3	N_bin1	N_bin2	N_bin3
1	6.64%	17.36%	31.07%	45.06%	10.71%	13.71%	13.99%		71729748.65	91810582.91	93702230.2	8.79E+07	1.13E+08	1.15E+08
2	13.80%	29.93%	46.80%	61.39%	16.12%	16.88%	14.59%		107958851.9	112990563.4	97699613.9	1.32E+08	1.39E+08	1.20E+08
3	24.75%	45.24%	62.81%	75.70%	20.49%	17.56%	12.89%		137184190.6	117599764.2		1.68E+08	1.44E+08	
4	38.77%	60.92%	76.54%	86.29%	22.16%	15.61%	9.76%							
5	53.72%	74.41%	86.49%	92.95%	20.69%	12.07%	6.47%							
6	67.01%	84.20%	92.64%	96.55%	17.20%	8.43%	3.92%							
7	76.35%	89.98%	95.79%	98.20%	13.63%	5.81%	2.41%							
8	76.83%	90.25%	95.93%	98.27%	13.42%	5.67%	2.34%							
	P(V<V1)	P(V<V2)	P(V<V3)	P(V<V4)	P(V1<V<V2)	P(V2<V<V3)	P(V3<V<V4)		t_bin1	t_bin2	t_bin3	N_bin1	N_bin2	N_bin3
1	67.12%	84.28%	92.68%	96.58%	17.16%	8.40%	3.90%		114875266.9			3.46E+08		
2	80.43%	92.22%	96.90%	98.73%	11.79%	4.68%	1.83%							
3	89.69%	96.61%	98.85%	99.59%	6.92%	2.24%	0.74%							
4	95.16%	98.69%	99.62%	99.88%	3.53%	0.93%	0.26%							
5	97.93%	99.54%	99.89%	99.97%	1.61%	0.35%	0.08%							
6	99.15%	99.84%	99.97%	99.99%	0.69%	0.13%	0.03%							
7	99.61%	99.94%	99.99%	100.00%	0.32%	0.05%	0.01%							
8	99.63%	99.94%	99.99%	100.00%	0.31%	0.05%	0.01%							

		ELP (N-S)Suburban Terrain probabilities								seconds in each bin			cycles in each bin		
Segment		P(V<V1)	P(V<V2)	P(V<V3)	P(V<V4)	P(V1<V<V2)	P(V2<V<V3)	P(V3<V<V4)		t_bin1	t_bin2	t_bin3	N_bin1	N_bin2	N_bin3
1		0.01%	0.05%	0.22%	0.66%	0.04%	0.17%	0.44%		292221.7858	1143531	2950706	1.03E+05	4.01E+05	1.04E+06
2		0.03%	0.19%	0.72%	1.88%	0.16%	0.53%	1.17%		1089250.545	3536393	7809587	3.82E+05	1.24E+06	2.74E+06
3		0.11%	0.61%	1.97%	4.55%	0.50%	1.36%	2.58%		3370240.586	9115339	17290746	1.18E+06	3.20E+06	6.07E+06
4		0.35%	1.64%	4.57%	9.38%	1.29%	2.93%	4.80%		8649417.239	19622459	32162428	3.04E+06	6.89E+06	1.13E+07
5		0.93%	3.65%	8.91%	16.44%	2.73%	5.26%	7.53%		18258316.77	35209139	50431723	6.41E+06	1.24E+07	1.77E+07
6		1.94%	6.62%	14.50%	24.56%	4.69%	7.88%	10.06%		31386427.63	52732318	67382478	1.10E+07	1.85E+07	2.37E+07
7		2.91%	9.15%	18.80%	30.31%	6.24%	9.65%	11.51%		41777561.47	64601396	77073214	1.47E+07		
8		1.70%	5.97%	13.32%	22.92%	4.27%	7.36%	9.60%		28578554.81	49252207	64275047			
		P(V<V1)	P(V<V2)	P(V<V3)	P(V<V4)	P(V1<V<V2)	P(V2<V<V3)	P(V3<V<V4)		t_bin1	t_bin2	t_bin3	N_bin1	N_bin2	N_bin3
1		12.56%	27.93%	44.49%	59.15%	15.38%	16.56%	14.66%		102946094.7	1.11E+08	98125943	1.26E+08	1.36E+08	1.20E+08
2		22.73%	42.65%	60.30%	73.60%	19.93%	17.64%	13.30%		133431622.2	1.18E+08	89030416	1.64E+08	1.45E+08	1.09E+08
3		35.97%	58.06%	74.20%	84.60%	22.09%	16.15%	10.40%		147912550	1.08E+08		1.81E+08	1.33E+08	
4		50.49%	71.74%	84.65%	91.79%	21.25%	12.91%	7.15%							
5		63.83%	82.03%	91.35%	95.84%	18.20%	9.32%	4.49%							
6		73.96%	88.58%	95.06%	97.84%	14.63%	6.48%	2.77%							
7		79.24%	91.58%	96.59%	98.59%	12.34%	5.01%	2.00%							
8		72.20%	87.53%	94.50%	97.55%	15.32%	6.97%	3.05%							
		P(V<V1)	P(V<V2)	P(V<V3)	P(V<V4)	P(V1<V<V2)	P(V2<V<V3)	P(V3<V<V4)		t_bin1	t_bin2	t_bin3	N_bin1	N_bin2	N_bin3
1		78.78%	91.33%	96.47%	98.53%	12.55%	5.14%	2.06%		84060835.62			2.53E+08		
2		88.46%	96.09%	98.64%	99.50%	7.63%	2.55%	0.87%							
3		94.37%	98.42%	99.53%	99.85%	4.05%	1.11%	0.32%							
4		97.49%	99.42%	99.85%	99.96%	1.92%	0.43%	0.11%							
5		98.93%	99.79%	99.95%	99.99%	0.86%	0.16%	0.04%							
6		99.52%	99.92%	99.98%	100.00%	0.40%	0.07%	0.01%							
7		99.71%	99.96%	99.99%	100.00%	0.24%	0.04%	0.01%							
8		99.44%	99.90%	99.98%	100.00%	0.46%	0.08%	0.02%							

APPENDIX B:
HMIP RELIABILITY ANALYSIS
(Steps 11 and 12)

	San Antonio							Dallas/Fort Worth						
S_{Ri} (no GS)	Open	γ_i	$(\gamma_i SR_i)^3$		Suburban	γ_i	$(\gamma_i SR_i)^3$	Open	γ_i	$(\gamma_i SR_i)^3$		Suburban	γ_i	$(\gamma_i SR_i)^3$
0.030	3.81E+04	0.00002	0.00		1.05E+05	0.00006	0.00	9.71E+02	0.00000	0.00		3.98E+03	0.00000	0.00
0.047	1.39E+05	0.00008	0.00		3.42E+05	0.00018	0.00	6.34E+03	0.00000	0.00		2.26E+04	0.00001	0.00
0.049	1.36E+05	0.00008	0.00		3.23E+05	0.00017	0.00	5.72E+03	0.00000	0.00		1.93E+04	0.00001	0.00
0.068	3.53E+05	0.00020	0.00		7.94E+05	0.00042	0.00	2.53E+04	0.00002	0.00		8.06E+04	0.00004	0.00
0.077	4.31E+05	0.00025	0.00		9.22E+05	0.00049	0.00	3.13E+04	0.00002	0.00		9.28E+04	0.00005	0.00
0.112	9.75E+05	0.00056	0.00		1.91E+06	0.00101	0.00	1.08E+05	0.00007	0.00		2.88E+05	0.00015	0.00
0.124	4.17E+05	0.00024	0.00		8.51E+05	0.00045	0.00	2.77E+04	0.00002	0.00		7.62E+04	0.00004	0.00
0.196	1.15E+06	0.00066	0.00		2.14E+06	0.00113	0.00	1.28E+05	0.00008	0.00		3.12E+05	0.00016	0.00
0.225	1.09E+06	0.00063	0.00		1.88E+06	0.00100	0.00	1.09E+05	0.00007	0.00		2.38E+05	0.00013	0.00
0.283	2.33E+06	0.00134	0.00		3.98E+06	0.00211	0.00	3.83E+05	0.00024	0.00		8.48E+05	0.00045	0.00
0.354	2.64E+06	0.00152	0.00		4.20E+06	0.00223	0.00	4.26E+05	0.00027	0.00		8.45E+05	0.00044	0.00
0.389	2.36E+06	0.00136	0.00		3.37E+06	0.00178	0.00	3.31E+05	0.00021	0.00		5.55E+05	0.00029	0.00
0.403	8.24E+07	0.04740	0.00		1.18E+08	0.06243	0.00	3.57E+07	0.02227	0.00		6.40E+07	0.03360	0.00
0.409	2.95E+06	0.00170	0.00		1.65E+06	0.00088	0.00	4.56E+05	0.00028	0.00		1.98E+05	0.00010	0.00
0.448	3.86E+06	0.00222	0.00		4.12E+06	0.00218	0.00	6.76E+05	0.00042	0.00		7.43E+05	0.00039	0.00
0.513	4.78E+06	0.00275	0.00		7.12E+06	0.00377	0.00	1.11E+06	0.00070	0.00		2.03E+06	0.00107	0.00
0.612	5.09E+06	0.00293	0.00		6.84E+06	0.00362	0.00	1.12E+06	0.00070	0.00		1.75E+06	0.00092	0.00
0.634	1.11E+08	0.06401	0.00		1.42E+08	0.07514	0.00	6.77E+07	0.04225	0.00		1.05E+08	0.05525	0.00
0.664	1.28E+08	0.07381	0.00		1.65E+08	0.08728	0.00	7.37E+07	0.04601	0.00		1.14E+08	0.06013	0.00
0.704	7.65E+06	0.00440	0.00		8.07E+06	0.00427	0.00	2.07E+06	0.00129	0.00		2.24E+06	0.00118	0.00
0.886	8.36E+06	0.00481	0.00		1.07E+07	0.00567	0.00	2.60E+06	0.00162	0.00		3.81E+06	0.00200	0.00
0.919	1.24E+08	0.07154	0.00		1.44E+08	0.07641	0.00	9.67E+07	0.06040	0.00		1.34E+08	0.07015	0.00
1.020	1.17E+07	0.00676	0.00		1.23E+07	0.00649	0.00	4.40E+06	0.00275	0.00		4.71E+06	0.00248	0.00
1.045	1.50E+08	0.08612	0.00		1.73E+08	0.09135	0.00	1.17E+08	0.07277	0.00		1.58E+08	0.08304	0.00
1.513	1.48E+08	0.08537	0.00		1.56E+08	0.08282	0.00	1.43E+08	0.08949	0.00		1.74E+08	0.09131	0.00
1.684	1.76E+08	0.10124	0.00		2.05E+08	0.10855	0.01	1.29E+08	0.08061	0.00		1.75E+08	0.09209	0.00
2.545	5.80E+08	0.33339	0.61		5.23E+08	0.27669	0.35	7.47E+08	0.46650	1.67		7.49E+08	0.39332	1.00
2.650	1.78E+08	0.10242	0.02		1.88E+08	0.09941	0.02	1.71E+08	0.10673	0.02		2.05E+08	0.10767	0.02
4.089	3.84E+06	0.00221	0.00		3.84E+06	0.00203	0.00	6.74E+06	0.00421	0.00		6.74E+06	0.00354	0.00
	1738251460		0.64		1889629025		0.38	1601125606		1.70		1903458931		1.03
		S_{RE}	**0.86**			S_{RE}	**0.72**		S_{RE}	**1.19**			S_{RE}	**1.01**

Houston								Austin							
Open	γ_i	$(\gamma_i SR_i)^3$		Suburban	γ_i	$(\gamma_i SR_i)^3$		Open	γ_i	$(\gamma_i SR_i)^3$		Suburban	γ_i	$(\gamma_i SR_i)^3$
6.80E+03	0.00000	0.00		2.41E+04	0.00001	0.00		3.79E+03	0.00000	0.00		1.42E+04	0.00001	0.00
3.59E+04	0.00002	0.00		1.10E+05	0.00007	0.00		2.18E+04	0.00001	0.00		7.11E+04	0.00003	0.00
3.33E+04	0.00002	0.00		9.80E+04	0.00006	0.00		2.00E+04	0.00001	0.00		6.21E+04	0.00003	0.00
1.20E+05	0.00008	0.00		3.27E+05	0.00020	0.00		7.80E+04	0.00004	0.00		2.27E+05	0.00011	0.00
1.47E+05	0.00010	0.00		3.78E+05	0.00023	0.00		9.61E+04	0.00005	0.00		2.62E+05	0.00013	0.00
4.22E+05	0.00027	0.00		9.73E+05	0.00058	0.00		2.97E+05	0.00016	0.00		7.24E+05	0.00035	0.00
1.35E+05	0.00009	0.00		3.26E+05	0.00020	0.00		8.69E+04	0.00005	0.00		2.21E+05	0.00011	0.00
4.99E+05	0.00032	0.00		1.07E+06	0.00064	0.00		3.51E+05	0.00019	0.00		7.93E+05	0.00039	0.00
4.44E+05	0.00029	0.00		8.73E+05	0.00053	0.00		3.06E+05	0.00017	0.00		6.30E+05	0.00031	0.00
1.24E+06	0.00080	0.00		2.40E+06	0.00144	0.00		9.39E+05	0.00051	0.00		1.92E+06	0.00093	0.00
1.39E+06	0.00090	0.00		2.47E+06	0.00148	0.00		1.05E+06	0.00057	0.00		1.95E+06	0.00095	0.00
1.16E+06	0.00075	0.00		1.79E+06	0.00108	0.00		8.49E+05	0.00046	0.00		1.36E+06	0.00066	0.00
6.62E+07	0.04293	0.00		1.01E+08	0.06094	0.00		6.22E+07	0.03393	0.00		1.01E+08	0.04941	0.00
1.52E+06	0.00098	0.00		7.44E+05	0.00045	0.00		1.14E+06	0.00062	0.00		5.31E+05	0.00026	0.00
2.11E+06	0.00137	0.00		2.29E+06	0.00138	0.00		1.62E+06	0.00088	0.00		1.77E+06	0.00086	0.00
3.01E+06	0.00195	0.00		4.89E+06	0.00294	0.00		2.45E+06	0.00133	0.00		4.16E+06	0.00203	0.00
3.12E+06	0.00202	0.00		4.48E+06	0.00269	0.00		2.51E+06	0.00137	0.00		3.72E+06	0.00181	0.00
9.84E+07	0.06386	0.00		1.30E+08	0.07825	0.00		1.02E+08	0.05543	0.00		1.43E+08	0.06974	0.00
1.12E+08	0.07257	0.00		1.50E+08	0.08991	0.00		1.14E+08	0.06195	0.00		1.61E+08	0.07847	0.00
5.13E+06	0.00333	0.00		5.48E+06	0.00329	0.00		4.32E+06	0.00235	0.00		4.63E+06	0.00226	0.00
5.95E+06	0.00386	0.00		8.03E+06	0.00483	0.00		5.16E+06	0.00281	0.00		7.19E+06	0.00351	0.00
1.15E+08	0.07442	0.00		1.34E+08	0.08078	0.00		1.28E+08	0.06984	0.00		1.60E+08	0.07788	0.00
8.98E+06	0.00583	0.00		9.47E+06	0.00570	0.00		8.15E+06	0.00444	0.00		8.64E+06	0.00422	0.00
1.38E+08	0.08955	0.00		1.61E+08	0.09653	0.00		1.54E+08	0.08407	0.00		1.90E+08	0.09272	0.00
1.38E+08	0.08947	0.00		1.43E+08	0.08600	0.00		1.67E+08	0.09088	0.00		1.83E+08	0.08944	0.00
1.61E+08	0.10440	0.01		1.90E+08	0.11441	0.01		1.76E+08	0.09609	0.00		2.20E+08	0.10713	0.01
5.05E+08	0.32744	0.58		4.28E+08	0.25721	0.28		6.96E+08	0.37962	0.90		6.28E+08	0.30640	0.47
1.65E+08	0.10731	0.02		1.72E+08	0.10351	0.02		1.99E+08	0.10875	0.02		2.19E+08	0.10681	0.02
7.78E+06	0.00505	0.00		7.78E+06	0.00468	0.00		6.24E+06	0.00340	0.00		6.24E+06	0.00304	0.00
1541422704		0.61		1663376269		0.31		1834181793		0.93		2050369766		0.51
	S_{RE}	**0.85**			S_{RE}	**0.68**			S_{RE}	**0.98**			S_{RE}	**0.80**

	El Paso									
	Open	γ_i	$(\gamma_i SR_i)^3$		Suburban	γ_i	$(\gamma_i SR_i)^3$			
	1.46E+04	0.00001	0.00		4.99E+04	0.00003	0.00			
	7.27E+04	0.00005	0.00		2.13E+05	0.00014	0.00			
	6.82E+04	0.00005	0.00		1.92E+05	0.00013	0.00			
	2.29E+05	0.00016	0.00		5.94E+05	0.00039	0.00			
	2.80E+05	0.00019	0.00		6.86E+05	0.00046	0.00			
	7.54E+05	0.00051	0.00		1.64E+06	0.00109	0.00			
	2.60E+05	0.00018	0.00		6.04E+05	0.00040	0.00			
	8.91E+05	0.00060	0.00		1.82E+06	0.00121	0.00			
	8.06E+05	0.00055	0.00		1.52E+06	0.00101	0.00			
	2.05E+06	0.00140	0.00		3.77E+06	0.00250	0.00			
	2.32E+06	0.00157	0.00		3.92E+06	0.00260	0.00			
	1.98E+06	0.00134	0.00		2.97E+06	0.00197	0.00			
	8.51E+07	0.05777	0.00		1.20E+08	0.07972	0.00			
	2.55E+06	0.00173	0.00		1.31E+06	0.00087	0.00			
	3.46E+06	0.00235	0.00		3.72E+06	0.00247	0.00			
	4.61E+06	0.00313	0.00		7.13E+06	0.00473	0.00			
	4.85E+06	0.00329	0.00		6.72E+06	0.00446	0.00			
	1.11E+08	0.07554	0.00		1.34E+08	0.08924	0.00			
	1.29E+08	0.08793	0.00		1.59E+08	0.10584	0.00			
	7.59E+06	0.00515	0.00		8.04E+06	0.00534	0.00			
	8.47E+06	0.00575	0.00		1.10E+07	0.00730	0.00			
	1.16E+08	0.07847	0.00		1.23E+08	0.08156	0.00			
	1.21E+07	0.00822	0.00		1.27E+07	0.00841	0.00			
	1.39E+08	0.09440	0.00		1.48E+08	0.09807	0.00			
	1.23E+08	0.08334	0.00		1.16E+08	0.07672	0.00			
	1.67E+08	0.11341	0.01		1.82E+08	0.12105	0.01			
	3.60E+08	0.24434	0.24		2.73E+08	0.18108	0.10			
	1.48E+08	0.10037	0.02		1.41E+08	0.09361	0.02			
	4.15E+07	0.02820	0.00		4.15E+07	0.02757	0.00			
	1472421776		0.27		1505825774		0.13			
		S_{RE}	**0.65**			S_{RE}	**0.50**			

	SAT Open				SAT Sub				DFW Open				DFW Sub		
# of yrs.	N	β	p_f		N	β	p_f		N	β	p_f		N	β	p_f
1	34765029	6.57	0.00%		37792580	7.64	0.00%		32022512	4.42	0.00%		38069179	5.20	0.00%
2	69530058	4.91	0.00%		75585161	5.97	0.00%		64045024	2.76	0.29%		76138357	3.54	0.02%
3	104295088	3.93	0.00%		113377741	5.00	0.00%		96067536	1.78	3.74%		114207536	2.56	0.52%
4	139060117	3.24	0.06%		151170322	4.31	0.00%		128090049	1.09	13.75%		152276715	1.87	3.05%
5	173825146	2.71	0.34%		188962902	3.78	0.01%		160112561	0.56	28.91%		190345893	1.34	9.05%
6	208590175	2.27	1.16%		226755483	3.34	0.04%		192135073	0.12	45.29%		228415072	0.90	18.41%
7	243355204	1.90	2.86%		264548063	2.97	0.15%		224157585	-0.25	59.93%		266484250	0.53	29.81%
8	278120234	1.58	5.69%		302340644	2.65	0.41%		256180097	-0.57	71.64%		304553429	0.21	41.70%
9	312885263	1.30	9.71%		340133224	2.36	0.90%		288202609	-0.85	80.36%		342622608	-0.07	52.92%
10	347650292	1.05	14.79%		377925805	2.11	1.74%		320225121	-1.11	86.60%		380691786	-0.33	62.78%
11	382415321	0.82	20.70%		415718385	1.88	2.99%		352247633	-1.34	90.93%		418760965	-0.55	71.05%
12	417180350	0.61	27.16%		453510966	1.67	4.71%		384270146	-1.55	93.88%		456830144	-0.76	77.75%
13	451945380	0.42	33.88%		491303546	1.48	6.92%		416292658	-1.74	95.88%		494899322	-0.96	83.04%
14	486710409	0.24	40.60%		529096127	1.30	9.61%		448315170	-1.92	97.23%		532968501	-1.13	87.15%
15	521475438	0.07	47.12%		566888707	1.14	12.75%		480337682	-2.08	98.13%		571037679	-1.30	90.31%
16	556240467	-0.08	53.29%		604681288	0.98	16.27%		512360194	-2.24	98.73%		609106858	-1.45	92.70%
17	591005496	-0.23	59.02%		642473868	0.84	20.10%		544382706	-2.38	99.14%		647176037	-1.60	94.51%
18	625770526	-0.37	64.25%		680266449	0.70	24.17%		576405218	-2.52	99.41%		685245215	-1.74	95.88%
19	660535555	-0.49	68.97%		718059029	0.57	28.39%		608427730	-2.65	99.60%		723314394	-1.87	96.90%
20	695300584	-0.62	73.17%		755851610	0.45	32.71%		640450243	-2.77	99.72%		761383573	-1.99	97.67%
21	730065613	-0.74	76.89%		793644190	0.33	37.03%		672472755	-2.89	99.81%		799452751	-2.11	98.24%
22	764830642	-0.85	80.15%		831436771	0.22	41.32%		704495267	-3.00	99.86%		837521930	-2.22	98.67%
23	799595672	-0.95	82.98%		869229351	0.11	45.52%		736517779	-3.11	99.91%		875591108	-2.33	99.00%
24	834360701	-1.06	85.44%		907021932	0.01	49.58%		768540291	-3.21	99.93%		913660287	-2.43	99.24%
25	869125730	-1.15	87.57%		944814512	-0.09	53.49%		800562803	-3.31	99.95%		951729466	-2.53	99.42%
26	903890759	-1.25	89.39%		982607093	-0.18	57.21%		832585315	-3.40	99.97%		989798644	-2.62	99.56%
27	938655788	-1.34	90.96%		1020399673	-0.27	60.73%		864607827	-3.49	99.98%		1027867823	-2.71	99.66%
28	973420817	-1.43	92.30%		1058192254	-0.36	64.04%		896630340	-3.58	99.98%		1065937002	-2.80	99.74%
29	1008185847	-1.51	93.45%		1095984834	-0.44	67.14%		928652852	-3.66	99.99%		1104006180	-2.88	99.80%
30	1042950876	-1.59	94.42%		1133777415	-0.53	70.02%		960675364	-3.74	99.99%		1142075359	-2.96	99.85%
31	1077715905	-1.67	95.25%		1171569995	-0.60	72.70%		992697876	-3.82	99.99%		1180144537	-3.04	99.88%
32	1112480934	-1.75	95.96%		1209362576	-0.68	75.17%		1024720388	-3.90	100.00%		1218213716	-3.12	99.91%
33	1147245963	-1.82	96.56%		1247155156	-0.75	77.45%		1056742900	-3.97	100.00%		1256282895	-3.19	99.93%
34	1182010993	-1.89	97.07%		1284947737	-0.83	79.54%		1088765412	-4.04	100.00%		1294352073	-3.26	99.94%
35	1216776022	-1.96	97.51%		1322740317	-0.89	81.46%		1120787924	-4.11	100.00%		1332421252	-3.33	99.96%
36	1251541051	-2.03	97.88%		1360532898	-0.96	83.21%		1152810437	-4.18	100.00%		1370490431	-3.40	99.97%
37	1286306080	-2.09	98.19%		1398325478	-1.03	84.81%		1184832949	-4.25	100.00%		1408559609	-3.47	99.97%
38	1321071109	-2.16	98.46%		1436118059	-1.09	86.27%		1216855461	-4.31	100.00%		1446628788	-3.53	99.98%
39	1355836139	-2.22	98.68%		1473910639	-1.15	87.59%		1248877973	-4.37	100.00%		1484697967	-3.59	99.98%
40	1390601168	-2.28	98.87%		1511703220	-1.22	88.79%		1280900485	-4.43	100.00%		1522767145	-3.65	99.99%
41	1425366197	-2.34	99.04%		1549495800	-1.27	89.88%		1312922997	-4.49	100.00%		1560836324	-3.71	99.99%
42	1460131226	-2.40	99.18%		1587288381	-1.33	90.87%		1344945509	-4.55	100.00%		1598905502	-3.77	99.99%
43	1494896255	-2.46	99.30%		1625080961	-1.39	91.76%		1376968021	-4.61	100.00%		1636974681	-3.83	99.99%
44	1529661285	-2.51	99.40%		1662873542	-1.44	92.57%		1408990534	-4.66	100.00%		1675043860	-3.88	99.99%
45	1564426314	-2.56	99.48%		1700666122	-1.50	93.30%		1441013046	-4.72	100.00%		1713113038	-3.94	100.00%
46	1599191343	-2.62	99.56%		1738458703	-1.55	93.95%		1473035558	-4.77	100.00%		1751182217	-3.99	100.00%
47	1633956372	-2.67	99.62%		1776251283	-1.60	94.55%		1505058070	-4.82	100.00%		1789251396	-4.04	100.00%
48	1668721401	-2.72	99.67%		1814043864	-1.65	95.08%		1537080582	-4.87	100.00%		1827320574	-4.09	100.00%
49	1703486431	-2.77	99.72%		1851836444	-1.70	95.57%		1569103094	-4.92	100.00%		1865389753	-4.14	100.00%
50	1738251460	-2.82	99.76%		1889629025	-1.75	96.00%		1601125606	-4.97	100.00%		1903458931	-4.19	100.00%
Years	Cycles	β	p_f		Years	Cycles	β		Years	Cycles	β		Years	Cycles	β
3.6	125012315	3.50	0.02%		5.6	211950805	3.50		1.5	46938297	3.50		2.0	77334247	3.50

IAH Open			IAH Sub			RMMA Open			RMMA Sub		
N	β	p_f	N	β	p_f	N	β	p_f	N	β	p_f
30828454	6.97	0.00%	33267525	8.40	0.00%	36683636	5.53	0.00%	41007395	6.73	0.00%
61656908	5.30	0.00%	66535051	6.73	0.00%	73367272	3.87	0.01%	82014791	5.07	0.00%
92485362	4.33	0.00%	99802576	5.76	0.00%	110050908	2.90	0.19%	123022186	4.10	0.00%
123313816	3.64	0.01%	133070102	5.07	0.00%	146734543	2.21	1.37%	164029581	3.41	0.03%
154142270	3.11	0.09%	166337627	4.53	0.00%	183418179	1.67	4.74%	205036977	2.87	0.21%
184970724	2.67	0.38%	199605152	4.10	0.00%	220101815	1.23	10.88%	246044372	2.43	0.75%
215799179	2.30	1.08%	232872678	3.73	0.01%	256785451	0.86	19.40%	287051767	2.06	1.96%
246627633	1.98	2.40%	266140203	3.41	0.03%	293469087	0.54	29.37%	328059163	1.74	4.08%
277456087	1.69	4.50%	299407728	3.12	0.09%	330152723	0.26	39.74%	369066558	1.46	7.22%
308284541	1.44	7.46%	332675254	2.87	0.21%	366836359	0.01	49.72%	410073953	1.21	11.38%
339112995	1.21	11.25%	365942779	2.64	0.41%	403519994	-0.22	58.77%	451081349	0.98	16.41%
369941449	1.00	15.76%	399210305	2.43	0.75%	440203630	-0.43	66.66%	492088744	0.77	22.10%
400769903	0.81	20.83%	432477830	2.24	1.25%	476887266	-0.62	73.32%	533096139	0.58	28.21%
431598357	0.63	26.29%	465745355	2.06	1.96%	513570902	-0.80	78.83%	574103534	0.40	34.50%
462426811	0.47	31.95%	499012881	1.90	2.89%	550254538	-0.97	83.30%	615110930	0.23	40.78%
493255265	0.31	37.67%	532280406	1.74	4.08%	586938174	-1.12	86.88%	656118325	0.08	46.88%
524083719	0.17	43.31%	565547932	1.60	5.52%	623621809	-1.27	89.73%	697125720	-0.07	52.67%
554912173	0.03	48.75%	598815457	1.46	7.22%	660305445	-1.40	91.98%	738133116	-0.20	58.09%
585740628	-0.10	53.92%	632082982	1.33	9.18%	696989081	-1.53	93.74%	779140511	-0.33	63.08%
616569082	-0.22	58.76%	665350508	1.21	11.38%	733672717	-1.66	95.12%	820147906	-0.46	67.62%
647397536	-0.34	63.25%	698618033	1.09	13.80%	770356353	-1.77	96.19%	861155302	-0.57	71.71%
678225990	-0.45	67.37%	731885559	0.98	16.41%	807039989	-1.89	97.03%	902162697	-0.69	75.36%
709054444	-0.56	71.12%	765153084	0.87	19.19%	843723625	-1.99	97.68%	943170092	-0.79	78.60%
739882898	-0.66	74.51%	798420609	0.77	22.10%	880407260	-2.09	98.19%	984177488	-0.89	81.45%
770711352	-0.76	77.55%	831688135	0.67	25.12%	917090896	-2.19	98.58%	1025184883	-0.99	83.96%
801539806	-0.85	80.26%	864955660	0.58	28.21%	953774532	-2.29	98.89%	1066192278	-1.09	86.14%
832368260	-0.94	82.68%	898223185	0.49	31.34%	990458168	-2.38	99.13%	1107199674	-1.18	88.05%
863196714	-1.03	84.83%	931490711	0.40	34.50%	1027141804	-2.46	99.31%	1148207069	-1.26	89.70%
894025168	-1.11	86.72%	964758236	0.31	37.65%	1063825440	-2.55	99.46%	1189214464	-1.35	91.13%
924853622	-1.19	88.39%	998025762	0.23	40.78%	1100509076	-2.63	99.57%	1230221860	-1.43	92.37%
955682077	-1.27	89.85%	1031293287	0.15	43.86%	1137192711	-2.71	99.66%	1271229255	-1.51	93.43%
986510531	-1.35	91.14%	1064560812	0.08	46.88%	1173876347	-2.78	99.73%	1312236650	-1.59	94.35%
1017338985	-1.42	92.27%	1097828338	0.00	49.82%	1210559983	-2.86	99.79%	1353244046	-1.66	95.14%
1048167439	-1.49	93.25%	1131095863	-0.07	52.67%	1247243619	-2.93	99.83%	1394251441	-1.73	95.82%
1078995893	-1.56	94.11%	1164363389	-0.14	55.44%	1283927255	-3.00	99.86%	1435258836	-1.80	96.41%
1109824347	-1.63	94.87%	1197630914	-0.20	58.09%	1320610891	-3.07	99.89%	1476266231	-1.87	96.91%
1140652801	-1.70	95.52%	1230898439	-0.27	60.64%	1357294527	-3.13	99.91%	1517273627	-1.93	97.34%
1171481255	-1.76	96.10%	1264165965	-0.33	63.08%	1393978162	-3.20	99.93%	1558281022	-2.00	97.71%
1202309709	-1.82	96.59%	1297433490	-0.40	65.41%	1430661798	-3.26	99.94%	1599288417	-2.06	98.03%
1233138163	-1.88	97.03%	1330701015	-0.46	67.62%	1467345434	-3.32	99.95%	1640295813	-2.12	98.30%
1263966617	-1.94	97.41%	1363968541	-0.52	69.72%	1504029070	-3.38	99.96%	1681303208	-2.18	98.54%
1294795071	-2.00	97.74%	1397236066	-0.57	71.71%	1540712706	-3.44	99.97%	1722310603	-2.24	98.74%
1325623525	-2.06	98.02%	1430503592	-0.63	73.59%	1577396342	-3.49	99.98%	1763317999	-2.29	98.91%
1356451980	-2.11	98.27%	1463771117	-0.69	75.36%	1614079978	-3.55	99.98%	1804325394	-2.35	99.06%
1387280434	-2.17	98.49%	1497038642	-0.74	77.03%	1650763613	-3.60	99.98%	1845332789	-2.40	99.19%
1418108888	-2.22	98.68%	1530306168	-0.79	78.60%	1687447249	-3.66	99.99%	1886340185	-2.46	99.30%
1448937342	-2.27	98.85%	1563573693	-0.84	80.07%	1724130885	-3.71	99.99%	1927347580	-2.51	99.39%
1479765796	-2.32	98.99%	1596841219	-0.89	81.45%	1760814521	-3.76	99.99%	1968354975	-2.56	99.47%
1510594250	-2.37	99.12%	1630108744	-0.94	82.75%	1797498157	-3.81	99.99%	2009362371	-2.61	99.54%
1541422704	-2.42	99.23%	1663376269	-0.99	83.96%	1834181793	-3.86	99.99%	2050369766	-2.66	99.60%
Years	Cycles	β	Years	Cycles	β	Years	Cycles	β	Years	Cycles	β
4.2	130792227	3.50	7.7	255857021	3.50	2.3	85592629	3.50	3.8	157737881	3.50

ELP Open				ELP Sub					
N	β	p_f		N	β	p_f			
29448436	9.03	0.00%		30116515	10.80	0.00%			
58896871	7.36	0.00%		60233031	9.14	0.00%			
88345307	6.39	0.00%		90349546	8.16	0.00%			
117793742	5.70	0.00%		120466062	7.47	0.00%			
147242178	5.16	0.00%		150582577	6.94	0.00%			
176690613	4.73	0.00%		180699093	6.50	0.00%			
206139049	4.36	0.00%		210815608	6.13	0.00%			
235587484	4.03	0.00%		240932124	5.81	0.00%			
265035920	3.75	0.01%		271048639	5.53	0.00%			
294484355	3.50	0.02%		301165155	5.27	0.00%			
323932791	3.27	0.05%		331281670	5.05	0.00%			
353381226	3.06	0.11%		361398186	4.84	0.00%			
382829662	2.87	0.21%		391514701	4.64	0.00%			
412278097	2.69	0.36%		421631217	4.47	0.00%			
441726533	2.53	0.58%		451747732	4.30	0.00%			
471174968	2.37	0.89%		481864248	4.15	0.00%			
500623404	2.23	1.30%		511980763	4.00	0.00%			
530071839	2.09	1.84%		542097279	3.86	0.01%			
559520275	1.96	2.51%		572213794	3.73	0.01%			
588968710	1.84	3.32%		602330310	3.61	0.02%			
618417146	1.72	4.29%		632446825	3.49	0.02%			
647865581	1.61	5.40%		662563341	3.38	0.04%			
677314017	1.50	6.68%		692679856	3.28	0.05%			
706762452	1.40	8.10%		722796372	3.17	0.08%			
736210888	1.30	9.68%		752912887	3.08	0.11%			
765659323	1.21	11.39%		783029403	2.98	0.14%			
795107759	1.12	13.23%		813145918	2.89	0.19%			
824556194	1.03	15.20%		843262434	2.80	0.25%			
854004630	0.94	17.26%		873378949	2.72	0.33%			
883453065	0.86	19.42%		903495464	2.64	0.42%			
912901501	0.78	21.66%		933611980	2.56	0.53%			
942349937	0.71	23.96%		963728495	2.48	0.65%			
971798372	0.63	26.31%		993845011	2.41	0.80%			
1001246808	0.56	28.70%		1023961526	2.34	0.97%			
1030695243	0.49	31.12%		1054078042	2.27	1.17%			
1060143679	0.42	33.54%		1084194557	2.20	1.39%			
1089592114	0.36	35.97%		1114311073	2.13	1.64%			
1119040550	0.30	38.39%		1144427588	2.07	1.92%			
1148488985	0.23	40.79%		1174544104	2.01	2.23%			
1177937421	0.17	43.17%		1204660619	1.95	2.58%			
1207385856	0.11	45.51%		1234777135	1.89	2.95%			
1236834292	0.05	47.81%		1264893650	1.83	3.36%			
1266282727	0.00	50.06%		1295010166	1.77	3.81%			
1295731163	-0.06	52.26%		1325126681	1.72	4.29%			
1325179598	-0.11	54.40%		1355243197	1.66	4.80%			
1354628034	-0.16	56.49%		1385359712	1.61	5.35%			
1384076469	-0.21	58.51%		1415476228	1.56	5.94%			
1413524905	-0.27	60.47%		1445592743	1.51	6.56%			
1442973340	-0.31	62.36%		1475709259	1.46	7.21%			
1472421776	-0.36	64.19%		1505825774	1.41	7.90%			
	Cycles	β			Cycles	β			
10.0	294378866	3.50		20.9	630756871	3.50			

	San Antonio							Dallas/Fort Worth						
S_{Ri} (no GS)	Open	γ_i	$(\gamma_i SR_i)^3$		Suburban	γ_i	$(\gamma_i SR_i)^3$	Open	γ_i	$(\gamma_i SR_i)^3$		Suburban	γ_i	$(\gamma_i SR_i)^3$
0.021	1.43E+04	0.00001	0.00		4.67E+04	0.00003	0.00	2.65E+02	0.00000	0.00		1.36E+03	0.00000	0.00
0.033	5.70E+04	0.00005	0.00		1.64E+05	0.00012	0.00	1.92E+03	0.00000	0.00		8.50E+03	0.00001	0.00
0.037	5.58E+04	0.00005	0.00		1.56E+05	0.00012	0.00	1.75E+03	0.00000	0.00		7.36E+03	0.00001	0.00
0.048	1.56E+05	0.00014	0.00		4.06E+05	0.00030	0.00	8.41E+03	0.00001	0.00		3.27E+04	0.00003	0.00
0.058	1.93E+05	0.00017	0.00		4.79E+05	0.00035	0.00	1.06E+04	0.00001	0.00		3.87E+04	0.00003	0.00
0.084	4.68E+05	0.00041	0.00		1.06E+06	0.00078	0.00	4.01E+04	0.00005	0.00		1.29E+05	0.00011	0.00
0.095	1.87E+05	0.00016	0.00		4.48E+05	0.00033	0.00	9.50E+03	0.00001	0.00		3.25E+04	0.00003	0.00
0.149	5.63E+05	0.00049	0.00		1.20E+06	0.00089	0.00	4.86E+04	0.00005	0.00		1.45E+05	0.00012	0.00
0.171	5.38E+05	0.00047	0.00		1.09E+06	0.00080	0.00	4.21E+04	0.00005	0.00		1.15E+05	0.00010	0.00
0.216	1.22E+06	0.00106	0.00		2.38E+06	0.00176	0.00	1.59E+05	0.00018	0.00		4.22E+05	0.00036	0.00
0.251	3.67E+07	0.03192	0.00		5.81E+07	0.04293	0.00	1.13E+07	0.01273	0.00		2.31E+07	0.01966	0.00
0.269	1.41E+06	0.00123	0.00		2.59E+06	0.00191	0.00	1.82E+05	0.00021	0.00		4.41E+05	0.00038	0.00
0.321	1.30E+06	0.00113	0.00		2.19E+06	0.00162	0.00	1.49E+05	0.00017	0.00		3.16E+05	0.00027	0.00
0.389	2.73E+06	0.00237	0.00		4.61E+06	0.00341	0.00	5.18E+05	0.00058	0.00		1.13E+06	0.00096	0.00
0.395	5.79E+07	0.05037	0.00		8.18E+07	0.06042	0.00	2.61E+07	0.02933	0.00		4.61E+07	0.03929	0.00
0.439	6.49E+07	0.05648	0.00		9.17E+07	0.06779	0.00	2.75E+07	0.03091	0.00		4.81E+07	0.04103	0.00
0.500	2.52E+06	0.00219	0.00		3.37E+06	0.00249	0.00	3.87E+05	0.00044	0.00		5.91E+05	0.00050	0.00
0.505	3.01E+06	0.00262	0.00		4.67E+06	0.00345	0.00	5.51E+05	0.00062	0.00		1.06E+06	0.00090	0.00
0.572	7.35E+07	0.06401	0.00		9.46E+07	0.06988	0.00	4.38E+07	0.04924	0.00		6.87E+07	0.05863	0.00
0.580	2.99E+06	0.00260	0.00		2.49E+06	0.00184	0.00	4.96E+05	0.00056	0.00		3.79E+05	0.00032	0.00
0.692	8.86E+07	0.07710	0.00		1.12E+08	0.08305	0.00	5.28E+07	0.05944	0.00		8.09E+07	0.06897	0.00
0.731	5.24E+06	0.00456	0.00		7.61E+06	0.00563	0.00	1.37E+06	0.00154	0.00		2.42E+06	0.00207	0.00
0.787	5.25E+06	0.00457	0.00		6.68E+06	0.00493	0.00	1.26E+06	0.00142	0.00		1.81E+06	0.00154	0.00
1.001	9.99E+07	0.08693	0.00		1.16E+08	0.08569	0.00	7.64E+07	0.08592	0.00		1.05E+08	0.08918	0.00
1.130	1.04E+08	0.09057	0.00		1.34E+08	0.09869	0.00	5.94E+07	0.06686	0.00		9.19E+07	0.07841	0.00
1.140	8.39E+06	0.00730	0.00		1.02E+07	0.00757	0.00	2.81E+06	0.00317	0.00		3.84E+06	0.00328	0.00
1.476	4.62E+08	0.40214	0.21		4.69E+08	0.34694	0.13	4.83E+08	0.54374	0.52		5.63E+08	0.47985	0.35
1.778	1.22E+08	0.10600	0.01		1.40E+08	0.10380	0.01	9.43E+07	0.10616	0.01		1.28E+08	0.10896	0.01
4.916	3.34E+06	0.00291	0.00		3.34E+06	0.00247	0.00	5.87E+06	0.00660	0.00		5.87E+06	0.00500	0.00
	1149087307		0.22		1353169798		0.14	888690329		0.52		1172289798		0.36
		S_{RE}	**0.60**			S_{RE}	**0.52**		S_{RE}	**0.81**			S_{RE}	**0.71**

	Houston							Austin						
	Open	γ_i	$(\gamma_i SR_i)^3$		Suburban	γ_i	$(\gamma_i SR_i)^3$	Open	γ_i	$(\gamma_i SR_i)^3$		Suburban	γ_i	$(\gamma_i SR_i)^3$
	2.08E+03	0.00000	0.00		9.11E+03	0.00001	0.00	1.10E+03	0.00000	0.00		5.17E+03	0.00000	0.00
	1.22E+04	0.00001	0.00		4.58E+04	0.00004	0.00	7.07E+03	0.00001	0.00		2.83E+04	0.00002	0.00
	1.14E+04	0.00001	0.00		4.11E+04	0.00003	0.00	6.52E+03	0.00001	0.00		2.50E+04	0.00002	0.00
	4.46E+04	0.00004	0.00		1.47E+05	0.00012	0.00	2.78E+04	0.00002	0.00		9.78E+04	0.00007	0.00
	5.58E+04	0.00005	0.00		1.74E+05	0.00014	0.00	3.49E+04	0.00003	0.00		1.16E+05	0.00008	0.00
	1.75E+05	0.00017	0.00		4.82E+05	0.00040	0.00	1.18E+05	0.00010	0.00		3.45E+05	0.00025	0.00
	5.15E+04	0.00005	0.00		1.52E+05	0.00013	0.00	3.18E+04	0.00003	0.00		9.96E+04	0.00007	0.00
	2.12E+05	0.00021	0.00		5.45E+05	0.00045	0.00	1.43E+05	0.00013	0.00		3.89E+05	0.00028	0.00
	1.91E+05	0.00019	0.00		4.58E+05	0.00038	0.00	1.27E+05	0.00011	0.00		3.20E+05	0.00023	0.00
	5.75E+05	0.00057	0.00		1.31E+06	0.00109	0.00	4.16E+05	0.00037	0.00		1.01E+06	0.00072	0.00
	2.60E+07	0.02555	0.00		4.53E+07	0.03765	0.00	2.25E+07	0.01980	0.00		4.17E+07	0.02978	0.00
	6.63E+05	0.00065	0.00		1.40E+06	0.00116	0.00	4.80E+05	0.00042	0.00		1.07E+06	0.00076	0.00
	5.71E+05	0.00056	0.00		1.09E+06	0.00091	0.00	4.04E+05	0.00036	0.00		8.05E+05	0.00058	0.00
	1.56E+06	0.00153	0.00		2.96E+06	0.00246	0.00	1.21E+06	0.00107	0.00		2.44E+06	0.00174	0.00
	4.71E+07	0.04637	0.00		7.10E+07	0.05906	0.00	4.48E+07	0.03942	0.00		7.18E+07	0.05129	0.00
	5.17E+07	0.05089	0.00		7.81E+07	0.06495	0.00	4.84E+07	0.04258	0.00		7.73E+07	0.05528	0.00
	1.29E+06	0.00127	0.00		1.85E+06	0.00153	0.00	9.67E+05	0.00085	0.00		1.42E+06	0.00101	0.00
	1.69E+06	0.00166	0.00		2.90E+06	0.00241	0.00	1.31E+06	0.00115	0.00		2.34E+06	0.00168	0.00
	6.48E+07	0.06371	0.00		8.65E+07	0.07192	0.00	6.65E+07	0.05851	0.00		9.44E+07	0.06751	0.00
	1.59E+06	0.00157	0.00		1.27E+06	0.00106	0.00	1.21E+06	0.00106	0.00		9.50E+05	0.00068	0.00
	7.80E+07	0.07674	0.00		1.03E+08	0.08530	0.00	8.01E+07	0.07052	0.00		1.12E+08	0.07981	0.00
	3.47E+06	0.00342	0.00		5.47E+06	0.00455	0.00	2.90E+06	0.00255	0.00		4.77E+06	0.00341	0.00
	3.34E+06	0.00329	0.00		4.48E+06	0.00373	0.00	2.74E+06	0.00241	0.00		3.77E+06	0.00269	0.00
	9.20E+07	0.09046	0.00		1.08E+08	0.08972	0.00	1.02E+08	0.08986	0.00		1.27E+08	0.09080	0.00
	9.06E+07	0.08911	0.00		1.21E+08	0.10054	0.00	9.19E+07	0.08087	0.00		1.30E+08	0.09276	0.00
	6.16E+06	0.00606	0.00		7.84E+06	0.00652	0.00	5.44E+06	0.00478	0.00		7.11E+06	0.00508	0.00
	4.26E+08	0.41882	0.24		4.20E+08	0.34947	0.14	5.32E+08	0.46803	0.33		5.58E+08	0.39920	0.20
	1.12E+08	0.11040	0.01		1.31E+08	0.10862	0.01	1.25E+08	0.11017	0.01		1.54E+08	0.11029	0.01
	6.77E+06	0.00666	0.00		6.77E+06	0.00563	0.00	5.43E+06	0.00478	0.00		5.43E+06	0.00388	0.00
	1016819878		0.25		1202737511		0.15	1136306941		0.34		1398914242		0.21
		S_{RE}	**0.63**			S_{RE}	**0.53**		S_{RE}	**0.70**			S_{RE}	**0.60**

	El Paso						
	Open	γ_i	$(\gamma_i SR_i)^3$		Suburban	γ_i	$(\gamma_i SR_i)^3$
	4.59E+03	0.00000	0.00		1.94E+04	0.00002	0.00
	2.56E+04	0.00002	0.00		9.15E+04	0.00008	0.00
	2.40E+04	0.00002	0.00		8.29E+04	0.00007	0.00
	8.86E+04	0.00008	0.00		2.76E+05	0.00023	0.00
	1.11E+05	0.00010	0.00		3.26E+05	0.00027	0.00
	3.27E+05	0.00030	0.00		8.46E+05	0.00070	0.00
	1.03E+05	0.00009	0.00		2.91E+05	0.00024	0.00
	3.94E+05	0.00036	0.00		9.59E+05	0.00079	0.00
	3.61E+05	0.00033	0.00		8.25E+05	0.00068	0.00
	9.97E+05	0.00092	0.00		2.14E+06	0.00178	0.00
	4.03E+07	0.03707	0.00		6.70E+07	0.05551	0.00
	1.15E+06	0.00106	0.00		2.31E+06	0.00191	0.00
	1.01E+06	0.00093	0.00		1.85E+06	0.00153	0.00
	2.51E+06	0.00231	0.00		4.49E+06	0.00372	0.00
	6.35E+07	0.05835	0.00		8.89E+07	0.07364	0.00
	7.18E+07	0.06604	0.00		1.02E+08	0.08462	0.00
	2.17E+06	0.00200	0.00		3.02E+06	0.00250	0.00
	2.74E+06	0.00252	0.00		4.48E+06	0.00371	0.00
	7.68E+07	0.07063	0.00		9.35E+07	0.07740	0.00
	2.64E+06	0.00242	0.00		2.14E+06	0.00177	0.00
	9.27E+07	0.08526	0.00		1.12E+08	0.09269	0.00
	5.18E+06	0.00476	0.00		7.74E+06	0.00641	0.00
	5.09E+06	0.00468	0.00		6.62E+06	0.00548	0.00
	9.53E+07	0.08764	0.00		1.00E+08	0.08321	0.00
	1.08E+08	0.09909	0.00		1.33E+08	0.11001	0.00
	8.58E+06	0.00788	0.00		1.06E+07	0.00874	0.00
	3.55E+08	0.32661	0.11		3.05E+08	0.25222	0.05
	1.14E+08	0.10527	0.01		1.21E+08	0.10013	0.01
	3.61E+07	0.03324	0.00		3.61E+07	0.02993	0.00
	1087608207		0.13		1207614660		0.06
		S_{RE}	**0.50**			S_{RE}	**0.40**

	SAT Open				SAT Sub				DFW Open				DFW Sub		
# of yrs.	N	β	p_f		N	β	p_f		N	β	p_f		N	β	p_f
1	22981746	10.15	0.00%		27063396	10.77	0.00%		17773807	8.66	0.00%		23445796	8.87	0.00%
2	45963492	8.49	0.00%		54126792	9.11	0.00%		35547613	6.99	0.00%		46891592	7.20	0.00%
3	68945238	7.51	0.00%		81190188	8.13	0.00%		53321420	6.02	0.00%		70337388	6.23	0.00%
4	91926985	6.82	0.00%		108253584	7.44	0.00%		71095226	5.33	0.00%		93783184	5.54	0.00%
5	114908731	6.29	0.00%		135316980	6.91	0.00%		88869033	4.79	0.00%		117228980	5.01	0.00%
6	137890477	5.85	0.00%		162380376	6.47	0.00%		106642839	4.36	0.00%		140674776	4.57	0.00%
7	160872223	5.48	0.00%		189443772	6.10	0.00%		124416646	3.99	0.00%		164120572	4.20	0.00%
8	183853969	5.16	0.00%		216507168	5.78	0.00%		142190453	3.67	0.01%		187566368	3.88	0.01%
9	206835715	4.88	0.00%		243570564	5.50	0.00%		159964259	3.38	0.04%		211012164	3.60	0.02%
10	229817461	4.62	0.00%		270633960	5.24	0.00%		177738066	3.13	0.09%		234457960	3.34	0.04%
11	252799208	4.40	0.00%		297697355	5.01	0.00%		195511872	2.90	0.19%		257903755	3.11	0.09%
12	275780954	4.19	0.00%		324760751	4.81	0.00%		213285679	2.69	0.36%		281349551	2.90	0.18%
13	298762700	3.99	0.00%		351824147	4.61	0.00%		231059485	2.50	0.62%		304795347	2.71	0.33%
14	321744446	3.82	0.01%		378887543	4.44	0.00%		248833292	2.32	1.01%		328241143	2.53	0.56%
15	344726192	3.65	0.01%		405950939	4.27	0.00%		266607099	2.16	1.55%		351686939	2.37	0.89%
16	367707938	3.50	0.02%		433014335	4.12	0.00%		284380905	2.00	2.27%		375132735	2.21	1.34%
17	390689684	3.35	0.04%		460077731	3.97	0.00%		302154712	1.86	3.17%		398578531	2.07	1.93%
18	413671431	3.21	0.07%		487141127	3.83	0.01%		319928518	1.72	4.28%		422024327	1.93	2.67%
19	436653177	3.08	0.10%		514204523	3.70	0.01%		337702325	1.59	5.60%		445470123	1.80	3.58%
20	459634923	2.96	0.15%		541267919	3.58	0.02%		355476131	1.47	7.13%		468915919	1.68	4.66%
21	482616669	2.84	0.22%		568331315	3.46	0.03%		373249938	1.35	8.87%		492361715	1.56	5.92%
22	505598415	2.73	0.31%		595394711	3.35	0.04%		391023745	1.24	10.80%		515807511	1.45	7.35%
23	528580161	2.63	0.43%		622458107	3.24	0.06%		408797551	1.13	12.91%		539253307	1.34	8.96%
24	551561908	2.52	0.58%		649521503	3.14	0.08%		426571358	1.03	15.19%		562699103	1.24	10.73%
25	574543654	2.43	0.77%		676584899	3.04	0.12%		444345164	0.93	17.61%		586144899	1.14	12.65%
26	597525400	2.33	0.99%		703648295	2.95	0.16%		462118971	0.84	20.15%		609590695	1.05	14.70%
27	620507146	2.24	1.25%		730711691	2.86	0.21%		479892777	0.75	22.79%		633036491	0.96	16.89%
28	643488892	2.15	1.57%		757775087	2.77	0.28%		497666584	0.66	25.51%		656482287	0.87	19.18%
29	666470638	2.07	1.93%		784838483	2.69	0.36%		515440391	0.57	28.29%		679928083	0.79	21.56%
30	689452384	1.99	2.34%		811901879	2.61	0.46%		533214197	0.49	31.10%		703373879	0.71	24.02%
31	712434131	1.91	2.81%		838965275	2.53	0.57%		550988004	0.41	33.93%		726819674	0.63	26.53%
32	735415877	1.83	3.34%		866028671	2.45	0.71%		568761810	0.34	36.77%		750265470	0.55	29.09%
33	758397623	1.76	3.93%		893092066	2.38	0.87%		586535617	0.26	39.58%		773711266	0.48	31.67%
34	781379369	1.69	4.58%		920155462	2.31	1.06%		604309423	0.19	42.36%		797157062	0.41	34.26%
35	804361115	1.62	5.29%		947218858	2.24	1.27%		622083230	0.12	45.11%		820602858	0.34	36.85%
36	827342861	1.55	6.06%		974282254	2.17	1.50%		639857037	0.06	47.79%		844048654	0.27	39.43%
37	850324607	1.48	6.89%		1001345650	2.10	1.77%		657630843	-0.01	50.41%		867494450	0.20	41.98%
38	873306354	1.42	7.78%		1028409046	2.04	2.07%		675404650	-0.07	52.96%		890940246	0.14	44.50%
39	896288100	1.36	8.73%		1055472442	1.98	2.40%		693178456	-0.14	55.44%		914386042	0.08	46.97%
40	919269846	1.30	9.73%		1082535838	1.92	2.77%		710952263	-0.20	57.83%		937831838	0.02	49.39%
41	942251592	1.24	10.79%		1109599234	1.86	3.17%		728726069	-0.26	60.13%		961277634	-0.04	51.75%
42	965233338	1.18	11.90%		1136662630	1.80	3.60%		746499876	-0.31	62.35%		984723430	-0.10	54.05%
43	988215084	1.12	13.06%		1163726026	1.74	4.07%		764273683	-0.37	64.47%		1008169226	-0.16	56.29%
44	1011196830	1.07	14.27%		1190789422	1.69	4.58%		782047489	-0.43	66.50%		1031615022	-0.21	58.45%
45	1034178577	1.01	15.52%		1217852818	1.63	5.12%		799821296	-0.48	68.44%		1055060818	-0.27	60.54%
46	1057160323	0.96	16.81%		1244916214	1.58	5.70%		817595102	-0.53	70.29%		1078506614	-0.32	62.56%
47	1080142069	0.91	18.14%		1271979610	1.53	6.31%		835368909	-0.58	72.06%		1101952410	-0.37	64.49%
48	1103123815	0.86	19.50%		1299043006	1.48	6.97%		853142715	-0.64	73.73%		1125398206	-0.42	66.36%
49	1126105561	0.81	20.90%		1326106402	1.43	7.65%		870916522	-0.68	75.32%		1148844002	-0.47	68.14%
50	1149087307	0.76	22.32%		1353169798	1.38	8.37%		888690329	-0.73	76.82%		1172289798	-0.52	69.85%
Years	Cycles	β	p_f		Years	Cycles	β		Years	Cycles	β		Years	Cycles	β
16.0	367023890	3.50	0.02%		20.7	559487551	3.50		8.6	152305746	3.50		9.4	219517436	3.50

IAH Open				IAH Sub				RMMA Open				RMMA Sub		
N	β	p_f		N	β	p_f		N	β	p_f		N	β	p_f
20336398	10.15	0.00%		24054750	10.98	0.00%		22726139	9.12	0.00%		27978285	9.72	0.00%
40672795	8.49	0.00%		48109500	9.32	0.00%		45452278	7.45	0.00%		55956570	8.05	0.00%
61009193	7.52	0.00%		72164251	8.35	0.00%		68178416	6.48	0.00%		83934855	7.08	0.00%
81345590	6.83	0.00%		96219001	7.66	0.00%		90904555	5.79	0.00%		111913139	6.39	0.00%
101681988	6.29	0.00%		120273751	7.12	0.00%		113630694	5.25	0.00%		139891424	5.85	0.00%
122018385	5.85	0.00%		144328501	6.68	0.00%		136356833	4.82	0.00%		167869709	5.42	0.00%
142354783	5.48	0.00%		168383252	6.31	0.00%		159082972	4.45	0.00%		195847994	5.05	0.00%
162691181	5.16	0.00%		192438002	5.99	0.00%		181809111	4.13	0.00%		223826279	4.73	0.00%
183027578	4.88	0.00%		216492752	5.71	0.00%		204535249	3.84	0.01%		251804564	4.44	0.00%
203363976	4.63	0.00%		240547502	5.46	0.00%		227261388	3.59	0.02%		279782848	4.19	0.00%
223700373	4.40	0.00%		264602253	5.23	0.00%		249987527	3.36	0.04%		307761133	3.96	0.00%
244036771	4.19	0.00%		288657003	5.02	0.00%		272713666	3.15	0.08%		335739418	3.75	0.01%
264373168	4.00	0.00%		312711753	4.83	0.00%		295439805	2.96	0.15%		363717703	3.56	0.02%
284709566	3.82	0.01%		336766503	4.65	0.00%		318165944	2.78	0.27%		391695988	3.38	0.04%
305045964	3.65	0.01%		360821253	4.49	0.00%		340892082	2.62	0.44%		419674273	3.22	0.06%
325382361	3.50	0.02%		384876004	4.33	0.00%		363618221	2.46	0.69%		447652558	3.06	0.11%
345718759	3.35	0.04%		408930754	4.18	0.00%		386344360	2.32	1.03%		475630842	2.92	0.18%
366055156	3.22	0.06%		432985504	4.05	0.00%		409070499	2.18	1.47%		503609127	2.78	0.27%
386391554	3.09	0.10%		457040254	3.92	0.00%		431796638	2.05	2.02%		531587412	2.65	0.40%
406727951	2.96	0.15%		481095005	3.79	0.01%		454522777	1.93	2.70%		559565697	2.53	0.57%
427064349	2.85	0.22%		505149755	3.68	0.01%		477248915	1.81	3.52%		587543982	2.41	0.80%
447400746	2.73	0.31%		529204505	3.57	0.02%		499975054	1.70	4.48%		615522267	2.30	1.08%
467737144	2.63	0.43%		553259255	3.46	0.03%		522701193	1.59	5.58%		643500552	2.19	1.42%
488073542	2.53	0.58%		577314005	3.36	0.04%		545427332	1.49	6.83%		671478836	2.09	1.83%
508409939	2.43	0.76%		601368756	3.26	0.06%		568153471	1.39	8.21%		699457121	1.99	2.32%
528746337	2.33	0.98%		625423506	3.17	0.08%		590879609	1.30	9.74%		727435406	1.90	2.89%
549082734	2.24	1.24%		649478256	3.07	0.11%		613605748	1.21	11.39%		755413691	1.81	3.54%
569419132	2.16	1.55%		673533006	2.99	0.14%		636331887	1.12	13.16%		783391976	1.72	4.27%
589755529	2.07	1.91%		697587757	2.90	0.18%		659058026	1.03	15.04%		811370261	1.64	5.10%
610091927	1.99	2.33%		721642507	2.82	0.24%		681784165	0.95	17.02%		839348545	1.55	6.01%
630428325	1.91	2.80%		745697257	2.74	0.30%		704510304	0.87	19.09%		867326830	1.48	7.00%
650764722	1.84	3.32%		769752007	2.67	0.38%		727236442	0.80	21.23%		895305115	1.40	8.09%
671101120	1.76	3.91%		793806758	2.59	0.48%		749962581	0.72	23.44%		923283400	1.33	9.25%
691437517	1.69	4.55%		817861508	2.52	0.58%		772688720	0.65	25.69%		951261685	1.25	10.50%
711773915	1.62	5.26%		841916258	2.45	0.71%		795414859	0.58	27.99%		979239970	1.18	11.82%
732110312	1.55	6.02%		865971008	2.38	0.86%		818140998	0.52	30.30%		1007218255	1.12	13.21%
752446710	1.49	6.85%		890025758	2.32	1.02%		840867137	0.45	32.64%		1035196539	1.05	14.67%
772783108	1.42	7.74%		914080509	2.25	1.21%		863593275	0.39	34.98%		1063174824	0.99	16.19%
793119505	1.36	8.68%		938135259	2.19	1.42%		886319414	0.32	37.31%		1091153109	0.92	17.76%
813455903	1.30	9.68%		962190009	2.13	1.65%		909045553	0.26	39.63%		1119131394	0.86	19.39%
833792300	1.24	10.74%		986244759	2.07	1.91%		931771692	0.20	41.94%		1147109679	0.80	21.06%
854128698	1.18	11.85%		1010299510	2.01	2.20%		954497831	0.15	44.21%		1175087964	0.75	22.76%
874465095	1.13	13.00%		1034354260	1.96	2.51%		977223970	0.09	46.44%		1203066248	0.69	24.50%
894801493	1.07	14.21%		1058409010	1.90	2.86%		999950108	0.03	48.64%		1231044533	0.64	26.27%
915137891	1.02	15.45%		1082463760	1.85	3.23%		1022676247	-0.02	50.79%		1259022818	0.58	28.06%
935474288	0.96	16.74%		1106518510	1.80	3.63%		1045402386	-0.07	52.89%		1287001103	0.53	29.86%
955810686	0.91	18.07%		1130573261	1.74	4.06%		1068128525	-0.12	54.94%		1314979388	0.48	31.68%
976147083	0.86	19.43%		1154628011	1.69	4.52%		1090854664	-0.17	56.94%		1342957673	0.43	33.50%
996483481	0.81	20.82%		1178682761	1.64	5.01%		1113580802	-0.22	58.87%		1370935958	0.38	35.32%
1016819878	0.76	22.23%		1202737511	1.60	5.53%		1136306941	-0.27	60.75%		1398914242	0.33	37.14%
Years	Cycles	β		Years	Cycles	β		Years	Cycles	β		Years	Cycles	β
16.0	325239765	3.50		22.6	543991246	3.50		10.4	235927723	3.50		13.3	373052318	3.50

	ELP Open				ELP Sub			
	N	β	p_f		N	β	p_f	
	21752164	11.61	0.00%		24152293	12.99	0.00%	
	43504328	9.94	0.00%		48304586	11.33	0.00%	
	65256492	8.97	0.00%		72456880	10.36	0.00%	
	87008657	8.28	0.00%		96609173	9.67	0.00%	
	108760821	7.75	0.00%		120761466	9.13	0.00%	
	130512985	7.31	0.00%		144913759	8.69	0.00%	
	152265149	6.94	0.00%		169066052	8.32	0.00%	
	174017313	6.62	0.00%		193218346	8.00	0.00%	
	195769477	6.33	0.00%		217370639	7.72	0.00%	
	217521641	6.08	0.00%		241522932	7.47	0.00%	
	239273805	5.85	0.00%		265675225	7.24	0.00%	
	261025970	5.64	0.00%		289827518	7.03	0.00%	
	282778134	5.45	0.00%		313979811	6.84	0.00%	
	304530298	5.27	0.00%		338132105	6.66	0.00%	
	326282462	5.11	0.00%		362284398	6.49	0.00%	
	348034626	4.95	0.00%		386436691	6.34	0.00%	
	369786790	4.81	0.00%		410588984	6.19	0.00%	
	391538954	4.67	0.00%		434741277	6.06	0.00%	
	413291119	4.54	0.00%		458893571	5.93	0.00%	
	435043283	4.42	0.00%		483045864	5.80	0.00%	
	456795447	4.30	0.00%		507198157	5.69	0.00%	
	478547611	4.19	0.00%		531350450	5.58	0.00%	
	500299775	4.08	0.00%		555502743	5.47	0.00%	
	522051939	3.98	0.00%		579655037	5.37	0.00%	
	543804103	3.88	0.01%		603807330	5.27	0.00%	
	565556267	3.79	0.01%		627959623	5.17	0.00%	
	587308432	3.70	0.01%		652111916	5.08	0.00%	
	609060596	3.61	0.02%		676264209	5.00	0.00%	
	630812760	3.53	0.02%		700416503	4.91	0.00%	
	652564924	3.44	0.03%		724568796	4.83	0.00%	
	674317088	3.37	0.04%		748721089	4.75	0.00%	
	696069252	3.29	0.05%		772873382	4.68	0.00%	
	717821416	3.22	0.06%		797025675	4.60	0.00%	
	739573581	3.14	0.08%		821177968	4.53	0.00%	
	761325745	3.07	0.11%		845330262	4.46	0.00%	
	783077909	3.01	0.13%		869482555	4.39	0.00%	
	804830073	2.94	0.16%		893634848	4.33	0.00%	
	826582237	2.88	0.20%		917787141	4.26	0.00%	
	848334401	2.82	0.24%		941939434	4.20	0.00%	
	870086565	2.75	0.29%		966091728	4.14	0.00%	
	891838730	2.70	0.35%		990244021	4.08	0.00%	
	913590894	2.64	0.42%		1014396314	4.02	0.00%	
	935343058	2.58	0.49%		1038548607	3.97	0.00%	
	957095222	2.53	0.58%		1062700900	3.91	0.00%	
	978847386	2.47	0.67%		1086853194	3.86	0.01%	
	1000599550	2.42	0.78%		1111005487	3.81	0.01%	
	1022351714	2.37	0.90%		1135157780	3.75	0.01%	
	1044103878	2.32	1.03%		1159310073	3.70	0.01%	
	1065856043	2.27	1.17%		1183462366	3.65	0.01%	
	1087608207	2.22	1.32%		1207614660	3.61	0.02%	
	Years	Cycles	β		Years	Cycles	β	
	29.3	637732983	3.50		52.2	1261679456	3.50	

	San Antonio							Dallas/Fort Worth						
S_{Ri} (no GS)	Open	γ_i	$(\gamma_i SR_i)^3$		Suburban	γ_i	$(\gamma_i SR_i)^3$	Open	γ_i	$(\gamma_i SR_i)^3$		Suburban	γ_i	$(\gamma_i SR_i)^3$
0.030	1.82E+05	0.00008	0.00		4.55E+05	0.00019	0.00	8.02E+03	0.00000	0.00		2.90E+04	0.00001	0.00
0.047	5.71E+05	0.00026	0.00		1.27E+06	0.00055	0.00	4.32E+04	0.00002	0.00		1.36E+05	0.00005	0.00
0.048	5.79E+05	0.00026	0.00		1.26E+06	0.00054	0.00	4.08E+04	0.00002	0.00		1.23E+05	0.00005	0.00
0.068	1.28E+06	0.00057	0.00		2.60E+06	0.00111	0.00	1.47E+05	0.00007	0.00		4.13E+05	0.00016	0.00
0.076	1.57E+06	0.00070	0.00		3.07E+06	0.00132	0.00	1.84E+05	0.00008	0.00		4.88E+05	0.00019	0.00
0.110	3.12E+06	0.00140	0.00		5.60E+06	0.00240	0.00	5.41E+05	0.00024	0.00		1.28E+06	0.00051	0.00
0.112	1.59E+06	0.00071	0.00		3.03E+06	0.00130	0.00	1.73E+05	0.00008	0.00		4.36E+05	0.00017	0.00
0.176	3.75E+06	0.00168	0.00		6.46E+06	0.00277	0.00	6.54E+05	0.00029	0.00		1.46E+06	0.00058	0.00
0.201	3.78E+06	0.00169	0.00		6.24E+06	0.00267	0.00	6.01E+05	0.00027	0.00		1.26E+06	0.00050	0.00
0.255	6.64E+06	0.00297	0.00		1.05E+07	0.00451	0.00	1.66E+06	0.00074	0.00		3.35E+06	0.00133	0.00
0.317	7.77E+06	0.00348	0.00		1.17E+07	0.00503	0.00	1.92E+06	0.00086	0.00		3.60E+06	0.00143	0.00
0.370	1.37E+08	0.06118	0.00		1.81E+08	0.07766	0.00	7.46E+07	0.03337	0.00		1.22E+08	0.04821	0.00
0.378	1.61E+07	0.00720	0.00		1.42E+07	0.00607	0.00	5.20E+06	0.00233	0.00		4.29E+06	0.00170	0.00
0.400	7.67E+06	0.00343	0.00		1.09E+07	0.00468	0.00	1.70E+06	0.00076	0.00		2.89E+06	0.00115	0.00
0.459	1.23E+07	0.00550	0.00		1.73E+07	0.00739	0.00	4.24E+06	0.00190	0.00		7.25E+06	0.00287	0.00
0.583	1.64E+08	0.07335	0.00		1.94E+08	0.08291	0.00	1.22E+08	0.05459	0.00		1.72E+08	0.06826	0.00
0.589	1.94E+08	0.08672	0.00		2.32E+08	0.09930	0.00	1.37E+08	0.06135	0.00		1.95E+08	0.07733	0.00
0.592	1.30E+07	0.00583	0.00		1.57E+07	0.00671	0.00	3.78E+06	0.00169	0.00		5.00E+06	0.00198	0.00
0.630	1.39E+07	0.00621	0.00		1.84E+07	0.00788	0.00	4.65E+06	0.00208	0.00		7.23E+06	0.00286	0.00
0.743	2.11E+07	0.00946	0.00		2.44E+07	0.01043	0.00	9.00E+06	0.00402	0.00		1.13E+07	0.00448	0.00
0.844	1.66E+08	0.07434	0.00		1.78E+08	0.07640	0.00	1.54E+08	0.06904	0.00		1.93E+08	0.07659	0.00
0.912	1.97E+07	0.00884	0.00		2.47E+07	0.01057	0.00	8.99E+06	0.00402	0.00		1.30E+07	0.00514	0.00
0.926	2.00E+08	0.08963	0.00		2.15E+08	0.09187	0.00	1.87E+08	0.08343	0.00		2.31E+08	0.09156	0.00
1.329	2.42E+08	0.10843	0.00		2.64E+08	0.11315	0.00	2.15E+08	0.09598	0.00		2.69E+08	0.10662	0.00
1.341	1.80E+08	0.08043	0.00		1.76E+08	0.07529	0.00	2.02E+08	0.09055	0.00		2.24E+08	0.08868	0.00
1.666	2.16E+08	0.09683	0.00		2.13E+08	0.09111	0.00	2.43E+08	0.10874	0.01		2.68E+08	0.10615	0.01
2.280	5.96E+08	0.26674	0.22		5.00E+08	0.21423	0.12	8.49E+08	0.37984	0.65		7.78E+08	0.30823	0.35
3.026	4.63E+06	0.00207	0.00		4.63E+06	0.00198	0.00	8.13E+06	0.00363	0.00		8.13E+06	0.00322	0.00
Total	2.23E+09		0.23		2.34E+09		0.13	2.24E+09		0.66		2.53E+09		0.36
		S_{RE}	0.62			S_{RE}	0.50		S_{RE}	0.87			S_{RE}	0.71

Houston							Austin						
Open	γ_i	$(\gamma_i SR_i)^3$		Suburban	γ_i	$(\gamma_i SR_i)^3$	Open	γ_i	$(\gamma_i SR_i)^3$		Suburban	γ_i	$(\gamma_i SR_i)^3$
4.60E+04	0.00002	0.00		1.43E+05	0.00007	0.00	2.77E+04	0.00001	0.00		9.18E+04	0.00004	0.00
1.99E+05	0.00010	0.00		5.40E+05	0.00027	0.00	1.31E+05	0.00005	0.00		3.77E+05	0.00015	0.00
1.94E+05	0.00010	0.00		5.09E+05	0.00025	0.00	1.26E+05	0.00005	0.00		3.50E+05	0.00014	0.00
5.65E+05	0.00029	0.00		1.36E+06	0.00067	0.00	4.01E+05	0.00017	0.00		1.02E+06	0.00040	0.00
7.00E+05	0.00036	0.00		1.61E+06	0.00079	0.00	4.98E+05	0.00021	0.00		1.21E+06	0.00047	0.00
1.71E+06	0.00087	0.00		3.50E+06	0.00173	0.00	1.31E+06	0.00054	0.00		2.83E+06	0.00110	0.00
6.79E+05	0.00035	0.00		1.50E+06	0.00074	0.00	4.76E+05	0.00020	0.00		1.11E+06	0.00043	0.00
2.05E+06	0.00105	0.00		4.00E+06	0.00198	0.00	1.57E+06	0.00065	0.00		3.24E+06	0.00126	0.00
1.97E+06	0.00100	0.00		3.66E+06	0.00181	0.00	1.49E+06	0.00062	0.00		2.89E+06	0.00112	0.00
4.31E+06	0.00220	0.00		7.56E+06	0.00374	0.00	3.56E+06	0.00147	0.00		6.59E+06	0.00256	0.00
5.02E+06	0.00255	0.00		8.31E+06	0.00411	0.00	4.14E+06	0.00171	0.00		7.18E+06	0.00279	0.00
1.18E+08	0.05989	0.00		1.64E+08	0.08082	0.00	1.18E+08	0.04876	0.00		1.74E+08	0.06768	0.00
1.16E+07	0.00591	0.00		9.95E+06	0.00492	0.00	1.02E+07	0.00421	0.00		8.58E+06	0.00334	0.00
4.71E+06	0.00240	0.00		7.26E+06	0.00359	0.00	3.79E+06	0.00157	0.00		6.07E+06	0.00236	0.00
9.11E+06	0.00464	0.00		1.37E+07	0.00679	0.00	8.11E+06	0.00336	0.00		1.28E+07	0.00499	0.00
1.50E+08	0.07652	0.00		1.80E+08	0.08901	0.00	1.65E+08	0.06848	0.00		2.11E+08	0.08203	0.00
1.76E+08	0.08972	0.00		2.15E+08	0.10628	0.00	1.91E+08	0.07899	0.00		2.47E+08	0.09598	0.00
8.99E+06	0.00458	0.00		1.12E+07	0.00556	0.00	7.68E+06	0.00318	0.00		9.81E+06	0.00382	0.00
1.02E+07	0.00518	0.00		1.43E+07	0.00708	0.00	8.98E+06	0.00372	0.00		1.31E+07	0.00511	0.00
1.69E+07	0.00861	0.00		2.00E+07	0.00990	0.00	1.58E+07	0.00655	0.00		1.92E+07	0.00746	0.00
1.54E+08	0.07866	0.00		1.64E+08	0.08097	0.00	1.84E+08	0.07617	0.00		2.08E+08	0.08078	0.00
1.61E+07	0.00822	0.00		2.11E+07	0.01042	0.00	1.54E+07	0.00637	0.00		2.09E+07	0.00812	0.00
1.86E+08	0.09479	0.00		1.97E+08	0.09741	0.00	2.22E+08	0.09186	0.00		2.49E+08	0.09693	0.00
2.25E+08	0.11455	0.00		2.44E+08	0.12073	0.00	2.63E+08	0.10893	0.00		3.02E+08	0.11731	0.00
1.64E+08	0.08334	0.00		1.54E+08	0.07621	0.00	2.11E+08	0.08745	0.00		2.11E+08	0.08216	0.00
1.97E+08	0.10034	0.00		1.87E+08	0.09260	0.00	2.54E+08	0.10517	0.01		2.55E+08	0.09926	0.00
4.89E+08	0.24901	0.18		3.78E+08	0.18692	0.08	7.16E+08	0.29644	0.31		5.90E+08	0.22929	0.14
9.38E+06	0.00478	0.00		9.38E+06	0.00464	0.00	7.53E+06	0.00312	0.00		7.53E+06	0.00293	0.00
1.96E+09		0.19		2.02E+09		0.09	2.42E+09		0.32		2.57E+09		0.15
	S_{RE}	0.58			S_{RE}	0.44		S_{RE}	0.68			S_{RE}	0.54

				El Paso				
	Open	γ_i	$(\gamma_i SR_i)^3$		Suburban	γ_i	$(\gamma_i SR_i)^3$	
	9.36E+04	0.00005	0.00		2.79E+05	0.00016	0.00	
	3.78E+05	0.00021	0.00		9.70E+05	0.00055	0.00	
	3.71E+05	0.00021	0.00		9.27E+05	0.00053	0.00	
	1.00E+06	0.00056	0.00		2.27E+06	0.00130	0.00	
	1.24E+06	0.00069	0.00		2.68E+06	0.00153	0.00	
	2.80E+06	0.00157	0.00		5.38E+06	0.00307	0.00	
	1.22E+06	0.00068	0.00		2.56E+06	0.00146	0.00	
	3.37E+06	0.00188	0.00		6.19E+06	0.00353	0.00	
	3.29E+06	0.00184	0.00		5.81E+06	0.00332	0.00	
	6.50E+06	0.00364	0.00		1.07E+07	0.00611	0.00	
	7.58E+06	0.00425	0.00		1.19E+07	0.00678	0.00	
	1.39E+08	0.07777	0.00		1.77E+08	0.10104	0.00	
	1.63E+07	0.00915	0.00		1.43E+07	0.00815	0.00	
	7.30E+06	0.00409	0.00		1.08E+07	0.00616	0.00	
	1.26E+07	0.00705	0.00		1.78E+07	0.01019	0.00	
	1.55E+08	0.08660	0.00		1.68E+08	0.09618	0.00	
	1.86E+08	0.10411	0.00		2.08E+08	0.11858	0.00	
	1.30E+07	0.00731	0.00		1.59E+07	0.00907	0.00	
	1.42E+07	0.00793	0.00		1.90E+07	0.01085	0.00	
	2.18E+07	0.01223	0.00		2.51E+07	0.01435	0.00	
	1.41E+08	0.07881	0.00		1.35E+08	0.07692	0.00	
	2.04E+07	0.01142	0.00		2.52E+07	0.01442	0.00	
	1.69E+08	0.09485	0.00		1.63E+08	0.09296	0.00	
	2.11E+08	0.11817	0.00		2.10E+08	0.11989	0.00	
	1.31E+08	0.07317	0.00		1.11E+08	0.06340	0.00	
	1.58E+08	0.08831	0.00		1.36E+08	0.07785	0.00	
	3.13E+08	0.17540	0.06		2.15E+08	0.12305	0.02	
	5.01E+07	0.02804	0.00		5.01E+07	0.02859	0.00	
	1.79E+09		0.07		1.75E+09		0.03	
		S_{RE}	0.50			S_{RE}	0.40	

	SAT Open				SAT Sub				DFW Open				DFW Sub		
# of yrs.	N	b	p_f		N	b	p_f		N	b	p_f		N	b	p_f
1	44662625.95	8.37714	0		46706055.2	9.765973687	0.00000		44720464.33	5.889465338	1.93724E-09		50502367.48	7.064964854	8.03246E-13
2	89325251.9	6.713622375	9.49252E-12		93412110.39	8.102451446	0		89440928.65	4.225943097	1.18971E-05		101004735	5.401442613	3.30535E-08
3	133987878	5.74	0.00%		140118166	7.13	0.00%		134161393	3.25	0.06%		151507102	4.43	0.00%
4	178650504	5.05	0.00%		186824221	6.44	0.00%		178881857	2.56	0.52%		202009470	3.74	0.01%
5	223313130	4.51	0.00%		233530276	5.90	0.00%		223602322	2.03	2.13%		252511837	3.20	0.07%
6	267975756	4.08	0.00%		280236331	5.47	0.00%		268322786	1.59	5.60%		303014205	2.76	0.28%
7	312638382	3.71	0.01%		326942386	5.10	0.00%		313043250	1.22	11.14%		353516572	2.39	0.83%
8	357301008	3.39	0.04%		373648442	4.78	0.00%		357763715	0.90	18.44%		404018940	2.07	1.90%
9	401963634	3.10	0.10%		420354497	4.49	0.00%		402484179	0.62	26.89%		454521307	1.79	3.66%
10	446626259	2.85	0.22%		467060552	4.24	0.00%		447204643	0.36	35.82%		505023675	1.54	6.19%
11	491288885	2.62	0.44%		513766607	4.01	0.00%		491925108	0.13	44.65%		555526042	1.31	9.51%
12	535951511	2.41	0.79%		560472662	3.80	0.01%		536645572	-0.07	52.96%		606028410	1.10	13.54%
13	580614137	2.22	1.32%		607178718	3.61	0.02%		581366036	-0.27	60.50%		656530777	0.91	18.16%
14	625276763	2.04	2.05%		653884773	3.43	0.03%		626086501	-0.44	67.15%		707033145	0.73	23.23%
15	669939389	1.88	3.02%		700590828	3.27	0.05%		670806965	-0.61	72.90%		757535512	0.57	28.58%
16	714602015	1.72	4.24%		747296883	3.11	0.09%		715527429	-0.76	77.78%		808037880	0.41	34.06%
17	759264641	1.58	5.73%		794002938	2.97	0.15%		760247894	-0.91	81.86%		858540247	0.27	39.54%
18	803927267	1.44	7.49%		840708994	2.83	0.23%		804968358	-1.05	85.25%		909042615	0.13	44.90%
19	848589893	1.31	9.50%		887415049	2.70	0.35%		849688822	-1.18	88.04%		959544982	0.00	50.06%
20	893252519	1.19	11.75%		934121104	2.58	0.50%		894409287	-1.30	90.32%		1010047350	-0.12	54.96%
21	937915145	1.07	14.22%		980827159	2.46	0.70%		939129751	-1.42	92.18%		1060549717	-0.24	59.55%
22	982577771	0.96	16.88%		1027533214	2.35	0.94%		983850215	-1.53	93.69%		1111052085	-0.35	63.81%
23	1027240397	0.85	19.71%		1074239270	2.24	1.25%		1028570680	-1.64	94.90%		1161554452	-0.46	67.73%
24	1071903023	0.75	22.66%		1120945325	2.14	1.62%		1073291144	-1.74	95.89%		1212056820	-0.56	71.30%
25	1116565649	0.65	25.72%		1167651380	2.04	2.06%		1118011608	-1.84	96.68%		1262559187	-0.66	74.54%
26	1161228275	0.56	28.85%		1214357435	1.95	2.58%		1162732072	-1.93	97.32%		1313061554	-0.75	77.47%
27	1205890901	0.47	32.01%		1261063490	1.86	3.17%		1207452537	-2.02	97.83%		1363563922	-0.84	80.09%
28	1250553527	0.38	35.20%		1307769546	1.77	3.85%		1252173001	-2.11	98.25%		1414066289	-0.93	82.44%
29	1295216153	0.30	38.37%		1354475601	1.68	4.60%		1296893465	-2.19	98.58%		1464568657	-1.02	84.53%
30	1339878778	0.21	41.51%		1401181656	1.60	5.44%		1341613930	-2.27	98.85%		1515071024	-1.10	86.38%
31	1384541404	0.14	44.60%		1447887711	1.52	6.37%		1386334394	-2.35	99.07%		1565573392	-1.18	88.03%
32	1429204030	0.06	47.63%		1494593766	1.45	7.38%		1431054858	-2.43	99.24%		1616075759	-1.25	89.48%
33	1473866656	-0.01	50.57%		1541299821	1.37	8.46%		1475775323	-2.50	99.38%		1666578127	-1.33	90.77%
34	1518529282	-0.09	53.43%		1588005877	1.30	9.63%		1520495787	-2.57	99.50%		1717080494	-1.40	91.90%
35	1563191908	-0.16	56.18%		1634711932	1.23	10.87%		1565216251	-2.64	99.59%		1767582862	-1.47	92.89%
36	1607854534	-0.22	58.83%		1681417987	1.17	12.19%		1609936716	-2.71	99.66%		1818085229	-1.54	93.76%
37	1652517160	-0.29	61.37%		1728124042	1.10	13.57%		1654657180	-2.78	99.73%		1868587597	-1.60	94.53%
38	1697179786	-0.35	63.79%		1774830097	1.04	15.01%		1699377644	-2.84	99.77%		1919089964	-1.67	95.21%
39	1741842412	-0.42	66.10%		1821536153	0.97	16.51%		1744098109	-2.90	99.82%		1969592332	-1.73	95.80%
40	1786505038	-0.48	68.30%		1868242208	0.91	18.07%		1788818573	-2.96	99.85%		2020094699	-1.79	96.31%
41	1831167664	-0.54	70.38%		1914948263	0.85	19.67%		1833539037	-3.02	99.87%		2070597067	-1.85	96.77%
42	1875830290	-0.59	72.34%		1961654318	0.80	21.31%		1878259502	-3.08	99.90%		2121099434	-1.91	97.16%
43	1920492916	-0.65	74.20%		2008360373	0.74	22.99%		1922979966	-3.14	99.91%		2171601802	-1.96	97.51%
44	1965155542	-0.70	75.95%		2055066429	0.68	24.70%		1967700430	-3.19	99.93%		2222104169	-2.02	97.81%
45	2009818168	-0.76	77.60%		2101772484	0.63	26.43%		2012420895	-3.25	99.94%		2272606537	-2.07	98.08%
46	2054480794	-0.81	79.14%		2148478539	0.58	28.18%		2057141359	-3.30	99.95%		2323108904	-2.12	98.31%
47	2099143420	-0.86	80.59%		2195184594	0.53	29.95%		2101861823	-3.35	99.96%		2373611272	-2.18	98.52%
48	2143806046	-0.91	81.95%		2241890649	0.48	31.73%		2146582288	-3.40	99.97%		2424113639	-2.23	98.70%
49	2188468672	-0.96	83.22%		2288596705	0.43	33.51%		2191302752	-3.45	99.97%		2474616007	-2.28	98.86%
50	2233131297	-1.01	84.41%		2335302760	0.38	35.30%		2236023216	-3.50	99.98%		2525118374	-2.32	98.99%
Years	Cycles	b	p_f		Years	Cycles	b		Years	Cycles	b		Years	Cycles	b
7.63066431	340805505.8	3.50002	0		13.60778805	635566100	3.50055		2.705639839	120997469.9	3.500697625		4.417313538	223084791.6	3.49975516

	IAH Open				IAH Sub				RMMA Open				RMMA Sub		
	N	b	p_f		N	b	p_f		N	b	p_f		N	b	p_f
	39275276.73	9.142198514	0		40459702.32	10.97270778	0		48309845.99	7.443192109	4.91829E-14		51436020.41	9.048695598	0
	78550553.45	7.478676273	3.75255E-14		80919404.65	9.309185537	0		96619691.99	5.779669868	3.74237E-09		102872040.8	7.385173356	7.61613E-14
	117825830	6.51	0.00%		121379107	8.34	0.00%		144929538	4.81	0.00%		154308061	6.41	0.00%
	157101107	5.82	0.00%		161838809	7.65	0.00%		193239384	4.12	0.00%		205744082	5.72	0.00%
	196376384	5.28	0.00%		202298512	7.11	0.00%		241549230	3.58	0.02%		257180102	5.19	0.00%
	235651660	4.84	0.00%		242758214	6.67	0.00%		289859076	3.14	0.08%		308616122	4.75	0.00%
	274926937	4.47	0.00%		283217916	6.30	0.00%		338168922	2.77	0.28%		360052143	4.38	0.00%
	314202214	4.15	0.00%		323677619	5.98	0.00%		386478768	2.45	0.71%		411488163	4.06	0.00%
	353477491	3.87	0.01%		364137321	5.70	0.00%		434788614	2.17	1.50%		462924184	3.78	0.01%
	392752767	3.62	0.01%		404597023	5.45	0.00%		483098460	1.92	2.76%		514360204	3.52	0.02%
	432028044	3.39	0.04%		445056726	5.22	0.00%		531408306	1.69	4.57%		565796225	3.29	0.05%
	471303321	3.18	0.07%		485516428	5.01	0.00%		579718152	1.48	6.95%		617232245	3.09	0.10%
	510578597	2.99	0.14%		525976130	4.82	0.00%		628027998	1.29	9.90%		668668265	2.89	0.19%
	549853874	2.81	0.25%		566435833	4.64	0.00%		676337844	1.11	13.36%		720104286	2.72	0.33%
	589129151	2.64	0.41%		606895535	4.47	0.00%		724647690	0.94	17.26%		771540306	2.55	0.54%
	628404428	2.49	0.64%		647355237	4.32	0.00%		772957536	0.79	21.50%		822976327	2.39	0.83%
	667679704	2.34	0.96%		687814939	4.17	0.00%		821267382	0.64	25.99%		874412347	2.25	1.23%
	706954981	2.21	1.37%		728274642	4.04	0.00%		869577228	0.51	30.63%		925848367	2.11	1.73%
	746230258	2.08	1.90%		768734344	3.91	0.00%		917887074	0.38	35.32%		977284388	1.98	2.37%
	785505535	1.95	2.54%		809194046	3.78	0.01%		966196920	0.25	39.99%		1028720408	1.86	3.15%
	824780811	1.84	3.32%		849653749	3.67	0.01%		1014506766	0.14	44.57%		1080156429	1.74	4.08%
	864056088	1.72	4.24%		890113451	3.55	0.02%		1062816612	0.02	49.01%		1131592449	1.63	5.15%
	903331365	1.62	5.29%		930573153	3.45	0.03%		1111126458	-0.08	53.26%		1183028469	1.52	6.38%
	942606641	1.52	6.49%		971032856	3.35	0.04%		1159436304	-0.18	57.30%		1234464490	1.42	7.76%
	981881918	1.42	7.82%		1011492558	3.25	0.06%		1207746150	-0.28	61.10%		1285900510	1.32	9.28%
	1021157195	1.32	9.29%		1051952260	3.15	0.08%		1256055996	-0.38	64.66%		1337336531	1.23	10.95%
	1060432472	1.23	10.89%		1092411963	3.06	0.11%		1304365842	-0.47	67.96%		1388772551	1.14	12.74%
	1099707748	1.15	12.61%		1132871665	2.98	0.15%		1352675688	-0.55	71.02%		1440208572	1.05	14.65%
	1138983025	1.06	14.44%		1173331367	2.89	0.19%		1400985534	-0.64	73.83%		1491644592	0.97	16.67%
	1178258302	0.98	16.37%		1213791070	2.81	0.25%		1449295380	-0.72	76.41%		1543080612	0.89	18.78%
	1217533579	0.90	18.39%		1254250772	2.73	0.32%		1497605226	-0.80	78.76%		1594516633	0.81	20.98%
	1256808855	0.82	20.48%		1294710474	2.66	0.40%		1545915072	-0.87	80.91%		1645952653	0.73	23.24%
	1296084132	0.75	22.64%		1335170177	2.58	0.49%		1594224918	-0.95	82.85%		1697388674	0.66	25.55%
	1335359409	0.68	24.85%		1375629879	2.51	0.60%		1642534764	-1.02	84.61%		1748824694	0.59	27.91%
	1374634685	0.61	27.11%		1416089581	2.44	0.73%		1690844610	-1.09	86.20%		1800260714	0.52	30.29%
	1413909962	0.54	29.39%		1456549284	2.37	0.88%		1739154456	-1.16	87.64%		1851696735	0.45	32.69%
	1453185239	0.48	31.70%		1497008986	2.31	1.05%		1787464302	-1.22	88.93%		1903132755	0.38	35.10%
	1492460516	0.41	34.01%		1537468688	2.24	1.25%		1835774148	-1.29	90.09%		1954568776	0.32	37.50%
	1531735792	0.35	36.32%		1577928391	2.18	1.46%		1884083994	-1.35	91.14%		2006004796	0.26	39.89%
	1571011069	0.29	38.63%		1618388093	2.12	1.70%		1932393840	-1.41	92.07%		2057440816	0.20	42.25%
	1610286346	0.23	40.91%		1658847795	2.06	1.97%		1980703686	-1.47	92.91%		2108876837	0.14	44.58%
	1649561623	0.17	43.17%		1699307498	2.00	2.26%		2029013532	-1.53	93.66%		2160312857	0.08	46.87%
	1688836899	0.12	45.40%		1739767200	1.95	2.58%		2077323378	-1.58	94.33%		2211748878	0.02	49.12%
	1728112176	0.06	47.60%		1780226902	1.89	2.93%		2125633224	-1.64	94.94%		2263184898	-0.03	51.32%
	1767387453	0.01	49.75%		1820686605	1.84	3.31%		2173943070	-1.69	95.47%		2314620919	-0.09	53.47%
	1806662729	-0.05	51.85%		1861146307	1.78	3.72%		2222252916	-1.75	95.95%		2366056939	-0.14	55.56%
	1845938006	-0.10	53.90%		1901606009	1.73	4.16%		2270562762	-1.80	96.38%		2417492959	-0.19	57.59%
	1885213283	-0.15	55.90%		1942065711	1.68	4.63%		2318872608	-1.85	96.77%		2468928980	-0.24	59.56%
	1924488560	-0.20	57.85%		1982525414	1.63	5.13%		2367182454	-1.90	97.11%		2520365000	-0.29	61.47%
	1963763836	-0.25	59.73%		2022985116	1.58	5.66%		2415492300	-1.95	97.41%		2571801021	-0.34	63.31%
	Years	Cycles	b		Years	Cycles	b		Years	Cycles	b		Years	Cycles	b
	10.49443133	412171694.4	3.500276186		22.50278324	910455911.3	3.500113393		5.170927567	249806714.4	3.499940568		10.09441342	519216454.7	3.500041825

	ELP Open				ELP Sub			
	N	b	p_f		N	b	p_f	
	35715486.64	11.68318007	0		35022784.54	13.81156136	0	
	71430973.29	10.01965783	0		70045569.08	12.14803912	0	
	107146460	9.05	0.00%		105068354	11.17	0.00%	
	142861947	8.36	0.00%		140091138	10.48	0.00%	
	178577433	7.82	0.00%		175113923	9.95	0.00%	
	214292920	7.38	0.00%		210136707	9.51	0.00%	
	250008407	7.01	0.00%		245159492	9.14	0.00%	
	285723893	6.69	0.00%		280182276	8.82	0.00%	
	321439380	6.41	0.00%		315205061	8.54	0.00%	
	357154866	6.16	0.00%		350227845	8.29	0.00%	
	392870353	5.93	0.00%		385250630	8.06	0.00%	
	428585840	5.72	0.00%		420273414	7.85	0.00%	
	464301326	5.53	0.00%		455296199	7.66	0.00%	
	500016813	5.35	0.00%		490318984	7.48	0.00%	
	535732300	5.18	0.00%		525341768	7.31	0.00%	
	571447786	5.03	0.00%		560364553	7.16	0.00%	
	607163273	4.88	0.00%		595387337	7.01	0.00%	
	642878760	4.75	0.00%		630410122	6.87	0.00%	
	678594246	4.62	0.00%		665432906	6.75	0.00%	
	714309733	4.49	0.00%		700455691	6.62	0.00%	
	750025220	4.38	0.00%		735478475	6.50	0.00%	
	785740706	4.26	0.00%		770501260	6.39	0.00%	
	821456193	4.16	0.00%		805524044	6.29	0.00%	
	857171679	4.06	0.00%		840546829	6.18	0.00%	
	892887166	3.96	0.00%		875569613	6.09	0.00%	
	928602653	3.86	0.01%		910592398	5.99	0.00%	
	964318139	3.77	0.01%		945615183	5.90	0.00%	
	1000033626	3.69	0.01%		980637967	5.81	0.00%	
	1035749113	3.60	0.02%		1015660752	5.73	0.00%	
	1071464599	3.52	0.02%		1050683536	5.65	0.00%	
	1107180086	3.44	0.03%		1085706321	5.57	0.00%	
	1142895573	3.37	0.04%		1120729105	5.49	0.00%	
	1178611059	3.29	0.05%		1155751890	5.42	0.00%	
	1214326546	3.22	0.06%		1190774674	5.35	0.00%	
	1250042033	3.15	0.08%		1225797459	5.28	0.00%	
	1285757519	3.08	0.10%		1260820243	5.21	0.00%	
	1321473006	3.02	0.13%		1295843028	5.15	0.00%	
	1357188492	2.95	0.16%		1330865812	5.08	0.00%	
	1392903979	2.89	0.19%		1365888597	5.02	0.00%	
	1428619466	2.83	0.23%		1400911382	4.96	0.00%	
	1464334952	2.77	0.28%		1435934166	4.90	0.00%	
	1500050439	2.71	0.33%		1470956951	4.84	0.00%	
	1535765926	2.66	0.39%		1505979735	4.78	0.00%	
	1571481412	2.60	0.46%		1541002520	4.73	0.00%	
	1607196899	2.55	0.54%		1576025304	4.68	0.00%	
	1642912386	2.49	0.63%		1611048089	4.62	0.00%	
	1678627872	2.44	0.73%		1646070873	4.57	0.00%	
	1714343359	2.39	0.84%		1681093658	4.52	0.00%	
	1750058846	2.34	0.96%		1716116442	4.47	0.00%	
	1785774332	2.29	1.09%		1751139227	4.42	0.00%	
	Years	Cycles	b		Years	Cycles	b	
	30.2566191	1080629875	3.500016589		73.44017996	2572079599	3.50022259	

	San Antonio							Dallas/Fort Worth						
S_{Ri} (no GS)	Open	γ_i	$(\gamma_i SR_i)^3$		Suburban	γ_i	$(\gamma_i SR_i)^3$	Open	γ_i	$(\gamma_i SR_i)^3$		Suburban	γ_i	$(\gamma_i SR_i)^3$
0.022	7.61E+04	0.00005	0.00		2.22E+05	0.00012	0.00	2.50E+03	0.00000	0.00		1.11E+04	0.00001	0.00
0.025	2.62E+05	0.00016	0.00		6.63E+05	0.00036	0.00	1.41E+04	0.00001	0.00		5.23E+04	0.00003	0.00
0.034	2.59E+05	0.00016	0.00		6.67E+05	0.00037	0.00	1.49E+04	0.00001	0.00		5.72E+04	0.00003	0.00
0.040	7.73E+05	0.00048	0.00		1.73E+06	0.00095	0.00	7.06E+04	0.00005	0.00		2.26E+05	0.00013	0.00
0.050	6.22E+05	0.00039	0.00		1.45E+06	0.00079	0.00	5.56E+04	0.00004	0.00		1.87E+05	0.00011	0.00
0.058	1.65E+06	0.00102	0.00		3.35E+06	0.00184	0.00	2.26E+05	0.00016	0.00		6.39E+05	0.00037	0.00
0.085	7.84E+05	0.00049	0.00		1.72E+06	0.00094	0.00	6.64E+04	0.00005	0.00		2.04E+05	0.00012	0.00
0.134	2.01E+06	0.00124	0.00		3.92E+06	0.00215	0.00	2.79E+05	0.00020	0.00		7.44E+05	0.00043	0.00
0.151	2.02E+06	0.00126	0.00		3.83E+06	0.00211	0.00	2.59E+05	0.00019	0.00		6.54E+05	0.00038	0.00
0.194	3.80E+06	0.00235	0.00		6.76E+06	0.00371	0.00	7.70E+05	0.00055	0.00		1.83E+06	0.00106	0.00
0.234	6.71E+07	0.04160	0.00		9.86E+07	0.05419	0.00	2.68E+07	0.01928	0.00		4.97E+07	0.02881	0.00
0.237	4.51E+06	0.00279	0.00		7.68E+06	0.00422	0.00	9.13E+05	0.00066	0.00		2.03E+06	0.00118	0.00
0.271	1.08E+08	0.06718	0.00		1.43E+08	0.07854	0.00	5.80E+07	0.04180	0.00		9.33E+07	0.05412	0.00
0.321	4.50E+06	0.00279	0.00		7.33E+06	0.00403	0.00	8.27E+05	0.00060	0.00		1.70E+06	0.00099	0.00
0.343	7.60E+06	0.00471	0.00		1.19E+07	0.00653	0.00	2.19E+06	0.00157	0.00		4.35E+06	0.00252	0.00
0.368	9.42E+07	0.05840	0.00		1.23E+08	0.06779	0.00	5.33E+07	0.03840	0.00		8.57E+07	0.04971	0.00
0.427	1.31E+08	0.08138	0.00		1.55E+08	0.08523	0.00	9.62E+07	0.06927	0.00		1.35E+08	0.07820	0.00
0.506	8.76E+06	0.00543	0.00		1.30E+07	0.00716	0.00	2.47E+06	0.00178	0.00		4.55E+06	0.00264	0.00
0.506	8.50E+06	0.00527	0.00		1.18E+07	0.00648	0.00	2.12E+06	0.00153	0.00		3.48E+06	0.00202	0.00
0.533	1.09E+08	0.06739	0.00		1.30E+08	0.07116	0.00	7.93E+07	0.05714	0.00		1.13E+08	0.06567	0.00
0.561	1.29E+07	0.00797	0.00		1.44E+07	0.00792	0.00	3.97E+06	0.00286	0.00		4.73E+06	0.00275	0.00
0.618	1.34E+08	0.08319	0.00		1.45E+08	0.07959	0.00	1.23E+08	0.08854	0.00		1.54E+08	0.08923	0.00
0.733	1.33E+07	0.00822	0.00		1.83E+07	0.01004	0.00	5.16E+06	0.00372	0.00		8.63E+06	0.00501	0.00
0.797	1.47E+07	0.00909	0.00		1.90E+07	0.01042	0.00	5.47E+06	0.00394	0.00		8.21E+06	0.00476	0.00
0.907	1.57E+08	0.09764	0.00		1.89E+08	0.10371	0.00	1.11E+08	0.08008	0.00		1.58E+08	0.09185	0.00
0.959	2.01E+07	0.01244	0.00		2.45E+07	0.01346	0.00	1.01E+07	0.00725	0.00		1.41E+07	0.00815	0.00
1.380	5.38E+08	0.33329	0.10		5.06E+08	0.27778	0.06	6.47E+08	0.46603	0.27		6.84E+08	0.39655	0.16
1.428	1.63E+08	0.10112	0.00		1.75E+08	0.09617	0.00	1.52E+08	0.10917	0.00		1.88E+08	0.10907	0.00
3.629	4.05E+06	0.00251	0.00		4.05E+06	0.00222	0.00	7.10E+06	0.00511	0.00		7.10E+06	0.00411	0.00
	1612878395		0.10		1820101863		0.06	1388518041		0.27		1724556539		0.17
		S_{RE}	**0.47**			S_{RE}	**0.39**		S_{RE}	**0.65**			S_{RE}	**0.55**

	Houston							Austin						
	Open	γ_i	$(\gamma_i SR_i)^3$		Suburban	γ_i	$(\gamma_i SR_i)^3$	Open	γ_i	$(\gamma_i SR_i)^3$		Suburban	γ_i	$(\gamma_i SR_i)^3$
	1.60E+04	0.00001	0.00		6.06E+04	0.00004	0.00	9.22E+03	0.00001	0.00		3.74E+04	0.00002	0.00
	7.47E+04	0.00005	0.00		2.37E+05	0.00015	0.00	4.65E+04	0.00003	0.00		1.57E+05	0.00008	0.00
	7.71E+04	0.00005	0.00		2.50E+05	0.00016	0.00	4.85E+04	0.00003	0.00		1.68E+05	0.00009	0.00
	3.00E+05	0.00021	0.00		8.18E+05	0.00051	0.00	2.04E+05	0.00012	0.00		5.93E+05	0.00031	0.00
	2.39E+05	0.00017	0.00		6.80E+05	0.00042	0.00	1.62E+05	0.00010	0.00		4.92E+05	0.00025	0.00
	7.99E+05	0.00056	0.00		1.92E+06	0.00119	0.00	5.85E+05	0.00035	0.00		1.50E+06	0.00077	0.00
	2.92E+05	0.00020	0.00		7.70E+05	0.00048	0.00	1.96E+05	0.00012	0.00		5.49E+05	0.00028	0.00
	9.78E+05	0.00068	0.00		2.24E+06	0.00139	0.00	7.18E+05	0.00043	0.00		1.74E+06	0.00090	0.00
	9.43E+05	0.00066	0.00		2.07E+06	0.00129	0.00	6.82E+05	0.00041	0.00		1.58E+06	0.00082	0.00
	2.24E+06	0.00156	0.00		4.54E+06	0.00282	0.00	1.77E+06	0.00107	0.00		3.82E+06	0.00197	0.00
	5.24E+07	0.03663	0.00		8.30E+07	0.05166	0.00	4.83E+07	0.02908	0.00		8.13E+07	0.04204	0.00
	2.65E+06	0.00185	0.00		5.10E+06	0.00317	0.00	2.10E+06	0.00126	0.00		4.26E+06	0.00220	0.00
	9.28E+07	0.06486	0.00		1.28E+08	0.07976	0.00	9.24E+07	0.05566	0.00		1.35E+08	0.06996	0.00
	2.52E+06	0.00176	0.00		4.59E+06	0.00286	0.00	1.96E+06	0.00118	0.00		3.74E+06	0.00193	0.00
	5.24E+06	0.00366	0.00		9.02E+06	0.00561	0.00	4.47E+06	0.00269	0.00		8.13E+06	0.00420	0.00
	8.19E+07	0.05727	0.00		1.12E+08	0.06970	0.00	8.29E+07	0.04992	0.00		1.21E+08	0.06232	0.00
	1.20E+08	0.08398	0.00		1.44E+08	0.08969	0.00	1.32E+08	0.07922	0.00		1.67E+08	0.08656	0.00
	5.99E+06	0.00419	0.00		9.70E+06	0.00604	0.00	5.08E+06	0.00306	0.00		8.65E+06	0.00447	0.00
	5.50E+06	0.00385	0.00		8.20E+06	0.00510	0.00	4.55E+06	0.00274	0.00		7.03E+06	0.00364	0.00
	9.95E+07	0.06954	0.00		1.20E+08	0.07494	0.00	1.09E+08	0.06551	0.00		1.40E+08	0.07248	0.00
	9.11E+06	0.00637	0.00		1.05E+07	0.00652	0.00	7.90E+06	0.00476	0.00		9.20E+06	0.00476	0.00
	1.25E+08	0.08728	0.00		1.33E+08	0.08301	0.00	1.48E+08	0.08907	0.00		1.68E+08	0.08672	0.00
	1.03E+07	0.00719	0.00		1.51E+07	0.00941	0.00	9.42E+06	0.00567	0.00		1.45E+07	0.00752	0.00
	1.12E+07	0.00782	0.00		1.53E+07	0.00949	0.00	1.01E+07	0.00610	0.00		1.43E+07	0.00742	0.00
	1.43E+08	0.10009	0.00		1.75E+08	0.10885	0.00	1.55E+08	0.09330	0.00		2.01E+08	0.10372	0.00
	1.69E+07	0.01181	0.00		2.14E+07	0.01331	0.00	1.65E+07	0.00995	0.00		2.17E+07	0.01123	0.00
	4.81E+08	0.33591	0.10		4.30E+08	0.26728	0.05	6.40E+08	0.38543	0.15		6.09E+08	0.31486	0.08
	1.52E+08	0.10603	0.00		1.61E+08	0.10007	0.00	1.81E+08	0.10879	0.00		2.03E+08	0.10506	0.00
	8.19E+06	0.00572	0.00		8.19E+06	0.00509	0.00	6.57E+06	0.00396	0.00		6.57E+06	0.00340	0.00
	1430642223		0.10		1607404573		0.05	1660396994		0.16		1934286632		0.09
		S_{RE}	**0.47**			S_{RE}	**0.38**		S_{RE}	**0.54**			S_{RE}	**0.44**

	El Paso							
	Open	γ_i	$(\gamma_i SR_i)^3$		Suburban	γ_i	$(\gamma_i SR_i)^3$	
	3.36E+04	0.00002	0.00		1.21E+05	0.00008	0.00	
	1.48E+05	0.00010	0.00		4.46E+05	0.00030	0.00	
	1.52E+05	0.00011	0.00		4.66E+05	0.00031	0.00	
	5.54E+05	0.00039	0.00		1.42E+06	0.00094	0.00	
	4.42E+05	0.00031	0.00		1.18E+06	0.00078	0.00	
	1.37E+06	0.00096	0.00		3.08E+06	0.00204	0.00	
	5.44E+05	0.00038	0.00		1.36E+06	0.00090	0.00	
	1.68E+06	0.00117	0.00		3.60E+06	0.00238	0.00	
	1.64E+06	0.00115	0.00		3.41E+06	0.00226	0.00	
	3.55E+06	0.00248	0.00		6.71E+06	0.00444	0.00	
	7.40E+07	0.05167	0.00		1.10E+08	0.07279	0.00	
	4.21E+06	0.00294	0.00		7.59E+06	0.00502	0.00	
	1.16E+08	0.08103	0.00		1.48E+08	0.09816	0.00	
	4.09E+06	0.00285	0.00		7.05E+06	0.00466	0.00	
	7.62E+06	0.00532	0.00		1.22E+07	0.00809	0.00	
	9.95E+07	0.06945	0.00		1.24E+08	0.08233	0.00	
	1.28E+08	0.08908	0.00		1.38E+08	0.09130	0.00	
	8.75E+06	0.00611	0.00		1.34E+07	0.00883	0.00	
	8.30E+06	0.00579	0.00		1.18E+07	0.00783	0.00	
	1.06E+08	0.07381	0.00		1.15E+08	0.07589	0.00	
	1.30E+07	0.00907	0.00		1.47E+07	0.00971	0.00	
	1.15E+08	0.08020	0.00		1.08E+08	0.07164	0.00	
	1.37E+07	0.00955	0.00		1.88E+07	0.01246	0.00	
	1.51E+07	0.01054	0.00		1.96E+07	0.01297	0.00	
	1.54E+08	0.10717	0.00		1.71E+08	0.11303	0.00	
	2.06E+07	0.01438	0.00		2.48E+07	0.01637	0.00	
	3.54E+08	0.24695	0.04		2.70E+08	0.17880	0.02	
	1.38E+08	0.09653	0.00		1.31E+08	0.08680	0.00	
	4.37E+07	0.03051	0.00		4.37E+07	0.02891	0.00	
	1432980287		0.04		1512145264		0.02	
		S_{RE}	**0.35**			S_{RE}	**0.27**	

	SAT Open				SAT Sub				DFW Open				DFW Sub		
# of yrs.	N	β	p_f		N	β	p_f		N	β	p_f		N	β	p_f
1	32257568	11.17	0.00%		36402037	12.14	0.00%		27770361	9.17	0.00%		34491131	9.79	0.00%
2	64515136	9.51	0.00%		72804075	10.47	0.00%		55540722	7.51	0.00%		68982262	8.13	0.00%
3	96772704	8.54	0.00%		109206112	9.50	0.00%		83311082	6.54	0.00%		103473392	7.15	0.00%
4	129030272	7.85	0.00%		145608149	8.81	0.00%		111081443	5.85	0.00%		137964523	6.46	0.00%
5	161287840	7.31	0.00%		182010186	8.28	0.00%		138851804	5.31	0.00%		172455654	5.93	0.00%
6	193545407	6.87	0.00%		218412224	7.84	0.00%		166622165	4.87	0.00%		206946785	5.49	0.00%
7	225802975	6.50	0.00%		254814261	7.47	0.00%		194392526	4.50	0.00%		241437915	5.12	0.00%
8	258060543	6.18	0.00%		291216298	7.15	0.00%		222162887	4.18	0.00%		275929046	4.80	0.00%
9	290318111	5.90	0.00%		327618335	6.86	0.00%		249933247	3.90	0.00%		310420177	4.52	0.00%
10	322575679	5.65	0.00%		364020373	6.61	0.00%		277703608	3.65	0.01%		344911308	4.26	0.00%
11	354833247	5.42	0.00%		400422410	6.38	0.00%		305473969	3.42	0.03%		379402439	4.03	0.00%
12	387090815	5.21	0.00%		436824447	6.17	0.00%		333244330	3.21	0.07%		413893569	3.83	0.01%
13	419348383	5.02	0.00%		473226485	5.98	0.00%		361014691	3.02	0.13%		448384700	3.63	0.01%
14	451605951	4.84	0.00%		509628522	5.80	0.00%		388785052	2.84	0.22%		482875831	3.46	0.03%
15	483863519	4.67	0.00%		546030559	5.64	0.00%		416555412	2.68	0.37%		517366962	3.29	0.05%
16	516121086	4.52	0.00%		582432596	5.48	0.00%		444325773	2.52	0.59%		551858093	3.14	0.09%
17	548378654	4.37	0.00%		618834634	5.34	0.00%		472096134	2.38	0.88%		586349223	2.99	0.14%
18	580636222	4.24	0.00%		655236671	5.20	0.00%		499866495	2.24	1.26%		620840354	2.85	0.22%
19	612893790	4.11	0.00%		691638708	5.07	0.00%		527636856	2.11	1.75%		655331485	2.72	0.32%
20	645151358	3.98	0.00%		728040745	4.95	0.00%		555407216	1.99	2.36%		689822616	2.60	0.47%
21	677408926	3.87	0.01%		764442783	4.83	0.00%		583177577	1.87	3.09%		724313746	2.48	0.65%
22	709666494	3.75	0.01%		800844820	4.72	0.00%		610947938	1.76	3.95%		758804877	2.37	0.89%
23	741924062	3.65	0.01%		837246857	4.61	0.00%		638718299	1.65	4.95%		793296008	2.26	1.18%
24	774181630	3.55	0.02%		873648894	4.51	0.00%		666488660	1.55	6.08%		827787139	2.16	1.53%
25	806439198	3.45	0.03%		910050932	4.41	0.00%		694259021	1.45	7.36%		862278270	2.06	1.95%
26	838696765	3.35	0.04%		946452969	4.32	0.00%		722029381	1.36	8.76%		896769400	1.97	2.44%
27	870954333	3.26	0.06%		982855006	4.23	0.00%		749799742	1.27	10.29%		931260531	1.88	3.01%
28	903211901	3.18	0.07%		1019257044	4.14	0.00%		777570103	1.18	11.95%		965751662	1.79	3.65%
29	935469469	3.09	0.10%		1055659081	4.06	0.00%		805340464	1.09	13.71%		1000242793	1.71	4.38%
30	967727037	3.01	0.13%		1092061118	3.98	0.00%		833110825	1.01	15.57%		1034733923	1.63	5.19%
31	999984605	2.93	0.17%		1128463155	3.90	0.00%		860881186	0.93	17.53%		1069225054	1.55	6.08%
32	1032242173	2.86	0.21%		1164865193	3.82	0.01%		888651546	0.86	19.57%		1103716185	1.47	7.05%
33	1064499741	2.78	0.27%		1201267230	3.75	0.01%		916421907	0.78	21.67%		1138207316	1.40	8.10%
34	1096757309	2.71	0.34%		1237669267	3.68	0.01%		944192268	0.71	23.83%		1172698447	1.33	9.23%
35	1129014877	2.64	0.41%		1274071304	3.61	0.02%		971962629	0.64	26.04%		1207189577	1.26	10.44%
36	1161272444	2.57	0.50%		1310473342	3.54	0.02%		999732990	0.57	28.28%		1241680708	1.19	11.71%
37	1193530012	2.51	0.61%		1346875379	3.47	0.03%		1027503350	0.51	30.54%		1276171839	1.12	13.06%
38	1225787580	2.44	0.73%		1383277416	3.41	0.03%		1055273711	0.44	32.82%		1310662970	1.06	14.46%
39	1258045148	2.38	0.86%		1419679454	3.35	0.04%		1083044072	0.38	35.10%		1345154101	1.00	15.93%
40	1290302716	2.32	1.02%		1456081491	3.29	0.05%		1110814433	0.32	37.38%		1379645231	0.94	17.45%
41	1322560284	2.26	1.19%		1492483528	3.23	0.06%		1138584794	0.26	39.65%		1414136362	0.88	19.02%
42	1354817852	2.20	1.38%		1528885565	3.17	0.08%		1166355155	0.20	41.89%		1448627493	0.82	20.62%
43	1387075420	2.15	1.59%		1565287603	3.11	0.09%		1194125515	0.15	44.11%		1483118624	0.76	22.27%
44	1419332988	2.09	1.83%		1601689640	3.06	0.11%		1221895876	0.09	46.30%		1517609754	0.71	23.95%
45	1451590556	2.04	2.08%		1638091677	3.00	0.13%		1249666237	0.04	48.44%		1552100885	0.65	25.66%
46	1483848123	1.98	2.36%		1674493714	2.95	0.16%		1277436598	-0.01	50.55%		1586592016	0.60	27.39%
47	1516105691	1.93	2.66%		1710895752	2.90	0.19%		1305206959	-0.07	52.60%		1621083147	0.55	29.13%
48	1548363259	1.88	2.99%		1747297789	2.85	0.22%		1332977319	-0.12	54.61%		1655574278	0.50	30.89%
49	1580620827	1.83	3.34%		1783699826	2.80	0.26%		1360747680	-0.17	56.57%		1690065408	0.45	32.65%
50	1612878395	1.78	3.72%		1820101863	2.75	0.30%		1388518041	-0.21	58.47%		1724556539	0.40	34.42%
Years	Cycles	β	p_f		Years	Cycles	β		Years	Cycles	β		Years	Cycles	β
24.5	789012911	3.50	0.02%		36.6	1331323513	3.50		10.6	295460254	3.50		13.7	474108270	3.50

IAH Open			IAH Sub			RMMA Open			RMMA Sub		
N	β	p_f	N	β	p_f	N	β	p_f	N	β	p_f
28612844	11.39	0.00%	32148091	12.67	0.00%	33207940	10.08	0.00%	38685733	11.11	0.00%
57225689	9.73	0.00%	64296183	11.01	0.00%	66415880	8.42	0.00%	77371465	9.45	0.00%
85838533	8.76	0.00%	96444274	10.04	0.00%	99623820	7.44	0.00%	116057198	8.48	0.00%
114451378	8.07	0.00%	128592366	9.35	0.00%	132831760	6.75	0.00%	154742931	7.79	0.00%
143064222	7.53	0.00%	160740457	8.81	0.00%	166039699	6.22	0.00%	193428663	7.25	0.00%
171677067	7.09	0.00%	192888549	8.37	0.00%	199247639	5.78	0.00%	232114396	6.81	0.00%
200289911	6.72	0.00%	225036640	8.00	0.00%	232455579	5.41	0.00%	270800128	6.44	0.00%
228902756	6.40	0.00%	257184732	7.68	0.00%	265663519	5.09	0.00%	309485861	6.12	0.00%
257515600	6.12	0.00%	289332823	7.40	0.00%	298871459	4.81	0.00%	348171594	5.84	0.00%
286128445	5.87	0.00%	321480915	7.15	0.00%	332079399	4.55	0.00%	386857326	5.59	0.00%
314741289	5.64	0.00%	353629006	6.92	0.00%	365287339	4.32	0.00%	425543059	5.36	0.00%
343354133	5.43	0.00%	385777098	6.71	0.00%	398495279	4.12	0.00%	464228792	5.15	0.00%
371966978	5.24	0.00%	417925189	6.52	0.00%	431703218	3.92	0.00%	502914524	4.96	0.00%
400579822	5.06	0.00%	450073281	6.34	0.00%	464911158	3.75	0.01%	541600257	4.78	0.00%
429192667	4.89	0.00%	482221372	6.17	0.00%	498119098	3.58	0.02%	580285989	4.61	0.00%
457805511	4.74	0.00%	514369463	6.02	0.00%	531327038	3.43	0.03%	618971722	4.46	0.00%
486418356	4.59	0.00%	546517555	5.87	0.00%	564534978	3.28	0.05%	657657455	4.31	0.00%
515031200	4.46	0.00%	578665646	5.74	0.00%	597742918	3.14	0.08%	696343187	4.18	0.00%
543644045	4.33	0.00%	610813738	5.61	0.00%	630950858	3.01	0.13%	735028920	4.05	0.00%
572256889	4.20	0.00%	642961829	5.48	0.00%	664158798	2.89	0.19%	773714653	3.92	0.00%
600869734	4.09	0.00%	675109921	5.37	0.00%	697366737	2.77	0.28%	812400385	3.81	0.01%
629482578	3.98	0.00%	707258012	5.26	0.00%	730574677	2.66	0.39%	851086118	3.70	0.01%
658095422	3.87	0.01%	739406104	5.15	0.00%	763782617	2.55	0.53%	889771851	3.59	0.02%
686708267	3.77	0.01%	771554195	5.05	0.00%	796990557	2.45	0.71%	928457583	3.49	0.02%
715321111	3.67	0.01%	803702287	4.95	0.00%	830198497	2.35	0.93%	967143316	3.39	0.04%
743933956	3.57	0.02%	835850378	4.85	0.00%	863406437	2.26	1.19%	1005829048	3.29	0.05%
772546800	3.48	0.02%	867998470	4.76	0.00%	896614377	2.17	1.50%	1044514781	3.20	0.07%
801159645	3.40	0.03%	900146561	4.68	0.00%	929822317	2.08	1.86%	1083200514	3.12	0.09%
829772489	3.31	0.05%	932294653	4.59	0.00%	963030256	2.00	2.28%	1121886246	3.03	0.12%
858385334	3.23	0.06%	964442744	4.51	0.00%	996238196	1.92	2.76%	1160571979	2.95	0.16%
886998178	3.15	0.08%	996590835	4.43	0.00%	1029446136	1.84	3.30%	1199257712	2.87	0.20%
915611023	3.08	0.10%	1028738927	4.36	0.00%	1062654076	1.76	3.90%	1237943444	2.80	0.26%
944223867	3.00	0.13%	1060887018	4.28	0.00%	1095862016	1.69	4.57%	1276629177	2.72	0.32%
972836711	2.93	0.17%	1093035110	4.21	0.00%	1129069956	1.62	5.30%	1315314909	2.65	0.40%
1001449556	2.86	0.21%	1125183201	4.14	0.00%	1162277896	1.55	6.09%	1354000642	2.58	0.49%
1030062400	2.79	0.26%	1157331293	4.07	0.00%	1195485836	1.48	6.95%	1392686375	2.51	0.60%
1058675245	2.73	0.32%	1189479384	4.01	0.00%	1228693775	1.41	7.87%	1431372107	2.45	0.72%
1087288089	2.66	0.39%	1221627476	3.94	0.00%	1261901715	1.35	8.85%	1470057840	2.38	0.86%
1115900934	2.60	0.46%	1253775567	3.88	0.01%	1295109655	1.29	9.90%	1508743573	2.32	1.01%
1144513778	2.54	0.55%	1285923659	3.82	0.01%	1328317595	1.23	11.00%	1547429305	2.26	1.19%
1173126623	2.48	0.65%	1318071750	3.76	0.01%	1361525535	1.17	12.15%	1586115038	2.20	1.39%
1201739467	2.42	0.77%	1350219842	3.70	0.01%	1394733475	1.11	13.36%	1624800770	2.14	1.60%
1230352312	2.37	0.90%	1382367933	3.65	0.01%	1427941415	1.05	14.62%	1663486503	2.09	1.84%
1258965156	2.31	1.04%	1414516025	3.59	0.02%	1461149355	1.00	15.92%	1702172236	2.03	2.11%
1287578000	2.26	1.20%	1446664116	3.54	0.02%	1494357294	0.94	17.26%	1740857968	1.98	2.40%
1316190845	2.21	1.37%	1478812207	3.49	0.02%	1527565234	0.89	18.64%	1779543701	1.93	2.71%
1344803689	2.15	1.56%	1510960299	3.43	0.03%	1560773174	0.84	20.06%	1818229434	1.87	3.05%
1373416534	2.10	1.77%	1543108390	3.38	0.04%	1593981114	0.79	21.50%	1856915166	1.82	3.41%
1402029378	2.05	2.00%	1575256482	3.33	0.04%	1627189054	0.74	22.98%	1895600899	1.77	3.81%
1430642223	2.01	2.25%	1607404573	3.29	0.05%	1660396994	0.69	24.47%	1934286632	1.73	4.23%
Years	Cycles	β	Years	Cycles	β	Years	Cycles	β	Years	Cycles	β
26.8	767291039	3.50	45.7	1469738075	3.50	15.5	515121674	3.50	23.9	923266530	3.50

ELP Open				ELP Sub			
N	β	p_f		N	β	p_f	
28659606	13.42	0.00%		30242905	15.29	0.00%	
57319211	11.75	0.00%		60485811	13.63	0.00%	
85978817	10.78	0.00%		90728716	12.65	0.00%	
114638423	10.09	0.00%		120971621	11.96	0.00%	
143298029	9.55	0.00%		151214526	11.43	0.00%	
171957634	9.12	0.00%		181457432	10.99	0.00%	
200617240	8.75	0.00%		211700337	10.62	0.00%	
229276846	8.43	0.00%		241943242	10.30	0.00%	
257936452	8.14	0.00%		272186147	10.02	0.00%	
286596057	7.89	0.00%		302429053	9.76	0.00%	
315255663	7.66	0.00%		332671958	9.53	0.00%	
343915269	7.45	0.00%		362914863	9.33	0.00%	
372574875	7.26	0.00%		393157769	9.13	0.00%	
401234480	7.08	0.00%		423400674	8.96	0.00%	
429894086	6.92	0.00%		453643579	8.79	0.00%	
458553692	6.76	0.00%		483886484	8.64	0.00%	
487213298	6.62	0.00%		514129390	8.49	0.00%	
515872903	6.48	0.00%		544372295	8.35	0.00%	
544532509	6.35	0.00%		574615200	8.22	0.00%	
573192115	6.23	0.00%		604858106	8.10	0.00%	
601851721	6.11	0.00%		635101011	7.98	0.00%	
630511326	6.00	0.00%		665343916	7.87	0.00%	
659170932	5.89	0.00%		695586821	7.76	0.00%	
687830538	5.79	0.00%		725829727	7.66	0.00%	
716490144	5.69	0.00%		756072632	7.56	0.00%	
745149749	5.60	0.00%		786315537	7.47	0.00%	
773809355	5.51	0.00%		816558442	7.38	0.00%	
802468961	5.42	0.00%		846801348	7.29	0.00%	
831128567	5.34	0.00%		877044253	7.21	0.00%	
859788172	5.25	0.00%		907287158	7.13	0.00%	
888447778	5.18	0.00%		937530064	7.05	0.00%	
917107384	5.10	0.00%		967772969	6.97	0.00%	
945766990	5.02	0.00%		998015874	6.90	0.00%	
974426595	4.95	0.00%		1028258779	6.83	0.00%	
1003086201	4.88	0.00%		1058501685	6.76	0.00%	
1031745807	4.82	0.00%		1088744590	6.69	0.00%	
1060405413	4.75	0.00%		1118987495	6.62	0.00%	
1089065018	4.69	0.00%		1149230401	6.56	0.00%	
1117724624	4.62	0.00%		1179473306	6.50	0.00%	
1146384230	4.56	0.00%		1209716211	6.44	0.00%	
1175043836	4.50	0.00%		1239959116	6.38	0.00%	
1203703441	4.45	0.00%		1270202022	6.32	0.00%	
1232363047	4.39	0.00%		1300444927	6.26	0.00%	
1261022653	4.33	0.00%		1330687832	6.21	0.00%	
1289682259	4.28	0.00%		1360930737	6.15	0.00%	
1318341864	4.23	0.00%		1391173643	6.10	0.00%	
1347001470	4.18	0.00%		1421416548	6.05	0.00%	
1375661076	4.13	0.00%		1451659453	6.00	0.00%	
1404320681	4.08	0.00%		1481902359	5.95	0.00%	
1432980287	4.03	0.00%		1512145264	5.90	0.00%	
Years	Cycles	β		Years	Cycles	β	
62.3	1785399189	3.50		136.0	4111566580	3.50	

	San Antonio							Dallas/Fort Worth						
S_{Ri} (no GS)	Open	γ_i	$(\gamma_i SR_i)^3$		Suburban	γ_i	$(\gamma_i SR_i)^3$	Open	γ_i	$(\gamma_i SR_i)^3$		Suburban	γ_i	$(\gamma_i SR_i)^3$
0.035	5.91E+04	0.00003	0.00		1.59E+05	0.00008	0.00	1.75E+03	0.00000	0.00		6.95E+03	0.00000	0.00
0.056	2.07E+05	0.00010	0.00		4.97E+05	0.00024	0.00	1.09E+04	0.00001	0.00		3.75E+04	0.00002	0.00
0.060	2.05E+05	0.00010	0.00		4.79E+05	0.00023	0.00	9.99E+03	0.00001	0.00		3.29E+04	0.00001	0.00
0.081	5.09E+05	0.00026	0.00		1.11E+06	0.00053	0.00	4.16E+04	0.00002	0.00		1.28E+05	0.00006	0.00
0.095	6.24E+05	0.00032	0.00		1.31E+06	0.00062	0.00	5.19E+04	0.00003	0.00		1.50E+05	0.00007	0.00
0.129	6.18E+05	0.00031	0.00		1.25E+06	0.00060	0.00	4.73E+04	0.00002	0.00		1.29E+05	0.00006	0.00
0.138	1.36E+06	0.00069	0.00		2.62E+06	0.00125	0.00	1.72E+05	0.00009	0.00		4.44E+05	0.00020	0.00
0.204	1.63E+06	0.00083	0.00		2.99E+06	0.00143	0.00	2.07E+05	0.00011	0.00		4.99E+05	0.00023	0.00
0.252	1.60E+06	0.00081	0.00		2.80E+06	0.00133	0.00	1.85E+05	0.00010	0.00		4.12E+05	0.00019	0.00
0.295	3.18E+06	0.00161	0.00		5.36E+06	0.00256	0.00	5.91E+05	0.00031	0.00		1.29E+06	0.00059	0.00
0.397	3.70E+06	0.00188	0.00		5.91E+06	0.00282	0.00	6.82E+05	0.00036	0.00		1.37E+06	0.00062	0.00
0.490	1.05E+08	0.05302	0.00		1.45E+08	0.06918	0.00	5.03E+07	0.02617	0.00		8.65E+07	0.03932	0.00
0.499	8.64E+06	0.00438	0.00		7.67E+06	0.00366	0.00	2.17E+06	0.00113	0.00		1.82E+06	0.00083	0.00
0.505	3.55E+06	0.00180	0.00		5.27E+06	0.00252	0.00	5.83E+05	0.00030	0.00		1.04E+06	0.00047	0.00
0.575	6.44E+06	0.00326	0.00		9.56E+06	0.00456	0.00	1.70E+06	0.00088	0.00		3.10E+06	0.00141	0.00
0.685	6.50E+06	0.00329	0.00		8.00E+06	0.00382	0.00	1.42E+06	0.00074	0.00		1.94E+06	0.00088	0.00
0.772	1.34E+08	0.06795	0.00		1.65E+08	0.07899	0.00	8.94E+07	0.04653	0.00		1.33E+08	0.06053	0.00
0.795	7.20E+06	0.00365	0.00		9.98E+06	0.00476	0.00	1.84E+06	0.00096	0.00		3.01E+06	0.00137	0.00
0.829	1.56E+08	0.07930	0.00		1.95E+08	0.09313	0.00	9.88E+07	0.05146	0.00		1.48E+08	0.06721	0.00
1.079	1.18E+07	0.00600	0.00		1.40E+07	0.00668	0.00	3.91E+06	0.00204	0.00		5.07E+06	0.00230	0.00
1.118	1.44E+08	0.07276	0.00		1.61E+08	0.07692	0.00	1.21E+08	0.06303	0.00		1.60E+08	0.07280	0.00
1.151	1.13E+07	0.00572	0.00		1.47E+07	0.00704	0.00	4.00E+06	0.00208	0.00		6.10E+06	0.00277	0.00
1.298	1.69E+07	0.00858	0.00		1.93E+07	0.00923	0.00	7.61E+06	0.00396	0.00		9.45E+06	0.00429	0.00
1.304	1.73E+08	0.08771	0.00		1.93E+08	0.09227	0.00	1.46E+08	0.07614	0.00		1.91E+08	0.08670	0.00
1.803	2.06E+08	0.10460	0.01		2.34E+08	0.11164	0.01	1.65E+08	0.08603	0.00		2.17E+08	0.09867	0.01
1.889	1.64E+08	0.08320	0.00		1.68E+08	0.07999	0.00	1.70E+08	0.08861	0.00		1.98E+08	0.09010	0.00
2.837	1.97E+08	0.10006	0.02		2.02E+08	0.09643	0.02	2.04E+08	0.10622	0.03		2.36E+08	0.10723	0.03
3.393	6.03E+08	0.30573	1.12		5.14E+08	0.24557	0.58	8.43E+08	0.43897	3.30		7.88E+08	0.35783	1.79
4.902	4.06E+06	0.00206	0.00		4.06E+06	0.00194	0.00	7.12E+06	0.00370	0.00		7.12E+06	0.00323	0.00
	1972978375		1.15		2094785857		0.61	1920675593		3.34		2200785367		1.83
		S_{RE}	**1.05**			S_{RE}	**0.85**		S_{RE}	**1.49**			S_{RE}	**1.22**

	Houston							Austin						
	Open	γ_i	$(\gamma_i SR_i)^3$		Suburban	γ_i	$(\gamma_i SR_i)^3$	Open	γ_i	$(\gamma_i SR_i)^3$		Suburban	γ_i	$(\gamma_i SR_i)^3$
	1.16E+04	0.00001	0.00		3.99E+04	0.00002	0.00	6.61E+03	0.00000	0.00		2.41E+04	0.00001	0.00
	5.82E+04	0.00003	0.00		1.73E+05	0.00010	0.00	3.61E+04	0.00002	0.00		1.14E+05	0.00005	0.00
	5.51E+04	0.00003	0.00		1.58E+05	0.00009	0.00	3.38E+04	0.00002	0.00		1.02E+05	0.00004	0.00
	1.86E+05	0.00011	0.00		4.92E+05	0.00027	0.00	1.24E+05	0.00006	0.00		3.48E+05	0.00015	0.00
	2.30E+05	0.00013	0.00		5.77E+05	0.00032	0.00	1.54E+05	0.00007	0.00		4.08E+05	0.00018	0.00
	2.17E+05	0.00013	0.00		5.19E+05	0.00028	0.00	1.43E+05	0.00007	0.00		3.61E+05	0.00016	0.00
	6.32E+05	0.00036	0.00		1.42E+06	0.00078	0.00	4.55E+05	0.00022	0.00		1.08E+06	0.00047	0.00
	7.59E+05	0.00044	0.00		1.60E+06	0.00088	0.00	5.47E+05	0.00026	0.00		1.22E+06	0.00053	0.00
	7.07E+05	0.00041	0.00		1.40E+06	0.00077	0.00	5.01E+05	0.00024	0.00		1.04E+06	0.00046	0.00
	1.80E+06	0.00104	0.00		3.42E+06	0.00188	0.00	1.40E+06	0.00066	0.00		2.80E+06	0.00122	0.00
	2.08E+06	0.00120	0.00		3.70E+06	0.00203	0.00	1.61E+06	0.00077	0.00		3.00E+06	0.00131	0.00
	8.68E+07	0.05008	0.00		1.28E+08	0.06999	0.00	8.40E+07	0.03981	0.00		1.31E+08	0.05731	0.00
	5.61E+06	0.00324	0.00		4.85E+06	0.00266	0.00	4.64E+06	0.00220	0.00		3.96E+06	0.00173	0.00
	1.88E+06	0.00109	0.00		3.06E+06	0.00168	0.00	1.43E+06	0.00068	0.00		2.41E+06	0.00105	0.00
	4.27E+06	0.00246	0.00		6.92E+06	0.00380	0.00	3.57E+06	0.00169	0.00		6.06E+06	0.00265	0.00
	3.96E+06	0.00228	0.00		5.11E+06	0.00280	0.00	3.18E+06	0.00151	0.00		4.19E+06	0.00183	0.00
	1.21E+08	0.06969	0.00		1.53E+08	0.08401	0.00	1.28E+08	0.06087	0.00		1.73E+08	0.07565	0.00
	4.71E+06	0.00272	0.00		7.01E+06	0.00385	0.00	3.91E+06	0.00185	0.00		6.04E+06	0.00264	0.00
	1.39E+08	0.08038	0.00		1.79E+08	0.09832	0.00	1.46E+08	0.06907	0.00		1.98E+08	0.08676	0.00
	8.63E+06	0.00498	0.00		1.06E+07	0.00580	0.00	7.59E+06	0.00360	0.00		9.50E+06	0.00415	0.00
	1.33E+08	0.07687	0.00		1.49E+08	0.08204	0.00	1.53E+08	0.07261	0.00		1.83E+08	0.07994	0.00
	8.46E+06	0.00488	0.00		1.17E+07	0.00641	0.00	7.57E+06	0.00359	0.00		1.09E+07	0.00475	0.00
	1.38E+07	0.00795	0.00		1.62E+07	0.00887	0.00	1.31E+07	0.00621	0.00		1.57E+07	0.00686	0.00
	1.61E+08	0.09262	0.00		1.79E+08	0.09841	0.00	1.85E+08	0.08756	0.00		2.19E+08	0.09562	0.00
	1.91E+08	0.10992	0.01		2.17E+08	0.11924	0.01	2.15E+08	0.10196	0.01		2.59E+08	0.11312	0.01
	1.52E+08	0.08746	0.00		1.51E+08	0.08276	0.00	1.89E+08	0.08949	0.00		1.99E+08	0.08709	0.00
	1.82E+08	0.10517	0.03		1.82E+08	0.10008	0.02	2.27E+08	0.10746	0.03		2.39E+08	0.10467	0.03
	5.02E+08	0.28960	0.95		3.96E+08	0.21736	0.40	7.26E+08	0.34434	1.59		6.10E+08	0.26668	0.74
	8.21E+06	0.00474	0.00		8.21E+06	0.00451	0.00	6.59E+06	0.00313	0.00		6.59E+06	0.00288	0.00
	1734168698		0.99		1822137300		0.44	2108844597		1.64		2286615161		0.78
		S_{RE}	**1.00**			S_{RE}	**0.76**		S_{RE}	**1.18**			S_{RE}	**0.92**

					El Paso		
	Open	γ_i	$(\gamma_i SR_i)^3$		Suburban	γ_i	$(\gamma_i SR_i)^3$
	2.47E+04	0.00002	0.00		8.12E+04	0.00005	0.00
	1.16E+05	0.00007	0.00		3.29E+05	0.00020	0.00
	1.11E+05	0.00007	0.00		3.04E+05	0.00019	0.00
	3.48E+05	0.00022	0.00		8.73E+05	0.00054	0.00
	4.30E+05	0.00027	0.00		1.02E+06	0.00064	0.00
	4.11E+05	0.00026	0.00		9.37E+05	0.00058	0.00
	1.10E+06	0.00069	0.00		2.33E+06	0.00145	0.00
	1.32E+06	0.00082	0.00		2.65E+06	0.00165	0.00
	1.25E+06	0.00078	0.00		2.38E+06	0.00148	0.00
	2.90E+06	0.00181	0.00		5.21E+06	0.00324	0.00
	3.37E+06	0.00210	0.00		5.69E+06	0.00353	0.00
	1.08E+08	0.06697	0.00		1.45E+08	0.09026	0.00
	8.45E+06	0.00526	0.00		7.41E+06	0.00460	0.00
	3.12E+06	0.00194	0.00		4.88E+06	0.00303	0.00
	6.36E+06	0.00396	0.00		9.74E+06	0.00605	0.00
	6.17E+06	0.00384	0.00		7.76E+06	0.00482	0.00
	1.31E+08	0.08162	0.00		1.51E+08	0.09409	0.00
	7.07E+06	0.00440	0.00		1.01E+07	0.00626	0.00
	1.55E+08	0.09645	0.00		1.83E+08	0.11364	0.00
	1.21E+07	0.00751	0.00		1.44E+07	0.00893	0.00
	1.29E+08	0.08000	0.00		1.31E+08	0.08110	0.00
	1.16E+07	0.00721	0.00		1.52E+07	0.00947	0.00
	1.75E+07	0.01088	0.00		1.99E+07	0.01237	0.00
	1.55E+08	0.09631	0.00		1.57E+08	0.09777	0.00
	1.89E+08	0.11773	0.01		1.98E+08	0.12319	0.01
	1.29E+08	0.08012	0.00		1.16E+08	0.07197	0.00
	1.55E+08	0.09658	0.02		1.42E+08	0.08798	0.02
	3.29E+08	0.20485	0.34		2.31E+08	0.14367	0.12
	4.38E+07	0.02728	0.00		4.38E+07	0.02724	0.00
	1606927902		0.38		1609304335		0.15
		S_{RE}	**0.72**			S_{RE}	**0.53**

	SAT Open				SAT Sub				DFW Open				DFW Sub		
# of yrs.	N	β	p_f		N	β	p_f		N	β	p_f		N	β	p_f
1	39459567	4.85	0.00%		41895717	6.22	0.00%		38413512	2.36	0.91%		44015707	3.48	0.03%
2	78919135	3.19	0.07%		83791434	4.56	0.00%		76827024	0.70	24.25%		88031415	1.82	3.47%
3	118378702	2.22	1.33%		125687151	3.58	0.02%		115240536	-0.27	60.82%		132047122	0.84	19.97%
4	157838270	1.53	6.35%		167582869	2.89	0.19%		153654047	-0.97	83.28%		176062829	0.15	43.95%
5	197297837	0.99	16.11%		209478586	2.36	0.92%		192067559	-1.50	93.33%		220078537	-0.38	64.93%
6	236757405	0.55	29.03%		251374303	1.92	2.74%		230481071	-1.94	97.37%		264094244	-0.82	79.42%
7	276216972	0.18	42.75%		293270020	1.55	6.05%		268894583	-2.31	98.95%		308109951	-1.19	88.31%
8	315676540	-0.14	55.48%		335165737	1.23	10.93%		307308095	-2.63	99.57%		352125659	-1.51	93.46%
9	355136107	-0.42	66.29%		377061454	0.95	17.17%		345721607	-2.91	99.82%		396141366	-1.79	96.36%
10	394595675	-0.67	74.96%		418957171	0.69	24.36%		384135119	-3.16	99.92%		440157073	-2.05	97.97%
11	434055242	-0.90	81.65%		460852889	0.47	32.06%		422548631	-3.39	99.97%		484172781	-2.28	98.86%
12	473514810	-1.11	86.67%		502748606	0.26	39.85%		460962142	-3.60	99.98%		528188488	-2.48	99.35%
13	512974377	-1.30	90.37%		544644323	0.07	47.41%		499375654	-3.79	99.99%		572204196	-2.68	99.63%
14	552433945	-1.48	93.07%		586540040	-0.11	54.49%		537789166	-3.97	100.00%		616219903	-2.85	99.78%
15	591893512	-1.65	95.02%		628435757	-0.28	60.96%		576202678	-4.14	100.00%		660235610	-3.02	99.87%
16	631353080	-1.80	96.42%		670331474	-0.43	66.76%		614616190	-4.29	100.00%		704251318	-3.17	99.93%
17	670812647	-1.95	97.42%		712227191	-0.58	71.86%		653029702	-4.44	100.00%		748267025	-3.32	99.96%
18	710272215	-2.08	98.14%		754122909	-0.72	76.30%		691443214	-4.57	100.00%		792282732	-3.46	99.97%
19	749731782	-2.21	98.66%		796018626	-0.85	80.11%		729856725	-4.70	100.00%		836298440	-3.59	99.98%
20	789191350	-2.34	99.03%		837914343	-0.97	83.37%		768270237	-4.83	100.00%		880314147	-3.71	99.99%
21	828650917	-2.45	99.29%		879810060	-1.09	86.12%		806683749	-4.94	100.00%		924329854	-3.83	99.99%
22	868110485	-2.57	99.49%		921705777	-1.20	88.45%		845097261	-5.06	100.00%		968345562	-3.94	100.00%
23	907570052	-2.67	99.62%		963601494	-1.30	90.39%		883510773	-5.16	100.00%		1012361269	-4.05	100.00%
24	947029620	-2.77	99.72%		1005497211	-1.41	92.02%		921924285	-5.27	100.00%		1056376976	-4.15	100.00%
25	986489187	-2.87	99.80%		1047392929	-1.50	93.38%		960337797	-5.36	100.00%		1100392684	-4.25	100.00%
26	1025948755	-2.97	99.85%		1089288646	-1.60	94.50%		998751309	-5.46	100.00%		1144408391	-4.34	100.00%
27	1065408322	-3.06	99.89%		1131184363	-1.69	95.44%		1037164820	-5.55	100.00%		1188424098	-4.43	100.00%
28	1104867890	-3.14	99.92%		1173080080	-1.78	96.22%		1075578332	-5.64	100.00%		1232439806	-4.52	100.00%
29	1144327457	-3.23	99.94%		1214975797	-1.86	96.86%		1113991844	-5.72	100.00%		1276455513	-4.60	100.00%
30	1183787025	-3.31	99.95%		1256871514	-1.94	97.39%		1152405356	-5.80	100.00%		1320471220	-4.68	100.00%
31	1223246592	-3.39	99.96%		1298767231	-2.02	97.83%		1190818868	-5.88	100.00%		1364486928	-4.76	100.00%
32	1262706160	-3.46	99.97%		1340662949	-2.10	98.20%		1229232380	-5.96	100.00%		1408502635	-4.84	100.00%
33	1302165727	-3.54	99.98%		1382558666	-2.17	98.50%		1267645892	-6.03	100.00%		1452518342	-4.91	100.00%
34	1341625295	-3.61	99.98%		1424454383	-2.24	98.75%		1306059403	-6.10	100.00%		1496534050	-4.98	100.00%
35	1381084862	-3.68	99.99%		1466350100	-2.31	98.96%		1344472915	-6.17	100.00%		1540549757	-5.05	100.00%
36	1420544430	-3.75	99.99%		1508245817	-2.38	99.13%		1382886427	-6.24	100.00%		1584565464	-5.12	100.00%
37	1460003997	-3.81	99.99%		1550141534	-2.45	99.28%		1421299939	-6.30	100.00%		1628581172	-5.19	100.00%
38	1499463565	-3.88	99.99%		1592037251	-2.51	99.40%		1459713451	-6.37	100.00%		1672596879	-5.25	100.00%
39	1538923132	-3.94	100.00%		1633932969	-2.57	99.49%		1498126963	-6.43	100.00%		1716612587	-5.31	100.00%
40	1578382700	-4.00	100.00%		1675828686	-2.63	99.58%		1536540475	-6.49	100.00%		1760628294	-5.37	100.00%
41	1617842267	-4.06	100.00%		1717724403	-2.69	99.64%		1574953987	-6.55	100.00%		1804644001	-5.43	100.00%
42	1657301835	-4.12	100.00%		1759620120	-2.75	99.70%		1613367498	-6.61	100.00%		1848659709	-5.49	100.00%
43	1696761402	-4.17	100.00%		1801515837	-2.81	99.75%		1651781010	-6.66	100.00%		1892675416	-5.55	100.00%
44	1736220970	-4.23	100.00%		1843411554	-2.86	99.79%		1690194522	-6.72	100.00%		1936691123	-5.60	100.00%
45	1775680537	-4.28	100.00%		1885307271	-2.91	99.82%		1728608034	-6.77	100.00%		1980706831	-5.66	100.00%
46	1815140105	-4.34	100.00%		1927202989	-2.97	99.85%		1767021546	-6.83	100.00%		2024722538	-5.71	100.00%
47	1854599672	-4.39	100.00%		1969098706	-3.02	99.87%		1805435058	-6.88	100.00%		2068738245	-5.76	100.00%
48	1894059240	-4.44	100.00%		2010994423	-3.07	99.89%		1843848570	-6.93	100.00%		2112753953	-5.81	100.00%
49	1933518807	-4.49	100.00%		2052890140	-3.12	99.91%		1882262081	-6.98	100.00%		2156769660	-5.86	100.00%
50	1972978375	-4.54	100.00%		2094785857	-3.17	99.92%		1920675593	-7.03	100.00%		2200785367	-5.91	100.00%
Years	Cycles	β	p_f		Years	Cycles	β		Years	Cycles	β		Years	Cycles	β
1.8	69332249	3.50	0.02%		3.1	130211533	3.50		0.6	23907513	3.50		1.0	43634465	3.50

IAH Open			IAH Sub			RMMA Open			RMMA Sub		
N	β	p_f	N	β	p_f	N	β	p_f	N	β	p_f
34683374	5.53	0.00%	36442746	7.35	0.00%	42176892	3.85	0.01%	45732303	5.43	0.00%
69366748	3.86	0.01%	72885492	5.68	0.00%	84353784	2.19	1.44%	91464606	3.76	0.01%
104050122	2.89	0.19%	109328238	4.71	0.00%	126530676	1.21	11.24%	137196910	2.79	0.26%
138733496	2.20	1.40%	145770984	4.02	0.00%	168707568	0.52	30.03%	182929213	2.10	1.80%
173416870	1.66	4.82%	182213730	3.48	0.02%	210884460	-0.01	50.47%	228661516	1.56	5.91%
208100244	1.23	11.03%	218656476	3.05	0.12%	253061352	-0.45	67.34%	274393819	1.12	13.03%
242783618	0.86	19.62%	255099222	2.68	0.37%	295238244	-0.82	79.37%	320126123	0.76	22.51%
277466992	0.53	29.64%	291541968	2.35	0.93%	337415136	-1.14	87.28%	365858426	0.43	33.20%
312150366	0.25	40.05%	327984714	2.07	1.91%	379592027	-1.42	92.26%	411590729	0.15	43.96%
346833740	0.00	50.03%	364427460	1.82	3.44%	421768919	-1.68	95.31%	457323032	-0.10	54.02%
381517113	-0.23	59.08%	400870206	1.59	5.59%	463945811	-1.90	97.16%	503055335	-0.33	62.92%
416200487	-0.44	66.94%	437312952	1.38	8.35%	506122703	-2.11	98.27%	548787639	-0.54	70.49%
450883861	-0.63	73.58%	473755698	1.19	11.71%	548299595	-2.31	98.94%	594519942	-0.73	76.75%
485567235	-0.81	79.05%	510198444	1.01	15.58%	590476487	-2.48	99.35%	640252245	-0.91	81.82%
520250609	-0.97	83.49%	546641190	0.85	19.87%	632653379	-2.65	99.60%	685984548	-1.07	85.86%
554933983	-1.13	87.05%	583083936	0.69	24.47%	674830271	-2.80	99.75%	731716852	-1.23	89.05%
589617357	-1.27	89.87%	619526682	0.55	29.26%	717007163	-2.95	99.84%	777449155	-1.37	91.54%
624300731	-1.41	92.09%	655969428	0.41	34.14%	759184055	-3.09	99.90%	823181458	-1.51	93.47%
658984105	-1.54	93.84%	692412174	0.28	39.02%	801360947	-3.22	99.93%	868913761	-1.64	94.96%
693667479	-1.66	95.20%	728854920	0.16	43.81%	843537839	-3.34	99.96%	914646064	-1.76	96.12%
728350853	-1.78	96.26%	765297666	0.04	48.46%	885714731	-3.46	99.97%	960378368	-1.88	97.01%
763034227	-1.89	97.08%	801740412	-0.07	52.91%	927891623	-3.57	99.98%	1006110671	-1.99	97.69%
797717601	-2.00	97.72%	838183158	-0.18	57.13%	970068515	-3.67	99.99%	1051842974	-2.10	98.21%
832400975	-2.10	98.22%	874625904	-0.28	61.10%	1012245407	-3.78	99.99%	1097575277	-2.20	98.62%
867084349	-2.20	98.61%	911068650	-0.38	64.79%	1054422298	-3.87	99.99%	1143307581	-2.30	98.93%
901767723	-2.29	98.91%	947511396	-0.47	68.22%	1096599190	-3.97	100.00%	1189039884	-2.39	99.17%
936451097	-2.38	99.14%	983954142	-0.56	71.38%	1138776082	-4.06	100.00%	1234772187	-2.48	99.35%
971134471	-2.47	99.33%	1020396888	-0.65	74.27%	1180952974	-4.15	100.00%	1280504490	-2.57	99.49%
1005817845	-2.56	99.47%	1056839634	-0.74	76.91%	1223129866	-4.23	100.00%	1326236793	-2.66	99.60%
1040501219	-2.64	99.58%	1093282380	-0.82	79.31%	1265306758	-4.31	100.00%	1371969097	-2.74	99.69%
1075184593	-2.72	99.67%	1129725126	-0.90	81.49%	1307483650	-4.39	100.00%	1417701400	-2.82	99.76%
1109867967	-2.79	99.74%	1166167872	-0.97	83.45%	1349660542	-4.47	100.00%	1463433703	-2.89	99.81%
1144551340	-2.87	99.79%	1202610618	-1.05	85.22%	1391837434	-4.54	100.00%	1509166006	-2.97	99.85%
1179234714	-2.94	99.83%	1239053364	-1.12	86.82%	1434014326	-4.61	100.00%	1554898310	-3.04	99.88%
1213918088	-3.01	99.87%	1275496110	-1.19	88.24%	1476191218	-4.68	100.00%	1600630613	-3.11	99.91%
1248601462	-3.07	99.89%	1311938856	-1.25	89.52%	1518368110	-4.75	100.00%	1646362916	-3.18	99.93%
1283284836	-3.14	99.92%	1348381602	-1.32	90.67%	1560545002	-4.82	100.00%	1692095219	-3.24	99.94%
1317968210	-3.20	99.93%	1384824348	-1.38	91.69%	1602721894	-4.88	100.00%	1737827522	-3.30	99.95%
1352651584	-3.27	99.95%	1421267094	-1.45	92.61%	1644898786	-4.94	100.00%	1783559826	-3.37	99.96%
1387334958	-3.33	99.96%	1457709840	-1.51	93.42%	1687075678	-5.00	100.00%	1829292129	-3.43	99.97%
1422018332	-3.39	99.96%	1494152586	-1.57	94.14%	1729252569	-5.06	100.00%	1875024432	-3.49	99.98%
1456701706	-3.44	99.97%	1530595332	-1.62	94.79%	1771429461	-5.12	100.00%	1920756735	-3.55	99.98%
1491385080	-3.50	99.98%	1567038078	-1.68	95.37%	1813606353	-5.18	100.00%	1966489039	-3.60	99.98%
1526068454	-3.56	99.98%	1603480824	-1.74	95.88%	1855783245	-5.23	100.00%	2012221342	-3.66	99.99%
1560751828	-3.61	99.98%	1639923570	-1.79	96.33%	1897960137	-5.29	100.00%	2057953645	-3.71	99.99%
1595435202	-3.66	99.99%	1676366316	-1.84	96.73%	1940137029	-5.34	100.00%	2103685948	-3.76	99.99%
1630118576	-3.71	99.99%	1712809062	-1.89	97.09%	1982313921	-5.39	100.00%	2149418251	-3.82	99.99%
1664801950	-3.77	99.99%	1749251808	-1.95	97.41%	2024490813	-5.44	100.00%	2195150555	-3.87	99.99%
1699485324	-3.81	99.99%	1785694554	-1.99	97.70%	2066667705	-5.49	100.00%	2240882858	-3.92	100.00%
1734168698	-3.86	99.99%	1822137300	-2.04	97.95%	2108844597	-5.54	100.00%	2286615161	-3.96	100.00%

Years	Cycles	β	Years	Cycles	β	Years	Cycles	β	Years	Cycles	β
2.3	80650346	3.50	5.0	180919178	3.50	1.2	48811061	3.50	2.2	101994039	3.50

ELP Open				ELP Sub		
N	β	p_f		N	β	p_f
32138558	8.04	0.00%		32186087	10.21	0.00%
64277116	6.37	0.00%		64372173	8.55	0.00%
96415674	5.40	0.00%		96558260	7.58	0.00%
128554232	4.71	0.00%		128744347	6.89	0.00%
160692790	4.17	0.00%		160930434	6.35	0.00%
192831348	3.74	0.01%		193116520	5.91	0.00%
224969906	3.37	0.04%		225302607	5.54	0.00%
257108464	3.05	0.12%		257488694	5.22	0.00%
289247022	2.76	0.29%		289674780	4.94	0.00%
321385580	2.51	0.60%		321860867	4.69	0.00%
353524138	2.28	1.12%		354046954	4.46	0.00%
385662696	2.07	1.90%		386233040	4.25	0.00%
417801254	1.88	2.99%		418419127	4.06	0.00%
449939812	1.70	4.42%		450605214	3.88	0.01%
482078371	1.54	6.20%		482791301	3.71	0.01%
514216929	1.38	8.33%		514977387	3.56	0.02%
546355487	1.24	10.79%		547163474	3.41	0.03%
578494045	1.10	13.55%		579349561	3.28	0.05%
610632603	0.97	16.58%		611535647	3.15	0.08%
642771161	0.85	19.83%		643721734	3.02	0.13%
674909719	0.73	23.25%		675907821	2.91	0.18%
707048277	0.62	26.79%		708093907	2.79	0.26%
739186835	0.51	30.42%		740279994	2.69	0.36%
771325393	0.41	34.08%		772466081	2.59	0.49%
803463951	0.31	37.74%		804652168	2.49	0.64%
835602509	0.22	41.36%		836838254	2.39	0.83%
867741067	0.13	44.92%		869024341	2.30	1.06%
899879625	0.04	48.39%		901210428	2.22	1.34%
932018183	-0.04	51.75%		933396514	2.13	1.65%
964156741	-0.13	54.98%		965582601	2.05	2.02%
996295299	-0.20	58.08%		997768688	1.97	2.43%
1028433857	-0.28	61.03%		1029954774	1.90	2.90%
1060572415	-0.35	63.83%		1062140861	1.82	3.43%
1092710973	-0.43	66.48%		1094326948	1.75	4.01%
1124849531	-0.50	68.98%		1126513035	1.68	4.65%
1156988089	-0.56	71.32%		1158699121	1.61	5.34%
1189126647	-0.63	73.52%		1190885208	1.55	6.10%
1221265205	-0.69	75.57%		1223071295	1.48	6.91%
1253403763	-0.75	77.49%		1255257381	1.42	7.78%
1285542321	-0.82	79.27%		1287443468	1.36	8.70%
1317680879	-0.87	80.92%		1319629555	1.30	9.67%
1349819437	-0.93	82.45%		1351815641	1.24	10.70%
1381957996	-0.99	83.87%		1384001728	1.19	11.78%
1414096554	-1.04	85.19%		1416187815	1.13	12.91%
1446235112	-1.10	86.40%		1448373902	1.08	14.08%
1478373670	-1.15	87.52%		1480559988	1.02	15.29%
1510512228	-1.20	88.55%		1512746075	0.97	16.54%
1542650786	-1.25	89.49%		1544932162	0.92	17.83%
1574789344	-1.30	90.37%		1577118248	0.87	19.15%
1606927902	-1.35	91.17%		1609304335	0.82	20.50%

Years	Cycles	β	Years	Cycles	β
6.6	212873198	3.50	16.4	527661010	3.50

	San Antonio							Dallas/Fort Worth						
S_{Ri} (w/ GS)	Open	γ_i	$(\gamma_i SR_i)^3$		Suburban	γ_i	$(\gamma_i SR_i)^3$	Open	γ_i	$(\gamma_i SR_i)^3$		Suburban	γ_i	$(\gamma_i SR_i)^3$
0.022	2.76E+04	0.00002	0.00		8.64E+04	0.00005	0.00	6.38E+02	0.00000	0.00		3.11E+03	0.00000	0.00
0.035	1.04E+05	0.00007	0.00		2.86E+05	0.00017	0.00	4.30E+03	0.00000	0.00		1.80E+04	0.00001	0.00
0.039	1.03E+05	0.00007	0.00		2.78E+05	0.00017	0.00	3.98E+03	0.00000	0.00		1.60E+04	0.00001	0.00
0.051	2.69E+05	0.00019	0.00		6.73E+05	0.00041	0.00	1.77E+04	0.00001	0.00		6.52E+04	0.00004	0.00
0.061	3.35E+05	0.00023	0.00		8.03E+05	0.00049	0.00	2.25E+04	0.00002	0.00		7.82E+04	0.00005	0.00
0.085	3.33E+05	0.00023	0.00		7.76E+05	0.00047	0.00	2.07E+04	0.00002	0.00		6.86E+04	0.00004	0.00
0.089	7.74E+05	0.00053	0.00		1.68E+06	0.00102	0.00	7.97E+04	0.00006	0.00		2.45E+05	0.00016	0.00
0.133	9.40E+05	0.00065	0.00		1.96E+06	0.00119	0.00	9.81E+04	0.00008	0.00		2.83E+05	0.00018	0.00
0.167	9.32E+05	0.00064	0.00		1.86E+06	0.00113	0.00	8.91E+04	0.00007	0.00		2.41E+05	0.00016	0.00
0.193	1.93E+06	0.00133	0.00		3.66E+06	0.00222	0.00	3.00E+05	0.00024	0.00		7.70E+05	0.00050	0.00
0.264	2.29E+06	0.00157	0.00		4.13E+06	0.00251	0.00	3.56E+05	0.00029	0.00		8.47E+05	0.00055	0.00
0.278	5.52E+07	0.03794	0.00		8.33E+07	0.05062	0.00	2.01E+07	0.01618	0.00		3.86E+07	0.02503	0.00
0.310	2.23E+06	0.00154	0.00		3.82E+06	0.00232	0.00	3.13E+05	0.00025	0.00		6.84E+05	0.00044	0.00
0.382	4.19E+06	0.00288	0.00		6.94E+06	0.00422	0.00	9.43E+05	0.00076	0.00		2.02E+06	0.00131	0.00
0.438	8.07E+07	0.05553	0.00		1.09E+08	0.06604	0.00	4.22E+07	0.03393	0.00		7.02E+07	0.04550	0.00
0.482	9.21E+07	0.06332	0.00		1.25E+08	0.07567	0.00	4.55E+07	0.03652	0.00		7.54E+07	0.04883	0.00
0.488	4.81E+06	0.00331	0.00		7.50E+06	0.00456	0.00	1.06E+06	0.00085	0.00		2.07E+06	0.00134	0.00
0.565	4.53E+06	0.00312	0.00		6.52E+06	0.00396	0.00	8.81E+05	0.00071	0.00		1.51E+06	0.00098	0.00
0.635	9.64E+07	0.06632	0.00		1.18E+08	0.07175	0.00	6.56E+07	0.05271	0.00		9.69E+07	0.06278	0.00
0.706	7.89E+06	0.00543	0.00		1.14E+07	0.00695	0.00	2.46E+06	0.00197	0.00		4.37E+06	0.00283	0.00
0.758	1.16E+08	0.08003	0.00		1.41E+08	0.08574	0.00	7.94E+07	0.06382	0.00		1.15E+08	0.07446	0.00
0.784	7.42E+06	0.00510	0.00		8.55E+06	0.00520	0.00	1.83E+06	0.00147	0.00		2.27E+06	0.00147	0.00
0.890	8.64E+06	0.00594	0.00		1.16E+07	0.00705	0.00	2.57E+06	0.00206	0.00		4.04E+06	0.00262	0.00
1.049	1.35E+08	0.09296	0.00		1.65E+08	0.10035	0.00	8.70E+07	0.06989	0.00		1.26E+08	0.08142	0.00
1.098	1.23E+08	0.08472	0.00		1.37E+08	0.08296	0.00	1.06E+08	0.08522	0.00		1.37E+08	0.08884	0.00
1.289	1.28E+07	0.00883	0.00		1.63E+07	0.00989	0.00	5.24E+06	0.00421	0.00		7.67E+06	0.00497	0.00
1.652	1.48E+08	0.10171	0.00		1.63E+08	0.09918	0.00	1.27E+08	0.10202	0.00		1.62E+08	0.10471	0.01
1.802	5.43E+08	0.37333	0.30		5.13E+08	0.31152	0.18	6.49E+08	0.52155	0.83		6.90E+08	0.44666	0.52
4.919	3.62E+06	0.00249	0.00		3.62E+06	0.00220	0.00	6.34E+06	0.00509	0.00		6.34E+06	0.00411	0.00
	1454169257		0.31		1645547607		0.18	1244965581		0.84		1543694286		0.53
		S_{RE}	**0.68**			S_{RE}	**0.57**		S_{RE}	**0.94**			S_{RE}	**0.81**

	Houston							Austin						
	Open	γ_i	$(\gamma_i SR_i)^3$		Suburban	γ_i	$(\gamma_i SR_i)^3$	Open	γ_i	$(\gamma_i SR_i)^3$		Suburban	γ_i	$(\gamma_i SR_i)^3$
	4.63E+03	0.00000	0.00		1.92E+04	0.00001	0.00	2.54E+03	0.00000	0.00		1.13E+04	0.00001	0.00
	2.52E+04	0.00002	0.00		8.98E+04	0.00006	0.00	1.51E+04	0.00001	0.00		5.73E+04	0.00003	0.00
	2.40E+04	0.00002	0.00		8.27E+04	0.00006	0.00	1.42E+04	0.00001	0.00		5.21E+04	0.00003	0.00
	8.67E+04	0.00007	0.00		2.70E+05	0.00019	0.00	5.57E+04	0.00004	0.00		1.86E+05	0.00011	0.00
	1.09E+05	0.00008	0.00		3.23E+05	0.00022	0.00	7.04E+04	0.00005	0.00		2.22E+05	0.00013	0.00
	1.03E+05	0.00008	0.00		2.95E+05	0.00020	0.00	6.60E+04	0.00004	0.00		2.00E+05	0.00011	0.00
	3.22E+05	0.00025	0.00		8.42E+05	0.00058	0.00	2.23E+05	0.00015	0.00		6.23E+05	0.00036	0.00
	3.93E+05	0.00031	0.00		9.74E+05	0.00067	0.00	2.74E+05	0.00018	0.00		7.20E+05	0.00041	0.00
	3.71E+05	0.00029	0.00		8.75E+05	0.00060	0.00	2.54E+05	0.00017	0.00		6.33E+05	0.00036	0.00
	9.99E+05	0.00078	0.00		2.20E+06	0.00151	0.00	7.49E+05	0.00050	0.00		1.75E+06	0.00101	0.00
	1.18E+06	0.00092	0.00		2.44E+06	0.00169	0.00	8.87E+05	0.00059	0.00		1.94E+06	0.00111	0.00
	4.17E+07	0.03244	0.00		6.84E+07	0.04715	0.00	3.76E+07	0.02524	0.00		6.55E+07	0.03767	0.00
	1.09E+06	0.00085	0.00		2.12E+06	0.00146	0.00	8.04E+05	0.00054	0.00		1.63E+06	0.00094	0.00
	2.60E+06	0.00202	0.00		4.81E+06	0.00331	0.00	2.10E+06	0.00141	0.00		4.11E+06	0.00236	0.00
	6.88E+07	0.05349	0.00		9.74E+07	0.06712	0.00	6.81E+07	0.04568	0.00		1.02E+08	0.05891	0.00
	7.71E+07	0.05992	0.00		1.10E+08	0.07577	0.00	7.51E+07	0.05037	0.00		1.13E+08	0.06521	0.00
	2.95E+06	0.00229	0.00		5.08E+06	0.00350	0.00	2.37E+06	0.00159	0.00		4.29E+06	0.00247	0.00
	2.61E+06	0.00203	0.00		4.08E+06	0.00281	0.00	2.05E+06	0.00137	0.00		3.32E+06	0.00191	0.00
	8.73E+07	0.06788	0.00		1.09E+08	0.07544	0.00	9.33E+07	0.06263	0.00		1.25E+08	0.07160	0.00
	5.62E+06	0.00437	0.00		8.81E+06	0.00607	0.00	4.88E+06	0.00327	0.00		8.03E+06	0.00461	0.00
	1.05E+08	0.08191	0.00		1.31E+08	0.09005	0.00	1.13E+08	0.07567	0.00		1.48E+08	0.08525	0.00
	4.78E+06	0.00371	0.00		5.68E+06	0.00392	0.00	3.94E+06	0.00264	0.00		4.76E+06	0.00274	0.00
	6.03E+06	0.00469	0.00		8.63E+06	0.00595	0.00	5.18E+06	0.00348	0.00		7.69E+06	0.00442	0.00
	1.21E+08	0.09400	0.00		1.52E+08	0.10457	0.00	1.27E+08	0.08527	0.00		1.68E+08	0.09673	0.00
	1.15E+08	0.08904	0.00		1.27E+08	0.08722	0.00	1.33E+08	0.08895	0.00		1.55E+08	0.08936	0.00
	1.01E+07	0.00787	0.00		1.35E+07	0.00928	0.00	9.38E+06	0.00630	0.00		1.29E+07	0.00744	0.00
	1.37E+08	0.10683	0.01		1.51E+08	0.10434	0.01	1.59E+08	0.10662	0.01		1.85E+08	0.10628	0.01
	4.86E+08	0.37813	0.32		4.37E+08	0.30120	0.16	6.46E+08	0.43328	0.48		6.17E+08	0.35504	0.26
	7.32E+06	0.00569	0.00		7.32E+06	0.00505	0.00	5.88E+06	0.00394	0.00		5.88E+06	0.00338	0.00
	1286116172		0.32		1450814946		0.17	1489971980		0.48		1739026929		0.27
		S_{RE}	**0.69**			S_{RE}	**0.55**		S_{RE}	**0.78**			S_{RE}	**0.65**

					El Paso			
	Open	γ_i	$(\gamma_i SR_i)^3$		Suburban	γ_i	$(\gamma_i SR_i)^3$	
	1.00E+04	0.00001	0.00		4.00E+04	0.00003	0.00	
	5.17E+04	0.00004	0.00		1.75E+05	0.00013	0.00	
	4.95E+04	0.00004	0.00		1.63E+05	0.00012	0.00	
	1.68E+05	0.00013	0.00		4.94E+05	0.00036	0.00	
	2.10E+05	0.00016	0.00		5.90E+05	0.00043	0.00	
	2.02E+05	0.00016	0.00		5.47E+05	0.00040	0.00	
	5.82E+05	0.00045	0.00		1.43E+06	0.00103	0.00	
	7.10E+05	0.00055	0.00		1.66E+06	0.00120	0.00	
	6.79E+05	0.00052	0.00		1.52E+06	0.00110	0.00	
	1.68E+06	0.00129	0.00		3.45E+06	0.00250	0.00	
	1.98E+06	0.00153	0.00		3.87E+06	0.00280	0.00	
	6.10E+07	0.04694	0.00		9.44E+07	0.06827	0.00	
	1.87E+06	0.00144	0.00		3.44E+06	0.00249	0.00	
	4.02E+06	0.00309	0.00		6.97E+06	0.00504	0.00	
	8.67E+07	0.06674	0.00		1.13E+08	0.08174	0.00	
	1.00E+08	0.07704	0.00		1.33E+08	0.09622	0.00	
	4.58E+06	0.00353	0.00		7.47E+06	0.00541	0.00	
	4.18E+06	0.00322	0.00		6.27E+06	0.00454	0.00	
	9.65E+07	0.07429	0.00		1.09E+08	0.07895	0.00	
	8.00E+06	0.00616	0.00		1.18E+07	0.00853	0.00	
	1.17E+08	0.08969	0.00		1.31E+08	0.09486	0.00	
	7.23E+06	0.00556	0.00		8.44E+06	0.00611	0.00	
	8.70E+06	0.00669	0.00		1.19E+07	0.00860	0.00	
	1.39E+08	0.10666	0.00		1.60E+08	0.11581	0.00	
	1.10E+08	0.08465	0.00		1.08E+08	0.07809	0.00	
	1.33E+07	0.01021	0.00		1.68E+07	0.01215	0.00	
	1.32E+08	0.10186	0.00		1.31E+08	0.09443	0.00	
	3.60E+08	0.27730	0.12		2.77E+08	0.20040	0.05	
	3.91E+07	0.03007	0.00		3.91E+07	0.02828	0.00	
	1299453015		0.14		1382022958		0.06	
		S_{RE}	**0.51**			S_{RE}	**0.38**	

	SAT Open				SAT Sub				DFW Open				DFW Sub		
# of yrs.	N	β	p_f		N	β	p_f		N	β	p_f		N	β	p_f
1	29083385	8.73	0.00%		32910952	9.70	0.00%		24899312	6.73	0.00%		30873886	7.31	0.00%
2	58166770	7.06	0.00%		65821904	8.03	0.00%		49798623	5.06	0.00%		61747771	5.65	0.00%
3	87250155	6.09	0.00%		98732856	7.06	0.00%		74697935	4.09	0.00%		92621657	4.68	0.00%
4	116333541	5.40	0.00%		131643809	6.37	0.00%		99597246	3.40	0.03%		123495543	3.99	0.00%
5	145416926	4.86	0.00%		164554761	5.83	0.00%		124496558	2.86	0.21%		154369429	3.45	0.03%
6	174500311	4.43	0.00%		197465713	5.40	0.00%		149395870	2.43	0.76%		185243314	3.01	0.13%
7	203583696	4.06	0.00%		230376665	5.03	0.00%		174295181	2.06	1.98%		216117200	2.64	0.41%
8	232667081	3.74	0.01%		263287617	4.71	0.00%		199194493	1.74	4.12%		246991086	2.32	1.01%
9	261750466	3.45	0.03%		296198569	4.42	0.00%		224093805	1.45	7.30%		277864972	2.04	2.07%
10	290833851	3.20	0.07%		329109521	4.17	0.00%		248993116	1.20	11.49%		308738857	1.79	3.70%
11	319917237	2.97	0.15%		362020474	3.94	0.00%		273892428	0.97	16.54%		339612743	1.56	5.96%
12	349000622	2.76	0.29%		394931426	3.73	0.01%		298791739	0.76	22.26%		370486629	1.35	8.86%
13	378084007	2.57	0.51%		427842378	3.54	0.02%		323691051	0.57	28.38%		401360514	1.16	12.36%
14	407167392	2.39	0.84%		460753330	3.36	0.04%		348590363	0.39	34.69%		432234400	0.98	16.37%
15	436250777	2.23	1.30%		493664282	3.20	0.07%		373489674	0.23	40.98%		463108286	0.81	20.79%
16	465334162	2.07	1.91%		526575234	3.04	0.12%		398388986	0.07	47.08%		493982172	0.66	25.50%
17	494417547	1.93	2.70%		559486186	2.90	0.19%		423288297	-0.07	52.88%		524856057	0.51	30.39%
18	523500933	1.79	3.68%		592397139	2.76	0.29%		448187609	-0.21	58.30%		555729943	0.38	35.34%
19	552584318	1.66	4.85%		625308091	2.63	0.43%		473086921	-0.34	63.28%		586603829	0.25	40.27%
20	581667703	1.54	6.22%		658219043	2.51	0.61%		497986232	-0.46	67.81%		617477715	0.12	45.09%
21	610751088	1.42	7.79%		691129995	2.39	0.84%		522885544	-0.58	71.89%		648351600	0.01	49.75%
22	639834473	1.31	9.55%		724040947	2.28	1.14%		547784855	-0.69	75.53%		679225486	-0.11	54.20%
23	668917858	1.20	11.48%		756951899	2.17	1.50%		572684167	-0.80	78.75%		710099372	-0.21	58.40%
24	698001243	1.10	13.59%		789862851	2.07	1.93%		597583479	-0.90	81.59%		740973257	-0.31	62.33%
25	727084629	1.00	15.84%		822773804	1.97	2.44%		622482790	-1.00	84.08%		771847143	-0.41	65.99%
26	756168014	0.91	18.22%		855684756	1.88	3.03%		647382102	-1.09	86.26%		802721029	-0.51	69.37%
27	785251399	0.82	20.71%		888595708	1.79	3.71%		672281414	-1.18	88.15%		833594915	-0.60	72.47%
28	814334784	0.73	23.30%		921506660	1.70	4.47%		697180725	-1.27	89.79%		864468800	-0.68	75.31%
29	843418169	0.64	25.95%		954417612	1.61	5.32%		722080037	-1.35	91.22%		895342686	-0.77	77.89%
30	872501554	0.56	28.65%		987328564	1.53	6.26%		746979348	-1.44	92.44%		926216572	-0.85	80.23%
31	901584939	0.48	31.39%		1020239516	1.45	7.29%		771878660	-1.51	93.50%		957090458	-0.93	82.34%
32	930668325	0.41	34.14%		1053150469	1.38	8.41%		796777972	-1.59	94.41%		987964343	-1.00	84.25%
33	959751710	0.33	36.89%		1086061421	1.30	9.61%		821677283	-1.66	95.20%		1018838229	-1.08	85.96%
34	988835095	0.26	39.62%		1118972373	1.23	10.89%		846576595	-1.74	95.87%		1049712115	-1.15	87.50%
35	1017918480	0.19	42.32%		1151883325	1.16	12.24%		871475906	-1.81	96.45%		1080586000	-1.22	88.87%
36	1047001865	0.13	44.99%		1184794277	1.10	13.67%		896375218	-1.87	96.95%		1111459886	-1.29	90.10%
37	1076085250	0.06	47.60%		1217705229	1.03	15.16%		921274530	-1.94	97.37%		1142333772	-1.35	91.20%
38	1105168636	0.00	50.15%		1250616181	0.97	16.71%		946173841	-2.00	97.74%		1173207658	-1.42	92.18%
39	1134252021	-0.07	52.64%		1283527134	0.90	18.32%		971073153	-2.07	98.05%		1204081543	-1.48	93.05%
40	1163335406	-0.13	55.05%		1316438086	0.84	19.97%		995972464	-2.13	98.32%		1234955429	-1.54	93.82%
41	1192418791	-0.19	57.38%		1349349038	0.78	21.67%		1020871776	-2.19	98.56%		1265829315	-1.60	94.51%
42	1221502176	-0.24	59.64%		1382259990	0.73	23.41%		1045771088	-2.24	98.76%		1296703201	-1.66	95.13%
43	1250585561	-0.30	61.81%		1415170942	0.67	25.17%		1070670399	-2.30	98.93%		1327577086	-1.71	95.67%
44	1279668946	-0.36	63.89%		1448081894	0.61	26.97%		1095569711	-2.35	99.07%		1358450972	-1.77	96.16%
45	1308752332	-0.41	65.89%		1480992846	0.56	28.78%		1120469023	-2.41	99.20%		1389324858	-1.82	96.58%
46	1337835717	-0.46	67.81%		1513903799	0.51	30.60%		1145368334	-2.46	99.31%		1420198743	-1.88	96.96%
47	1366919102	-0.51	69.63%		1546814751	0.46	32.43%		1170267646	-2.51	99.40%		1451072629	-1.93	97.30%
48	1396002487	-0.56	71.38%		1579725703	0.41	34.27%		1195166957	-2.56	99.48%		1481946515	-1.98	97.60%
49	1425085872	-0.61	73.04%		1612636655	0.36	36.11%		1220066269	-2.61	99.55%		1512820401	-2.03	97.87%
50	1454169257	-0.66	74.61%		1645547607	0.31	37.94%		1244965581	-2.66	99.61%		1543694286	-2.08	98.10%
Years	Cycles	β	p_f		Years	Cycles	β		Years	Cycles	β		Years	Cycles	β
8.8	256781089	3.50	0.02%		13.2	435075465	3.50		3.8	95541443	3.50		4.9	151222796	3.50

IAH Open			IAH Sub			RMMA Open			RMMA Sub		
N	β	p_f	N	β	p_f	N	β	p_f	N	β	p_f
25722323	8.92	0.00%	29016299	10.22	0.00%	29799440	7.61	0.00%	34780539	8.64	0.00%
51444647	7.26	0.00%	58032598	8.55	0.00%	59598879	5.95	0.00%	69561077	6.98	0.00%
77166970	6.29	0.00%	87048897	7.58	0.00%	89398319	4.98	0.00%	104341616	6.00	0.00%
102889294	5.60	0.00%	116065196	6.89	0.00%	119197758	4.28	0.00%	139122154	5.31	0.00%
128611617	5.06	0.00%	145081495	6.35	0.00%	148997198	3.75	0.01%	173902693	4.78	0.00%
154333941	4.62	0.00%	174097794	5.92	0.00%	178796638	3.31	0.05%	208683231	4.34	0.00%
180056264	4.25	0.00%	203114092	5.55	0.00%	208596077	2.94	0.16%	243463770	3.97	0.00%
205778588	3.93	0.00%	232130391	5.23	0.00%	238395517	2.62	0.44%	278244309	3.65	0.01%
231500911	3.65	0.01%	261146690	4.94	0.00%	268194956	2.34	0.97%	313024847	3.37	0.04%
257223234	3.40	0.03%	290162989	4.69	0.00%	297994396	2.09	1.85%	347805386	3.12	0.09%
282945558	3.17	0.08%	319179288	4.46	0.00%	327793836	1.86	3.16%	382585924	2.89	0.19%
308667881	2.96	0.15%	348195587	4.25	0.00%	357593275	1.65	4.96%	417366463	2.68	0.37%
334390205	2.77	0.28%	377211886	4.06	0.00%	387392715	1.46	7.27%	452147001	2.49	0.65%
360112528	2.59	0.48%	406228185	3.88	0.01%	417192154	1.28	10.06%	486927540	2.31	1.05%
385834852	2.42	0.77%	435244484	3.72	0.01%	446991594	1.11	13.29%	521708079	2.14	1.61%
411557175	2.27	1.16%	464260783	3.56	0.02%	476791034	0.96	16.91%	556488617	1.99	2.35%
437279499	2.12	1.68%	493277082	3.42	0.03%	506590473	0.81	20.83%	591269156	1.84	3.28%
463001822	1.99	2.34%	522293381	3.28	0.05%	536389913	0.68	24.98%	626049694	1.70	4.42%
488724145	1.86	3.16%	551309680	3.15	0.08%	566189353	0.55	29.27%	660830233	1.57	5.77%
514446469	1.73	4.14%	580325978	3.03	0.12%	595988792	0.42	33.64%	695610771	1.45	7.33%
540168792	1.62	5.29%	609342277	2.91	0.18%	625788232	0.31	38.01%	730391310	1.33	9.10%
565891116	1.51	6.61%	638358576	2.80	0.26%	655587671	0.19	42.33%	765171849	1.22	11.07%
591613439	1.40	8.09%	667374875	2.69	0.36%	685387111	0.09	46.54%	799952387	1.12	13.22%
617335763	1.30	9.74%	696391174	2.59	0.48%	715186551	-0.02	50.61%	834732926	1.01	15.53%
643058086	1.20	11.53%	725407473	2.49	0.64%	744985990	-0.11	54.51%	869513464	0.92	17.98%
668780409	1.10	13.46%	754423772	2.40	0.83%	774785430	-0.21	58.21%	904294003	0.82	20.56%
694502733	1.01	15.53%	783440071	2.31	1.06%	804584869	-0.30	61.71%	939074541	0.73	23.23%
720225056	0.93	17.70%	812456370	2.22	1.33%	834384309	-0.39	65.00%	973855080	0.64	25.98%
745947380	0.84	19.97%	841472669	2.13	1.64%	864183749	-0.47	68.06%	1008635619	0.56	28.78%
771669703	0.76	22.33%	870488968	2.05	2.00%	893983188	-0.55	70.91%	1043416157	0.48	31.62%
797392027	0.68	24.74%	899505267	1.97	2.42%	923782628	-0.63	73.55%	1078196696	0.40	34.47%
823114350	0.61	27.21%	928521566	1.90	2.88%	953582067	-0.71	75.98%	1112977234	0.32	37.31%
848836674	0.53	29.72%	957537864	1.82	3.41%	983381507	-0.78	78.22%	1147757773	0.25	40.14%
874558997	0.46	32.24%	986554163	1.75	3.98%	1013180947	-0.85	80.27%	1182538311	0.18	42.93%
900281320	0.39	34.78%	1015570462	1.68	4.62%	1042980386	-0.92	82.14%	1217318850	0.11	45.68%
926003644	0.32	37.31%	1044586761	1.62	5.31%	1072779826	-0.99	83.85%	1252099389	0.04	48.37%
951725967	0.26	39.82%	1073603060	1.55	6.06%	1102579265	-1.05	85.41%	1286879927	-0.02	50.99%
977448291	0.19	42.31%	1102619359	1.49	6.87%	1132378705	-1.12	86.82%	1321660466	-0.09	53.54%
1003170614	0.13	44.77%	1131635658	1.42	7.73%	1162178145	-1.18	88.11%	1356441004	-0.15	56.01%
1028892938	0.07	47.18%	1160651957	1.36	8.65%	1191977584	-1.24	89.27%	1391221543	-0.21	58.39%
1054615261	0.01	49.54%	1189668256	1.30	9.62%	1221777024	-1.30	90.33%	1426002082	-0.27	60.69%
1080337585	-0.05	51.84%	1218684555	1.25	10.65%	1251576463	-1.36	91.28%	1460782620	-0.33	62.90%
1106059908	-0.10	54.09%	1247700854	1.19	11.72%	1281375903	-1.41	92.14%	1495563159	-0.39	65.01%
1131782231	-0.16	56.27%	1276717153	1.13	12.84%	1311175343	-1.47	92.92%	1530343697	-0.44	67.03%
1157504555	-0.21	58.39%	1305733452	1.08	14.01%	1340974782	-1.52	93.62%	1565124236	-0.49	68.96%
1183226878	-0.26	60.43%	1334749750	1.03	15.22%	1370774222	-1.58	94.26%	1599904774	-0.55	70.80%
1208949202	-0.32	62.41%	1363766049	0.98	16.46%	1400573662	-1.63	94.83%	1634685313	-0.60	72.54%
1234671525	-0.37	64.31%	1392782348	0.93	17.75%	1430373101	-1.68	95.34%	1669465852	-0.65	74.20%
1260393849	-0.42	66.14%	1421798647	0.88	19.06%	1460172541	-1.73	95.80%	1704246390	-0.70	75.77%
1286116172	-0.46	67.89%	1450814946	0.83	20.41%	1489971980	-1.78	96.22%	1739026929	-0.75	77.26%

Years	Cycles	β	Years	Cycles	β	Years	Cycles	β	Years	Cycles	β
9.6	246516775	3.50	16.4	476306632	3.50	5.5	165347005	3.50	8.5	296263549	3.50

ELP Open				ELP Sub			
N	β	p_f		N	β	p_f	
25989060	10.99	0.00%		27640459	12.94	0.00%	
51978121	9.33	0.00%		55280918	11.27	0.00%	
77967181	8.36	0.00%		82921377	10.30	0.00%	
103956241	7.67	0.00%		110561837	9.61	0.00%	
129945302	7.13	0.00%		138202296	9.07	0.00%	
155934362	6.69	0.00%		165842755	8.64	0.00%	
181923422	6.32	0.00%		193483214	8.27	0.00%	
207912482	6.00	0.00%		221123673	7.95	0.00%	
233901543	5.72	0.00%		248764132	7.66	0.00%	
259890603	5.47	0.00%		276404592	7.41	0.00%	
285879663	5.24	0.00%		304045051	7.18	0.00%	
311868724	5.03	0.00%		331685510	6.97	0.00%	
337857784	4.84	0.00%		359325969	6.78	0.00%	
363846844	4.66	0.00%		386966428	6.60	0.00%	
389835905	4.49	0.00%		414606887	6.44	0.00%	
415824965	4.34	0.00%		442247347	6.28	0.00%	
441814025	4.19	0.00%		469887806	6.14	0.00%	
467803085	4.06	0.00%		497528265	6.00	0.00%	
493792146	3.93	0.00%		525168724	5.87	0.00%	
519781206	3.80	0.01%		552809183	5.75	0.00%	
545770266	3.69	0.01%		580449642	5.63	0.00%	
571759327	3.57	0.02%		608090102	5.52	0.00%	
597748387	3.47	0.03%		635730561	5.41	0.00%	
623737447	3.37	0.04%		663371020	5.31	0.00%	
649726508	3.27	0.05%		691011479	5.21	0.00%	
675715568	3.17	0.08%		718651938	5.12	0.00%	
701704628	3.08	0.10%		746292397	5.03	0.00%	
727693688	3.00	0.14%		773932857	4.94	0.00%	
753682749	2.91	0.18%		801573316	4.86	0.00%	
779671809	2.83	0.23%		829213775	4.77	0.00%	
805660869	2.75	0.30%		856854234	4.70	0.00%	
831649930	2.68	0.37%		884494693	4.62	0.00%	
857638990	2.60	0.46%		912135152	4.55	0.00%	
883628050	2.53	0.57%		939775612	4.47	0.00%	
909617111	2.46	0.69%		967416071	4.40	0.00%	
935606171	2.39	0.84%		995056530	4.34	0.00%	
961595231	2.33	1.00%		1022696989	4.27	0.00%	
987584291	2.26	1.18%		1050337448	4.21	0.00%	
1013573352	2.20	1.39%		1077977907	4.14	0.00%	
1039562412	2.14	1.62%		1105618367	4.08	0.00%	
1065551472	2.08	1.87%		1133258826	4.02	0.00%	
1091540533	2.02	2.16%		1160899285	3.97	0.00%	
1117529593	1.97	2.46%		1188539744	3.91	0.00%	
1143518653	1.91	2.80%		1216180203	3.86	0.01%	
1169507714	1.86	3.17%		1243820662	3.80	0.01%	
1195496774	1.80	3.56%		1271461122	3.75	0.01%	
1221485834	1.75	3.98%		1299101581	3.70	0.01%	
1247474894	1.70	4.44%		1326742040	3.65	0.01%	
1273463955	1.65	4.92%		1354382499	3.60	0.02%	
1299453015	1.60	5.43%		1382022958	3.55	0.02%	

Years	Cycles	β	Years	Cycles	β
22.7	589745219	3.50	51.0	1410201829	3.50

	San Antonio								Dallas/Fort Worth						
S_{Ri} (no GS)	Open	γ_i	$(\gamma_i SR_i)^3$		Suburban	γ_i	$(\gamma_i SR_i)^3$		Open	γ_i	$(\gamma_i SR_i)^3$		Suburban	γ_i	$(\gamma_i SR_i)^3$
0.032	1.55E+05	0.00007	0.00		3.90E+05	0.00016	0.00		6.41E+03	0.00000	0.00		2.35E+04	0.00001	0.00
0.050	4.92E+05	0.00021	0.00		1.11E+06	0.00046	0.00		3.53E+04	0.00002	0.00		1.13E+05	0.00004	0.00
0.053	4.97E+05	0.00022	0.00		1.09E+06	0.00046	0.00		3.31E+04	0.00001	0.00		1.02E+05	0.00004	0.00
0.073	1.12E+06	0.00049	0.00		2.29E+06	0.00096	0.00		1.22E+05	0.00005	0.00		3.48E+05	0.00013	0.00
0.083	1.37E+06	0.00060	0.00		2.71E+06	0.00113	0.00		1.53E+05	0.00007	0.00		4.10E+05	0.00016	0.00
0.085	1.39E+06	0.00060	0.00		2.66E+06	0.00111	0.00		1.43E+05	0.00006	0.00		3.64E+05	0.00014	0.00
0.120	2.76E+06	0.00120	0.00		5.00E+06	0.00210	0.00		4.57E+05	0.00020	0.00		1.10E+06	0.00042	0.00
0.134	3.32E+06	0.00144	0.00		5.77E+06	0.00242	0.00		5.52E+05	0.00024	0.00		1.25E+06	0.00048	0.00
0.194	5.96E+06	0.00259	0.00		9.54E+06	0.00399	0.00		1.43E+06	0.00061	0.00		2.91E+06	0.00111	0.00
0.224	3.34E+06	0.00145	0.00		5.58E+06	0.00234	0.00		5.09E+05	0.00022	0.00		1.08E+06	0.00041	0.00
0.353	6.99E+06	0.00304	0.00		1.07E+07	0.00447	0.00		1.66E+06	0.00071	0.00		3.15E+06	0.00121	0.00
0.379	6.92E+06	0.00300	0.00		9.97E+06	0.00418	0.00		1.48E+06	0.00063	0.00		2.55E+06	0.00098	0.00
0.416	1.45E+08	0.06291	0.00		1.90E+08	0.07974	0.00		8.12E+07	0.03473	0.00		1.31E+08	0.05018	0.00
0.441	1.61E+07	0.00697	0.00		1.51E+07	0.00631	0.00		5.25E+06	0.00224	0.00		4.77E+06	0.00183	0.00
0.512	1.12E+07	0.00487	0.00		1.59E+07	0.00666	0.00		3.73E+06	0.00159	0.00		6.45E+06	0.00247	0.00
0.596	1.27E+07	0.00552	0.00		1.70E+07	0.00714	0.00		4.11E+06	0.00176	0.00		6.49E+06	0.00248	0.00
0.652	1.20E+07	0.00522	0.00		1.47E+07	0.00614	0.00		3.38E+06	0.00144	0.00		4.58E+06	0.00175	0.00
0.655	1.71E+08	0.07434	0.00		2.00E+08	0.08390	0.00		1.31E+08	0.05581	0.00		1.82E+08	0.06976	0.00
0.864	1.83E+07	0.00796	0.00		2.31E+07	0.00969	0.00		8.08E+06	0.00346	0.00		1.18E+07	0.00453	0.00
0.918	2.03E+08	0.08809	0.00		2.41E+08	0.10077	0.00		1.47E+08	0.06287	0.00		2.07E+08	0.07926	0.00
0.948	1.71E+08	0.07445	0.00		1.82E+08	0.07640	0.00		1.63E+08	0.06953	0.00		2.01E+08	0.07712	0.00
1.026	1.97E+07	0.00858	0.00		2.30E+07	0.00965	0.00		8.18E+06	0.00350	0.00		1.05E+07	0.00401	0.00
1.234	2.59E+07	0.01127	0.00		2.92E+07	0.01222	0.00		1.43E+07	0.00612	0.00		1.75E+07	0.00671	0.00
1.444	2.07E+08	0.08974	0.00		2.19E+08	0.09190	0.00		1.96E+08	0.08396	0.00		2.41E+08	0.09219	0.00
1.500	2.51E+08	0.10887	0.00		2.71E+08	0.11357	0.00		2.27E+08	0.09691	0.00		2.81E+08	0.10778	0.00
1.881	2.21E+08	0.09584	0.01		2.15E+08	0.09017	0.00		2.52E+08	0.10783	0.01		2.75E+08	0.10541	0.01
1.977	5.96E+08	0.25890	0.13		4.91E+08	0.20562	0.07		8.71E+08	0.37223	0.40		7.79E+08	0.29834	0.21
2.091	1.83E+08	0.07958	0.00		1.78E+08	0.07444	0.00		2.10E+08	0.08979	0.01		2.30E+08	0.08798	0.01
3.395	4.53E+06	0.00197	0.00		4.53E+06	0.00190	0.00		7.95E+06	0.00340	0.00		7.95E+06	0.00304	0.00
	2301765491		0.15		2388056995		0.08		2339026334		0.42		2610439224		0.23
		S_{RE}	**0.53**			S_{RE}	**0.44**			S_{RE}	**0.75**			S_{RE}	**0.61**

	Houston							Austin						
	Open	γ_i	$(\gamma_i SR_i)^3$		Suburban	γ_i	$(\gamma_i SR_i)^3$	Open	γ_i	$(\gamma_i SR_i)^3$		Suburban	γ_i	$(\gamma_i SR_i)^3$
	3.76E+04	0.00002	0.00		1.19E+05	0.00006	0.00	2.25E+04	0.00001	0.00		7.54E+04	0.00003	0.00
	1.67E+05	0.00008	0.00		4.57E+05	0.00022	0.00	1.09E+05	0.00004	0.00		3.17E+05	0.00012	0.00
	1.61E+05	0.00008	0.00		4.28E+05	0.00021	0.00	1.04E+05	0.00004	0.00		2.92E+05	0.00011	0.00
	4.81E+05	0.00024	0.00		1.17E+06	0.00057	0.00	3.37E+05	0.00014	0.00		8.74E+05	0.00033	0.00
	5.95E+05	0.00029	0.00		1.38E+06	0.00067	0.00	4.19E+05	0.00017	0.00		1.03E+06	0.00039	0.00
	5.75E+05	0.00028	0.00		1.29E+06	0.00062	0.00	3.99E+05	0.00016	0.00		9.41E+05	0.00036	0.00
	1.47E+06	0.00073	0.00		3.06E+06	0.00149	0.00	1.12E+06	0.00045	0.00		2.46E+06	0.00093	0.00
	1.78E+06	0.00088	0.00		3.50E+06	0.00170	0.00	1.35E+06	0.00054	0.00		2.80E+06	0.00107	0.00
	3.80E+06	0.00188	0.00		6.74E+06	0.00327	0.00	3.11E+06	0.00124	0.00		5.82E+06	0.00221	0.00
	1.71E+06	0.00085	0.00		3.21E+06	0.00156	0.00	1.27E+06	0.00051	0.00		2.51E+06	0.00095	0.00
	4.43E+06	0.00220	0.00		7.44E+06	0.00361	0.00	3.62E+06	0.00145	0.00		6.37E+06	0.00242	0.00
	4.17E+06	0.00207	0.00		6.52E+06	0.00316	0.00	3.33E+06	0.00133	0.00		5.42E+06	0.00206	0.00
	1.26E+08	0.06223	0.00		1.72E+08	0.08365	0.00	1.27E+08	0.05074	0.00		1.85E+08	0.07025	0.00
	1.16E+07	0.00577	0.00		1.08E+07	0.00523	0.00	1.02E+07	0.00409	0.00		9.40E+06	0.00357	0.00
	8.20E+06	0.00406	0.00		1.25E+07	0.00607	0.00	7.23E+06	0.00289	0.00		1.16E+07	0.00440	0.00
	9.19E+06	0.00456	0.00		1.31E+07	0.00636	0.00	8.05E+06	0.00322	0.00		1.19E+07	0.00453	0.00
	8.19E+06	0.00406	0.00		1.04E+07	0.00506	0.00	6.95E+06	0.00278	0.00		9.06E+06	0.00344	0.00
	1.57E+08	0.07804	0.00		1.86E+08	0.09042	0.00	1.75E+08	0.06997	0.00		2.20E+08	0.08358	0.00
	1.48E+07	0.00735	0.00		1.96E+07	0.00950	0.00	1.40E+07	0.00561	0.00		1.93E+07	0.00731	0.00
	1.85E+08	0.09176	0.00		2.23E+08	0.10835	0.00	2.02E+08	0.08091	0.00		2.58E+08	0.09812	0.00
	1.59E+08	0.07901	0.00		1.67E+08	0.08101	0.00	1.91E+08	0.07664	0.00		2.13E+08	0.08107	0.00
	1.56E+07	0.00776	0.00		1.88E+07	0.00914	0.00	1.45E+07	0.00583	0.00		1.79E+07	0.00681	0.00
	2.24E+07	0.01112	0.00		2.57E+07	0.01249	0.00	2.25E+07	0.00902	0.00		2.65E+07	0.01006	0.00
	1.92E+08	0.09517	0.00		2.01E+08	0.09751	0.00	2.31E+08	0.09239	0.00		2.56E+08	0.09731	0.00
	2.33E+08	0.11543	0.01		2.50E+08	0.12139	0.01	2.74E+08	0.10994	0.00		3.11E+08	0.11827	0.01
	2.00E+08	0.09926	0.01		1.88E+08	0.09142	0.01	2.60E+08	0.10421	0.01		2.59E+08	0.09827	0.01
	4.80E+08	0.23787	0.10		3.62E+08	0.17568	0.04	7.14E+08	0.28607	0.18		5.74E+08	0.21798	0.08
	1.66E+08	0.08242	0.01		1.55E+08	0.07514	0.00	2.16E+08	0.08664	0.01		2.14E+08	0.08126	0.00
	9.17E+06	0.00455	0.00		9.17E+06	0.00445	0.00	7.36E+06	0.00295	0.00		7.36E+06	0.00280	0.00
	2017388894		0.12		2061210543		0.06	2496496591		0.20		2632985276		0.10
		S_{RE}	**0.50**			S_{RE}	**0.39**		S_{RE}	**0.59**			S_{RE}	**0.47**

	El Paso						
	Open	γ_i	$(\gamma_i SR_i)^3$		Suburban	γ_i	$(\gamma_i SR_i)^3$
	7.70E+04	0.00004	0.00		2.33E+05	0.00013	0.00
	3.18E+05	0.00018	0.00		8.29E+05	0.00047	0.00
	3.11E+05	0.00017	0.00		7.87E+05	0.00044	0.00
	8.60E+05	0.00047	0.00		1.98E+06	0.00112	0.00
	1.06E+06	0.00058	0.00		2.33E+06	0.00132	0.00
	1.04E+06	0.00057	0.00		2.21E+06	0.00125	0.00
	2.44E+06	0.00134	0.00		4.77E+06	0.00269	0.00
	2.94E+06	0.00162	0.00		5.47E+06	0.00309	0.00
	5.79E+06	0.00318	0.00		9.64E+06	0.00544	0.00
	2.88E+06	0.00158	0.00		5.14E+06	0.00290	0.00
	6.77E+06	0.00372	0.00		1.07E+07	0.00606	0.00
	6.53E+06	0.00359	0.00		9.78E+06	0.00552	0.00
	1.47E+08	0.08068	0.00		1.85E+08	0.10418	0.00
	1.63E+07	0.00898	0.00		1.53E+07	0.00863	0.00
	1.14E+07	0.00630	0.00		1.64E+07	0.00928	0.00
	1.29E+07	0.00711	0.00		1.76E+07	0.00992	0.00
	1.20E+07	0.00659	0.00		1.48E+07	0.00838	0.00
	1.60E+08	0.08810	0.00		1.72E+08	0.09723	0.00
	1.89E+07	0.01042	0.00		2.37E+07	0.01340	0.00
	1.93E+08	0.10626	0.00		2.13E+08	0.12038	0.00
	1.43E+08	0.07888	0.00		1.36E+08	0.07652	0.00
	2.04E+07	0.01122	0.00		2.38E+07	0.01344	0.00
	2.64E+07	0.01450	0.00		2.93E+07	0.01652	0.00
	1.73E+08	0.09494	0.00		1.64E+08	0.09256	0.00
	2.16E+08	0.11875	0.01		2.12E+08	0.11997	0.01
	1.58E+08	0.08702	0.00		1.35E+08	0.07641	0.00
	2.98E+08	0.16416	0.03		2.00E+08	0.11297	0.01
	1.31E+08	0.07208	0.00		1.10E+08	0.06213	0.00
	4.90E+07	0.02694	0.00		4.90E+07	0.02765	0.00
	1817767386		0.05		1770948167		0.03
		S_{RE}	**0.37**			S_{RE}	**0.30**

	SAT Open				SAT Sub				DFW Open				DFW Sub		
# of yrs.	N	β	p_f		N	β	p_f		N	β	p_f		N	β	p_f
1	46035310	9.34	0.00%		47761140	10.67	0.00%		46780527	6.87	0.00%		52208784	8.08	0.00%
2	92070620	7.68	0.00%		95522280	9.00	0.00%		93561053	5.21	0.00%		104417569	6.42	0.00%
3	138105929	6.71	0.00%		143283420	8.03	0.00%		140341580	4.24	0.00%		156626353	5.45	0.00%
4	184141239	6.02	0.00%		191044560	7.34	0.00%		187122107	3.55	0.02%		208835138	4.76	0.00%
5	230176549	5.48	0.00%		238805699	6.80	0.00%		233902633	3.01	0.13%		261043922	4.22	0.00%
6	276211859	5.04	0.00%		286566839	6.37	0.00%		280683160	2.57	0.50%		313252707	3.78	0.01%
7	322247169	4.67	0.00%		334327979	6.00	0.00%		327463687	2.20	1.38%		365461491	3.41	0.03%
8	368282479	4.35	0.00%		382089119	5.67	0.00%		374244214	1.88	2.99%		417670276	3.09	0.10%
9	414317788	4.07	0.00%		429850259	5.39	0.00%		421024740	1.60	5.49%		469879060	2.81	0.25%
10	460353098	3.82	0.01%		477611399	5.14	0.00%		467805267	1.35	8.91%		522087845	2.56	0.53%
11	506388408	3.59	0.02%		525372539	4.91	0.00%		514585794	1.12	13.18%		574296629	2.33	1.00%
12	552423718	3.38	0.04%		573133679	4.70	0.00%		561366320	0.91	18.17%		626505414	2.12	1.70%
13	598459028	3.19	0.07%		620894819	4.51	0.00%		608146847	0.72	23.67%		678714198	1.93	2.70%
14	644494337	3.01	0.13%		668655959	4.33	0.00%		654927374	0.54	29.49%		730922983	1.75	4.01%
15	690529647	2.84	0.22%		716417098	4.17	0.00%		701707900	0.37	35.44%		783131767	1.58	5.66%
16	736564957	2.69	0.36%		764178238	4.01	0.00%		748488427	0.22	41.35%		835340552	1.43	7.65%
17	782600267	2.54	0.55%		811939378	3.87	0.01%		795268954	0.07	47.09%		887549336	1.28	9.97%
18	828635577	2.41	0.81%		859700518	3.73	0.01%		842049480	-0.06	52.56%		939758121	1.15	12.59%
19	874670886	2.28	1.14%		907461658	3.60	0.02%		888830007	-0.19	57.69%		991966905	1.02	15.47%
20	920706196	2.15	1.57%		955222798	3.48	0.03%		935610534	-0.32	62.44%		1044175690	0.89	18.59%
21	966741506	2.04	2.09%		1002983938	3.36	0.04%		982391060	-0.43	66.79%		1096384474	0.78	21.89%
22	1012776816	1.92	2.72%		1050745078	3.25	0.06%		1029171587	-0.55	70.74%		1148593259	0.66	25.32%
23	1058812126	1.82	3.46%		1098506218	3.14	0.08%		1075952114	-0.65	74.29%		1200802043	0.56	28.85%
24	1104847436	1.71	4.32%		1146267358	3.04	0.12%		1122732641	-0.75	77.47%		1253010827	0.46	32.43%
25	1150882745	1.62	5.29%		1194028497	2.94	0.16%		1169513167	-0.85	80.30%		1305219612	0.36	36.03%
26	1196918055	1.52	6.39%		1241789637	2.85	0.22%		1216293694	-0.95	82.81%		1357428396	0.26	39.61%
27	1242953365	1.43	7.60%		1289550777	2.76	0.29%		1263074221	-1.04	85.02%		1409637181	0.17	43.14%
28	1288988675	1.34	8.93%		1337311917	2.67	0.38%		1309854747	-1.12	86.96%		1461845965	0.09	46.59%
29	1335023985	1.26	10.37%		1385073057	2.58	0.49%		1356635274	-1.21	88.66%		1514054750	0.00	49.94%
30	1381059294	1.18	11.91%		1432834197	2.50	0.62%		1403415801	-1.29	90.15%		1566263534	-0.08	53.19%
31	1427094604	1.10	13.55%		1480595337	2.42	0.77%		1450196327	-1.37	91.45%		1618472319	-0.16	56.30%
32	1473129914	1.02	15.28%		1528356477	2.35	0.94%		1496976854	-1.44	92.58%		1670681103	-0.23	59.28%
33	1519165224	0.95	17.09%		1576117617	2.27	1.15%		1543757381	-1.52	93.56%		1722889888	-0.31	62.12%
34	1565200534	0.88	18.97%		1623878756	2.20	1.38%		1590537907	-1.59	94.41%		1775098672	-0.38	64.81%
35	1611235844	0.81	20.91%		1671639896	2.13	1.65%		1637318434	-1.66	95.15%		1827307457	-0.45	67.36%
36	1657271153	0.74	22.91%		1719401036	2.06	1.95%		1684098961	-1.73	95.80%		1879516241	-0.52	69.76%
37	1703306463	0.68	24.95%		1767162176	2.00	2.28%		1730879487	-1.79	96.35%		1931725026	-0.58	72.01%
38	1749341773	0.61	27.02%		1814923316	1.94	2.65%		1777660014	-1.86	96.84%		1983933810	-0.65	74.13%
39	1795377083	0.55	29.13%		1862684456	1.87	3.05%		1824440541	-1.92	97.26%		2036142595	-0.71	76.10%
40	1841412393	0.49	31.24%		1910445596	1.81	3.50%		1871221068	-1.98	97.62%		2088351379	-0.77	77.95%
41	1887447702	0.43	33.37%		1958206736	1.75	3.98%		1918001594	-2.04	97.93%		2140560164	-0.83	79.66%
42	1933483012	0.37	35.50%		2005967876	1.69	4.50%		1964782121	-2.10	98.20%		2192768948	-0.89	81.26%
43	1979518322	0.32	37.62%		2053729016	1.64	5.07%		2011562648	-2.15	98.44%		2244977733	-0.94	82.74%
44	2025553632	0.26	39.73%		2101490155	1.58	5.67%		2058343174	-2.21	98.64%		2297186517	-1.00	84.11%
45	2071588942	0.21	41.83%		2149251295	1.53	6.31%		2105123701	-2.26	98.82%		2349395302	-1.05	85.38%
46	2117624252	0.15	43.90%		2197012435	1.48	6.99%		2151904228	-2.32	98.97%		2401604086	-1.11	86.56%
47	2163659561	0.10	45.94%		2244773575	1.42	7.71%		2198684754	-2.37	99.10%		2453812870	-1.16	87.64%
48	2209694871	0.05	47.95%		2292534715	1.37	8.47%		2245465281	-2.42	99.22%		2506021655	-1.21	88.65%
49	2255730181	0.00	49.92%		2340295855	1.32	9.26%		2292245808	-2.47	99.32%		2558230439	-1.26	89.57%
50	2301765491	-0.05	51.86%		2388056995	1.28	10.09%		2339026334	-2.52	99.41%		2610439224	-1.31	90.42%
Years	Cycles	β	p_f		Years	Cycles	β		Years	Cycles	β		Years	Cycles	β
11.4	525135102	3.50	0.02%		19.8	945529850	3.50		4.1	190765926	3.50		6.7	352398939	3.50

IAH Open			IAH Sub			RMMA Open			RMMA Sub		
N	β	p_f	N	β	p_f	N	β	p_f	N	β	p_f
40347778	10.14	0.00%	41224211	11.79	0.00%	49929932	8.46	0.00%	52659706	10.00	0.00%
80695556	8.47	0.00%	82448422	10.12	0.00%	99859864	6.80	0.00%	105319411	8.34	0.00%
121043334	7.50	0.00%	123672633	9.15	0.00%	149789795	5.83	0.00%	157979117	7.37	0.00%
161391112	6.81	0.00%	164896843	8.46	0.00%	199719727	5.14	0.00%	210638822	6.68	0.00%
201738889	6.28	0.00%	206121054	7.92	0.00%	249649659	4.60	0.00%	263298528	6.14	0.00%
242086667	5.84	0.00%	247345265	7.48	0.00%	299579591	4.16	0.00%	315958233	5.70	0.00%
282434445	5.47	0.00%	288569476	7.12	0.00%	349509523	3.79	0.01%	368617939	5.33	0.00%
322782223	5.15	0.00%	329793687	6.79	0.00%	399439455	3.47	0.03%	421277644	5.01	0.00%
363130001	4.86	0.00%	371017898	6.51	0.00%	449369386	3.19	0.07%	473937350	4.73	0.00%
403477779	4.61	0.00%	412242109	6.26	0.00%	499299318	2.94	0.16%	526597055	4.48	0.00%
443825557	4.38	0.00%	453466320	6.03	0.00%	549229250	2.71	0.34%	579256761	4.25	0.00%
484173335	4.17	0.00%	494690530	5.82	0.00%	599159182	2.50	0.62%	631916466	4.04	0.00%
524521112	3.98	0.00%	535914741	5.63	0.00%	649089114	2.31	1.05%	684576172	3.85	0.01%
564868890	3.80	0.01%	577138952	5.45	0.00%	699019046	2.13	1.65%	737235877	3.67	0.01%
605216668	3.64	0.01%	618363163	5.29	0.00%	748948977	1.97	2.47%	789895583	3.50	0.02%
645564446	3.48	0.02%	659587374	5.13	0.00%	798878909	1.81	3.51%	842555288	3.35	0.04%
685912224	3.34	0.04%	700811585	4.99	0.00%	848808841	1.67	4.79%	895214994	3.20	0.07%
726260002	3.20	0.07%	742035796	4.85	0.00%	898738773	1.53	6.32%	947874699	3.07	0.11%
766607780	3.07	0.11%	783260006	4.72	0.00%	948668705	1.40	8.10%	1000534405	2.94	0.17%
806955558	2.95	0.16%	824484217	4.60	0.00%	998598637	1.28	10.11%	1053194110	2.81	0.25%
847303336	2.83	0.23%	865708428	4.48	0.00%	1048528568	1.16	12.34%	1105853816	2.70	0.35%
887651113	2.72	0.33%	906932639	4.37	0.00%	1098458500	1.05	14.76%	1158513522	2.58	0.49%
927998891	2.61	0.45%	948156850	4.26	0.00%	1148388432	0.94	17.36%	1211173227	2.48	0.66%
968346669	2.51	0.60%	989381061	4.16	0.00%	1198318364	0.84	20.11%	1263832933	2.38	0.88%
1008694447	2.41	0.79%	1030605272	4.06	0.00%	1248248296	0.74	22.97%	1316492638	2.28	1.14%
1049042225	2.32	1.02%	1071829482	3.97	0.00%	1298178228	0.65	25.92%	1369152344	2.18	1.45%
1089390003	2.23	1.29%	1113053693	3.88	0.01%	1348108159	0.56	28.94%	1421812049	2.09	1.82%
1129737781	2.14	1.62%	1154277904	3.79	0.01%	1398038091	0.47	32.00%	1474471755	2.01	2.25%
1170085559	2.06	1.99%	1195502115	3.70	0.01%	1447968023	0.38	35.06%	1527131460	1.92	2.73%
1210433336	1.97	2.41%	1236726326	3.62	0.01%	1497897955	0.30	38.12%	1579791166	1.84	3.29%
1250781114	1.90	2.90%	1277950537	3.54	0.02%	1547827887	0.22	41.16%	1632450871	1.76	3.91%
1291128892	1.82	3.44%	1319174748	3.47	0.03%	1597757819	0.15	44.14%	1685110577	1.69	4.60%
1331476670	1.75	4.04%	1360398959	3.39	0.03%	1647687750	0.07	47.07%	1737770282	1.61	5.36%
1371824448	1.67	4.70%	1401623169	3.32	0.04%	1697617682	0.00	49.93%	1790429988	1.54	6.18%
1412172226	1.61	5.42%	1442847380	3.25	0.06%	1747547614	-0.07	52.70%	1843089693	1.47	7.08%
1452520004	1.54	6.21%	1484071591	3.18	0.07%	1797477546	-0.14	55.38%	1895749399	1.40	8.04%
1492867782	1.47	7.06%	1525295802	3.12	0.09%	1847407478	-0.20	57.97%	1948409104	1.34	9.07%
1533215560	1.41	7.96%	1566520013	3.06	0.11%	1897337409	-0.27	60.45%	2001068810	1.27	10.16%
1573563337	1.35	8.93%	1607744224	2.99	0.14%	1947267341	-0.33	62.83%	2053728515	1.21	11.31%
1613911115	1.28	9.95%	1648968435	2.93	0.17%	1997197273	-0.39	65.11%	2106388221	1.15	12.52%
1654258893	1.23	11.02%	1690192645	2.87	0.20%	2047127205	-0.45	67.27%	2159047927	1.09	13.78%
1694606671	1.17	12.15%	1731416856	2.81	0.24%	2097057137	-0.51	69.33%	2211707632	1.03	15.09%
1734954449	1.11	13.33%	1772641067	2.76	0.29%	2146987069	-0.56	71.29%	2264367338	0.98	16.45%
1775302227	1.06	14.55%	1813865278	2.70	0.34%	2196917000	-0.62	73.14%	2317027043	0.92	17.86%
1815650005	1.00	15.82%	1855089489	2.65	0.40%	2246846932	-0.67	74.88%	2369686749	0.87	19.30%
1855997783	0.95	17.13%	1896313700	2.60	0.47%	2296776864	-0.72	76.53%	2422346454	0.81	20.78%
1896345560	0.90	18.47%	1937537911	2.54	0.55%	2346706796	-0.78	78.09%	2475006160	0.76	22.29%
1936693338	0.85	19.85%	1978762122	2.49	0.63%	2396636728	-0.83	79.55%	2527665865	0.71	23.82%
1977041116	0.80	21.26%	2019986332	2.44	0.72%	2446566660	-0.88	80.93%	2580325571	0.66	25.38%
2017388894	0.75	22.69%	2061210543	2.40	0.83%	2496496591	-0.92	82.22%	2632985276	0.61	26.96%

Years	Cycles	β	Years	Cycles	β	Years	Cycles	β	Years	Cycles	β
15.9	641119975	3.50	31.6	1301038740	3.50	7.9	395236681	3.50	15.0	790901138	3.50

ELP Open				ELP Sub			
N	β	p_f		N	β	p_f	
36355348	12.46	0.00%		35418963	14.08	0.00%	
72710695	10.80	0.00%		70837927	12.42	0.00%	
109066043	9.82	0.00%		106256890	11.45	0.00%	
145421391	9.13	0.00%		141675853	10.76	0.00%	
181776739	8.60	0.00%		177094817	10.22	0.00%	
218132086	8.16	0.00%		212513780	9.78	0.00%	
254487434	7.79	0.00%		247932743	9.41	0.00%	
290842782	7.47	0.00%		283351707	9.09	0.00%	
327198130	7.19	0.00%		318770670	8.81	0.00%	
363553477	6.93	0.00%		354189633	8.56	0.00%	
399908825	6.70	0.00%		389608597	8.33	0.00%	
436264173	6.50	0.00%		425027560	8.12	0.00%	
472619520	6.30	0.00%		460446523	7.93	0.00%	
508974868	6.13	0.00%		495865487	7.75	0.00%	
545330216	5.96	0.00%		531284450	7.58	0.00%	
581685564	5.80	0.00%		566703413	7.43	0.00%	
618040911	5.66	0.00%		602122377	7.28	0.00%	
654396259	5.52	0.00%		637541340	7.15	0.00%	
690751607	5.39	0.00%		672960303	7.02	0.00%	
727106955	5.27	0.00%		708379267	6.89	0.00%	
763462302	5.15	0.00%		743798230	6.78	0.00%	
799817650	5.04	0.00%		779217193	6.66	0.00%	
836172998	4.93	0.00%		814636157	6.56	0.00%	
872528345	4.83	0.00%		850055120	6.46	0.00%	
908883693	4.73	0.00%		885474083	6.36	0.00%	
945239041	4.64	0.00%		920893047	6.26	0.00%	
981594389	4.55	0.00%		956312010	6.17	0.00%	
1017949736	4.46	0.00%		991730973	6.09	0.00%	
1054305084	4.38	0.00%		1027149937	6.00	0.00%	
1090660432	4.30	0.00%		1062568900	5.92	0.00%	
1127015780	4.22	0.00%		1097987863	5.84	0.00%	
1163371127	4.14	0.00%		1133406827	5.77	0.00%	
1199726475	4.07	0.00%		1168825790	5.69	0.00%	
1236081823	4.00	0.00%		1204244753	5.62	0.00%	
1272437170	3.93	0.00%		1239663717	5.55	0.00%	
1308792518	3.86	0.01%		1275082680	5.48	0.00%	
1345147866	3.79	0.01%		1310501643	5.42	0.00%	
1381503214	3.73	0.01%		1345920607	5.35	0.00%	
1417858561	3.67	0.01%		1381339570	5.29	0.00%	
1454213909	3.61	0.02%		1416758533	5.23	0.00%	
1490569257	3.55	0.02%		1452177497	5.17	0.00%	
1526924604	3.49	0.02%		1487596460	5.11	0.00%	
1563279952	3.43	0.03%		1523015423	5.06	0.00%	
1599635300	3.38	0.04%		1558434387	5.00	0.00%	
1635990648	3.32	0.04%		1593853350	4.95	0.00%	
1672345995	3.27	0.05%		1629272313	4.89	0.00%	
1708701343	3.22	0.06%		1664691277	4.84	0.00%	
1745056691	3.17	0.08%		1700110240	4.79	0.00%	
1781412039	3.12	0.09%		1735529203	4.74	0.00%	
1817767386	3.07	0.11%		1770948167	4.69	0.00%	
Years	Cycles	β		Years	Cycles	β	
41.8	1519177996	3.50		82.2	2912486880	3.50	

	San Antonio							Dallas/Fort Worth						
S_{Ri} (no GS)	Open	γ_i	$(\gamma_i SR_i)^3$		Suburban	γ_i	$(\gamma_i SR_i)^3$	Open	γ_i	$(\gamma_i SR_i)^3$		Suburban	γ_i	$(\gamma_i SR_i)^3$
0.020	6.52E+04	0.00004	0.00		1.92E+05	0.00010	0.00	2.03E+03	0.00000	0.00		9.17E+03	0.00000	0.00
0.031	2.25E+05	0.00013	0.00		5.86E+05	0.00030	0.00	1.24E+04	0.00001	0.00		4.80E+04	0.00003	0.00
0.035	2.27E+05	0.00013	0.00		5.80E+05	0.00030	0.00	1.16E+04	0.00001	0.00		4.36E+04	0.00002	0.00
0.045	5.48E+05	0.00031	0.00		1.29E+06	0.00067	0.00	4.67E+04	0.00003	0.00		1.59E+05	0.00008	0.00
0.054	6.80E+05	0.00039	0.00		1.54E+06	0.00080	0.00	5.93E+04	0.00004	0.00		1.92E+05	0.00010	0.00
0.057	6.88E+05	0.00040	0.00		1.52E+06	0.00079	0.00	5.56E+04	0.00004	0.00		1.73E+05	0.00009	0.00
0.079	1.47E+06	0.00084	0.00		3.01E+06	0.00156	0.00	1.93E+05	0.00012	0.00		5.52E+05	0.00029	0.00
0.090	1.79E+06	0.00103	0.00		3.52E+06	0.00183	0.00	2.38E+05	0.00015	0.00		6.41E+05	0.00034	0.00
0.130	3.42E+06	0.00197	0.00		6.15E+06	0.00320	0.00	6.67E+05	0.00043	0.00		1.60E+06	0.00085	0.00
0.155	1.80E+06	0.00104	0.00		3.45E+06	0.00179	0.00	2.21E+05	0.00014	0.00		5.66E+05	0.00030	0.00
0.242	8.00E+07	0.04602	0.00		1.15E+08	0.05970	0.00	3.44E+07	0.02205	0.00		6.20E+07	0.03284	0.00
0.245	4.08E+06	0.00234	0.00		7.02E+06	0.00365	0.00	7.95E+05	0.00051	0.00		1.79E+06	0.00095	0.00
0.283	4.07E+06	0.00234	0.00		6.71E+06	0.00349	0.00	7.21E+05	0.00046	0.00		1.51E+06	0.00080	0.00
0.354	6.96E+06	0.00401	0.00		1.10E+07	0.00571	0.00	1.93E+06	0.00124	0.00		3.90E+06	0.00206	0.00
0.381	1.08E+08	0.06231	0.00		1.39E+08	0.07201	0.00	6.56E+07	0.04197	0.00		1.02E+08	0.05414	0.00
0.421	1.25E+08	0.07209	0.00		1.62E+08	0.08401	0.00	7.18E+07	0.04598	0.00		1.12E+08	0.05942	0.00
0.446	8.05E+06	0.00463	0.00		1.21E+07	0.00628	0.00	2.20E+06	0.00141	0.00		4.09E+06	0.00217	0.00
0.497	1.24E+07	0.00714	0.00		1.44E+07	0.00748	0.00	3.80E+06	0.00244	0.00		4.77E+06	0.00253	0.00
0.523	7.83E+06	0.00451	0.00		1.10E+07	0.00572	0.00	1.90E+06	0.00122	0.00		3.17E+06	0.00168	0.00
0.552	1.21E+08	0.06979	0.00		1.41E+08	0.07336	0.00	9.40E+07	0.06017	0.00		1.30E+08	0.06890	0.00
0.645	1.23E+07	0.00708	0.00		1.71E+07	0.00891	0.00	4.65E+06	0.00298	0.00		7.88E+06	0.00417	0.00
0.663	1.46E+08	0.08422	0.00		1.69E+08	0.08792	0.00	1.14E+08	0.07283	0.00		1.55E+08	0.08205	0.00
0.695	1.73E+08	0.09946	0.00		2.02E+08	0.10506	0.00	1.27E+08	0.08140	0.00		1.74E+08	0.09210	0.00
0.823	1.37E+07	0.00787	0.00		1.79E+07	0.00931	0.00	4.96E+06	0.00318	0.00		7.58E+06	0.00401	0.00
0.960	1.45E+08	0.08356	0.00		1.53E+08	0.07970	0.00	1.40E+08	0.08968	0.00		1.70E+08	0.09020	0.00
0.991	1.89E+07	0.01088	0.00		2.33E+07	0.01212	0.00	9.25E+06	0.00593	0.00		1.31E+07	0.00695	0.00
1.094	1.75E+08	0.10047	0.00		1.84E+08	0.09577	0.00	1.68E+08	0.10758	0.00		2.02E+08	0.10707	0.00
1.461	5.61E+08	0.32271	0.10		5.13E+08	0.26638	0.06	7.08E+08	0.45358	0.29		7.22E+08	0.38216	0.17
3.610	3.97E+06	0.00228	0.00		3.97E+06	0.00206	0.00	6.96E+06	0.00445	0.00		6.96E+06	0.00368	0.00
	1738538679		0.11		1924414763		0.06	1561677615		0.29		1888605373		0.18
		S_{RE}	**0.48**			S_{RE}	**0.39**		S_{RE}	**0.66**			S_{RE}	**0.56**

Houston								Austin							
	Open	γ_i	$(\gamma_i SR_i)^3$		Suburban	γ_i	$(\gamma_i SR_i)^3$		Open	γ_i	$(\gamma_i SR_i)^3$		Suburban	γ_i	$(\gamma_i SR_i)^3$
	1.32E+04	0.00001	0.00		5.09E+04	0.00003	0.00		7.57E+03	0.00000	0.00		3.11E+04	0.00002	0.00
	6.50E+04	0.00004	0.00		2.14E+05	0.00013	0.00		4.06E+04	0.00002	0.00		1.43E+05	0.00007	0.00
	6.28E+04	0.00004	0.00		2.01E+05	0.00012	0.00		3.88E+04	0.00002	0.00		1.33E+05	0.00006	0.00
	2.05E+05	0.00013	0.00		5.91E+05	0.00035	0.00		1.38E+05	0.00008	0.00		4.25E+05	0.00021	0.00
	2.57E+05	0.00017	0.00		7.09E+05	0.00042	0.00		1.74E+05	0.00010	0.00		5.10E+05	0.00025	0.00
	2.49E+05	0.00016	0.00		6.65E+05	0.00039	0.00		1.66E+05	0.00009	0.00		4.70E+05	0.00023	0.00
	6.96E+05	0.00045	0.00		1.69E+06	0.00100	0.00		5.05E+05	0.00028	0.00		1.31E+06	0.00063	0.00
	8.52E+05	0.00055	0.00		1.97E+06	0.00116	0.00		6.20E+05	0.00034	0.00		1.52E+06	0.00074	0.00
	1.98E+06	0.00128	0.00		4.07E+06	0.00240	0.00		1.55E+06	0.00085	0.00		3.39E+06	0.00164	0.00
	8.22E+05	0.00053	0.00		1.83E+06	0.00108	0.00		5.89E+05	0.00032	0.00		1.39E+06	0.00067	0.00
	6.41E+07	0.04160	0.00		9.86E+07	0.05817	0.00		6.02E+07	0.03314	0.00		9.84E+07	0.04759	0.00
	2.36E+06	0.00153	0.00		4.59E+06	0.00271	0.00		1.85E+06	0.00102	0.00		3.81E+06	0.00184	0.00
	2.24E+06	0.00146	0.00		4.14E+06	0.00244	0.00		1.73E+06	0.00095	0.00		3.34E+06	0.00162	0.00
	4.73E+06	0.00307	0.00		8.24E+06	0.00486	0.00		4.00E+06	0.00220	0.00		7.37E+06	0.00357	0.00
	9.57E+07	0.06209	0.00		1.27E+08	0.07492	0.00		9.87E+07	0.05432	0.00		1.39E+08	0.06737	0.00
	1.09E+08	0.07084	0.00		1.47E+08	0.08650	0.00		1.11E+08	0.06100	0.00		1.58E+08	0.07628	0.00
	5.42E+06	0.00352	0.00		8.90E+06	0.00525	0.00		4.57E+06	0.00251	0.00		7.87E+06	0.00381	0.00
	8.77E+06	0.00569	0.00		1.05E+07	0.00619	0.00		7.58E+06	0.00417	0.00		9.24E+06	0.00447	0.00
	5.00E+06	0.00324	0.00		7.58E+06	0.00447	0.00		4.11E+06	0.00226	0.00		6.46E+06	0.00312	0.00
	1.12E+08	0.07257	0.00		1.31E+08	0.07752	0.00		1.25E+08	0.06864	0.00		1.56E+08	0.07542	0.00
	9.45E+06	0.00613	0.00		1.41E+07	0.00830	0.00		8.58E+06	0.00472	0.00		1.34E+07	0.00650	0.00
	1.35E+08	0.08755	0.00		1.57E+08	0.09286	0.00		1.51E+08	0.08290	0.00		1.86E+08	0.09012	0.00
	1.58E+08	0.10259	0.00		1.88E+08	0.11071	0.00		1.73E+08	0.09538	0.00		2.17E+08	0.10500	0.00
	1.03E+07	0.00671	0.00		1.43E+07	0.00843	0.00		9.30E+06	0.00512	0.00		1.34E+07	0.00646	0.00
	1.35E+08	0.08758	0.00		1.40E+08	0.08271	0.00		1.63E+08	0.08973	0.00		1.80E+08	0.08692	0.00
	1.58E+07	0.01026	0.00		2.03E+07	0.01196	0.00		1.54E+07	0.00845	0.00		2.05E+07	0.00990	0.00
	1.62E+08	0.10526	0.00		1.69E+08	0.09958	0.00		1.96E+08	0.10775	0.00		2.15E+08	0.10407	0.00
	4.93E+08	0.31975	0.10		4.25E+08	0.25059	0.05		6.73E+08	0.37008	0.16		6.17E+08	0.29832	0.08
	8.03E+06	0.00521	0.00		8.03E+06	0.00474	0.00		6.44E+06	0.00355	0.00		6.44E+06	0.00312	0.00
	1541793466		0.10		1694804538		0.05		1817579083		0.16		2067807117		0.09
		S_{RE}	**0.47**			S_{RE}	**0.37**			S_{RE}	**0.54**			S_{RE}	**0.44**

					El Paso			
	Open	γ_i	$(\gamma_i SR_i)^3$		Suburban	γ_i	$(\gamma_i SR_i)^3$	
	2.79E+04	0.00002	0.00		1.03E+05	0.00007	0.00	
	1.29E+05	0.00009	0.00		4.01E+05	0.00026	0.00	
	1.25E+05	0.00008	0.00		3.82E+05	0.00025	0.00	
	3.82E+05	0.00025	0.00		1.04E+06	0.00067	0.00	
	4.78E+05	0.00032	0.00		1.24E+06	0.00080	0.00	
	4.68E+05	0.00031	0.00		1.18E+06	0.00076	0.00	
	1.21E+06	0.00080	0.00		2.74E+06	0.00177	0.00	
	1.47E+06	0.00098	0.00		3.20E+06	0.00206	0.00	
	3.17E+06	0.00211	0.00		6.07E+06	0.00391	0.00	
	1.44E+06	0.00096	0.00		3.04E+06	0.00196	0.00	
	8.79E+07	0.05844	0.00		1.26E+08	0.08134	0.00	
	3.77E+06	0.00250	0.00		6.89E+06	0.00444	0.00	
	3.66E+06	0.00243	0.00		6.41E+06	0.00413	0.00	
	6.94E+06	0.00461	0.00		1.13E+07	0.00728	0.00	
	1.13E+08	0.07480	0.00		1.36E+08	0.08759	0.00	
	1.32E+08	0.08796	0.00		1.64E+08	0.10542	0.00	
	8.00E+06	0.00531	0.00		1.24E+07	0.00796	0.00	
	1.25E+07	0.00833	0.00		1.47E+07	0.00945	0.00	
	7.60E+06	0.00505	0.00		1.10E+07	0.00710	0.00	
	1.15E+08	0.07634	0.00		1.20E+08	0.07753	0.00	
	1.27E+07	0.00844	0.00		1.77E+07	0.01141	0.00	
	1.39E+08	0.09206	0.00		1.45E+08	0.09334	0.00	
	1.68E+08	0.11177	0.00		1.81E+08	0.11686	0.00	
	1.41E+07	0.00935	0.00		1.85E+07	0.01193	0.00	
	1.20E+08	0.07960	0.00		1.09E+08	0.07034	0.00	
	1.95E+07	0.01294	0.00		2.37E+07	0.01524	0.00	
	1.44E+08	0.09581	0.00		1.33E+08	0.08541	0.00	
	3.46E+08	0.22986	0.04		2.53E+08	0.16311	0.01	
	4.29E+07	0.02849	0.00		4.29E+07	0.02762	0.00	
	1504794609		0.04		1551727851		0.02	
		S_{RE}	**0.35**			S_{RE}	**0.26**	

	SAT Open				SAT Sub				DFW Open				DFW Sub		
# of yrs.	N	β	p_f		N	β	p_f		N	β	p_f		N	β	p_f
1	34770774	10.85	0.00%		38488295	11.95	0.00%		31233552	8.69	0.00%		37772107	9.45	0.00%
2	69541547	9.19	0.00%		76976591	10.29	0.00%		62467105	7.03	0.00%		75544215	7.79	0.00%
3	104312321	8.22	0.00%		115464886	9.32	0.00%		93700657	6.06	0.00%		113316322	6.82	0.00%
4	139083094	7.53	0.00%		153953181	8.63	0.00%		124934209	5.37	0.00%		151088430	6.13	0.00%
5	173853868	6.99	0.00%		192441476	8.09	0.00%		156167762	4.83	0.00%		188860537	5.59	0.00%
6	208624641	6.55	0.00%		230929772	7.65	0.00%		187401314	4.39	0.00%		226632645	5.15	0.00%
7	243395415	6.18	0.00%		269418067	7.28	0.00%		218634866	4.02	0.00%		264404752	4.78	0.00%
8	278166189	5.86	0.00%		307906362	6.96	0.00%		249868418	3.70	0.01%		302176860	4.46	0.00%
9	312936962	5.58	0.00%		346394657	6.68	0.00%		281101971	3.42	0.03%		339948967	4.18	0.00%
10	347707736	5.33	0.00%		384882953	6.43	0.00%		312335523	3.17	0.08%		377721075	3.93	0.00%
11	382478509	5.10	0.00%		423371248	6.20	0.00%		343569075	2.94	0.16%		415493182	3.70	0.01%
12	417249283	4.89	0.00%		461859543	5.99	0.00%		374802628	2.73	0.32%		453265290	3.49	0.02%
13	452020057	4.70	0.00%		500347838	5.80	0.00%		406036180	2.54	0.56%		491037397	3.30	0.05%
14	486790830	4.52	0.00%		538836134	5.62	0.00%		437269732	2.36	0.91%		528809505	3.12	0.09%
15	521561604	4.35	0.00%		577324429	5.45	0.00%		468503285	2.19	1.41%		566581612	2.96	0.16%
16	556332377	4.20	0.00%		615812724	5.30	0.00%		499736837	2.04	2.07%		604353719	2.80	0.26%
17	591103151	4.05	0.00%		654301019	5.15	0.00%		530970389	1.89	2.91%		642125827	2.65	0.40%
18	625873924	3.92	0.00%		692789315	5.02	0.00%		562203942	1.76	3.95%		679897934	2.52	0.59%
19	660644698	3.79	0.01%		731277610	4.89	0.00%		593437494	1.63	5.19%		717670042	2.39	0.85%
20	695415472	3.66	0.01%		769765905	4.76	0.00%		624671046	1.50	6.63%		755442149	2.26	1.18%
21	730186245	3.55	0.02%		808254200	4.65	0.00%		655904598	1.39	8.28%		793214257	2.15	1.59%
22	764957019	3.43	0.03%		846742496	4.53	0.00%		687138151	1.28	10.11%		830986364	2.04	2.09%
23	799727792	3.33	0.04%		885230791	4.43	0.00%		718371703	1.17	12.13%		868758472	1.93	2.68%
24	834498566	3.23	0.06%		923719086	4.33	0.00%		749605255	1.07	14.31%		906530579	1.83	3.38%
25	869269339	3.13	0.09%		962207381	4.23	0.00%		780838808	0.97	16.64%		944302687	1.73	4.19%
26	904040113	3.03	0.12%		1000695677	4.13	0.00%		812072360	0.87	19.10%		982074794	1.64	5.10%
27	938810887	2.94	0.16%		1039183972	4.04	0.00%		843305912	0.78	21.66%		1019846902	1.54	6.12%
28	973581660	2.86	0.21%		1077672267	3.96	0.00%		874539465	0.70	24.31%		1057619009	1.46	7.25%
29	1008352434	2.77	0.28%		1116160562	3.87	0.01%		905773017	0.61	27.02%		1095391117	1.37	8.48%
30	1043123207	2.69	0.36%		1154648858	3.79	0.01%		937006569	0.53	29.78%		1133163224	1.29	9.82%
31	1077893981	2.61	0.45%		1193137153	3.71	0.01%		968240122	0.45	32.56%		1170935332	1.21	11.25%
32	1112664755	2.54	0.56%		1231625448	3.64	0.01%		999473674	0.38	35.35%		1208707439	1.14	12.78%
33	1147435528	2.46	0.69%		1270113743	3.56	0.02%		1030707226	0.30	38.13%		1246479546	1.06	14.39%
34	1182206302	2.39	0.84%		1308602039	3.49	0.02%		1061940778	0.23	40.89%		1284251654	0.99	16.07%
35	1216977075	2.32	1.02%		1347090334	3.42	0.03%		1093174331	0.16	43.61%		1322023761	0.92	17.83%
36	1251747849	2.25	1.21%		1385578629	3.35	0.04%		1124407883	0.09	46.29%		1359795869	0.85	19.65%
37	1286518622	2.19	1.44%		1424066924	3.29	0.05%		1155641435	0.03	48.90%		1397567976	0.79	21.52%
38	1321289396	2.12	1.69%		1462555220	3.22	0.06%		1186874988	-0.04	51.46%		1435340084	0.72	23.44%
39	1356060170	2.06	1.97%		1501043515	3.16	0.08%		1218108540	-0.10	53.94%		1473112191	0.66	25.39%
40	1390830943	2.00	2.28%		1539531810	3.10	0.10%		1249342092	-0.16	56.34%		1510884299	0.60	27.38%
41	1425601717	1.94	2.62%		1578020105	3.04	0.12%		1280575645	-0.22	58.66%		1548656406	0.54	29.39%
42	1460372490	1.88	2.99%		1616508401	2.98	0.14%		1311809197	-0.28	60.90%		1586428514	0.48	31.41%
43	1495143264	1.83	3.39%		1654996696	2.93	0.17%		1343042749	-0.33	63.05%		1624200621	0.43	33.44%
44	1529914037	1.77	3.83%		1693484991	2.87	0.20%		1374276302	-0.39	65.11%		1661972729	0.37	35.47%
45	1564684811	1.72	4.30%		1731973286	2.82	0.24%		1405509854	-0.44	67.09%		1699744836	0.32	37.50%
46	1599455585	1.66	4.80%		1770461582	2.76	0.29%		1436743406	-0.50	68.97%		1737516944	0.27	39.51%
47	1634226358	1.61	5.34%		1808949877	2.71	0.33%		1467976958	-0.55	70.77%		1775289051	0.21	41.51%
48	1668997132	1.56	5.91%		1847438172	2.66	0.39%		1499210511	-0.60	72.48%		1813061158	0.16	43.49%
49	1703767905	1.51	6.52%		1885926467	2.61	0.45%		1530444063	-0.65	74.11%		1850833266	0.11	45.45%
50	1738538679	1.46	7.16%		1924414763	2.56	0.52%		1561677615	-0.70	75.65%		1888605373	0.07	47.37%
Years	Cycles	β	p_f		Years	Cycles	β		Years	Cycles	β		Years	Cycles	β
21.4	744373383	3.50	0.02%		33.9	1302910454	3.50		8.7	271890175	3.50		12.0	451456587	3.50

IAH Open				IAH Sub				RMMA Open				RMMA Sub		
N	β	p_f		N	β	p_f		N	β	p_f		N	β	p_f
30835869	11.20	0.00%		33896091	12.66	0.00%		36351582	9.77	0.00%		41356142	10.98	0.00%
61671739	9.53	0.00%		67792182	11.00	0.00%		72703163	8.11	0.00%		82712285	9.32	0.00%
92507608	8.56	0.00%		101688272	10.03	0.00%		109054745	7.14	0.00%		124068427	8.34	0.00%
123343477	7.87	0.00%		135584363	9.34	0.00%		145406327	6.45	0.00%		165424569	7.65	0.00%
154179347	7.34	0.00%		169480454	8.80	0.00%		181757908	5.91	0.00%		206780712	7.12	0.00%
185015216	6.90	0.00%		203376545	8.36	0.00%		218109490	5.47	0.00%		248136854	6.68	0.00%
215851085	6.53	0.00%		237272635	7.99	0.00%		254461072	5.10	0.00%		289492996	6.31	0.00%
246686955	6.21	0.00%		271168726	7.67	0.00%		290812653	4.78	0.00%		330849139	5.99	0.00%
277522824	5.92	0.00%		305064817	7.39	0.00%		327164235	4.50	0.00%		372205281	5.71	0.00%
308358693	5.67	0.00%		338960908	7.14	0.00%		363515817	4.25	0.00%		413561423	5.45	0.00%
339194562	5.44	0.00%		372856998	6.91	0.00%		399867398	4.02	0.00%		454917566	5.22	0.00%
370030432	5.23	0.00%		406753089	6.70	0.00%		436218980	3.81	0.01%		496273708	5.01	0.00%
400866301	5.04	0.00%		440649180	6.51	0.00%		472570562	3.62	0.01%		537629850	4.82	0.00%
431702170	4.86	0.00%		474545271	6.33	0.00%		508922143	3.44	0.03%		578985993	4.64	0.00%
462538040	4.70	0.00%		508441361	6.17	0.00%		545273725	3.27	0.05%		620342135	4.48	0.00%
493373909	4.54	0.00%		542337452	6.01	0.00%		581625307	3.12	0.09%		661698277	4.32	0.00%
524209778	4.40	0.00%		576233543	5.87	0.00%		617976888	2.97	0.15%		703054420	4.18	0.00%
555045648	4.26	0.00%		610129634	5.73	0.00%		654328470	2.84	0.23%		744410562	4.04	0.00%
585881517	4.13	0.00%		644025724	5.60	0.00%		690680052	2.71	0.34%		785766704	3.91	0.00%
616717386	4.01	0.00%		677921815	5.48	0.00%		727031633	2.58	0.49%		827122847	3.79	0.01%
647553256	3.89	0.00%		711817906	5.36	0.00%		763383215	2.47	0.68%		868478989	3.67	0.01%
678389125	3.78	0.01%		745713997	5.25	0.00%		799734797	2.35	0.93%		909835131	3.56	0.02%
709224994	3.67	0.01%		779610087	5.14	0.00%		836086378	2.25	1.23%		951191274	3.45	0.03%
740060864	3.57	0.02%		813506178	5.04	0.00%		872437960	2.15	1.59%		992547416	3.35	0.04%
770896733	3.47	0.03%		847402269	4.94	0.00%		908789542	2.05	2.03%		1033903558	3.25	0.06%
801732602	3.38	0.04%		881298360	4.85	0.00%		945141123	1.95	2.54%		1075259701	3.16	0.08%
832568471	3.29	0.05%		915194450	4.76	0.00%		981492705	1.86	3.12%		1116615843	3.07	0.11%
863404341	3.20	0.07%		949090541	4.67	0.00%		1017844287	1.78	3.79%		1157971985	2.98	0.14%
894240210	3.12	0.09%		982986632	4.58	0.00%		1054195868	1.69	4.53%		1199328128	2.90	0.19%
925076079	3.04	0.12%		1016882723	4.50	0.00%		1090547450	1.61	5.36%		1240684270	2.82	0.24%
955911949	2.96	0.16%		1050778813	4.42	0.00%		1126899032	1.53	6.28%		1282040412	2.74	0.31%
986747818	2.88	0.20%		1084674904	4.35	0.00%		1163250613	1.46	7.27%		1323396555	2.66	0.39%
1017583687	2.81	0.25%		1118570995	4.27	0.00%		1199602195	1.38	8.35%		1364752697	2.59	0.48%
1048419557	2.73	0.31%		1152467086	4.20	0.00%		1235953777	1.31	9.51%		1406108839	2.52	0.59%
1079255426	2.67	0.38%		1186363176	4.13	0.00%		1272305358	1.24	10.74%		1447464982	2.45	0.72%
1110091295	2.60	0.47%		1220259267	4.06	0.00%		1308656940	1.17	12.04%		1488821124	2.38	0.87%
1140927165	2.53	0.57%		1254155358	4.00	0.00%		1345008522	1.11	13.41%		1530177266	2.31	1.04%
1171763034	2.47	0.68%		1288051449	3.93	0.00%		1381360103	1.04	14.84%		1571533409	2.25	1.23%
1202598903	2.41	0.81%		1321947539	3.87	0.01%		1417711685	0.98	16.33%		1612889551	2.19	1.44%
1233434773	2.34	0.95%		1355843630	3.81	0.01%		1454063267	0.92	17.88%		1654245693	2.13	1.68%
1264270642	2.29	1.11%		1389739721	3.75	0.01%		1490414848	0.86	19.47%		1695601836	2.07	1.94%
1295106511	2.23	1.29%		1423635812	3.69	0.01%		1526766430	0.80	21.10%		1736957978	2.01	2.23%
1325942380	2.17	1.50%		1457531902	3.64	0.01%		1563118012	0.75	22.77%		1778314120	1.95	2.55%
1356778250	2.12	1.72%		1491427993	3.58	0.02%		1599469593	0.69	24.47%		1819670263	1.90	2.89%
1387614119	2.06	1.96%		1525324084	3.53	0.02%		1635821175	0.64	26.19%		1861026405	1.84	3.27%
1418449988	2.01	2.22%		1559220175	3.48	0.03%		1672172757	0.58	27.94%		1902382547	1.79	3.67%
1449285858	1.96	2.51%		1593116265	3.42	0.03%		1708524338	0.53	29.70%		1943738690	1.74	4.11%
1480121727	1.91	2.82%		1627012356	3.37	0.04%		1744875920	0.48	31.47%		1985094832	1.69	4.57%
1510957596	1.86	3.16%		1660908447	3.32	0.04%		1781227502	0.43	33.25%		2026450975	1.64	5.07%
1541793466	1.81	3.52%		1694804538	3.28	0.05%		1817579083	0.38	35.03%		2067807117	1.59	5.59%
Years	Cycles	β		Years	Cycles	β		Years	Cycles	β		Years	Cycles	β
24.7	762225985	3.50		45.5	1543916918	3.50		13.7	496206896	3.50		22.6	932931067	3.50

ELP Open				ELP Sub			
N	β	p_f		N	β	p_f	
30095892	13.48	0.00%		31034557	15.60	0.00%	
60191784	11.82	0.00%		62069114	13.93	0.00%	
90287677	10.85	0.00%		93103671	12.96	0.00%	
120383569	10.16	0.00%		124138228	12.27	0.00%	
150479461	9.62	0.00%		155172785	11.74	0.00%	
180575353	9.18	0.00%		186207342	11.30	0.00%	
210671245	8.81	0.00%		217241899	10.93	0.00%	
240767137	8.49	0.00%		248276456	10.61	0.00%	
270863030	8.21	0.00%		279311013	10.33	0.00%	
300958922	7.96	0.00%		310345570	10.07	0.00%	
331054814	7.73	0.00%		341380127	9.84	0.00%	
361150706	7.52	0.00%		372414684	9.63	0.00%	
391246598	7.33	0.00%		403449241	9.44	0.00%	
421342490	7.15	0.00%		434483798	9.26	0.00%	
451438383	6.98	0.00%		465518355	9.10	0.00%	
481534275	6.83	0.00%		496552912	8.94	0.00%	
511630167	6.68	0.00%		527587469	8.80	0.00%	
541726059	6.55	0.00%		558622026	8.66	0.00%	
571821951	6.42	0.00%		589656583	8.53	0.00%	
601917843	6.29	0.00%		620691140	8.41	0.00%	
632013736	6.18	0.00%		651725697	8.29	0.00%	
662109628	6.07	0.00%		682760254	8.18	0.00%	
692205520	5.96	0.00%		713794811	8.07	0.00%	
722301412	5.86	0.00%		744829368	7.97	0.00%	
752397304	5.76	0.00%		775863925	7.87	0.00%	
782493197	5.66	0.00%		806898482	7.78	0.00%	
812589089	5.57	0.00%		837933039	7.69	0.00%	
842684981	5.49	0.00%		868967596	7.60	0.00%	
872780873	5.40	0.00%		900002153	7.52	0.00%	
902876765	5.32	0.00%		931036710	7.44	0.00%	
932972657	5.24	0.00%		962071267	7.36	0.00%	
963068550	5.17	0.00%		993105824	7.28	0.00%	
993164442	5.09	0.00%		1024140381	7.21	0.00%	
1023260334	5.02	0.00%		1055174939	7.14	0.00%	
1053356226	4.95	0.00%		1086209496	7.07	0.00%	
1083452118	4.88	0.00%		1117244053	7.00	0.00%	
1113548010	4.82	0.00%		1148278610	6.93	0.00%	
1143643903	4.75	0.00%		1179313167	6.87	0.00%	
1173739795	4.69	0.00%		1210347724	6.81	0.00%	
1203835687	4.63	0.00%		1241382281	6.75	0.00%	
1233931579	4.57	0.00%		1272416838	6.69	0.00%	
1264027471	4.51	0.00%		1303451395	6.63	0.00%	
1294123363	4.46	0.00%		1334485952	6.57	0.00%	
1324219256	4.40	0.00%		1365520509	6.52	0.00%	
1354315148	4.35	0.00%		1396555066	6.46	0.00%	
1384411040	4.30	0.00%		1427589623	6.41	0.00%	
1414506932	4.24	0.00%		1458624180	6.36	0.00%	
1444602824	4.19	0.00%		1489658737	6.31	0.00%	
1474698717	4.14	0.00%		1520693294	6.26	0.00%	
1504794609	4.09	0.00%		1551727851	6.21	0.00%	
Years	Cycles	β		Years	Cycles	β	
64.1	1927909553	3.50		154.6	4798632116	3.50	